This document is:

Ikegami, H., ed. *Third International Conference on Cold Fusion, "Frontiers of Cold Fusion"*. 1992, Universal Academy Press, Inc., Tokyo, Japan: Nagoya Japan. 698.

The printed book is in one volume, but this version has been split into two parts to facilitate downloading.

This is Part 2, page 253 to page 698:

http://lenr-canr.org/acrobat/IkegamiHthirdintera.pdf

Part 1, title page to page 252, is here:

http://lenr-canr.org/acrobat/IkegamiHthirdinter.pdf

Materials and Hydrogen Behavior

Hydrogen/Deuterium Concentration in Pd under Cathodic Polarization

Michio ENYO

Catalysis Research Center, Hokkaido University,

Kita 11 Nishi 10, Kita-ku, Sapporo, 060 JAPAN

ABSTRACT

Effective hydrogen pressure at hydrogen evolving cathode is discussed in connection with the mechanism of the hydrogen electrode reaction. A Nernst type expression involving hydrogen overpotential is not generally applicable. Experimental results on Pd and Pd-Ag alloy cathodes with and without addition of catalytic poison are presented. The highest pressure observed was *ca.* 10^6 atm at 0.25 A cm^{-2}, 30℃.

1. INTRODUCTION

The high reducing power of hydrogen evolving cathode in aqueous solution has been often quoted by the term *Nascent hydrogen*. An increasing attention is now paid on this phenomenon as the high activity of hydrogen produced by the hydrogen electrode reaction (HER) on Pd, or the hydrogen/deuterium concentration derived thereof in Pd, is believed to be one of the most vital factors involved in the alleged cold fusion.

The concentration of hydrogen in metal/alloy specimen should in general be determined by the pressure of hydrogen to which it is exposed, through the hydrogen absorption isotherm of Pd-H system. Alternatively, at the electrode at which HER is taking place, one may think of a hypothetical hydrogen pressure (which may be identified with the cavity pressure[1]) and the latter should in some way be related to the hydrogen overpotential. It is believed that hydrogen entry into metal takes place *via.* hydrogen adatom H(a) which is the intermediate of the HER.[1,2] In other words, evaluation of the hypothetical hydrogen pressure may be reduced to the evaluation of chemical potential of H(a) during actual

FRONTIERS OF COLD FUSION

progress of HER: Twice of the latter can be equated with that of the hypothetical hydrogen gas.

As demonstrated earlier[3-6], a Nernst-type expression to correlate the equivalent hydrogen pressure, $\bar{P}_{H_2}$, to the overpotential, η, as in **Eqn.(1)**,

$$-\eta = (RT/2F) \ln \bar{P}_{H_2} / P_{H_2,eq} \qquad (1)$$

is not generally justifiable. Thus, DeLuccia, Yamakawa and Nanis[7] carried out combined experimental observations of hydrogen permeation rates through a mild steel membrane electrode when its one face is exposed to gaseous hydrogen or alternatively to an electrochemical system where HER takes place. Experimentally observed relationship between such hydrogen pressures and overpotential values so as to yield the same rates of hydrogen permeation, reproduced in **Fig.1(A)**, indicated that the corresponding hydrogen pressure was far lower than expected from a Nernst-type relation applied to the overpotential (dotted line). This is a clear indication that a revision of the model is necessary. A quantitative description will be discussed below.

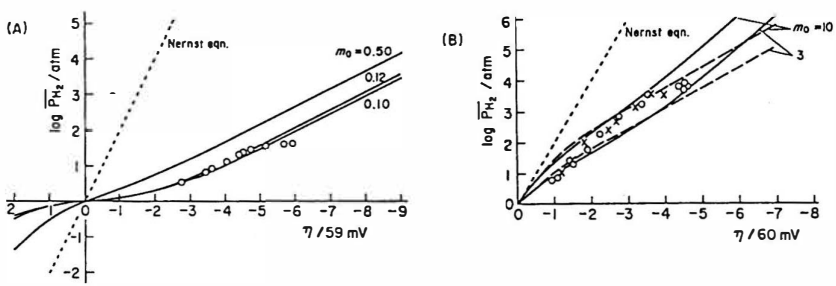

Fig.1. Equivalent hydrogen pressure *vs.* hydrogen overpotential relation. In both figures, the dotted lines represent **Eqn.(1)**, namely, a Nernst equation applied to η.
(A) On mild steel electrode observed by DeLuccia *et al.*[7] at 25 ℃. Solid lines are calculated for the Volmer-Tafel reaction route on the basis of the Langmuir isotherm with m_0 = 0.50, 0.12 (the best fit case) and 0.10.
(B) On Pd foil electrode[5] at 30 ℃. Solid lines (Langmuir isotherm) and broken lines (Temkin isotherm) are calculated with m_0 = 10 or 3.

2. SHORT SUMMARY OF ELECTRODE KINETICS

(1) Basic Kinetic Equations

Only an outline of the analysis[6] will be presented below. Basic equations involved are;

(i) the relationship which connects the Gibbs free energy decrease $-\Delta G$ (the reaction affinity) of the overall reaction, with $-\Delta g_s$, that shared by the consecutive elementary step s,

$$-\Delta G = nF\eta = \sum_s \nu_s(-\Delta g_s) \qquad (2)$$

where ν_s is the stoichiometric number of step s.

(ii) that between the step affinity and the forward and backward rates, v_{+s} and v_{-s}, of that step,

$$-\Delta g_s = -RT \ln v_{+s}/v_{-s} \qquad (3)$$

(iii) that connecting the forward-to-backward rate ratio of the overall reaction V_+/V_-, and such ratios of elementary steps,

$$V_+/V_- = \prod_s v_{+s}/v_{-s} \qquad (4)$$

(iv) a steady-state relationship connecting the overall net rate and step net rates,

$$V_+ - V_- = (v_{+s} - v_{-s})/\nu_s \qquad (5)$$

(2) The case of Hydrogen Electrode Reaction

As substantiated[6] well, HER on many electrocatalytically active metals obey the Volmer-Tafel reaction route,

$$H^+ + e^- \xrightarrow{\text{Volmer}} H(a), \qquad 2\,H(a) \xrightarrow{\text{Tafel}} H_2$$

In this case, **Eqn.(2)** is reduced to,

$$-\Delta G = 2F\eta = -(2\Delta g_V + \Delta g_T) \qquad (6)$$

It is convenient, as will be seen later, to define the affinity distribution parameter m as,

$$m \equiv \Delta g_T/\Delta g_V \qquad (7)$$

The function for m can be derived as below: From **Eqn.(5)** for these two steps,

$$v_{-V}(v_{+V}/v_{-V} - 1)/2 = v_{-T}(v_{+T}/v_{-T} - 1)$$

Hence, giving appropriate rate expressions[6] for v_{-V} and v_{-T} and using **Eqn.(3)** for v_{+V}/v_{-V}, *etc.* which involves $-\Delta g_V$, *etc.*, an equation which involves m and η may be derived, although in a transcendental form. Thence, m at any values of η can be computed, provided that appropriate rate expressions for v_{-V}, *etc*, together with other kinetic parameters are given.

It can be shown that m near equilibrium, denoted by

m_0, is related to the exchange current densities of the two elementary steps as,

$$m_0 = i_{0V} / i_{0T} \qquad (8)$$

This can be evaluated experimentally *e.g.* from transient measurements, isotope tracer expoeriments[8], *etc.*

3. QUANTITATIVE TREATMENT OF THE EQUIVALENT HYDROGEN PRESSURE

The equivalent hydrogen pressure can be formulated as follows: If no unique rate-determining step (RDS) exists, or the reaction is kinetically under mixed-control, then the chemical potential, $\mu(H)$, of H(a) in steady-state should be determined by a balance between Volmer and Tafel steps, and the pressure would be lower than that given by **Eqn.(1)**. As $-\Delta g_T$ is given on the one hand by the following relation which is readily derived from **Eqns.(6) and (7)**,

$$-\Delta g_T = 2mF\eta / (m + 2) \qquad (9)$$

and related, on the other hand, to $\mu(H_2)$ as,

$$-\Delta g_T = 2\,\mu(H) - \mu(H_2) = \mu(H_2) - \mu(H_2) \qquad (10)$$

it is straight-forward to calculate $\bar{P}_{H_2}$ from m and η.

The above-quoted data on Fe can be quantitatively accounted for by choosing a suitable value for m_0; the value found in this particular case was *ca.* 0.12. No independent datum is available for m_0 for Fe, but the value appears to be reasonable if one refers to the datum, *ca.* 1 for Ni, which has been obtained from the isotope tracer work[8], and accepts a similarity between HER kinetics on these metals.

4. ANALYSIS OF OVERPOTENTIAL TRANSIENTS

(1) Basic Transient Equations

Direct experimental evaluation of $\mu(H)$ is not necessarily easy but it can be made conveniently on Pd, or perhaps on other hydrogen absorbing metals/alloys, through the observation of overpotential transients, due to the existence of a large pool for H(a) in the form of absorbed hydrogen, namely, H(Pd). A general equation to describe overpotential transient with time for the Volmer-Tafel route may be written, based on the mass-balance condition with respect to electric charge, as,[6]

$$C\frac{d\eta}{dt} = i - i_{0V}\{\gamma_{\uparrow} e^{\beta f\eta} - \gamma_{\downarrow} e^{-(1-\beta)f\eta}\} \qquad (11)$$

with, if one accepts the Frumkin-Temkin isotherm for

hydrogen adsorption,

$$\gamma_{\uparrow} = \frac{\theta}{\theta_0} \exp\{ \delta u (\theta - \theta_0) \} \quad (12)$$

and

$$\gamma_{\downarrow} = \frac{1-\theta}{1-\theta_0} \exp\{ -(1-\delta) u (\theta - \theta_0) \} \quad (13)$$

where C is the double layer capacitance of the electrode, i_{0V} is the exchange current density of Volmer step, θ is the surface coverage with H(a), $u \equiv U/RT$ in which U is the interaction energy parameter in the adsorption isotherm, δ $(0<\delta<1)$ is a constant, β is the symmetry factor, $f \equiv F/RT$, and those with subscript 0 indicate quantities at equilibrium of HER.

(2) Overpotential Decay Transients

Upon interruption of the polarization current after a state of steady polarization is reached, the overpotential initially decays rapidly at the expense of the electric charge accumulated on the electrode through the Volmer step. This decay ends within a very short time, with the time constant $\tau \approx 10^{-3}$s for Pd in acidic solutions which is determined by values of C and effective polarization resistance R_V (which is overpotential-dependent) of the Volmer process, namely, $\tau = R_V C$.

The decay of η practically stops when the electrode potential reached the point which corresponds to the value practically fixed by the level of μ(H) that was realized during the steady-state polarization, namely, immediately before the moment of the current interruption. At that point, effectively, $C(d\eta/dt)$ becomes 0 in **Eqn.(11)**. With $i = 0$ (current is off), the value of η at that moment, called[9] η_2', is given as,

$$\eta_2' = (RT/F) \ln \gamma \quad (14)$$

where $\gamma \equiv \gamma_{\uparrow} / \gamma_{\downarrow}$. This Nernst-type relation may be accepted because, at this moment after the double layer discharge, Volmer reaction should practically be in quasi-equilibrium.

It can readily be seen from **Eqns.(12)** and **(13)** that γ is equal to the variation of activity a(H) of H(a) as

$$\gamma = a(H) / a(H)_0 \quad (15)$$

It is clear, referring to **Eqns.(10)** and **(14)**, that

$$-\eta_2' = (RT/2F) \ln P_{H2}/P_{H2,eq} \quad (16)$$

This is of a similar form with, but definitely different from, **Eqn.(1)**. Thus, **Eqn.(1)** should hold if $\eta_2' = \eta$ (rate-determining Tafel mechanism) but should be lower than that if $\eta_2' < \eta$ or no growth with η if $\eta_2' = 0$ (rate-determining Volmer mechanism).

The overpotential decay transients are very informative: First, the affinity value allotted to Tafel step is given by η_2' and second, the initial rapid portion which is allotted to Volmer step is then obtained ($\eta_1' + \eta_2' = \eta$). Accordingly, one can directly observe m on Pd HER at any value of η, because $-2\Delta g_V = F\eta_1'$ and $-\Delta g_T = F\eta_2'$, and hence the equivalent hydrogen pressure.

5. EXPERIMENTAL RESULTS ON PALLADIUM ELECTRODE

(1) Decay Transients on Pd

An extensive work on the overpotential transients has been carried out on Pd.[3-5] Thanks to its high ability of absorption of hydrogen, galvanostatic overpotential rise and decay transients on Pd hydrogen electrode are clearly separated into two portions each, one with the time constant of *ca.* 10^{-3}s (in acidic solutions) and the other *ca.* 10^3s (or longer) for $\sim 10\mu$m (or thicker) Pd foil.

Experimentally, η_2' was clearly defined on the decay transients as shown in **Fig.2**, (A) on Pd electrode in H_2SO_4 and (B) on $Pd_{60}Ag_{40}$ alloy electrode in H_2SO_4 + thiourea; this also indicates that diffusion (and the ingress/egress rate of hydrogen) is sufficiently rapid in those cases.

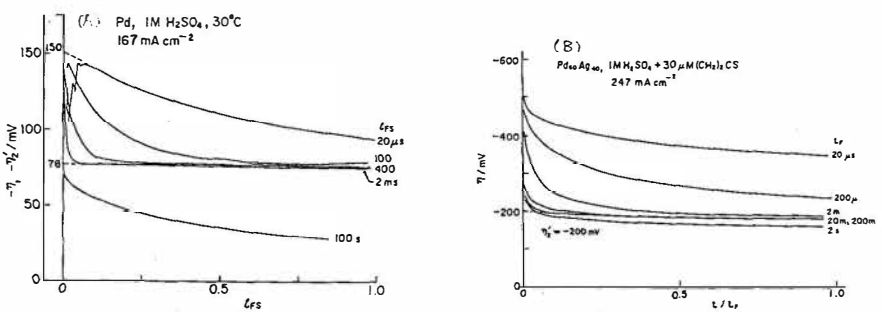

Fig.2. Typical galvanostatic overpotential decay transients at 30 ℃ on: (A) Pd electrode in 1*M* H_2SO_4, (B) Pd-Ag alloy electrode in 1*M* H_2SO_4 + 30 μM $(CH_2)_2CS$, 30 ℃. Abscissa is given in unit of full-scale time, t_{FS}, assigned to each curves.

Tafel plots of η and η_2' on Pd and Pd-Ag alloy electrodes in 1*M* H_2SO_4 are plotted in **Fig.3.** It may be seen that no systematic influence of alloy composition upon η was noted; the electrocatalytic activity was, as usual, strongly influenced by its surface condition, *etc.*. On the other hand, η_2' was much more stable and practically independent of the alloy composition.

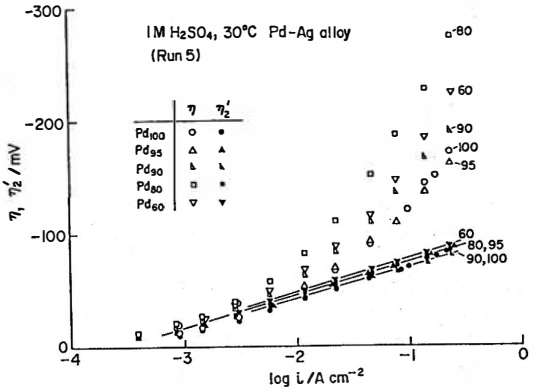

Fig.3. Tafel Plots of η and the slowly decaying overpotential component η_2' on Pd and Pd-Ag alloy electrodes. 1M H_2SO_4, 30 ℃.

Typical results of evaluation of $\overline{P}_{H2}$ from η_2' on Pd in 1M H_2SO_4 are shown above in **Fig.1(B)**. The data are not at all in agreement with **Eqn.(1)**. On the other hand, it is noteworthy that they are satisfactorily interpreted by the theoretical curves calculated with m_0 of 3~10, which is observed from the overpotential decay transient, as seen by solid lines calculated on the basis of Langmuir adsorption isotherm, or dotted lines on the Temkin isotherm with U arbitrarily taken as 5 (u = 5RT in $U \equiv u/RT$).

(2) Effects of Catalytic Poisons

A numerous investigations have been carried out on poisons in catalysis, but not much is known as to on which elementary steps they are exerting effects. Such effects of poisons on elementary steps are clearly observable on Pd. For example, tetrabutylammonium ion was effective to retard Volmer step. On the other hand, thiourea was effective in retarding Tafel step. It is evident from the discussion presented above that the latter may be an effective additive to Pd HER system if one is to increase hydrogen in Pd. Other additives, I^-, CN^-, SCN^-, As_2O_3, *etc.* were found to have intermediate characters, exerting comparable degrees of poisoning effects on both Volmer and Tafel steps. It may be interesting to investigate other additives and accumulate information on their poisoning effects on various elementary steps.

Similar results in 1M H_2SO_4 with the addition of 10 or 30 μM $(CH_2)_2CS$ are plotted in **Figs.4 and 5** for Pd and $Pd_{80}Ag_{20}$ electrodes, respectively. It is evident that overpotential values, especially η_2', are much larger in the presence of thiourea: The latter reaches the value

as high as *ca.* -200 mV at 0.25 A cm^{-2} and this value corresponds to the equivalent hydrogen pressure of some 10^6 atm according to **Eqn.(16)**. This level of hydrogen pressure would correspond to the atomic ratio H/Pd of *ca.* 1.0 at 30℃ according to an empirical relation,

$$H/Pd = 0.70 + 0.05 \log P_{H_2}/atm \quad (30\ ℃) \qquad (17)$$

which may be derived on the basis of the absorption isotherm reported by Frieske and Wicke[10].

Attention was paid so far to the catalytic effects on the elementary steps of HER, but there may be similar effects on the mobility of H(a), in particular on the ingress/egress of hydrogen at the surface-to-bulk layer. In this connection, CN^- [11] and CO[12] were reported to retard such steps: Systematic studies may lead us to have more detailed picture of the effects of poisons on various catalytic reactions.

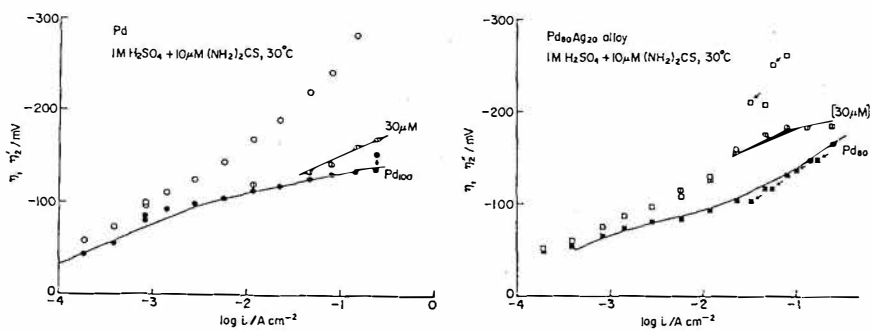

Fig.4(left). Tafel Plots of η (open symbols) and the slowly decaying overpotential component η_2' (full or half closed symbols) on Pd electrode. 1*M* H_2SO_4 + 10 (and 30) μM $(CH_2)_2CS$, 30 ℃.

Fig.5(right). Tafel Plots of η (open symbols) and the slowly decaying overpotential component η_2' (full or half closed symbols) on $Pd_{80}Ag_{20}$ alloy electrode. 1*M* H_2SO_4 + 10 (and 30) μM $(CH_2)_2CS$, 30 ℃.

(3) Characterization of η_2' by Anodic Stripping

It seems important to confirm if the electrode potential at and after the moment of observation of η_2' is indeed maintained because of high concentration of H(a), and hence of H(Pd). Characterization in this respect was conducted by application of an anodic stripping charge and observing the response of the electrode potential.

The amount of anodic charge to be applied should be much larger than that required to remove a monolayer of H(a). If the electrode potential is locked up *e.g.* by any unknown adsorbed substance, then the potential after the anodic stripping would be anywhere far apart from the potential at which the stripping was started. On the other hand, if H(a) is supplied by rapid ingress/egress of H/Pd, then the potential after the stripping should quickly recover the original value.

Such tests are shown in **Fig.6**. Successive anodic pulses with the charge up to 114 mC cm^{-2} (curves 1-4) were applied after observing η_2' (*ca.* -135 mV in this example), but in each time the original electrode potentials were restored. Only after application of 972 mC cm^{-2} (curve 5), *ca.* 15 mV of potential shift was noted. On the other hand, the amount of electricity needed to remove monolayer of H(a) should be roughly 0.5 mC cm^{-2} (roughness factor was usually *ca.* 2). Namely, the electrode restores its negative potential even after application of anodic stripping charges that correspond to almost 10^3 times of the charge which corresponds to a monolayer of H(a). This seems to be a sufficient evidence to prove that the electrode after cathodization as described above indeed contains hydrogen of the amount evaluated from η_2'.

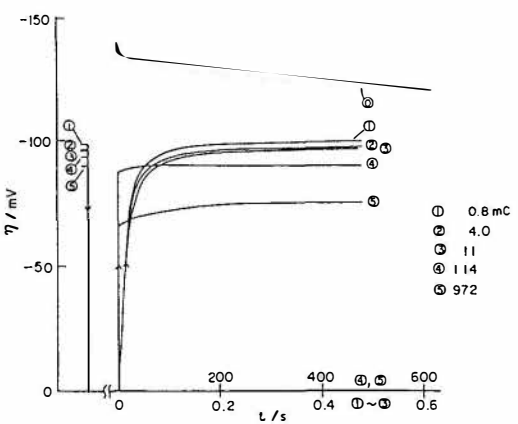

Fig.6. Electrode potential decay (curve 0) after observation of η_2' (*ca.*-135 mV) and change of electrode potential after application of various amounts of anodic stripping charge. 0.8 mC cm^{-2} (curve 1), 4.0 (2), 11 (3), 114 (4), and 972 (5). $Pd_{90}Ag_{10}$ electrode, 1*M* H_2SO_4, 30 ℃.

The quick recovery (<0.1s) of potential after the application of anodic stripping charge in **Fig.6** indicates that the rate of recovery of hydrogen by the outward diffusion from the bulk of Pd as well as by the egress process at the surface zone is sufficiently rapid as compared with that of escape of hydrogen by the Tafel step. This may be an evidence in support of the model that hydrogen is confined in Pd because of slowness of the Tafel step, and hence augmentation of the concentration is made possible by the use of catalytic poisons that retard that rate: Otherwise, the rate of escape of hydrogen should be too rapid during the electrolysis that no significant accumulation of hydrogen up to such a high level as reported above by cathodization may be possible.

REFERENCES

1). J.O'M.Bockris and A.K.N.Reddy, *Modern Electrochemistry*, Plenum Press, New York (1970), p.1333.
2). J.O'M.Bockris and P.K.Subramanyan, Electrochim.Acta, **16**, 2169 (1971).
3). M.Enyo and T.Maoka, J.Electroanal.Chem.,**108**, 277 (1980).
4). M.Enyo, J.Electroanal.Chem., **134**, 75 (1982)
5). T.Maoka and M.Enyo, Electrochim.Acta, **26**, 607, 615 (1981)
6). M.Enyo, *The comprehensive Treatise of Electrochemistry*, vol.7, Ed. by B. E. Conway and J.O'M. Bockris, Plenum, New York (1983), *pp.* 241-300.
7). J.J.DeLuccia, K.Yamakawa and L.Nanis, private communication: S.Yoshizawa and K.Yamakawa, Denki kagaku (J.Electrochem.Soc., Jpn), **39**, 845 (1971).
8). M.Enyo, in *Modern Aspects of Electrochemistry*, no.**11**, ed. by B.E.Conway and J.O'M.Bockris, Plenum, New York, (1975). pp.251-314.
9). A.N.Frumkin and N.Aladjalova, Actaphysicochim. URSS, **19**, 1 (1944).
10). H.Frieske and E.Wicke, Ber.Bunsenges.Phys.Chem., **77**, 48 (1973).
11). J.McBreen, J.Electroanal.Chem., **287**, 279 (1990).
12). A.Czerwinski, S.Zamponi and R.Marassi, J.Electroanal.Chem., **304**, 233 (1991).

The ABC's of the Hydrogen-Metal System

Y. FUKAI
Department of Physics, Chuo University
Kasuga, Bunkyo-ku, Tokyo 112

ABSTRACT

Some basic properties of the hydrogen-metal system are described with particular attention paid to the availability of close D-D pairs in metals. A brief description is also given of the behavior of energetic D^+ ions during their passage through a metal lattice.

1. Introduction

There appears to be a general expectation that the occurrence of "cold fusion" phenomena, if any, is connected to some unusual and hitherto unknown behaviors of hydrogen in metals, especially in Pd. The purpose of this paper is to describe some basic properties of the hydrogen-metal system, the ABC's, the knowledge of which must be shared by everyone in this community. (For more details including most recent results, see Fukai 1993).

Roughly speaking, there are two ways for nuclear fusion to take place. The first, the ordinary way, is that the fusion occurs in the course of collision of two nuclei having energies high enough to overcome the mutual Coulomb repulsion. The second is that two nuclei are held at sufficiently short distances so that the nuclear fusion can be induced by the tunneling through the Coulomb barrier. As by definition the real "cold" fusion refers to the second (static) mechanism, most of the

FRONTIERS OF COLD FUSION

discussions given below are on the equilibrium properties of the hydrogen-metal system, more specifically, the state of D-D pairs in metals. Only a brief description will be given of some properties that are relevant to dynamical processes.

A measure of the internuclear distance that produces observable fusion rates is given by the calculation of Koonin and Nauenberg (1989). They calculated fusion rates in diatomic hydrogen molecules of various isotopic composition, and their dependence on the internuclear distance by varying the hypothetical electron mass. Their results showed that the fusion rate depends nearly exponentially on the distance, and that for the d-d fusion rate to be 10^{-20} s^{-1}, the distance should be ~0.015nm. The question is whether there is any way to hold D-D pairs in metals at such a short distance. For comparison, at the distance of a D_2 molecule (0.074nm), the fusion rate amounts to only 10^{-64} s^{-1}, which is completely negligible.

2. Distance between hydrogen atoms in metals

Hydrogen atoms enter interstitial sites in metal lattices to form metallic alloys. The heat of solution h_s is different for different metal species, and for a given metal, varies with the hydrogen concentration as shown in Fig. 1 (Fukai 1993). In all the cases, the concentration dependence of h_s is similar. The

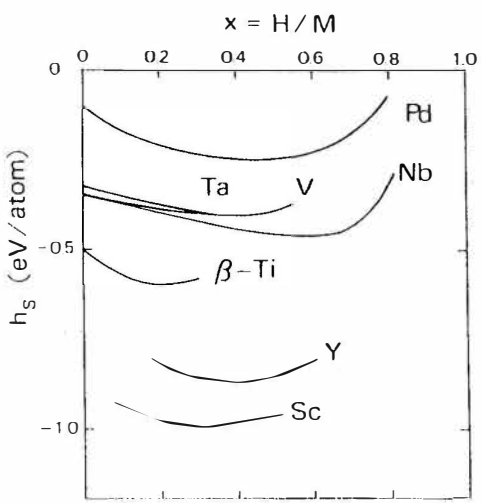

Fig. 1 The heat of solution of hydrogen in some metals as a function of hydrogen concentration. For data sources, see Fukai 1993.

overall lattice expansion caused by hydrogen atoms facilitates the dissolution of hydrogen at the beginning, but the short-range repulsion between hydrogen atoms gradually comes into play at higher concentrations.

In Pd, the heat of solution is $h_S = -0.106$ eV at the infinite dilution, but it crosses zero at x = [H]/[Pd] ≈ 0.84, and becomes positive thereafter (Flanagan and Lynch 1975). This implies that near the composition $x \approx 0.84$, there can be large concentration fluctuations in the hydriding process (e.g. by electrolysis), and at higher concentrations, PdH_x decomposes exothermically (by giving off heat). For D in Pd, the heat-of-solution curve is shifted by 0.026 eV upward (Wicke 1985), but the overall behavior is nearly the same.

There is an empirical rule that interstitial hydrogen atoms do not come closer than 0.21nm, another manifestation of the short-range mutual repulsion. In cases where the distance between neighboring interstitial sites is shorter than 0.21nm interstitial sites are only partially filled with hydrogens, either orderly or disorderly.

Maps showing the average D-density distribution can be Fourier-reconstructed from neutron diffraction data. Care must be taken in interpreting the density maps in disordered phases: whereas the maps indicate that hydrogens are distributed evenly over all the closely-spaced interstitial sites, the actual situation should be that they occupy only a small fraction of sites by trying to keep away from each other. In ordered phases, on the other hand, D-density maps provide useful information on the potential field for hydrogen atoms. Figure 2 shows D-density maps of ß-$VD_{0.51}$, an ordered phase of the V-D system (Okada 1980). The distribution of D atoms is very strongly anisotropic, indicating that the potential is steeply increasing in the c-direction and is slowly-varying in the a-b direction. The amplitude of potential undulations can be estimated from the excitation energies to highly excited vibrational states (observed by inelastic neutron scattering) and the activation energies of diffusion at high temperatures where the migration proceeds essentially via jumps over saddle points (Fukai and Sugimoto 1992, Fukai 1993). Thus, a measure of potential undulations can be given as 0.5~1eV.

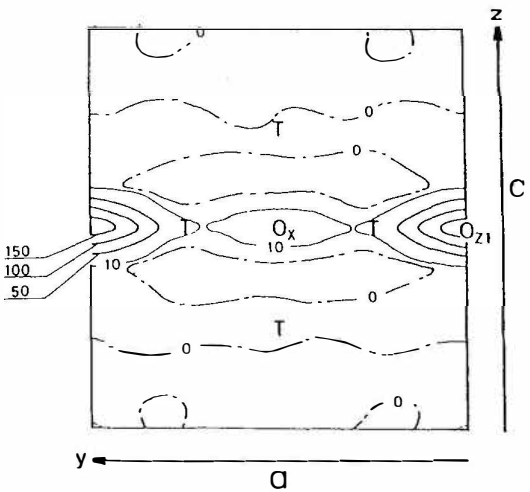

Fig. 2 D-density map in β-$VD_{0.51}$ (Okada 1980).

A possibility of hydrogen atoms coming a little closer arises when they are trapped by lattice defects, more specifically, by vacancies. Numerous experiments performed on the defect-trapping of hydrogen atoms have shown that in many metals a vacancy can trap as many as six hydrogen atoms with binding energies of the order of ~0.5 eV (Myers et al. 1989). This does not imply that six hydrogen atoms are jammed in a very narrow space by replacing one metal atom. Rather, it is more appropriate to regard them as occupying six interstitial sites nearest to the vacancy. The actual configuration of D trapped by vacancies in Pd determined by the channeling method is depicted in Fig. 3 (Besenbacher et al. 1990). Hydrogen atoms are displaced slightly towards the

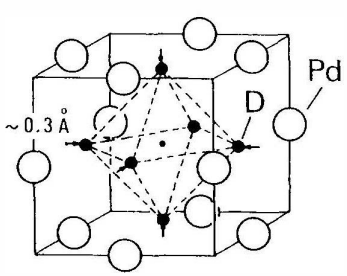

Fig. 3 Configuration of six D atoms trapped at a vacancy in Pd (Besenbacher et al. 1989).

center of a vacancy, and the mutual distance between them ($\approx$ 0.185nm) is certainly smaller than the normal distance in a stoichiometric PdD ($\approx$ 0.28nm). Recently, a number of calculations have been performed on the electronic structure and energies of hydrogen pairs in Pd (Wang et al. 1989, Sun and Tománek 1989, Lam and Yu 1989), and all the calculations agree in that the equilibrium pair distance becomes longer than the internuclear separation in a molecule.

3. Possibility of close D-D pairs in metals

It may be appropriate here to specify more clearly the requirement to be placed on the D-D distance. The ordinary procedure to calculate the fusion rate Λ is to evaluate the wave function of the relative motion of two D nuclei at the separation of $\rho \sim 10^{-14}$ m, where nuclear interactions occur; viz. $\Lambda = A|\Psi(\rho)|^2$. This procedure is not applicable to a D-D pair in a metal because the potential field arising from interactions with metal atoms is fixed in position relative to the metal lattice, and therefore the separation of space variables into the center-of-mass and the relative coordinate cannot be made. However, the following considerations show that potential undulations in metals do not affect the problem seriously.

At small pair separations, the interaction potential can be written in any case as

$$V(r) \rightarrow e^2/r + V_o. \qquad (1)$$

In a free space, the electronic energy is that of the He atom, $V_o = -51.8$ eV. The calculation of Koonin and Nauenberg (1989) which correctly incorporated this screening energy gave the D-D fusion rate ten orders of magnitude larger than the previous calculation which neglected this term ($V_o = 0$) (Van Siclen and Jones 1986). Judging from these results, the effect of potential undulations in metals, being only 0.5~1 eV, should not change the order of magnitude of the Koonin-Nauenberg's calculation. Thus, the requirement on the pair separation of ~0.015nm applies equally well to D-D pairs in metals.

The following discussions show that there is no way to sustain such close D-D pairs in any solids.

Let us consider the balance of forces exerted by the repulsion between two D atoms in a pair and the counteracting force arising from the distorted interatomic bonds of the surrounding lattice.

The repulsive force is estimated as $f_p \approx e^2/r^2 \approx 1 \times 10^{-6}$N at $r \approx 0.015$nm, whereas the lattice force per bond can be estimated as $f_b \approx (c_{11}/N_o) \cdot (\Delta l/l)$, where N_o is the number of bonds per unit area. Substituting the values appropriate for Pd ($c_{11} = 2.3 \times 10^{11}$ N/m^2, $N_o = 6.6 \times 10^{18}$ m^{-2}) and for large strains of $\Delta l/l \sim 1/3$, the counteracting force is estimated to be $f_b \approx 1 \times 10^{-8}$ N at the largest. Thus, interatomic bonds in Pd are not strong enough to counteract the forces exerted by the close D-D pair. In fact, there is no solid on earth which is strong enough to sustain D-D pairs at such short distances. What actually happens is that the D-D pair relaxes to a distance where the force balance can be realized.

The same conclusion can be reached from energy considerations. The energy of a D-D pair in a metal can be approximated by the value in a free space; $V(r) \approx 44.2$ eV at $r \approx 0.015$nm. The electronic energy corrections in a metal should be ~ 1eV at the largest. On the other hand, formation energies of lattice defects are much smaller; ~ 1.5 eV for a vacancy and ~ 5 eV for an interstitial atom in a metal of a melting point of $T_m \approx 2000$K (these values roughly scale with T_m). This implies that a close D-D pair, if once created, should immediately transfer its energy to the surrounding lattice to attain some lower-energy configuration; even the creation of a number of lattice defects is energetically more favorable.

It may be added that the use of a screened Coulomb potential $(e^2/r)\ e^{-\alpha r}$ for the first term of eq.(1) is erroneous. A literal application of a Thomas-Fermi formula which describes the screening by a dense electron gas gives a screening length of $\alpha^{-1} = [4\pi e^2 N(E_F)]^{-1/2}$, which becomes as small as ~0.02nm in Pd. This is a consequence of a peculiar situation in Pd that the Fermi energy E_F happens to fall on a very pronounced peak of the density of states $N(E)$. Calculations showed, however, that this peak arises from 4d electrons of Pd which are strongly localized on Pd atoms and therefore do not participate in the screening of nuclear charges in interstitial sites (Papaconstantopoulos et al. 1978). No such electrons are

available in metals that are effective in screening a singly-charged particle in such vicinities.

The screening would be more effective if there were negatively charged particles heavier than electrons. Indeed, when an electron in a D_2 molecule is replaced with a negative muon (μ^-) which is about 200 times heavier than an electron, the screening radius is reduced by this factor and the fusion probability is increased to 10^9 s^{-1}. However, the use of the "effective mass" of conduction electrons in this context is a mistake. Conduction electrons behave as if they had a large mass when they travel over many atomic distances as waves. The concept of effective mass is simply inapplicable to the problem of static charge screening.

The upper bound for a d-d fusion rate in metals was calculated by Leggett and Baym (1989) by including possible many body effects, and was found to be very small ($\sim 10^{-47}$ s^{-1}), in agreement with the present discussions.

Thus, we cannot expect any measurable d-d fusion to occur in metals as long as we stay within the static regime.

Needless to say, the probability of realizing a close D-D pair configuration by thermal excitation is negligibly small, being $e^{-44.2eV/kT} \approx 10^{-770}$ at room temperature.

4. Effects of high pressure

Here I describe the pressure dependence of the distance between hydrogen atoms in elemental hydrogen and in hydrogen-metal systems.

Elemental hydrogen under normal pressure is an aggregate of stable covalent molecules weakly bound with each other by van der Waals interactions. Thus, the interatomic distance within a molecule ($\approx$ 0.074 nm) is much shorter than intermolecular distances, and a large compressibility of the elemental hydrogen results from the compression of the latter. In contrast, the pressure dependence of the former is very peculiar. The frequency of the stretching vibration, which reflects the bond strength in a molecule, increases with pressure up to $\sim$ 40 GPa but turns into a decrease thereafter. The decrease goes through a discontinuity at $\sim$ 150 GPa and continues on to $\sim$ 250 GPa where the sample becomes gradually more opaque (a phenomenon indicative of an electronic band

closure which leads eventually to a semi-conductive or semi-metallic state) (Hemley and Mao 1988, Mao and Hemley 1989). These observations imply that as more electrons tend to participate in the bonding between molecules at higher pressures, the bonding within the molecules becomes weaker and the interatomic distance correspondingly longer. Theoretical calculations predict that the metallization of hydrogen proceeds in two steps; a molecular crystal → an intermediate metallic structure with a remnant molecular bonding → monatomic metal (Brovman et al. 1972, Barbee et al. 1989). It is only after the monatomic metallic structure is realized that the minimum distance between hydrogen atoms decreases with pressure.

Fukai (1991) pointed out that the hydrogen volume in metallic enviornments, including interstitial hydrogen and elemental metallic hydrogen, follows a universal compression curve, which can be expressed to a good approximation by the Vinet-type formula,

$$p=3K_0(1-y)y^{-2}e^{\eta(1-y)} \quad , \quad y=(V/V_0)^{1/3}$$

with the bulk modulus K_0=99.2 GPa, the initial volume V_0=2.96 $\times 10^{-3}$ nm^3 and η=4.47. Using this equation of state, we can estimate the pressure required to reduce the interatomic distance to $\sim$ 0.015 nm. The value comes out to be 1.3×10^6 GPa (6.2×10^5 GPa for 0.02 nm), which is of the order of magunitude of the center pressure of the Jovian planets, Jupiter and Saturn. The occurrence of a piezonuclear fusion is only possible at these extremely high pressures hardly attainable in laboratory experiments.

5. Dynamical processes of D^+'s in metals

Let us consider a nuclear fusion to be caused by the collision of incident energetic D^+'s with D^+'s in a metal lattice.

As the reaction cross section $\sigma(E)$ increases steeply with the energy of an incoming D nucleus, the total probability of occurrence of such events depends solely on the availability of high-energy D nuclei. Cosmic rays and the acceleration of fracture-induced D^+'s by transient electric fields built up across

the cracks (fracto-fusion) have been proposed as possible sources of such energetic particles.

In this section, I consider the fate of incident D^+'s with energies of 1~500 keV after entering a metal lattice, whatever their source may be. At these energies, the incoming D^+'s gradually lose their energies by interactions with conduction electrons, and finally come to rest by creating lattice defects when their energies decrease to ~10 eV. As the relation between the incident energy E_0 and the total path length λ_0 is approximately given by $\lambda_0 \propto \sqrt{E_0}$ in this energy range, the energy of an incident D^+ decreases to $E = E_0 (\lambda_0 - l)^2/\lambda_0^2$ after straggling over a distance l from the surface. For D^+ in Pd, $\lambda_0 = 0.1\mu m$ for $E_0 = 3$ keV. The rapid dissipation of incident energies restricts the possibility of nuclear fusion to within a thin surface layer.

In special cases when the direction of an incident beam lies within ~ 1^o of some principal crystal axes or planes, the penetration depth is increased by an order of magnitude (the ion channeling), and the nuclear fusion rate will be enhanced accordingly. The enhancement can be rather important because the beam of incident D^+'s is concentrated near the center of channels where most of the interstitial D^+'s (targets) are located.

Another effect of high-energy incident particles is to create a number of knocked-on D^+'s which may induce additional fusion events. This effect is most important when incident particles are neutrons; the energy of neutrons can be transferred efficiently to hydrogens to create energetic D^+'s.

In any case, it must be emphasized that the high-energy particles must be prepared outside solid samples. Particle energies are always dissipated in solids, especially the energies of charged particles in metals. The acceleration of any particles in metals up to the order of kev is simply impossible.

Finally, I wish to rectify the misconception that strong electric fields built up across the thin double layer near the electrode may induce some nuclear events. It is not the magnitude of field strengths but the energy acquired from the electric field that matters. The energy of D^+'s acquired by acceleration across the double layer is ~ 0.1eV at the largest, which is completely negligible for nuclear events.

6. Conclusion

The properties described here are the very ABC's of the hydrogen-metal systems. In seeking for a mechanism of cold fusion phenomena, one should not ignore these ABC's but find some way to circumvent difficulties posed by them. The difficulties are great for the occurrence of nuclear fusion events, not to speak of the excess heat release. Even greater difficulties are expected for other fusion reactions involving pairs with higher-valence nuclei or three-body interactions. The hydrogen-metal systems, with all these ABC's are by no means friendly to cold nuclear fusion.

7. References

Barbee,T.W., III, A.Garcia , and M.L.Cohen, 1989, *Phys. Rev. Lett.*, 62, 1150

Besenbacher,F., B.B.Nielsen, J.K.Nφrskov, S.M.Myers, and P.Nordlander, 1990, *J. Fusion Energy*, **9**, 257.

Brovman, E.G., Yu.Kagan, and A.Kholas, 1972, *Zh. Eksp. Teor. Fiz.*, 62, 1492 (*Sov.Phys. JETP*, 35, 783).

Flanagan,T.B. and J.F.Lynch, 1975, *J. Phys. Chem.*, **79**, 444.

Fukai,Y., 1991, *J. Less-Common Met.*, 172, 8

Fukai,Y., 1993, *The Metal-Hydrogen System - Basic Bulk Properties* (Springer Series in Materials Science, vol. 21, Heidelberg, to be published January 1993.)

Fukai,Y. and H.Sugimoto, 1992, *Diffusion in Solids, Unsolved Problems*. Ed. by G.E.Murch (Trans Tech Publ.), p.87.

Hemley, R.J. and H.K.Mao, 1988, *Phys. Rev. Lett.*, 61, 857

Koonin,S.E. and S.M.Nauenberg, 1989, *Nature*, **339**, 690.

Lam,P.K. and R.Yu, 1989, *Phys. Rev. Lett.*, **63**, 1895.

Leggett,A.J. and G.Baym, 1989, *Phys. Rev. Lett.* **63**, 191.

Mao, H.K. and R.J.Hemley, 1989, *Science*, 244, 1462

Myers,S.M., P.M.Richards, W.R.Wampler, and F.Besenbacher, 1989, *J. Nucl. Mater.*, **165**, 9.

Okada,I., 1980, Master's Thesis, Tohoku University (Unpublished).

Papaconstantopoulos,D.A., B.M.Klein, E.N.Economu, and L.L.Boyer, 1978, *Phys. Rev.*, B **17**, 141.

Sun,Z. and D.Tománek, 1989, *Phys. Rev. Lett.*, **63**, 59.

Van Siclen,C.D. and S.E.Jones, 1986, *J. Phys.* G **12**, 213.

Wang,X.W., S.G.Louie, and M.L.Cohen, 1989, *Phys. Rev.* B **40**, 5822.

Wicke,E., 1985, Z. *Phys. Chem. N.F.* **143**, 1.

Some Observations Related to the Presence of Hydrogen and Deuterium in Palladium

DR COUPLAND, ML DOYLE, JW JENKINS, JHF NOTTON, RJ POTTER and DT THOMPSON
Johnson Matthey Technology Centre, Sonning Common, Reading, RG4 9NH, UK

ABSTRACT

Surface and bulk analytical work carried out on palladium rod samples returned to Johnson Matthey by Fleischmann and Pons indicates that a number of elements, including platinum and lithium were deposited on the surface during electrolysis in D_2O. Surface analysis via time of flight SIMS indicates that the Li^6/Li^7 isotope ratio is unusually low but no original reference is available.

One electrolysed rod exhibited recovery of part of the wrought microstructure which would ordinarily require a temperature of > ca. 200°C, and another rod showed recrystallisation of a portion of its length and this would normally require a temperature of > ca 300°C. These effects, which were observed at the ends of the rods away from the spot welds, cannot readily be explained by known processing history, and could not be reproduced by filing or sawing.

Temperature programmed hydrogen absorption/desorption profile measurements on a range of palladium samples indicate wide differences in properties; for example a rod electrolysed in aqueous LiOH solution absorbed hydrogen more readily than a similar rod electrolysed in aqueous NaOH. This technique would therefore seem to be of value in characterising the palladium electrode.

Electrochemical measurements conducted in H_2O show that there are significant differences between the behaviour of Pd in LiOH, and in NaOH and KOH solutions.

FRONTIERS OF COLD FUSION

1 Analysis of Palladium Rods Returned to JMTC by Fleischmann and Pons

Three of the rods, which had been loaned by JM, were returned from Utah and analysed:

Rod 1: 4mm diameter,10cm long, as received condition.

Rod 2: 2mm diameter,9cm long,used as cathode at 64mA/cm^2

Rod 3: 2mm diameter,1.2cm long,used as cathode at 512mA/cm^2

1.1 Surface Analysis

SEM analysis using a Cambridge Stereoscan 250 Mark II fitted with Princeton Gamma Tech (PGT) System 4 energy dispersive X-ray analyser indicated cracks and scratches on the surface, with the intensity of features increasing from Rod 1 to Rod 3. There was no significant surface contamination on Rod 1 but iron, copper, platinum and zinc were detected on the used rods. SEM EDAX analysis profile plots for percentages of these four elements for various positions along the rod for a penetration depth of one micron indicated platinum concentrations of up to 9% for Rod 3 and up to 2% Pt for Rod 2. The other elements were present in lower percentages (usually <1%).

XPS analysis was undertaken with a Kratos XSAM 800 surface analyser using a beam of argon ions at 4keV to etch back the surface until the bulk metal was reached. Elements found were oxygen, nitrogen, sodium, chlorine and palladium on Rod 1; oxygen, sodium, silicon and platinum on Rod 2; and oxygen, silicon, iron, sodium, platinum, zinc and copper on Rod 3. Spectral line overlaps interfered with the detection and measurement of lithium in the presence of iron. Instead of a sharp demarcation at the palladium surface the impurities showed a gradual fall off. This is interpreted as an effect of the roughness of the surface with a surface film of variable thickness within the analysis area.

Time of flight SIMS analysis has been carried out on the two palladium Rods 1 and 2. A Cambridge Mass Spectrometry TOF SIMS instrument was used, and it was operated so that not more than one monolayer of metal

was ablated in a twenty minute period during spectrum collection, so that isotope ratio measurements were not confused by depth profiling effects. The surface of the sample was ablated by a gallium ion beam. This has the advantage that oxide species are not present to complicate the mass spectrum as is normally the case when an oxygen ion beam is used. The palladium isotope values measured for the two rods are closely similar, but differ somewhat from values quoted in the literature.

ISOTOPE	VIRGIN ROD No.1	USED ROD No.2	LITERATURE VALUES
102	1.28	1.31	0.92
104	11.58	11.50	10.43
105	22.96	23.77	22.33
106	28.00	28.39	27.23
108	25.25	23.90	26.70
110	10.91	11.10	12.36

Figure 1. TOF SIMS Pd isotope ratios(%)

ISOTOPE	REPLICATE MEASUREMENTS			LITERATURE VALUES
6	4.0	4.8	4.7	7.5
7	96.0	95.3	95.3	92.5

Figure 2. TOF SIMS Li isotope ratios(%)

No lithium was detected at the centre of the rod. Lithium was detected at a very low level on Rod 1 after the removal of four monolayers and only as the isotope of mass 7; this was considered to be a trace contaminant. After the removal of four monolayers on Rod 2 a larger amount of lithium was detected with both isotopes being found. The measured values for isotope 6 seem to be consistently different from the expected values. So far as can be ascertained from an inspection of the mass spectra there is no possibility of a significant interference with isotope 7 so that the effect is considered to be real. There was no opportunity to measure the ratio on the lithium used in the electrolysis cell.

Overall conclusions from the surface analysis results were that platinum was detected on the electrolysed rods by all the methods used, and O, Si, Fe, Na, Zn, Cu, Li, Cl were also detected. The Pt, Cu, Fe, and Zn were present as metals.

1.2 Bulk Analysis

Spectrographic analysis for trace impurities is normally made on pure metals produced by JM. The batch analysis for the materials supplied to Fleischmann and Pons is given in Figure 3. Samples for ICP were dissolved in aqua regia in closed containers (to minimise loss of Ru). Rods 1 and 2 were analysed in quadruplicate and Rod 3 in duplicate. Results are given in Figure 4. Li and Pt show increases from Rod 1 to Rod 3. B, Al, Cu and Au values are substantially constant, low levels of Rh and Ru were found in all these analyses.

Element	Ingot 1 ppm	Ingot 2 ppm
Al	5	10
B	20	20
Ca	30	30
Cr	2	3
Cu	10	10
Fe	10	10
Ni	1	1
Ag	1	1
Pt	10	10
Au	30	30

Mg and Si were detected at levels below 1 ppm.

Figure 3 Spectrographic bulk analysis

INSTRUMENT USED - VG Plasma Quad PQ2.

Element	ROD 1 ppm	ROD 2 ppm	ROD 3 ppm
Li	6	9	12
B	25	25	31
Al	7	8	9
Cu	13	14	15
Zn	< 1	< 1	6
Rh	1	1	2
Ru	0.6	0.4	0.3
Au	13	13	13
Pt	6	16	27
Pb	0.2	0.3	0.6

Elements not detected:
< 0.1 ppm Bi, Th, U, Ta, Re, Hf, In.
< 0.2 ppm Hg, Tl, Os, Ir, Cs, Ba, Sb, Nb, Mo, Y, Sr, Rb, Mn, Co and all lanthanides.
< 1 ppm W, Te, Zr, Ga.
< 2 ppm Ni, Mg, Ti.
<5 ppm Ge.
< 10 ppm Cr.
Not determined:- Cd, Ag, V, Na, Ca, Si, P, K, As, Fe, Se and halogens.

Figure 4 ICP-Mass Spec bulk analysis

1.3 Metallography

The end of Rod 2 furthest from the spot weld exhibited microstructural variation from the norm, i e recovered grain structure, which would be consistent for instance with temperatures of greater than 200°C having been generated for a short period. Rod 3 showed complete recrystallisation over a distance of approximately 4mm from the non-spot welded end, consistent with a temperature of greater than 300°C having been generated. However we do not know the total history of the rods after they passed out of our hands so we cannot independently draw definite conclusions.

Vigorous filing and sawing of virgin and hydrogenated rods did not produce this recrystallisation phenomenon.

2. Temperature Programmed Hydrogen Absorption/Desorption on Various Palladium Samples

2.1 Temperature Programmed Absorption/Desorption Technique

Hydrogen absorption and desorption is measured by monitoring changes in the exit hydrogen concentration of a 10% hydrogen in nitrogen stream passing over the sample at a slow rate (25ml per minute). The sample itself can be heated or cooled at a linear rate. The method allows for the measurement of very small amounts of hydrogen and the temperature at which it is absorbed (or reacted) and desorbed. Typically the temperature is cycled between ambient and 400°C at 5°C per minute, one complete cycle therefore lasting some three hours. For samples which have been electrolytically charged the total hydrogen content, usually expressed as H/Pd atomic ratio, and the temperature at which the hydrogen is desorbed can both be measured. The latter reflects the combined effects of changes in hydride structure, changes in the cleanliness and catalytic effectiveness of the surface, and the effects of changes in surface to volume ratio reflecting changes in physical dimensions. Changes in the results between successive cycles can reflect changes in the surface, i.e. reactivation, which can occur during the high temperature part of the desorption cycle.

Our rationale for making such measurements lies in our belief that the differences which seem to occur amongst different palladium samples should be related to their ability to trap hydrogen or deuterium under non-equilibrium conditions, particularly under conditions of incipient temperature increases.

2.2 Measurement of Palladium Hydride/Deuteride Decomposition/Formation

Figure 5 shows typical literature data for the decomposition and formation of palladium deuteride and palladium hydride at one atmosphere pressure as the temperature is changed. As the temperature of a loaded sample is increased, one might expect a rather sharp evolution of hydrogen or deuterium at a relatively low temperature, say below 100°C, as the beta-hydride decomposes, followed by a small loss as the temperature increases and the alpha-hydride decomposes. Cooling the sample should incur a hysteresis effect, absorption taking place at a lower temperature than the

corresponding desorption. These temperatures should be lower for a deuterided sample than one which has been hydrided. Figure 6 gives the Pd-H phase diagram.

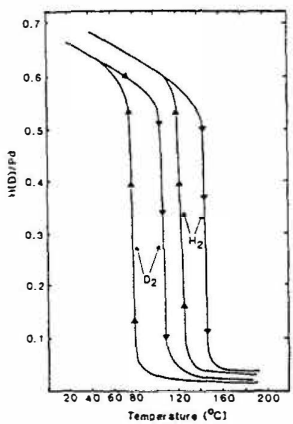

Figure 5. Absorption/Desorption of H or D at 1 atm vs temperature (Sieverts)

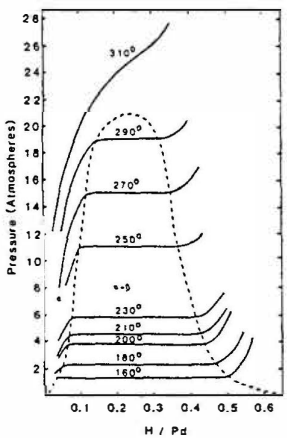

Figure 6. Pd-H Phase Diagram

Since the samples available were very different in geometry and surface condition, the magnitude of the peaks cannot be compared, but this technique does give an indication of the absorption/desorption characteristics of the samples.

The palladium hydride decomposition within these massive electrode samples can be very difficult and in some cases the temperature rises close to the critical temperature (ca 300°C) before decomposition occurs. Figure 7 shows the qualitative results for decomposition of six different samples of various surface to volume ratios. From this figure it is seen that for the palladium sponge and the palladium wire the results are very much what we might have expected from information on hydride formation shown in Figure 5, i e a sharp decomposition at around 100°C. With the 2mm rod, however, there is a marked shift in decomposition temperature with no evidence of significant gas evolution at 100°C. One might expect that the difficulty that the gas would have in permeating to the surface might explain this observation, at least in

part. The results for the 4mm, 6.3mm, and 8mm rods do not however seem to fit this simple explanation so some other factor(s) would seem to be involved. Since the 2 and 4mm rods are from the original experiments in which excess heat was observed, and the 8mm rod was tested at the same time and apparently failed to generate excess heat, we would like to identify these factors. There would seem to be a possible connection between the hydride stability as determined in this way and the heat generation under electrolytic conditions, in line with our original rationale.

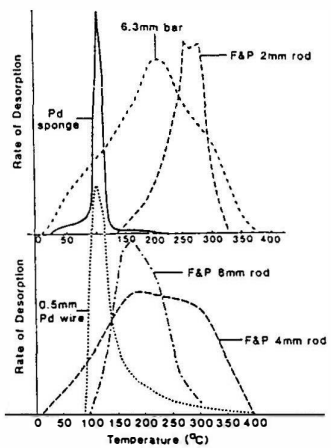

Figure 7. TPD curves for Pd hydride samples

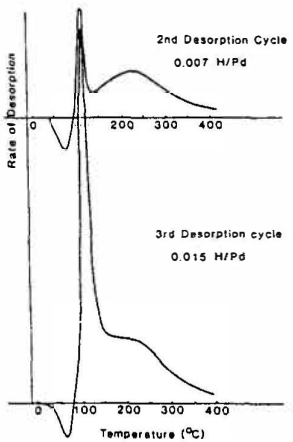

Figure 8. Sequential TPD on hydrided Rod 1

An indication of the effect of surface poisoning can be obtained by repeating the absorption/desorption cycles as indicated in Figure 8 for the same 4mm rod as used previously. When re-hydriding in the absorption apparatus with 10% hydrogen for a relatively short time the hydrogen uptakes are much less, as shown. What is most striking is that a significant desorption spike is now seen at 100°C and this increases substantially for the third cycle. In both cases a second desorption peak is recorded above 200°C which seems to correspond with the peak observed after electrolytic charging.

2.3 Comparison Between Rehydriding Characteristics of Pd Electrolysed in 0.1M LiOH and 0.1M NaOH

One other interesting observation, another part of the mystery and possibly another part of the solution is shown in Figure 9. This concerns part re-hydriding in the hydrogen absorption apparatus of two similar 6.3mm bar samples hydrided electrolytically in 0.1M LiOH and 0.1M NaOH electrolytes respectively. The initial desorption results were identical, giving broad peaks with maxima at 200°C (see Figure 7). Upon cooling the samples in hydrogen the results shown in Figure 9 were obtained:

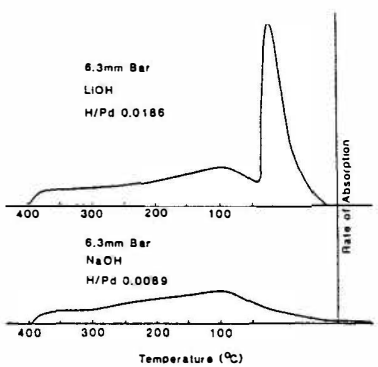

Figure 9. Rehydriding of 6.3mm Pd bar samples electrolysed in 0.1M LiOH and 0.1M NaOH

These results indicate that similar hydrogen re-absorptions occur at elevated temperatures, but there is a marked difference at the lower temperature, where the sample treated in LiOH absorbed hydrogen readily, but that treated in NaOH did not: in fact the pattern of the NaOH case was similar to that of an untreated rod. The low temperature absorption obtained in the LiOH experiment was matched by a corresponding low temperature desorption peak on the next desorption cycle.

Clearly the temperature programmed absorption/desorption measurements described above are indicating large sample differences. Interpreting how these differences arise and how they can be manipulated to an advantage is very much an open question.

The conclusions from the temperature programmed absorption/desorption results are that Pd sponge and Pd wire behaved as expected, but Pd rods gave a range of results probably dependent to some extent on the surface condition of the Pd. The rod electrolysed in LiOH absorbed hydrogen more readily than the similar rod electrolysed in NaOH.

3. Electrochemical Measurements in H_2O

3.1 Galvanostatic Charging of Pd Electrodes

In order to establish whether there are major differences between 'Pd hydride' formed by electrolysis in LiOH and other alkali metal hydroxides, a series of galvanostatic charge/discharge experiments have been carried out on Pd foil and rod electrodes in LiOH, NaOH, and KOH solutions. The charging process is highly sensitive to surface conditions in all of the electrolytes examined. In one experiment LiOH, 60°C), which as yet we have been unable to reproduce, the overpotential during charging reached a maximum and then steadily declined and the electrode subsequently acted as an efficient hydrogen evolver (Figure 10):

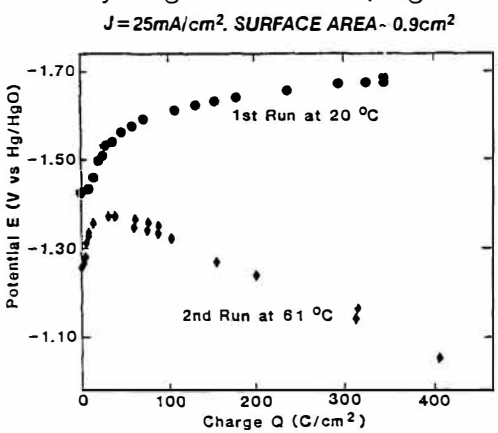

Figure 10. Galvanostatic charging curves for 0.05cm thick Pd foil in 0.1M LiOH at 20 and 61°C

The result obtained with LiOH electrolyte at 60°C could possibly be explained by the surface of the Pd electrode becoming progressively covered with Pt from the anode. The galvanostatic charging experiments carried out to date give (with one exception) similar results in the

three electrolytes tested. However there is some tentative evidence to suggest that galvanostatic discharge is somewhat inhibited in the case of LiOH.

The 'steady state' voltammograms given in Figure 11 show that palladium electrochemistry is sensitive to the nature of the alkali metal cation present. The comparatively diminished re-oxidation wave in the LiOH system is consistent with the galvanostatic discharge behaviour, i e some form of inhibition for the hydride dissolution reaction is present. However, the possibility that a surface Pd-Li alloy is involved cannot be ruled out.

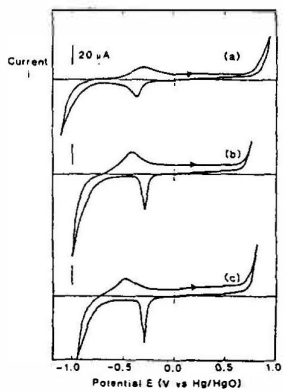

Figure 11. Steady state voltammograms for a Pd disc electrode (surface area $3.1 \times 10^{-2} cm^2$) in (a) 0.1M LiOH, (b) 0.1M NaOH, and (c) 0.1M KOH. 20°C, sweep rate 30mV/sec

Our conclusions from the electrochemical measurements in light water are that palladium electrochemistry is sensitive to the nature of the alkali metal cation and there are significant differences in the results obtained for LiOH, compared with those for NaOH and KOH solutions.

Acknowledgements

The authors thank members of the Analytical Department (JMTC) for the SEM EDAX, XPS, TOF SIMS and bulk analysis measurements. These include Drs P Whitehead, D R Hepburn, J A Busby and Mr M J Lovell.

Deuterium Concentration Profiles and Crystallization Anomalies in Electrolytically Deuterated Titanium Plates

B.ESCARPIZO, J.F.FERNANDEZ, F.CUEVAS, J.TORNERO, and C.SANCHEZ
Universidad Autónoma de Madrid
Cantoblanco 28049. Madrid
SPAIN

ABSTRACT

Deuterium concentration and distribution profiles in electrolytically deuterated Ti plates have been obtained by Elastic Recoil Detection (E.R.D.), Rutherford Back Scattering (R.B.S.) and X-ray diffraction (XRD). It has been found that D/Ti ratio remains constant (≈1.65) up to a penetration which depends on the electrolysis time and then it goes down steeply to ≈0.05. The formed deuteride (TiD_x, $x \approx 1.65$) exhibits some preferred orientations and its texture depends on that of the original Ti plate. The relevance of these data in relation to electrolytic cold fusion experiments is discussed.

1. Introduction

It has been emphasized by different authors that cold fusion phenomena may only be expected whenever high deuterium concentrations (stoichiometric ratio or even higher) be reached in the deuterated metal. Many papers have dealt with this problem in deuterated Pd cathodes but not enough attention has been paid to other metals like Ti and only a few papers have discussed the real atomic ratios (D/Ti) that can be obtained by electrolytic loading. On the other hand, a second condition that seems to be needed to observe cold fusion phenomena is that non equilibrium conditions (produced by any internal or external agent) must exist in the deuterated metal. In this context the knowledge of the real structure and texture of the formed deuterides and of their inhomogeneities becomes relevant. In this paper we dealt with both problems: deuterium concentration profiles in electrolytically formed TiD_x are presented and discussed. Some anomalies in the TiD_x crystallization have also been observed and correlated with the texture of the original Ti plates.

FRONTIERS OF COLD FUSION

2. Experimental

Electrolytic Ti plates (≈15·15·1 mm) were polished and etched. After thoroughly cleaning with D_2O they were used as cathodes in an electrolytic cell with two Pt plates as anodes. After loading for ~ 1000 h with current densities of about 500 mA/cm^2 the Ti cathodes were again cleaned and cut in several pieces (≈5·5·1 mm) to be used in different analysis. After these steps, it was observed that Ti pieces presented a slight deformation as shown in Fig 1. No attempt was made to correct the plate curvature.

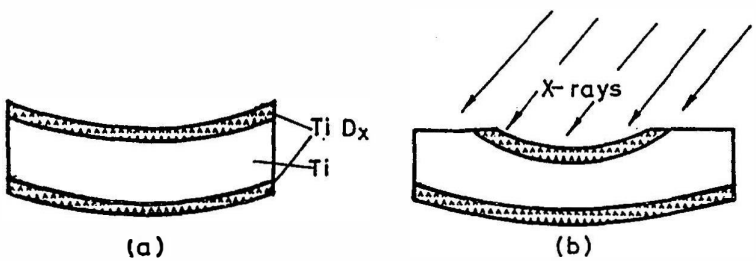

Figure 1. Deuterated Ti pieces (ETi24) as used for ERD and XRD measurements.

Deuterium concentration profiles in two Ti cathodes (ETi20 and ETi24) have been obtained by ERD and RBS techniques (experimental set up shown in Fig 2). The penetration depth of the α-particles (1.6 Mev) is around 0.5 μm with spot size ≈1 mm^2. In order to get quantitative deuterium concentrations the cross section of the elastic $^4He(^2H,^2H)^4He$ reaction must be known. Besenbacher et al. calculated this cross section from 0.8 to 2.3 Mev and recoil angles from 0° to 35° with a ∓5% uncertainty. The most important problem in our

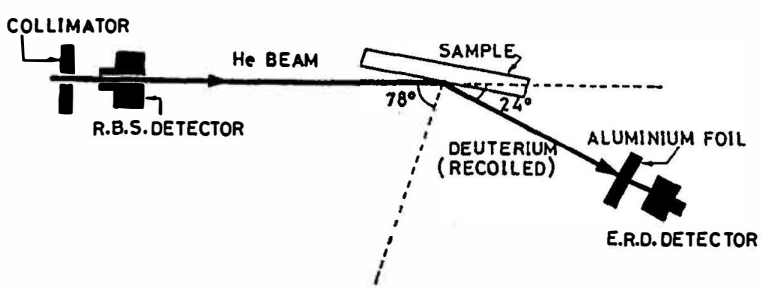

Figure 2. Experimental set-up used in ERD and RBS experiments (LNETI, Lisbon, Portugal).

measurements was the maximum Ti depth accessible to the ^4He ions. To overcome this difficulty a layer of the formed deuteride was removed after each ERD measurement by polishing (0.25 μm diamond powder) the sample.

In the same deuterated Ti-cathodes X-ray diffraction patterns were obtained and results from ETi24 are now presented. A Philips machine mod. PW1140 was used. Penetration depth of the Cu Kα line was ≃5 μm. The X-ray spot covered fully the investigated plate.

3. Results

It was detected that a deposit was formed during electrolysis at the cathode surface. Analysis (both by ERD and XRD) of this surface layer showed that it was composed by nickel oxide, magnesium oxide and small traces of Pt. Some details on the characteristics of this layer were reported at the Como Conference (B. Escarpizo et al 1991): This surface deposit was removed by polishing before accomplishing ERD and XRD measurements.

Typical results from ERD-RBS measurements together with the RUMP fit are shown in Fig.3 and 4. It is apparent that the near surface fit of the spectrum is not as good as that of the flat zone. Deuterium concentrations were obtained from the spectrum flat zone. Results obtained after removing several layers are shown in Fig 5 up to a penetration of 200 μm for both ETi20 and ETi24. Although it is difficult to know the depth scale error it has been estimated to be < 10% after micrometric measurements before the first and after the last polishing.

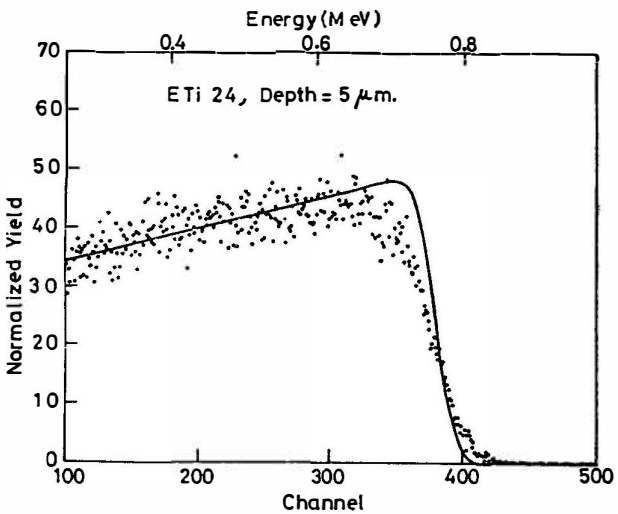

Figure 3. ERD spectrum and RUMP fit from ETi24.

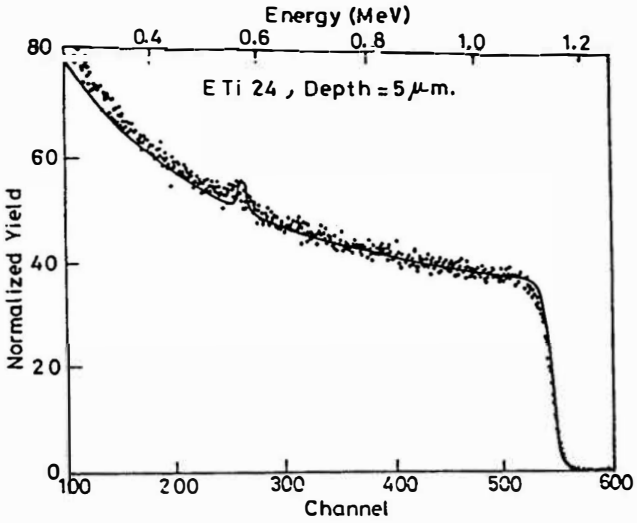

Figure 4. RBS spectrum obtained in parallel with the ERD data of Fig.3.

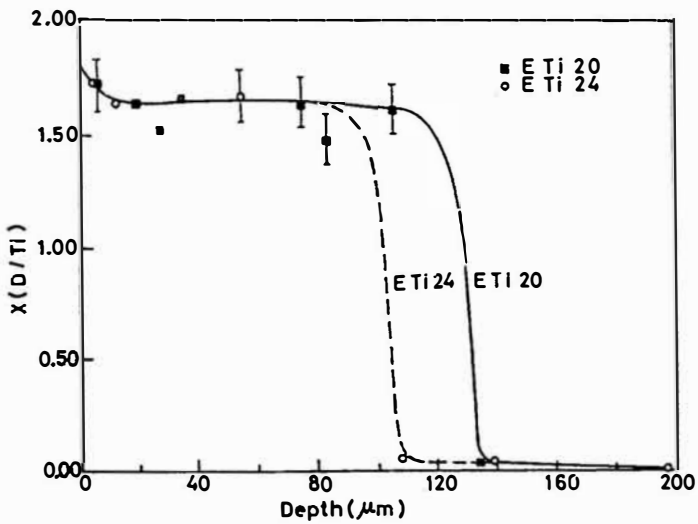

Figure 5. Deuterium concentration profiles in ETi20 and ETi2 cathodes as obtained from ERD data.

Both samples show a similar behaviour: an initial zone(≤ 10 μm) where D concentration is not clearly defined followed by an extended region, up to 120 μm, where D/Ti remains constant an equal to ≃ 1.65. After that a step decrease of D/Ti takes place within a thickness of around 20 μm. This region is more clearly seen in ETi20 than in ETi24 due to the experimental points of Fig.5. Finally a very low atomic ratio (from 0.05 to 0.005) is measured up to penetrations of ≃ 200 μm (more clearly seen in ETi24 sample).

Fig.6 shows evolution of some peak intensities with depth from XRD patterns obtained with ETi24. Maximun D penetration depth is confirmed by spectra of Fig.6 as far as the intensities of all detected TiDx peaks go down to zero at a depth of 110-120 μm in ETi24. Fig.6a shows the evolution of (220) peak of TiDx. In Fig.6b intensities of the (311) TiDx and (103) Ti peaks are plotted. The first one corresponds to d= 1.342 Å and the second one to d= 1.332 Å, and only a peak appeared in the pattern at the same 2θ; so we have concluded that the intensity of this peak should be the summed intensities of both (311) TiDx and (103) Ti peaks. Finally in Fig.6c the intensity of (222) TiDx peak is shown . Several other peak intensities from the XRD patterns could have been selected to be plotted but the three ones in Fig.6 make a full representation of the whole.

4. Discussion

First important result we must emphasized is that D penetration depth in our samples is confirmed by both types of measurements, ERD-RBS and XRD. In the experimental conditions used in the electrolytic loading a maximum D penetration of 110-120 μm is produced. But we must say that different D penetration depths into Ti will be produced if the electrolysis experimental conditions (time and current density) are changed. This conclusion is confirmed by results from different authors (Brauer et al. 1983, Briand et al. 1990, Sevilla et al. 1991). Brauer et al. used electrolysis times ranging from 5 to 100 s. and current densities from 5 to 200 mA/cm^2. They obtained H concentration profiles of the same shape as those shown in Fig.5 and maximum H/Ti ratios of the order of 1.65, very close to those from ETi20 (1.60) and ETi24(1.68). Penetration depths < 1μm were recorded in their experiments. On the other hand, Briand et al. concluded that D penetration is 2-3 μm and that TiD_2 is formed. They used an electrolysis time of 1-3 h. and 8 mA currents. Sevilla et al. proposed that D penetration should be of the order of 20 μm. As can be seen from Fig.5 of this paper the existence of a thin layer close to the surface region with D/Ti > 1.6 can not be disregarded. So we can conclude that at best higher D concentrations (close to D/Ti ≃ 2) would be produced in a surface layer (≤ 1μm) of the deuterated Ti plate. In the rest of the piece a limiting (D/Ti) concentration of ≃ 1.6-1.7 seems to exist although we must say that other authors (Millenbach et al. 1982, Dus et al. 1992) have reached different conclusions on this point. Millenbach et al. formed TiD_x (x=1.78) samples with 20 mA/cm^2, but the H concentrations were determined by

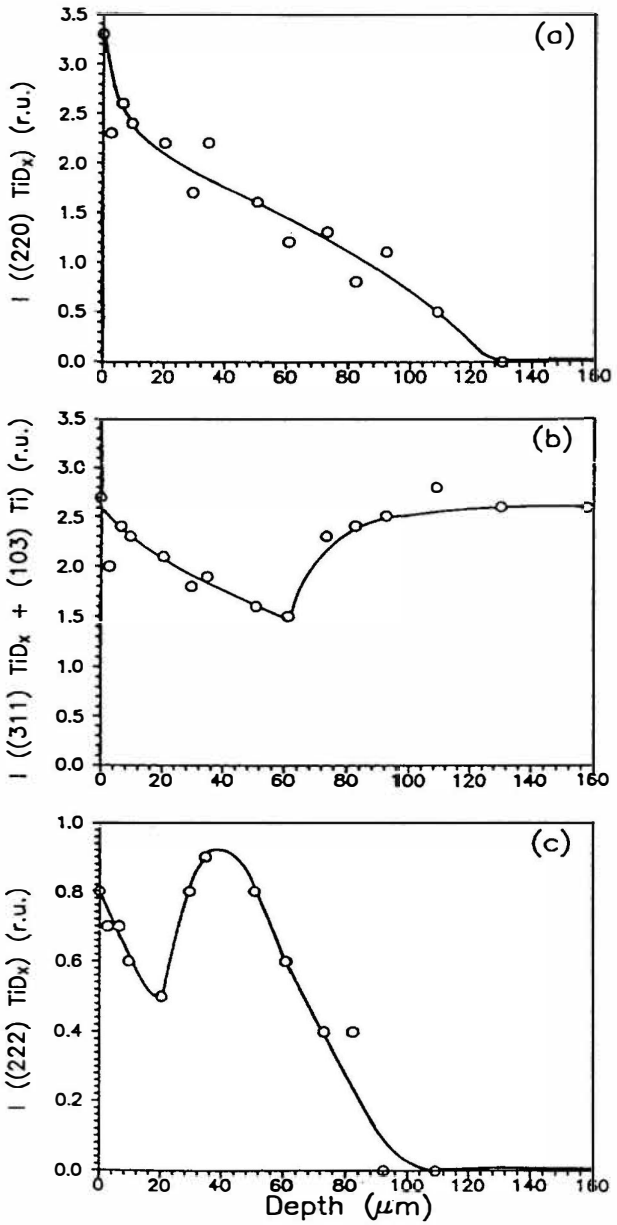

Figure 6. XRD peak intensities versus penetration depth in TIDx formed in ETi24. (a) →(200) peak. (b) →(311) TiDx and (103) Ti peaks. (c) →(222) TIDx peak.

comparing lattice parameter measurements with those from calibrated samples. This method is not a direct one and accuracy of the measurements could be questionable. Dus et al. prepared Ti thin films (300 Å) and studied H absorption from gas phase at temperatures between 78°K and 298°K. They found that the maximum H/Ti is temperature dependent and x=2 was obtained at R.T. Probably these results are not incongruent with our data as far as layers close to the surface of the electrolytically deuterated pieces are taken into account.

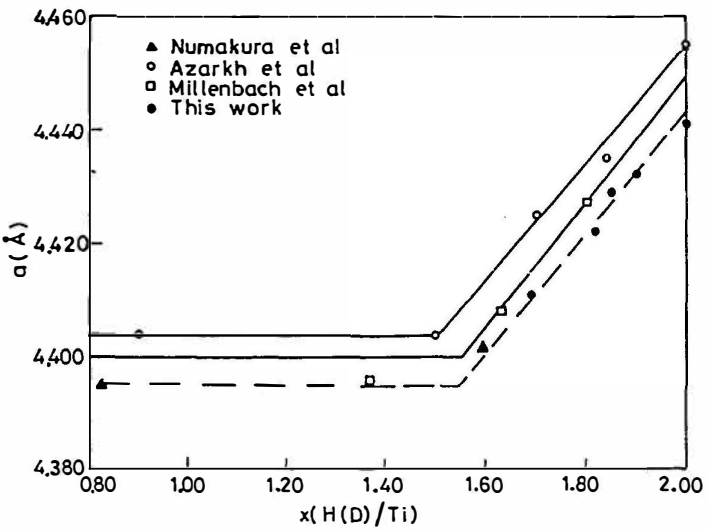

Figure 7. Variation of lattice parameter with atomic ratio, H(D)/Ti, in the H-Ti system.

From the above considerations a limit in the D concentration in electrochemically loaded Ti is a real possibility. Energetic reasons may explain these concentration limit. The change in the TiD_x (TiH_x) lattice parameter as a function of H(D)/Ti and the phase diagram of the H-Ti system are shown in Fig.7 and 8. The boundary between phases α and δ seems to establish the limit of the H/Ti ratio at room temperature.

Finally, anomalies in the crystallization of TiD_x (Fig.6) are well explained by examining the texture of the Ti plate before being deuterated (Fig.9). Due to the production process some preferred orientations are also observed. We must emphasize that the (002) Ti and (222) TiD_x peaks correspond to planes of highest packing in the hexagonal and cubic lattices of Ti and TiD_x respectively.

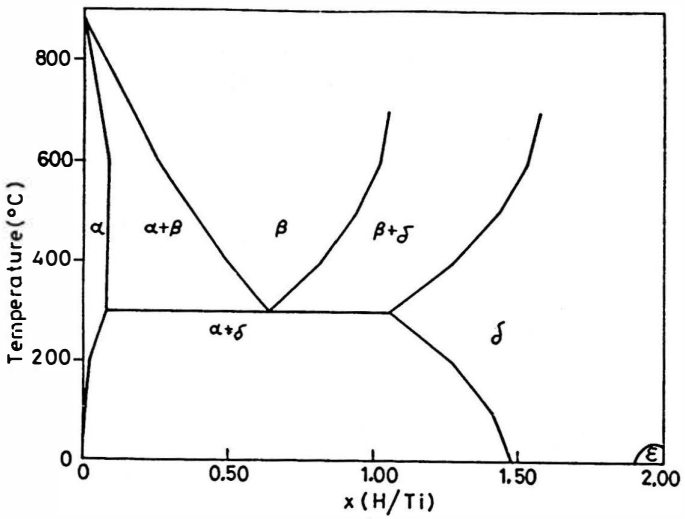

Figure 8. Phase diagram of the H-Ti system.

5. Conclusions

From this papers the following conclusions can be drawn.

a) Nuclear results from several cold fusion experiments in Ti (Jones et al. 1989, Sanchez et al.. 1989) should be corrected in relation to the fusion reaction rates when given per cubic centimeter of the deuterated cathode material.

b) More investigations have to be done to find the experimental way of improving the D/Ti ratio in electrolytic loading.

c) Every piece of metal to be used as cathode in a cold fusion experiment has to be previously investigated. Anomalies in texture (and other properties) might be well related to the non equilibrium conditions required to trigger cold fusion reactions.

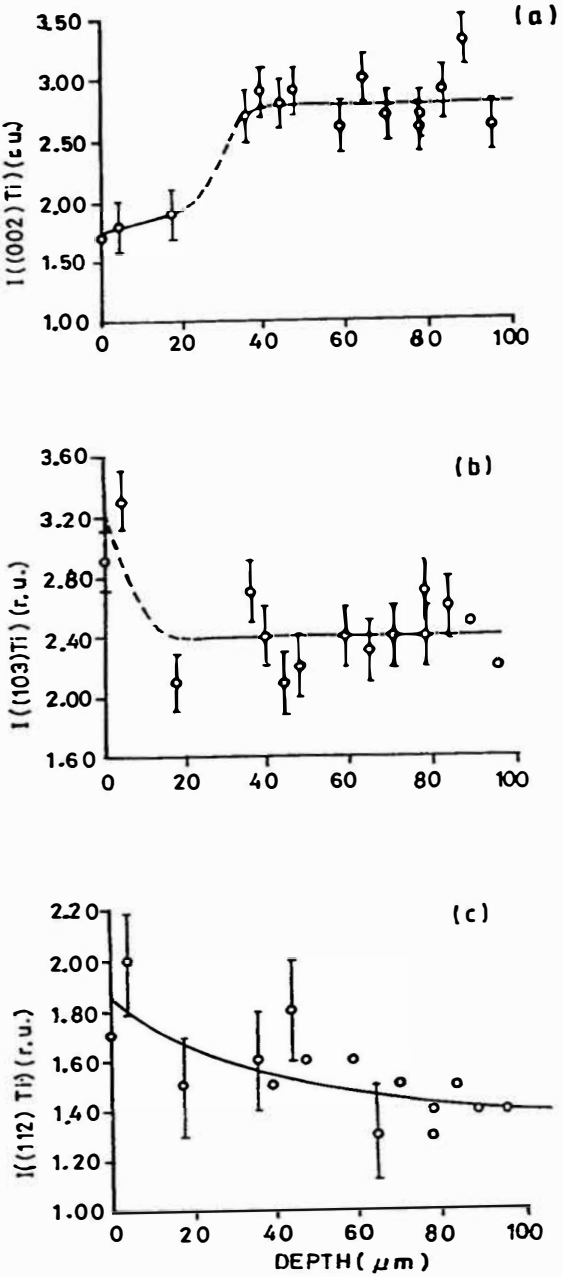

Figure 9. XRD peak intensities versus penetration depth from a Ti plate similar to ETi24. (a) → (002) peak, (b) → (103) peak, (c) → (112) peak.

6. References

1. Besenbacher, F. et al., 1986, Instruments and Methods in Physics Research, B 15, 459.
2. Brauer,E. et al.,1983, Ber. Bunsenges Phys. Chem.,87,341.
3. Briand, J.P. et al., 1990, Physics letters A, 145, 187.
4. Dus,R. et al., 1992, Surface Science to be published.
5. Escarpizo, B. et al., 1991, The Science of Cold Fusion, Conference Proceedings, 33. Bolonia, Italia. pp 15-20.
6. Jones, S. E. et al, 1989, Nature, 338,737.
7. Millenbach, P. and Given, M., 1982, Journal of Less Common Metals, 87, 179.
8. Sanchez, C. et al., 1989, Solid State Communications, 21, 1039.
9. Sevilla J. et al., 1990, Fusion Technology, 19, 188.

7. Acknowledgements

This work has been supported by CICYT (Spain) under contract MAT-90-0053. The authors recognized the support from Fundacion Banco Exterior (Madrid, Spain). Thanks are given to Profs. Soares and da Silva (LNETI, Lisbon, Portugal) for allowing and helping us with the RBS-ERD measurements.

Theory and Modeling

Coherent and Semi-Coherent Neutron Transfer Reactions

Peter L. HAGELSTEIN
Massachusetts Institute of Technology
Research Laboratory of Electronics
Cambridge, Massachusetts 02139

ABSTRACT

Neutron transfer reactions are proposed to account for anomalies reported in Pons-Fleischmann experiments. The prototypical reaction involves the transfer of a neutron (mediated by low frequency electric or magnetic fields) from a donor nucleus to virtual continuum states, followed by the capture of the virtual neutron by an acceptor nucleus. In this work we summarize basic principles, recent results and the ultimate goals of the theoretical effort.

1. Introduction

The past three and a half years has seen a considerable number of reports of observations of anomalies in metal deuteride systems; reports of the various and diverse effects can be found in the pages of this conference proceeding. We may summarize some of the effects currently being claimed:

1. Reproducible excess power generation in palladium electrolysis experiments carried out in a basic (LiOD) heavy water electrolye. The excess power has been reported at levels as high as 10 times the electrical IV input power. The observed excess energy at many laboratories exceeds 50 MJ/mole (500 eV/atom) of Pd, and can therefore not be accounted for by chemistry; it is of nuclear origin.

2. Anomalous neutron emission in electrolytic and gas-loaded metal deuterides.

3. Anomalous excess tritium production, unaccompanied by commensurate neutron production.

4. Fast anomalous fast ion emission from metal deuterides.

5. Anomalous gamma emission from metals involved in electrolytic and gas-loading deuterium experiments.

6. Claimed production of ^{4}He.

FRONTIERS OF COLD FUSION

7. Excess power generation in light water experiments involving nickel cathodes and K_2CO_3 electrolyte.

The experimental evidence in support of the various claims varies in quantity and quality. I regard the evidence in support of the excess power production in heavy water experiments to be sufficiently strong that it could be conservatively accepted as experimental fact at this point. The evidence for ^{4}He production, for example, is interesting; but it would be useful to obtain more confirmation to be certain that the effect is indeed what has been claimed.

There has been very little in the way of significant technical input from skeptics during the past several years. The principal criticisms which one hears repeated involve either that (1) the experiments are not done by competent experimentalists; or that (2) there is no effect, it is all noise; or finally that (3) if the heat is nuclear, then there must be commensurate neutron emission – since there is not, then the heat is of some other origin.

We recognize the first as an *ad hominum* attack which is in of itself devoid of technical content; if true, it would make the more relevant job of technical criticism easier. The second is an argument which was used effectively in 1989; but is not so convincing in 1992. Some of the SRI excess power measurements exceed 50 σ; Pons and Fleischmann point out that a watch and a knowledge of the heat of vaporization of water as it is vigorously boiled away is sufficient to verify that the excess power production is ten times the input IV electrical power in their experiments.

The third argument is more insidious, since it presupposes the conclusion. If one rejects the possibility of a new physical nuclear reaction mechanism, then one is forced to the conclusion stated. Having rejected the experimental results, there is no motivation to consider possible new reaction mechanisms. A tight and self-consistent argument, it is one which has generally been adopted by the physics community; it is also an argument which seems to require a fully-developed theory to refute. This argument is one which is probably most responsible for the antagonism on the part of the physics community in the US, and ultimately is responsible for nearly complete absence of research support in the US in the field.

Our point of view in the work described in this manuscript is that we accept the experimental claims to the degree merited by the evidence, and seek possible theoretical explanations. It should be noted that actually doing so entails very significant non-technical hardships, as we have found from experience; this course of action is not recommended for others.

2. Fusion Reactions

Nuclear fusion requires that two nuclei approach each other to within range to interact, typically fermis. Since nuclei are positively charged, the resulting Coulomb repulsion makes it difficult in general to nuclei to get close enough together to fuse. One approach to overcoming the Coulomb barrier is to arrange for the nuclei to be very energetic (as is done in magnetic fusion experiments or in stellar plasmas), or else to arrange for significant tunneling (as in muon catalyzed fusion). Skeptics were quick to point out that conditions in a metal hydride near room temperature does not lead either to sufficient kinetic energies or screening to lead to observable anomalous

fusion rates.

Heat production in Pons-Fleischmann experiments is hard to explain theoretically through a fusion mechanism. Not only would a mechanism have to exist that would allow nuclei to get sufficiently close to fuse, but a second mechanism would also have to exist to modify the expected fusion reaction channels. For example, *dd*-fusion yields $n + {}^3He$ or $p + t$ for primary reaction products; neither of these paths occur in Pons-Fleischmann experiments to a degree commensurate with the excess heat. Many workers in the field think that the ^{4}He branch is somehow favored, and there seems to be some evidence supporting significant ^{4}He production; it is hard to understand quite how this could occur from a theoretical point of view.

The field got its name "cold fusion" originally from early speculations concerning the source of heat and neutrons from the first electrochemistry experiments showing anomalous results. Although the anomalous neutron emission may have a component due to *dd*-fusion, the heat production is very hard to reconcile with fusion as described above. Reported observations of several of the other anomalies (fast ion emission, gamma emission and light water experiments) would be even harder to account for with a fusion mechanism.

For these and other reasons, we have concluded that whatever is going on, the heat production is simply not due to fusion. It must be nuclear, which implies that we must consider new basic reaction pathways.

3. Neutron Transfer Reactions

The first fundamental problem with fusion reactions occuring in a lattice at room temperature is the presence of a Coulomb barrier. A possible way around this which we have proposed is to pursue reactions which involve the transfer of neutrons from nuclei. A neutron is charge neutral, so that no Coulomb barrier occurs. Very significant other problems occur, but at least we no longer have to face the Coulomb barrier. A prototypical neutron transfer reaction (shown in Figure 1) would involve the transfer of a neutron from a donor nucleus (such as deuterium) to an acceptor nucleus (we have considered ^{2}H, ^{6}Li, ^{10}B and Pd isotopes as possible acceptor nuclei).

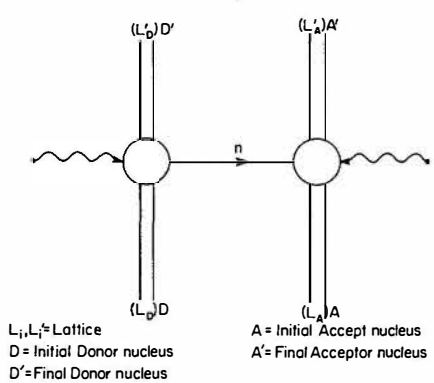

Figure 1: Two-step virtual neutron transfer reaction from a donor nucleus to an acceptor nucleus.

The second fundamental problem with fusion reactions is the problem of reconciling the reaction products with the experimentally observed products. In this case, if a neutron is to somehow go from one nucleus to another, we would expect to see primary or secondary capture gammas; these are observed at a low rate, down by many orders of magnitude from the heat-producing reaction rates.

There is a more severe problem which occurs with neutron transfer reactions, and that is how would a neutron be transferred off of a nucleus to start such a reaction? The neutron is tightly bound (2.225 MeV binding energy for a deuteron), and it cannot be expected to be transferred off of a nucleus without good reason. A neutron can be removed from a deuteron through photodisintegration with a gamma or fast particle (see Figure 2), but almost any other proposed means of doing so will requre new physics. It can be shown that a lattice has no means of transferring sufficient energy to a neutron to ionize it short of accelerating an electron or ion up to MeV energy and kinetically knocking it out.

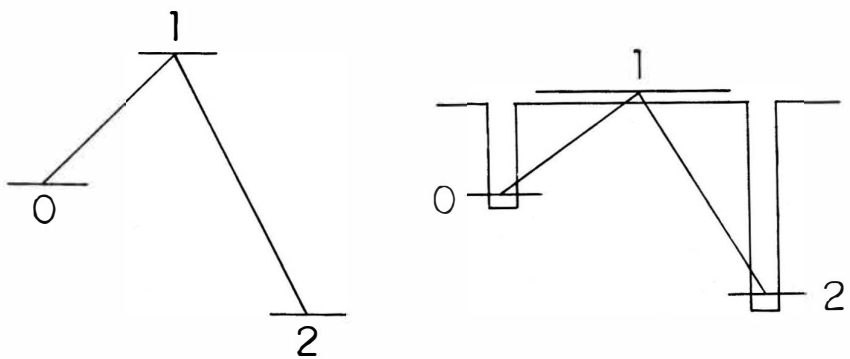

Figure 2: (a) Resonance transitions involving a real intermediate state driven by a laser. (b) Resonant neutron transfer reaction driven by a gamma.

Our approach[1-4] to this basic problem is to work with virtual neutrons by considering two-sep reactions which proceed through a virtual intermediate state. There is no way to arrange for sufficient energy to ionize a neutron in a lattice in room temperature, but there is a way (at least in principle) for continuum neutron states to be intermediate states driven off of resonance as part of a two-step reaction (as long as whatever happens at the other end is energetically allowed). This type of reaction is illustrated schematically in Figure 3.

Virtual particles are known in various branches of physics, including nuclear physics. It is a rather easy exercise to show that a virtual neutron which is off-resonant by multiple MeV will not go further than a few fermis from its parent nucleus in free space. If the nucleus to which the neutron were being transferred were within fermis, then such a constraint would not hinder the overall reaction; the Coulomb barrier unfortunately prevents this.

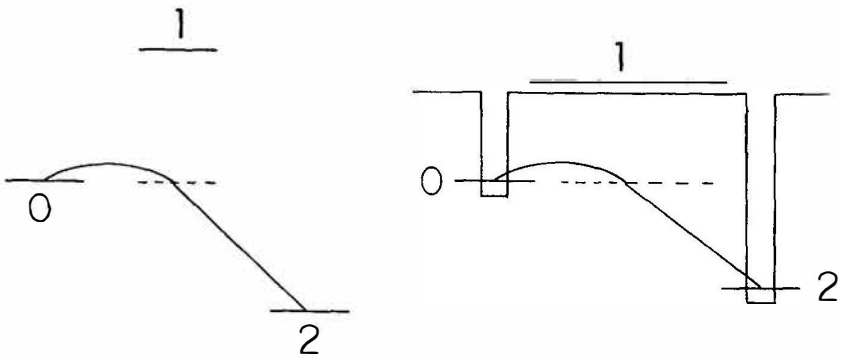

Figure 3: (a) Raman transitions involving a virtual intermediate state driven by a laser. (b) Off-resonant neutron transfer reaction driven by a low frequency electric or magnetic field.

Consequently, we are faced with the problem of arranging to get a virtual neutron from one nucleus to another over Angstrom distances, seemingly in the face of known physics saying that it can't be done. The demonstration that a virtual neutron doesn't stray appreciably from its point of origin is a free-space argument; we wondered whether long range interactions were possible in a lattice.

4. Virtual Neutron Transfer

The theory for two-step reactions which involve a virtual intermediate state is well known, and the reaction rate for a transition from state 0 through a virtual intermediate state 1 to a final state 2 can be determined from Fermi's Golden Rule through

$$\Gamma = \frac{2\pi}{\hbar} | < \Psi_2 | H_{21} (E_0 - H_1)^{-1} H_{10} | \Psi_0 > |^2 \rho(E_2) \tag{1}$$

where state 1 is driven at the frequency of state 0. This would correspond, for example, to a reaction where a neutron is transferred from a deuteron to virtual continuum states by a DC magnetic field, and subsequently gamma captured elsewhere onto an acceptor nucleus.

The Green's function for the virtual neutron is included in the term written symbolically as $(E_0 - H_1)^{-1}$, and which actually means to compute Ψ_1 from

$$(E_0 - H_1)\Psi_1 = H_{10}\Psi_0 \tag{2}$$

and then plug into

$$\Gamma = \frac{2\pi}{\hbar} | < \Psi_2 | H_{21} | \Psi_1 > |^2 \rho(E_2) \tag{3}$$

The Hamiltonians which occur in the theory are second-quantized operators which are appropriate for a many-particle description of the system. We may reduce

the problem down to its barest essentials if we focus on the wavefunction for the virtual neutron in the idealized case that there is only one deuteron in the lattice

$$(\Delta E - H_n)\psi_n(\mathbf{r}) = < \psi_p(\mathbf{r}_p)| - \mu \cdot \mathbf{B}|\Psi_D(\mathbf{r}_p, \mathbf{r}) > \tag{4}$$

ΔE is the energy deficit of the virtual neutron (on the order of -2.225 MeV), H_n is the Hamiltonian of the neutron, and ψ_n is the virtual neutron wavefunction. The term on the right hand side is the source for the neutron, which is due to the deuteron in a magnetic field.

The virtual neutron wavefunction can be calculated in terms of the Green's function through

$$\psi_n(\mathbf{r}) = \int G(\mathbf{r}|\mathbf{r}_0) < \psi_p(\mathbf{r}_p)| - \mu \cdot \mathbf{B}|\Psi_D(\mathbf{r}_p, \mathbf{r}_0) > \tag{5}$$

where the Green's function satisfies

$$(\Delta E - H_n)G(\mathbf{r}|\mathbf{r}_0) = \delta^3(\mathbf{r} - \mathbf{r}_0) \tag{6}$$

The behavior of the Green's function determines the character of the virtual neutron wavefunction, and we can determine whether virtual neutrons will be able to transfer more than a few fermis by studying the associated neutron Green's function. In the case where the neutron is assumed not to interact with the lattice after being formed, we would take the neutron Hamiltonian to be

$$H_n = -\frac{\hbar^2 \nabla^2}{2M_n} \tag{7}$$

and calculate the neutron Green's function to be

$$G(\mathbf{r}|\mathbf{r}_0) = -\frac{1}{4\pi}\frac{2M_n}{\hbar^2}\frac{e^{-\sqrt{\frac{2M_n|\Delta E|}{\hbar^2}}|\mathbf{r}|}}{|\mathbf{r}|} \tag{8}$$

This result assumes that the proton recoil is taken up by the lattice. We see that the range of the virtual neutron is severely limited to $(\hbar^2/2M_n|\Delta E|)^{1/2}$, which evaluates to about 3 fm for this example. This is the origin of the argument that a virtual neutron simply does not go very far from its point of origin.

We may include the primary effects of the lattice in the problem by including the nuclear potential responsible for Bragg scattering. In this case we take the neutron Hamiltonian to be

$$H_n = -\frac{\hbar^2 \nabla^2}{2M_n} + V(\mathbf{r}) \tag{9}$$

where the potential $V(\mathbf{r})$ is assumed to be periodic, and is expanded in terms of reciprocal lattice vectors $\mathbf{K}$ to give

$$V(\mathbf{r}) = \sum_{\mathbf{K}} V_{\mathbf{K}} e^{i\mathbf{K}\cdot\mathbf{r}} \tag{10}$$

We are able to solve for the Green's function approximately in this case. We find that the Green's function is dominated by a local piece which is very nearly equal to the non-interacting Green's function described above, plus an additional very small long range piece which is induced by the periodic potential

$$G(\mathbf{r}|\mathbf{r}_0) = G(\mathbf{r}|\mathbf{r}_0)|_{V=0} + \Delta G(\mathbf{r}|\mathbf{r}_0) \tag{11}$$

This long range piece is calculated to be equal to

$$\Delta G(\mathbf{r}|\mathbf{r}_0) = -\frac{1}{|\Delta E|^2}\sum_{\mathbf{K}} \delta^2(\mathbf{r}_\perp - (\mathbf{r}_0)_\perp)\frac{1}{\pi}|\mathbf{k}_r|\Big\{|V_{\mathbf{K}}|\sin[\frac{1}{2}\mathbf{K}\cdot(\mathbf{r}-\mathbf{r}_0)]f_1(\mathbf{k}_r\cdot(\mathbf{r}-\mathbf{r}_0))$$
$$+\frac{1}{2}\Big[V_{\mathbf{K}}^* e^{\frac{i}{2}\mathbf{K}\cdot(\mathbf{r}+\mathbf{r}_0)} + V_{\mathbf{K}} e^{-\frac{i}{2}\mathbf{K}\cdot(\mathbf{r}+\mathbf{r}_0)}\Big] f_2(\mathbf{k}_r\cdot(\mathbf{r}-\mathbf{r}_0))\Big\} \tag{12}$$

where $\mathbf{k}_r$ is the extinction vector for normal Bragg reflection

$$\mathbf{k}_r = \frac{2M_n|V_{\mathbf{K}}|}{\hbar^2|\mathbf{K}|^2}\mathbf{K} \tag{13}$$

and where f_1 and f_2 are auxiliary functions defined by

$$f_1(t) = \frac{\pi}{2t}[I_1(t) - \mathbf{L}_1(t)] \tag{14}$$

$$f_2(t) = 1 - \frac{\pi}{2}[I_1(t) - \mathbf{L}_1(t)] \tag{15}$$

In these formulas, I_1 is a modified Bessel function of first order, and $\mathbf{L}_1$ is a modified Struve function of first order.

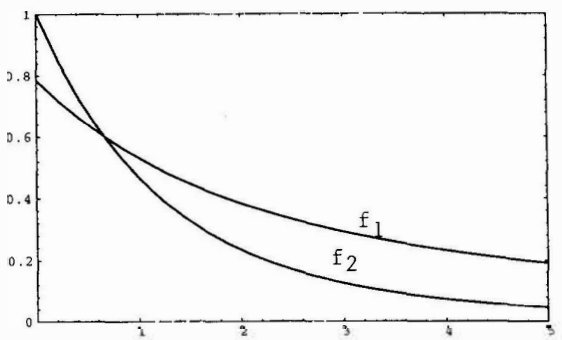

Figure 4: Auxiliary functions $f_1(x)$ and $f_2(x)$.

We may use these results to compute rates for second order gamma emission through

$$\Gamma = \int |\Delta\psi(\mathbf{r})|^2\Big[\sum_j N_j(\mathbf{r})(\sigma_j v)_0\Big]d^3\mathbf{r} \tag{16}$$

where $N_j(\sigma_j v)_0$ is the gamma capture rate for isotope j for the virtual neutron. In the presence of a magnetic field of 100 KGauss, the second order gamma emission rate is estimated to be near 10^{-60} $\sec^{-1}$/deuteron in PdD.

5. Resonance Exchange Scattering

We have succeeded in obtaining a long range contribution to the virtual neutron Green's function which is capable of delocalizing a neutron over a micron scale length. Unfortunately the associated rates for second order reactions through such a mechanism are calculated to be neglible.

This result bodes unfavorably for neutron transfer reaction mechanisms unless some new physics can be found which would improve the virtual neutron density. While searching for possible resonant mechanisms, we noted that the capture of a neutron onto a proton to form a deuteron would be resonant if the neutron originated from a deuteron initially. Certainly protons exist in the Pd rods at a the few per cent level in the excess heat experiments.

We have modeled the incoherent version of the process assuming that the initial deuteron is perturbed by a small amount δE, but that all subsequent captures and re-emissions occur in the Mossbauer limit of no phonon generation. In this case, the neutron Hamiltonian is modified to become

$$H_n = -\frac{\hbar^2\nabla^2}{2M_n} + V(\mathbf{r}) + W(\mathbf{r}) \tag{17}$$

where the operator $W(\mathbf{r})$ satisfies

$$W(\mathbf{r})\psi_n(\mathbf{r}) = \sum_i < \psi_p^{(i)}(\mathbf{r}_p)|-\mu\cdot\mathbf{B}|\Psi_D^{(i)}(\mathbf{r}_p,\mathbf{r}) > \frac{1}{\delta E} < \Psi_D^{(i)}(\mathbf{r}'_p,\mathbf{r}')|-\mu\cdot\mathbf{B}|\psi_p^{(i)}(\mathbf{r}'_p)\psi_n(\mathbf{r}') \tag{18}$$

Since the operator is of the form of an exchange term, we have termed the effect resonant exchange scattering.

The exchange operator leads to Bragg scattering on the same footing as the direct neutron potential considered in the last section. We may expand

$$W(\mathbf{r})e^{i\mathbf{k}\cdot\mathbf{r}} = \sum_{\mathbf{K}} W_{\mathbf{k}-\mathbf{K},\mathbf{k}} e^{i(\mathbf{k}-\mathbf{K})\cdot\mathbf{r}} \tag{19}$$

where the expansion coefficients $W_{\mathbf{k}-\mathbf{K},\mathbf{k}}$ are computed to be

$$W_{\mathbf{k}-\mathbf{K},\mathbf{k}} = \frac{|\mu\cdot\mathbf{B}|^2}{\delta E}\left[\frac{16\alpha_p\alpha_D}{(\alpha_p+\alpha_D)^2}\right]^{3/2}\frac{V_N}{V_{cell}} e^{-|\mathbf{k}|^2/2(\alpha_p+\alpha_D)} e^{-|\mathbf{k}-\mathbf{K}|^2/2(\alpha_p+\alpha_D)} \sum_j e^{i\mathbf{K}\cdot\mathbf{R}_j} \tag{20}$$

where the proton wavefunctions are parametrized by $\psi_p \sim e^{-\alpha_p|\mathbf{r}-\mathbf{R}_i|^2/2}$, and where the center of mass of the deuteron wavefunctions is parametrized by $\Psi_D \sim e^{-\alpha_D|\mathbf{r}-\mathbf{R}_i|^2/}$ In this expression, V_N is the nuclear volume, and V_{cell} is the lattice unit cell volume. The summation over j includes proton sites in the unit cell, and

$$|\mu \cdot \mathbf{B}|^2 = \sum_{M_S} |\, <^1 S, 0| - \mu \cdot \mathbf{B}|^3 S, M_S > |^2 \tag{21}$$

The exchange terms can be added to the direct terms in the development of the Green's function in the presence of resonance exchange scattering; our results of the last section can be applied here with the modification

$$V_{\mathbf{K}} \longrightarrow V_{\mathbf{K}} + W_{\mathbf{k}-\mathbf{K},\mathbf{k}} \tag{22}$$

Unfortunately, the expansion coefficients $W_{\mathbf{k}-\mathbf{K},\mathbf{k}}$ for the incoherent version of this new process are smaller by very roughly four orders of magnitude from the expansion coefficients $V_{\mathbf{K}}$ for direct potential scattering.

It appears that a coherent enhancement of the effect may be possible. The resonant exchange scattering matrix element computed in second quantization is given formally by

$$W^{(c)}_{\mathbf{k}-\mathbf{K},\mathbf{k}} =< \mathbf{k} - \mathbf{K}, L|\hat{H}_{-\mu\cdot\mathbf{B}} \frac{1}{\delta E} \hat{H}_{-\mu\cdot\mathbf{B}}|\mathbf{k}, L > \tag{23}$$

The evaluation of this expression yields

$$W^{(c)}_{\mathbf{k}-\mathbf{K},\mathbf{k}} = \sum_{i,j} \sum_{\alpha_p,\alpha_{p'}} \sum_{\alpha_D,\alpha_{D'}} \frac{1}{\delta E} < \psi^{(i)}_p \psi_{n,\mathbf{k}-\mathbf{K}}| - \mu \cdot \mathbf{B}|\Psi^{(i)}_D >< \Psi^{(j)}_D| - \mu \cdot \mathbf{B}|\psi^{(i)}_p \psi_{n,\mathbf{k}} >$$

$$< \hat{b}^{\dagger}_{p,\alpha_p}(i)\hat{b}_{D,\alpha_D}(i)\hat{b}^{\dagger}_{D,\alpha_{D'}}(j)\hat{b}_{p,\alpha_{p'}}(j) > \tag{24}$$

Using the parametrization of the proton and deuteron orbitals described above, this leads to a result which can be cast as

$$W^{(c)}_{\mathbf{k}-\mathbf{K},\mathbf{k}} = \sum_{\alpha_p,\alpha_{p'}} \sum_{\alpha_D,\alpha_{D'}} \frac{1}{\delta E} < \chi(\alpha_p)\chi(\alpha_n)|-\mu\cdot\mathbf{B}|\chi(\alpha_D) >< \chi(\alpha_{D'})|-\mu\cdot\mathbf{B}|\chi(\alpha_{p'})\chi(\alpha_n) >$$

$$\left[\frac{16\alpha_p\alpha_D}{(\alpha_p+\alpha_D)^2}\right]^{3/2} \frac{V_N}{V} e^{-|\mathbf{k}|^2/2(\alpha_p+\alpha_D)} e^{-|\mathbf{k}-\mathbf{K}|^2/2(\alpha_p+\alpha_D)} \left[\sum_j e^{i\mathbf{K}\cdot\mathbf{R}_j}\right] < \hat{\Sigma}_-[\alpha_p\alpha_n\alpha_D]\hat{\Sigma}_+[\alpha_{p'}\alpha_n\alpha_{D'}] > \tag{25}$$

This result is the coherent generalization of equation (20), and differs in the presence of possible coherence factors, which are expectation values over the many-particle operators $\hat{\Sigma}_-[\alpha_p\alpha_n\alpha_D] = \sum_i \hat{b}^{\dagger}_{p,\alpha_p}(i)\hat{b}_{D,\alpha_D}(i)$ and $\hat{\Sigma}_+[\alpha_{p'}\alpha_n\alpha_{D'}] >= \sum_j \hat{b}^{\dagger}_{D,\alpha_{D'}}(j)\hat{b}_{p,\alpha_{p'}}(j)$ These operators satisfy commuation relations identical to those of spin operators, and permit the construction of eigenstates analogous to spin states. Such states were studied by Dicke, and lead to coherent enhancements of matrix elements of the sort which appear in equation (25).

It has not been demonstrated yet that any particular mechanism is capable of producing the requisite Dicke states which would lead to a coherent enhancement of the resonant exchange scattering. It is our belief that diffusion in the quantum limit would cause phase-preserving delocalization of hydrogen isotopes in a metal

hydride, and that this would lead to the production of anomalous effects observed in Pons-Fleischmann experiments. If this is true, then we would obtain

$$W^{(c)}_{\mathbf{k}-\mathbf{K},\mathbf{k}} \sim N_{coh} W_{\mathbf{k}-\mathbf{K},\mathbf{k}} \tag{26}$$

The coherence number could be on the order of the number of sites enclosed in a cube with a volume which is on the order of $V_{coh} = L^3_{coh}$, where the scale length would be determined through $L_{coh} \sim \sqrt{D\tau}$, and where D is the quantum diffusion coefficient and τ is the phase destruction time (which we cojecture will be the NMR T_2 time). If so, the coherence numbers of $N_{coh} \sim 10^{10}$ may be attainable, which would cause the coherent version of the resonant exchange scattering to dominate the virtual neutron dynamics. This limit would require a more sophisticated calculation for the Green's function than the perturbative result given above.

6. Summary and Conclusions

We have proposed new coherent neutron transfer reactions to account for the anomalies which are associated with Pons-Fleischmann experiments. In this paper we have discussed the problems associated with the presence of a virtual neutron in a second order reaction, and we have summarized recent progress which we have made to date. Although lattice effects can cause a significant delocaliztion of the virtual neutron wavefunction, they are insufficient to lead to observable reaction rates. The coherent version of the new resonant exchange scattering mechanism which we have found appears to have the potential to provide large theoretical rates. If our conjecture is correct, the mechanism would be specific to deuterium in metal hydrides with high diffusion coefficients at room temperature.

Heat production in the theory could come from at least two reaction pathways. The neutron transfer could occur to the ground state of the acceptor (such as ^{6}Li or ^{10}B, and the energy transfer could occur to the lattice via the gap jumping mechanism which we have found in an earlier work[3]. Alternatively, the neutron transfer could occur to a relatively long-lived excited state of an acceptor nucleus (perhaps a Pd isotope), which might subsequently alpha decay.

References

1. P. L. HAGELSTEIN, "Coherent and Semi-Coherent Neutron Transfer Reactions I: The Interaction Hamiltonian," *Fusion Tech.* **22**, 172-180, (1992).

2. P. L. HAGELSTEIN, "Coherent and Semi-Coherent Neutron Transfer Reactions II: Transition Operators," submitted to *Fusion Tech.*, (1992)

3. P. L. HAGELSTEIN, "Coherent and Semi-Coherent Neutron Transfer Reactions III: Phonon Generation," to appear in *Fusion Tech.* (1992)

4. P. L. HAGELSTEIN, "Coherent and Semi-Coherent Neutron Transfer Reactions IV: Two-Step Reactions and Virtual Neutrons," submitted to *Fusion Tech.* November (1992)

Nuclear Fusion in Condensed Matter

V.ROMODANOV, V.SAVIN, Ya.SKURATNIK*, Yu.TIMOFEEV

142109, Podolsk, Moscow Region, Zheleznodorozhnaya 24, RI of SPA LUTCH. Fax. 095-137-9384
*Moscow, SRPCI named after Karpov

ABSTRACT

On the basis of the analysis of the energy loss by a fast particle in a solid it is supposed that the most probable energy range for the reactions of nuclear fusion in condensed media is in the range of the reduced energy of the interacting particles from ε_0 to ε_2 ($\sim$(10-400)$\cdot$1.6$\cdot$10^{-19} J for D-D reactions).

The tritium generation rate has increased by four orders of magnitude, while increasing the specific power by a factor of four, and it has reached the value of 10^9 atom$\cdot$s^{-1} when the neutron-to-tritium yield ratio is in the range from 10^{-7} to 10^{-9}.

The possibility of performing the reactions of nuclear fusion in condensed media between deuterium and target atoms at low energies is shown on the basis of the high-energy β-radiation recording, the isotopic target composition change and the radiography results.

1. Introduction

Investigation of nuclear fusion in condensed matter (NFCM) was performed according to the following stages: from groundless hopes to systematic search for some effects published before and to detection of the conditions under which these effects take place.

We were the first to use deuterium ion bombardment of different targets out of the powerful glow discharge medium for systematic investigation of the NFCM effects /1-3/.

The aim of this work is to determine the optimal range of the NFCM energies when bombarding different

FRONTIERS OF COLD FUSION

targets with accelerated deuterium ions and to define the neutron-to-tritium yield ratio more exactly.

2. Model concepts

As a basis of the model of deuterons interaction in a solid it is supposed that the fusion reaction between them will be possible when two deuterons and one atom of the target matrix hit one intersite cell. In this case the reaction must be threshold (the energy of displacement of the crystalline matrix atom is $(10-30)\cdot 1.6\cdot 10^{-19}$ J for different materials) and the collisions of the deuterons between each other and the target atoms are studied in the energy range exceeding the threshold one on the basis of the analysis of the energy lost by fast particles in a solid. This is possible at be having correlation between local (nuclear) and integral (atoms) collisions. Such an analysis is developed rather well for other fields of physics, in particular, for studying solid surface sputtering /4/.

In terms of this analysis we supposed that one of the possible energy intervals for nuclear fusion is defined by the ratio of the elastic (nuclear) and nonelastic (electronic) losses when accelerated particles move in a solid.

The energy transfer from the moving ion to the target atoms as a result of the elastic collisions is called nuclear deceleration and as a result of the nonelastic collisions - electronic deceleration. The dimensionless values of the current coordinate R and energy E are used in the theory of ion path in amorphous substances, developed by J.Lindhard, M.Scharff, H.E.Schioett (LSS) /5/.

$$\varepsilon \equiv E \left(\frac{M_2}{M_1+M_2} \right) / \frac{Z_1 \cdot Z_2 \cdot e^2}{a_{TF}} ,$$

$$\rho \equiv R \left(\frac{M_1 \cdot M_2}{(M_1+M_2)^2} \right) \cdot 4\pi a_{TF}^2$$

where R - energy of the incident particle; M_1 and M_2 - masses of the incident particle and the target atoms, respectively; Z_1 and Z_2 - atomic numbers; a_{TF} - Thomas-Fermi shielding distance; e - electron charge.

The total average energy losses are equal to the sum of the losses caused by the nuclear and electronic deceleration:

$$-\frac{dE}{dR} = N\,/S_n(E) + S_e(E)/,$$

where $S_n(E)$ - nuclear decelerative ability; N - avera-

ge number of atoms per target volume unit: $S_e(E)$ - electronic decelerative ability.

Only one universal curve which is supposed to be true for all ion-target combinations can be found by varying $(d\mathcal{E}/d\rho)_n$ depending on $\mathcal{E}$ (fig.1). The peak of the nuclear loss curve corresponds to $\mathcal{E}_1 \approx 0.35$.

The specific electronic losses are the following:

$$\left(-\frac{d\mathcal{E}}{d\rho}\right)_e = K_e \cdot \mathcal{E}^{0.5}$$

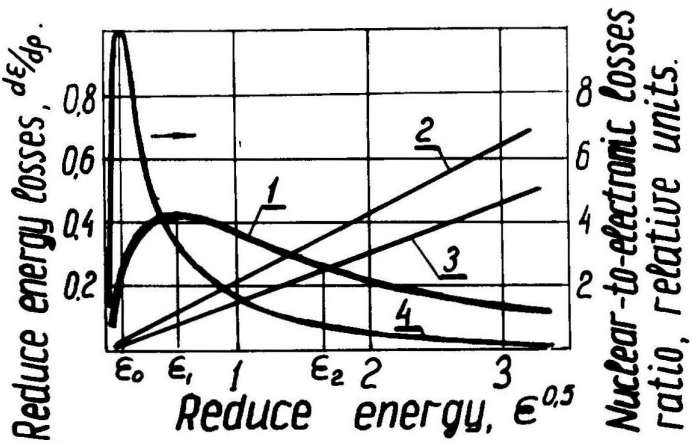

Fig. 1. Reduced energy losses $d\mathcal{E}/d\rho$ versus the reduced energy $\mathcal{E}^{0.5}$

1 - nuclear (elastic) losses, Thomas-Fermi potential; 2 - electronic losses, K_e=0.2; 3 - electronic losses, K_e=0.15; 4 - nuclear - to - electronic losses ratio (K_e=0.2)

The values K_e for most of the deuterium ion - target combinations is in the range 0.1-3.

For deuterium ions bombarding the condensed deuterium the calculated energy of the maximum nuclear losses corresponds to $30 \cdot 1.6 \cdot 10^{-19}$ J and the maximum ratio of nuclear-to-electronic losses according to P.Sigmund /4/ corresponds to the energy $7 \cdot 1.6 \cdot 10^{-19}$ J.

Thus, the maximum of the absorbed energy of the atom collisions is near the nuclear loss maximum corresponding to the energy $\mathcal{E}_1$ (see fig. 1) and the energy, absorbed when the particles collide, decreases considerably after the electronic losses exceed the nuclear ones, that corresponds to the energy $\mathcal{E}_2$ (see fig. 1). In view of the above-mentioned we consider that the most probable range of the NFCM energy is from $\mathcal{E}_0$ up to $\mathcal{E}_2$, the calculated values of which for some

ion-target combinations are given in Table 1. In this Table one can see that depending on the used ion-target combination of the interacting elements the energy of the maximum nuclear losses can reach a few hundreds of keV. According to the accepted model the nuclear interaction efficiency for moderate ion fluxes when using accelerated ions, can be estimated by the coefficient similar to the sputtering one. We called it the nuclear interaction coefficient which is the ratio of the amount of one of the nuclear reaction products to the number of the ions incident on the target made of the given material:

$$Y_n = \frac{\text{number of formed particles}}{\text{number of incident ions}}$$

Table 1

Characteristic energy values for different combinations of deuterium interaction with elements

Target	K_e	E_o, eV	E_1, eV	E_2, eV
^{2}H	0.09	7	30	370
^{7}Li	0.18	9	70	470
^{9}Be	0.21	10	100	510
^{11}B	0.24	11	130	610
^{23}Na	0.42	14	310	730
^{24}Mg	0.43	15	350	760
^{27}Al	0.48	15	380	980
^{45}Sc	0.73	18	700	720
^{48}Ti	0.77	18.1	740	740
^{51}V	0.81	18.4	780	670
^{89}Y	1.29	22.3	1530	400
^{91}Zr	1.31	22.5	1580	410
^{93}Nb	1.34	22.7	1630	360
^{232}Th	2.93	39	4520	-

The reaction product yield isn't supposed to depend on the density of the bombarding ion flux.

3. Experimental procedure and results

The plant construction and the experimental procedure of recording neutrons and tritium, which are

brought about when bombarding different targets by accelerated deuterium ions, are deseribed in /2/. The discharge unit of the plant is designed according to the diode circuit of the direct current in which the specimen of the cathode is bombarded by the deuterium ions out of the glow discharge plasma when the positive potential is applied to the anode. The lamellar specimens ~130 mm in diameter and from 0.05 up to 1 mm thick, located on the cooled substrate, as well as the cylindrical and rod ones having 5-20 mm in diameter were studied. The deuterium containing protium (up to 5% in atomic fractions) and tritium (up to $(5-7)\cdot10^{-10}$%) and having the pressure within $10-5\cdot10^{4}$ Pa was used as a gas which generated plasma. The ion energy changed within $(20-10^{4})\cdot1.6\cdot10^{-19}$ J both at the expense of the supply voltage and at the expense of changing the plasma generating gas pressure in the plant chamber. The current density was $25-5\cdot10^{3}$ A·m^{-2} and the speciment temperature was from 300 up to 2100K.

The thermal effects of the fusion reactions were determined by two methods at the experimental unit the diagram of which is shown in fig.2. The heat flow obtained as a result of the supposed nuclear fusion reaction was determined by measuring the temperature difference both in the measurement section at the temperatures up to 1000K and along the both sides of the weld at the temperatures higher than 1300K by the pyrometer OMP-54. The accuracy of such measurements didn't exceed ±50%.

Some results of measuring the tritium fluxes and their neutron ratio, when irradiating a number of elements by the accelerated deuterium ions out of the glow discharge plasma, are given in Table 2. In this table one can see that β-activity of the plasma-generating gas considerably exceeds the initial one after the gas exposure in the plant chamber under the above-mentioned experimental conditions. The most stable results on tritium generation were obtained when bombarding the erbium and molybdenum specimens by the accelerated deuterium ions and the maximum results were obtained for the niobium specimens. The recorded tritium fluxes were within $10^{5}-10^{9}$ atom·s^{-1}. The unexpectedly high rate of tritium generation (~10^{8} atom·s^{-1}) was obtained when bombarding a material which doesn't generate any hydrides under normal conditions, e.g. when bombarding tungsten.

The recorded neutron-to-tritium flux ratio is from 10^{-3} up to 10^{-9} and mainly depends on the recorded tritium fluxes. Therefore, one shouldn't consider it final.

The tritium content in the near-surface layer of

the specimens after the ion bombardment didn't correspond to its content in gas. The analysis made in the flow detector according to the procedure of measuring the electron spectrum depending on the energy (MSU /6/) showed that after the deuterium ion bombardment

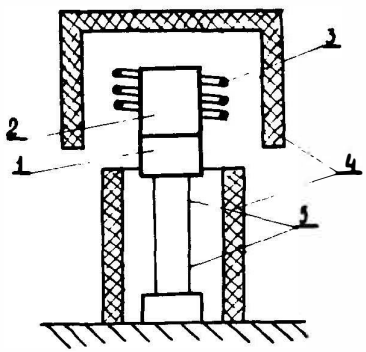

Fig. 2. The diagram of the device for thermal effect determination

1 - molybdenum specimen base; 2 - a part of the hydride-generating material; 3 - anode; 4 - ceramic insulators; 5 - thermocouples

the averaged tritium concentration in the near-surface niobium layer was 10^{7}-10^{8} atom·s^{-2} and in the near-surface tungsten layer (the tritium concentration in gas phase was less by an order of magnitude) the tritium concentration was within $5\cdot10^{9}$-$5\cdot10^{10}$ atom·cm^{-2} The energy spectrum of the radiation from the niobium surface (fig.3) is close to the curve of the tritium β-decay.

The nuclear interaction coefficient when generating tritium (specific flux) versus the bombarding deuteron energy is shown in fig. 4. The feature of the dependence is a threshold availability in the range 70-150·1.6·10^{-19} J. When increasing the bombarding ion energy for the materials under investigation, the nuclear interaction coefficient has increased from 10^{-14}

Table 2

Ratio of neutron and tritium fluxes when irradiating a number of materials by deuterium ions

Material	Process parameters			Background pulse / 100 s	Reduced activity in view of background, Bc/ml	Ratio of deuterium activities after and before experiments	Tritium atom flux, atom/s	Nuclear interaction coefficient, atom/ion	Neutron-to-tritium flux ratio	
	E, eV	T, K	τ, h						min	max
D_2	-	-	-	240	130	-	-	-	-	-
Y	40	1170	80	210	290	2.2	$1.2 \cdot 10^5$	$4.1 \cdot 10^{-15}$	$8.5 \cdot 10^{-6}$	$1.7 \cdot 10^{-3}$
Y	80	1270	23	250	$1.2 \cdot 10^3$	9.2	$4.5 \cdot 10^6$	$1.6 \cdot 10^{-12}$	$2.2 \cdot 10^{-7}$	$4.4 \cdot 10^{-5}$
Mo	125	1470	10	150	$6 \cdot 10^3$	46	$4.5 \cdot 10^6$	$9.2 \cdot 10^{-12}$	$2.2 \cdot 10^{-7}$	$4.4 \cdot 10^{-5}$
Mo	100	970	10	170	$1.6 \cdot 10^3$	12.3	$1.8 \cdot 10^7$	$5.9 \cdot 10^{-12}$	$5.5 \cdot 10^{-8}$	$1.1 \cdot 10^{-5}$
Nb	75	1170	162	230	$4.7 \cdot 10^4$	$3.6 \cdot 10^2$	10^7	$3.8 \cdot 10^{-13}$	10^{-7}	$2 \cdot 10^{-5}$
Nb	80	1170	60	700	$3 \cdot 10^6$	$2.3 \cdot 10^4$	$1.7 \cdot 10^9$	$6.8 \cdot 10^{-11}$	$0.6 \cdot 10^{-9}$	$1.8 \cdot 10^{-7}$
Nb	100	1670	8	240	$5.5 \cdot 10^4$	$4.2 \cdot 10^2$	$0.9 \cdot 10^9$	$1.2 \cdot 10^{-10}$	$1.1 \cdot 10^{-9}$	$2.2 \cdot 10^{-7}$
Er	50	1070	140	460	$1.2 \cdot 10^3$	9.6	$3.1 \cdot 10^5$	$9.9 \cdot 10^{-15}$	$3.2 \cdot 10^{-6}$	$6.4 \cdot 10^{-4}$
Er	70	1270	6	530	$8.9 \cdot 10^2$	6.8	$1.5 \cdot 10^7$	$3.2 \cdot 10^{-12}$	$6.7 \cdot 10^{-8}$	$1.3 \cdot 10^{-5}$
Ta	70	1570	110	350	$3.1 \cdot 10^3$	23.5	$9.6 \cdot 10^5$	$3.6 \cdot 10^{-14}$	$1.1 \cdot 10^{-6}$	$2.1 \cdot 10^{-4}$
Ta	90	1670	5	180	$1.6 \cdot 10^3$	12.3	$3.4 \cdot 10^7$	$7.3 \cdot 10^{-12}$	$2.9 \cdot 10^{-8}$	$5.9 \cdot 10^{-6}$
W	70	1500	115	600	$8.5 \cdot 10^5$	$6.5 \cdot 10^3$	$2.5 \cdot 10^8$	$9.1 \cdot 10^{-12}$	$4 \cdot 10^{-9}$	$8 \cdot 10^{-7}$
W	110	1670	10	760	$1.3 \cdot 10^4$	10^2	$1.7 \cdot 10^8$	$2.5 \cdot 10^{-11}$	$5.8 \cdot 10^{-9}$	$1.2 \cdot 10^{-6}$

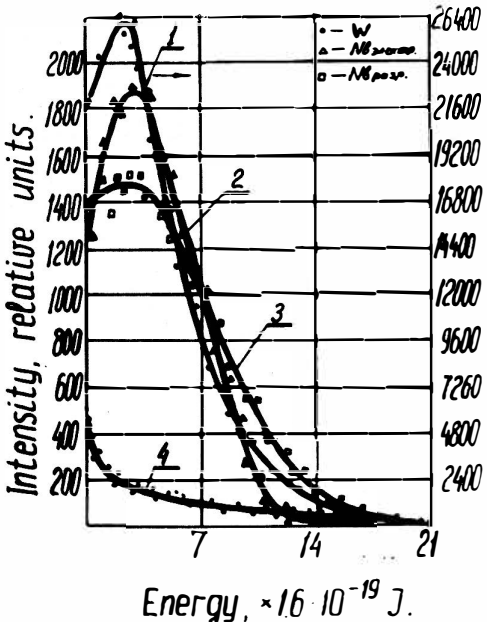

Fig. 3. The energy spectrum of β-radiation on surfaces of different materials

1 - tungsten after ion bombardment ($E=70 \cdot 1.6 \cdot 10^{-19}$ J, T=1500K, τ=115 h); 2 - niobium after having been saturated with tritium by means of electrolysis; 3 -niobium after ion bombardment ($E=75 \cdot 1.6 \cdot 10^{-19}$J, T=1170K, τ=162 h); 4 - starting tungsten

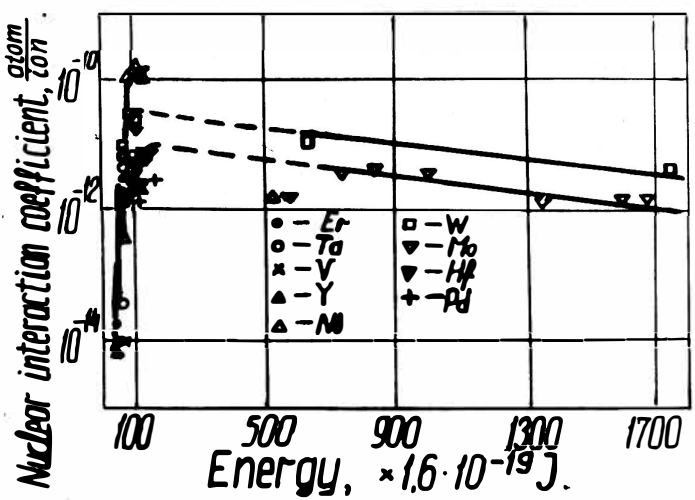

Fig.4. The nuclear interaction coefficient when generating tritium versus the energy of the bombarding deuterium ions for different target materials

-10^{-13} atom·ion^{-1} up to 10^{-11} - 10^{-10} atom·ion^{-1}. The average value of the threshold energy is by an arder of magnitude higher than the $\mathcal{E}_0$ estimation made according to Sigmund and 2-5 times higher than the displacement threshold ((10-30)·1.6·10^{-19} J). One failed to determine explicit the energy corresponding to the maximum values of Y_n. It is supposed to be in the range (200-400)·1.6·10^{-19} J. This energy is almost by an order of magnitude higher than $\mathcal{E}_1$(30·1.6·10^{-19} J) for the deuterium target, that may be caused by the metallic matrix effect. The obtained, rather low values of the energies of the maximum nuclear interaction can be also connected with the features of the experimental procedure, according to which the experiments with the deuteron energies exceeding 500·1.6·10^{-19} J were performed at lower pressures of the plasma-generating gas and, therebefore, at lower deuterium concentrations in a metal.

Thus, all the reproduced and reliable NFCM results can be most effectively obtained in the range of the energies of the bombarding deuterium ions from 100·1.6·10^{-19} J up to 500·1.6·10^{-19}J.

The availability of the radiation from the surface is also verified by the specimen radiography (fig.5). The radiogram with the total exposure of two emulsion layers 0.02-0.03 mm thick, located on the both

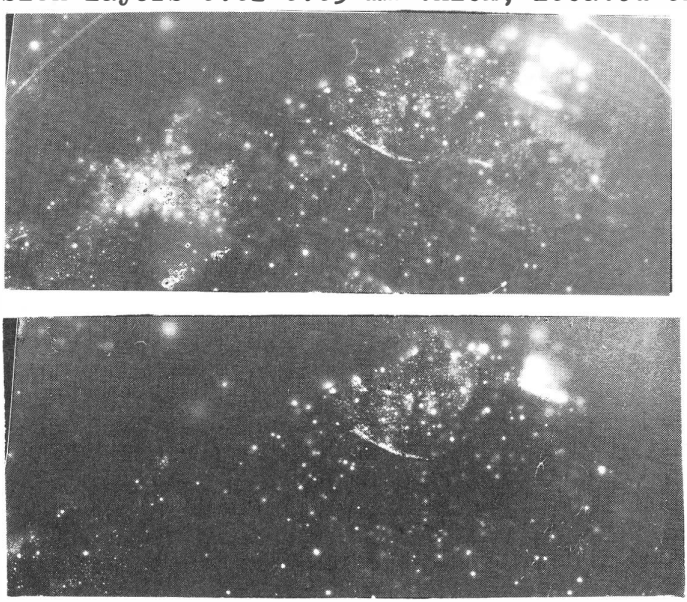

a

b

Fig.5. The yttrium specimen radiogram (T=1170K, τ =80 h):
a-starting film; b-the emulsion layer adjacent to the cpecimen is removed

sides of the triacetate base 0.16-0.18 mm thick (see fig.5a),as well as with the exposure of the same film but with the removed emulsion layer directly adjacent to the specimen (see fig.5b) is shown for yttrium. One can see that the film is pointwise exposed from the outside, though the number of the points is less. The outer emulsion layer was probably exposed at the expense of availability of the particles or radiation having a higher penetration rather than at the expense of the radiation caused by the tritium β-decay.

The recording of β-radiation from the yttrium specimen surface, with the gas detector the thereshold energy 160 keV and the efficiency 60%, allowed to record the count level excess over the background up to 12% and to measure the time response of the decay (Table 3).

Table 3

β-radiation pulse count rate versus time for yttrium after ion bombardment ($E=110 \cdot 1.6 \cdot 10^{-19}$ J, $I=0.3$ A, $\tau=24$ h)

Time (counting origin-bombardment finish), h	1	7	31	79
Counting rate (minus background), pulse$\cdot s^{-1}$	0.12 ± 0.10	0.055 ± 0.048	0.031 ± 0.021	0.015 ± 0.0

According to the estimation the $^{90}_{39}Y$ generation rate is equal to $1 \cdot 10^{-1}$ atom$\cdot s^{-1}$, that accounts for 10^{-6} of the tritium generation rate.

The results of the thermal balance measurement (fig.6) are compared with the calculated temperature difference for the total power 1, for the supposedly maximum power dissipating at the specimen of the cathod 3 and accounting for 50% of the total one, for the minimun power dissipating at the specimen of the cathode 4 and accounting for 30% of the total one and for the experimentally measured one 2. In comparison with the estimations of the heat coming to the specimen of the cathode the maximum excess for the total applied power 70 W at the temperature $\sim$ 600K was from 30% up to 100% supposedly as a result of the nuclear fusion reaction.

The tungsten and niobium specimens were investigated before and after the deuterium ion bombardment at the device MS-720IM by the secindary ion mass-spectrometry (SIMS) method. The ratios of the intensities of

the mass peaks of the specimens under study in the initial state and after the ion bombardment are given in Table 4.

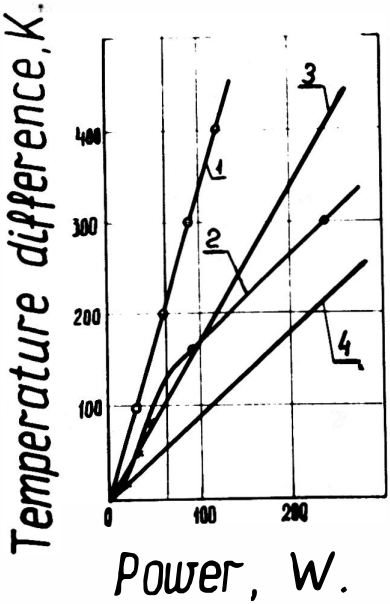

Fig. 6. The temperature difference versus the applied power

1 - calculational dependence for the total power; 2 - experimental dependence; 3 - estimation for the maximum power dissipated at the cathode; 4 - estimation for the minimum power dissipated at the anode

Table 4

Change in the ratio of the ion current of the elements to that of the light isotope of the specimen material as a result of the deuterium ion bombardment

Mass, AMU	Ion current ratio			
	Initial niobium	Niobium after bombardment	Initial tungsten	Tungsten after bombardment
93	1	1	-	-
94	0.07	0.7	-	-
182	-	-	1	1
183	-	-	0.69	0.76
184	-	-	1.25	1.16
185	-	-	0.16	0.24
186	-	-	0.01	0.86
187	-	-	0.16	0.18

The peak of the 94^{th} mass in the niobium-spectrum has considerably increased after the deuterium ion bombardment. In this case the presence of the 95^{th} mass (NbD) hasn't been detected.

Thus, the emulsion exposure from the outside during the radiographic experiments, availability of the high-energy β-radiation as well as the isotopic composition change registered by the SIMS mean that at relatively low energies the following NFCM reactions are possible not only between the deuterium atoms but also between the deuterium and target atoms:

$$^{93}_{41}Nb + {}^{2}_{1}H \longrightarrow {}^{94}_{41}Nb + {}^{1}_{1}H + 5\ MeV.$$

4. Conclusion

1. The threshold character of the dependence of the nuclear interaction rate on the energy of the bombarding deuterium ions has been detected in the NFCM reactions. When increasing the ion energy by a factor of two (from $50 \cdot 1.6 \cdot 10^{-19}$ J up to $100 \cdot 1.6 \cdot 10^{-19}$ J), the tritium generation rate has increased by 2-4 orders of magnitude.

2. The new energy range ($(100\text{-}500) \cdot 1.6 \cdot 10^{-19}$J) allowing to increase the reproducibility and reliability of the experiments was determined for the NFCM investigation.

3. It is shown that the dependence of the nuclear interaction coefficients on the atomic number of the target element isn't monotonic. The highest values of the nuclear interaction coefficient were obtained for niobium ($\sim 10^{-10}$ atom$\cdot$ion^{-1}) and for tungsten and hafnium ($\sim 10^{-11}$ atom$\cdot$ion^{-1}).

4. The tritium fluxes reaching the value of 10^{9} atom$\cdot$s^{-1} and the neutron fluxes close to the background ones don't allow yet to consider the neutron-to-tritium flux ratio at the level 10^{-9}-10^{-7} to be the final value.

5. The calorimetric measurements shouldn't be interpreted unambiguously yet because of the low sensitivity and accuracy of the experiments. The subsequent increase in the measurement accuracy and matching between the generated heat and the other NFCM products is required.

6. The data on radiography, high-energy β-radiation recording as well as on changing in the isotopic composition of the target show that at relatively low energies the NFCM reactions between the deuterium and target atoms, which are similar to the deuterium-deuterium reactions, are possible.

Acknowledgement

The authors are grateful to Dr.V.A.Modin for his assistance in the experimental plant development, Dr. S.G.Korneev for the high-energy γ-and β-activity measurements as well as Prof. R.N.Kuzmin and Dr. P.O.Revokatov for investigating tritium on the specimen surface.

References

1. V.A.Romodanov, V.I.Savin, M.V.Shakhurin, V.T.Chernyavsky, A.E.Pustovit.
Nuclear fusion in a solid. -
International Conference on Radiative Material Science. Alushta, May 22-25, 1990. Poster report 1-100. Theses of the reports. Kharkov, 1990, 1-95, part II, p. 80 (in Russian).
2. V.A.Romodanov, V.I.Savin, M.V.Shakhurin, V.T.Chernyavsky, A.E.Pustovit. Nuclear fusion in a solid.-
Zhurnal tekhnicheskoy fiziki, 1991, volume 61, issue 5, p. 122-125 (in Russian).
3. V.A.Romodanov, V.I.Savin, Ya.B.Skuratnik, Yu.M.Timofeev.
Reactions of nuclear fusion in condensed matter.-
Voprosy atomnoj nauki i tekhniki. Ser.: Radiation damage physics and radiation technology. 1992, Issue 1 (58), 2 (5-), p. 73-82. (in Russian).
4. Sputtering by Particle Bombardment I.
Physical sputtering of single-element solids. -
Edited by Behrisch.
Springer - Verlag.
Berlin-Heidelberg-New York, 1981.
5. D.Palmer. Ion implantation progress. -
In: Ion implantation into semiconductors and other materials. Edited by V.S.Vavilov. Novosti fiziki tvyordogo tela.
Issue 10. Moscow, Mir, 1980- 330 p. (in Russian).
6. R.N.Kuz'min, E.M.Sakharov, B.N.Shvilkin, A.P.Kuprin, P.O.Revokatov.
Observation of fast neutrons and tritium during electrolysis of heavy water. -
Institute for Nuclear Physics, Moscow State University. Moscow, USSR. Preprint - 90 - 58%204, 1990, - 12 p.

Condensed Matter Effects for Cold and Hot Fusion

Y. E. KIM, M. RABINOWITZ*, R. A. RICE, and J.-H. YOON
Department of Physics, Purdue University
West Lafayette, IN 47907
USA
*Electric Power Research Institute
Palo Alto, CA 94303
USA

ABSTRACT

In dense plasmas, the ensemble of fusing particles has a significant exchange of kinetic and potential energies. Because of this condensed matter effect (CME), the higher Z nuclei thus have a larger reduction in fusion rates. Our proposed solution of the solar neutrino problem finds a larger reduction for $^7Be(p,\gamma)^8B$ than for $p(p,e^+\nu_e)D$. Our CME predictions are consistent with neutrino detection experiments. CME have broad ranging astrophysical implications; may account for the anomalous branching ratio in cold fusion; and may be testable in laboratory beam fusion experiments with solid targets.

1. Introduction

It has recently been shown [1,2] that the conventional nuclear physics description of fusion reaction rates needs to be modified in laboratory and astrophysical environments due to CME. The conventional fusion rate R_{conv} for nuclear fusion reactions between two nuclei is written as $R_{conv} \propto \langle \sigma v \rangle$ where v is the relative velocity representing the incident flux and σ is the fusion cross–section. However, in condensed matter environments, R_{conv} needs to be modified to a new expression $R_{new} \propto \langle \tilde{\sigma} \overline{v} \rangle$, where $\tilde{\sigma}$ is a modified fusion cross–section and $\overline{v}$ is an average velocity of the incident particle in condensed matter which can differ significantly from the incident velocity. As a specific application of our new formulation of R_{new} to hot fusion, condensed matter effects for the solar neutrino problem will be presented. Application of our new formulation to cold fusion rates explaining the anomalous branching ratio for deuterium–deuterium fusion is in progress.

FRONTIERS OF COLD FUSION

2. Effective Flux Velocity

For the purpose of obtaining quantitative estimates of CME, we use a "shifted" screened Coulomb potential with an interior square–well nuclear potential $V_s(r)$:

$$V_s(r) = \begin{cases} -V_0 \,, & r < r_N \\ Z_i Z_j e^2 \left(\frac{1}{r} - \frac{1}{r_s}\right) \,, & r_s > r \geq r_N \\ 0 \,, & r_e > r \geq r_s \end{cases} \qquad (1)$$

For a number density of condensed (target) matter, n, and elastic cross–section σ_e, the mean free path is $\lambda_e = (n\sigma_e)^{-1} = r_e - r_2$ and for the fusion cross–section σ_f, $\lambda_f = (1/n\sigma_f) + r_2 = (\lambda_e\sigma_e/\sigma_f) + r_2$, where r_2 is chosen as the classical distance of closest approach (turning point) for a given barrier. The average interatomic distance is $\sim 2r_e$ in condensed matter. Then the average velocity ($\propto$ effective flux) can be written as $\langle v\rangle = \lambda_f/[(\sigma_e/\sigma_f)(t_i + t_0) + t_B + t_N]$ $= [(r_e - r_2)(\sigma_e/\sigma_f) + r_2]/[(t_i + t_0)(\sigma_e/\sigma_f) + t_B + t_N]$ where t_i, t_0, t_B and t_N are the times for the incident particles to traverse distances $(r_e - r_s)$, $(r_s - r_2)$, $(r_2 - r_N)$, and r_N, respectively. For the case of $\sigma_e >> \sigma_f$, $\langle v\rangle$ reduces to $\langle v\rangle \approx \overline{v} = (r_e - r_2)(t_i + t_0) = [(r_e - r_s) + (r_s - r_2)]/(t_i + t_0)$.

The traversal time $t(j) = t_0$ of the incident particle i in the presence of the barrier due to the target species j can be estimated in the WKB approximation for the case of $V_s(r)$, eq. (1), with $E < B = V_s(r_N)$ as $t(j) = \int_{r_2(j)}^{r_s(j)} [(2/\mu_{ij})|E - V_s(r)|]^{-1/2} dr$ where $\mu_{ij} = m_i m_j/(m_i + m_j)$. Using $t(j)$, we calculate $\overline{v}(v)$ and $F(E) = \overline{v}/v$ as a function of v or $E = \mu v^2/2$. Our calculations show that $\overline{v} \leq v$ where v is given by $v = v_i = (r_e - r_s)/t_i$.

3. Fusion Rates

The conventional fusion rate between two species of nuclei, i and j, with number densities n_i and n_j is conventionally written as $R_{conv} = [n_i n_j/(1 + \delta_{ij})]\langle\sigma v\rangle_{conv}$ where

$$\langle\sigma v\rangle_{conv} = \int d^3v_i \int d^3v_j f(\vec{v}_i) f(\vec{v}_j) v\sigma(v) = \int \sigma(v) v f(v) d^3v \qquad (2)$$

with kinetic energy $E = \mu v^2/2$, in the center of mass (CM) frame and the Maxwell–Boltzmann velocity distribution, $f(v) = (\mu/2\pi kT)^{3/2} \exp(-\mu v^2/2kT)$ where μ is the reduced mass.

Because of the continuous exchange of kinetic and potential energies in dense plasmas, the original velocity $\vec{v}$ whose distribution is described by $f(\vec{v})$ $= (\mu/2\pi kT)^{3/2} \exp(-\mu v^2/2kT)$ is reduced to $\overline{v} = u(v) < v$. The original pair total energy, $m_i v_i^2/2 + m_j v_j^2/2 = (m_i + m_j)V^2/2 + \mu v^2/2$, becomes $(m_i + m_j)V^2/2 + \mu u^2/2 + W(u)$ where $W(u)$ is the potential energy, $W(u)$ $= \mu v^2/2 - \mu u^2/2$. Therefore, the original velocity distributions $f(\vec{v}_i) f(\vec{v}_j) =$ $f(\vec{V}) f(\vec{v})$ are replaced by $f(\vec{V}) f(u)$ where $f(u)$ is given by $f(u) = (\mu/2\pi kT)^{3/2}$

$\exp[-(\mu u^2/2 + W)/kT]$. Since $f(u)$ does not conserve particle number due to $\int f(u)d^3u \neq 1$, $f(u)$ is replaced by $\tilde{f}(u)$, $\tilde{f}(u) = f(u)\ d^3v/d^3u = (\mu/2\pi kT)^{3/2}$ $\exp(-\mu v^2/2kT)\ d^3v/d^3u$ which gives particle number conservation $\int \tilde{f}(u)d^3u = 1$.

The velocity $\overline{v}$ is the appropriate value to be used for the fusion rate rather than $v(= v_i)$ which has been used in the conventional eq. (2). For dense astrophysical or laboratory plasmas, when a projectile particle i moves through the plasma with velocity $u = \overline{v}$, the probability of a fusion reaction per unit path length of the projectile is given by $P_x = n_j\sigma$ where n_j is the number of target nuclei per unit volume of the plasma. Because of the elastic scattering processes described previously, the projectile traversal distance per unit time is u, and not v. Then the fusion reaction probability for the projectile path length per unit time is $P = uP_x = un_j\sigma$. The rate at which n_i projectiles per unit volume, each moving with a speed $u(v)$ but in random directions, will react is then $R(u) = n_iuP_x = (n_iu)(n_j\sigma)$. If a projectile velocity distribution $\tilde{f}(u)$ is given, then the new fusion rate is given by $R_{new} = [n_in_j/(1 + \delta_{ij})]\langle\sigma v\rangle_{new}$ where

$$\begin{aligned} \langle\sigma v\rangle_{new} &= \int \sigma(u)u\tilde{f}(u)d^3u = \int \sigma(u)uf(v)d^3v \\ &= \left(\frac{8}{\pi\mu}\right)^{1/2}\frac{1}{(kT)^{3/2}}\int_0^\infty \sigma(\overline{E})F(E)E\exp\left(-\frac{E}{kT}\right)dE\ , \end{aligned} \tag{3}$$

and $\overline{E} = EF^2(E)$. We note that $\langle\sigma v\rangle_{new} \leq \langle\sigma v\rangle_{conv}$.

4. Results

The new fusion rate formula, eq. (3), is applied to the solar neutrino problem. Table 1 shows our results of applying CME reduction factors of $\langle\sigma v\rangle_{new}/\langle\sigma v\rangle_{conv} = 0.79$ and 0.48 for $p(p, e^+\nu_e)D$ and $^7Be(p,\gamma)^8B$, respectively, to the standard solar model (SSM) calculations of Refs. [3], [4], and [5]. Data collection periods (month.year – month.year) are indicated for Refs. [6] and [7].

The observed neutrino flux due to $^7Be(p,\gamma)^8B(e^+\nu_e)^8Be^*(\alpha)^4He$ by the Kamiokande-II detector [10,11] is $2.7\times10^6(1\pm0.11\ (\text{stat.})\pm0.13\ (\text{syst.}))\ \text{cm}^{-2}s^{-1}$ compared with the SSM result [3] of $5.7\times10^6\ \text{cm}^{-2}s^{-1}$. Our result of applying the CME reduction factor of $\langle\sigma v\rangle_{new}/\langle\sigma v\rangle_{conv} = 0.48$ yields $2.74\times10^6\ \text{cm}^{-2}s^{-1}$. which agrees with the experimental data [10,11].

5. Conclusions

We conclude that anomalies in both hot and cold fusion have a common origin in CME. It is noteworthy that overlooked CME may supply both the solution to the long standing solar neutrino problem, as well as an explanation for the anomalous branching ratio for $D - D$ fusion.

Table 1. Comparison of CME results with the experimental data [6–9].

	Rate $R_{\nu_e}^{Cl}$ with ^{37}Cl Detector (SNU)			Rate $R_{\nu_e}^{Ga}$ with ^{71}Ga Detector (SNU)		
Neutrino reaction	BU [3]	TCCD [4]	BPML [5]	BU [3]	TCCD [4]	BPML [5]
$p(p, e^+\nu_e)D$ (CME)	0	0	0	70.8 (56.0)	70.6 (55.8)	70.0 (55.3)
$p(p + e^-, \nu_e)D$	0.2	0.2	0.22	3.1	2.8	3.0
$^7Be(e^-, \nu_e)^7Li$	1.2	1.0	1.06	35.8	30.6	32.5
$^8B(e^+\nu_e)^8Be^*$ (CME)	6.2 (3.0)	4.1 (2.0)	5.73 (2.75)	13.8 (6.6)	9.3 (4.5)	13.1 (6.3)
$^{13}N(e^+\nu_e)^{13}C$	0.1	0.1	0.1	3.0	3.9	3.53
$^{15}O(e^+\nu_e)^{15}N$	0.3	0.4	0.318	4.9	6.5	5.58
SSM Total	8.0 ± 1.0 ($1\,\sigma$)	5.8 ± 1 ($1\,\sigma$)	7.43	131.5^{+7}_{-6} ($1\,\sigma$)	124 ± 5 ($1\,\sigma$)	127.7
SSM + CME Total	4.0	3.7	4.45	109.5	104.5	106.2
Experimental Results	(3.70 – 85) [6]: 2.1 ± 0.3 (3.70 – 3.88) [7]: 2.33 ± 0.25 (8.86 – 3.88) [7]: 4.2 ± 0.7			GALLEX [8]: $83 \pm 19 \pm 8$ SAGE [9]: $20^{+15}_{-20} \pm 32$		

References

1. Y. E. Kim et al., "Condensed Matter Effects on Nuclear Fusion Rates in Laboratory and Astrophysical Environments" to be published.
2. Y. E. Kim et al., "High Density Fusion and the Solar Neutrino Problem" to be published.
3. J. N. Bahcall and M. H. Pinsonneault, to be published in Rev. Mod. Phys.
4. S. Turck-Chièze et al., 1988, Astrophys. J., 335, 415.
5. G. Berthomieu et al., to be published in Astronomy and Astrophysics.
6. J. K. Rowley et al., 1985, AIP Conf. Proc. No. 126 (1985), p. 1.
7. R. Davis, Jr., 1988, Proceedings of the 13th International Conference on Neutrino Physics and Astrophysics, Neutrino '88, edited by J. Schneps et al. (World Scientific, Singapore, 1988), p. 518.
8. P. Anselmann et al. (GALLEX), 1992, Phys. Lett., B285, 376.
9. A. I. Abazov et al. (SAGE), 1991, Phys. Rev. Lett. 67, 3332.
10. K. S. Hirata et al., 1989, Phys. Rev. Lett., 63, 16.
11. K. S. Hirata et al., 1990, Phys. Rev. Lett., 65, 1297; 1991, Phys. Rev., D44, 3786.

New Hydrogen Energies in Specially Structured Dense Media : Capillary Chemistry and Capillary Fusion

Jean-Pierre VIGIER
Université P. et M. Curie, CNRS URA 769
Tour 22-12, 4me étage - Boîte 142, 75005 PARIS

ABSTRACT

The analysis of presently observed facts suggests that excess heat (above break-even) and concomittant cold fusion processes result from two different mechanisms which have a common origin in e.m. current behaviour in dense media (the Ampère forces). They both result from already known properties of nuclear forces and quantum mechanics.

1. Introduction

The present 1992 Nagoya Conference clearly illustrates the existing gap between growing evidence of new phenomena, tied to the presence of hydrogen and deuterium, in various types of electrodes. It can now be stated

A) that one has demonstrated the Fleischmann-Pons claim that there exists a significantly (now reproductible) excess heat (above break-even)
1) in electrolytic heavy water phenomena (see their new experiment)
2) in specially prepared palladium plates coated with deuterium oxide and gold (see Yamaguchi et al.)
3) in glow-discharges on deuterated palladium (see Kucherov et al.)

FRONTIERS OF COLD FUSION

This property has also been observed in zinc, titanium etc: the most striking being in tungsten bronze (see Barabushkin-Kabir et al.). Apparently there is growing evidence
- that the initial non reproductibility of such experiments is related (as shown by Kabir) with defects (cracks etc.) in certain samples utilized
- that excess heat grows with current intensities (i.e. with conductivity) in electrolysis and with increased loading of the electrode with heavy water or deuterium
- that it appears with a time delay (varying from minutes to hours) after the loading reaction starts
- that due to the variety of material utilized, it does not result from known chemical reactions

B) The observation of very small quantities of "fusion ashes" i.e. neutrons, He^3, He^4, tritium (and charged particles) but the essential fact remains

1) that if they result (as believed by the author) from already known nuclear reactions (D+D etc.) *these are not, by very far, in sufficient quantities to explain the observed excess heat*

2) that these fusion reactions occur in conditions of temperature where there is no apparent possibility to explain in this way how the corresponding ions overcome their Coulomb repulsive barrier: hence their name "cold fusion".

3) that there is nevertheless an apparent correlation between neutron production (whether continuous or in bursts) with this excess heat production.

C) that the excess heat phenomena also appears *in the total absence of fusion ashes* in various set-ups utilizing hydrogen and ordinary light water. I only mention here the Baraboshkin-Kabir, Srinavasan and Yamaguchi experiments. This new fact evidently cannot be explained by fusion mechanisms and implies the appearance (tied to H and D properties) of a new still unknown chemical type of phenomena. The facts A) B) C) evidently imply the following set of immediate evident questions:

1) Where does the excess heat come from? For heavy water or fusable conductors such as deuterium lithium etc? For light water or hydrogen? Has it the same origin or not?

2) Why are such experiments not always reproducible with apparently similar samples? Does this result from structured differences in the same products? or not?

3) Why is there a delay in time?

4) What is the origin or the observed energy bursts? Why are they correlated with neutron bursts?

5) If excess heat does not come from fusion and/or known chemical reactions in various types of electrodes what is its nature and its relation with observed fusion processes?.

In the presence of such facts and questions two main theoretical attitudes are possible.

1) We are observing something entirely new in the nuclear domain in the presence of condensed matter: i.e. fusion is tied to some structured properties of palladium (loaded with deuterium or heavy water) related to its lattice reactions (i.e. phonon propagation etc) or collective resonance reactions of fusing plasma enclosed within lattice structures. This is the line now followed by most theoreticians starting with Prof. Preparata on this panel.

My criticism of this is 1) that this line does not (to my knowledge) explain point C). 2) that it does not explain the gap between the quantity of fusion ashes) (i.e. nuclear fusion reacitons) observed and the excess heat itself.

2) that (within of course the present energy interval utilized)

- the present nuclear theory is valid: including the various branching rations of the D+D reactions

- that the present quantum mechanics formalism is also valid in that field

- that the interpretation of the facts A)B)C) to explain A) and C) simultaneously thus implies the observation/action of new specific physical properties tied to the geometrical structure of the electrodes and/or absorption loaded material.

A) modifies both $H^+ + H^+$ and $D^+ + D^+$ reactions in order to obtain excess heat in terms of a new chemical-type reaction compatible with quantum mechanics.

B) explains simultaneously the apparition (in very small quantities) of the observed fusion reactions: at least for very low intensity currents.

C) leads to reasonable predictions for new types of experiments.

&1. Charged particle Concentrations in Capillary Conductors

Within this later frame let me present here some facts and assumptions which (in my opinion) should be introduced as founding stones of a forthcoming developed model of the (presently known) facts presented at this Nagoya Conference. The first class of new facts now experimentally related with new current properties in condensed matter have been known and confirmed for some time. They are known to specialists as consequences of the action of the "Ampère Forces" empirically discovered long ago by Ampère (1823) and recently revived/justified by Graneau[1], Phipps[2], Rambaut and Vigier[3] and very recently by Saumont[4]. This force (which does not contradict presently known laws of classical and quantum electrodynamics for free charged particles) represents the collective interactions of charged current elements (i.e. of a mixture of positive ions with orbital and conducting electrons) presents the new remarkable characteristic of introducing unknown (now confirmed by experiment[4]) longitudinal repulsive forces between colinear current elements. Written in the usual notations (DFmn is a Newtonian force of repulsion (if positive) or attraction (if negative) between two current elements of length d_m and d_n and passing currents i_m and i_n respectively. The angle of inclination between the elements is ε and α and β are the inclinations of the elements to the distance vector r_{mn}) we have

$$\Delta F_{mn} = -\frac{\mu_0}{4\pi} i_m \cdot i_n \cdot \frac{dm \cdot dn}{r_{mn}^2} \left(2\cos\varepsilon - 3\cos\alpha\cos\beta\right) \quad (1)$$

which gives for the longitudinal force

$$\Delta F_{mn} = \frac{\mu_0}{4\pi} \cdot i_m \cdot i_n \frac{dm \cdot dn}{r_{mn}^2} \quad (2)$$

This longitudinal force in gaze ous liquid and solid conductors has been shown (as illustrated in the two following figures (1) and (2) to distort the usual current i.e

Fig.1

Fig. 1 showing how a tungsten conductor is cut into pieces called usually (beads". The tungsten wire is photographed during the currentpause (Uppsala expeirments).

Fig.2

Sketch of an X-ray photograph of deuterium fibre fragmentation

has the evident consequences of creating standing longitudinal current concentrations in conductors i.e. to split them into string of beads which interrupt the current at high intensities. This creation of strings of (repulsive) current concentrations correspond to the nodes of the longitudinal standing waves of wavelength 1/n (with n integer) which appears between the extremities of a limited current with fixed end points separated by a distance 1. If an electrode contains rows of capillaries the ionization or injected currents thus induces (as a quasi-static wave system is created) the possibility of screening effects (which induce fusion) or, as we shall see, new ion-electron-ion systems which might explain excess heat.

§2. Interpretation of Excess heat in terms of a new type of chemical reactions

Two different physical consequences can be derived from the existence of the current beads on the behaviour of ionized ions i.e. the creation of hitherto unknown very tightly bound states $H^+ + H^+ + e^- = \bar{H}_2^+$ and $D^+ + D^+ + e^- = \bar{D}_2^+$ states which correspond to the combination of two ions which rotate rapidly in stable type Bohr orbits around an electron squeezed between them. This new type three body system corresponds to a new unknown quasi-molecular state (whose stability will be discussed later). As we shall now limit ourselves here to a simplified calculation. This corresponds for deuterium (according to the usual formalism) to binding energies of the order ~50 kev which account for the excess heat released without appreciable fusion contribution. [This idea first suggested by Barut (in a private communication) was also proposed (with the same 50 kev binding energy) by Gryzinski in Gamov type analysis (Nature 338 (1989) 712) of the collision between (H or D) ions and atoms]. The electron's orbit flattens perpendicular to the line of the colliding ions . It can be squeezed between them and stabilized there by the surrounding electron cloud. [This method of quantization and the role of intervening electrons explains some types of observed regular collective motions (i.e. cluster formations) which can contain triangular, tetrahedral cubic... configurations which move collectively and have been observed to have strongly enhanced (by many orders of magnitude with individual particles)]. This configuration naturally arises when the Ampère force cuts the current into beads in a capillary since the situation of the ions then resembles what happens to fast going cars which crash successively into each other during a slowdown (accident) on a modern highway. This situation is very different from the usual quantum mechanical interpretation of chemical phenomena i.e. of the normal states of H_2^+ and D_2^+ which are assumed (according to the Born-Oppenheimer approximation) to correspond to the rapid motion of the electron in the field of two almost fixed nuclei. If one first neglects the spin and considers two masses M (with charges z) rotating at a distance r from a mass m (charge z) i.e.

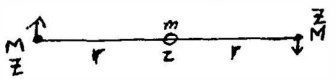

this gives the Hamiltonian

$$H = \frac{2p^2}{2M} + \alpha\left(\frac{2Z_3}{r} + \frac{Z^2}{2r}\right)$$

which when quantized by the usual Bohr-Sommerfeld method $\int p\,dq = nh$ with ($\hbar = c = 1$) i.e. fields $p = -(m\alpha/n)(2z + Z/2)Z$) i.e. energy levels $E_n = -\frac{1}{4}\frac{M\alpha^2 Z^2 (2z + \frac{Z}{2})^2}{n^2}$

- For the H_e atom this yields $E_0 = -6{,}12$ Ryd close to the observed value -5,69 Ryd.

- For $\bar{H}_2^+$ and $\bar{D}_2^+$ the Bohr energy levels are approached by $E_n = -(9/16)(M\alpha^2/n^2)$ which correspond to ground states of 28,1 kev and 56,2 kev for $\bar{H}_2^+$ and $\bar{D}_2^+$ of course. This crude calculation should/can be extended to include spin-spin and spin-orbit calculations and also made relativistic (a detailed calculation is submitted for publication) using an effective potential

$$V(R = 2r) = (L(L+1)/MR^2 - (3\alpha/R) + 4(\alpha/m)^{1/2}R^{-3/2}n$$

which yields very different minimal values and $1/M\alpha$ (Bohr radius for the proton) for $\bar{H}_2^+$. At short distances spin-spin interactions grow like 1/r3 (compared to $1/r^2$ for Coulomb interactions. Spin-orbit interactions (i.e. $V_{LS} = e\,M_e((\vec{L}\cdot\vec{S})/Mr^3) \simeq M\alpha^4(M/m)$) are of the order of 10 kev (40 kev for D) i.e. comparable to the Coulomb potential. They are attractive or repulsive according to the sign of $\vec{L}.\vec{S} = (1/2)(J(J+1) - L(L+1) - 3/4)$ so that the attractive case can increase the binding energy to stabilize the new configurations and thus help fusion tunnelling in some cases.

This model implies evident consequences

- Evidently the excess heat energy obtained with H_2^+ is one fourth of the amount obtained with $\bar{D}_2^+$

This heat depends on the number of $\bar{H}_2^+$ and $\bar{D}_2^+$ (or light and heavy water $\bar{H}_2O$ and $\bar{D}_2O$) i.e. on the loading of the capillaries contained in electrodes. Excess heat is created only when they are formed i.e. not necessarily immediately since individual capillaries' internal situation evolve with time.

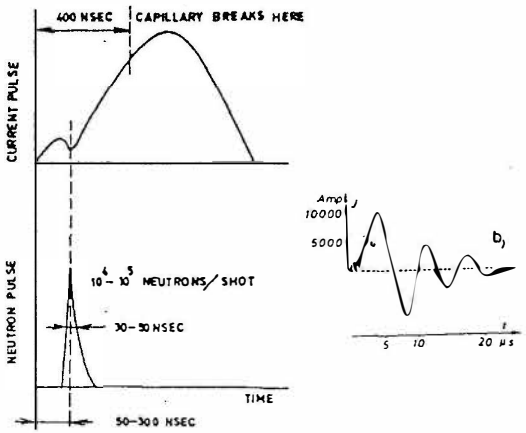

Fig.3. Drawings reproducted from the refs. [14] and [16] showing the principal elements which describe the capillary fusion experiments performed by Lochte-Holtgreven et al. [14] F.C. Young et al. N.R.L. 20 (1983) 439. [16] J.D. Sethian et al. P.R.L. 59 (1987) 585.

There exists the possibility to start chain formation of $\bar{H}_2^+$ or $\bar{D}_2^+$ which would explain heat bursts i.e. fusion waves of the Winterberg type. After some time the reaction stops and the new compound molecules ($\bar{H}_2^+$, $\bar{D}_2^+$) leave the system for good.

We now come to the question of "cold fusion".

§3. Cold Fusion Process in Capillaries

If one recalls that in some experiments there exists a correlation between excess heat and neutron emission and accept the fact that the later cannot explain the former the simplest possibility is to attribute both a common origin i.e. the beads of current concentration described above. Since it is evident that in $D^+ + D^+$ ion fusion the ions do not have a sufficient velocity to overcome the repulsive Coulomb barrier the only possibilities left are

- to assume a screening mechanism (i.e. lowering of the barrier followed by tunneling) tied to electron concentrations: a process discussed by many participants here (also supported by Rambaut and myself[5]).

For lack of space and time I will not discuss it here but only recall/indicate that it has been analyzed in various ways in the literature... and even extended to possible double screening processes (electrons plus ions) by Rambaut.

- to assume that the presence of an electron between two ions leads to unstable quantum closely bound quasi molecular quantum states which facilitate tunneling[5]. The existence of these new types of cold fusion mechanism opens interesting new possibilities for research and future utilisation. From the observed correlation between excess heat neutron emission and injected current pulses of the type utilized in capillary fusion (of z-pinch) one may obtain excess energy which mainly originates in this case from fusion processes. This is already strongly suggested by capillary experiments initiated in France (presently developed in Belgrade using $Li(ND_4)_3$ as conductor by Professor Marič on my suggestion) which shows growing neutron fluxes with growing current intensity (at significantly intensities) plus increasing neutron fluxes with decreasing capillary diameter.. They evidently justify the results obtained in Kiel some time ago by Lochte-Holtgreven and are represented in Fig. 3 . In Belgrade as in z-pinch experiments (by Sethian et al. (PRL [16]) one has obtained neutron bursts of $\sim 10^{12}$ neutrons in a few nanoseconds in frozen deuterium threads) by shooting $\sim 10^6$A in a few nanoseconds. Evidently the neutron flux grows like a high power (~8 or 10) of the current intensity. The Belgrade experiments suggest that big efforts should be made 1) to reduce the time duration of the triggering current pulses 2) to build fast switches to suppress the input current (second maximum in Fig. 3) after the Ampère force has cut it itself (see the first maximum of Fig. 3)

Conclusion

From this too brief analysis one can derive some experimental proposals and recall two quotations

A) New experiments are urgently needed

1) Redo all experiments presented here with heavy and light water (or with hydrogen and deuterium

2) Look at clustering theoretically and experimentally and look for radiation emitted by $\bar{H}_2^+$ and $\bar{D}_2^+$.

3) Push forward microscopic structural analysis of palladium bronze etc to look for capillaries (seen in bronze by Kabir) and compare systematically successful and unsuccessful samples

4) Try high current intensity very short current discharges in various situations (in conducting fusion material) to see if they increase excess heat production using loaded electrodes to increase the effect.

B) A big theoretical open minded effort is evidently needed

1) As stated by Einstein "Humanity is w.r.t. modern science like an inexperienced harseman on a wild horse". Evidently the wild horse of cold fusion has left the stable and is presently running

2) As stated to me long ago by Yukawa himself "When new facts appear the true theoretician should adapt his theories to these facts not the reverse. We are still far from a correct disantanglement of facts in condensed matter.

References

(1) P. Graneau, Ampère-Newmann electrodynamics in metal. Hadronic Press (1983).

(2) T.E. Phipps, Phys.Lett.A 14 (1990) 6.

(3) H. Rambaut and J.P. Vigier, Phys.Lett.A 142 (1989) 447 and 148 (1990) 229.

(4) R.Saumont, Phys.Lett.A 165 (1992) 310.

(5) See the summary of our proposals given by M. Rambaut. Phys.Lett.A. 163 (1992) 335.

Activity Review

Cold Fusion Researches in China - From Confirmation to Analyzing the Mechanism

Xing Zhong LI.

Department of Physics, Tsinghua University

Beijing 100084 CHINA

ABSTRACT

While the number of activities was decreasing, the quality of the research activities on cold fusion was improved in the third year. Neutron emissions from the glow discharge tube with flowing deuterium gas are addressed to confirm the anomalous nuclear phenomenon. "Combined Resonance Tunneling" and the concept of "Semi–Resonance" are proposed to be the possible mechanism.

1、General Situation

After the Como conference some institutes slowed down their steps due to the unfavorable atmosphere about the cold fusion (the close of National Institute of Cold Fusion at Utah etc.), or due to the difficulties in repetition. However, the cold fusion researcher in China survived and the quality of researches improved. Enlightened by the discharge tube experiment at Institute of Southwestern Nuclear Physics and Chemistry [3] in 1989, Professor Long He–Qing of Sichuan Institute of Material and Technology continuously improved his glow discharge tube experiment and obtained the evidences of anomalous neutron emission. The emission rate has been enhanced by a factor of ten in a year and it is reproducible. Institute of Applied Physics and Computational Mathematics helped in theoretical calculation to show that those neutron emissions were not caused by any beam–target effect or hot fusion. Furthermore, two days continuous neutron emission was monitored in an electrolytic cell at Institute of Southwestern Nuclear Physics and Chemistry also. The neutron energy distribution after slowing down was comparable with the standard neutron source. An accident of the explosion of electrolytic cell there was analyzed, and it was found that the energy released was much more than

FRONTIERS OF COLD FUSION

that from any possible chemical reactions.

Tsinghua University persists its "dry" experiment with CR–39 solid nuclear track detector. The resistance of palladium wire was measured in situ in a pressurized vessel to watch the evolution of a deuterized palladium wire. The Silicon Surface Barrier Detector (SSD) was used to detect the energetic charged particles in real time. Searching in the combination of parameters (pressure, temperature, loading ratio etc.), we expected to find the precursor of the burst signals in the SSD. In the same time Tsinghua University Group proposed the "Combined Resonance Tunneling" and the concept of "Semi–Resonance", [1] which may provide the possible mechanism to explain why the Coulomb barrier is penetrated at low incident energy and why the small nuclear scale reactions are affected by the large crystal scale parameters.

The team at Southwestern Institute of Physics continued their experiments in the deuterium plasma of magnetic mirror machine and in a coaxial AC discharge tube. The bursts of neutrons appeared once and once again. The experiments persist, although the leader of that team was in a cancer disease.

The China Institute of Atomic Energy measured the time–behavior of the signals after the bursts, in order to distinguish the neutron signal from electronic noise in a temperature cycling of metal (Ti)–deuterium system.

Beijing Normal University resumed their electrolytic cell experiment with a palladium electrode from Russia shortly before the conference, and the neutron signals were found again.

Xiamen University made a helium detection system, which is able to detect 4×10^8 helium atoms in deuterium matrix. A Zr–Al pump system was set up for separation of helium from deuterium.

Chengdu University of Science and Technology attempted to correlate the excess heat with helium production in an electrolytic cell with titanium electrode. The mass–spectrometer measured different results from the Ti sample above the electrolyte surface and the Ti sample beneath the electrolyte surface.

Institute of Chemistry, Academy of Science, proposed a State–Field Theory of Thermodynamics which implies a critical value of heat dissipation during the electrolytic process in the cell. It is claimed that cold fusion is possible only if the heat dissipation is higher than this critical value.

University of Science and Technology of China, Graduate School in Beijing observed energetic charged particles not only from the deuterized palladium, but also from the $Y_1Ba_2Cu_3O_{7-\delta}$ superconductor / Deuterium system, using CR–39 technique.

2、Continuous Neutron Emission from Glow Discharge Tube

As a strong evidence of the anomalous nuclear phenomenon, the neutron emission from the glow discharge tube has been carefully studied since April 19, 1989. It is found that the metal film on the surface of glass bulb and the flowing deuterium gas are two key points to make neutron emission reproducible. The emission rate has been enhanced from 10^3 n / sec to 10^4 n / sec; therefore, the neutron emission can be con-

firmed by activation method which is free from the electromagnetic noise. Indium foil and iridium foil are used as activation detectors, both of them give the same results for the average neutron influx, $\sim 10^4$ n/ (m^2 • sec). [2]

The energy spectrum of the neutron emission was measured by the fast neutron curtain to distinguish the neutrons from hot fusions. If there was beam–target effect to produce the d–d fusion, the energy of neutron should have been less than 2.45MeV. However, the energy spectrum showed clearly that there were two groups of neutrons, one group had the energy greater than 2.45MeV, and another group had the energy less than 2.45MeV. The number ratio of the first to the second group was greater than 9. Consequently, this neutron emission confirmed the existence of anomalous nuclear effect in deuterium / solid systems.

The interest point is that palladium turns out to be not necessary for neutron emission. Platinum, niobium, tungsten, palladium, silver, copper, molybdenum and iron are all tried as an electrode material. All of them have the neutron emission, the difference consists in the quantity of neutrons, which is the greatest for Pt and the least for iron.

3、 "Combined Resonance Tunneling" and "Semi–Resonance".

Even if we might reproduce the anomalous nuclear phenomenon once and once again, we might not be able to convince ourselves thoroughly if we do not have any model or theory to explain it. Among the long list of questions, the first is how the Coulomb barrier is penetrated at such a low incident energy; the second is why the parameter variation in crystal scale has an effect on the reaction in nuclear scale, i.e. why the operation in 10^{-8}cm has an effect in 10^{-13}cm.

In fact, these two questions were solved in fission reactor already, since the neutron needs not to penetrate any Coulomb barrier, and the resonance energy levels at low energy make it possible to control the nuclear reaction by careful design of the neutron slowing–down process in terms of macroscopic parameters. However, in the fusion reaction, Coulomb barrier is inevitable, and no resonance energy level has been found at low energy after 20 year searching. Fortunately, looking at the energy spectrum of ^{4}He nucleus there is a "Semi–Resonance" level at low energy. [2] "Semi–Resonance" is not a resonance, but it is an energy level just in the mid of two resonance levels. When two deuterons approach each other with zero energy, the energy of two deuteron system is 23.8MeV higher than the ground level of ^{4}He. We noticed that there are two excited states of ^{4}He at energy levels of 25.5MeV and 22.1 MeV. 23.8 MeV energy level is just in the mid of these two resonances. Since "Semi–Resonance" is not a resonance, the penetration of single Coulomb barrier at "Semi–Resonance" energy level is still impossible. Nevertheless, the combination of two "Semi–Resonance" by a resonance in crystal lattice might be penetrated together. This is proved by Quantum Mechanic tunneling theory. A new formalism for W.K.B. approximation is proposed to facilitate the calculation. In parallel, a microwave experiment is done to prove this conclusion of wave mechanics.

4、Future Plan

After the confirmation of the anomalous nuclear phenomenon, the next step should be more oriented towards mechanism. It would be a long term basic research project, and the international academic exchange is encouraged. An international diagnostic team to detect the neutron emission from glow discharge tube and calibrate the energy spectrum of the neutrons is suggested.

Invited talks about the could fusion status have been given at the National Congress of Chinese Nuclear Physics Society (Xian 1991) and at the International Conference on Laser–Plasma Interaction (Shanghai, 1992), and will be given at International Conference on Plasma Physics (Changsha, 1993). The scientific community is changing the attitude towards this new hydrogen energy source. We may expect a new discipline of science, "Solid State Nuclear Physics", soon.

5、Acknowledgements

This work is supported by the State Commission of Science and Technology, Natural Science Foundation of China and Tsinghua University. Chinese colleagues in cold fusion research are gratefully acknowledged for their advanced information.

6、References

〔1〕 Li, X.Z., et al., The Proceedings of ICCF3.
〔2〕 Long, H.Q., et al., The Proceedings of ICCF3.
〔3〕 Xiong, R.H., et al., The Proceedings of the First Symposium on Cold Fusion in China, Beijing, May 10, 1990, P.187.

Cold Fusion Researches in Russia

Vladimir TSAREV

Lebedev Physical Institute
117924 Moscow, Leninsky Prospect 53
RUSSIA

ABSTRACT

A review of cold fusion researches in the former Soviet Union during the past year is presented.

1. Introduction

I am supposed to report on a progress in cold fusion (CF) studies in our country since the last conference at Como. A year ago in Italy I demonstrated a figure which illustrated the CF geography in the USSR [27]. Now an analogous picture is shown in Fig. 1 where instead of fusion we have fission and disintegration into fragments. The time is not very favourable for science nowadays. Nevertheless, in spite of numerous breaks in economic, commercial, and cultural connections and inter-ethnic conflicts, we try to retain our scientific collaboration and friendly relations with all our colleagues from the ex-soviet republics. That's why, despite the title suggested for my talk, I'll speak on CF activity existing both in Russia and other ex-soviet republics. At Como I presented the results of more than 80 papers from about 45 Institutes and laboratories. Today these numbers are about four times less, but still there are some interesting results, both experimental and theoretical. Since the Como Conference two workshops on CF were organized in our country: "Hydrogen chemistry and technology", November 26-28, 1991, Ekaterinburg, Chairman Prof. A.N. Baraboshkin, and "Diffusive-cooperative phenomena in metal-hydrogen systems", September 15-19, 1992, Donetsk, Chairman Prof. V.A. Goltsov. While discussing the results submitted at these workshops I'll quote the published Abstracts as "Ekaterinburg" and

FRONTIERS OF COLD FUSION

Figure 1. Cold Fusion and Fission in the Former USSR´92

"Donetsk" (Part I and Part II).

2. Experimental Results

I'll begin with the experiment which, from my point of view, might be most original and promising, if its results are confirmed.

2.1. CF in Tungsten-Bronze Structures

A distinctive feature of the experiments [16], which have been carried out by a group from Institute of High-temperature Electrochemistry and Ural Polytechnucal Institute (Ekaterinburg) is the utilization of material which is new for CF experiments: oxidized sodium-tungsten bronze Na_xWO_3. Various degrees of tungsten valency states in bronze, rigidity of the tungsten-oxygen octahedral frame and high mobility of the alkaline metal ions allow one to produce specific structures with extensive channels and ionic conductivity.

Bronze monocrystals of 8 to 12 mm size were placed in a vacuum chamber (10^{-5} to 10^{-6} mm Hg) and subjected to heating in the presence of electric field. Then the system was cooled down to the room temperature and filled with hydrogen or with deuterium. Crystal temperature and neutron- and gamma radiation were registered. A typical neutron background was 1 to 7 h^{-1}.

In experiments with hydrogen no statistically significant increase of neutron- or gamma signal was observed. At the same time in all, more than 80 experiments with deuterium, an increase in the background as high as 2 to 20 times (during 10 min after filling with deuterium) was registered by a neutron counter. In the experiments with both H_2 and D_2 a crystal temperature elevation (typically 1 to 25 $^oC^2$) was observed, which corresponds to 2 to 50 J. For the same crystals the heat effect for D_2 was few times larger than for H_2. The results observed from 11.11.90 to 03.04.92 are summarized in Table 1.

A most striking feature of the experiment is 100% reproducibility of the neutron signals. From our previous experience in CF it is very hard to believe such "ideal" behaviour. (Systematics? Special role of channels?). As to the heat effects, heating with H_2 points to the "chemical" origin, whereas a greater effect for D_2 needs further study. Unfortunately, hurried attempts to do so at Lebedev Institute and Lugansk failed due to some technological reasons.

Table 1. Data on CF in Na_xWO_3 Bronze

Gas	Date of Experiment	Number of Experiments		neutrons, signal/BG	sample heating °C	positive results %
		Positive Results	Negative Results			
H_2	11.11.90-10.09.91	0	31	0	0.1-25	0
D_2	16.10.91-09.09.92	93	0	10^3-10^7	0.7-50	100
D_2	20.02.92	5	0	2-10	1-3	100
H_2	20.02.92	0	5	0	0.1	0
D_2	03.04.92	4	0	1.7-3	0.7-3	100
D_2	16.10.91	1	0	$1.2 \cdot 10^7$	0.01	100
D_2	06.11.91	1	0	6	22.5	100
D_2	04.12.91	1	0	$5.5 \cdot 10^5$	0.5	100
D_2	03.04.92	2	0	2-4	1.5	100

2.2. CF in Gas Discharge

During the past year three groups which employed the gas discharge for deuterium loading in CF experiments continued their work. This technique was already discussed at Como [27] and in [28], so I'll not go into details, but justrefer to the most essential results.

The most ambitious data were presented by A.B. Karabut et al. group from "Luch" (Podol'sk, Moscow District)[17]. They observed with Pd cathodes ($1 cm^2$, 100 μ thick) a high heat excess $Q/Q \simeq 500\%$, $P \simeq 33$ w and very energetic charged particles with energies up to about 16 MeV. They registered numbers of lines with E_γ (MeV)= = 1.6±0.1; 1.8±0.1; 2.2±0.1; 3.0±0.1; 3.5±0.1; 4.1±0.1; 5.2±0.1; 5.7±0.1; 7.6±0.1; 9.4±0.2; 12.2±0.4; 16.0±0.6. The source intensity is estimated as 10^5-10^7 charged particles per second, which is still about three orders of magnitude less than the energy excess.

The other group from the same Institute (V.A. Romodanov et al.) continued their tritium measurements during D_2 gas discharge [22]. They claimed about four orders of magnitude increase in tritium production under about four times increase of input power and the rate of total tritium yield up to 10^9 atoms$\cdot s^{-1}$ for a typical ion energy of 40 to 80 eV.

The Tomsk group reported their results on neutron-, gamma-, and charged particle registration during glow

discharge [1 4]. They used scintillation counter with n/γ separation and semiconductor detector for charged particles. During D_2-loading and cooling with liquid N_2 of Nb foils they observed 1.5 to 1.7 increase of neutron signal, but no increase for gammas and charged particles.

2.3. Interaction of Ti with LiD Vapour in Electric Discharge

The Institute of High-temperature Electrochemistry group continued their experiments with high temperature electrolysis in the Ti_1/D_2, LiD/LiD/Ti_2 system (see [27, 28] for earlier results). During the past year they analysed 103 gamma spectra measured at various thermocycling [24]. In 67 spectra an excess above the background was observed and some lines, not seen in the background spectra, were registered. The authors attributed the difference in gamma spectra observed for anodes and cathodes to possible reactions with Li on Ti cathodes.

2.4. Loading from Gas Phase

The Ural Polytechnical Institute group carried out D_2 gas loading and thermocycling of samples made of Pd, Ti, TiFe and some other alloys [19]. The temperature cycling interval 500-650 °C corresponds to $\alpha \rightarrow \alpha + \beta$ phase transitions for TiFe. Neutron pulses up to a 10^1-10^2 times background level were registered during cooling down to room temperature in vacuum for all materials.

In the experiment performed by the Lugansk-Donetsk-Lebedev Institute group [10] neutron-, acoustic- and electromagnetic emissions were registered during gas-phase deuterium loading of Pd, Nb, steel, and $LaNi_5$ samples in mainly non-equilibrium conditions created by multiple thermo-cryo-cycling. They confirmed their previous results (see [27,28]) with good statistics and a signal-to-background ratio of the order of ten.

2.5. Search for CF of Deuterium Implanted in Solid Samples

Cold fusion studies based on deuterium ion implantation method were actively carried out of late years by the Kharkov group (V.F. Zelensky et al., see [27,28]). Recently another Kharkov group (V.P. Bozko et al.) reported their results from the ion implantation experiment based on non-traditional approach [3]. The idea is to use the kinematic ratio to determine the acts of deuterium nucleus fusion on the background of DD-reactions, which is realized in the process of solid sample irra-

diation with accelerated deuterium ions. They used targets made of Be, C, Al, Si, Ti, Cu, Mo, Pd, Ta, W and Pb. In the first series of measurements (water cooling of targets) a noticeable increase in counts was observed only for Mo. The effect was estimated as $\Lambda \simeq 10^{-18}$ $(DD)^{-1}$ s^{-1}. In the second series (liquid nitrogen cooling) positive results were observed for Al, Ti, Cu and Mo. The estimate for Mo was $\Lambda \simeq 10^{-17}$ $(DD)^{-1}$ s^{-1}.

2.6. Neutron-, Acoustic-, and Electromagnetic Emission Registration during LiD Hydratation in Heavy Water

A weak neutron emission during LiD hydratation in D_2O was recently reported by the Novosibirsk group (see [27,28]). In order to check this "nuclear chemofusion" the Lugansk-Lebedev-Institute of Physical Chemistry group performed a similar experiment [11] using a highly efficient low background registration complex. The total amount of LiD (and LiH in control experiments) was about 30 g. Fast and slow neutrons were registered with γ/n separation with efficiency of 8 to 40%. For the total 30 h of measurements, in one series of 2 h duration 5 bursts were registered with a signal-to-background ratio 10 to 100 (The background level was ~ 5 h^{-1}).

2.7. Search for Neutron Emission during Percussion Destruction of LiD, TiD_x and Some Other Materials

The experimental situation with the so-called "nuclear-mechanofusion" is controversial. The B.V. Deryagin group reprted positive results from mechanical fracture of heavy ice, LiD crystals, and from friction and mechanical activation of Ti surfaces and Ti cavitation in the presence of D (see [26,27]). However, negative results were reported as well [21,25,29].

In order to check neutron emission during juvenile surface creation in some deuterium-containing materials the Lugansk-Kharkov-Lebedev group [12] studied percussion destruction of LiD crystals ($\Sigma m \simeq 10$ g), TiD_x tablets ($x = 1$ to 2; $\Sigma m \simeq 40$ g) and $Al_2(SO_4)_2$, $K_2SO_4 24D_2O$ crystals ($\Sigma m \simeq 15$ g). The resulted dispersion was about 0.5 to 2 m^2/g. A high detector efficiency for both fast and slow neutron registration and background suppression allowed one the registration of about two orders of magnitude smaller neutron signals than was claimed in the Deryagin's works. The results of the experiment are negative and set up the limit $\Lambda < 10^{-24}$ $(DD)^{-1} s^{-1}$.

2.8. Search for Nuclear Emission in Deuterium-Containing Systems during Phase Transitions

The Lugansk-Lebedev-Institute of High-temperature

Electrochemistry group carried out experimental search for nuclear emission during phase transitions in $Al_2(SO_4)_3$, K_2SO_4 $24D_2O$, $KNaC_4H_4O_6 \cdot 4D_2O$ and NbD_x [13]. Neutrons were registered by a high efficiency detector described in Part 3 of this talk. Tritium was measured with a scintillation counter and mass spectrometer. In some experimental series in order to improve the signal-to--background ratio and to study fine time structure of the events in the $(1\text{-}256) \cdot 10^{-6}$ s intervals, neutron bursts and neutron-acoustic-electromagnetic signal correlations were studied. No statistically significant signal above the background was registered, and the estimated limit on the reaction constant was $\Lambda < 10^{-24}$ $(DD)^{-1}$ s^{-1}.

2.9. CF Studies during Electrolysis

A CF stusy with traditional D_2O electrolysis was carried out in Chemical Physics Institute [6] and in Kharkov Institute of Monocrystals [8] and it also revealed pulsed neutron and proton emissions.

The Lugansk-Donetsk-Lebedev Institute group measured neutron-, acoustic-, and electromagnetic radiation during D_2O electrolysis with Pd, Nb and steel cathodes and confirmed their earlier result (see [27,28]) with better statistics.

2.10. Related Studies

In conclusion of this experimental section I would like to mention two more papers which, although do not deal with nuclear products of heat registration, nevertheless may be relevant to understanding the CF mechanism.

The L'viv State University group [18] registered the electroluminescence emission during electrolysis of heavy and ordinary water. The idea was to check the "fracto-acceleration model" (see [26]) which predicted correlation of CF and electromagnetic radiation caused by the crystal fracture.

It has been observed that for the stimulation of electromagnetic emission it is worthwhile to carry out preliminary electrolysis with a current density 2.5 to 7.5 mA/cm^2 for 1 to 2.5 h and then to increase the current density (i) to 12.5 - 125 mA/cm^2. The electromagnetic emission intensity reached 50 to 10^4 pulses per second, while for $i \geq 25$ mA/cm^2 a jump increase in radiation intensity up to $\simeq 10^5$ s^{-1} was observed. In experiments with ordinary water no similar jump increase was registered.

The formation of "supersatureted" (unstable) hydride phases (with D/Pd >1, D/Ti> 2) in the near-surface

layer during non-equilibrium sorbing/desorbing was hypothesized in [26] in connection with CF. Recently such possibility received some experimental support. A group from Institute of Physical Chemistry [20] observed that, after some thermic treatment, hydrogen did not produce a well-known α- and β-volumetrical phases in Pd but concentrated in the near-surface layer up to $1.24 \cdot 10^{-4}$ $M \cdot cm^{-2}$ surface density. That was established by electric resistivity measuring and by means of hydrogen extraction. In Part 4 we shall also discuss some theoretical results indicative of supersaturated layer formation.

3. Detectors

Of late years few groups in Russia and Ukraine built some original highly effective detecting systems for CF studies. I shall mention here in brief the detectors constructed by the Novosibirsk-, Lebedev Institute-, and Lugansk groups. Unfortunately, due to the problems mentioned in the Introduction only the Lugansk group was able to exploit their system effectively for a wide range of CF studies.

This group, in collaboration with some other Russian and Ukrainian groups, built a high efficiency low background automated ("on-line" regime) registration complex for correlation measurements in CF experiments [9]. The complex makes possible to search for neutron groups ($n \geq 2$) in 1 to 256 μs time intervals and for events with "rigit" correlations (within 20 μs) of neutron-, acoustic-, and electromagnetic signals. The time of appearance of the correlated events and some of their parameters (the time shifts between components, the number of pulses in a chosen time interval for each channel) are registered in real time mode and recorded on magnetic tape. Dead time is $\leq 10^{-3}$ s.

Registration of both fast and slow neutron signals and γ/n separation were used to increase the neutron identification reliability and to suppress the background to the level of $\simeq 3 \cdot 10^{-3}$ with 8 to 40% efficiency.

The Novosibirsk group improved their detector that had been previously used in "chemo-nuclear-fusion" experiment (see [27,28]). They constructed [1] a new version of neutron spectrometer with about 4π geometry operated in the 1 to 5 MeV energy range with a good γ/n discrimination. The efficiency is about 10% at the $2 \cdot 10^{-3}$ s^{-1} background level and permits one to measure a neutron energy spectrum at a very low intensity of the source.

The Lebedev Institute group designed, constructed and tested two new original detectors for simultaneous (or separate) measuring of proton and neutron emission [15].

The charged particle detector consists of two electrolytic cells filled with heavy and ordinary water. The bottom of each cell is made of 0.1 mm palladium foil and serves as a cathode and an input window of a proton detector. A method for the external cathode surface protection is developed to prevent leakage of deuterium (or hydrogen) from Pd. A proton detector-identifier contains a gas-filled wire proportional chamber and a scintillator CsI(Tl) detector.

The neutron detector gives the time, space and amplitude information on emission of single neutrons and neutron bursts. The detector includes a neutron hodoscope made of 5 cm thick plastic scintillator rods. The hodoscope is used simultaneously as a fast neutron detector (according to recoil protons), a neutron moderator and a detector of secondary gamma quanta which are produced due to thermal neutron capture in a cadmium foil surrounding each hodoscope element. Information is analysed by CAMAC electronics and multichannel time interval analyzer on line with IBM PC computer.

4. Theoretical Models

The problem of theoretical description of CF mechanism turned out to be not simpler than the problem of its unambiguous experimental proof. Meanwhile the urgent need of a "reasonable" model is dictated not only by obvious wish to understand the nature of the phenomenon. In the current, still very uncertain, experimental situation a working hypothesis that would be trustworthy and could correlate a large amount of observations and give some predictions might prove to be very useful to stimulate the experiments. Not the last is a "psychological factor": demonstration of CF permissibility in principle couldremove objections of sceptics who do not admit the CF wet idea.

Recently a promising "nonstationary" mechanism of rather a general quantum mechanical nature was suggested by the Lebedev Institute group [5]. The cause for fusion in the model is an enhancement of barrier penetrability aroused by appearance of high-momentum components in the deuteron wave function due to violation of its stationarity in solid state. (Similar effect was demonstrated recently [4] in a one-dimensional electron tunneling problem). CF rate was calculated by solving the Schrödinger equation for both the three-dimensional rectangular and the Coulomb potentials, when the "binding" part of the potential underwent instantaneous change. The latter might be caused by ionization, phase transition, irradiation, fracture, etc. The most essential feature of the model is a power but not exponential (Gamov fac-

tor) decrease of penetration probability. As a result, the total fusion probability for a DD pair in "favourable" conditions may be $\sim 10^{-8} - 10^{-14}$. If the nonstationarity is caused by fracture, it may result in up to 10^5-10^8 fusions per cm^3 of hydride.

Another "synergetic" hypothesis was suggested in [7]. The idea is that the self-organization of matter in nonequilibrium D-containing system with dissipative structure formation and separation of subsystems could result in distortion of the Boltzmann energy distribution and increase the probability for a deuteron to have an energy sufficient for fusion.

An attempt to take into account, for CF, the real density distribution in a crystal was made in [30] for PdD_x. For the deuteride ground state it results only in 10 to 20 orders of magnitude increase of the DD fusion rate with respect to the deuterium gas of a corresponding density. However, the fusion rate may reach an experimentally observed level, if the charge density is redistributed owing to some physical-chemical processes. The electromagnetic radiation following fracture may also change the Coulomb potential and increase the fusion rate considerably.

The idea of a possible formation of supersaturated zones near the surface [26] was recently studied theoretically [2,23]. The diffusion equation was analysed with a nonlinear concentration dependence of the diffusivity and with special nonequilibrium boundary regimes of "peaking" type for a time dependence of the current density $\sim (t - t_0)^{-\alpha}$, $\alpha > 0$. It has been shown that in such situation any boundary peaking regime results in the formation of inhomogeneous space structures near the surface.

5. Acknoledgements

I want to express my deep gratitude to the Organizing Committee and especially to Prof. H. Ikegami for great efforts in organizing my visit to ICCF3 and for financial support.

6. References

1. Arzhannikov A.V. et al., 1991, INF preprint 91-121, Novosibirsk.
2. Baraboshkin A.N. et al., 1992, Donetsk, 2, 4.
3. Bozko V.P. et al., 1992, Donetsk, 1, 13.
4. Casero R. et al., 1991, Univ. Autonoma de Madrid preprint.
5. Chechin V.A. et al., 1992, submitted to Fusion Technology.

6. Dalidchik F.I. et al., 1991, Ekaterinburg, 34.
7. Filimonov V.A., 1992, J.Radioanal.Nucl.Chem.,162,99.
8. Galunov N.Z. et al., 1992, Donetsk, 1, 16.
9. Gavrilyuk A.Yu. et al., 1992, Donetsk, 1, 20.
10. Golubnichij P.I. et al., 1992, Donetsk, 1,19.
11. Golubnichij P.I. et al., 1992, Donetsk, 1,26.
12. Golubnichij P.I. et al., 1992, Donetsk, 2,8.
13. Golubnichij P.I. et al., 1992, Donetsk, 1,25.
14. Gorbachev A.F. et al., 1991, Ekaterinburg, 44.
15. Grishin V.M. et al., 1992, contibution to this Conference.
16. Kaliev K.A. et al., 1992, Donetsk, 1,12.
17. Karabut A.B. et al., 1991, Ekaterinburg, 35.
18. Koval'tchuk E.P. et al., 1992, Donetsk, 1,17.
19. Lobanov V.V. et al., 1992, Donetsk, 1,5.
20. Lyakhov B.F. et al., 1991, Ekaterinburg, 6.
21. Price P.B., 1990, Nature 334, 542.
22. Romodanov V.A. et al., 1991, Ekaterinburg, 45.
23. Samgin A.L. et al., 1992, contribution to this Conference.
24. Sannikov V.I. et al., 1992, Donetsk, 2,6.
25. Sobotka L.G. et al., 1990, Nature 334, 601.
26. Tsarev V.A., 1990, Sov. Phys. Uspekhi 33, 881.
27. Tsarev V.A., 1991, Proc. ICCF2, Como, 319-336.
28. Tsarev V.A., Worledge D.H., 1992, Fusion Technology, 22, 138.
29. Zelensky V.F. et al., 1991, Voprosy Atomnoj Nauki i Tekhniki, 2, 46.
30. Demidenko V.S. et al., 1992, Donetsk, 1,18.

Cold Fusion Research in Italy

F. Scaramuzzi
ENEA, Area INN, Dip. Sviluppo Tecnologie di Punta,
CRE Frascati, C.P. 65, 00044 Frascati, Roma,
ITALY

1. The strange geography of Cold Fusion

In the last three and a half years many experiments have been performed in the field known with the conventional name of "Cold Fusion" (CF), and a number of theories have attempted to interpret them and to assess them in a coherent picture. Differently from other fields in science, this area has grown in a quite strange atmosphere: the most striking aspect of it is the anomalous "geography" of the activities, meaning by this term the different kind of development that research activities in this field have had in different countries.

Before outlining this geography, it could be worth trying to envisage the causes of this anomalous behaviour. One important feature is indeed the difficulty in reproducing most of the experiments in the field. Of course, this feature can be interpreted in positive as a proof of the great complexity of the phenomena under investigation, and in negative as the demonstration that the claimed effects do not exist. Both positions have been brought forward and are still existent: the increasing number of good quality positive experiments, and the improvements in reproducibility seem not to have changed the prevalent scepticism of the scientific community. Anyway, the lack of reproducibility is not the only cause of the scepticism: other features concur in creating it. In particular, the fact that the observed phenomena, if interpreted as nuclear phenomena in condensed matter, cannot be explained by the presently accepted knowledge on nuclear physics. Most striking of all, the experiments showing the production of "excess heat" pose a very intriguing problem: the large amount of energy produced cannot be explained in terms of any known chemical reaction; at the same time, the missing emission of energetic particles (neutrons, tritons, etc.) is in contrast with the expectations on nuclear reactions between energetic nuclei in

FRONTIERS OF COLD FUSION

quasi-vacuum (e.g., plasma), the only ones that are well known presently. All these features are at the basis of the scepticism, which is the cause of the "strange geography"; this will be briefly described in the following.

Even though it is difficult to perform a clear classification among the countries, an attempt is made to identify groups with similar behaviours.

- The first group consists of the countries in which an official and substantial research activity is going on, with continuous interactions among operating groups. In this group Japan excels, counting also on the commitment of Industry and, more recently, of Government (Ministry of International Trade and Industry, MITI). Russia (better, the former USSR), China and India can be assigned to this group as well.
- The development of CF in the USA puts this country in a very peculiar position. On one side there are many scientists active in the field, as it is witnessed by the large number of participants to this conference (55), second only to Japan. On the other side, it has to be noted that, with the important exception of EPRI (Electric Power Research Institute), no Federal Agency, nor University, is substantially funding research in CF.
- As far as Europe is concerned, Italy and, to a lesser extent, Spain perform a consistent activity, with moderate funding by state Agencies and/or Universities. The activity in Italy, third for number of participants to this Conference (20), is the subject of this paper, and will be treated in more detail in the following.
- The most striking feature in this "geography" is the almost total absence of research activities in the rest of Europe. Here, after the negative results obtained in the experiments performed in the spring-summer of 1989, mostly under the request of Euratom, every interest in CF seems to have disappeared.

2. Italian Agencies and Universities active in Cold Fusion

In fact, Italy could also belong to the first group, since many Agencies and Universities are moderately funding research in CF, and the scientists involved in this field have made a few attempts to coordinate each other, organizing meetings and conferences, both national and international (Varenna in 1989, Frascati in 1990, Como in 1991, Torino in 1992). However, up to now the activity has been mostly the fruit of the personal initiative of the scientists, and never a coordinated proposal of Agencies and Universities. No position on the scientific validity of the subject has been officially taken and the funds dedicated to CF have been rather modest.

The Agencies are the following:

- INFN (National Institute for Nuclear Physics): it is dedicated to fundamental studies in nuclear and subnuclear physics, and is strongly connected with Universities all around the Country. Most of the funding to CF in Italy comes from this Agency, and is

particularly dedicated to the development of sophisticated nuclear detectors.

- CNR (National Research Council): it is the State Agency for Research and operates in all fields of Science, mostly through its own Research Institutes, but also through funding of other research institutions, such as Universities. It has contributed to CF mostly through its Chemistry Committee.
- ISS (National Institute for Health): it is an Agency with a wide range of interests in Science, performing research mostly aimed to solve problems of health. Its Physics Laboratory is funding research in CF.
- ENEA (Agency for New Technologies, Energy and Environment): formerly the State Agency for Nuclear Energy, it has been recently restructured with the assignment of wider research tasks. After the first success of a Frascati Group in 1989, research in CF has been performed on a modest resource level and mostly on voluntary basis: recently the new Board of Administration has expressed an interest in the field, that hopefully will bring to a serious commitment of this Agency in CF.
- Various Universities participate to research activities, most of them in collaboration, or with the funding of the above Agencies: among them the Universities of Torino, Milano, Padova, Trieste, Bologna, Roma 1, Catania.
- Up to now Industry has been totally absent in this field.

In order to have a feeling about the amount of investments in Italy on CF, the figure referring to 1992 amounts to about 0.5 million dollars, not including expenses for personnel. A number of about 70 scientists, mostly working part-time, is committed all around the Country in research on CF.

3. Italian Research on Cold Fusion

The Italian participation to this Conference is a good representation of the research going on in this field, even though some active groups did not send contributions. Eleven abstracts were submitted and were accepted for presentation to ICCF3, coming from nine groups. The experimental papers range from gas loading to electrolysis, from nuclear particle detection to heat excess measurement. There is also a substantial contribution of theoretical papers. Eight of the papers were eventually presented at ICCF3, and the reader will find them in these proceedings.[1-8] Three of the papers have not been submitted, for the impossibility of the authors to attend ICCF3: they are all theoretical papers, and will be shortly described hereafter.

- The first (authors A. Tenenbaum and E. Tabet, of INFN, ISS and University of Rome 1) investigates a mechanism of D-D fusion taking place in the lattice of a metal undergoing rapid thermal transients: the abrupt release of elastic energy stored in the metal during the absorption of deuterium could produce micro-hot fusion, which could explain the detection of nuclear particles in gas loading experiments.[9]

- The second (author A. Scalia, of the University of Catania) investigates the behaviour of the fusion cross-section, as a function of the energy of the nucleons, for very low energies.[10]
- The third (authors L. Fonda of the University of Trieste, and G.L. Shaw of the University of California at Irvine) analyzes the hypothesis that CF could be catalysed by a not confined quark compound.[11]

Among the activities not presented at all at ICCF3, two are worth mentioning: that of a Padova Group, and that of a Bologna Group. Their most relevant results will be shortly outlined hereafter.

- Padova (CNR and University): two main kinds of experiments have been performed:
  - Study of the dynamics of D and H-charging in Pd sheets (gas loading), as a function of temperature, reaching D/Pd ratios in the range 0.8-0.9; when working with D, a quite substantial emission of charged particles has been detected with the help of CR-39 detectors, amounting, if interpreted as D-D fusions, to 10^{-19} fusions per second per couple of deuterons.[12]
  - The detection of neutrons emitted by D-charged Ti plates (gas loading), under vacuum after temperature cycles, measured with an advanced detector, has shown the emission of neutron bursts, clearly above background, with energies of about 2.5 MeV.[13]
- Bologna (INFN and University): experiments on the detection of neutrons from D-charged Pd (electrolysis) and Ti (gas loading) have been performed extensively under the Gran Sasso Laboratory of INFN, a well equipped Laboratory more than 1000 m under ground, where the background of neutrons is about one thousandth of the value at sea level. A particularly advanced detector system has been developed, able to clearly discriminate neutrons from gamma's, with a time resolution in the order of 10 ns, and the ability to measure the energy of the neutrons. None of the experiments performed up to now has shown the emission of neutrons that could be ascribed to CF effects.[14]

4. Some relevant results

Among the many results in CF research contributed by the Italian scientific community, two of the experiments presented at this Conference deserve a particular mention, and will be recalled in the following.

- The experiment by B. Stella et al.[5] performed in the Gran Sasso Laboratory of INFN, in which a sample of deuterated Pd has been stimulated with a neutron flux, while the emission of neutrons was detected at right angle with the neutron beam. The result is qualitatively interesting: it is possible to state that the rate of neutron emission, when the D-charged Pd is stimulated, is higher than the rate obtained with Pd without D. This seems to be a clear indication that the combination of the two, Pd and D, is responsible for nuclear reactions that manifest themselves with the emission of neutrons, confirming the role of the lattice in this new kind of nuclear events.

- The experiment by L. Bertalot et al. [8] performed at the ENEA Centre of Frascati has provided a novel approach to the heat excess experiments in heavy water with Pd cathode. Taking a couple of features from the Takahashi experiment (see also this Conference), i.e., the "hi-lo" technique and the flow calorimeter, this experiment tries to address the problem of the motion of D atoms in the Pd lattice at high D/Pd ratios. In order to do so, the cathode is mounted in such a way as to face on one side the electrolytic cell and on the other D_2 gas: measuring the permeation of the gas into or out of the cathode seems to be a powerful tool to investigate the heat excess production. The experiment provides a quite convincing confirmation of the heat excess production, with maxima up to about 10 times the heat input at low currents, and to 100% of the heat input at high currents, and presents stimulating correlations between the heat produced and some meaningful parameters, such as the period of the hi-lo procedure, the overpotential across the cell, and the D-permeation into the cathode. A transport model, also presented at ICCF3 [2] nicely interprets these correlations.

Among the contributions of the Italian community to CF research it has to be remembered the theory of G. Preparata et al., [15] which, with a very interesting approach, tries to explain the most intriguing issue in CF, i.e., the possible nuclear nature of the heat excess. Preparata's theory invokes a collective and coherent interaction between the D-nuclei and the plasmas in the lattice (electrons and nuclei), to justify the high rate of D-D fusions and the transformation of the mass defect energy of the reaction into heat, rather than in the well known processes taking place at high energy and in quasi-vacuum.

5. Conclusions

The lack of official commitment and effective support by the Research Agencies and by the Universities has not prevented Italian scientists from being quite active in performing research in CF. On the other side, it has to be acknowledged that no formal vetoes have been interposed to the free initiative of scientists in this field: on the contrary, some of the Agencies and Universities have moderately funded such an effort.

The quality of the experiments performed in Italy has been increasingly good, and the results obtained are rather outstanding in the general panorama of CF. But it is time to perform a more coordinated effort, keeping in mind that material science aspects, such as the characteristics of the materials used, play a very important role in the development of this topic. Thus, a much more intense effort is required in order to obtain a more substantial progress in the field.

The increasingly convincing results obtained by the whole CF community (this Conference has been particularly comforting in this respect), and the example of the Japanese Government and Industry, which appear to be determined to promoting research in this field, have changed the panorama of CF. There are now signs that also the

Italian scientific authorities could consider favouring research in this field in the near future.

6. References

1. G. Preparata (INFN and University of Milano), Theory of Cold Fusion in Deuterated Palladium, this Conference
2. A. De Ninno, V. Violante (ENEA, Frascati), "Quasi-Plasma" Transport Model in Deuterium Overloaded Palladium Cathodes, this Conference
3. D. Gozzi, P.L. Cignini, R. Caputo, M. Tomellini, E. Cisbani, S. Frullani, F. Garibaldi, M. Jodice, G.M. Urciuoli (INFN, ISS and University of Roma 1), Experiment with Global Detection of the Cold Fusion Products, this Conference
4. B. Stella, M. Alessio, M. Corradi, F. Croce, F. Ferrarotto, S. Improta, N. Iucci, V. Milone, G. Villoresi, F. Celani, A. Spallone (INFN and University of Roma 1), The FERMI Apparatus and a Measurement of Tritium Production in an Electrolytic Experiment, this Conference.
5. B. Stella, M. Corradi, F. Ferrarotto, V. Milone, F. Celani, A. Spallone (INFN and University of Roma 1), Evidence for Stimulated Emission of Neutrons in Deuterated Palladium, this Conference
6. E. Botta, T. Bressani, D. Calvo, A. Feliciello, P. Gianotti, L. Lamberti, M. Agnello, F. Iazzi, B. Minetti, A. Zecchina (INFN and University of Torino), Measurement of 2.5 MeV Neutron Emission from Ti/D and Pd/D Systems, this Conference
7. F. Celani, A. Spallone, P. Tripodi, A. Nuvoli (INFN, Frascati), Measurements of Excess Heat and Tritium during Self-Biased Pulsed Electrolysis of Pd-D_2O, this Conference
8. L. Bertalot, F. De Marco, A. De Ninno, A. La Barbera, F. Scaramuzzi, V. Violante, P. Zeppa (ENEA, Frascati), Study of the Deuterium Charging in Palladium by the Electrolysis of Heavy Water: Search for Heat Excess and Nuclear Ashes, this Conference
9. A. Tenenbaum, E. Tabet (INFN, ISS and University of Roma 1), Temporal Sequence of Nuclear Signals in a "Dry" Cold Fusion Experiment, abstract presented to this Conference
10. A. Scalia (University of Catania), Anomalies in Nuclear Fusion for Light Systems at Very Low Energy, abstract presented to this Conference
11. L. Fonda, G.L. Shaw (University of Trieste and University of California at Irvine), Anti-Diquark Catalysis of Cold Fusion, abstract presented to this Conference
12. C. Manduchi, G. Zannoni, G. Milli, L. Riccardi, G. Mengoli, M. Fabrizio (CNR and University of Padova), paper submitted to "Nuovo Cimento"
13. C. Manduchi (University of Padova), private communication
14. C. Moroni (INFN and University of Bologna), private communication
15. T. Bressani, E. Del Giudice, G. Preparata (INFN and Universities of Milano and Torino), 1989, Nuovo Cimento 101A,

845; G. Preparata, Proceedings of the "First Annual Conference on Cold Fusion", National Cold Fusion Institute, Salt Lake City (USA), 91 (1990)

II. Contributed Papers

Chapter I
Excess Heat

Study of Deuterium Charging in Palladium by the Electrolysis of Heavy Water: Search for Heat Excess and Nuclear Ashes

L. BERTALOT[a], F. DE MARCO[a], A. DE NINNO, A. LA BARBERA[b], F. SCARAMUZZI, V. VIOLANTE[a], P. ZEPPA[c]
ENEA, Area INN, Dip. Sviluppo Tecnologie di Punta, CRE Frascati, C.P. 65 - 00044 Frascati, Rome, Italy

ABSTRACT

The production of heat excess (HE) in electrolytic cells with heavy water and palladium cathodes is, in Cold Fusion, the experiment that has had more confirmations, even though still doubts are cast on its nuclear origin. Furthermore, the correlation of HE with some features of the experiment seems to be well established, the most convincing of which is a threshold in the D/Pd ratio. What is yet not quite clear is how to obtain a high D/Pd ratio, since this feature seems to depend both on the material and on the procedures adopted for the electrolysis. In this paper we will propose a novel approach to this problem, which permits to correlate HE with other features of the experiment. In particular, we try to study the transport of matter across the palladium lattice during the electrolysis. A model, proposed by two of us (ADN e VV), and presented in this Conference, helps to interpret the experimental results, and gives interesting hints for future research.

As far as the nuclear nature of the HE is concerned, it seems today clear that the only serious way to address this problem consists in performing experiments in which the presence of "nuclear ashes" is searched, ^4He nuclei being the most likely to be found. Such an experiment has been performed once[1], and needs confirmation. We plan to perform an experiment in which the production of ^4He nuclei can be detected in the gases evolving from the electrolytic-cell, in coincidence with the production of HE. A cryogenic system able to separate ^4He from other gases, including D_2, has been designed, and preliminary data on its behaviour are presented.

1. The electrolysis experiment

Three main features characterize this experiment:

FRONTIERS OF COLD FUSION

- The "hi-lo" technique, introduced by the Osaka Group[2], consisting in alternating low current to high current: the influence of its period on the heat production has been investigated.
- A particular geometry has been adopted, in which the cathode is immersed on one side in the electrolytic solution, while the other side faces a vacuum tight ambient in which gaseous D_2 (or H_2) is introduced: measuring the pressure variation of the gas gives information on its permeation through the cathode, thought as a membrane.
- In order to address the problem of poisoning of the cathode surface, which can be responsible for preventing high D/Pd ratios to be reached, a palladium anode has been used. Poisoning is produced by impurities present in the electrolytic solution, by dissolution of the anode, and by chemical reactions between the solution and all materials in contact with it. In our cell, the palladium anode is slowly but continuously dissolved, and conversely palladium is deposited on the cathode surface, thus regenerating it, by creating new active sites for the adsorption of D (or H). [This technique has also been used by the SRI Group[3].]

The experimental procedure starts with D_2 gas on the gas side of the cathode (pressures up to 1 bar) and an inert gas, say Ar, on the other side. The aim of this step is to favour charging of D in Pd from the gas, thus starting the electrolysis when already a non-zero D/Pd ratio has been achieved (remember that the diffusion coefficient of D in Pd is strongly dependent on D/Pd ratio, increasing by two orders of magnitude when the ratio changes from zero to 0.6). Up to now this procedure has not given reproducible results, the initial D/Pd ratio varying from 0.1 to 0.5, both obtained in a few days of gas loading. Once this first phase has been performed, the electrolytic solution is introduced and electrolysis starts. The experiment is aimed mainly to obtaining information about the presence of "density waves" in the lattice, by looking at the D_2 flow variations into and out of the gas side, and to the voltage variations across the cell (at constant current), and correlating them with the HE detected.

The electrolytic cell (Fig.1) is made out of glass (Pyrex) and teflon, to minimize poisoning. The connectors for both electrodes are in Ni coated by teflon. The area of the plane electrodes is 1 or 2 cm^2 (thickness, respectively 250 or 500 μm). The distance between electrodes is 3 mm, obtained with a rigid mounting. The electrodes have been previously brought to either 200 or 900°C, and then rapidly quenched in liquid N_2: under an electronic microscope the average linear dimension of grains is ≈20μm. A solution of LiOD, 0.1M in heavy water (for blanks, LiOH, 0.1M in light water) has been used, and tests made in the course of experiments have shown no change in molarity.

The calorimetry is obtained by circulating a thermoregulated water flow (< 1 cm^3/s, T = 25 ± 0.1°C) in a cylindrical glass heat exchanger symmetrically immersed in the cell (see Fig.1), and measuring the difference in temperature between inlet and outlet of the water in the heat exchanger. The cell is separated from the

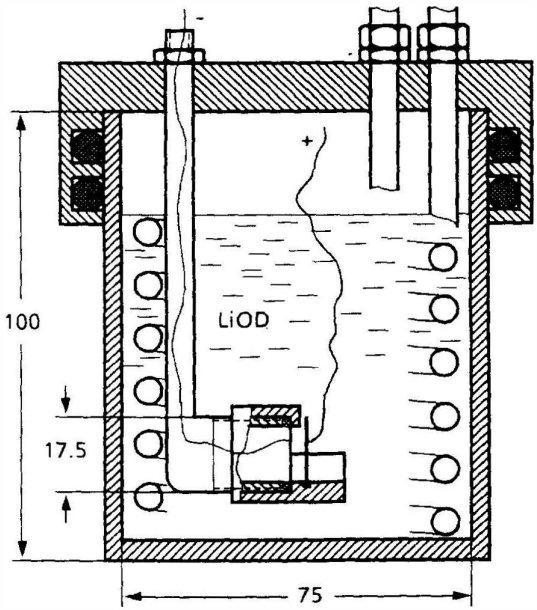

Figure 1. Schematic drawing of electrolytic cell and calorimeter.

external ambient by a 20 cm-thick polyethylene layer: variations in the room temperature have a negligible effect if kept within ≈2°C, which was the case during the experiments. In addition, the temperature difference between the thermostat and the cell is also recorded, as a check. Both temperatures are measured by nanovoltmeters, whose data are collected by a PC-based acquisition system. Calibration is performed with the help of an electrical resistor immersed in the cell, not far from the electrodes: the response is linear within 10% up to 25 W. The maximum error in measuring HE is ±25 mW.

Besides the two temperature differences, the pressure on the gaseous side of the cathode and the voltage across the cell (which is run at constant current), are measured and recorded.

2. Results

HE was detected in 3 experiments, both during the low current and the high current regimes, and was not detected in 1 blank test. During the three positive runs, the production of HE was not continuous and it was possible to correlate it to other features of the experiment, as explained below: thus, extended periods occurred in which no HE was produced, even though working with heavy water. This feature, together with the absence of heat production in the blank, seems to us a good test for the reliability of the

experiment. The HE reached a maximum value of ≈3 W (60-80 W/cm3) for both low and high currents, with a corresponding maximum of ≈10 times the heat input for low currents and about twice the heat input for high currents.

In the different runs we have tried to study the response of the system to the following parameters:

1. The period of the hi-lo procedure.
2. The current intensity and the voltage across the cell, in the two regimes.
3. The pressure variation on the gas side.

Here we will describe our results following this classification:

1. The semi-period was in the range 2500 - 10,000 s. The lower limit is imposed by the thermal relaxation time of the calorimeter. In Fig.2 the dependence of the measured HE on the semi-period is shown for one of the runs. In the first 120 hours of the experiment, not shown in the graph, the semi-period was of 10,000 s, and no HE was detected. In the last 150 hours, also not shown in the graph, no excess was measured, in spite of the low semi-period (4500 s): a posteriori, we found that, most probably because of the continuous migration of Pd from the anode to the cathode, holes had been produced in the anode, thus altering the geometry of the electric field: we think that this event is responsible for

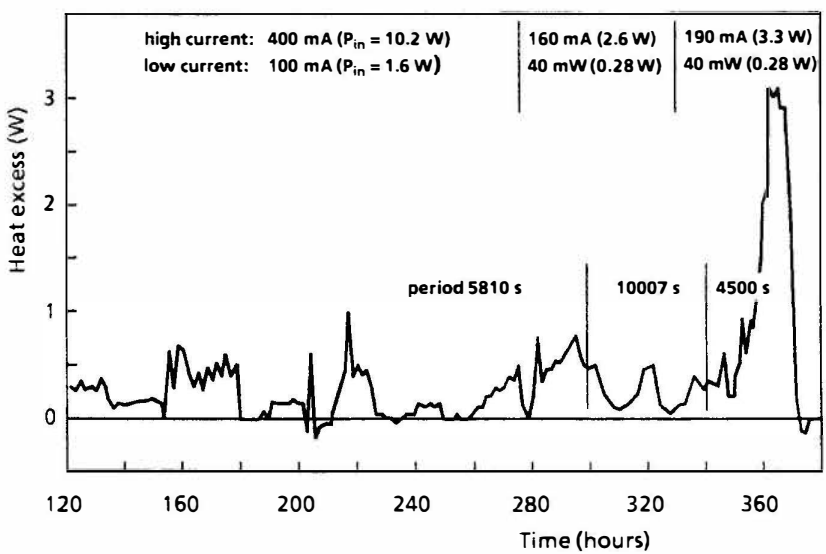

Figure 2. The HE in one of our runs as a function of time. Note that around hour 360 the maximum HE, of about 3 W, was obtained.

stopping the production of HE. The data presented show that the shorter periods are more likely to give HE.
2. In all our positive experiments we could find no significant correlation between the production of HE and the intensity of the electrolytic current. On the contrary, we found that the voltage across the cell is a significant parameter: we can measure an increase in time of the voltage across the cell, for the same current, and we find that HE is produced only when this voltage is high enough. In Fig.3 this correlation is shown. This "overpotential" can probably be related to the D/Pd ratio in the cathode.
3. We find that the permeation of gaseous D_2 in both directions through the cathode, thought as a membrane, during an electrolysis without HE, depends on the absolute value of the pressure on the gas side and on the electrolytic current intensity, with different values for high and low currents. When HE is present, we find that the gas preferentially goes into the cathode, and that there is no

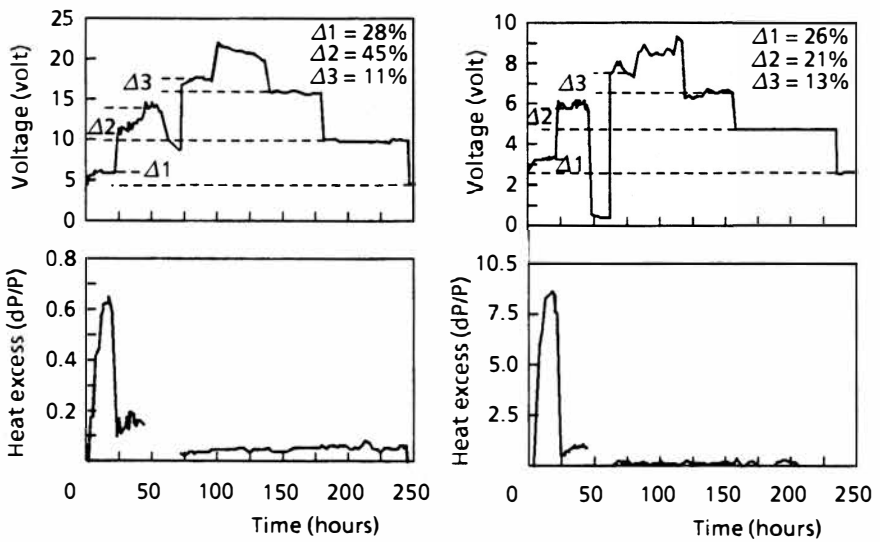

Figure 3. On the same time scale HE and voltage across the cell are reported for another run: the two graphs on the left refer to high current mode, those on the right to low current. The semi-period was 2500 s. Four current regimes were used (lo-hi): 7-50, 50-200, 100-400 and 150-600 mA/cm^2. Current was first increased and then decreased. In the last part of the graphs, where HE was negligible, the voltage is lower: the Δ's represent the "overpotential" when HE is produced. The lack of data for HE around hour 50 is due to misfunctioning of the acquisition system.

longer a difference in the gas flow between high and low current modes. An example of the two behaviours is shown in Fig.4.

3. Conclusions on the electrolysis experiments

The following conclusions can be drawn from this experiment:
- The production of HE in electrolytic cells with heavy water and palladium cathodes has been confirmed. The use of Pd anodes has presumably improved the quality of the surface, by regenerating it continuously, thus favouring deuterium charging of the cathode. The correlation of the overpotential with HE seems to indicate that the overpotential is a function of the D/Pd ratio.
- The novel geometry proposed, with the cathode facing on one side the electrolyte and on the other D_2 gas, permits to study the motion of D in Pd during electrolysis, by measuring the pressure variations on the gas side: a model tending to describe this motion and to correlate it to HE is presented in this Conference by two of us (ADN and VV).

4. ^{4}He separation

A first approximation cryostat has been realized, aimed to separate ^{4}He from other gases. The gas mixture to be processed flows through a "bed" with an extended surface kept at liquid helium temperature (4.2 K): on it all gases, with the exception of helium, will be condensed, with an extremely low residual vapour

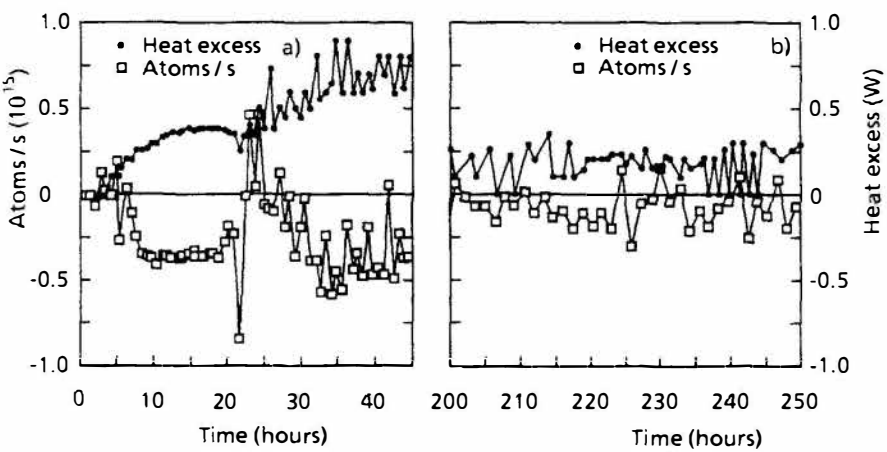

Figure 4. The flow of gas through the cathode, thought as a membrane, during electrolysis: positive values mean out of the cathode; negative, into the cathode. (a) Substantial HE is produced; (b) negligible HE is produced. Note that these data refer to the same run of Fig.3.

pressure. At the end of this cryogenic path, the uncondensed gas (helium) meets a plate coated with activated charcoal, in loose thermal contact with the 4.2 K bath: on it helium is totally adsorbed. The accumulated adsorbed helium can eventually be desorbed by heating the plate: the loose thermal contact prevents the rest of the cryostat from changing temperature. Typically, the charcoal coated plate can be brought to ≈ 40 K, while the rest of the cryostat does not exceed ≈ 6 K. The desorbed helium is then pumped through a mass spectrometer.

A test with atmospheric air has been performed with success, separating the ^4He in it contained ($5.4 \cdot 10^{-4}$%). Tests on the separation of ^4He from D_2 are in course.

Acknowledgments

The authors are grateful to Mess.rs D. Lecca, G. Lollobattista and F. Marini for their skilled cooperation in the costruction of the apparatus and in the execution of the experimental run.

Footnotes and References

a: Associazione EURATOM-ENEA sulla Fusione, Centro Ricerche Energia Frascati, C.P. 65 - 00044 Frascati, Rome, Italy
b: ENEA, Casaccia, INN/PCM;
c: ENEA, Casaccia, NUC/RIN.

1. Miles M.H.,Bush B.F.,Ostrom G.S.,Lagowski J.J., The Science of Cold Fusion, Proceedings of the II Annual Conference on Cold Fusion, Published by the Italian Physical Society, Bologna, Italy, pag. 363, 1991
2. Takahashi A.,Iida T.,Takeuchi T.,Mega A., to be published on J. Appl. Electromagnetics in Materials
3. McKubre M. , private communication
4. Johnson Matthey, Materials Technology U.K.

Cold Fusion Reaction Products and Behaviour of Deuterium Absorption in Pd Electrode

Tadahiko MIZUNO, Tadashi AKIMOTO, Kazuhisa AZUMI
Dept. Nuclear Eng., Fac. Eng. Hokkaido Univ.
Michio ENYO
Catalysis Research Center, Hokkaido Univ.

ABSTRACT

Excess heat generation from Pd electrode during cathodic polarization in D_2O-LiOD solution was investigated as a function of D/Pd loading ratio. The excess heat was observed when a Pd sample was filled with deuterium to D/Pd $\approx$ 0.90 by cathodic charging. The excess heat (H_{ex}) increased with D/Pd in an exponential manner ; the H_{ex} was of the order of magnitude of 0.1 watt/cm^2 at D/Pd $\simeq$ 1.0.

Experimental

Electrolysis was performed in a closed cell which was made of stainless steel and having a Pt black recombination catalyst located at the upper inner part of the cell. The lid of the cell accepted two with different area Pt anodes , Pd cathode, three temperature sensor connectors, a pressure gauge connector and a gas sampling port.

The cell was set in a constant temperature space which was surrounded by a water reservoir of $\pm$ 0.1 ℃ stability. The electrolyte was stirred by a magnetic stirrer which was set under the cell. Temperature was measured within 0.03℃ of accuracy by means of three digital voltmeters connected to each thermocouples (T.C.); these were fixed at various part in the cell. The other junctions of each T.C. were immersed in the water bath.

The temperature change during electrolysis was calibrated by operating two of Pt electrodes with various electric current. Experiments were performed at around 100℃ and current density of several hundred mA/cm^2.

FRONTIERS OF COLD FUSION

Experimental results

Figure 1 shows a change of D/Pd loading ratio, temperature and cell voltage during electrolysis with 0.2A/cm^2. The deuterium absorption process showed two steps; the first step occurred immediately after the start of electrolysis and the second step started when the loading ratio reached the value of β phase. The absorption rate in the second step was slower than the first step by two orders of magnitude.

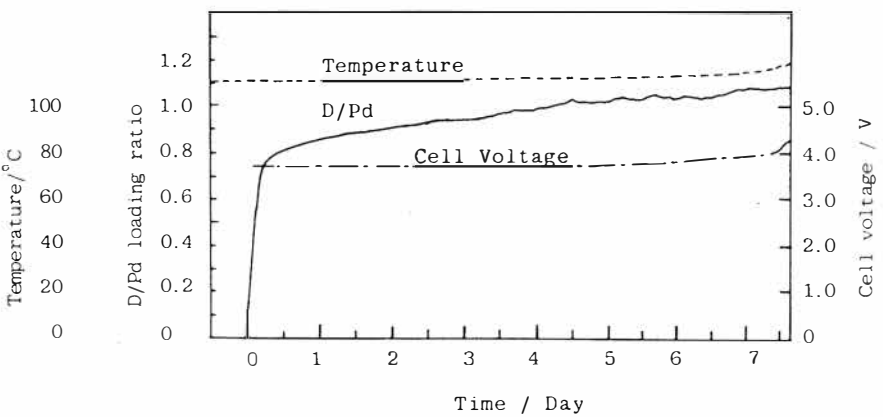

Fig.1 Changes of D/Pd loading ratio, temperature and cell voltage during electrolysis with 0.2A/cm^2 in 0.5 M/dm^3 LiOD solution.

The loading ratio attained after the slow step was completed was dependent on the electrolysis conditions such as temperature and current density. The D/Pd ratio reached 1.1 after 7 days of electrolysis. In this case, temperature and cell voltage started to increase after 7 days of electrolysis ; this may be caused by an increase of resistivity of the Pd metal due to high concentration of deuterium absorption.

The excess heat production was observed when the D/Pd ratio reached to almost unity; it continued and still increased with further increase of D/Pd ratio. The H_{ex} generation was apparently dependent on the D/Pd loading ratio, but not on

cathodic current density. The relationship between H_{ex} and D/Pd ratio was investigated by changing the temperature and the current density. After 7 days of electrolysis with $0.2A/cm^2$, the current density was increased step by step up to $0.4A/cm^2$, and at each steps it was kept for 7 days. The loading ratio usually reached to a constant value within a day.

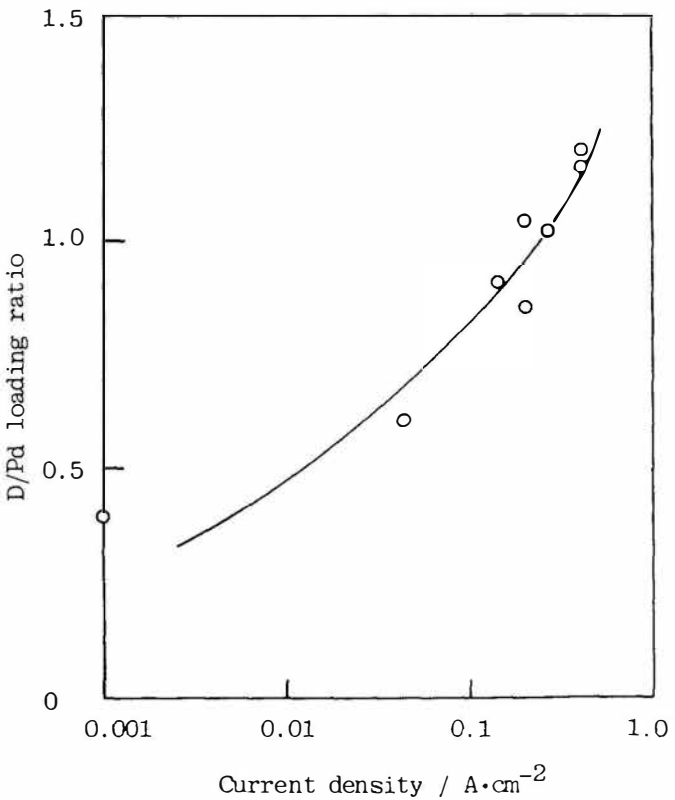

Fig.2 Effect of cathodic current density on the D/Pd loading ratio.

Figure 2 summarizes the effect of cathodic current density on the D/Pd loading ratio. The loading ratio of unity could be obtained by electrolysis of $0.2A/cm^2$ at 100℃. The D/Pd value at the lowest current density of $0.001A/cm^2$ showed a tendency to increase; the value shown in Fig.2 was obtained after 7 days.

Figure 3 shows the relationship between H_{ex} and D/Pd ratio obtained under various electrolysis conditions. The H_{ex} seems to increase exponentially with the D/Pd loading ratio, but its precise form is still not clear. The H_{ex} generation was $0.07\ w/cm^2$ when the D/Pd ratio was close to unity.

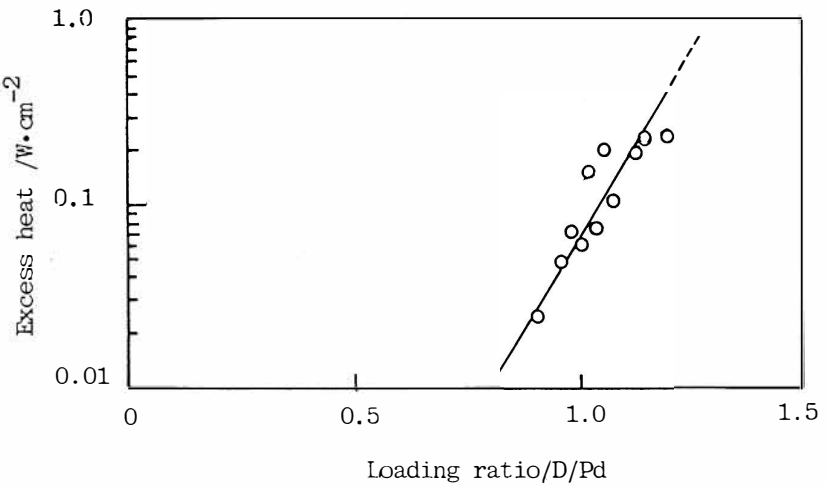

Fig.3 Relationship between H_{ex} and D/Pd ratio obtained under various electrolysis condition.

Observation of Excess Heat during Electrolysis of 1M LiOD in a Fuel Cell Type Closed Cell

Norifumi HASEGAWA, Keiji KUNIMATSU, *Tamio OHI, *Toshihisa TERASAWA.
IMRA JAPAN CO., LTD. *AISIN MATERIAL R&D CO., LTD.
2-3-6 Techno Park Shimonopporo, Atsubetsu-Ku, Sapporo 004, Japan
*5-50 Hachiken-Cho, Kariya, Aichi 448, Japan

ABSTRACT

Measurement of the excess heat generation during electrolysis of 1M LiOD has been conducted in a closed cell pressurerized by deuterium gas in which a fuel cell type gas diffusion electrode was employed as an anode, and a platinized platinum electrode served as the RHE for determination of hydrogen overvoltage at the palladium cathode. This has allowed us simultaneous determination of both excess heat generation and deuterium loading ratio, D/Pd, in the course of long term electrolysis which lasted for nearly two months.

Dependence of excess heat generation on D/Pd has been observed up to D/Pd = 0.88 with the maximum output/input ratio of 1.35. The minimum D/Pd to produce the excess heat has been found around 0.83-0.84.

Dependence of D/Pd on the overvoltage and the dependence of the excess heat generation on the D/Pd suggest that the dependence of the excess heat generation on the current density reported originally by Fleischmann and Pons and later by Storms can be interpreted in terms of the dependence of the loading ratio on the electrolysis current density. In other words, higher current density is necessary to maintain the high loading ratio.

1. Introduction

Since Fleischmann and Pons et al,[1] reported their observation of large amounts of excess heat during the electrolysis of heavy water with a Pd cathode, laboratories around the world have attempted to reproduce their results. It has been shown recently that the phenomenon of excess heat generation is closely related to achievement of deuterium loading ratio D/Pd greater than 0.9[2]. The purpose of the present investigation is to find the quantitative relation between excess heat generation and the deuterium loading ratio in the palladium cathode.

2. Experimental

2-1. Measurement of deuterium loading ratio

Electrolysis was conducted in a hermetically sealed cell containing 1M LiOD and pressurized by deuterium gas in which a fuel cell anode partially immersed in the electrolyte served as an anode as shown in Figs. 1 and 2. The gas diffusion layer of the fuel cell anode was modified by an additional composite layer made from PTFE membrane filter and a carbon paper to facilitate the deuterium gas supply through the layer when the anode is partially immersed in the electrolyte. The electrode reactions at anodes and cathodes are given by,

Anode $D_2 \rightarrow 2D^+ + 2e^-$.

Cathode $2D^+ + 2e^- \rightarrow D_2$ or $D_{(Pd)}$.

The over all reaction is given by $D_2 \rightarrow 2D_{(Pd)}$.

The deuterium loading ratio is determined from the D_2 pressure decrease after initiation of electrolysis and can be monitored in-situ throughout the electrolysis. The electrolysis was conducted by using Pd and Ni cathode (4mm ϕ × 18.5mm) at the initial pressure of 7Kgf/cm^2 by changing the current density between 50 and 1000mA/cm^2. The Pt/Pt electrode was placed dose to the cathode and this served as the RHE(Reversible Hydrogen Electrode) for the measurement of the hydrogen overvoltage at the cathode. The overvoltage reported in the present study has been corrected for the ohmic overvoltage which was measured by galvanostatic pulse experiment. After installation of the cell in the high pressure vessel, air in the vessel was evacuated and the cell was filled with D_2. Before electrolysis, the potential of the Pd electrode was kept 1000mV against the anode to avoid deuterium absorption into the Pd cathode.

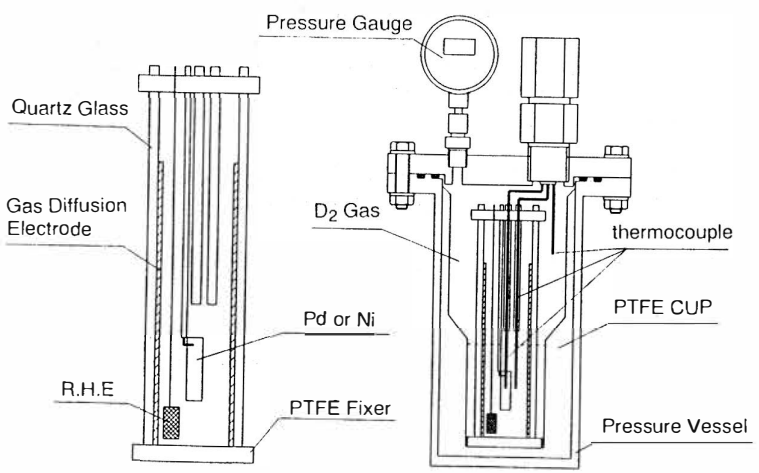

Fig-1 Electrolysis geometry

Fig-2 Structure of the pressure vessel

2-2. Detection of excess heat

Detection of excess heat at cathode was conducted by measuring the temperature rise in the cathode by a thermocouple inserted in it through a hole (1.5mm × 7mm) made at it's top. The temperature rise was first observed as a function of input power for the Ni cathode. The relation between the temperature rise and the input power thus observed served as a calibration curve. The Ni cathode was then replaced by a palladium cathode and the relation between the temperature rise and input power was measured. The estimation of the excess heat was conducted by comparing the temperature rise for a given input power

between the Ni and Pd cathodes. The cell was totally submerged in a water bath in which temperature was regulated at 10℃ or 30℃ ±0.1℃.

4. Result and Discussion

Figure-3 compares the relation between the temperature rise in the cathode and input power observed by Ni cathode, given by the straight line, and by Pd cathode. The calibration curve obtained by Ni cathode makes a good straight line while the data points observed by Pd cathode lie on the calibration line up to the input power of ca 1W, above which, however, they lie above the calibration line.

A similar experiment was conducted in 1M LiOH to see if the deviation of the palladium data from the calibration line demonstrated in Fig.3 is characteristic of the palladium/deuterium system.

Figure-4 shows the result obtained for the palladium/hydrogen system, in which there is a close agreement between the palladium data and the calibration line obtained by using a Ni cathode. We conclude from Figs.3 and 4 that the temperature change observed in the palladium cathode in 1M LiOD is caused by joule heating due to the input power as well as by additional excess heat generation in the palladium cathode. The excess heat generation calculated from Fig.3 are related to the deuterium loading ratio in ways as shown in Figs.5 and 6.

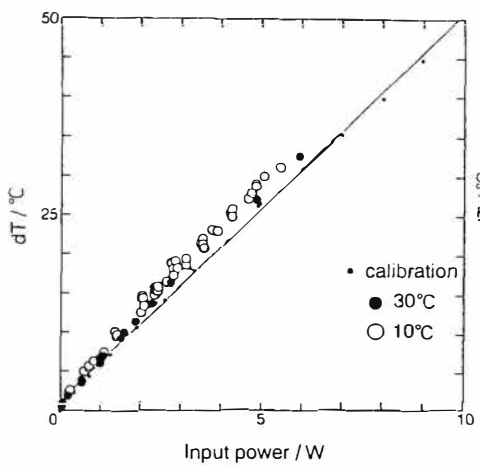

Fig.3 Comparison of the relation between temperature rise in cathode and input power observed with Ni and Pd electrodes in 1M LiOD.

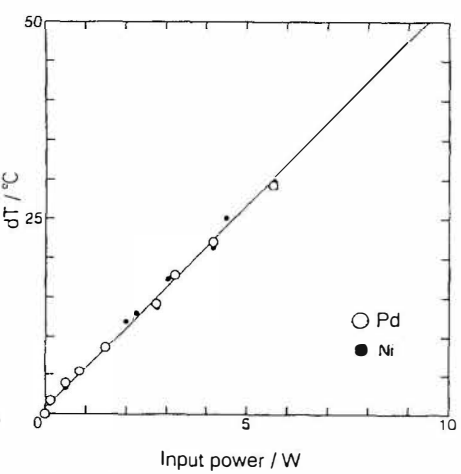

Fig.4 Comparison of the relation between temperature rise in cathode and input power observed with Ni and Pd electrodes in 1M LiOH at 10℃.

Figure-5 hows the variation of D/Pd and excess heat generation during the two months period of electrolysis. The excess heat generation started several days after the initiation of electrolysis and continued for over fifty days during which the electrolysis current density was varied between 50 and 1000 mA/cm^2 and the bath temperature was changed between 10℃ and 30℃.

The relation between loading ratio and the excess heat generation derived from Fig. 5 is shown in Fig. 6. The clear dependence of the excess heat generation on D/Pd is evident in Fig. 6. We can notice also that the critical D/Pd to give rise to the excess heat generation is around 0.83. The critical D/Pd value found in the present study is lower by

0.05 than that reported by SRI[2]. The origin of the different values of the critical D/Pd for the excess heat generation is not clear at the moment.

It could be related to the different methods employed for the determination of D/Pd, i.e, electrical resistivity measurement at SRI and pressure measurement during electrolysis using a fuel cell anode.

Figure-7 shows the dependence of the loading ratio on the overvoltage at the palladium cathode. At 30 ℃ (bath temperature) we can see a steady increase of the loading ratio with overvoltage, while change of the loading ratio is much smaller at 10 ℃ (bath temperature) in the current density range studied. It is evident from the dependence at 10 ℃ that higher current density is necessary to achieve D/Pd closer to unity. The relation between the excess heat generation and the current density reported originally by Fleischmann and Pons [3] and later by Storms [4] for the excess heat normalized for the unit surface area could be understood in terms of the overvoltage (current density) dependence of the loading ratio as shown in Fig. 7.

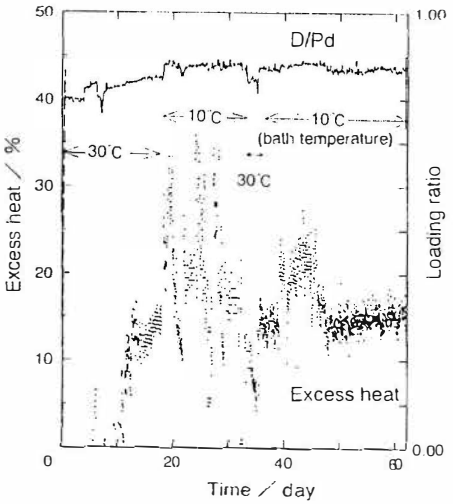

Fig.5 Change of loading ratio and excess heat generation in Pd during electrolysis in 1M LiOD.

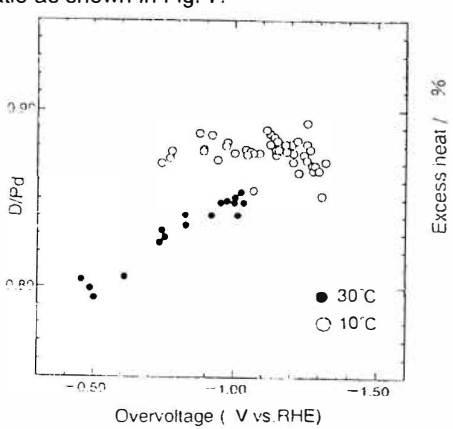

Fig.7 Dependence of deuterium loading ratio on overvoltage at 10℃ and 30℃ in 1M LiOD.

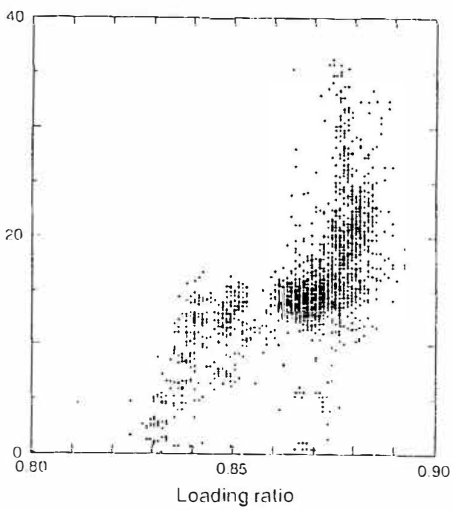

Fig.6 Dependence of excess heat generation on D/Pd in 1M LiOD.

5 Reference

(1) M.Fleischmann, S.Pons, J Electroanal.Chem., **263**,187(1989)
(2) Michael C.H. Mckubre Review of fatal accident at SRI January 2,1992
(3) M.Fleischmann, S.Pons, J Electroanal.Chem., **33**,332(1992)
(4) E.Storms, Fusion Technology. **433**,20,(1991)

On the Explosion in a Deuterium/Palladium Electrolytic System

Zhang Xinwei, Zhang Wushou
Institute of Applied Physics and Computational Mathematics
P.O.Box 8009, Beijing 100088, PRC
Wang Dalun, Chen Suhe, Fu Yibei, Fan Daxiao, Chen Wenjiang
Institute of Southwest Nuclear Physics and Chemistry

Abstract

An explosion in a D / Pd electrolytic system is analyzed, it is not chemical explosion but cold fusion reaction. A possible mechanism of cold fusion is suggested in this paper.

Keywords

explosion, cold fusion, Deuterium / Palladium electrolytic system

1. Introduction

Since the announcement of cold fusion by Fleishmann and Pons[1], there have been a lot of research works on D / Pd system in the world; a lot of explosion in D / Pd systems especially in D / Pd electrolytic systems have happened, the explosion happened at SRI International[2] was a famous one. It was suggested that explosion in D / Pd systems is caused by Oxygen / Deuterium recombination[2]. In our D / Pd electrolytic experiments, three explosions happened in April 1991, after measuring remains of an explosion, we induce another conclusion: explosion caused by cold fusion in Pd tube.

2. Electrolytic cell and explosion case

The electrolytic system was composed of a glass measuring cylinder (Φ25.5 $\times$ Φ23 $\times$ 186mm, $\sim$ 80ml), heavy water ($\sim$ 39cm^3), Pd tube (Φ1.67 $\times$ Φ0.67 $\times$ 80mm) cathod and Pt wire anode, a rubber plug of round platform (Φ27 $\times$ Φ21 $\times$ 22mm, $\sim$15.5g) stretched in measuring cylinder about 12mm and sealed the top of the cylinder but a blowhole(Φ3mm, gas could escape through it), the volume of gas above heavy water in the cylinder was about 33.3cm^3. The cell was placed in a water bath ($\sim$530ml light water in it).

There had been three explosions in these D / Pd electrolytic systems in April 1991. In two explosions, the rubber plug with Pd tube and Pt wire had

flown off about 1.5–2 meter away, the bottom of cell had been blown out, D_2O in cell had been mixed with H_2O in bath. Because no one on the scene of explosions, the tempeature of water in bath was measured about half hour after one explosion happened, it raised 5 ° C. Before the explosion, the applied voltage on cell was 7.5V and current was 260mA, it had been running for about 50 hours.

3. Explosion analysis

First, tempearture of 530ml water raise 5 ° C, it need $\Delta Q = 1.1 \times 10^4 J$ at least (conduction of heat is not concerned).

Second, as a result of simulation test, it need 2.1Kg force for the plug flying off, corresponding excess pressure $\Delta P = 5.12 \times 10^4 Pa$, it is to say that the minimum pressure in gas cylinder of cell is $1.53 \times 10^5 Pa$. Because of the electrolytic cell is a open system, the D_2 and O_2 gas producted in electrolysis can escape from the blowhole easily, so the excess pressure in cell can't accumulate generally; but, if only there is a lot of gas be producted in short time (τ) in cell and high excess pressure is formed, the gas can't escape through the small hole efficiently, so the rubber plug is pushed out and flying off, the bottom of cell is blown out resulting rocket action. Leading to this result, there are two possible cases:

<1> O_2 / D_2 recombination causes chemical explosion. Volume of gas cylinder in cell is $33.3cm^3$, calculating the release heat Q by the best O_2 / D_2 mixing ratio.

$$2D_2 + O_2 = 2D_2O + 67.8Kcal$$

Q = 281J. It is more less than the practical heat.

We consider another limit situation, the space above heavy water in cell is filled with O_2 gas and O_2 combines with D_2 gas released from Pd tube in short time to form water, the corresponding heat is 843J, it is only $\frac{1}{13}$ of the practical heat and this kind of heat can't heat up heavy water efficiently, so the practical explosion can't be caused by chemical reaction.

<2> Heat burst caused by cold fusion in Pd tube. Lots of heat released makes the tempearture of Pd tube raises thousands degrees and heavy water around it vaporized rapidly, the heavy water vapor makes the pressure in cell increases speedly and explosion happens.

We can estimate the upper limit of τ

$$\tau = \frac{L}{V_{eff}} = L\sqrt{\frac{\rho_0}{\Delta P}}\left(\frac{\Phi}{\Phi_1}\right)^2$$

where L = 8cm (height of gas cylinder), $\Delta P = 5.12 \times 10^4 Pa$, $\Phi = 2.3cm$ (inner diamter of the cell), $\Phi_1 = 0.3cm$ (effective diamter of hole), $\rho_0 = 0.0009g / cm^3$ (density of heavy water vapor of 1 atm).

the result is $\tau = 0.0579S$

the energy production rate is

$$P \geqslant P_{min} = \frac{\Delta Q}{\tau V} = 1.11 \times 10^6 W / cm^3 (Pd)$$

V is volume of Pd tube, $V = 0.147 cm^3$.

The heat burst in the explosion reached MW per cm^3Pd.

There had been an explosion in a D / Pd electrolytic system at SRI International on January 2, 1992 too, because it may be a close system and the parameters are complex, we can't reach clear conclusion on it, but it is possible that it was a cold nuclear fusion explosion too.

3. A proposal for mechanism of cold fusion

Where such large excess heat comes from? Why the heat mismatches products nucleus? it is puzzle for us and very difficult to explain within the domain of the physical and chemical knowledge now availabe, it is possible that new physics appear in it. Two year ago, the first author of this paper provided a hypothesis as follows[3]:

A small part of the rest energy MC^2 connected with the rest mass M of deuterium can be transformed directly into utilizable energy, this process called as RDTME can be written into the form that

$$D_1 + D_2 \longrightarrow D_3 + D_4 + \varphi \qquad \cdots(1)$$

in which D_i(i = 1–4) represent deuterons with rest mass M_i respectively, and ,

$$M_3 = M_1 - \Delta M_1, \qquad M_4 = M_2 - \triangle M_2 \qquad \cdots(2)$$

$\varphi = (\triangle M_1 + \triangle M_2)c^2 > 0$ is the energy which can be released as the kinetic energy of electron, deuterons and / or the energy of photon. It seems that the value of φ mainly distributes from 1 ev to 20 kev.

The reaction mentioned above takes place only under certain specific artificial circumstances with, especially, some kind of electronic screen. The condition under which F–P's cold fusion takes place is one of these specific artificial circumstances.

Furthermore, we suggest a possible mechanism of excess heat released in RDTME .

In PdDx , TiDx or other Deuterium / Metal system, when a free electron transits to a specific state in which the electron can screen the coulomb repulsive force between two D nuclei i.e. the electron comes into a bound state, the photon may be emitted. Due to some possible yet unknown relation between the electromagnetic interaction and the strong interaction, D nuclei may provide a energy $(\triangle M)\, c^2$ connecting with its rest mass M_D to the electron, then, the electron can get back to the initial state and emit photon again. This process may repeate several times under certain specifical conditions, as a result,the excess heat is released continuously.

We devided the screen state in which the electrons can get into two kinds: weak screen(w–s) and strong screen(s–s).When the electrons transit to w–s state, only lower energy photons are emitted without any traditional light nucleus fusion taking place; When the electrons transit to s–s state, besides the

energetic photons being emitted, various fusions of deuterium may sometimes be ignited. Obviously,the probability that the electrons get into w–s.state is much more large than that the electrons get into s–s state, so the production of excess heat is far more than that of the nuclear particles . Thus the puzzle of the huge mismatch between the excess heat and the nuclear reaction generating particles is solved naturally. At the same time, we may understand the possible correlation existing between the branching ratio of cold fusion and the temperature, pressure and other enviroment parameters in the PdDx or other Deuterium / Metal Systems.

The screening effect existing between two deuterons caused by the mobile electrons and deuterium ions D^+ in the lattice of PdDx etc. have been discussed in many papers. This effect can make the coulomb repulsive barrier weaker , then may enhance, perhaps greatly, the probability of fusion taking place between the low energy deuterons. But the screening mechanism have not yet explained the mismatch between the excess heat and the fusion products as well as the such large fusion rate obtained in the experiments.

Similarly to the reaction (1), the fusion reaction between protons and between proton and deuteron can take place too. That is to say, the light–water–electrolysis can also generate the excess heat in spite of small.

Reference

(1) M.Fleishmann, S.Pons and M.Hawkins, J.Electroanal. Chem. 261 (1989)301

(2) New Scientist January 11, 1992

(3) Zhang Xinwei et al.,

Ⅱ Annual conference on cold Fusion, June 29–July 4, 1991, Como Italy

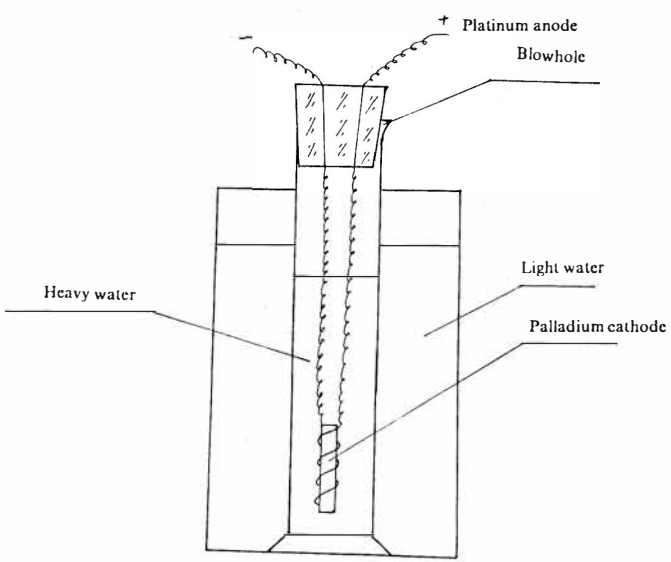

Fig.1 Experimental set–up

Measurements of D/Pd and Excess Heat during Electrolysis of LiOD in a Fuel-Cell Type Closed Cell Using a Palladium Sheet Cathode

Masafumi Kobayashi, Norio Imai, Norifumi Hasegawa, Akiko Kubota, Keiji Kunimatsu
IMRA JAPAN CO.,LTD.
3-6 Techno Park 2 Chome,Simonopporo,Atsubetsu-ku, Sapporo 004 Japan

ABSTRACT

Measurement of D/Pd and excess heat was carried out during electrolysis of LiOD in a fuel-cell type closed cell using two batches of palladium sheet cathodes. We applied the "saw-tooth" current mode and the following "L-H " current mode which was employed originally by Takahashi. Excess heat of 10-30% of input power was observed in experiment-A using a Pd sheet cathode that was one of the same batch used by Takahashi. But in experiment-B, the palladium sheet that was one of the different batch did not produce any measurable excess power. The saw-tooth mode and the L-H mode operation had no effect to enhance D/Pd.

1. Introduction

Takahashi,Iida,Takeuchi and Mega have reported [1] the production of excess power that exceeded 100 W/cm^3 in an open type electrolytic cell using a Pd sheet cathode. They suggested that the "saw-tooth mode" and the "L-H mode" operation might enhance D/Pd ratio more than 1.0 although measurement of D/Pd was not conducted in their study. We developed a fuel-cell type closed cell and the method of in-situ determination of D/Pd ratio during electrolysis.

The porpose of the present study is firstly to replicate Takahashi-type experiment in the fuel-cell type closed cell and secondly to investigate effect of saw-tooth and the L-H mode operation on the loading ratio. The results of simultanious determination of excess heat and D/Pd are reported.

2. Experimental

Fig.1 shows schematic view of the fuel-cell type closed electrolysis cell. A stainless steel pressure vessel was used with a PTFE cup fitted inside the vessel. Electrolyte was 150 ml 1M LiOD. The vessel filled with about 9 atm.D_2 was submerged in a water bath kept at constant temperature. A cold worked pure Pd plate (1mm thick 25 $\times$ 25mm) from Tanaka Kikinzoku Kogyo K.K. which was one of the same batch used by Takahashi was used in Experiment-A. A second similar Pd sheet which was prepared by the same method but is one of a different batch was used in Experiment-B. The Pd sheet

FRONTIERS OF COLD FUSION

cathode was supported by PTFE retainers as shown in Fig.1. Two sheets of gas diffusion type electrode (anode) were placed parallel to the Pd cathode. The minimum anode-cathode distances was 10mm(or 6mm) for both sides. Loading ratio, D/Pd, was calculated by measuring D_2 gas pressure and temperature. The electrolyte temperature was monitored by two thermocouples covered with PTFE tubes. Thermocouple-1(T-1) was located close to the upper part of Pd cathode. T-2 was placed at the middle point between the cathode(Pd) and anode. The calorimetric determination of excess heat was conducted by comparing the temper9ature rise in the electrolyte observed by Ni and Pd cathode respectively for a given input power assuming there is no excess heat generation for Ni cathode. We started the "pre-loading phase" with the "saw tooth current mode" between 0.25A and 4.0(5.0)A repeated every twenty minutes, which was continued for 7 days. From the 8th day we switched to the L-H current mode operation by changing the current between 0.25A and 4.2(5.0)A every six hours.

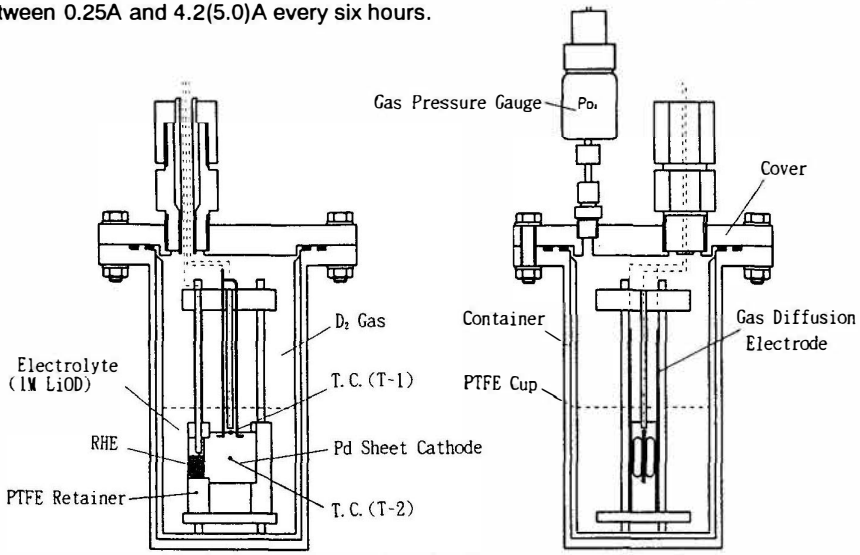

Fig.1 Fuel-cell type closed cell

Experimental conditions are shown as follows.

Table 1. Experimental conditions

	Experiment-A	Experiment-B
cathode material	Pd sheet 1st batch	Pd sheet 2nd batch
electrolyte	1M LiOD 150ml	1M LiOD 150ml
current	0.25A-4A 0.25A-4.2A	0.25A-5A
saw tooth cycle	20 min.	20 min.
saw tooth mode duration	1 week	1 week
L-H cycle	6 hr.	6 hr.
calibration	Ni sheet cathode	Ni sheet cathode
water bath temperature	20℃	20℃

3. Results and Discussion

Fig.2 shows D/Pd as a function of time during the electrolysis (Experiment-A). After

initiation of the saw-tooth mode operation, the loading ratio reached an almost constant value of 0.78 within two hours. The loading ratio remained constant for a week throughout the saw-tooth mode operation. On switching to the L-H mode operation, D/Pd varied between 0.77 and 0.79 during Low and High current mode period respectively. This suggests that the L-H current mode operation caused releasing and re-loading of deuterium. From the 13th day we changed the current of the L-H mode to 2A and 3.5A. And further, we changed the current to 1A and 3A from the 15th day. Then,D/Pd stayed almost constant at about 0.80.

Fig.3 shows solution temperature(T-1) as a function of time during the electrolysis (Experiment-A).The temperature does not reach its steady value during the saw-tooth current mode operation for a given current density due to its too short cycle time, while the electrolyte shows its steady temperature for the given current densities during the L-H current mode operation as shown in Fig.3.

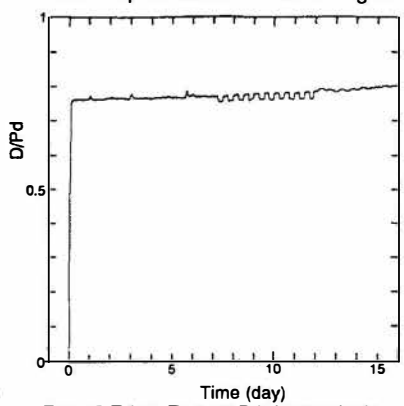

Fig.2 D/Pd vs. Time on Pd sheet cathode in 1M LiOD at 293K (Experiment-A)

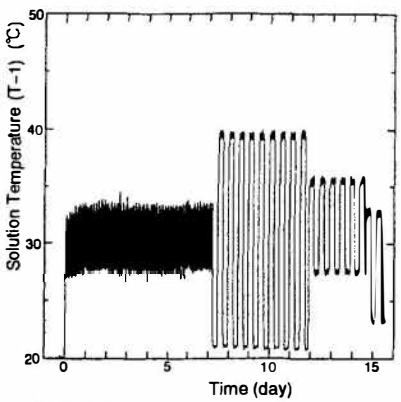

Fig.3 Solution Temperature (T-1) vs.Time on Pd sheet cathode in 1M LiOD at 293K (Experiment-A)

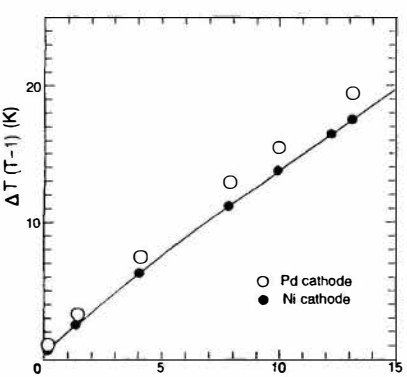

Fig.4 ΔT vs. Input Power on Ni or Pd sheet cathode in 1M LiOD at 293K (Experiment-A)

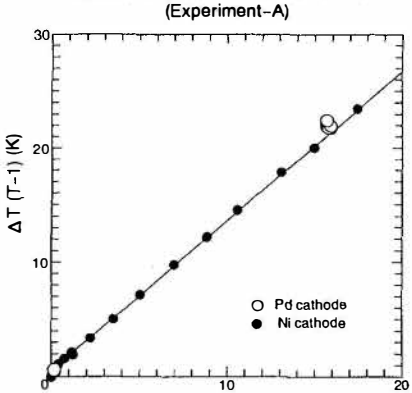

Fig.5 ΔT vs. Input Power on Ni or Pd sheet cathode in 1M LiOD at 293K (Experiment-B)

Fig.4 and Fig.5 show the relation between the change in solution temperature and input power for Experiment-A and B respectively. The relation is compared between the Ni and the Pd cathode . From Fig.6 and Fig.7 we conclude that excess heat of 10-30% with

respect to the input power was observed (Experiment-A), while there was no measurable excess heat for Experiment-B

In view of the low loading ratio around 0.80 in the present study, we further investigated effect of the way of holding the Pd sheet cathode by PTFE retainers on the loading ratio. The retainers hold the Pd cathode at the two edges making the edges of Pd umpolarized during electrolysis. The umpolarized edges may lead to release of deuterium during its loading. Fig.6 shows the H/Pd as a function of overvoltage ofserved in 1M LiOH in the absence and presence of the PTFE retainers. The Pd was hanging in solution by two Pd wires in the absence of the PTFE retainers. The higher H/Pd values were observed without retainers, which suggests that the unpolarised edges of Pd in the PTFE retainers are in fact releasing hydrogen while loading is going on at other parts of the Pd cathode.

We further investigated effect of the saw-tooth and the L-H mode operation on the loading ratio by observing the H/Pd under galvanostatic condition after the two succesive operations. Fig.7 shows the dependence of H/Pd on overvoltage observed at constant currents with and without the saw-tooth and the L-H mode operations before the galvanostatic steady state loading ratio measurement. No effect of preloading by the saw-tooth and the L-H mode operations was observed as shown in Fig.7.

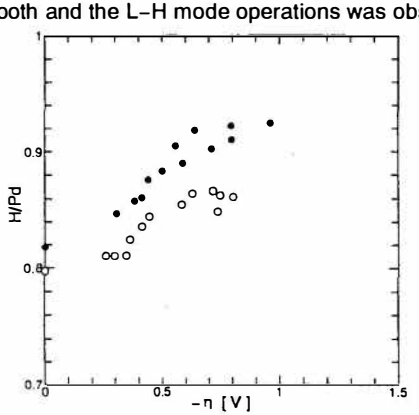

Fig.6 H/Pd vs. overvoltage on Pd sheet cathode with(○) or without (●) retainers

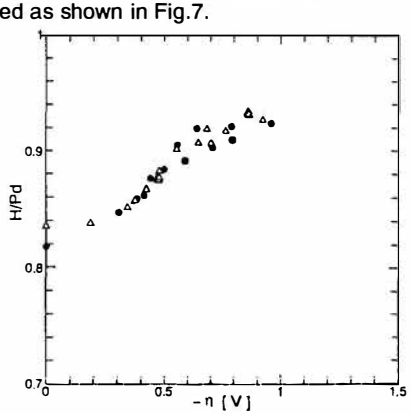

Fig.7 H/Pd vs. overvoltage on Pd sheet cathode with (△) or without (●) the saw-tooth and the L-H mode operation

4. Summary

The D/Pd ratio of 0.79～0.81 was observed on two batches of Pd sheet cathodes using the saw-tooth and the L-H mode operation. The low loading ratio suggests that the two modes operation has in fact little effect on improving the D/Pd.

Excess heat of 10～30% with respect to the input power was observed by only one of the Pd batches. The detection of the excess heat despite for the low D/Pd suggests that the two modes operation may lead to the higher local D/Pd than the average D/Pd on the Pd sheet cathode.

It is necessary to carry out further studies with better electrolysis geometry so that excess heat measurement can be conducted under higher D/Pd ratio.

5. References

[1] A.Takahashi, T.Iida, T.Takeuchi and A.Mega : Excess Heat and Nuclear Products by D_2O/Pd Electrolysis and Multibody Fusion, Submitted to International Journal of Applied Electromagnetics in Materials,1992.

[2] E.Storms , Fusion Technology, **433**,20,(1991)

Anomalous Heat Generation/Absorption in Pd/Pd/LiOD/D_2O/Pd Electrolysis System

Chi-Meen WAN, Swe-Kai CHEN, Chiao-Jiunn LINN, Chi-Yung LIANG, Chun-Jung LIN, Shuh-Biao CHU, and Chi-Chiao WAN

ABSTRACT

The annealed Pd cathode, which was deuterium-loaded for 3500 min, showed an anomalous heat generation. Anomalous heat absorption was regularly repeated from 4000th to 7500th min of deuterium loading in the same cell. The current density was 2700 mA/cm2. Total heat production was 0.3 to 3.3 MJ. Heat production of Pd per unit volume was 3.2 to 35.2 kJ/mm3. Total absorption was 22 kJ and absorption density was 217 J/mm3 in a typical absorption.

1.Introduction

Anomalous heat was reported by Pons and Fleischmann (1). Although it has been verified from many places, the reproducibility is still very poor. In the laboratory at National Tsing Hua University, Taiwan, the results are very similar. In more than 3 years, small excess heat has been characterized repeatedly(2). An anomalous heat in Pd /Pd/LiOD/D2O system was observed once at 2 pm on 28 December, 1991. There is another kind of phenomenon, anomalous heat absorption, which has not been reported, occurs repeatedly. Whether there is any relation between heat generation and absorption is very valuable to study, it is the purpose of this report to introduce the phenomena.

2.Experimental

Both cathode and anode are palladium wires with diameters of 3.2 & 0.35 mm, respectively. The surface area of the cathode is 2 cm2. Quartz tube with diameter 50 mm and height 100 mm is used as cell container. The containing D2O with 0.1M LiOD in the cell is 350ml, which is kept

FRONTIERS OF COLD FUSION

at constant level with an automatic D2O feeder. The charging current density is monotonically and stepwisely increased to 2700 mA/cm2 by a power supply until anomalous heat is generated.

The electrolysis cell is emerged in a water bath with a constant reference temperature. This temperature is kept by an Endocal RTE-220 Refrigerated Bath/Circulator (NESLAB; NH, USA). The RTE-220 bath is with a flow of 15 liters/min at 0 feed head and has a boost heater, which will come on if the bath temperature is 2.5 ℃ below the setpoint.

3.Results

I. The Phenomenon of Anomalous Heat Generation

Figs.1(a)-(b) show the records of cell and bath reference temperatures and DC power vs. time, respectively These figures show the anomalous heat. In order to assure that the anomalous heat was generated in the electrolysis cell, rather than from the bath, a similar experiment was performed. The bath temperature was suddenly increased to 100 ℃ to observe the response of the cell. The results is shown in Figs.2(a)-(b). The main difference between Figs.1 & 2 is the temperature change. There is a temperature decrease for bath on the left side of the peak in Fig.1(a), and for cell on the left in Fig.2(a). The temperature decrease before (ie, on the left of) a temperature peak is explained to be a resistance to temperature rise caused by another heat source. By this mechanism, one can assure that the temperature rise in Figs.1(a) & 2(a) were caused by a heat source in the cell and the bath, respectively. The generated heat in the cell shown in Fig.2(a) is at least 15℃x500ml+6.4℃x350ml = 77,240 Cal = 324,408 J. This would heat the water in the bath from 3509th to 3523-th min and from 85.4 to 100.4 ℃ (the 0.4 ℃ variation was an error recorded by computer). That is, the increasing rate of the bath heated by the cell is 1.07 ℃/min.

On the other hand, it can be calculated from Fig. 3(a) that the boost heater heats the bath water from 85.4 to 100.4 ℃ and from 3914 to 3933 min. The heating rate is 0.79 ℃/min. The heating rate by the cell is 35.7% higher than that by the boost heater. This means that the anomalous heat generated in the cell is at most 1086 W. (The heat generation for the boost heater is 800W.) Since the anomalous heat generation was from 3510th to 3560th min, the total heat generation in the cell is estimated to be at most 1086 W x 50 min x 60 sec = 3258 kJ. The size of palladium cathode is 3.2 mm in diameter, 20 mm in length. The volume of the cathode is 101.6 mm3. The unit volumic heat is thus from 3.2 to 35.2 kJ/mm3 if one assumes that the heat was totally generated by the cathode.

II.The Phenomenon of Anomalous Heat Absorption

Figs.3(a)-(b) show the records of anomalous heat absorption in the electrolysis cell. Fig.3(a) shows the temperature distribution in the cell (the upper three tangled curves) and reference temperature in the bath (the lower curve). The DC power, voltage, and current in the cell are shown in the upper, middle, and lower curves, respectively.

It can be seen from Fig.3(a) that the cell temperature decreases from 95 to 78 ℃ within 10 min and then recovers to 95 ℃. The reference temperature can rapidly drop by 4 ℃. These temperature drops occurred once every 500 to 600 min. The highest drop is 15 ℃. The anomalous heat generation and absorption happened in the same cell and the time interval between the heat generation and the 1st heat absorption is about 300 min. The typical heat absorption shown in Fig.3(a) is estimated to be

15 ℃ x 350 ml = 5250 Cal = 22,050 J.

The voltage and current were steadily decreased by a small rate until a temperature drop suddenly occurred and then increased to the original values (Fig.3(b)). The DC power drop for each cycle is about 10 W, ie, in 110± 5 W. For each drop, the dropping rate is more rapid than the temperature recovering rate. The dropping rate is at least 15℃/5min = 3℃/min. The unit volumic heat absorption is 22050 J/ 101.6 mm3 = 217 J/mm3.

4.Summary

In this experiment, a Pd/Pd/LiOD/D2O electrolysis system was used. The diameters of Pd for cathode and anode were 3.2 and 0.35 mm, respectively. In the case of quartz container, both anomalous heat generation and absorption were observed. The total heat production for anomalous heat burst in quartz container is calculated to be from 0.3 to 3.3 MJ and the unit volumic heat of Pd cathode is from 3.2 to 35.2 kJ/mm3. For heat absorption, the total heat involvement is 22kJ and 217J/mm3. The current density was 2700 mA/cm2.

The financial support of NSC, Republic of China, and National Tsing Hua University, to this work is gratefully acknowledged.

5. References

1. M.,Fleischmann, S.Pons, and M.Hawkins, J. Electroanal. Chem. 261 (1989) and 263 (1989).
2. C.S.Yang, C.Y.Liang, T.P.Perng, L.J.Yuan, C.M.Wan, and C.C.Wan, Proc. Cold Fusion Symp., 8th World Hydrogen Energy Conf., Honolulu, Hawaii, July 22-27, 1990, p.95, University of Hawaii.

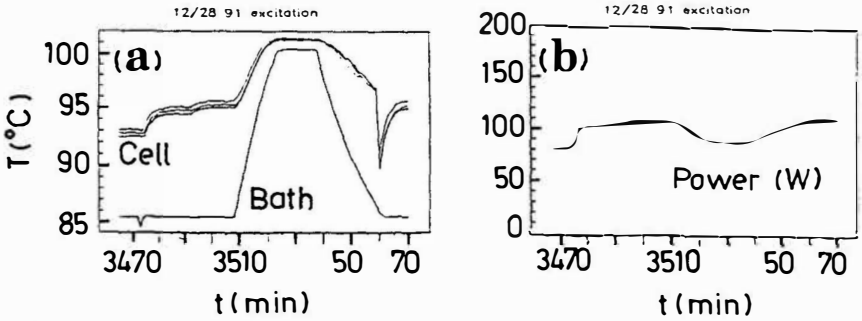

Figure 1. Records of System Temperature Increase (a) and Applied DC Power (b). (by heat generated in cell.)

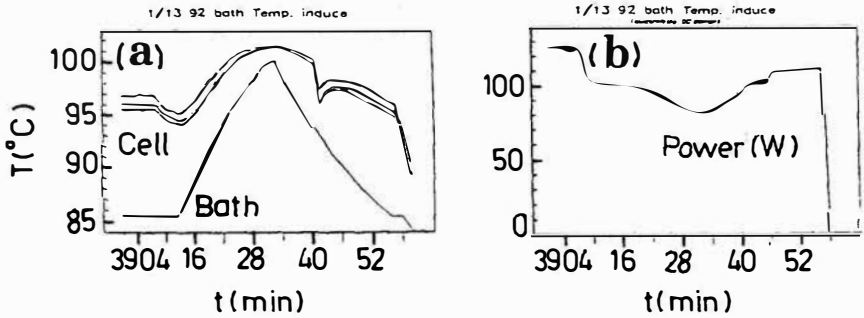

Figure 2. Records of System Temperature Increase (a) and Applied DC Power (b). (by boost heater.)

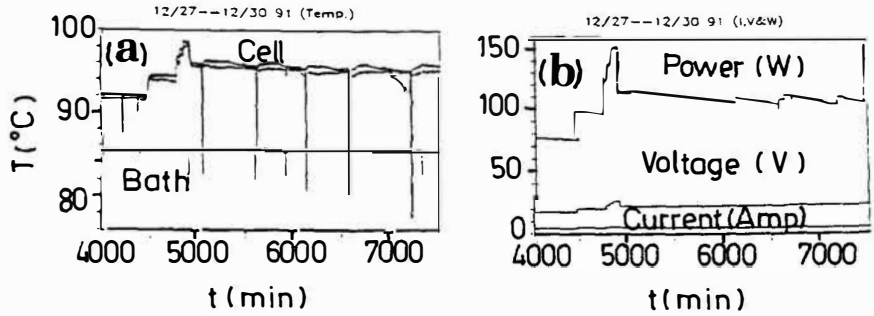

Figure 3. Records of System Temperature Drop (a) and Applied DC Power, Voltage, and Current (b) During Heat Absorption Inside the Cell.

Periodically Current-Controlled Electrolysis of D_2O/Pd System for Excess Heat Production

Hiroyuki MIYAMARU and Akito TAKAHASHI
Department of Nuclear Engineering, Osaka University, Yamadaoka, 2-1, Suita, Osaka, JAPAN

ABSTRACT

For the purpose of clarifying the correlation between current density and excess heat production in the D_2O/Pd electrolysis, a new measurement system with an open type calorimeter was constructed. An electrolysis cell was specially designed and applied current was changed every few hours. Some palladium plates were electrolyzed with various current densities. A slight excess heat was observed during step-up mode electrolysis of the palladium plate called the 1st batch. No excess heat was observed with other palladium plates. Though the relation between applied current patterns and excess heat level was not clear, this study suggests that palladium material feature has an important role in excess heat production.

Introduction

It has been suggested[1] that excess heat occurs near surface of Pd cathode. However, the correlation between current density and excess heat level is not clearly understood in the recent studies of cold fusion phenomena[2),3)]. The purpose of this study is to find a critical current density and appropriate current patterns which may trigger the excess heat production or enhance Pd/D ratio in palladium cathode. In the electrolysis, applied current is dynamically changed every few hours to scan various current densities. An open type calorimeter is specially designed to obtain rapid thermal response of the applied power. Multi-point measurement system is also established for the accurate

FRONTIERS OF COLD FUSION

evaluation of heat level.

Experimental

Figure 1(a) shows the illustration of an open type calorimeter for an electrolysis cell (D_2O/Pd + 0.3 mol/l LiOD). The cell and the measurement system are specially designed for the periodic electrolysis. An external cooling apparatus is installed to obtain rapid thermal response of the calorimeter. The temperature of water coolant is controlled to be 20°C±0.05°C. The influence of thermal gradient is minimized by a mechanical stirrer and multi-point measurement. Three thermocouples are installed to monitor electrolyte temperature at the top, middle and bottom of electrolyte. Another two thermocouples are installed in the inlet and outlet of cooling glass tube. The difference of coolant temperature is monitored to cross-check heat level. All the thermocouples are sealed with teflon coating.

The electrode assembly is shown in Fig. 1(b). The cathode is palladium plate (25mm x 25mm x 1mm) that was supplied by Tanaka Kikinzoku Kogyo K. K.. The anode is platinum wire mesh (25mm x 40 mm, 50 meshes/inch) that is attached on both sides of the cathode with 6mm spacing. This mesh anode is intended to uniform the deuterium charge into the palladium sheet. This assembly is set in the central part of the cylindrical cell.

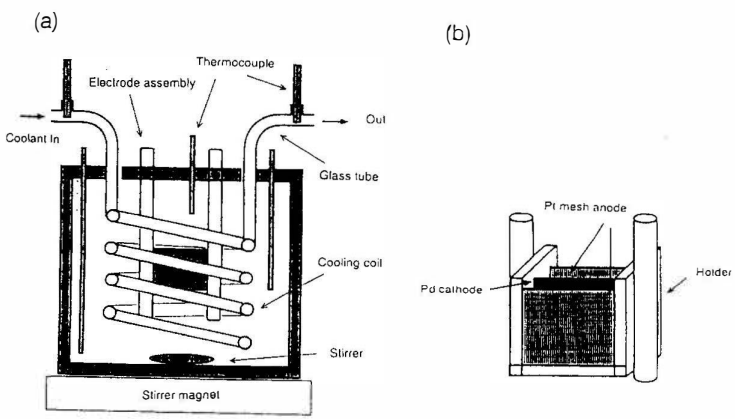

Fig.1(a) Cross sectional view of the calorimeter.
(b) Electrode assembly with an acrylic holder.

A gold plate is substituted for the palladium cathode and electrolyzed to obtain a calibration curve from 0.4 W to 120 W. Another calibration curve is obtained from the difference of the coolant temperature

between inlet and outlet. Measured temperature is converted into heat power level.

Results

Some palladium plates called the 1st, 2nd and 3rd batch were studied using this calorimeter and current patterns were changed respectively.

(a) Low-High electrolysis mode (L-H mode)

The palladium sheets of the 2nd and the 3rd batch were loaded with deuterium by L-H mode. Low current (30 mA/cm^2) and high current (300 mA/cm^2) were applied alternatively in each 5 hours interval. The amplitude of the input power ranged from 0.4 W to 60 W. Figure 2 shows the experimental result of L-H mode. Measured electrolyte temperature was converted into output power by the calibration curve. The bar shown in the figure indicates the output power including ±1 watt error level of this system and broken line indicates input power. No excess heat was observed with each palladium batch during one month run.

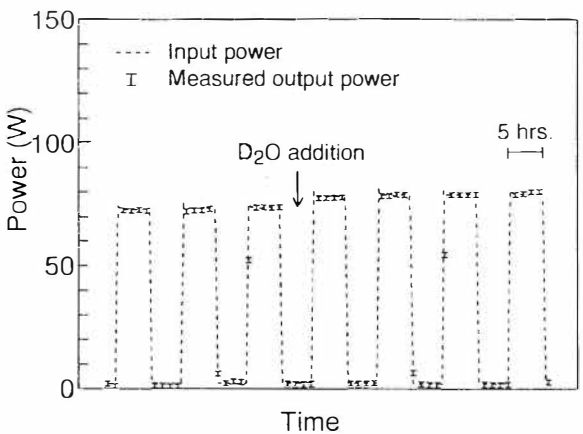

Fig.2 Experimental result of L-H mode (3rd batch)

(b)Step-up mode

Step-up mode electrolyses were performed for the 1st and the 3rd batch Pd cathodes. The current density was stepped up with 2 hours interval from 30mA/cm^2 to 400 mA/cm^2 in 6 steps and this cycle was repeated. One of the experimental results of step-up mode electrolysis is shown in fig. 3. A slight excess heat was observed during the electrolysis of the 1st batch Pd. Excess heat level was about 2 W (3 % excess

level). However, no excess heat was observed with the 3rd batch.

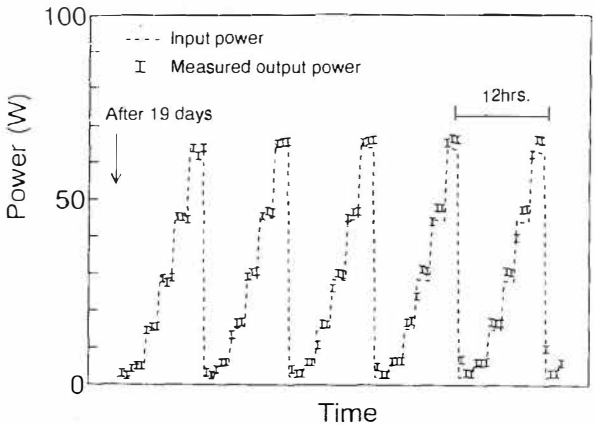

Fig.3 Experimental result of step-up mode (1st batch)

Conclusion

Cell temperature was slightly different at each point. This shows that thermal flow is produced by the bubbling, stirring and thermal conductivity effect in the cell. Since thermal flow path becomes unstable due to turbulent flow in electrolysis for long run, multi-point temperature measurement should be needed and total heat level must be calculated by the integrating heat levels at various points in the cell, so as to make calorimetry in precision.

Slight excess heat was observed during one month electrolysis by using the 1st batch palladium. Although the 3rd batch was treated with the same way of the 1st batch, no excess heat was observed. The relation between applied current density and excess heat production has not been clarified. On the experiments using the 1st batch and the 3rd batch, it is suggested that palladium material feature will have a important role in excess heat production. Qualification of Pd metal fabrication should be established to obtain systematic excess heat data.

Reference

1) E. Storms, Fusion Technology, 20, 443 (1991).
2) A. Takahashi et al., Int. J. Appl. Electromag. Mat. 106, 1-10 (1992).
3) M.C.H. McKubre et al., "The science of cold fusion" Proc. ACCF2, p419-443 (1992).

Some Lessons from 3 Years of Electrochemical Calorimetry

Michael E. MELICH
Physics Department Naval Postgraduate School
Monterey, Califomia 93943-5000 USA

Wilford N. HANSEN
Physics Department Utah State University
Logan, Utah 84322-4415 USA

Abstract

An analysis of the time series data from the 16 Harwell FPH electrochemical cells is being conducted. Using generally accepted calorimetric principles and detailed numerical analysis, the behavior of "cold fusion" output data is used to estimate the instrumental sensitivity and the time varying accuracy of the results of the experiments. In Harwell's D_2O Cell 3 there are more than ten time intervals where an unexplained power source or energy storage mechanism may be operating. A comparison to a previous analysis of Pons and Fleischmann data is made.

Introduction

With the cooperation of Harwell and its research team, Williams et al[2], we have obtained copies of the digital data, laboratory notebooks, and other records of the 1989 Harwell electrochemical calorimetry experiments on "cold fusion". With this information we have been able to explore the characteristics of their experimental design and their data thereby developing insight into the quality of the experimental results. These results are briefly compared to results of Hansen's [1] similar analysis of Pons and Fleischmann data.

Conclusions

- Characterizing the Instruments. Harwell's extensive variations in the timing and magnitude of the calibration heater power and the electrochemical current/voltage pose a robust test of models of the electrochemical calorimetry instrument.
- Experimental Protocol and Interpretability. The regularity of the experimental protocol used by Pons and Fleischmann as reported at ICCF2 by Hansen[1] produces significantly less ambiguity in interpretation of experimental results than those used by Harwell.
- Extractable Information. Regression techniques for estimating parameters in mathematical models can be applied to the Harwell data to extract more information than presented by Williams et al [2].
- Reliability of Data Sets. Not all operating regimes captured in the Harwell data can be described by the available models. However, performance over extensive time intervals are well described and can be used to accurately estimate heat transfer coefficients, anomalous power values, and experimental uncertainty.

FRONTIERS OF COLD FUSION

• Anomalous Power in Cell 3. Heavy water Cell 3 showed a marked temperature rise on more than ten occasions while its light water control Cell 4 showed no such rise. The power required to generate these increased temperatures is 100-200 mW. The input power to the cell was generally less than 1500 mW. The calorimetric error during these periods was approximately 1%.

Data Screening and Parameter Estimation

We have found in studying the Harwell data from their FPH cells that the accuracy to which they can be analyzed varies greatly from cell to cell and within a given cell. We have found that an effective way of finding "good" regions, i.e., those with small fluctuations in the estimated parameters, for analysis is to calculate the conductive heat transfer coefficient Kc using a "sliding" window of , say, ten points(30 min), which is moved over the entire time history of the cell. For this the excess heat, Qf, is temporarily assumed to be zero.

Plots of such running Kc values are shown in Figure 1a for heavy water Cell 5 and in Figure 1b for light water Cell 14. Cell 14 is obviously much better behaved

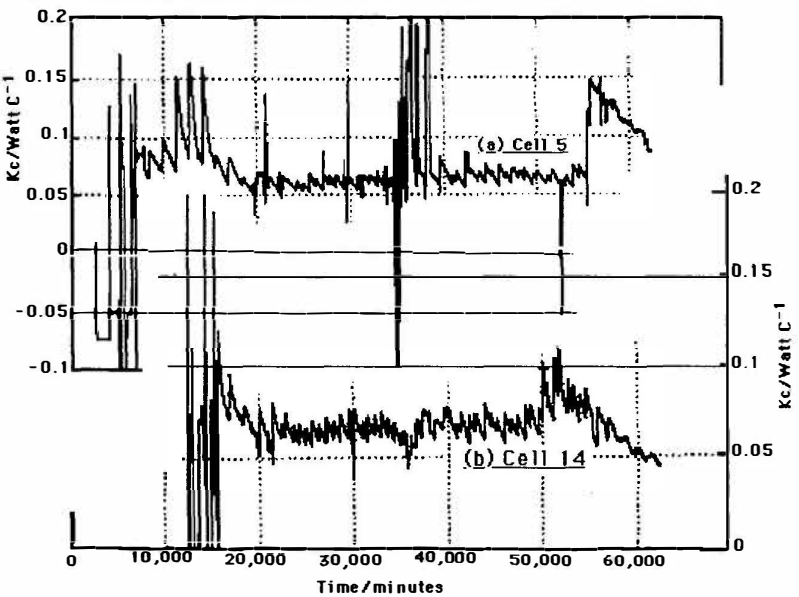

Figure 1. Thirty minute "sliding window" estimates of the conductive heat transfer coefficent for: (a) 41 days of operation of D_2O Cell5; (b) 36 days of operation of H_2O Cell 14.

than Cell 5. Ideally, Kc should remain constant. The large change with electrolyte height, the "tidal effect", is easily understood. The tidal variations and especially the wild gyrations are simply due to poor cell design and function.(Effects on performance and virtual elimination of the tidal variations in Pons and Fleischmann redesigned cells is described in Hansen[1].) Fortunately there is an abundance of FPH data, including many calibration pulses of known power. Sometimes the equations(Pons and Fleischmann equations are used here) don't fit the large changes in current and heater power, presumably because stirring ceases to be adequate or some other control breaks down. These regions become obvious from a study of

apparent Kc behavior. But where Kc is somewhat misbehaved the fit is good and a non-zero Qf would show up clearly.

These observations are illustrated in the Figure 1 and Table 1. Cell 14 is fairly well behaved from data point 5,500(18,850 min) out to 15,800(49,750 min). The many pulses and current gyrations in this region are well accommodated by the equations. In Cell 5, however, there are several regions where a reasonable fit cannot be achieved. It is simply fruitless to attempt fits in these regions. The data are faulty. Fits can still be had in good regions.

Table 1 shows the results of least squares optimization over various time intervals with simultaneous fitting of Kc and Qf. By choosing regions with calibration pulses and by avoiding a few bad regions, Qf can be determined to within about 0.01 watts. This is an order of magnitude better than the original analysis of these data presented by Williams[2].

Table 1. Estimated Kc and Qf for H_2O Cell 14. (Kr = 5×10^{-10} watts deg^{-4})

Time/minutes	Kc/Watts C^{-1}	Qf/ Watts
18,850-21,850	0.0659	-0.0072
20,500-23,350	0.0676	0.0028
23,350-25,350	0.0649	0.0091
29,350-32,350	(Failed to converge,	no good calibration pulse.)
33,850-36,850	0.0766*	0.0621*
38,350-41,350	0.0688	-0.0083
18,850-35,350	0.0682	0.0143
18,850-62,350	0.0698	0.0064
41,350-62,350	0.0757**	0.0206**

* Suspect estimates, see Figure 1.

** Data beyond 50,350 min is suspect, yet the estimate for average Qf is within 2% of zero.

Anomalous Power in Cell 3

Harwell Cells 1, 2, 3, and 4 were wired in series to a constant current source. Odd numbered cells had D_2O, even numbered cells H_2O. The Pd cathode of 6mm diameter by 10 mm length was in 0.1 molar NaOD in Cell 3 and 0.1 molar NaOH in Cell 4. Figure 2 shows a section of time series data covering the period 10,000 minutes to 30,000 minutes. The data collection started at 2,350 minutes and a 198 mA current was first applied at 2,632 minutes.

Compare the behavior of the temperature and input power traces for Cell 3 with those of Cell 4 starting at time 13,918 min, where the Cell 3 voltage jumps by 80 mV(not shown) and its temperature begins a much faster rise. The temperature rise is halted with the refilling of Cell 3 at time 14,197 min, which produces a voltage increase of 26 mV, while Cell 4 is refilled at 14,212 min producing a voltage drop of 39mV. The temperature change for Cell 3, T(14,197) - T(13,918) = 31.84 - 30.47 = 1.37 C; compare to Cell 4, T(14,212) - T(13,918) = 26.16 - 25.96 = 0.20 C. That is, over the same nearly 3 hour interval with the same electrical current in the same bath but with different electrolytes, Cell 3 experienced a 1.37/.20 = 6.85 greater temperature rise than Cell 4.

Subsequent to Cell 3's rapid temperature rise at 13,918 minutes it experiences a sequence of over 10 similar increases during the next 9 days. Throughout these anomalous increases in temperature in Cell 3, Cell 4 behaves "normally", i.e., it suffers no unexplained pulses of energy. Our initial estimate of the power associated with these anomalous temperature increases is 100-200 mW. The electrolytic current was under 300 mA and the potential was less than 5 V. There are calibration pulses which occur during these events. Further analysis of this data is warranted and underway.

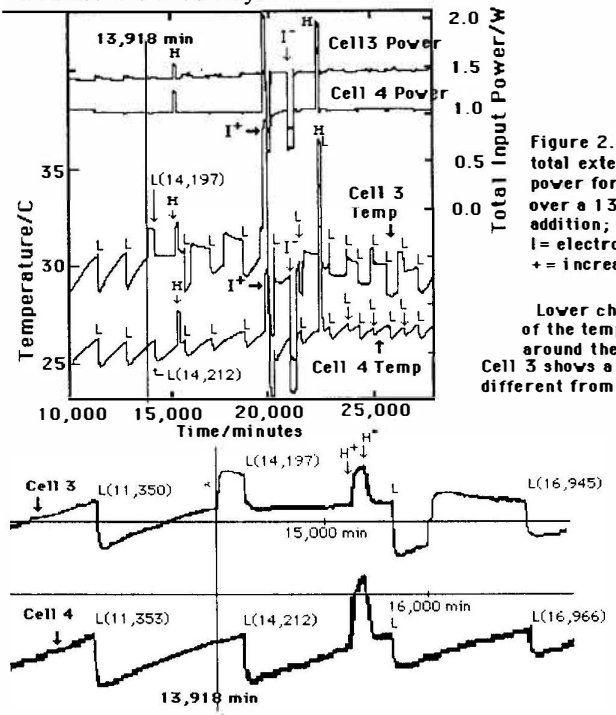

Figure 2. Temperature and total externally supplied input power for D_2O Cell 3 and H_2O over a 13 day period. L= liquid addition; H= heater pulse; I= electrolytic current change. + = increase; - = decrease.

Lower chart is an expansion of the temperature time series around the time 13,918 where Cell 3 shows a rise in temperature different from Cell 4.

List of Symbols/Nomenclature

Kc - Conductive heat transfer coefficient, W/degree C

Kr - Radiative heat transfer coefficient, W/degree C^4

Qf - Excess Heat, W

Points - Data point set, collected every three minutes in Harwell experiments

T(14,198) - Temperature at time 14,198 since starting time of Harwell experiments, may not be from starting time of particular Cell

L; L(19,128) - Liquid addition; at the particular indicated minute, e.g., 19128 minutes

References

1. Hansen, W.N. , 1992, *Proceedings of the II Annual Conference on Cold Fusion, Vol. 33 of the Conference Proceedings*, The Italian Physical Society, Bologna, p.491

2. Williams, D.E., et al, *Nature*, 342 (1989), 375

A Potential Shuttle Mechanism for Charging Hydrogen Species into Metals in Hydride-Containing Molten Salt Systems

Bor Yann LIAW[1] and Bruce E. LIEBERT[2]
Hawaii Natural Energy Institute[1] and Department of Mechanical Engineering[2], University of Hawaii, 2540 Dole St.
Honolulu, HI 96822, USA

ABSTRACT

This paper proposes a "shuttle mechanism" in the hydride-containing molten salts under severe charging conditions. Our previous work reported that the use of elevated-temperature deuteride-containing molten salts promises great potential for charging deuterium into metals for excess heat generation. Substantial excess heat was measured occasionally but was difficult to reproduce, which reduced the prospect of this technology. We believe an understanding of the reaction mechanism is critical for reproducibility.

The proposed "shuttle mechanism" is based on the interpretation of the polarization behavior for various cell operating conditions. An attempt has been made to understand the reaction(s) responsible for the excess heat generation in spite of the complexity of the electrochemistry of this molten-salt system compared to heavy-water electrolysis. We examined the oxidation potentials reported in the literature and compared with results obtained from polarization techniques.

1. Introduction

The reducing environment of the eutectic LiCl-KCl system incorporated with excess LiH has been proposed [2] for preparing "hydrogen-transparent" interfaces to enhance metal-hydrogen interactions without interference from surface oxides. It is particularly important for base metals, e.g. Ti, V, Nb, and Zr, that usually have oxides. The narrow stability of LiH at very reducing potentials is shown in Fig. 1. This narrow stability window of LiH, on the other hand, provides an additional potential range suitable for imposing a high hydrogen activity on metals, as the shaded areas in the figure show. We call this regime the "Window of Opportunity for Excess Heat (WOEH)." The lower limit of the WOEH starts from the reversible D^-/D_2 potential where the hydrogen partial pressure is 1 atm at the particular temperature. The upper limit is constrained typically by the chlorination of the specific metal.

The redox potential for metals in the eutectic LiCl-KCl system has been reported in the literature [6,7,9]. This information, although for equilibrium conditions, is useful for interpreting reactions during the

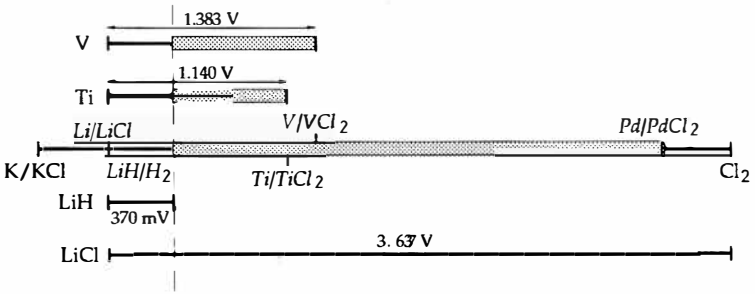

Figure 1. Immunity of V, Ti, and Pd in the molten salt melt at 700 K. The shaded areas represent the "Window of Opportunity for Excess Heat" (WOEH) for V, Ti, and Pd, respectively.

charging conditions and for selecting materials for molten salt cells. Pd exhibits a wide range of stability and thus has an optimal WOEH.

We reported two intriguing events of excess heat production using molten salt techniques [3-5]. Thermochemical considerations cannot explain the excess heat anomaly. ^{4}He enrichment found in the deuteride sample [3] seems to support the results reported by Bush et al. [1]. However, the complexity of the molten salt system causes difficulty in reproducing excess heat on demand. We believe a understanding of the electrochemical behavior of the molten salt system will help us achieve reproducible excess heat generation.

2. Methods

A typical molten salt cell comprises:

"LiAl"/Al | LiCl-KCl eutectic, excess LiD(H) | M; M=Pd or Mo.

The "LiAl"/Al mixture services as a secondary reference electrode as well as a Li reservior, while the choice of Pd or Mo depends on the need for D(H) absorption. The cell was operated in a controlled argon atmosphere with minimal oxygen and moisture content. Voltammetry was conducted using a PARC 173 potentiostat with a PARC 175 Universal Programmer or a HP-3325B Synthesizer/Function Generator.

3. Results

Fig. 2 is a cyclic voltammogram which displays a concentration dependence of the polarization behavior in a semi-quantitative manner. The relative concentration was calculated from the charge (by integrating the current over the time) involved during the polarization cycles. This result demonstrated that a continuous cycle has a noticeable effect on the polarization behavior at high potentials as LiD became depleted in the melt. Table 1 lists a series of possible reactions and their potentials obtained from the thermodynamic data [4].

4. Discussion

As we considered a number of possible reactions we found that:

1) Pd tends to evolve, rather than absorb, hydrogen, according to the reversible cell potentials. However, under a low-current-density charging, the absorption and hydride formation dominate, attributing to

overpotentials associated with each process.

2) The cyclic voltammogram (Fig. 2, curve a) displays two distinct peaks: one located at -307.7 mV and the other at about 150 mV vs. an "LiAl"/Al reference. The peak at -307.7 mV is assigned to the reversible Li^+/Li reaction, similar to that reported by Wen et al. [8]. The peak at about 150 mV is assigned to deuterium gas evolution (expected at 106.7 mV at 648 K). The gas evolution is almost irreversible, as expected, since no reverse peak is found. The curve also exhibits curvatures for activation and transport-limiting regimes, respectively.

3) According to the redox-potential series, we assume the cell reactions varied with LiD concentration in the melt, resulting in various chloride formations. The formation of $LiAlCl_4$ was expected at about 1.1 V. We detected Al deposition on Pd using the SEM/EDX technique. Al seems to result from a further oxidation of $AlCl_4^-$ at the anode. $ZnCl_2$ formation was next to follow, as Zn was also detected on the Pd surface by SEM/EDX. The Zn deposition might follow a similar route as $ZnCl_4^{2-}$ being oxidized to Zn on the Pd anode at potentials higher than 1.73 V.

4) The $FeCl_2$ formation occurs at about 2.02 V, while the $FeCl_3$ formation is at a higher potential of about 3.10 V. Fe was an impurity introduced by the current leads. The two reactions exemplify the corrosion of leads in the melt, which often caused failure of the cell.

5) Finally, an interesting shuttle reaction depicts the conversion of deuteride into deuteron at a potential higher than 2.148 V. The presence of the deuteron under the charging condition could lead to an intriguing consequence at the anode. This situation suggests that a substantial polarization could result in a high concentration of D^+ at the anode and D^- at the cathode. The influx of D^- accelerated by the strong electric field to impact the concentrated D^+ at the anode might have an unpredictable but significant effect on the excess heat production. One may also consider a dynamic shuttle process of which deuteride was stripped into deuteron at the anode and subsequently converted back to deuteride at the cathode.

From our reported polarization behavior in the excess heat events [4,5], we identified a possible scenario that corresponds to the excess heat process. Due to a similar cell resistance as to what a LiD-saturated cell exhibits, we conclude that the transport property of the cell after a long charging remained similar to the original; however, the reversible cell potential changed to about 1.995 V.

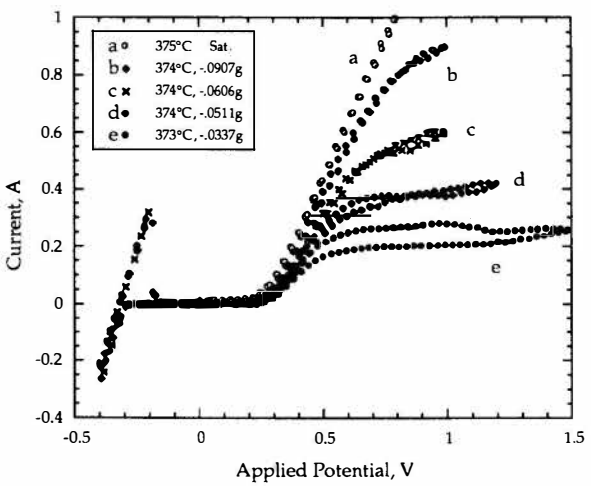

Figure 2. Polarization curves of an Al|LiCl-KCl eutectic, excess LiD|Mo cell.

Table 1. Free Energy and Enthalpy of Reactions in the Molten salt Pd-D System at 700 K

Reaction	ΔG, kJ mol^{-1}	Potential, V
1. x LiD + Pd + x Al = x "LiAl" + $PdD_{x\|x->0}$	26.363	0.273
2. x LiD + $PdD_{0.5}$ + x Al = x "LiAl" + $PdD_{0.5+x\|x->0}$	12.41	0.129
3. LiD + Al = "LiAl" + 0.5 D_2	7.00	0.073
4. 2 LiCl + $PdD_{0.5}$ + 2 Al = 2 "LiAl" + $PdCl_2$ + 0.25 D_2	606.637	3.143
5. 2 LiCl + Fe + 2 Al = 2 "LiAl" + $FeCl_2$	390.123	2.021
6. 3 LiCl + Fe + 3 Al = 3 "LiAl" + $FeCl_3$	898.839	3.105
7. 4 LiCl + 4 Al = 3 "LiAl" + $LiAlCl_4$	425.181	1.102
8. 2 LiCl + 2 Al + Zn = 2 "LiAl" + $ZnCl_2$	333.856	1.730
9. 0.5 LiCl + $PdD_{0.5}$ + 0.5 Al = 0.5 "LiAl" + 0.5 DCl + Pd	103.652	2.148

This potential seems related to $FeCl_2$ and/or D^+ formation. We further excluded the $FeCl_2$ formation to be solely responsible for excess heat based on the arguments of thermochemical data and mass balance. Therefore, it is most likely that the D^+ and D^- transport contributes to the current passing through the cell. Without an impeding surface layer, the high potential implies a high deuterium activity and loading in Pd.

5. Conclusions

1) D^+ formation may occur during high-current charging at over 2V, enhancing the deuterium loading for excess heat generation.
2) The $Fe/FeCl_2$ redox can help stabilize the D^+ formation.
3) The D^+/D^- shuttle process could maintain a high current at high potentials without exhausting LiD in the melt.
4) The control of the relative concentration of Li^+, Fe^{+2}, D^+, D^- and Cl^- in the melt seems crucial for the excess heat effect.

6. References

1. Bush, B.F. et al., 1991, J. Electroanal. Chem., 304, 271.
2. Deublein, G. and R.A. Huggins, 1989, J. Electrochem. Soc., 136, 2234.
3. Liaw, B.Y. et al., 1993, Fusion Technology, in press.
4. Liaw, B.Y. et al., 1992, Molten Salts, R.J. Gale, et al., eds., the 181st Electrochem. Society Meeting, May 17-22, 1992, St. Louis, MO, the Electrochem. Society, Inc., p.1.
5. Liaw, B.Y. et al., 1991, J. Electroanal. Chem., 319, 161.
6. Mamantov, G., 1987, Molten Salt Chemistry, NATO-ASI V. 202, G. Mamantov and R. Marassi, eds., D. Reidel Publishing Co., p.259.
7. Plambeck, J.A., 1980, Encyclopedia of Electrochemistry of the Elements, Vol. X, A.J. Bard, ed., Marcel Dekker, N. Y., p.11.
8. Wen, C.J. et al., 1979, J. Electrochem. Soc., 126, 2258.
9. Worrell, W.L. and J. Hladik, 1972, Physics of Electrolytes, Vol. 2, J. Hladik, ed., Academic Press, New York, p.747.

Experiments Supporting the Transmission Resonance Model for Cold Fusion in Light Water: I. Correlation of Isotopic and Elemental Evidence with Excess Heat

Robert T. BUSH and Robert D. EAGLETON
California State Polytechnic University, Pomona
Physics Department
3801 West Temple Avenue
Pomona, California 91768, USA

ABSTRACT

The experimental evidence cited here (Part I) in support of the Bush TRM Model was originally reported by Bush[2] in his paper, "A Light Water Excess Heat Reaction Suggests That 'Cold Fusion' May Be 'Alkali-Hydrogen Fusion.'" Excess heat production in electrolytic light water experiments was experimentally correlated with a shift not only in elemental abundance but also with an isotopic reversal in the case of a light water-based Rb_2CO_3 cell found to produce strontium. Part II[3] reports on more recent work correlating x-ray emissions with excess power for both a heavy water excess heat reaction and a light water excess heat reaction.

1. Introduction

Bush's three dimensional transmission resonance model (TRM)[2] predicts a unique variation in the excess power for an electrolytic cold fusion cell as a function of the applied current density and cell temperature. Previous experiments[4] involving heavy water yielded data in agreement with the predictions of this model[1,2]. The present paper cites more recent work with alkali ions in light water originally reported by Bush.[2] In that paper he hypothesized that the light water excess heat reaction with potassium carbonate originally reported by Mills and Kneizys[6] and the heavy water excess heat reaction of Fleischmann and Pons[5] are two sides of the same coin, the latter representing low energy nuclear processes at, or within, a metal lattice. These processes were hypothesized to involve the transfer of either a proton, deuteron, or triton, to an alkali nucleus, yielding three forms of "alkali-hydrogen fusion", respectively, as the prototype for a generalized low energy nuclear transmutation in a lattice[2]. ("Alkali nucleus" was taken to include hydrogen itself.) This form of fusion avoids two thorny problems inevitably cited by critics of "cold fusion;" viz. a spectacular insufficiency of neutrons, and of gamma rays. (X-ray emission, which would be

FRONTIERS OF COLD FUSION

expected in connection with the product nucleus is correlated with excess heat production in Part II.) Bush[2] hypothesized calcium and strontium, respectively, as the nuclear products in the cases of the light water excess heat effect employing alkali salts of potassium and rubidium, such as the carbonate or hydroxide. Excess heat production was correlated[2] with an elemental shift from potassium to calcium in support of the Bush TRM Model[1,2]. Here we give more details of the work reported by Bush[2] involving the elemental shift from rubidium to strontium and the isotopic reversal between Sr86 and Sr88 hypothesized and measured in the case of a light water-based rubidium carbonate cell.

2. Apparatus

The electrolytic cell employed is similar to that Fleishmann-Pons[5] with the following principal modifications: (a) the use of a *platinum black recombiner* in the cell to allow for *closed-cell operation*, (b) a *magnetic stirrer* that provides for more uniform electrolyte mixing, and (c) *Teflon* coating of all nonelectrode materials to reduce electrolyte contamination. It consists of a double wall pyrex vessel surrounded by a one inch thick layer of styrofoam. Cell temperature is regulated by controlling the temperature of the bath water which flows through the jacket surrounding the cell. Cell temperatures, current, and voltage data were monitored and logged using a MacIntosh IIx computer equipped with National Instrument's LabView software. Four type K thermocouples were used with each cell: one at the bath inlet port, one at the bath outlet port, and two within the electrolytic cell. The thermocouple voltages were converted to temperature by use of AD595AQ/9217 integrated circuit chips. This system permitted steady state temperature measurements with standard deviations of about 0.05 °C. Corrections for thermocouple temperature offsets were made within the software. The cells' current and voltage signals were logged from Fluke 45 dual display multimeters which were equipped with an IEEE bus. In the case of the light water cells the nickel sponge (nickel fibrex) cathode typically forms an open cylinder of thickness 0.5mm and radius about 1.5 cm, with a platinum wire positioned axially as the anode. Calibration is achieved by running the cell anodically, and can typically be checked on the fly.

3. Rubidium Carbonate Cell: Elemental and Isotopic Analysis and Correlation With Excess Heat.

Figures 1-4 on the last page show a mass spectrogram resulting from a SIMS analysis of the cathode of cell 53: [light water based 0.57M Rb_2CO_3 electrolyte (50 ml), platinum wire anode (18 cm long, 1mm diam.); sponge nickel (fibrex) cathode (45 cm^2 "area"); charging began 9:20PM, (2/1/92) (1 mA/cm^2); excess heat detected: (2/4/92); cell turned off: (3/25/92); peak excess power: 4.3W (Input: 6.34V/2.36A/14.96W, gain 28.7%), average excess power: (1.81 ± 0.37) W; total excess heat: **(6.4 ± 1.3) MJ.**] Fig. 1 shows the post-run, (0-100) amu ("atomic mass units") mass spectrum (spectrogram) with large signals for Rb85 and Rb86 and significant signals at mass numbers 86 and 88, which Bush[2] interpreted to correspond to strontium; viz. Sr86 and Sr88, respectively. {Note that the signal "bias" has been turned way up in going from the spectrum of Fig. 2: [(pre-run), (0-100)amu] in order to accomodate the large rubidium signals and to suppress noise. This can be guaged

by noting that the nickel signal (Ni) has been significantly reduced in going from Fig. 2 to Fig.1. In addition, the signals in Fig.2 between masses 66 and 100 that appeared in Fig.2 have, for the most part, been suppressed in Fig.1. The NiO signal at mass 74 was large enough in Fig.2 to still show up in Fig.1, but the original signals for mass numbers 86 and 88 in Fig.2 are clearly too small with the bias employed for the spectrum portrayed in Fig. 1 to contribute noticeably to he signals at 86 and 88 of the post-run spectrm. [The niobium (Nb) appearing in Fig. 1 was apparently the result of having employed the platinum anode of cell 53 in a previous cell, number 48, which had a reference electrode constructed from a platinum-coated niobium wire.] Now, the most striking feature of the post-run spectrum, as reported by Bush[2], is that the ratio of the strontium signals (86-to-88) is close to that of the rubidium signals (85-to-87), or about 2.59. Had the strontium been the result of contamination, one would expect to see the ratio of the strontium signals mirroring the normal abundance ratio for these isotopes; viz. about 0.12.

[It should be noted that, while the electrolyte was not analyzed for strontium, an analysis of the pre-and post-run for cell 49, a previous Rb_2CO_3 cell at Los Alamos (LANL) via arc spectroscopy showed no elemental strontium in either the post- or pre-run electrolyte samples from cell 49 down to a concentration of 50 ppb. (An earlier positive test of the electrolyte of cell 49 for strontium by Geo-Monitor, Inc.1 was probably flawed by the assumption that a linear extrapolation could be made in the case of a flame photometry device set with the "zero" not corresponding to 0 ppm for strontium.) In addition, a mass spectrometric study of similar electrolyte samples from cell 49 by West Coast Analytical Service, Inc of Santa Fe Springs, CA, showed no strontium isotopes down to a concentration of 5ppb. (The 5ppm reported in Bush's paper was an uncorrected typing error.) The anode was not analyzed for strontium. However, here, as in the case of the electrolyte, strontium in the post-run cathode resulting from contamination would have isotopically mirrored the natural abundance ratio rather than showing an isotopic reversal.] In his report, the SIMS operator specified the ratio of the post-run "strontium" signal to that for rubidium as 6.2×10^{-5}. Based upon the known rubidium concentration of the electrolyte and the excess heat measured for cell 53, Bush has recalculated a theoretical value for this ratio of $(7.4 \pm 1.5) \times 10^{-5}$, in good agrement with the above experimental value, and in support of his "alkali-hydrogen fusion" hypothesis[2]. (This replaces an earlier estimate of Bush[2] based upon an incomplete assessment of the excess heat for cell 53.) It is interesting to note that the SIMS operator reported the strontium as "rubidium hydride". However, although his mass spectroscope was incapable of distinguishing strontium from rubidium hydride, the latter is very unstable and known to dissociate at 27 C. As a measure of how patently absurd the hypothesis of rubidium hydride is, our contact at the national laboratory, who arranged the out-of-house SIMS test, points out that the signal in the mass spectrum for the much more stable rubidium oxide in Fig. 3 is lower than the signal for the so-called "rubidium hydride" of Fig.1. (It is sad to have to report that the highly competent SIMS operator was apparently sufficiently upset that he was analyzing the results of a "cold fusion" experiment that this, no doubt, influenced his choice of labelling for the masses 86 and 88 in the post-run spectrum of he report. In addition, because of the negativity surrounding cold fusion, both our helpful contact of noted expertise and integrity and his otherwise fine, and certainly prestigious, laboratory must remain anonymous for the

present time.) Thus, it is apparent that the signals at masses 86 and 88 of Fig. 1 more than likely represent strontium, in spectacular corroboration of the hypothesis of "alkali-hydrogen fusion"[2] in a metal lattice.

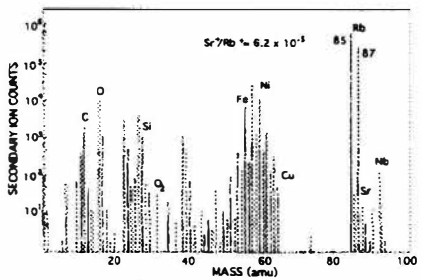

Figure 1. Cathode post-run mass spectrogram.

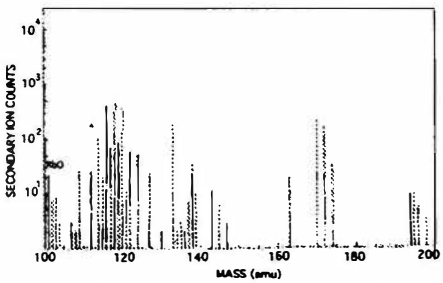

Figure 3. Cathode post-run mass spectrogram.

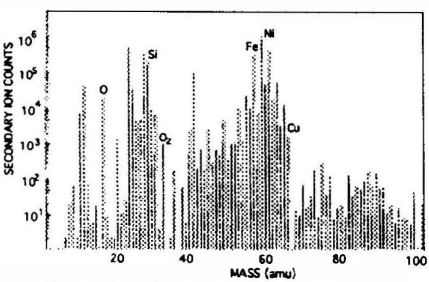

Figure 2. Cathode pre-run mass spectrogram.

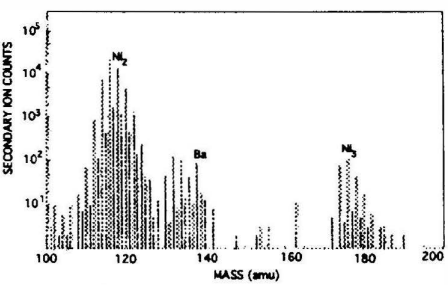

Figure 4. Cathode pre-run mass spectrogram.

Acknowledgments: These are listed once after Part II.[3]

References:

1. R. Bush, "'Cold Fusion': The Transmission Resonance Model Fits Data on Excess Heat, Predicts Optimal Trigger Points, and Suggests Nuclear Reaction Scenarios," Fusion Technol., 19, 313 (1991)
2. R. Bush, "A Light Water Excess Heat Reaction Suggests That 'Cold Fusion' May Be 'Alkali-Hydrogen Fusion'", Fusion Technol.,22, 301(1992)
3. R. Bush and R. Eagleton, "Experiments Supporting the Transmisssion Resonance Model for Cold Fusion in Light Water. II. Correlation of X-Ray Emission With Excess Power", Proceedings of the Third Annual Conference on Cold Fusion, Nagoya, Japan, Oct. 21-25, 1992.
4. R. Eagleton and R. Bush, "Calorimetric Evidence Supporting the Transmission Resonance Model for Cold Fusion", Fusion Technol., 20, 239 (1991).
5. M. Fleischmann and S. Pons, "Electrochemically Induced Nuclear Fusion of Deuterium," J. Electroanal. Chem., 261, 301 (1989)
6. R. Mills and K. Kneizys, Excess Heat Production by the Electrolysis of an Aqueous Potassium Carbonate Electrolyte and the Implications for Cold Fusion," Fusion Technol., 20, 65 (1991).

Experimental Studies Supporting the Transmission Resonance Model for Cold Fusion in Light Water: II Correlation of X-Ray Emission with Excess Power

R.T. BUSH and R. D. EAGLETON
Physics Department
California State Polytechnic University
3801 West temple Avenue, Pomona, CA, USA

ABSTRACT: Part I[3] presented evidence in support of Bush's TRM Model[1,2,4] and, in particular, his hypothesis of "alkali-hydrogen fusion" in a lattice as a prototype for cold fusion with both light and heavy water[2]. In Part II preliminary evidence is presented for x-ray emission accompanying both the heavy and light water excess heat effects in the form of both characteristic x-rays and bremmstrahlung. These studies had the unsatisfactory feature of low signal-to-noise, but the satisfactory features of reasonable statistics and excellent correlation. An interesting feature was that x-ray emission decreased somewhat after a cell was switched off, but then spiked upward to decay exponentially to the background level over a period of days. This emission was apparently associated with the desorption of hydrogen from the cathode. With the cell turned off it was also possible to study x-ray emission accompanying the thermal desorption of hydrogen by changing the cell temperature and studying x-ray emission as a function of cathode surface temperature. When this effect of x-rays accompanying desorption was factored in, Bush's TRM Model[1,2,4] appears to account for the correlation between x-ray emission and excess power.

1. Introduction:

Copious amounts of radiation, either in the form of neutrons or radiation , have not been reported in the case of either heavy water cold fusion cells (Fleischmann-Pons[5]) or light water cold fusion cells (Mills[6]), and this has been a puzzle. Bush points out that his TRM Model incorporating the hypothesis of "alkali-hydrogen fusion" in a lattice offers a solution to this puzzle: Thus, if much, or all, of the excitation energy goes into the kinetic energy of the product particle; e.g. a calcium nucleus in the case of a potassium nucleus adding a proton at, or

FRONTIERS OF COLD FUSION

just inside, the surface of a nickel lattice, one would expect radiation in the form of characteristic x-rays and bremmstrahlung, but no neutrons or gamma rays, which are far more penetrating. So, where are the x-rays? Tantalizing evidence has been achieved by researchers such as Miles and Ben Bush[7], who have had one instance in which a dental film placed inside a heavy water cell showed fogging in a case in which the cell was also known to be evidencing excess heat. In addition, Srinivasan[8] has seen evidence of extraordinary electron fluxes in cases of palladium and titanium loaded with either deuterium or hydrogen electrolytically or by gas-loading. It was primarily private communications from these two groups that encouraged Bush to look for x-rays with cells designed by Bush and Eagleton and built by Eagleton.

A limitation was that only one scintillation counter was available. Additionally, the emission was meager enough that it would not fog dental film positioned against the outer Styrofoam surfaces even for many days. However, by placing a scintillation tube on top of the cell, or as close as possible along side at the same height as the cathode (This orientation usually gave he best counting rates.) it was possible to attain data in support of the existence of both characteristic x-rays and bremmstrahlung and, also, to see two basic x-ray effects: 1. Qualitative and quantitative correlation of x-ray emission with excess power. 2. Qualitative and quantitative correlation of x-ray emission associated with the desorption of hydrogen from the cathode. The weight of the evidence provides support for Bush's three dimensional TRM Model[1,2,4] (Transmission Resonance Model). An unsatisfactory feature of these preliminary studies was the low signal-to-noise ratio of the data, which meant that one must often count for long periods of time (hours or days). (This aspect is apparently consistent with those studies in which previous experimentalists anticipated seeing a readily-measurable effect.) However, a significant ameliorating feature was that, whereas characteristic x-rays required days of counting and then about half that of background subtraction at relatively low excess power to see, correlations of x-ray emission with excess power could be observed for cases in which each x-ray data point required only about fifteen minutes, provided that the counts from many channels of a multi-channel analyzer were added together to establish a single data point. Thus, the sum of the counts resulting from bremmstrahlung and numerous characteristic x-rays was employed to establish a single data point. This enabled the pattern of x-ray data points to be correlated either qualitatively, or quantitatively, with the excess power data achieved with the calorimeter. The result was that poor signal-to-noise was considerably compensated by reasonable statistics and a high correlation resulting in a high level of confidence in the results. Reproducibility also appeared to be good.

2. Apparatus:

The electrolytic cell (light water case), calorimeter, and computerized data acquisition system were described in Part I[3]. For the heavy

water cell the anode-cathode configuration (platinum wire anode-palladium cathode) of the cell was close to that of Fleischmann-Pons[5]. X-ray measurements were performed using a Bicron 1.5 inch diameter NaI scintillation detector. An 811-3 multichannel analyzer PC board and software by Nucleus, Inc. of Oak Ridge, Tennessee were employed by Bush for x-ray counting.

3. Experiments with a Heavy Water Cell (Cell 58):

The electrolytic cell chosen for the initial studies attempting to correlate x-ray emission and excess heat, cell 58, had a cathode consisting of a (77% Pd/23% Ag)-alloy fabricated by Storms of Los Alamos. The platinum wire anode was wrapped uniformly around this thin flat cathode ala Takahashi. It took about 16 days of charging to produce any excess heat, with much current ramping along the way. Approximately 3 W was the highest excess power observed. (Cathode surface area: 4 cm^2. An unusual feature was that the electrolyte was 0.85M LiOD.)

Discovery of x-ray emission-vs.-current density fine structure mirroring that for excess power vs. current density and predicted by Bush's TRM Model.

Fig. 1 portrays this situation for which calorimetric data and x-ray data were taken simultaneously, and show a strong correlation based upon the similarity of the typical "hill-and-valley" curve familiar from Bush's TRM Model. If the charged product nucleus is given kinetic energy, and/or if electrons present are given some of the excess energy, x-rays should be produced due to the deceleration of the charges. Data points were the result of summing the results of a large number of energy channels.

Characteristic x-ray lines were observed:

Fig. 2 and Fig. 3 show apparent characteristic x-ray lines associated with platinum: Since the anode is of Pt, and part of this plates onto the cathode during electrolysis, this should not be surprising. Fig. 2 shows a characteristic Pt x-ray line centered at about channel 316 corresponding closely to the known energy of 75.6 keV. [Correspondence of the energies and channels was established via a calibration curve employing characteristic lines for such sources as Cs137 (32 keV x-ray line) and Co57 (122keV line).] Fig. 3 shows an apparent doublet of Pt x-ray lines centered at approximately the channels 272 and 280, corresponding, respectively, to the known Pt x-ray line energies of 65.1 keV and 66.8 keV. In all three cases note the reasonable Gaussian line shape. Fig. 4 is quite interesting: Apparent characteristic palladium x-ray lines centered at approximately channels 90,100, and 105 corresponding, respectively, to the known energies of about 21.1 keV, 23.8 keV, and 24.3 keV. Characteristic lines identified as those of silver are shown centered at channels 93, 107, and 109, corresponding, respectively, to the known Ag lines of 22.1 keV, 25.0 keV, and 25.5 keV. In addition, other lines in Fig. 4 have been identified as being associated with plausible typical impurities of Pd and Pt: A ruthenium peak is seen centered at about channel 82 corresponding to the known energy of

about 19.2 keV, and a rhodium peak is centered at about channel 87 corresponding to the known energy of about 20.1 keV. Apparently, then, the excess heat effect can be employed in conjunction with an x-ray counter and multi-channel analyzer to determine the presence of major metal impurities. Also, the presence of the x-rays (keV range) provides evidence of nuclear processes. With regard to x-rays potentially associated with energetic electrons, two possibilities suggest themselves: These electrons may result from internal conversion. Also, perhaps these are the electrons effecting the nuclear reaction via shielding, as in the case of the a "s-electrons" suggested by Bush[2].

After cell 58 was turned off, the x-ray counting rate initially decreased several percent for about a day and then spiked up in the time of about a day to a peak about 12% higher than when the cell was operating. The counting rate then decayed exponentially over a period of about nine days to the apparent background level later established by removing the cathode from the cell.

This behavior is seen from Fig. 5 and apparently is a different x-ray emission effect in that it is associated with the desorption of the deuterons from the cathode.

Based upon the finding of x-rays with a switched-off cell, Bush realized the possibility of looking for temperature-dependent x-ray emission peaks (sum of counts from large number of different channels) associated with the thermal desorption of deuterons.

Fig. 6 shows that the first attempt at this was reasonably successful. The solid curve is based upon Bush's TRM Model. The latter predicts this temperature dependence in the same manner that it predicts the temperature dependence for neutron emission in the case of the thermal desorption of deuterons; e.g. recall the well known -30 C line established for neutron emission. Thus, with an electrolytic cell in which the cell, and thus cathode, can be heated by heating the bath, x-ray, and probably neutron, temperature-dependent studies can be conducted by simply switching off the current as an alternative to more "conventional" calorimetric experiments. With reference to Fig. 6, it is absolutely mind-boggling that minor temperature changes of the cathode, e.g. going from 32C to 23.4C in this case, can result in a major increase in the real x-ray intensity.

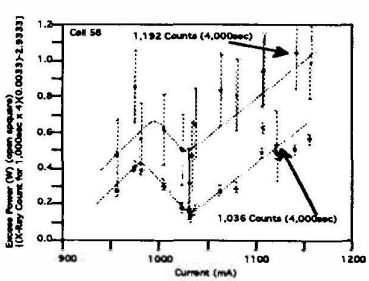

Figure 1. Excess Power 7 X-Ray Count vs Currentt

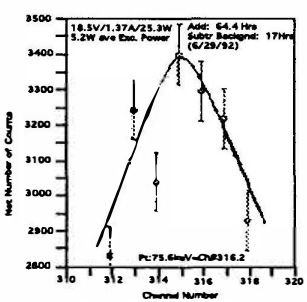

Figure 2. Net Counts vs. Channel Number.

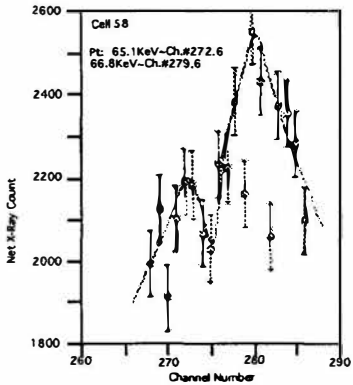

Figure 3. X-Ray Count vs. Channel Number

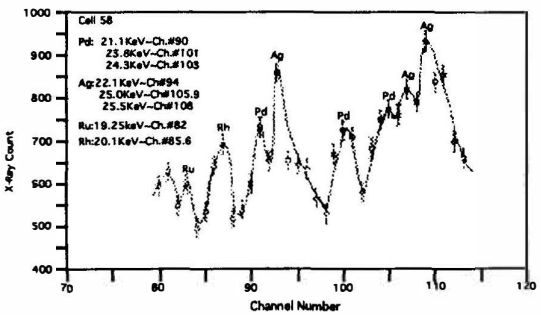

Figure 4. X-Ray Count vs. Channel Number

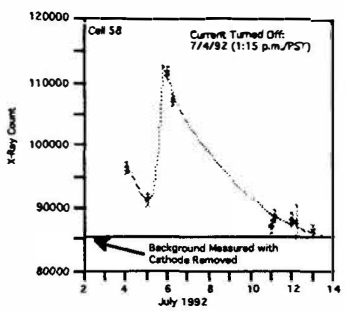

Figure 5. X-Ray Decay After Cell Turned Off

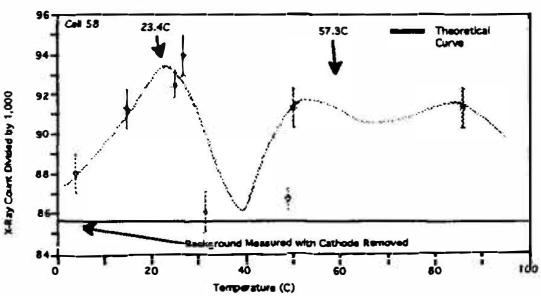

Figure 6. X-Ray Count: Thermal Desorption of Deuterons

4. Experiments with a Light Water Cell (Cell 62):

Cell 62 was a light water based 0.57M LiOH cell with the inside out anode-cathode configuration described in Part I[3] with the thin annulus (approx. 1 mm) of the cathode composed of sponge nickel (nickel fibrex).

Fig. 7 and Fig. 8, respectively, show a qualitative correlation between excess power and x-ray emission over a period of days at relatively low excess power. Apparent discrepancies in that correspondence can be accounted for by the x-ray emission effect associated with hydrogen desorption when the current (applied power) is very low, or off. Fig. 9 has the excess power and x-ray count data points included on the same plot. For this higher excess power range one again sees a qualitative correlation between excess power and x-ray emission, but in a higher excess power range. Finally, Fig. 10 exhibits the roughly linear relation between real x-ray count (actual count minus background) and excess power for this light water cell. (In cases where two real x-ray counts were the same, the excess powers were averaged to establish the point.)

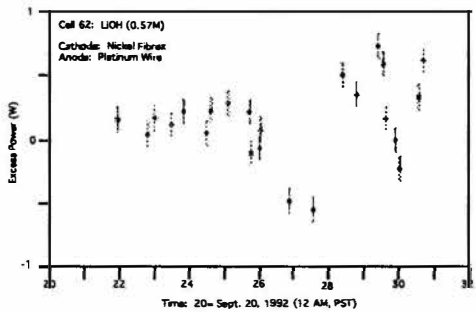

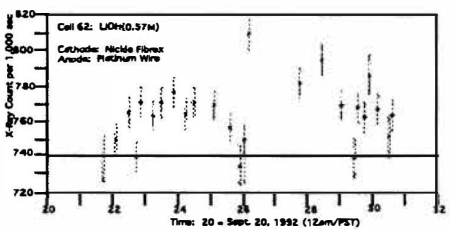

Figure 8. X-Ray Count vs. Time.

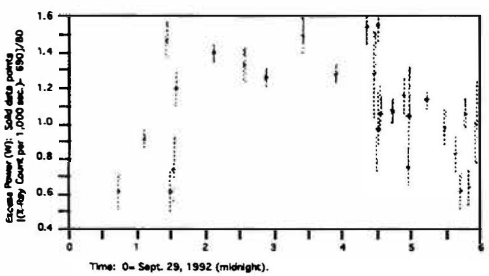

Figure 9. Experimental Correlation Between X-Ray Count and Excess Power

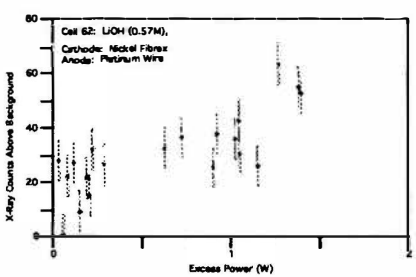

Figure 10. Real X-Ray Count vs. Excess Power

5. Conclusions:

In the case of heavy water cells with palladium cathodes it might be supposed that microcracking of the palladium results in high electric fields, with the resulting accelerated charged particles yielding x-rays upon deceleration. However, this argument could hardly be applied to the light water case, since the nickel cathode is presumably undergoing no microcracking. Applying Occam's razor suggests, then, that x-rays in the Pd case do not arise from microcracking. We conclude from these studies that x-rays have been systematically observed and studied, perhaps for the first time, for both the heavy - and light water cases and correlated with excess power. These studies strengthen the argument that the light water and heavy water excess heat effects are, indeed, nuclear effects. Coupled with the evidence adduced in Part I[3], we conclude that they also strengthen the case for Bush's hypothesis[2] of "cold fusion" as "alkali-hydrogen fusion" in a metal lattice, or as CAF ("Cold Alkali Fusion") (Suggested to Bush by Drexler[9].).

Acknowledgments

It is a pleasure to acknowledge Roger Bush, son of R.T. Bush, whose ingenious contributions have made possible our computerized data acquisition system. Pete Siegel of the Cal Poly Physics Department is thanked for help with the x-ray equipment and for encouraging Bush's search for x-rays. Hal Fox is appreciated for Dr. Eagleton's financial support for the Nagoya Conference and for his enthusiastic support of the Cal Poly Cold Fusion Project. Joe Ignat is thanked for providing funding for Dr. Bush to attend the Nagoya Conference, and for his general support and encouragement of our project. Tim Shoemaker is appreciated for his help in assembling the manuscripts. Southern California Edison, Inc. of Rosemead, CA, is especially thanked for their funding of our research. N.J. Kertamus of S.C.E. is thanked, in particular, for his interest and support. N. Srinivasan, Head of the Neutron Physics Division, B.A.R.C., Bombay India, has been especially encouraging of the Cal Poly research effort. Finally, we wish to thank H. Ikegami, Chairman, Secretariat, ICCF3, for his leadership in the planning of the Nagoya Conference. (These acknowledgments also apply to Part I[3].)

References

1. R. Bush, "'Cold Fusion': The Transmission Resonance Model Fits Data on Excess Heat, Predicts Optimal Trigger Points, and Suggests Nuclear Reaction Scenarios," Fusion Technol., **19**, 313 (1991).
2. R. Bush, "A Light Water Excess Heat Reaction Suggests That 'Cold Fusion' May Be 'Alkali-Hydrogen Fusion'," Fusion Technol.,**22**, 301(1992).

3. R. Bush and R. Eagleton, "Experiments Supporting the Transmission Resonance Model for Cold Fusion in Light Water. II. Correlation of X-Ray Emission With Excess Power", Proceedings of the Third Annual Conference on Cold Fusion, Nagoya, Japan, Oct. 21-25, 1992.
4. R. Eagleton and R. Bush, "Calorimetric Evidence Supporting the Transmission Resonance Model for Cold Fusion", Fusion Technol., 20, 239 (1991).
5. M. Fleischmann and S. Pons, "Electrochemically Induced Nuclear Fusion of Deuterium," J. Electroanal. Chem., 261, 301 (1989).
6. R. Mills and K. Kneizys, "Excess Heat Production by the Electrolysis of an Aqueous Potassium Carbonate Electrolyte and the Implications for Cold Fusion," Fusion Technol., 20, 65 (1991).
7. M. Miles and B. Bush (China Lake, CA), Private Communication, May 1992.
8. M. Srinivasan (BARC, Bombay, India), Private Communication, May 1992.
9. J. Drexler, Private Communication, October 1992.

Implications of Isoperibolic Electrode Calorimetry for Cold Fusion : The Silica Effect

Ernest E. CRIDDLE
Electrochemical Science & Technology Centre
University of Ottawa
Ottawa, Ontario, Canada K1N 6N5

ABSTRACT

Isoperibolic electrode calorimetry has demonstrated that four times as much heat is generated at the anode than at the cathode in D_2O. Experiments recognized that silica affected some results. Experiments in K_2CO_3 reported here identify silica as both a contributor to excess heat generation and as a factor in modifying the cell calibration constant. Implications for cold fusion will be discussed.

1. Introduction

An early attempt at the University of Ottawa (1) to replicate the work of Fleischmann and Pons (5) failed to produce excess heat. Analyses later found silica in the lithium metal and on both the palladium cathode and platinum anode along with traces of base metals.

Isoperibolic calorimetry (6) describes how heat, generated in a cell, establishes a temperature difference between that cell and its surroundings. Recent work (4) has described how each electrode in this cell may be potted separately with one side exposed to the electrolyte while the other contacts a thermocouple well which is potted in resin. Each half cell can then be treated as a separate isoperibolic electrode calorimeter. However, excess heat was not observed in LiOD.

Therefore, the work was shifted to ordinary water (9,10) where replication of excess heat seemed to be more easily accomplished. However, excess heat was not observed until contaminant silica was added as will be described.

FRONTIERS OF COLD FUSION

2. Methods

The cell and blank for 0.57M K_2CO_3 in H_2O were 75ml unsilvered dewars. The cathode of 38x40x0.03mm (30cm^2) Ni foil was spot welded to 2mm Ni rod and wound as a 5mm pitch spiral with about 1.3 turns. The 10x25mm Pt anode was spot welded to 0.5mm Pt wire. Both Ni and Pt were sheathed above the electrolyte. A 10Ω resistor served as calibration heater immersed in oil in a 5mm OD tube. Separate power supplies provided cell and heater current. The temperatures (of the cells and the bath), voltages and currents were monitored with an Acurex Autograph 800 data logger.

Well aged Ni was prepared for use by smoothing with a wooden dowel, rubbing with fine steel wool, degreasing in alcoholic KOH and coating with silica. Alternatively, it was polished with Tripoli, green rouge and blue rouge before degreasing and coating with 5mg silica.

Ottawa lab distilled water contains only 0.02ppm SiO_2; our K_2CO_3 contained 16ppm SiO_2. Fresh 0.57M K_2CO_3 contained 70ppm. Our best heating so far has been observed in 0.57M K_2CO_3 to which 100ppm SiO_2 and 10ppm $FeCl_3$ were added (Fe first, SiO_2 next, age, and add K_2CO_3). Following use, this solution was found to contain 100ppm SiO_2.

3. Results

Electrode heating vs input watts is plotted in Fig. 1 as reported elsewhere (4). The lower X-axis reflects the voltages of D_2 and O_2 evolution against Hg/HgO reference electrodes. These voltages project (at zero current) to zero watts on the upper x-axis. The cathodic evolution of D_2 from Pd slopes up to the left (at negative watts) while the anodic evolution of O_2 from Pt slopes up to the right. Fresh metals exhibited the greatest heat per watt. On aged metals, oxygen evolution yielded four times as much heat as hydrogen evolution.

Freshly prepared 0.3N LiOD provided different results. First, stirring was found to reduce cell heating per watt input. Second, both reference electrodes developed bubbles in their capillaries which interfered with their accuracy; bubbles became more numerous as the run progressed. When dismantled, both reference electrodes had white scale at the top of their electrolyte; the scale did not dissolve in acid and was probably silica. No bursts of heat were observed.

In K_2CO_3 electrolyte, cell and calibration heating were equal at first. Heating developed after 100ppm silica was added to the electrolyte. The highest heats seen in Fig. 2 were produced in K_2CO_3 with SiO_2 and $FeCl_3$ present. The sharp rise after the 24 hour calibration occurred when the aged Ni cathode was replaced with a freshly polished and silica coated Ni. The isothermal calibration points required about

two hours each with cell power turned off while resistive heating was fine tuned to hold the cell temperature constant.

Similar results were observed in Na_2CO_3 with SiO_2 and $FeCl_3$ contrary to the theory of Mills (9).

4. Discussion

Silica, found in chemicals and some lab distilled waters, dissolves from Pyrex at 5mg/cm^2/hr in alkaline solution. Its chemistry is complex (3,7). Various sizes and shapes of particles may exist as stable colloids. These deposit as a monolayer especially on grease free metal oxides; thereafter, VanDerWaals forces repel other colloidal particles. In a cold fusion cell, electrophoretic forces carry silica to the anode while tri and tetravalent metal ions with a silica sheath move to the cathode. There they cannot stick but form gels which may thicken the solution or adhere to the cell walls depending on their size, shape, porosity and thermophoretic forces. Aging could lead to changes.

Thus, in aged LiOD the calorimeters performed well. In fresh LiOD, silica gel trapped evolving gases which escaped into Luggin capillaries carrying some gel with them. Silica in K_2CO_3 solution, and coated on both Ni and Pt, enhanced the observations of excess heat. This may be true on Pd as well.

Lithium silicate gels at 80°C and dissolves when cooled; this contrasts to sodium and potassium silicates which gel when cold. Thus, operation with warm lithium deuterate could produce a gel and lead to heat retention and bumping.

It is possible that phase shifts in silica deposits could produce fusion products not unlike those observed in Pd-D and Ti-D systems (2,8) or as trace contaminants from fumaroles and volcanoes (11,12). Indeed, volcanoes may be produced when silicate rocks undergo phase changes and exhibit related phenomena.

5. Conclusions

It is concluded that four times more heat is generated during the evolution of oxygen from Pt than from the evolution of deuterium from Pd. Silica interfered with some observations and must be controlled before results are certain.

The presence of silica in 0.5M K_2CO_3 and Na_2CO_3 enhanced the observations of excess heat on Ni. A deliberate coating of silica on the anode and cathode also proved beneficial. This silica was also associated with changes in cell calibration constant.

It is concluded further that heating in our cells varied with the condition of silica coating the cathode, with stirring rate and with the

amount of silica that coated the cell walls. While phase changes are anticipated in silica involved in this system, and while such changes may give rise to excess heat and to some nuclear products, it was not determined whether significant heating occurred on anodes, cathodes, cell walls or in solution. Further work is required.

The financial support of EMR Canada, CANMET Alternative Energy Division, to this work is gratefully acknowledged.

6. References

1. Adams, W. A. et.al., presented at the 176th Meeting of The Electrochemical Society, Florida, 1989.
2. Beltyukov, I. L. et.al., Fusion Technology, Vol. 20, September 1991.
3. Brinker, C. J. and Scherer, G. W., Sol-Gel Science, Academic Press, 1991.
4. Criddle, E. E., 182nd Meeting of The Electrochemical Society, Toronto, 1992.
5. Fleischmann, M., Pons, S. and Hawkins, M., J. Electroanal. Chem. 261 (1989) and 263 (1989).
6. Gur, T. M. et.al. Special Symp. Proc. on Cold Fusion WHEC #8.
7. Iler, R.K., The Chemistry of Silica, Wiley, 1979.
8. Jorne, J., Fusion Technology, Vol. 19, March 1991.
9. Mills, R. L. and Kneizys, S. P., Fusion Technology, Vol. 20, August 1991.
10. Noninski, V. C., Fusion Technology, Vol. 21, March 1992.
11. Palmer, E. P., AIP Conf. Proc. 228, Provo, UT, 1990.
12. Sheely, E. V., AIP Conf. Proc. 228, Provo, UT, 1990.

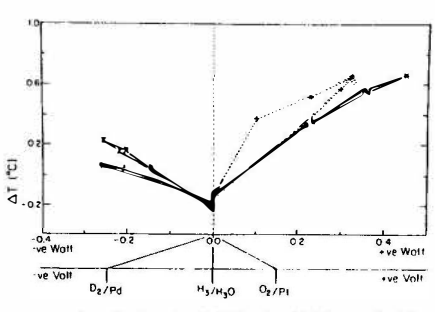

Fig.1. Cathode and anode heating vs wattages as derived from voltages and current.

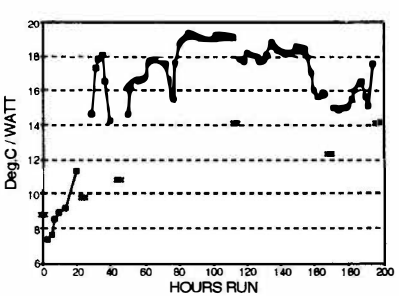

Fig.2. Variations in cell(-+-) and calibr.(x) heating in $K_2CO_3 + SiO_2 + FeCl_3$.

Excess Heat Production in Electrolysis of Potassium Carbonate Solution with Nickel Electrodes

Reiko NOTOYA and Michio ENYO
Catalysis Research Center, Hokkaido University
Kita-11, Nishi-10, Kita-ku, Sapporo 060
JAPAN

ABSTRACT

With the aim of realizing the potassium-proton cold fusion, the electrolysis of light water solution of potassium carbonate was carried out by means of porous nickel cathode. The cell was cooled by a constant rate air stream and maintained at 20°C during all the electrolysis. Typical results indicated that the excess heat production rate was proportional to the input power in the range of measurements(up to 2W) and the excess heat observed was 3 to 4 times greater than the input power, after corrected for the thermoneutral potential.

After the electrolysis, the calcium ion concentration in the electrolytes was measured by flame photospectrometry and the increases of calcium concentration in the electrolytes due to the electrolysis were found to be 3.2 to 4.4 ppm. These amounts are comparable to the amounts of the excess heat calcurated within the same order of magunitued.

1. Introduction

It was a shocking news that nuclear reactions of deuterium occurred on paradium cathode at room temperature[1]. The study of "cold fusion" has burst into flame throughout the world. Moreover, the novel type of the cold fusion in light water was suggested by Mills et al[2], last year. The majority of scientists still are doubtful about them, because of little reproducibility and consistence among the amounts of

FRONTIERS OF COLD FUSION

their products, heat emission and radiation. However, these systems are essentially the most popular ones for hydrogen evolution reaction. Matsuda's group had shown in their works[3] that several active metals for hydrogen evolution reaction, for example, nickel, formed considerable amounts of the alkali metallic intermediates during electrolysis of alkaline solutions. On the basis of them[3], the nuclear reaction of potassium was sufficiently likely and therefore warranting further investigation. The aim of this work was to obtain the unequivocal evidence of this nuclear reaction.

2. Experimentals

An electrolytic cell made of Pyrex glass was used for the experiment and equipped with 3 electrodes, these being, a 1 x 0.5 x 0.1 cm sintered nickel test-electrode, platinum counter and platinum reference electrodes. A 20 milli-liter light water's solution of potassium carbonate with a concentration of 0.5 mol per liter was used as the electrolyte, and stirred by bubbling hydrogen gas, with gas stream rate of 1.5 ml/min during the electrolysis. The nickel electrode was cathodically polarized by a stationary constant current from 0.01 to 0.70 ampere and the temperature of the electrolyte was measured. A standard nichrome heating wire with a resistance of 15 ohm was put in the cell for comparison. The electrolysis was carried out using the twin celles simultaneously, in order to confirm that the heat discharged was only by electrolysis. The twin cells were placed a thermostat chamber of the temperature held at 20.00 $\pm$0.01^{o}C during the electrolysis by air convection.

3. Results and Discussion

Figure 1 shows the typical relationship between the input power, W_{input}, given by electrolysis and the increase of electrolyte temperature, T. The input power, W_{input} is given by the following equation:

$$W_{input} = I(E - 1.482\ V), \qquad (1)$$

where I and E denote the current and the potential difference between the test electrode and the counter electrode. The 1.482 V value is due to the enthalpy change for $H_2O \rightarrow H_2 + (1/2)O_2$[4]. Figure 1 shows the electrolyte temperature increase for the standard resister(2) and that for electrolysis. It was found that the electrolyte temperature increased up to

54.2°C from the initial temperature of 20°C with the input power of 2.70 joule/sec and this temperature rise was proportional to the input power W_{input}, within the input power range of 0 to 2.7 joule/sec. The figure shows a linear relationship between the temperature increase and the input power W_{input} with a corelation coefficient of more than 0.999 for both lines. The line gradient for the cell is remarkably greater than that for the standard resister.

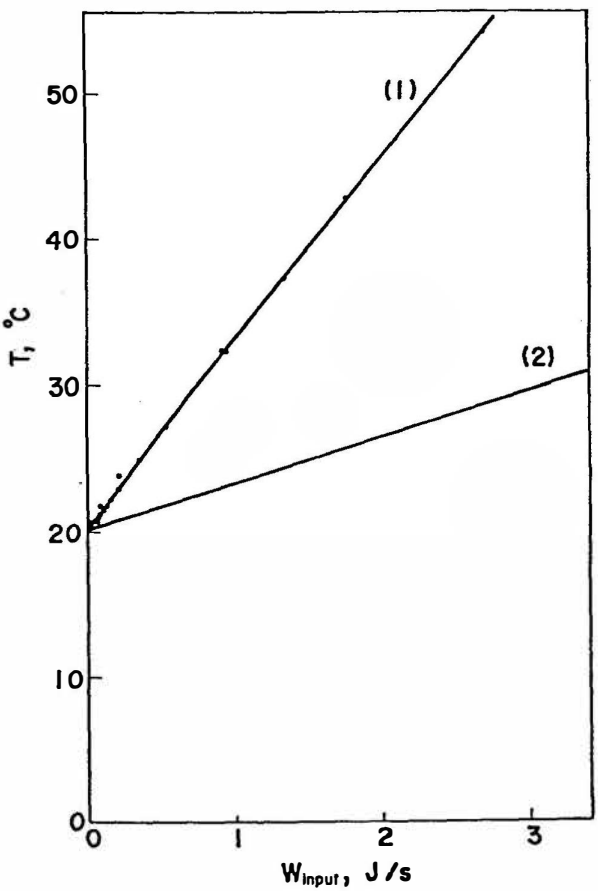

Figure 1. a. Relationship between temperature increase of electrolyte and input power W_{input} in the cell-(1) and as compared with the standard resister-(2).

The difference in the value of input power W_{input} between two lines at a given temperature, shown in this figure, can be defined as the excess heat. Figure 2 shows the relationship between the excess heat ΔW_{output} and the input power W_{input} observed in the cell. The excess heats determined from ten time-repeated experiments were found to be from 2.7 to 3.4 times more than W_{input}.

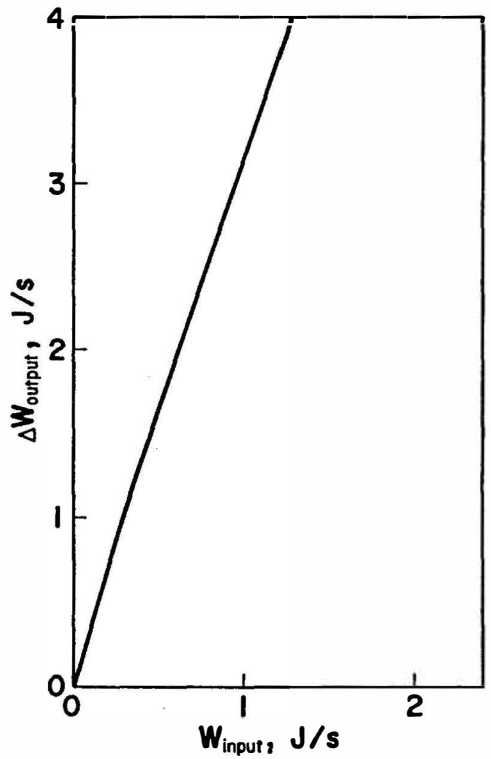

Figure 2. Amount of excess heat ΔW_{output} evolved during the electrolysis with input power W_{input} in 0.5 M K_2CO_3.

The calcium ion concentration in the electrolyte was measured by flame photospectrometry with an accuracy of ±0.02 ppm. In the same solution of 0.5 mol per liter potassium carbonate as the electrolyte, calcium ion was not detected, before use. In order to determine the background value, the calcium ion concentration in the solution of 20ml was poured into the electrolytic cell vessel equipped with the three

electrodes and the standard heater and put at 20°C without electrolysis, during the electrolysis of the working cell, which was made exactly the same as the former. The calibration line of the intensity of the spectrum for calcium plotted against it's concentration is shown in Figure 3. On the basis of this line, the calcium concentrations in the three samples of electrolyte after different conditions of electrolysis were found to be 24.7, 25.1 and 26.2 ppm when the background values, to be 21.5, 21.5 and 22.0. The increases of calcium concentration in the samples of electrolyte due to the electrolysis were determined to be 3.2, 3.6 and 4.2 ppm by use of these data. These increases of calcium concentration in the electrolytes are comparable to the total amounts of excess heats evolving in these electrolytes, within the same order of magunitued.

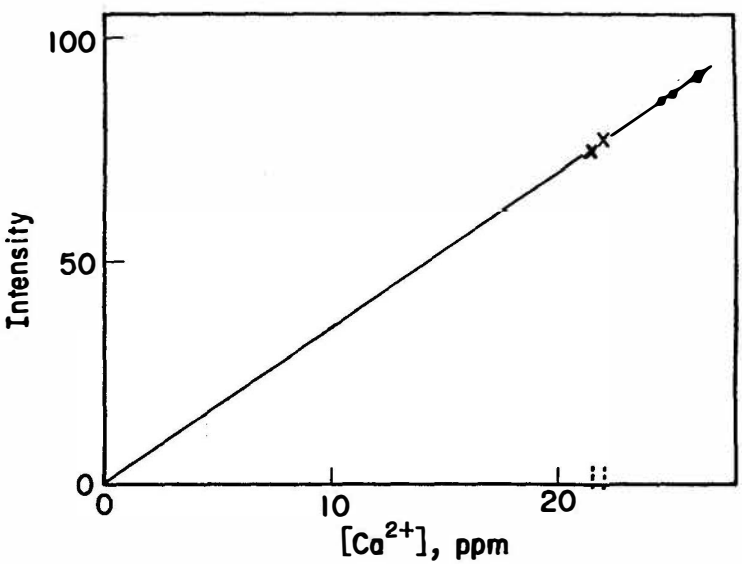

Figure 3. Intensities of flame photospectra of calcium with concentrations of calcium ion in the electrolytes after electrolysis(●) and in electrolytes put in cell without electrolysis(x).
A line shown in this figure is the caribration line for the calcium ion concentration.

Bush et al[4] proposed the possibility of nuclear reactions between potassium and proton as follows,

$$^{39}_{19}K + ^{1}_{1}H = ^{40}_{20}Ca + 8.33 \text{ MeV} \quad (2)$$

and

$$^{41}_{19}K + ^{1}_{1}H = ^{42}_{20}Ca + 10.3 \text{ MeV} \quad (3)$$

From the present work, it is not clear which of the 2 reactions, (2) or (3), was predominant in this system. A further investigation is being conducted at present to verify this.

4. List of Symbols

W_{input} = Input power, joule/sec
I = Current, amp
E = Potential difference, volt
T = Temperature, ^{o}C
ΔW_{output} = Excess Heat, joule/sec

5. References

1. Fleischmann, M. and Pons, S., 1989, J.Electroanal Chem., 261, 301.
2. Mills, R. and Kneizys, K., 1991, Fusion Technol., 19, 65.
3. Notoya, R. and Matsuda, A., 1966, J.Research Inst. Catal.,Hokkaido Univ., 14, 198.
4. Bush, R.T, 1991, Fusion Technol., 22, 301.

Excess Heat Produced during Electrolysis of H_2O on Ni, Au, Ag and Sn Electrodes in Alkaline Media

T.OHMORI and M.ENYO

Catalysis Research Center, Hokkaido University

Sapporo, 060, Japan

ABSTRACT

Excess heat evolution was measured on Ni, Au, Ag and Sn in aqueous K_2CO_3, Na_2CO_3, Na_2SO_4 and Li_2SO_4 solutions under galvanostatic electrolysis conditions. Steady evolution of excess heat in various electrode/electrolyte systems, but not in Ni/Na_2CO_3, Ni/Na_2SO_4 and Ni/Li_2SO_4, was observed for at least several days of observation. The largest excess heat observed was 907 mW on Sn in K_2SO_4.

Introduction

Mills and Kneizys reported a production of 130 mW excess heat in Ni/K_2CO_3-H_2O system [1]. Later, Bush reported 310 - 580 mW in the same system and claimed the detection of Ca of the amount that may correspond to the amount of excess energy [2]. The present study is aimed at the reproduction of their results on Ni, and further to investigate similar possibilities on several other metal electrodes. The reasoning of this extension is that the underpotential deposition (upd) of alkali metals is known to occur under high cathodic polarization [3].

Experimental

The electrolytic cell used was a 300 ml Pyrex glass vessel with a 5 cm thick silicon rubber stopper equipped with the test electrode, counter and reference electrodes, a thermocouple, inlet and outlet glass tubes for H_2 gas and a heater. The cell was placed in an air

FRONTIERS OF COLD FUSION

thermostat maintained at 25 ± 1 °C. The test electrodes used were plates of various metals (Ni, Au, Ag, Sn, etc). Surface of these electrodes was abraded with emery papers and then rinsed with ethyl alcohol and Milli-Q water in a ultrasonic bath. The counter electrode was a platinum net. The reference electrode was of a rhodium wire. The heater used for the cell constant measurement is a nichrome wire (1.6Ω) covered with a teflon tube (2 mm diam.).

The cell constant was measured by applying a current to the heater using 100 ml 0.5 M K_2CO_3 solution under stirring with a flow of H_2 gas (several ml per min.). The electrolyte solution was 100 ml of 0.5 M aqueous K_2CO_3, Na_2CO_3 and Li_2SO_4.
The electrolysis was conducted galvanostatically usually for 20 hours by passing a constant current of 1.0 A and the variations of input potential and the temperature rise were monitored by a pen recorder.

Results and Discussion

Figure 1 shows typical variations of the solution temperature with polarization time obtained on a Ni electrode in K_2CO_3 and Na_2CO_3 solutions. The time variations of input potential are also shown in this figure. It can be seen from this figure that the increase in temperature in K_2CO_3 is 1 - 1.3 °C larger than in Na_2CO_3 in spite of the fact that the levels of input

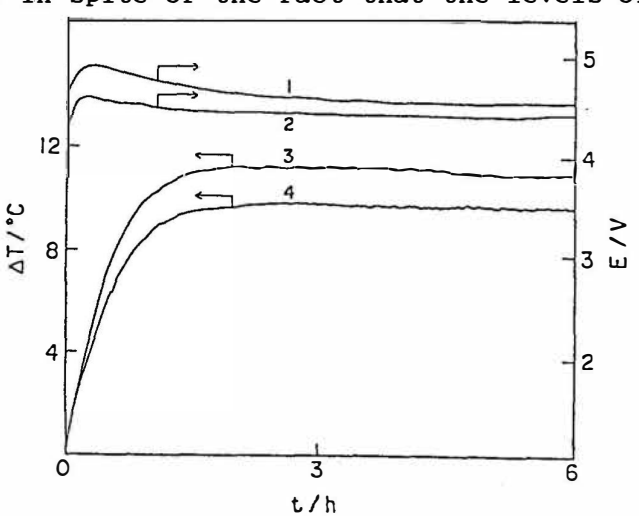

Fig.1 Variations of input potential and solution temperature with polarization time. (1),(4) in 0.5M Na_2CO_3, (2),(3) in 0.5 M K_2CO_3.

power are in the opposite order. The difference was essentially unchanged during the polarization over several days. This result indicates that a noticeable amount of excess heat is produced in Ni/K_2CO_3 system.

The rate of excess heat evolution R_{ex} was determined quantitatively from the shift of solution temperature ΔT and the applied electrolysis power R_{app} in the following way. The energy balance equation for the cell in a steady-state is

$$R_{ex} = R_{rx} + R_L - R_{app} \quad (1)$$

where R_{rx} is the rate of heat removed by the endothermic reaction $H_2O \rightarrow H_2 + 1/2O_2$, which is equal to the product of the thermoneutral potential (1.48 V for H_2O) and the polarization current I, and R_L is the thermal loss rate. The latter, when a steady-state is reached, is given by

$$R_L = \Delta T/k \quad (2)$$

from Eqns.(1) and (2) and using $R_{app} = EI$ where E is the total cell voltage, we have

$$R_{ex} = \Delta T/k - (E - 1.48)I \quad (3)$$

A preliminary heat measurement was first performed in the electrolysis on Au in 1M H_2SO_4 solution to check the precision of our method. Practically no excess heat was obtained in this system during 20 hours of observation. On the other hand, significant magnitudes of excess heat were observed on Ni, Au, Ag and Sn in K_2CO_3, Na_2CO_3, Na_2SO_4 and Li_2SO_4 solutions, except for Ni/Na_2CO_3, Ni/Na_2SO_4 and Ni/Li_2SO_4, as listed in Table 1 together with the data of cell potential and solution temperature shift. The excess heat evolution was almost steady, but a slight tendency to increase on prolonged time of polarization was noted. The largest excess heat evolution was observed on Sn electrode; the value reached after 65 hours of polarization was 907 mW, as compared with the input power of (4.95 - 1.48) x 1 = 3.47 W. The magnitude of the excess heat evolution increases in the order Ag < Ni < Au < Sn. It was noteworthy that the excess heat was noticeable also in Na_2CO_3 and Li_2SO_4 for Au, Ag and Sn.

The total summed-up amount of the excess energy evolved during the electrolysis is too large to be regarded as the heat of any chemical reaction. For instance, the total excees heat evolved in the electrolysis on the Sn electrode for 65 hours of polarization was evaluated to be 176 kJ. Even if one supposes that all the amount of Sn (1 g) of the electrode was reacted

with certain species in the system (which is not the case), the heat produced would at most be 9.3 kJ (for $Sn(OH)_4$) which is too small an amount to account for the excess heat observed.

Table 1 Rate of excess heat evolution on various metal electrodes

electrode	solution	E (V)	ΔT (°C)	R_{ex} (mW)
Ni	K_2CO_3	4.12	0.75	208
Ni	K_2CO_3	3.88	1.26	387
Ni	Na_2CO_3	3.94	0.02	6
Ni	Na_2SO_4	4.17	0.01	0
Ni	Li_2SO_4	4.50	0.01	0
Au	K_2CO_3	4.34	1.71	524
Au	Na_2CO_3	4.85	1.83	565
Au	Li_2SO_4	4.60	1.64	503
Ag	K_2CO_3	4.12	1.07	328
Ag	Li_2SO_4	5.10	0.31	95
Sn	K_2CO_3	5.04	2.31	708
Sn*	K_2CO_3	4.95	2.96	907
Sn	Na_2CO_3	5.07	0.73	224

* electrolyzed for 65 hours.

The excess heat evolution observed in many systems other than Ni/Na_2CO_3, Ni/Na_2SO_4 and Ni/Li_2SO_4 may suggest the following nuclear reactions.

$$_{19}K^{39} + {}_1P^1 \longrightarrow {}_{20}Ca^{40} + 8.3\ MeV \qquad (I)$$

$$_{11}Na^{23} + {}_1P^1 \longrightarrow {}_{12}Mg^{24} + 11\ MeV \qquad (II)$$

$$_3Li^6 + {}_1P^1 \longrightarrow {}_2He^4 + {}_2He^3 + 2.3\ MeV \qquad (III)$$

The excess heat evolution on Ni was observed only in K_2CO_3. On Ag and Sn, it was larger in K_2CO_3 than in Na_2CO_3 or Li_2SO_4 solutions. On Au, no large difference was observed between these electrolytes. These results may suggest that all the reactions (I), (II) and (III) occur in general, but the degree of the progress of each reaction depends on the nature of the electrode material, surface and bulk conditions of the electrode, adsorbed or upd species, etc.

1. Mills, R. L. and Kneizys, S. P., 1991, Fusion Technology, 20, 65.
2. Bush, R. T., 1992, Fusion Technology, 22, 301.
3. Ohmori, T. and Enyo, M., 1992, Electrochimica Acta, 37, 2021.

Chapter II
Nuclear Products

Measurement of 2.5 MeV Neutron Emission from Ti/D and Pd/D Systems

M. AGNELLO, E. BOTTA, T. BRESSANI, D. CALVO, A. FELICIELLO, P. GIANOTTI, F. IAZZI, C. LAMBERTI, B. MINETTI and A. ZECCHINA

ABSTRACT

A new set of measurements of neutron emission from gas (D_2 and H_2) loaded Ti and Pd systems has been carried out in the TOFUS experiment. The temperature and pressure controls of the gas loading apparatus were improved. The results concerning the Ti/D system show the presence of a small 2.5 MeV neutron emission, with a signal having a statistical significance of ~ 5σ. The results on the Pd/D system doesn't show a statistically significant signal (less ~ 2σ).

1. Introduction

Since the start of the debate about the occurrence of D-D fusion phenomena in the lattice of some metals like Pd and Ti, the detection of neutrons, in particular 2.5 MeV neutrons, has been considered as the most reliable signature of the effect. In order to clarify this point, a sophisticated neutron detector was designed and built for the TOFUS experiment and in a first set of measurements we observed a small amount of neutron emission following the loading of Ti shavings with gaseous D_2 [4], with a statistical significance of ~ 2.5 σ. After a number of improvements on the heating system of the apparatus a second set of measurements has been performed with a better control of the pressure and temperature of both the metal and the gas [1].

The results shown here concern the Ti/D and Pd/D systems: blank measurement on the Ti/H and Pd/H systems have been performed too, in the same way as those ones with D, in order to avoid possible variations of the performances of the scintillators and detector electronics due to the heating cycles.

2. Experimental set-up and description of the thermal cycles

Concerning the neutron detector, it has been already described in previous papers [1, 2, 3] and we just recall here the performances: the neutrons are detected by two blocks of plastic scintillators NE110 in coincidence (double scattering technique) and their energy is determined using a reconstruction method

FRONTIERS OF COLD FUSION

based on the measurement of the neutron Time of Flight (TOF) and of the impact position onto the scintillators.

A cylindrical cell is located in front of the first block and contains the metal: it can be loaded with gaseous D_2 or H_2 and degassed up to a vacuum of 10^{-11} bar. Two K-type thermocouples, the first one embebbed in the metal and the second one lying in the upper internal part of the cell, allow to monitor simultaneously the temperature of the metal and of the surrounding gas. The pressure of the gas is monitored too, by means of a piezoresistive pressure gauge located in the upper part of the cell.

For the Ti measurements, 20 g of high purity Ti sponge supplied by GINATTA TORINO TITANIUM SpA, were used. The operating thermal conditions of the Ti/gas system were chosen with the aim of exploring the dependence of the neutron emission, if any, upon the thermodynamic conditions. After the degasing step, a known amount of D_2 was dosed at room temperature. The Ti/D system was submitted to a number of thermal cycles consisting of a heating step from room temperature (~ 25°C) up to 540 °C at least (called run UP) followed by a cooling step to the room temperature (called run DOWN). During these cycles the gas flowed out and in the metal, as monitored by the increase and decrease of the pressure respectively and phase transitions occur in both UP and DOWN runs. During these repeated cycles, the morphology of the Ti gradually changes from sponge to a powder. This is due to the large strains associated with the hydride formation and phase transformations which cause the formation of internal cracks and fractures and ultimately lead to the crystals fragmentation.

The cycles were performed at two atomic ratios, 0.7 (~ 20% of the total data taking) and 1.8, i.e. near the saturation (~ 80% of the total data taking). For the higher loading runs the cycles in the Ti deuteride phase diagram were such that only the δ phase was concerned and therefore no phase transition was observed.

The duration of a run UP was ~ 100 minutes and the total number of runs UP was 12; an equal number of runs DOWN was performed, each one of ~ 250 minutes, followed by several hours (~ 13) at steady temperature for a total time of 13933 minutes. Also, 4 runs UP and 4 runs DOWN with Hydrogen gas (blank runs) having the same duration of those ones with Deuterium, were performed for a total time of 4631 minutes.

For the Pd measurements we used 54 g of metallic Pd in form of small cylinders, of diameter 1 mm and length ~ 2 mm. The operating thermal conditions were: 6 cycles UP from 20 °C to 350 °C and 6 cycles DOWN from 350 °C to 20 °C through α and β phases, for a total time of 2820 minutes with D_2 and the same with H_2; the atomic ratio was ~ 0.7. At the end of the experiment the small cylinders of Pd resulted to be transformed into small spheres due to the lattice strain release during the α–β phase transition producing the formation of internal cracks and dislocations.

If an emission of 2.5 MeV neutrons from the cell occurs, one expects that, by subtracting the spectra observed during the blank runs from those ones observed during the runs with D (all properly normalized in time) some excess should appear in the energy region around 2.5 MeV: in fact, looking at the Fig 1, where such a subtraction is reported, one sees that the energy channel between 2 and 3 MeV contains an excess of ~ 377 counts with a significance of about 3.9 standard deviation. Another way of searching for neutron excesses is that of subtracting from each run with D_2 filling the total spectrum obtained with H_2 filling, properly normalized in time. The counts in each channel were then obtained

as the weighted mean of the values obtained for each D_2 run and the error was calculated as the standard deviation. The result is shown by Fig.2 and no substantial difference is apparent between the two methods, apart the reduction of

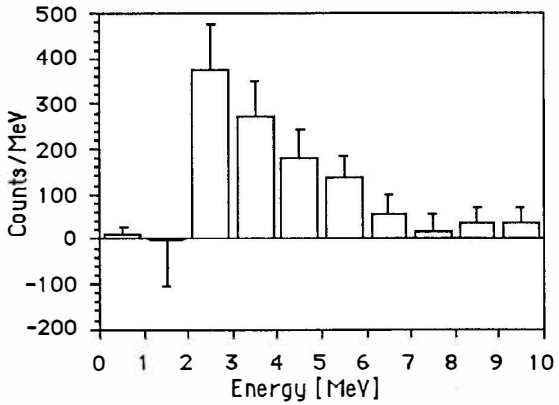

Fig.1 Difference between the neutron emission spectra observed in Ti/D and Ti/H systems: the error bars refer to the statistical error only and must be intended plus and minus.

the errors. The channel between 2 MeV and 3 MeV is again the most populated, at a 5.4σ level. As a further confirmation that the signal in this channel is not due to the subtraction method, such a procedure has been applied also to two halves of the total background measurements chosen at random obtaining a statistical fluctuation consistent with zero. An estimate of the neutron production per unit mass and time

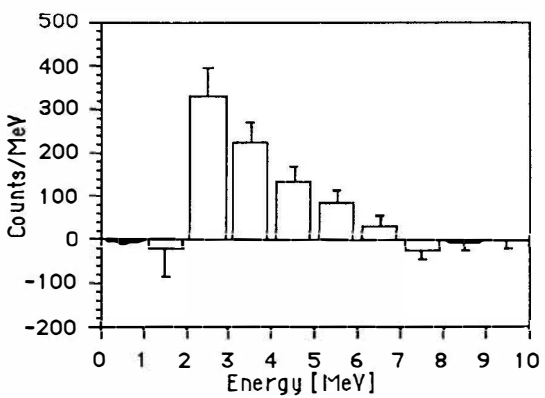

Fig.2 Spectrum of neutrons emitted from the Ti/D system (single runs analysis, as described in the text).

was made assuming that the neutron production rate was independent from time: on this basis a result of 0.11 ± 0.03 neutrons g^{-1} s^{-1} has been obtained.

As a final remark we point out the total absence of neutron bursts in our

measurements, never detected at the trigger level nor by the fast counters.

Concerning the measurements on the Pd/gas system, the total time for the data acquisition was considerably lower for both D_2 and H_2, with respect to the Ti:

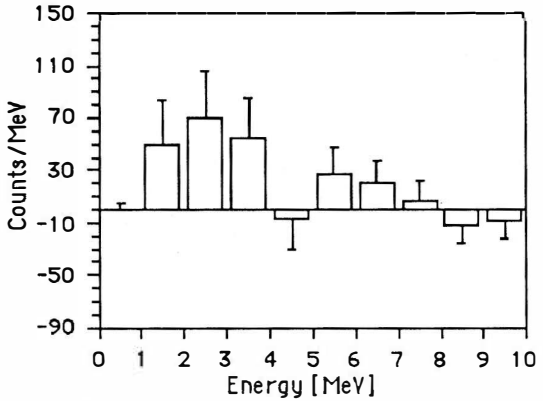

Fig.3 Difference between the neutron emission spectra observed in Pd/D and Pd/H systems: error bars as in Fig.1.

this was due to the decision of stopping the cycles when the Pd metal morphology showed to be highly modified with respect to the initial situation.

The same analysis applied to the Ti data was applied to the Pd runs and the result is shown by Fig.3: also in this case a small signal of ~ 70 events appears in the channel between 2 and 3 MeV, with the typical smearing on the nearest channels, but the statistical significance is small, less than 2 standard deviations. The neutron emission rate would be 0.02 ± 0.01 neutrons $g^{-1}s^{-1}$. Of course no burst has been counted.

3. Conclusions

In conclusion, we have confirmed with a greater statistical significance (5σ), the emission of 2.5 MeV neutrons from a Ti/D system submitted to thermodynamic cycles. No such a significant neutron emission was observed for the Pd/D system, again submitted to thermodynamic cycles corresponding to a crossing between the α and β phases. However, the neutron rate observed in this experiment is one order of magnitude lower than that observed in a previous experiment. We attribute this difference to the different nature of Ti metal used in the two experiments and we plan to repeat with the improved cell and with a further improvement in the neutron detector the measurement with the Ti shavings.

4. References

1. M. Agnello et al., in "The Science of Cold Fusion", Conf. Proc. Vol. 33, SIF, Bologna, 1991, p. 249.
2. G. Bonazzola et al., in "Understanding Cold Fusion Phenomena", Conf. Proc. Vol. 24, SIF, Bologna (1989) p. 313.
3. G. Bonazzola et al., NIM A299 (1990), 25.
4. T. Bressani et al., Conf. Proc. Vol. 33, SIF, Bologna, 1991, p. 105.

Evidence for Stimulated Emission of Neutrons in Deuterated Palladium

B. STELLA, M. CORRADI, F. FERRAROTTO, V. MILONE
INFN Roma and Dipart. di Fisica
Universita' "La Sapienza", P. A. Moro 2, 00185 Roma
F. CELANI, A. SPALLONE
INFN Frascati (Roma) - Italy

ABSTRACT

In order to study the effect of Palladium in cold fusion, metallic deuterated Pd samples have been irradiated with partly moderated Am/Be neutrons and the resulting neutron intensity has been measured by the FERMI apparatus, an efficient and sofisticated detector for moderated neutrons.

Once subtracted the vessel + (empty) Pd effect measured in "blank" runs, an excess of 13.0 ± 0.6 neutrons per sec. (≈ 4 % of the total measured rate) has been detected. Assuming 2.45 MeV energy for the neutrons emitted by the radiated sample, the resulting rate corresponds to several outgoing neutrons for every neutron impinging on the Pd-D sample. Similar measurements with Cadmium absorber gave lower effects. We don't observe any effect with gaseous deuterium.

The underlying process can be interpreted as d-d fusion in a Pd-D lattice perturbed by neutrons. The excess, predominantly due to thermal incident neutrons, demonstrates that the Palladium lattice strongly increases the probability for d-d fusion even almost at rest.

1. Introduction and methods

The main cognitive question concerning cold fusion is if the d-d fusion probability (almost) at rest inside deuterated metals like palladium (Pd-D) is many orders of magnitude larger than in vacuum and in the deuterium molecule. This is anyway not possible in Pd-D in a steady state, because the equilibrium d-d distance is much larger there than in the D_2 molecule.In fact all claimed evidences for cold fusion are connected to non static situations.

The main question can be approached by firing low energy deuterons to a Pd-D sample and detecting fusion products coming out. The cluster impact fusion experiments at

FRONTIERS OF COLD FUSION

Brookhaven [1] can be interpreted according to us (interpretation not considered by the authors) as a possibly positive answer (yet not including Pd). Results of accelerated single ions experiments have been reported at this conference. This approach suffers from a few drawbacks: 1) The ions explore only the surface of the sample; 2) fractal dimensions of the surface and field effects might play a role; 3) the metal surface is very often dirthened by different absorbed atoms; 4) the impinging energy cannot be so small to exclude "hot" fusion.

Our solution has been to use neutrons in order to perturb the equilibrium: the lower their energy the larger the effect (by elastic scattering), reducing the doubts of hot fusion. Moreover they explore the full volume of the sample. We use a moderated neutron source: repeated measurements with different moderators and absorbers can provide (by subtraction) the desired quasi-thermal projectile neutrons.

2. The experiment

As samples we have used metallic Pd, one cilinder (8 mm diameter, 2.5 cm length) and two square section wires (1.2 mm side, 3.0 cm length). They have been loaded in a stainless steel cell with 35 Atm. D_2 and low temperature thermic cycles. The loading has been measured first by pressure drop and then by mass, with a sensitivity of 10^{-4} g. We have found a D/Pd atomic ratio $\langle x \rangle = 0.71 \pm .01$ averaged over the full volume.

An Am/Be source (2660 neutrons/sec) has been put inside a moderator-collimator (fig. 1) made of poliethylene bulk and Cadmium walls. This "neutron gun" was designed by full MC simulation in order to have the maximum intensity of slow neutrons impinging on the target and the minimum number hitting directly the detector. A removable Cd sheet in front allows to change the spectral composition of the neutrons. The resulting spectra of the projectile neutrons in the two cases is shown in fig.2. The shaded area shows that by subtraction of two measurements we can obtain a

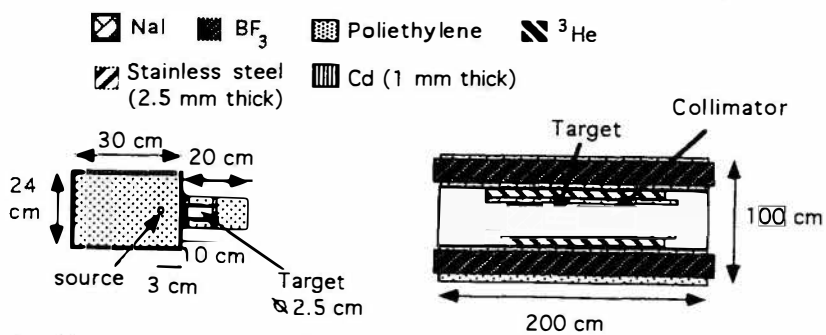

Fig. 1 : Longitudinal view of the collimator and of the FERMI apparatus

source enriched with thermal neutrons.

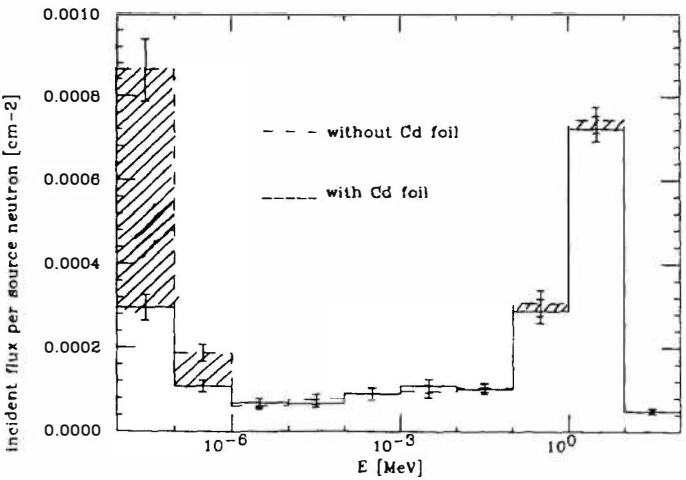

Fig. 2: Energy distribution of the relative neutron flux on the sample

As detector we have used FERMI apparatus, outlined in the previous contribution: it provides neutron detection with high efficiency for a broad range of energies, 0.5 MHz up to infinite time resolution for bursts, sofisticated electronics and data acquisition, full Monte Carlo simulation (experimentally tested), statistical energy determination. The experiment is setup inside the underground Gran Sasso laboratory, were the neutron background is 10^{-3} times lower than in Rome.

The Pd samples were put inside a stainless steel cell to be inserted in the detector (fig. 1) close to the neutron source. A poliethylene collar 2 cm thick surrounded the target cell. We have performed several blank measurements: 1) with cell in air; 2) with 35 bar D_2 in the cell; 3)cell with Pd in air, together with the main case of Pd-D in 35 bar D_2. Every measurement was repeated twice and every case was measured with and without Cd sheet in front of the source.

3. Results

The results are shown in table 1. The three columns concern the series of measurements with different neutron spectra: the third is the subtraction of the second from the first, to single out the effect of predominantly thermal neutrons.

Every column is a complete set of measurements, with blanks and repeated runs to check systematic errors (we find internal consistency of the data). The measurements with gaseous (incoherent) D_2 give a negligible effect, as expected by the simulation, which includes the neutron

Table 1 : rates in Hz for different experiments

Run type	No Cadmium	With Cadmium	Difference
Empty cell	298.54 ± .45	288.43 ± .46	
Pd sample	296.51 ± .39	286.60 ± .54	9.91 ± .67
Pd-D +D_2(35 bar)	309.54 ± .44	293.42 ± .54	16.12 ± .70
(Pd-D +D_2) - Pd	13.03 ± .59	6.82 ± .76	6.21 ± .96
Emitted neutron excess (MC eff.)	58.3 ± 2.6	30.5 ± 3.4	27.8 ± 4.3
Incident neutrons (MC)	11.3 ± 1.0	9.42 ± .92	1.86 ± .38
Excess/incident	5.16 ± .52	3.24 ± .48	14.9 ± 3.8

capture. After subtraction of the blank rates, we find an excess in both series with 22 and 9 (6.5 for the difference) standard deviations significance respectively and corresponding to 2 - 5 % of the total measured rate.

Our statistical energy determination (by distribution of counting rates of our 9 counters) has poor resolution in this case, due to the subtraction of large numbers. We then assume at present (we are working to improve the method) 2.45 MeV for the energy of the neutrons emitted by the samples. The corresponding efficiency was 22.3 %. With this number we determine the emitted rate of neutrons and comparing it with the incident one, we conclude that several neutrons have been emitted for every incident one. The last number to the right shows that most of the effect is due to thermal neutrons.

The results can be explained only by the influence of Pd lattice (since we don't find any effect with incoherent D_2). Fission neutrons (we have to check if our samples come from reactor) cannot likely account for the effect, because the measurement with Pd alone has been subtracted. We have checked other systematic errors.

4. Conclusions

We find an effect we attribute to multiple d-d fusion in Pd-D stimulated (perturbed) by thermal neutrons. The excess of several neutrons for every incident one implies that the Pd-D lattice has a far larger probability per unit time of emitting neutrons than the D_2 molecule.

We are checking if the time distribution of the events is consistent with our interpretation.The experiment is being repeated for confirmation.

References

1) Beuhler,R.J.;Friedlander,G.;Friedman,L.,1989,Phys. Rev. Lett.,63,1292;
Beuhler,R.J. et al.,1990,J. Phys. Chem.,94,7665.

"Cold" Fusion in a Complex Cathode

YOSHIAKI ARATA and YUE-CHANG ZHANG

Osaka University, 11-1 Mihogaoka Ibaraki, Osaka 567, Japan

ABSTRACT

A new cathode was developed, consisting of a nickel rod with a palladium layer applied by plasma spraying, the palladium layer activates the surface functions of the deuterated cathode. High reproducibility of a "cold" fusion reaction is confirmed by using this cathode.

INTRODUCTION

The authors have had a concept that the existence of microdefects is a necessary condition for cold fusion. A "complex cathode" with a sprayed layer of palladium including suitable microdefects has been developed and employed in a cold fusion experiment.[1]

Since the surface of the complex cathode has numerous microdefects such as cracks, porosity, boundary layer defects, lattice defects, dislocations, uneven surfaces, localized strain, etc compared with the surface of a cathode without a sprayed palladium layer, the actual surface area of the complex cathode was incommensurably larger than that of an ordinary palladium cathode. .

EXPERIMENT

The experimental arrangement consists of an electrosis cell, located in a cooling water basin.[2] Anode is a platinum tube, the cathode (see Fig. 1) consists of a 20-mm-diam x 50-mm-high nickel rod coated with a 300 μm surface layer of palladium, which was applied by plasma spraying in a low vacuum. [The abbreviations Pd(Ni) used herein to represent this complex cathode.] Neutrons were measured by using BF_3 and ^3He detectors.

The N-patterns actually measured with the BF_3 detector and mulitichannel analyzer are the puls height spectra of reactions A and B, as shown in Fig. 2. Through the wall effect in the detector with respect to reaction A, energy zone C is also formed.

Morefover, Fig. 2 shows N-patterns of the ^{252}Cf calibration neutron source

FRONTIERS OF COLD FUSION

and the Pd(Ni) cathode itself. The occurrence or nonoccurrence of the cold fusion reaction can be determined by using the ^{252}Cf N-patterns as the basis for comparison of the N-patterns of the cathode and of the background. To derive quantitative values for these N-patterns, the zones labeled (a), (b), (c), (d), and (e) in Fig. 2, each spanning 34 channels, were selected as regions of interest.

If the detector is not influenced by any disturbance (noise or background radiation), then (c)=(d)=(e)=0. When there is a disturbance, however, then usually (c)≈(d≈(e)≠0, and these values will increase in close proportion to the time elapsed. Hence, to use N-pattern data to derive a quantitative value for the intensity of a neutron flux radiated from any neutron source, it is necessary to consider the background Y_b arising from various sorts of disturbances, defined as

$$Y_b = \frac{(c) + (d) + (e)}{3}$$

We have located reaction A, which is regarded as the key phenomenon for demonstrating generation of neutron flux, in region of interest (a). That region's pulse count relates to the neutron flux valuation Y_N, Y_N=(a) - Y_b. When Y_N= 0, there is no neutron flux, and when Y_N has significant value, generation of a neutron flux is confirmed. When the experiment contineued the long period, Y_b is a key factor in demonstrating the existence of neutron flux generation as shown in Fing. 3..

Three Pd (Ni) cathodes were deuterated in an electrolyte of heavy water with 0.07M LiOH, and one Pd(Ni) cathode was hydrogenerated in light water with the same electrolyte content. Generation of neutrons from the deuterated cathodes was continuously detected, indicating the occurrence of cold fusion. The neutron measurement for the hydrogenerated cathode was virtually identical to the background level, indicating there was no neutron generation from the hydrogenerated cathode.

Figure 4 presents a comparison of the "N-patterns" (pulse-high spectra) observed after 120 h from the background, a deuterated cathode, and the hydrogenated cathode. To aid comparison, is also presents the N-pattern of a deuterated cathode after 192 h next to that of a calibrated neutron ^{252}Cf (2.6 10^3 n/s) after 30 min. of measurement. Figure 5, which is derived from observed N-patterns such as those in Fig.4, shows that similar results were repeatedly observed in several experiments on different dates. This is vital data, for it is the first reported confirmation of the reproducibility of cold fusion.

Neutrons were measured simultaneously by identically collaborated ^{3}He and BF_3 detectors, the measurements indicating that the deuterated cathodes are the neutron sources.[2]

REFERENCES

1. Y. ARATA and Y. C. ZHANG, "Corroborating Evidence for "Cold" Fusion Reaction, " Proc. Jpn. Acad., 66, Ser. B6 (1990)

6. Y. ARATA and Y. C. ZHANG, "Reproduced "Cold" Fusion Reaction using a

complex cathode", Fusion Technol., 22, 287 (1992).

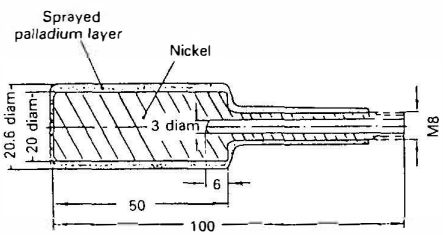

Fig. 1. Schematic of the complex cathode.

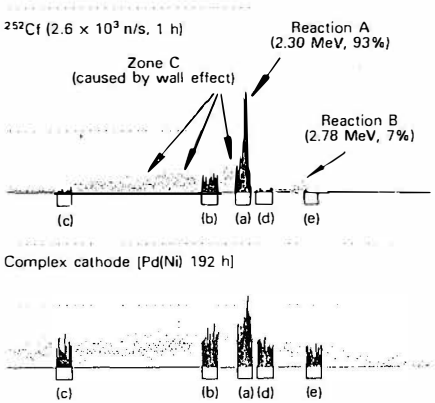

Fig. 2. Definition of Y_N and Y_b, in terms of 34-channel regions of interest of the N-pattern of the deuterated Pd(Ni) cathode, obtained by using a BF_3 detector and multichannel analyzer (MCA-7800, 1024 channels). The horizontal axis is channel number, the vertical axis is pulse height: Counts in channels (a) 500 through 533, (b) 430 through 463, (c) 137 through 170, (d) 543 through 576, and (e) 640 and 673.

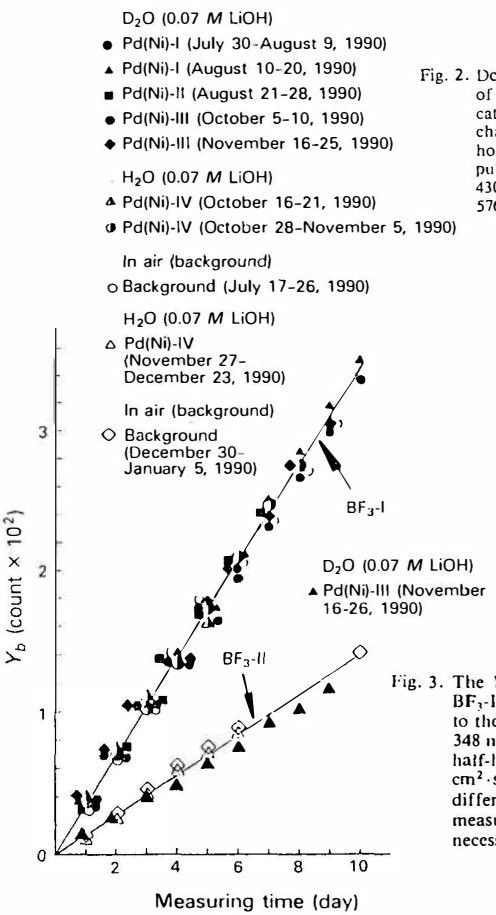

Fig. 3. The Y_b characteristics obtained by detectors BF_3-I and BF_3-II. The detectors are identical models manufactured to the same standards (Mitsubishi ND-8534-34-30; 25 × 348 mm; gas pressure 300 Torr; applied voltage 1.7 kV; half-handwidth 2.5 to 4%; neutron sensitivity 2.5 n/cm²·s; amplification factor 15). They nevertheless have different sensitivities, as indicated by the differing Y_b measurements; hence, for comparative purposes, it is necessary to use data from only the same detector.

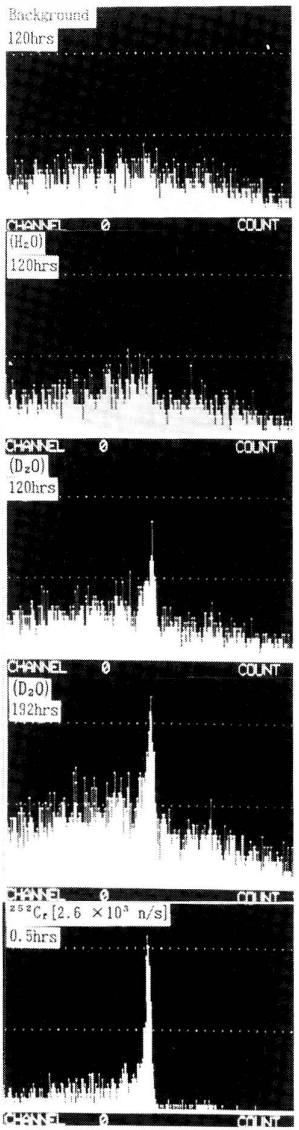

Fig. 4.

Comparison of N-patterns (pulse-height spectra) of the background, the hydrogenated complex cathode, two deuterated complex cathodes, and a calibrated ^{252}Cf neutron source, obtained by detector BF_3-I (full scale: 64 counts).

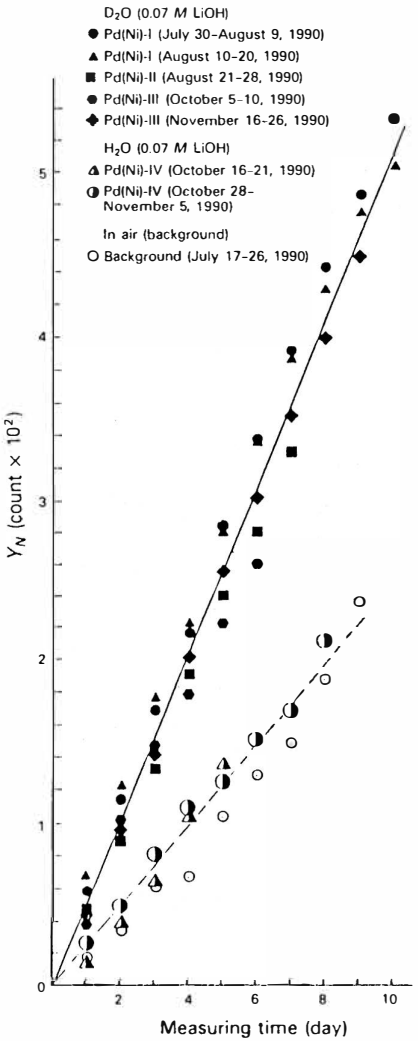

Fig. 5.

Comparison of Y_N characteristics of the background, the hydrogenated complex cathodes, and the deuterated complex cathodes, obtained by detector BF_3-I. Note that the characteristics of the background and the hydrogenated cathode are almost the same.

Neutron Measurements in a AC-Discharged Tube

W.X.Liang, D.M.Xu, G.Y.Zhang, Z.L.Yao, E.Y.Wang

Southwestern Institute of Physics

P.O.Box 432, Chengdu, Sichuan 610041 P.R.China

A schematic diagram of the device is shown in Fig.1. Discharge is produced by an AC voltage (300V-600V, 50Hz)applied between two Pd Coaxial elecerodes in a glass tube filling deuterium gas with pressure in the range of 0.1 to tens Torr. The neutron counts are recorded by two long Counters Consisting of BF_3 Counter. One of the neutron detectors is close to the glass tube and another is far away from glass tube for baokground noutron level measurements. After 20 minutes discharge cleaning with 350V AC at this time increasing the voltage to 500v, the neutron counts are suddenly increased to the level higher than 4 times of the background. Fiffteen minutes later increasing a little deuterium pressure again, the neutron counts rise to a level of 10 times higher than the bacground (see Fig.2).

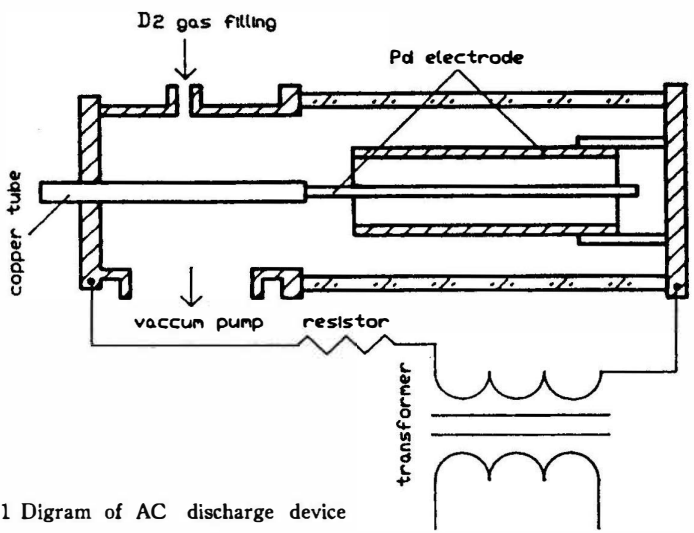

Fig. 1 Digram of AC discharge device

FRONTIERS OF COLD FUSION

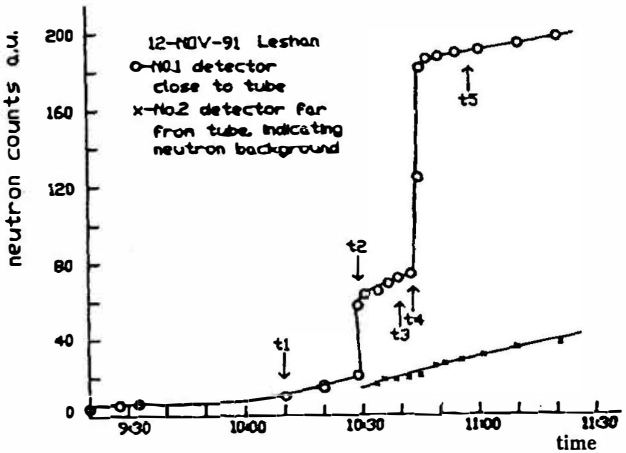

Fig.2 Neutron count changing with experiment condition changing. At time t1 starts gas filling and AC voltage is 350V, at t2 voltage raises from 350V to 500V, at t3 gas fills further, at t2 and t4 neutron counts increase suddenly, at t5 stops gas filling.

On the basis of traditional electrolysis proposed by Fleischmann and Pons, a electrolyzer consisting of Pd cathod and Pt anode placing in a solution of D_2O and LiOD is placed in a pulsed magnetic field to observe the effect of magnetic field upon the electrolysis. The width, peak hight and period of pulsed magetic field are as follows: 50 microsecond, 7 Tesla and 13 second respectively. One of above mentioned long counter is used to measure the neutrons from the electrlyzer. The neutron measurement results are indicated in Fig.3 from which one can see that the measured neutron counts with and without pulsed magnetic field appear to be same.

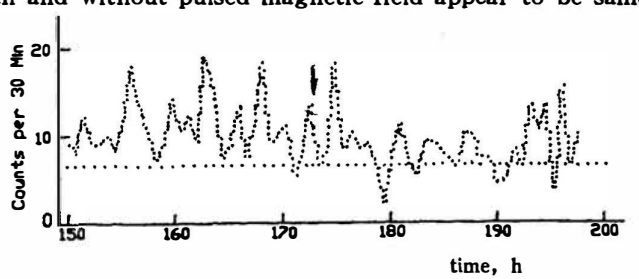

Fig.3 Neutron count changing with time. The arrow indicates the time applying pulsed magnetic field. The straight line denotes average neutron background counts.

References

1. Martin Fleischman and Stanley Pons, Submitted to Journal of Electronanalytical Chemistry, March 11, (1989).
2. Z.W.Li, Private communication, (1989).

Anomalous Effects in Deuterium/Metal Systems

Long Heqing, Sun Sihai, Liu Hongquan, Xie Renshou
Institute of Sichuan Material and Technology
Zhang Xinwei, Zhang Wushou
Institute of Applied Physics and Computational Mathematics
P.O.Box 8009, Beijing 100088, PRC

Abstract

Stable and high yield of neutron had been measured repeatedly in the glow discharge process of the flowing rare deuterium gas in a Deuterium / Metal system consisted of Pt, Nb, W, Cu, Mo, Ag or Fe with D respectively.

A layer of metal film which was deposited on the inner surface of glass reaction bulb in the glow discharge process and insulated from electrodes played key action on inducing anomalous effects repeatedly. Neutrons had been measured by activation detector (^{115}In, ^{193}Ir) and recoil proton neutron spectrometer; there was a continued spectrum in the energy range from 0.5Mev to 11Mev; The average neutron energy was 3.55Mev; different heights of peak appeared at (0.5–1.0)Mev, (3.0–3.5)Mev, (5.0–5.5)Mev, (8.0–8.5)Mev (9.0–9.5)Mev and (10.0–10.5)Mev; but the neutrons of (2.0–2.5)Mev interesting to people appeared in a valley of the energy spectrum and their yield was only 7–8% of the total yield of neutrons. The highest yield of neutron appeared in D / Pt system, the lowest appeared in D / Fe system, the highest average yield of neutron was 8.3×10^3n / s in D / Nb system (observed time 470min.), the yield of neutron burst was $(0.26–6.2) \times 10^6$n / s(time interval 0.1s).

Intense gamma–ray emission had been detected at same time, the average activity was 3.1×10^4Bq (detected time 175min.). There was a continued gamma spectrum in the energy range from tens Kev to > 20Mev, different heights of peak appeared at tens Kev (Point a), 3.4Mev (b) and 5.8Mev(C), The peaks of energy>7Mev were not quite certain.

The similar experiments were conducted many times with hydrogen or helium gas instead of deuterium but no neutron over background was detected.

Keywords

Deuterium / Metal systems, neutron spectrum, gamma spectrum, activation method, anomalous nuclear effect.

1. Introduction

FRONTIERS OF COLD FUSION

Since the announcement of cold fusion by Fleishmann and Pons[1], there have been a lot of research works on D / Pd or D / Ti system in the world, Eiichi Yamaguchi[2] had presented gigantic neutron bursts of $(1-2)\times 10^6$n / s in Mn–o / Pd: D / Au system, but no average yield and spectrum of neutron.

As for the neutron emission in anomalous nuclear effects, there were only yield of neutron burst and rough energy range but no stable neutron emission and energy spectrum in past papers. The reasons were <1> rate of neutron emission was low, <2> anomalous nuclear effects couldn't be controlled and repeated, so the neutron energy spectrum (NES) and gamma spectrum couldn't be measured exactly, our works have been getting on aiming these questions.

2. Experiments

As having presented[3], we had reached $\sim 10^2$n / s of average neutron yield in a D / Pd system by the dynamic low pressure gas discharge method. But it was far away for measuring NES and neutron activation. At latest, it was found by Long Heqing that there had been intense neutron and gamma–ray emission in Deuterium / Metal systems consisted of Deuterium with some Metals (as Pt, Nb, W···) except Pd or Ti. At present, high yield of neutron emission ($\sim 10^4$n / s averaged) could be lasting as you want. The features of this method are <1> electrode is made of Pt, Nb, W··· etc., <2> a film of metal (same as metal of electrode) is deposited on the inner surface of the reaction glass bulb and insulated from electrodes, <3> low pressure deuterium gas flow is supplied, <4> the parameters are suitable for glow discharge. When the applied voltage is greater than 17KV there will be intense neutron and gamma–ray emission to be observed.

The apparatus used in this work have been discribed in previous publication[3], but the measuring systems will be introduced in detail.

2.1 NES measurement

NES was measured by a recoil proton fast neutron scintillation spectrometer, it had low response for gamma–ray. The counts rate of gamma–ray, which emitted from ^{60}Co and its energy > 0.5Mev, was only 0.05%. It was interference–free efficicently. NES was transformed from proton–recoil spectrum measured in the experiments, the inverse matrix F^{-1} could be calculated from proton–recoil spectrum of ^{238}Pu–Be Neutron Source and its NES[4] so the neutron spectrum is given by

$$N = F^{-1}M \tag{2.1}$$

where M is column matrix of proton–recoil spectrum.

2.2 Activation

Activation was the most reliable neutron measurement method in a high electromagnetic interference environment. ^{115}In and ^{193}Ir active pieces were placed in paraffine slowing–down layer (7.5cm thick, it is 15cm from the center of reaction bulb) and irradiated for several hours, then measuring the activity by α, β measuring apparatus with low background.

2.3 Neutron burst

Neutron burst was defined of maximum counts in 0.1s in the experiments, the mono–channel output of spectrometer was linked with the entrance of computer (IPC–610) accross counting board, it could show the counts of every time interval (0.1s).

2.4 Gamma–spectrum measurement

A NaI scintillation counter was used as the gamma–ray spectrometer, the measurement efficiency was 0.8% for the gamma–ray emitted from ^{60}Co, the counts of background was 13CPS after shielding.

3. Results

3.1 Neutron yield

<1> Relative yield of neutron

Relative neutron yield of different D / M systems are shown in Table 1, these metals were chosen at random and neutron emission could be measured in all of D / M systems, the relative order was Pt, Nb, W, Pd, Ag, Cu, Mo and Fe.

<2> Activation

For scaling active pieces, similar experiments were conducted with ^{238}Pu–Be Neutron Source instead of the reaction bulb, the ^{238}Pu–Be Neutron Source was placed in "center of the reaction bulb" and irradiating for 20min., then neasuring the β activity of active pieces, the results are shown in Table 2. The effective distance in Table 2 was deduced from point source formula.

In experiments, the active pieces were bare ^{115}In pieces, ^{115}In pieces wraped by cadmium (Cd) and bare ^{193}Ir pieces, the results of D / Nb system are shown in Table 3, the average yield of neutron calculated from the average fluence rate was $2.64 \pm 0.36 \times 10^3$n / s. The results of D / Pt system are shown in Table 4, the average yield of neutron calculated by same method was $1.24 \pm 0.51 \times 10^4$n / s.

The measuring half life period of ^{116}In (53.03 ± 5.5min) and ^{194}Ir (19.6 ± 1.6hour) consisted well with standard value 54.1min and 19.4hour respectively.

The result of ^{115}In piece which wraped by cadinum and had been irradiated for 4 hours was background level.

<3> NES method

Less understanding of neutron distribution in anomalous nuclear effects, we assumed neutrons were emitted from a "point source" and the effective distance $R_{eff} = 8.7$cm was deduced from ^{238}Pu–Be Neutron Source instead of the reaction bulb at same condition.

The fluence rate of D / Nb system is shown in Table 5. The average neutron yield was $6.1 \pm 1.6 \times 10^3$n / s, the maximum average neutron yield was 8.3×10^3n / s (observed time 470min.). Comparing results of the two methods, it is consistent in 40% relative deviation.

3.2 Neutron Spectrum

From the NES of ^{238}Pu–Be Neutron Source[4] (shown in Fig.1) and the measured proton–recoil spectrum by our spectrometer. We calculated inverse matrix F^{-1} with formula(2–1) (Energy interval was chosen of $\Delta E = 0.5$Mev), the detection efficency of energy interval was calculated from the proton–recoil spectrum with the NES and is shown in Figure 2.

We had scaled the spectrometer by a 2.45Mev monoenergitic neutron

source, the channel was as same as of the ^{238}Pu–Be Neutron Source.

NES of D / Nb system is shown in Figure 3 (980min.) and Figure 4 (470min.). The results of Figure 3 was accumulation of that of Figure 4, their shape and peaks are consistent with each other. Because of low yield of neutron in D / Pd system, there was only NES of E< 6.0Mev in Figure 5. NES of D / Pt system is shown in Figure 6. NES of E< 6.0Mev of three systems are similar.

For D / Nb system, the interval of neutron energy was from 0.5Mev to 11.0Mev, the average energy was $\bar{E}_n$ = 3.55Mev, five different heights of peak appeared at (3.0–3.5)Mev, (5.0–5.5)Mev, (8.0–8.5)Mev, (9.0–9.5)Mev and (10.0–10.5)Mev. But the spectrum of D / Pt system was broken off in the interval of (8.5–10.5)Mev, it seemed that there were higher energy neutrons (E> 10.5Mev), there were five peaks too. The neutrons of (2.0–2.5)Mev interesting to people appeared in a valley of the energy spectrum and their yield was only 7–8% of the total yield of neutrons.

3.3 Gamma–ray

Gamma spectrometer was scaled by ^{22}Na, ^{60}Co and ^{137}Cs gamma–source. The results are shown in Table 6. But the spectrometer had some response for ^{241}Am gamma–source (0.05957Mev), so the data of low energy in Table 6 couldn't be used.

Gamma–spectrum of D / Nb system is shown in Figure 7. The interval of energy is from tens Kev to>20Mev, the peaks of E< 7Mev are obvious, they are tens Kev(point a), 3.4 Mev(b) and 5.8 Mev(c). The peaks of high energy are less clear because of low intensity, notably the yield of gamma–ray was about ten times of neutron.

3.4 Contrasted Experiments

The similar experiments were conducted with hydrogen gas and helium gas instead of deuterium but no neutron over background was detected.

The neutron counts for 70 minutes are shown in Figure 8 and Figure 9, there are 0.3CPM interference counts in 44–90 channel (corresponding 0.5–1Mev) because of 17–24KV high voltage appied in the experiments, it could be neglect.

4. Discussion and conclusion

4.1 Gas discharge process

In the dynamic low pressure gas discharge process, a lot of atom or atom cluster would be sputting from electrodes and depositing on the inner surface of reaction bulb to form a metal film. Plasma was formed in major part space between electrodes; in addition, there would be a accelerating field on the inner surface of metal film, it made $D^+(D_2^+)$ moving to the metal film. Other wise, the density of Deuterium was low in the electrodes because of high temperature on it. So the anomalous effects were caused by the metal film mainly but not the electrodes.

4.2 Contribution of Beam–Target neutron

As a result of calculating, the neutrons caused by beam–target effect were less than 100n / s, it was less than 2% of total neutrons. If there were a lot of neutrons caused by beam–target effect there would be a peak of (2.0–2.5)Mev

in the NES, just the opposite, there was no and the neutrons in there were only 7–8% of total neutrons.

Another fact was if the deuterium gas pressure added to 27–50Pa the counts of neutrons did not reduce obviously.

4.3 High energy neutrons

It seemed that there had been high energy neutrons in NES of D / Pt and D / Nb systems, because of our spectrometer limitation, the high energy neutrons (E > 11Mev) couldn't be determined. It needs advance research.

4.4 The action of metal

The metals in experiments were chosen at random, they don't take part in the primary reaction in anomalous nuclear effect at least, but the secondary reaction maybe, the coulomb barrier between deuterons may be reduced by metal help, so the reaction possibility rises notably. The peaks in NES and gamma–spectrum may be relate multi–body fusion. But simulation indicate, only multi–body fusion can't explain the peaks[5].

Acknowledg ments

The authors express their thanks to Mr. Wu sheng, Wu DongZhou, Zhou Ruyan for their discussion and supporting, thanks to members of taking part in the experiments for their combining and helping, especially thanks are due to Prof. Li Xinzhong for his help and support.

References

(1) M.Flieshmann, S.Pons and H.Hawkins, J.Electronal. Chem. 261, 301(1989)

(2) Eiichi, Yamaguchi et al., Jpn. J.Appl. Phys. 29, L666(1990)

(3) Long Heqing et al., The anomalous nuclear effects inducing by the dynamic low pressure gas discharge in D / Pd system (to be publishing in this proceeding)

(4) S.Block et al., Health Phys, 13, 1027(1967)

(5) Zhang Xinwei and Zhang Wushou et al.,(to be published)

Table 1 Relative neutron yield of different D / M systems

system	P_t–D	Nb–D	W–D	Pd–D	Ag–D	Cu–D	Mo–D	Fe–D
voltage (KV)	17–21	17–21	17–21	17–21	16–18	17–21	17–21	17–21
relative neutron yield	10.1	8.2	5.2	3.7	2.8	1.6	1.6	1.0

Table 2 Scaled results of ^{115}In active pieces

sample	half life (min.)	decay rate when stop irradiating (Bq)	fluence rate $\times 10^{-3}$ ($n / m^2 \cdot s$)	ratio of hot neutron fluence rate over activity $n \cdot m^{-3}s^{-1}Bq^{-1}$	effective distance (cm)	measuring apparatus
1*	52.03	158.8	4.91	3.09×10^2	11.9	BH–1216
	56.60	162.2	4.98	3.07×10^3	11.9	LB–1900
2*	54.03	114.5	3.7	3.28×10^3	13.7	BH–1216
	56.40	122.6	4.01	3.27×10^2	13.2	LB–1900
average value	54.8 ± 1.8	139.5 ± 21	4.41 ± 0.54	$3.18 \pm 0.10 \times 10^3$	12.7 ± 0.8	—

Table 5 Results of NES method of D / Nb system

Sample	1	2	3
fluence rate $\times 10^{-4}$ ($n / m^2 \cdot s$)	4.83	8.73	5.64

Table 6 Scaled results of energy–channel

gamma source	energy E, (Mev)	corresponding channel (n)	$\Delta E_\gamma / \Delta n$	$\Delta E_\gamma / \Delta n$
^{22}Na	1.274	217	0.0220	0.0237 ± 0.0012
^{60}Co	1.253	216	0.0246	
^{137}Cs	0.662	192	0.0245	

Table 3 Results of activation of D / Nb system

sample	half life	pure count rates (CPS)	decay rate (Bq)	fluence rate $\times 10^{-4}$ ($n / m^2 \cdot s$)	detecting limit (Bq)
1* 2* 3*	53.03 ± 5.5 min.	$2.60 \pm 0.46 \times 10^{-2}$ $2.44 \pm 0.49 \times 10^{-2}$ $2.43 \pm 0.43 \times 10^{-2}$	0.100 0.094 0.094	1.48 1.48 1.15	0.025 (BH–1216)
4**	—	0	—	—	0.025 (BH–1216)
5***	19.6 ± 1.6 hours	$3.12 \pm 0.39 \times 10^{-1}$	0.104	1.10	0.025 (BH–1216)

* ^{115}In ($\Phi 30 \times 0.087$mm)

** ^{115}In ($\Phi 30 \times 0.087$mm) wraped by Cd (0.5mm thick)

*** ^{193}Ir ($\Phi 40 \times 0.2$mm)

Table 4 Results of activation of D / Pt system

sample+	pure count rates (CPS)	decay rate (Bq)	fluence rate $\times 10^{-4}$ ($n / m^2 \cdot s$)	detecting limit (Bq)
1*	$6.93 \pm 0.80 \times 10^{-2}$	0.231	3.60	0.025 (BH–1216)
2*	$3.29 \pm 0.20 \times 10^{-1}$	0.658	8.67	0.020 (LB–1900)

\+ ^{115}In ($2 \times \Phi 50 \times 0.087$mm)

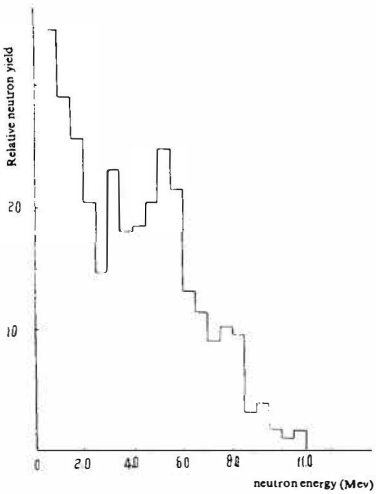

Fig. 1 ^{238}Pu–Be Source neutron spectrum

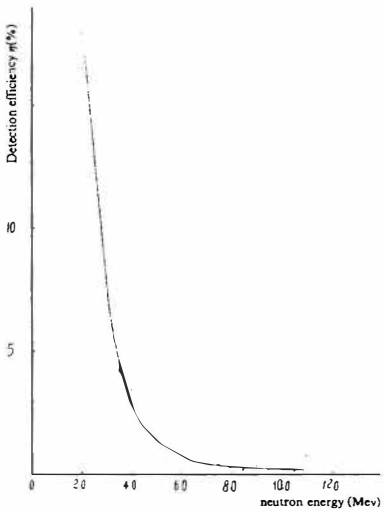

Fig. 2 Detection efficiency of fast neutron spectrometer neutron curtain in energy interval

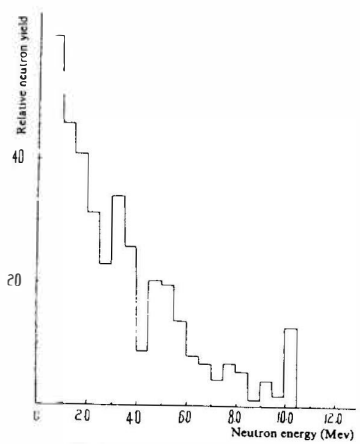

Fig. 4 Neutron spectrum of D / Nb system

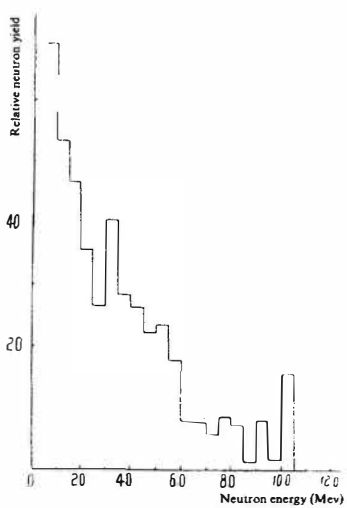

Fig. 3 Neutron spectrum of D / Nb system

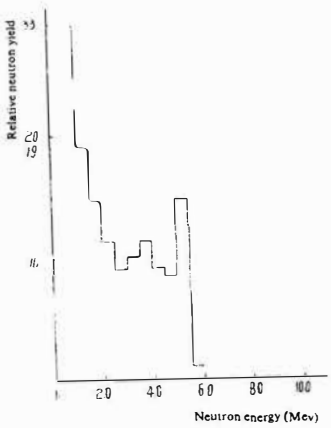

Fig.5 Neutron spectrum of D / Pd system

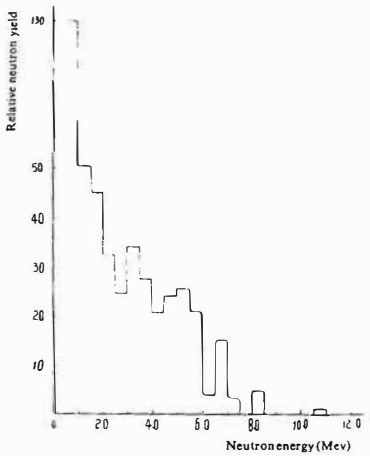

Fig.6 Neutron spectrum of D / Pt system

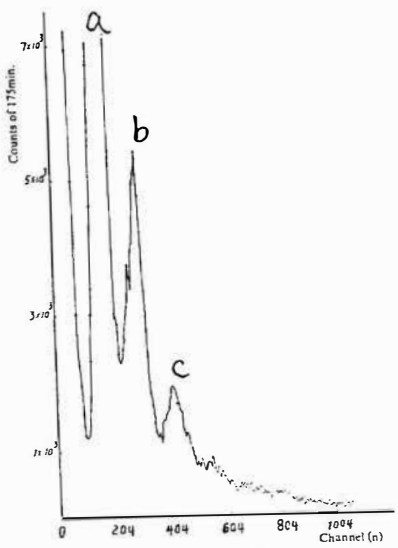

Fig.7 Gamma-spectrum of D / Nb system

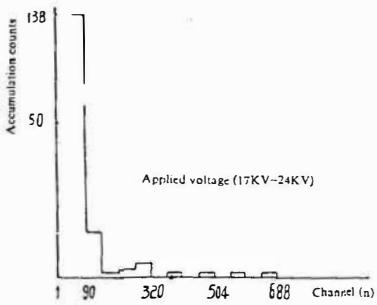

Fig.8 Counts of 70min. of H / Nb system

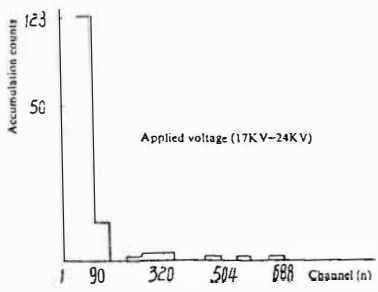

Fig.9 Counts of 70min. of He / Nb system

The Anomalous Nuclear Effects Inducing by the Dynamic Low Pressure Gas Discharge in a Deuterium/Palladium System

Long Heqing, Xie Renshou, Sun Sihai, Liu Hongquan, Gan Jinbang, Chen Bairong
Institute of Sichuan Material and Technology
Zhang Xinwei, Zhang Wushou
Institute of Applied Physics and Computational Mathematics
P.O.Box 8009, Beijing, PRC

Abstract

Neutron emission which average rate was 13–330 n / s and X–ray which average energy > eU_{max} were continuously detected from a gas discharge reaction bulb, these neutrons were divided into two groups of 2–2.5Mev and 2.5–7Mev, the emission of neutron was 100% reproducible.

Keywords

Deuterium / Palladium system, gas discharge, palladium film, Deuterium reaction

1. Introduction

Since April 1989, we had employed gas discharge activation in D / Pd system for absorbing and releasing deuterium experiment[1] similar to the of Xiong Riheng[2], Wada et al.[3]. Results of time distribution and rates of neutron emission were approximately to the same extent of Wada, but the first peak of neutron burst induced by the first discharge was more lower. And we had verfied the rate of neutron emission did not relate to D / Pd ratio obviously if the atom ratio of D / Pd$\geq$0.3, a "three electrodes" reaction bulb that we will introduce had similar result too. But the neutron yield was still higher and neutron emission was 100% reproducible.

2. Experiment

The apparatus used for fusion studies is shown schematically in Figure 1. It is composed of reaction bulb, vacuum system, source of hydrogen / deuterium, high voltage transformer and detection system etc..

The palladium rods were carried out in a reaction glass bulb of 200ml (Φ80mm, 2mm thick) with a pairs of electrode stems, the palladium 99.97% rods of 2mmΦ were fixed to the Kovar eletrode stems. Before experiment, Pd

FRONTIERS OF COLD FUSION

electrodes were cleaned, degassed and activeted, the atom ratio of D / Pd was up to 0.5–0.8 generally.

In the experiment, there would have been sputtered a layer of film (1–5μm thick) on the inner surface of reaction bulb, the distance of electrodes was about 50–60mm, the shortest distance bettween electrodes and palladium film was 10–15mm.

The high voltage was supplied by a 5KVA, 50Hz Alternating current transformer(YDJ5 / 50). The distributed capacity of source electrode to earth was 500PF.

Neutron was measured by a recoil–proton fast neutron scintillation counter with a mono–channel analyzer, they could discriminate the energy of neutron and sufficiently suppress the contamination of γ–ray. Background of neutron was 4–5 CPH.

X–ray was measured by a compensate energy thermoluminescence dosimeter, it could measure the dose of X–ray or γ–ray which energy was greater than 10 Kev.

Experiment procedure is summarized as follows.

1. At a constant pumping speed, the rate of deuterium gas flow was adjusted so the pressure was 4–13Pa, high voltage was applied to induce the dynamic low pressure gas discharge.

2. Deuterium gas was filled in the reaction bulb at room temperature, the time of absorbing deuterium was from several minutes to tens hours, then evacuating and discharging.

3. Results

Neutron measurement had carried out intermittently, every observation had continued from severl minutes to ~ 100 minutes (See Tab.1,2,3 and Fig.2). All of neutrons were divided into two groups[1], low energy group was 2–2.5Mev, the higher was 2.5–7Mev. The average rate of neutron emission was 13–330n / s. In experiments, we assumed: <1> the average energy of neutron was 2.45Mev and 4.5Mev separately; the relevant measurement efficiency was 2.38% and 0.38%; <2> neutrons were emitted from palladium film isotropical; the solid angle was about 5%. Neutron emission could be observed repeatedly if only the experiment parameters were suitable, the counts of neutron would be tend to background level after 20 minutes of the gas source was switched off. If the pressure was too low the counts of neutron would reduce obviously.

After saturate absorbing deuterium, while evacuating and discharging at same time, neutron emission had also been observed, but the rate was lower than the former and the reproducibility was only 60%, the neutron emission was happened in or after the short time of self sustaining discharge.

The palladium film could break to many pieces if it had absorbed deuterium supersaturated after used many times.

The same experiments were conducted with hydrogen gas instead of deuterium and the results are shown in Table 4 and Table 5, it indicats that neutron emission was background level and confirms that only deuterium–loaded system can emit neutrons.

X–ray was detected in the process of gas discharge. The accumulative maximum dose rate reached 70rem / h. Different thickness of Cu absorbing flats were applied and the accumulative dose is shown in Table 6, the plate was made of unitary copper material and didn't include the glass wall (2mm thick) of re-

action bulb and polythene wall (2.5mm thick) of dosemeter. Fit the data of Table 6:

Linear absorb cofficient $\mu = 199.7cm^{-1}$ was related to the average energy of X-ray $Ex \approx 37kev$, but the applied maximum voltage in experiments was 20KV, it corresponded to maximum voltage on the reaction bulb was only 15.5KV, it is to say that $eU_{max} = 15.5Kev < 37Kev$. If X-ray was induced by electron bremsstrablung and energy of electrons was continued, the maximum energy of electrons was about 50Kev.

4. Conclusion

It is possible that palladium film played a key role for gain the anomalous nuclear effect. In the experiment, regulating current limiter, there would be glow discharge occured, and palladium atom (or atom cluster) was sputtered from the tip of electrodes meanwhile, electrodes getting short, distance of electrodes getting long. The Tempreature of reaction bulb wall rised to 60–200 ° C at same time.

We occasinally observed added current pulse over the stable current signal, the average value of current pulse was ~ 1A, the maximum > 10A, and the characteristic time was several ms, but the current induced by glow discharge was less than 100mA. neutrons observed were mainly distributed in higher energy region of 2.5–7Mev, the production rate of higher energy neutrons was about 9 times of 2–2.5Mev lower energy meutrons, the maximum was 30 times, we had test this ratio repeatedly in applied voltage of 10–20KV, the most probably value was about 9.

Beacuse low gas pressure was carried out and high voltage was applied, it is suspected that neutrons were caused by beam–target effect. But beam–target effect was not mainly in fact, the reason are <1> 2.5–7Mev higher energy neutrons were observed and their production rate was higher than that of 2.0–2.5Mev, but the applied voltage on the reaction bulb was less than 15.5KV, it can't be explained by the classical Bean–Target Model[4]; <2> if neutrons were caused by beam–target effect, the yield of nutrons would increase when the gas pressure decreased, but results were close each other when gas pressure was 4Pa and 27Pa separately; <3> when the applied voltage increased, corresponding to beam–target model relately the yield of neutron would increased but this didn't happen (See Tab. 2) in the experiment. So the beam–target neutron was not mainly in there.

Acknowledgment

We appreciate the valuable discussions with Prof. Wu Sheng, Gao Guotong, Jian Guoqiang, Qin Youjun, Wu Dongzhou.

Reference

[1] Gao Guotong, Long Heqing,
II Annual conference on Cold Fusion, June 29–July 4, 1991, Como Italy
[2] Xiong Riheng et al. Proc of Conference On Cold Fusion, Beijing, China, May 1990
[3] N.Wada et al., Jap.J.Appl. Phys. 28 (1989) L2017
[4] Zhang Xinwei, Zhang Wushou (to be published)

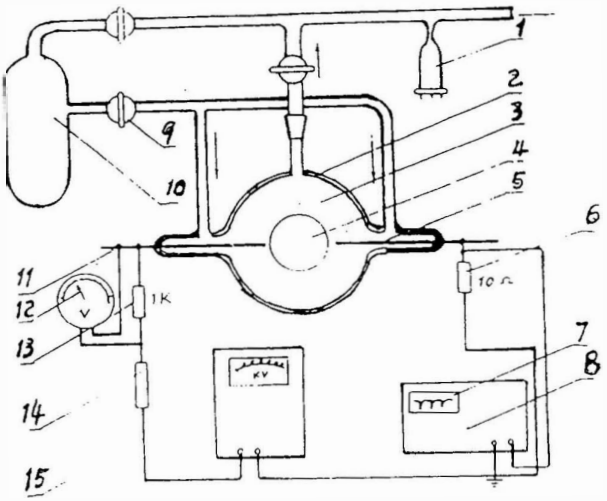

1. Vacuum gauge 2. palladium film 3. reaction bulb
4. neutron detector 5. earth electrode 6. sample resistence
7. sharp of current 8. oscilloscope 9. valve 10. gas source
11. sourle electrode 12. voltmeter 13. standard resistence
14. current limiter 15. high voltage source

Fig.1 Experimental set-up

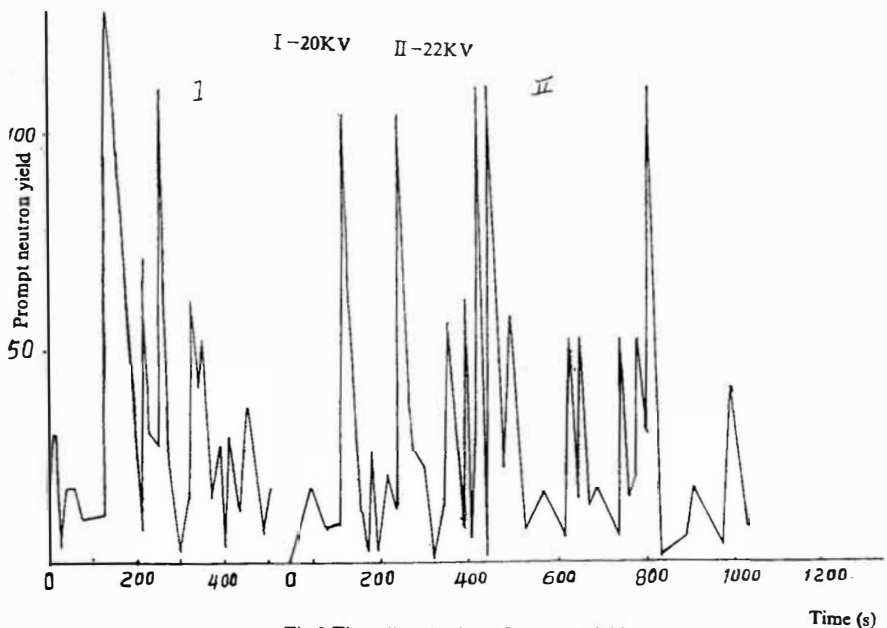

Fig.2 Time distrubution of neutron yield

Table 1 Neutron yield in the dynamic low pressure gas discharge process(16KV, 6Pa)

time (min.)		0.5	0.8	1.1	1.3	1.8	2.0	2.5	3.0	3.7	4.2	4.6
neutron counts	2–2.5(Mev)	1	1	2	5	6	7	8	8	9	9	10
	2.5–7(Mev)	1	3	4	6	7	11	13	15	15	16	17
average neutron yield (n / s)	2–2.5(Mev)	1.4	0.9	0.9	2.6	2.3	2.1	1.8	1.4	1.4	1.2	1.2
	2.5–7(Mev)	8.7	16.3	15.8	20.0	16.9	23.9	22.6	21.7	17.6	16.5	16.0
	sum	10.1	17.2	16.7	22.6	19.2	26.0	24.7	23.1	19.0	17.7	17.2

Table 2 Neutron yield in the dynamic gas discharge process (6～13Pa)

time (min.)		6.9	8.2	12.3	13.6	5.3	11.8	4.6	7.5
voltage (KV)		10	11	12	13	14	15	16	17
average neutron yield corresponding time interval (n / s)	2–2.5(Mev)	12.7	1.1	0.8	4.8	3.1	0.4	1.5	0.5
	2.5–7(Mev)	12.5	3.1	4.1	9.2	12.7	6.1	17.8	13.5
	sum	25.2	4.2	4.9	14.0	15.8	6.5	19.3	14.0
neutron yield ratio (2.5–7) / (2–2.5)		~1	2.8	5.1	1.9	4.1	14.5	11.8	29

Table 3 Neutron yield in pumping process after having absorbed deuterium for 2–3 minutes (4–13Pa)

time (min.)		0.8	3.0	3.4	3.8	4.6	4.8
voltage (KV)		10	11	12	13	14	14
average neutron yield corresponding time interval (n / s)	2–2.5(Mev)	0	0.2	0.2	0.2	0.2	41.7
	2.5–7(Mev)	5.2	1.4	1.3	1.0	1.0	280.4
	sum	5.2	1.7	1.5	1.2	1.2	332

Table 4 Neutron counts in the dynamic hydrogen gas discharge process (3–13Pa)

time (min.)		3.5	4.0	6.5	4.5	3.7	3.3	4.0	6.0
voltage (KV)		9–10	10–11	10–12	10–15	10–17	13–17	12–16	11–15
neutron counts	2–2.5(Mev)	0	0	1	0	0	0	0	0
	2.5–7(Mev)	0	0	2	0	0	0	0	0

Table 5 Neutron counts in pumping discharge process after absorbing hydrogen up to H / Pd = 0.76 (3–15Pa)

time (min.)		0.3	0.2	0.4	1.1	3.1	4.0	4.2	6.8
voltage (KV)		10	15	16	22	20–24	22–25	24–25	25
neutron counts	2–2.5(Mev)	0	0	0	0	0	0	0	0
	2.5–7(Mev)	0	0	0	0	0	0	0	0

Table 6 Data of X-ray absorbed dose

thickness of absorbing plate	absorbing dose of 0.01cm I_0(msv)	absorbing dose of different thickness I (msv)	I / I_0
0.02	5.598	0.521	9.31×10^{-2}
0.03	5.544	0.167	3.02×10^{-2}
0.04	4.951	0.0183	3.70×10^{-3}

Neutron Monitoring on Cold Fusion Experiments

L. J. YUAN*, C. M. WAN, C. Y. LIANG and S. K. CHEN
Materials Science Center, National Tsing Hua University
*Institute of Nuclear Science, National Tsing Hua University
Kuang Fu Road, Hsinchu, Taiwan 30043 R.O.C.

ABSTRACT

A helium-3 proportional detector was equipped with the experiment of Liaw-type electrolytic cell contained eutectic LiCl-KCl molten salt saturated by LiD electrolytic to collect the informations of the rate and the energy distribution of possible neutron produced during the electrolysis processes.

For long time monitoring, the significant reproducible neutron bursts appeared at several runs of cells during electrolytic processing. The neutron counting rate increased about a factor of two above the level of the background measurement. The pulse height signals were verified of neutron energy ranging from thermal up to 350 keV.

1. Introduction

Since the first report of discovery the neutron emission from cold fusion reaction by Jones et al. [1]. After that at least seven groups[2] have claimed both detections of neutron emission and excess heat production in the cell at room temperature. However, none of them has detected neutrons emission as well as both neutron emission and heat generation at elevated temperature.

In this report, we attempt to detect neutrons produced in LiCl-KCl molten salt saturated by LiD electrolytic at cell temperature about 400 °C.

2. Experimental Arrangement

The investigation of possible neutron esission has been carried out with similar to Liaw's LiCl-KCl molton salt saturated by LiD electrolytic. The cell design as shown in Fig. 1, the eutectic LiCl-KCl molten salt saturated with LiD electrolyte was filled in an aluminum can cathode with a Pd anode. An independent AC power driven furnace provided the reference temperature before the DC current

FRONTIERS OF COLD FUSION

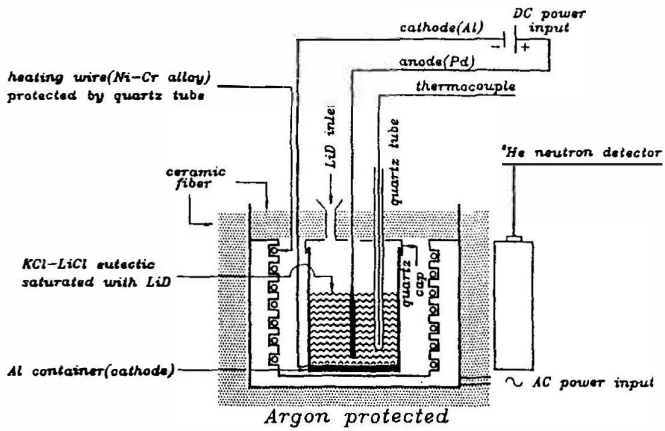

Fig. 1 A schmeatic configuration of the molten salt cell.

applied for electrolysis. A K-type thermocouple was used for the cell temperature measurement. The Pd anode immerged in the salt with surface area of about 3.8 - 5.7 cm^2. The whole experimental setup was operated in a glove box purged with Ar gas. The LiCl-KCl eutectic mixture was firstly melted by the AC power, which was kept the cell to get a stable reference working temperature, 390 °C. The cell then runing by applying a DC current for electrolytic process after LiD was added. Two grams of LiD were lasted up to 5 to 20 hours of electrolysis depending on the DC current applied. The duration for each addition of LiD is called a cycle of the process. A run in a cell usually contains 5 to 10 cycles. A helium-3 detector was also employed for continuous monitoring of neutrons. The detector efficiency was calibrated with a ^{239}Pu-^{13}C source of neutron emission rate $1.17X10^5$ ns^{-1}. Thus the efficiency of about 0.01% was obtained of this arrangement.

3. Results and Conclusions

For the neutron emission studies on LiCl-KCl molten salt experiments, several runs of different Pd diameter anode have been studied. The neutrons emission was obsevered on a 6 mm diameter Pd anode experiments, at 30 hours right after the DC charging current applied to the cell. The neutron counting rate jumped about twice higher then the background level. As indicated in Fig. 2, the cell runing about 215th to 270th hours (30 hrs. after the DC charging current applied), the neutron counting rate jumped from bockground level 5.51±0.44 cpm, to a higher value, 12.02±0.56 cpm. The cell temperature and the DC power applied in the cell compared with the neutrons during the electrolytic processing was shown in Fig. 3. From this figure it indicates that once the neutron emission is triggered the neutron counting rate is rather low relationship corresponding to the applied DC power. The cell temperature increase

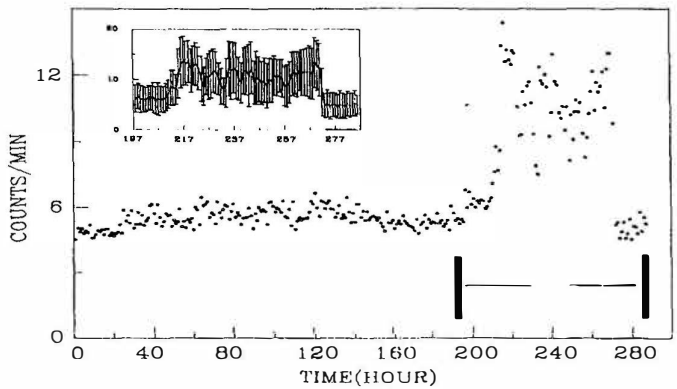

Fig. 2 Neutron counting rate of a 6 mm diameter Pd anode during electrolytic process.

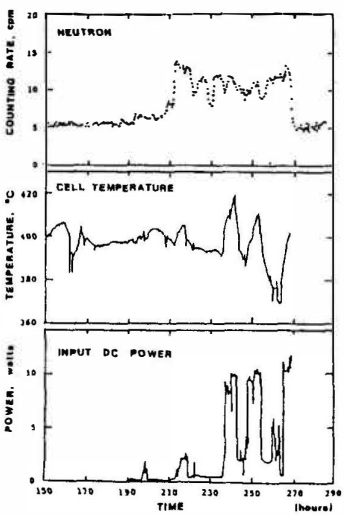

Fig. 3
(a) Neutron counting rate vs time.

(b) The cell temperature, power gain is estimated about 5 to 108 times of the input power.

(c) Input power of the cell, the cell started to electrolyze at hrs. 190, the current density was applied 18-800 mA/cm^2.

depends on the applied DC power. The estimated power gain in this case was about 5 to 108 times of the cell input power.

The neutorn emissions of an another experiment with the same anode diameter was shown in Fig. 4. The cell ran about 114th to 170th hours, the neutron counting rate also jumped from background level, 4.67±0.52 cpm to 7.43±0.62 cpm. The pulse height distributions of both background and cell run measurements were shown in Figs. 5(a) and 5(b), respectively. As comparsion with the background and the cell runs measurements, the counts from channel number 40 to 58 of figure 5(b) were significantly different from the the distribution of the background one. There was verified that the neutorns with energy above thermal up to 350 keV were collected during the cells were in electroytic processing. Above channel 58 the counts recorded on each channel fell almost the same level equivalent to the back-

ground.

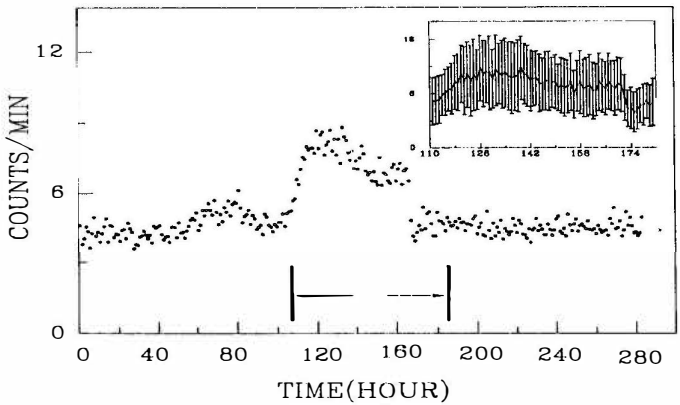

Fig. 4 Neutron emission of an another 6 mm diameter Pd anode was collected about 114th to 170th hours during electrolysis.

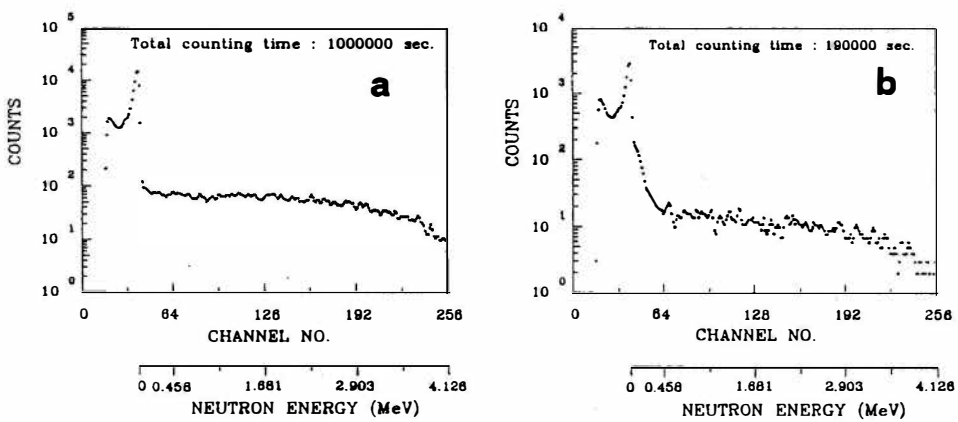

Fig. 5 (a) The pulse height distribution of neutron signals collected from background measurement, (b) from cell electrolysis.

At least three full runs of 6 mm diameter Pd anode electrolytic processes had neutron emissions being detected with equivalent same shape of neutron pulse height distribution. But in case of smaller diameter Pd anode e.g. 4.5 mm, was only large excess heat generation was observed. The neutron emission had not been detected yet in our experiment.

4. References

1. Jones, S. et.al., 1989, Nature, 338, 737.
2. Mallove, E., 1991, "Fire from Ice", Wiley, New York.

Neutron Emission from Palladium Electrodes in Deuterium Gas under Highly Non-uniform Electric Fiel

Hiroshi YAMADA, Norio SUGAYA, Tsuyoshi KAMIOKA,
Michiaki MATSUKAWA, Tamiya FUJIWARA and Koshichi NOTO
Faculty of Engineering, Iwate University
Ueda 4-3-5, Morioka 020
JAPAN

ABSTRACT

The fusion reproducibility in palladium(Pd) has been searched with the detection of excess neutron for point-to-plane electrode configuration in deuterium(D_2) and in hydrogen(H_2) gas atmosphere using a Pd, nickel(Ni) and tungusten(W) point. Excess neutron counts were observed using D_2 loaded Pd points under DC high-voltage applications. To the contrary, no count except background was observed with other points under the similar test condition. The observed highest counting rate of 61 counts for 10 seconds from the Pd is equivalent to the neutron emission of $\sim 1 \times 10^5$ n/(s·cm^3).

1. Introduction

Since the cold fusion was claimed to occur in Pd or Ti cathodes during electrysis of D_2O[1,2], a considerable number of research groups have investigated the fusion and many positive results have been obtained in these four years. In one of these studies, De Ninno et al. have found another simple methode of the cold fusion without the process of electrysis, that is, they have observed a spontaneous neutron emission from D_2 loaded Ti powder during the process of cooling with liquid nitrogen and heating[3].

In this short report, the experimental condition has been investigated to obtain more steady excess neutron emission with a point-to-plane electrode system in D_2 gas atmosphere using a ^{3}He thermal neutron detector. The experimental arrangement presented is simple and thus would assist a theoretical approach to the mechnism of the cold fusion.

2. Experimental

A neutron measurement system is used to detect 2.45 MeV neutrons from the D(d,n)^{3}He fusion branch. The system consists of a ^{3}He thermal neutron detector(Reuter-stokes: RS-P4-0806-207), a pre-amplifier(EG & G ORTEC: 142PC), an amplifier(EG & G ORTEC 590A single channel analyzer), a Timer-and-Counter(EG & ORTEC:996), a

FRONTIERS OF COLD FUSION

polyethylene inner moderator(500 mm long, 500 mm wide and 300 mm high), 1 mm thick Cd sheet reflector and ∿ 500 mm thick outer shielding of saturated boric acid solution in water. The polyethylene inner block, having a central cavity with a cylindrical shape of 140 mm in diameter and 100 mm high, enhances the efficiency of the ^{3}He counter by moderating fast neutron emitted from a cell. The polyethylene moderator is surrounded with the Cd sheet. The cell and the detector are positioned inside the central cavity. Signals from detector are fed to the single channel analyzer through the preamplifier and the amplifier. The counts are stored on a floppy disk using a personal computer. The electromagnetic noise related to high-voltage application is avoided by adjusting the preamplifier gain, the shaping time of the amplifier and the window of the single channel analyzer. The efficiency of the detector is ∿ 1 % using ^{252}Cf source with a neutron intensity of 2.3×10^{4} n/s. The average background of neutron flax without test cell is 8.6 cph after the adjusting. The background level is not so low, because the measurement system is directly positioned on the ground and is only covered with an upper thin roof.

The point-to-plane electrode system with gap spacing of ∿ 15 mm was in the closed cell filled with 2 atm pressure D_2 gas. The plane electrode was a brass disk of 30 mm diameter. A commercial Pd wire of 0.3 and 0.5 mm in diameter were cut to ∿ 30 mm in length to be the point electrodes. After polishing, the Pd points were vacuum annealed at 800 °C under a pressure less than 10^{-3} Torr for 3 hours and cooled to room temperature, follwed by loading of D_2 gas under 2 atm pressure for 24 hours. Next, the Pd point was set to the cell and kept in D_2 gas atmosphere of 2 atm pressure for 20 up to 40 hours under a DC 4.5 kV application in the neutron measurement system. The negative DC voltage was applied to the point electrode. Then a DC ∿ 10 kV, the lowest voltage for flashover, was applied to activate the Pd point electrode[4]. Just after several strokes of flashover, the DC voltage was immediately decreased to a slightly lower voltage than that for flashover. Ni and W points of similar size were used as reference electrodes under almost the same voltage amplitude with the aim of measuring the change in neutron counts. H_2 and air were also used as loading and enviroment reference gas.

3. Results and Discussion

The deuteron to Pd loading ratio was 0.66 at 24 hours after the start of loading. No excess count was usually observed until the activation by the flashover. An initial burst of neutron was detected after the several strokes of flashover in 8 out of 22 runs using D_2 loaded Pd points in D_2 gas atmosphere. However, such excess counts were once observed without any flashover, suggesting that the activation by flashover is not necessary for the neutron emission. The excess counts ceased when the applied voltage was removed. This indicates that the application of DC high voltage is a key factor for the fusion in this study. Counting rate significantly higher than the background level were observed in 6 runs out of the above positive 9 runs. But, 3 out of the remarkable 6 runs were carried out using a point. One of typical time behaviors of

neutron emission is shown in figure 1 (a); the rate is given by the counts summed up within 2 minutes. The time 0 in the figure shows the time when the last stroke of flashover took place. The average background of neutron flax of 0.29 counts per 2 minutes can be negligible in the figure. The average counting rate in figure 1 (a) is 96.5 counts per 2 minutes. Keeping into account the efficiency of the counter, the total number of emitted neutrons over 3 hours amounts to $\sim 1\times10^6$. The observed highest counting rate of 61 counts for 10 seconds, $\sim$ 2,500 times larger than the background counting rate, is equivalent to the emission of $\sim 1\chi10^5$ $n/(s\cdot cm^3)$ from the Pd electrode. In addition, excess neutron emission was also observed in H_2 gas atmosphere, as shown in figure 1 (b), and in air using D_2 loaded Pd point while these counting rate were lower than those in D_2 gas atmosphere. To the contrary, no count except background was observed with other points for all the 43 runs under the similar test condition, even though the point was H_2 loaded Pd in D_2 gas atmosphere. These results indicate that the fusion did not take place in the enviroment gas volume but in the Pd bulk or its surface. The number of positive runs to that of total runs for each condition is compiled into table 1. All the results allow us to conceive that a corona current of the order of 10 μA due to the DC high-voltage application would induce the transition of deuterons from octahedral sites in Pd to other sites[5] and that a multiplication of the transition would occur in the Pd bulk or its surface.

4. Conclusion

Nine out of twenty-two runs with D_2 loaded Pd points in D_2 gas atmosphere have given excess neutron counts under DC high-voltage applications. Furthermore, excess neutron emission was also observed in H_2 gas atmosphere and in air using D_2 loaded Pd point, while its counting rate was lower than that in D_2 gas atmosphere. This indicates that the fusion did not take place in enviroment gas volume but occured in Pd bulk or its surface. Corona current of the order of 10 μA due to the DC high-voltage application would be responsible to the continuous neutron emission by the fusion.

5. Acknowledgements

The authers would like to express their thanks to Professors N. Niimura in Tohoku University and T. Mizuno in Hokkaido University for the useful advice to constract the neutron measurement system. They are also grateful to Dr. T. Matsumoto of National Research Institute for Metals in Tokyo, Professors H. Horie, K. Mori and S. Mori in Iwate University for valuable information on metals.

6. References

1. M. Fleischmann and S. Pons, 1989, J. Electroanal. Chem., 261,301
2. S. E. Jones et al., 1989, Nature, 338, 737
3. A. De Ninno et al., 1989, Europhys. Lett., 9, 221
4. N. Wada and K. Nishizawa, 1989, Jpn. J. Appl. Phys., 28, L2017
5. A. Takahashi et al., 1991, Fusion Tech., 19, 182

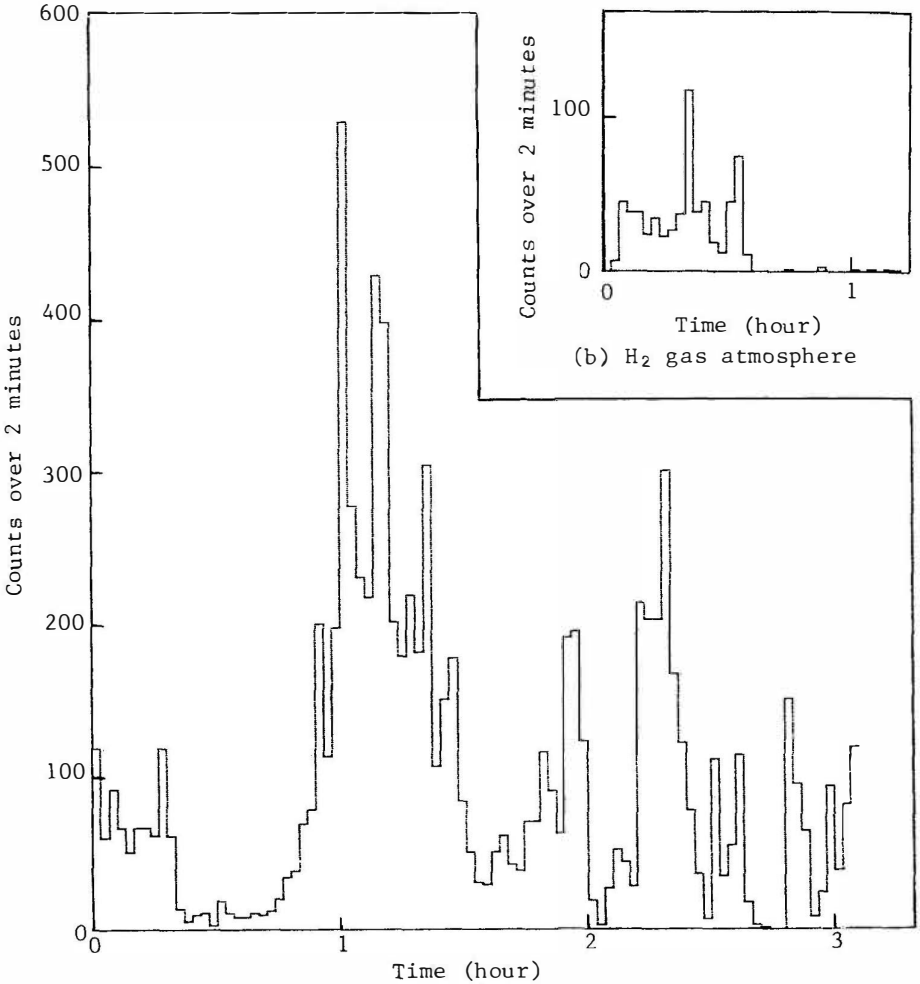

Fig. 1. Time dependence of neutron emission under negative DC ~ 9 kV application after the activation by flashovers.

Enviroment gas	Point and (loading gas)					
	Pd(D_2)	Pd(H_2)	Pd	W	Ni(D_2)	Ni
D_2	9/22	0/3	0/3	0/3	0/8	0/6
H_2	2/3	0/14	0/6			
Air	1/2					

Table 1. The number of positive runs to that of total runs for each condition.

Neutron Emission from Crushing Process of High Piezoelectric Matter in Deuterium Gas

T. SHIRAKAWA*, M. CHIBA[1)*], M. FUJII, K. SUEKI,
S. MIYAMOTO, Y. NAKAMITU[1)], H. TORIUMI[1)], T. UEHARA[1)],
H. MIURA[1)], T. WATANABE[1)], K.FUKUSHIMA[1)], T. HIROSE[1)],
T. SEIMIYA AND H. NAKAHARA
Department of Chemistry and Department of Physics[1)],
Faculty of Science, Tokyo Metropolitan University,
Minamiosawa, Hachioji, Tokyo, Japan 192-03.

ABSTRACT

We studied neutron emission from a crushing process of a Lithium-Niobate($LiNbO_3$) single crystal in deuterium gas atmosphere. We observed excess neutrons 3 counts / h with a confidence level of 99.95% that correspond 120 neutrons / h emission from process.

1. Introduction

In a solid crushing process, chemical bonds broken and ionic charges appear on the crushing surface. An activate state is induced by these charges. The mechanochemical reaction arise extraordinary chemical reactions. The charge may generate high electric field. deuterons are accelerated by the field and collide with target deuterides. Consequently, nuclear fusion occurs and neutrons emits. Kluev et al. and Derjaguin et al. have reported neutron emissions from deuterated metal due to the mechanochemical process[1,2].

We report a neutron emission from a crushing process of a high piezoelectric materials in deuterium gas using vibromill.

2. Experimental

We chose a single crystal of lithium niobate as the piezoelectric material. It has a high piezoelectric strain constant of 6.92×10^{-11} C/N(d_{15}) and a relatively low dielectric constant of 85.2(X_{11}^{T}). The generated

FRONTIERS OF COLD FUSION

voltage proportional to the piezoelectric strain constant and inverse proportional to the dielectric constant. The low conductivity ensures the charge retain after the charge unbalance of the fracturing process.

The mill was composed of a 500ml cup and a stainless steel ball (50 mm diameter) which vibrated at the frequency of 50 Hz with the vertical amplitude of 3 mm.

The neutrons were detected 10 ^{3}He proportional counters arrayed circularly in a cylindrical shaped paraffin block of 50 cm outer diameter and 10 cm inner diameter. The neutrons thermalized by the paraffin and reacted with ^{3}He making a proton and a tritium with a Q value of 760 keV. The pulse heights of output signals of the ^{3}He counters were digitized by analog to digital converters. The vibromill was set in the center of the cylindrical paraffin.

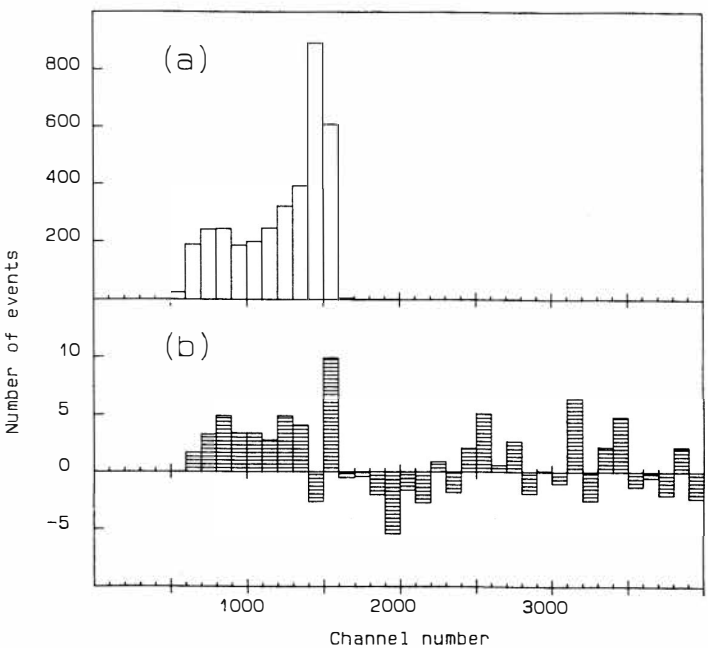

Figure 1. (a) shows ^{252}Cf emitted neutron distribution of counts over the channels of pulse height analyzer. The peak of 1500 channel in pulse height distribution corresponded the energy of 760 keV thermal neutron.

(b) shows pulse height distribution of excess emitted neutrons summation over lithium niobate + deuterium gas 12 samples. A neutron spectra was observed at 500-1600 channels. Reference was used 12 h averaging value back ground from 132 h.

3. Results and discussion

The pulse height distribution is shown in the figure 1 (a). In order to increase the signal to noise ratio, counts between 600 and 1599 channels were selected. The detection efficiency was measured to be 2.6% by a calibrated ^{252}Cf source.

The experiment was done in the low background facility at Nokogiri mountain. of The Cosmic-ray Research Institute, The University of Tokyo. It was located underground at the depth of 100 m water equivalent. The count rate of the background was observed 7.6 counts / h. The crushing for a sample was continued 1 hour duration. The crystal of lithium niobate was ca. 3 mm granule initially and after 15 min crushing the size was reduced to ca. 1 μm diameter. The figure 1 (b) shows the excess neutrons pulse height distribution of the summation of 12 samples of lithium niobate + D_2 system. It was compared with normalized 12 h background taken during 132 h. The sum of bbetween 1600 to 4000 channel counted neutron were scarcely slight 1.5. However 600 to 1599 channel counted neutrons were obviously excess 35.8. Table 1 shows the experimental results 16 samples on crushing process. Derjaguin et al.[2] observed excess neutron emission on $Ti+D_2O$

Table 1

sample & amount	neutrons (counts/hour)
Ti 10g + D_2O 8 ml	4
Pd 5g + D_2O 8 ml	5
$LiNbO_3$ 12g + D_2 101 kPa	11
$LiNbO_3$ 13g + D_2 101 kPa	12
$LiNbO_3$ 15g + D_2 1.1 kPa	18
$LiNbO_3$ 15g + D_2 6.6 kPa	12
$LiNbO_3$ 20g + D_2 16.6 kPa	11
$LiNbO_3$ 16g + D_2 13.2 kPa	5
$LiNbO_3$ 10g + D_2 24.7 kPa	8
$LiNbO_3$ 10g + D_2 25.7 kPa	9
$LiNbO_3$ 15g + D_2 101 kPa	9
$LiNbO_3$ 12g + D_2 101 kPa + LiD 2g	10
$LiNbO_3$ 12g + D_2 101 kPa + LiD 2g	13
$LiNbO_3$ 13g + D_2 101 kPa + LiD 2g	8
$LiNbO_3$ 12g + air 101 kPa	8
$LiNbO_3$ 10g + N_2 101 kPa	9

system. However we did not observe excess neutron in $Ti+D_2O$ or $Pd+D_2O$ systems. On the lithium niobate + deuterium gas system, we observed excess neutron emission over the background.
Neverthless, in air and N_2 +lithium niobate system, we did not observe excess neutrons. For intensify of the density of deuterium atoms, we add a lithium deuteride in the system. Also, on the lithium niobate + lithium deuteride + deuterium gas system, we observed excess neutrons. All the counts of the 12 runs of lithium niobate + deuterium gas system were 127 compared to the expected background of 91.2. If our observed background fluctuation was Gaussian distribution, we can calculate mean and standard deviation 91.2 and 9.5 respectively. The value 127 corresponds 0.05% probability if it was fluctuation of the background. So, we observed 35.8 excess neutrons in crushing process. These neutrons were emitted by an acceleration of deuterium at high voltage field in crushing process of high piezoelectric material.

4. conclusion

We conclude that the excess neutron (average 3 neutrons / hour) observed by mechanochemical crushing process of lithium niobate in deuterium gas with confidence level 99.95%. The D-D fusion reaction was occurred in the crushing process of lithium niobate crystals. We named this fusion reaction "Mechano neuclear reaction".

5.References

1. V. A. Kluev et al. 1984, Dokl. Phys. Chem. 279, 1027.
2. B. V. Derjaguin et al. 1989, Nature 341, 492.

A Search for Fracture-Induced Nuclear Fusion in Some Deuterium-Loaded Materials

Kenji WATANABE and Yuh FUKAI
Department of Physics, Chuo University, Kasuga,
Bunkyo-ku, 112 JAPAN
Nobuo NIIMURA* and Osamu KONNO*
*Laboratory of Nuclear Science, Faculty of Science,
Tohoku University, Mikamine 1-2, Sendai 982, JAPAN

ABSTRACT

Attempts to detect neutron emission attributable to D-D nuclear fusion accompanying fracture of deuterium-loaded materials have been carried out using a ball mill specially designed for this purpose.

Chips of Ti, Ti-alloys, Y and $YBa_2Cu_3O_{7-x}$, loaded with deuterium, were crushed in the ball mill to about 10μm in size in 60 or 120 minutes, and neutrons were counted by an array of 4～12 ^{3}He detectors sarrounding the ball mill. The signal-counting efficiency was 0.3～4%.

No positive signature has been obtained for the occurrence of fracture-induced fusion.

1. Introduction

Immediately aftre cold fusion phenomena were reported by Jones et al. (1989) and Fleischmann and Pons (1989), suggestions were made that a d-d fusion reaction could be induced during the crack propagation in deuterium-loaded materials (Cohen and Davies 1989, Mayer et al. 1989, Takeda and Takizuka 1989).

However, experimental evidence for the fracture-induced fusion has not been clear. In LiD, Klyuev et al.(1986) had reported neutron emissions during impact fracture, but recent experiments of Price (1990) using a track-reading plastic detector found no particle emission. Derjaguin et al.(1989) claimed to have observed neutron emission during vibromilling of a complex mixture of Ti chips, heavy water, deuterated polypropilenium and LiD. The implication of their experiment is hard to evaluate.

FRONTIERS OF COLD FUSION

The only clear-cut experiment performed so far in regard to the fracture-induced fusion is that of Dickinson et al. (1990), in which they observed emissions of photons, electrons and D^+ ions during the fracture of TiD_x, and a fairly large charge imbalance between the two cracked pieces of the sample. Although the energy of emitted D^+ ions was not determined in their experiment, there appears to be a possibility that it can be of the order of 10keV which is necessary to yield measurable fusion rates.

Our measurement have been performed to detect neutron emission attributable to d-d nuclear fusion accompany fracture of deuterium-loaded materials using a ball mill specially designed for this purpose.

2. Experimental Details

The deuterium and hydrogen loading of specimens were performed in a Sieverts-type apparatus. The specimens used are listed in Table 1.

Table 1. Samples

Sample	Shape;Size	Quantity
$TiD_{1.0}$	block;2～10 mm	400 g
$TiD_{1.9}$	block;2～10 mm	500 g
$YD_{2.9}$	block;2～10 mm	81 g
$Ti_{086}Al_{01}V_{004}D_{1.1}$	fragment;5～10 mm	260 g
$Ti_{086}Al_{01}V_{004}H_{1.1}$	fragment;5～10 mm	223 g
$Ti_{086}Al_{01}V_{004}D_{1.1}$	fragment;5～10 mm	177 g
$TiD_{1.3}$	plate;1mm thick	171 g
$TiH_{1.7}$	plate;1mm thick	177 g
$YBa_2Cu_3O_{7-x}D_{0.8}$	block;2～10 mm	147 g
$YBa_2Cu_3O_{7-x}H_{1.0}$	block;2～10 mm	147 g

The electrical resistivity of the specimens varies widely: $\sim 10^{-6}\Omega\cdot$m for Ti and Ti-alloy deuterides, $\sim$ 1 $\Omega\cdot$m for $YD_{2.6}$, and $\sim 10^{2}\Omega\cdot$m for the deuterides of $YBa_2Cu_3O_{7-X}$.

These samples were crushed in the ball mill (21cm in diameter, 13cm in width) to about 10μm in average size(Rosin-Rammler distribution) in a vacuum or 1 atm. of D_2 gas for 25～120 minutes at room temperature. The ball mill was surrounded by a polyethylene moderator (3cm thick), in which an array of 4～12 ^{3}He detectors (25mm in diameter, 15cm in active length) was located, and the whole assembly was shielded from outside radiation by borated water of 50 cm thickness.

Signals were counted by CAMAC scalers, and recorded in a microcomputer every 5 min. The signal-counting efficiency was measured by using ^{252}Cf neutron sources, to be 0.3 and 4% for four and twelve

detectors.

Measurements were made to check possible noises arising from the rotation of the ball mill by comparing background counts during the on- and off-time of the empty ball-mill operation. No difference was found.

It must be emphasised that the present experiment allows the use of much larger quantities of samples, and produces much larger area of freshly cracked surface, than any experiments reported so far.

3. Experimental Results

Each run of measurements consisted of neutron counting during the on- and off-period of the ball-mill operation consecutively.

Typical time-variations of neutron count rates are shown in figure 1 for $TiD_{1.0}$, $YBa_2Cu_3O_{7-x}D_{0.8}$ and $YBa_2Cu_3O_{7-x}H_{1.0}$.

No difference in the count rates of on- and off-periods can be observed in any of these runs.

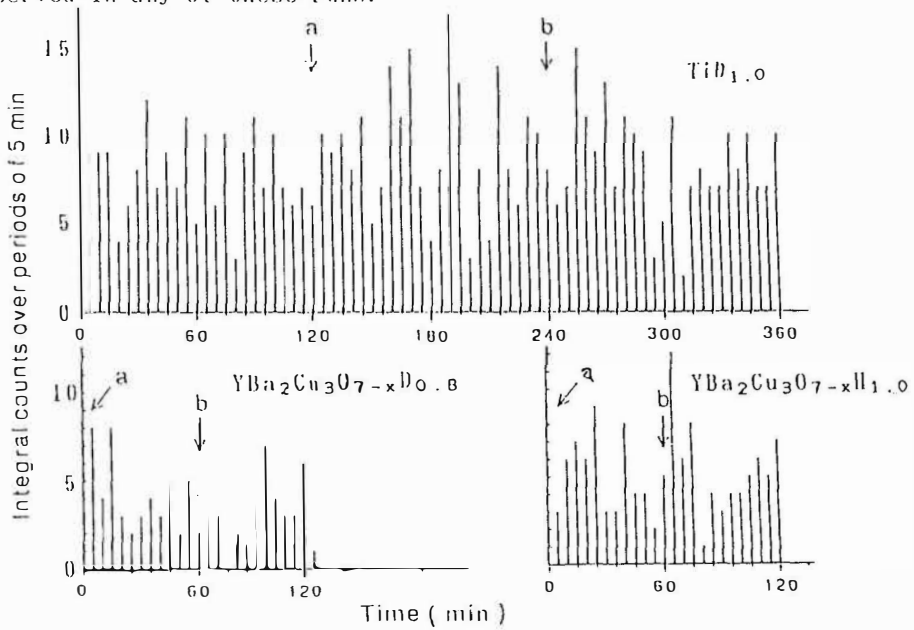

Figure 1. Time-variation of neutron count rates.
Arrow a: start, and b:stop of the crushing operation.

The average count rates observed for all the samples are listed in Table 2. Difference in the count rates during the on- and off-periods cannot be said to be meaningful.

Table 2. Count Rates(count/5min ± σ) and Duration

Sample	Crusing on Counts; Duration	Crushing off Counts; Duration
$TiD_{1.0}$	9.2±0.6; 120 min.	8.3±0.6; 120 min.
$TiD_{1.9}$	8.2±0.6; 120 min.	8.9±0.6; 120 min.
$YD_{2.9}$	8.8±1.3; 25 min.	7.8±1.2; 25 min.
$Ti_{0.86}Al_{0.1}V_{0.04}D_{1.1}$	6.5±0.5; 120 min.	2.5±0.3; 120 min.
$Ti_{0.86}Al_{0.1}V_{0.04}H_{1.1}$	3.1±0.3; 60 min.	2.9±0.2; 60 min.
$Ti_{0.86}Al_{0.1}V_{0.04}D_{1.1}$	4.3±0.6; 60 min.	5.2±0.7; 60 min.
$TiD_{1.3}$	5.6±0.7; 60 min.	6.0±0.7; 60 min.
$TiH_{1.7}$	4.8±0.7; 50 min.	4.1±0.6; 50 min.
$YBa_2Cu_3O_{7-x}D_{0.8}$	4.1±0.6; 60 min.	3.2±0.5; 60 min.
$YBa_2Cu_3O_{7-x}H_{1.0}$	5.0±0.6; 60 min.	5.4±0.7; 60 min.

4. Discussion

Let us start with a crude estimation of D-D fusion rates by assuming appropriate values. Let n_1 be the density of D^+ ions on unit surface of crack, δ the fraction of D^+ ions emitted and accelerated across the crack surfaces, λ the fusion reactions per one accelerated D^+ ion and dS/dt the rate of generation of fresh crack surface, then the total rate of D-D fusion is given by $\lambda_{tot} = n_1 \delta \lambda (dS/dt)\ s^{-1}$, which becomes $4 \times 10^3 \delta$ for experimented conditions of $TiD_{1.9}$. If we assume $\delta \simeq 10^{-5}$, and a voltage of 10kV across the crack gap of 10μm, we obtain λ_{tot} equal to the background counts. These values appear quite reasonable. Absence of any observable neutron emission suggests that some of these values were overestimated.

Admittedly, the efficiency of acceleration of D^+ ions depends critically the time of decay of the voltage across the crack surfaces. The present experiment is believed to have coverd a wide range of the decay time because, other things being equal, if should be proportional of the electrical resistivity.

Thus, the negative results of the present experiment, in spite of greatly enhanced sensitivities, put a rather stringent limit on the occurrence probability of the fracture-induced fusion.

5. References

1. Cohen, J. S. and Davies, J. D., 1989, Nature 338, 705.
2. Derjaguin, B. V. et al., 1989, Nature 341, 492.
3. Dickinson, J. T. et al., 1990, J. Mater. Res., 5, 109.
4. Fleischmann, M. and Pons, S. J., 1989, Electroanal. Chem. 261, 301.
5. Jones, S. E. et al., 1989, Nature 338, 737.
6. Klyuev, V. A. et al., 1986, Sov. tech. Lett. 12, 551.
7. Mayer F. J. et al., 1989, presented at Santa Fe Workshop on Cold Fusion Phenomena, Santa Fe, New Mexico, May 23-25.
8. Price, P. B., 1990, Nature 343, 542.
9. Takeda, T. Takizuka, T., 1989, J. Phys. Soc. Japan 58, 3073.

Search for Excess Heat, Neutron Emission and Tritium Yield from Electrochemically Charged Palladium in D_2O

Shigeru ISAGAWA, Yukio KANDA and Takenori SUZUKI

National Laboratory for High Energy Physics, KEK

1-1 Oho, Tsukuba-shi, Ibaraki-ken, 305 JAPAN

ABSTRACT

The electrolysis of heavy water is being investigated with two types of open calorimetric systems. Pd cathodes, Pt anodes and D_2O/0.1M LiOD electrolytes have been used. Until now no clear-cut heat bursts as reported have been observed. One exceptional phenomenon showing abnormal power imbalance without neutron and tritium anomalies was found, but has not been repeated under the similar experimental conditions. Neutron emission, on the other hand, as a very rare case showed an abnormal increase for only short term during one of another series of experiments. The increase of about 3.8σ above the background level lasted for 9 hours on the 20th day after starting the electrolysis. The emission rate amounts to about 27.2 ± 11.2 neutrons s^{-1}, which is equivalent to about 700 times as much as the background level. Neither excess heat nor tritium anomalies were, however, observed. The reason for the lack of repeatability of these experimental results is discussed.

1. Introduction

The generation of excess energy and possible products of nuclear interactions, as proposed by Fleischmann, Pons and Hawkins[2] and Jones et al.[4] has attracted much attention from scientific point of view of metal-hydrogen systems. We were particularly interested in observing by ourselves a "burst" of excess enthalpy lasting a long period of time and in experimentally making clear if it comes from nuclear reaction or not. Aiming to reproduce the claimed excess heat and neutron emission from electrochemical cell, power balance and radiation emission measurements have been continuously carried out[3] for more than 3 and a half years with several sets of open type cells consisting of Pd cathodes, Pt anodes and D_2O/0.1M LiOD electrolytes.

2. Electrochemical Cells

Two types of glass cells have been prepared as shown in Fig. 1; a) water-cooled cells with a cooling water jacket; b) thermally insulated dewar type cells immersed in constant temperature water baths. A variety of Pd rods have been tested as the cathode. Original materials of 99.8 % or 99 .95 % were delivered from Johnson

Matthey Company. They were as received, annealed *in vacuo* or remelt in Al_2O_3 crucibles with a UHV induction furnace. Electrolysis has normally been done in constant current mode, although the current was sometimes modulated in various manner. For a) type cells, relatively larger samples were used with a current density up to 1050 mA/cm^2. Power balance was checked by comparing the curve of cell temperature vs. input power with the calibration curve, or by measuring the flow rate and the temperature difference of inlet/outlet water in a cooling channel as shown in Fig. 2. For b) type cells, relatively smaller samples were used with a current density up to 840 mA/cm^2. Excess heat was monitored only by use of the calibration curve.

3. Measurement of Nuclear Products and Chemical Analysis

For neutron monitoring a single or a double rem counter system was used, in which dose meters of BF_3 and/or ^3He type were placed adjacent to the electrolysis cells (See Fig. 3). Tritium concentrations in the cells before, during and after electrolysis were intermitently measured with a liquid scintillation counter by an external standard method[3]. In order to check the hydrogen contamination during long-run electrolysis, a quantitative analysis of H/D ratio was also made by infrared spectrophotometry[1]. The Li concentration was measured by ion chromatography technique. Surface analysis of Pd samples was also done with EDX as well as SEM.

4. Results and Discussions

Although many indications of excess heat have been observed so far, almost all of them except one has been excluded as a ghost by further experimental reexamination. They were caused by; 1) freezing of electrolyte; 2) a change of calibration curve with time due to unexpected escape of Li from cells; 3) an observational error in measurement of temperature difference; 4) a change in calibration of flow rate of the cooling water. A typical example is shown in Fig. 4. Until now we have never observed a clear-cut heat burst as shown in the reference[2]. Only one example of abnormal power imbalance observed in an a) type cell has not been ruled out, however, even after re-calibration of the flow rate. Neutron and tritium showed no anomalies in this case. This phenomenon has not been repeated any more under the similar experimental conditions.

Neutron emission, on the other hand, showed an abnormal increase in one of a series of b) type experiments as summarized in Fig. 5. In these experiments four cells were installed together in each bath and two BF_3 counters (15 and 16 in Fig. 3) were used for neutron monitoring. On the 20th day after starting the electrolysis one (15) of the counters detected the increase of neutron emission, about 3.8σ above the background. It lasted for about 9 hours. Another counter (16) located 3m apart showed a small increase of counting rate, but in the limit of statistical error. No observation of solar neutrons associated with the large flare has been reported on this date. But one (6) of the four cells coincidentally showed a spontaneous increase in current. If this cell is thus assumed to be a neutron emission source, its net emission rate is equivalent to about 27.2±11.2 neutrons s^{-1}. This phenomenon also happened only once without accompanying any heat excess or abnormal increase of tritium.

Experiments were also carried out to check the contamination of D_2O with hydrogen from air during long-run electrolysis. The results proved that the D_2O or the electrolyte, and thus the Pd could be contaminated with unexpected amounts of hydrogen from air. It is reported that 0.9 D per one Pd is the critical threshold value to get the cold fusion phenomena. If this is the case, the hydrogen contamination could account for the lack of reproducibility of above mentioned experimental results.

5. Acknowledgement

The authors especially thank Professors K. Kondo and M. Miyajima for their kind helps to continue this investigation. Continuing encouragements of Professors H. Hirabayashi, Y. Kimura, H. Sugawara and K. Takata are also gratefully acknowledged.

6. References

1. Bosch, H.-S. et. al., 1989, J. Fusion Energy, 9, 165.
2. Fleischmann, M., Pons, S. and Hawkins, M., 1989, J. Electroanal. Chem., 261, 301 and 263, 187.
3. Isagawa, S., Kanda, Y., Kondo, K., Miyajima, M., Sasaki, S., Suzuki, T. and Yukawa, T., 1989, KEK Report, October, 89-15.
4. Jones, S. E. et. al., 1989, Nature, 338, 737.

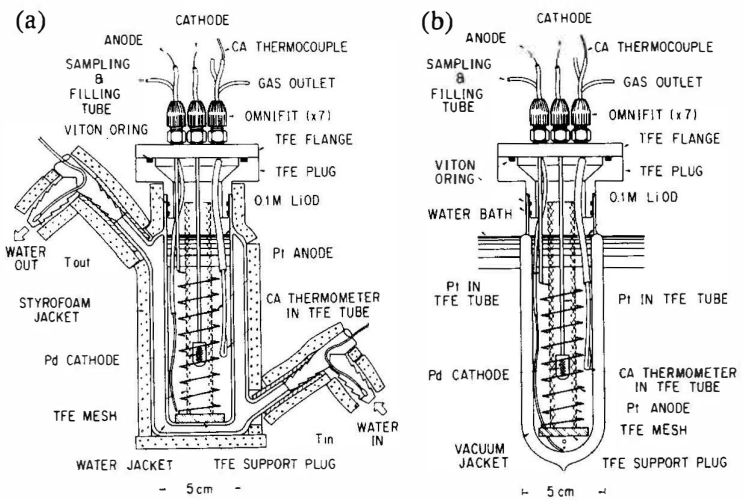

Figure 1.(a) Water-cooled cell, (b) Vacuum insulated dewar type cell.

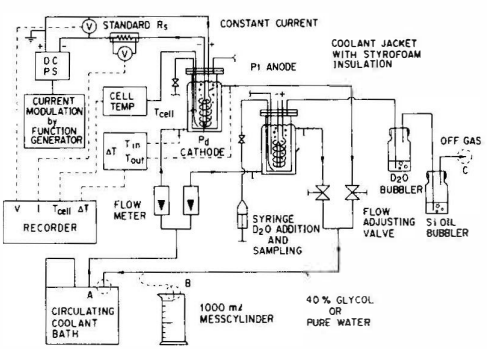

Figure 2. Schematic diagram of calorimetry of a) type cells. Coolant and gas flow rate can be calibrated at B and C positions, respectively.

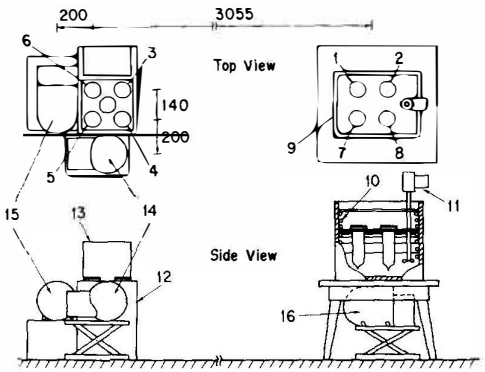

Figure 3. Setup of b) type experiment. 1 ~ 8 Dewar type cells in which 8 is for control experiment, 9 Coleman bath, 10 Cooling pipe, 11 Stirrer, 12 RTE220 bath, 13 Temperature controller, 14 ^{3}He rem-counter, 15, 16 BF_3 rem counters S/N 12254 and 9074, respectively.

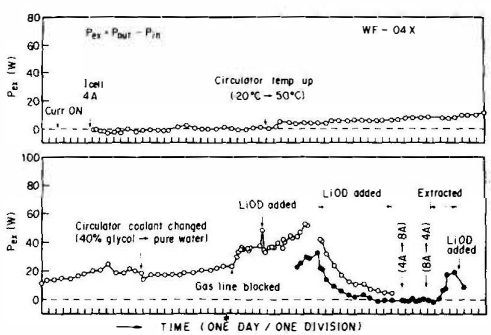

Figure 4. Change of virtual excess power with time. Filled circles denote the same data after flow rate re-calibration. Adjusting the Li content to the original value diminishes the virtual excess power to 0.

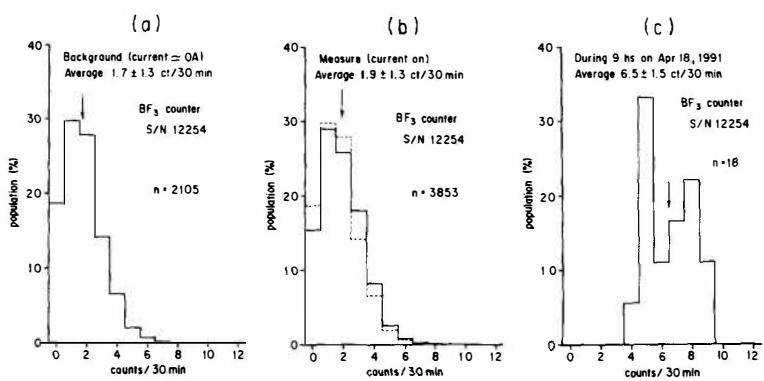

Figure 5. Frequency histograms of the neutron counter in a b) type experiment. Dotted line in (b) indicates the background as shown in (a). Fig. (c) shows the anomalously high counts lasting for 9 hours.

Measurement of Neutrons in Electrolysis at Low Temperature Range

Masatoshi FUJII, Masami CHIBA, Kenji FUKUSHIMA,
Motomi KATADA, Tachishige HIROSE, Kenichi KUBO,
Hiroaki MIURA, Shinya MIYAMOTO, Hiromichi NAKAHARA,
Yuki NAKAMITSU, Tsutomu SEIMIYA, Toshiaki SHIRAKAWA,
Keisuke SUEKI, Hideyuki TORIUMI, Torahiko UEHARA,
Toshihiro WATANABE, Tokyo Metropolitan University

ABSTRACT

We observed three neutron trains continuing 2 or 3h as the excess flux during an electrolysis of deuterated alcoholic electrolyte at low temperature range with Pd cathode for 1878h. Those were 22 counts/2h and two times of 27 counts/3h in the average background counts of 4/h. We could not find any excess in the other time intervals between 28.6ms and 1878h. The production rates of the 22 and 27 counts were $6.3X10^{-24}$ and $4.5X10^{-24}$/d-d/s during 2 and 3h, respectively. The confidence levels of neutron emission for 22/2h and 27/3h were 88% and 59%, respectively, estimated from the statistics. And for the total of the three trains, the confidence level became 98%.

1. Introduction

We focused our attention on the result of De Ninno et al.[1] who observed neutron emission changing temperature of titanium in pressurized deuterium gas. Neutrons emerged from the titanium in a particular temperature of 240 K. This temperature seems to be corresponding to the phase-transition of titanium hydrides. The change could make a cracks with a high electric field between the gaps which accelerated deuterons.

So, we carried out the first experiment for searching neutrons from an electrolysis changing the temperature between 200 K and 300 K in order to create the dynamic condition in palladium cathode. Additionally, the advantage of the electrolysis at the low temperature range is not only the capability of changing the temperature, but also increase of an absorbed amount of hydro-

FRONTIERS OF COLD FUSION

gen into palladium [2-4]. Furthermore, our detection system was constructed in attention with a time interval as wide range as possible, since we do not know how the neutron emission occurs in the time structure.

2. Methods

2.1 Neutron detection system

Neutron detection system was consisted of ten ^{3}He proportional gas counters (Reuter-Stokes, USA), which were inserted in a paraffin moderator shaped as a cylinder with a height of 30 cm, outer and inner diameter of 38 cm and 10 cm, respectively. Each couple of the ^{3}He counters was linked to a preamplifier. The pulse height data were recorded using a CAMAC PHADC. The event time was also stored to analyze the time structure of the neutron emissions. The pulse height data can be read out every 28.6 ms, which is limited by the CAMAC readout time.

Detection efficiency of neutrons was defined as number of detection per number of emitted in the cell which was measured by the ^{252}Cf neutron source placed at the palladium electrode position. The detection efficiency was 3.3 % selecting within -3σ to $+2\sigma$. The detection system was placed in Nkogiriyama underground laboratory, Institute for Cosmic Ray Research, University of Tokyo, which was covered with sandstone of 100 m water equivalent. The average of neutron background rate was about 4/h.

2.2 Electrolysis

The cell used in this work was made of quartz glass of 22 mm in inner diameter and 150 mm in length. The anode was a coiled shape made of a platinum wire of 0.5 mm in diameter and 500 mm in length. The palladium cathode electrode of 5 mm in diameter and 20 mm length was placed in the center of the platinum wire. We used an electrolyte as 2N DC1(37 wt% with 99% D; Aldrich Chemical Company, Inc.) of deuterated methanol (99.8 atom% D; ISOTEC Inc.) solution, whose freezing point was lower than 200 K.

The electrolysis was continued unexchanging the electrode but exchanging the electrolyte for about 2 weeks, because methanol was resolved into formaldehyde and formic acid which froze under the low temperature condition. The electrolysis was carried out with constant current mode which was repeated between -113.2 mA/cm^2 for 170 min. and -0.14 mA/cm^2 for 10 min. The total electrolysis duration was 1878 h, and the temperature of the electrolysis bath were kept at about 210 K.

The amount of absorbed deuterium was estimated by

the measurements of thermogravimetory (TG) and temperature programed desorption (TPD) spectra of mass number 2. In our electrolysis condition, the average ratio of deuterium was Pd:D=1:0.7.

3. Analysis and results

We studied the frequency distributions of the neutron count during the electrolysis of each time interval. The expected frequency distribution was deduced from the Poisson distribution substituting the average and the total counts of the time interval.

Searching from the time interval from 28.6 ms to 240 min, almost all the time interval frequency distributions were fit to the Poisson, but some anomalous events were observed in 120 and 180 time intervals (Fig. 1). They were one event of 22 counts/2h, which occurred at 31.01 days after the beginning of the electrolysis and two events of 27 counts/3h at 62.14 and 82.17 days, respectively. The pulse height distributions of the three events were similar to that of the 252Cf source data (e.g. fig. 2 shows the distribution of 22/2h train). Thus the counts of these events can be decided as the neutron signals. The neutron signals of these

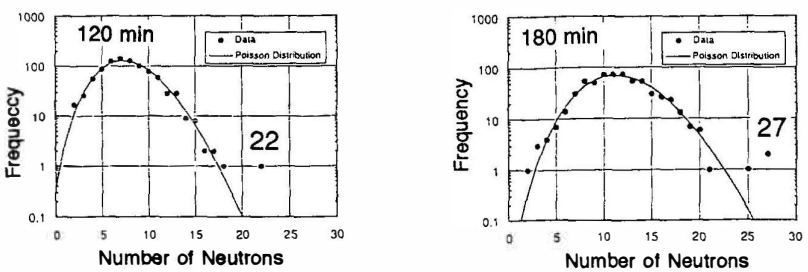

Fig. 1 Frequency distributin of 120 and 180 min

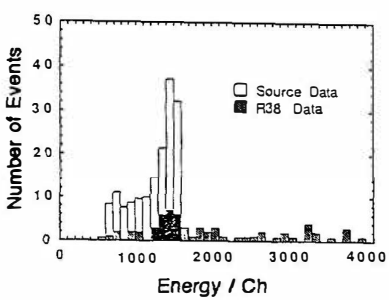

Fig. 2 Energy spectram

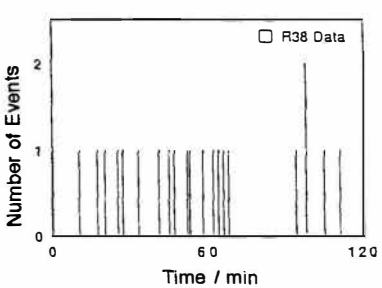

Fig. 3 Time distribution

events were distributed over the time duration (e.g. fig. 3 shows the time distribution of 22/2h train). This time distribution indicates that these emission phenomena is not both a continuous process during the electrolysis, and burst process.

Table 1. Summarize of the excess neutron emission.

No.	tp/d	td/h	C	P	m	n (PXm)	$EX10^{-24}$ /d-d/s
1	31.01	2	22	0.00013	939	0.12	6.3
2	62.14	3	27	0.00066	626	0.41	4.5
3	82.17	3	27	0.00066	626	0.41	4.5
Sum of three events		8	76	---	---	0.021	4.9
Total observation		1878 90/d	7437 3.96/h	---	---	--	---

tp:passage time, td:duration time, C:counts of neutron, P:probability, m:sampling number, n:frequency of appearance, E:emission rate.

A statistical analysis of these three events were summarized in table 1. These production rate of the 22 and 27 counts were $6.3X10^{-24}$ and $4.5X10^{-24}$/d-d/s during 2 and 3h, respectively. The confidence levels of neutron emission for 22/2h and 27/3h were 88% and 59%, respectively. For the total of the three trains, the confidence level became 98%.

Since the anomalous neutron emission intermittently occurs and continued a few hours, we will consider that the possible process of the neutron emission phenomena maybe related to the accumulation of stress and the creep mechanism of cathode material.

We would like to express our appreciation to Prof. K.Yamakoshi of The University of Tokyo to a facilities for a usage of the Nokogiriyama underground laboratory. The present study was partially supported by a Fund for Special Research Project at Tokyo Metropolitan University and a Grant-in-Aid for Scientific Research from the Ministry of Education, Science and Culture of Japan.

4. References

[1] De Ninno, A. et al., 1989, Europhys.Lett., 9, 221.
[2] Harper, J.M.E. et al., 1974, Phys.Lett., 47A, 69.
[3] Burger, J.P.et al.1975, Solid State Commun. 17, 277.
[4] Liu, D.R. et al., 1988, Acta. Metall., 36, 2597.

Limit on Fast Neutrons from DD Fusion in Deuterized Pd by Means of Ge Detector

E. Choi, H. Ejiri, and H. Ohsumi

Dep. of Phys., Osaka Univ., Toyonaka, Osaka 560. Japan.

Abstract

Search for fast neutrons from the electrochemically loaded Pd-D system at room temperature was made in order to study the possible d+d fusion there. A low-background high-resolution Ge detector surrounded by neutron scatterers was used to investigate the fast(1∼5 MeV) neutrons. The neutron flux was obtained by measuring yields of the γ-rays following inelastic scattering of the fast neutrons from nuclei in the scatterers. The observed spectrum shows no statistically significant excess of the γ-rays above background. The upper limit on the fusion rate was obtained as $\lambda_f < 1.6 \cdot 10^{-24}$ (ddn)fusions / [(dd pair) sec].

1. Introduction

Nuclear fusions such as d+d, d+t and others are strongly inhibitted at room temperature by the Coulomb barrier because the relative kinetic energy (temperature) is far below the barrier. The nuclear fusion at room temperature, however, might be much enhanced if the effective Coulomb barrier could be reduced slightly by possible modification of electric fields in the solid(metal) state[1-3]. This is the so-called cold fusion, in contrast to the hot fusion at high temperature. The hot fusion has been well established experimentally and theoretically since many decades in nuclear physics, and since many years in plasma physics. On the other hand there are no strong experimental evidences for the cold fusion so far.

It is crucial for experimental studies of the nuclear fusion to investigate the nuclear reaction products such as n, p, ^{3}He, and ^{3}H. Observation of just the heat (energy) excess in the macroscopic system does not prove the nuclear fusion at all since many chemical and solide-state contributions are hardly excluded as possible origines of the heat.

Many experimental surveys for the possible cold fusions have appeared, some supporting[4-8] and others disproving[9-15] the finite fusion at the room or cold temperature. Among them, search for the neutrons is one of most straightforward ways to prove the nuclear fusion since they arises only from nuclear reactions. Experimental studies of the neutron, however, are difficult because it has no charge. Recently we have suceeded in developing a new type of the high-sensitive detector for fast neutrons. It is very important to investigate experimentally the limit on the d+d fusion rate by using the new technique.

The present work reports the search for the fast neutrons from electrochemically loaded Pd-D system at the room temperature by means of the new detector. The

unique point is to use a high energy-resolution Ge detector to measure the fast neutrons. The principle is to measure the energy spectrum of γ-rays following inelastic scattering of the fast neutrons. The detector is sensitive to only the fast neutrons, and the γ-ray shows up as discrete peaks, corresponding to the nuclear excitation energies, in the continuum background spectrum. Consequently the signal can be clearly identified. The details of the detector has been given elsewhere[16].

2. Electrochemistry for the Pd-D system

The Pd-D system was made electrochemically by using Pd and Pt electrodes in the electrolysis of D_2O. The electrochemical cell was a cylindrical polyethylene bottle of 70mm in height and 60mm in diameter. The cathode was a massive palladium plate, 50mm wide by 50mm long, with a thickness of 2mm. The total mass of this electrode is 59.04g. The anode was made of two sheets of platinium samples, 50mm wide by 50mm long, with thickness of 0.2mm and the spacing of cathode-anode is 10mm. The two platinium sheets were mounted parallel to each other in one electrolytic cell, as shown in the insert of Fig. 1. The platinium electrodes used in the cell were spot-welded to a 0.5 mm diameter platinium wire.

The electrolyte was 99.9% pure heavy water(D_2O) with 0.1M LiCl. The electrolytic cell holded about 176.34g of the electrolyte. The top was closed except for two holes with 3mm diameter to release gas pressure. The electrolysis was operated in a constant current of 0.7A. The applied electric voltage was about 8V. We measured the weight of the Pd plate as a function of time during the electrolysis. The weight increased gradually and finally saturated at the fixed weight as shown in Fig. 2. The increase of the weight gives the total number of the deuterium atoms in the palladium plate.

3. Neutron measurements

In the present experiment use was made of the low- background Ge detector system ELEGANTS III(s)[16]. The detector system ELEGANTS III(s), together with the Pd-D electrochemical system, is shown in Fig. 1. The Ge detector used is the low-background 171cm^3 pure Ge detector, which has been primarily used as a central detector of ELEGANTS III[17,18] for measuring rare double beta decays of ^{76}Ge. The Ge detector is surrounded by 10cm thick OFHC (oxygen free high conductive copper) and 10cm thick lead shield. OFHC is known to be quite free from radioactive contamination, namely below the observable limit of 0.2ppb. The whole system is covered by active shields of 15mm thick plastic scintillators to reject charged cosmic rays. The electrolytic cell was placed in front of the Ge detector. The 16mm thick Fe plate, as the fast neuton scatterer, was inserted between the detector and the front of the cell, and the other Fe plate was also place at the backside of the cell(see Fig. 1). The ^{65}Cu and ^{63}Cu isotopes in the OFHC shield and the ^{74}Ge and ^{72}Ge isotopes in the detector itself were also used as the scatterers of the fast neutrons.

The efficiency of the neutron counter was measured by placing a ^{252}Cf source at the position of the cell. The ^{252}Cf source provided fission neutrons with intensity of $I_n(E_n)$=104 per sec and with the averagy energy of $E_n \sim 2.5$ MeV[16], which is

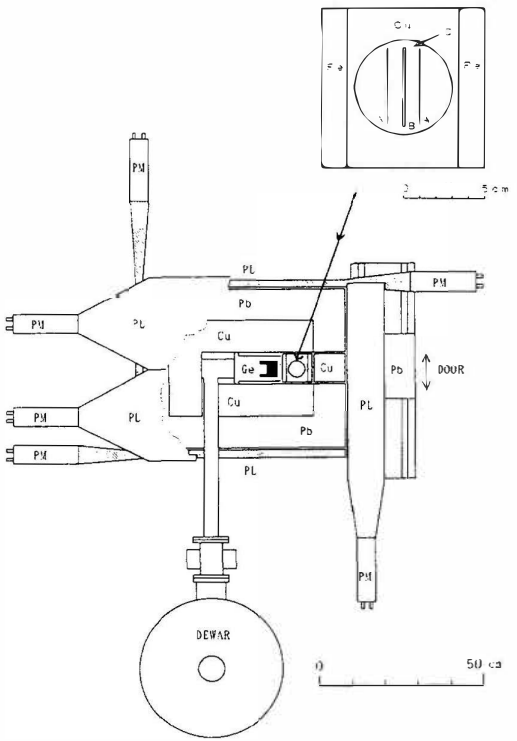

Figure 1. Top view of ELEGANTSIIIs
Ge, PL, PM, Cu, and Pb are the Ge-detector, the plastic scintillators, the photomultipliers, the copper shield(scatterer) bricks, and the lead shield bricks, respectively. The insert shows the enlarged view of the electrolytic cell(C) with the front and back iron scatterers(Fe). A and B in the cell are the Pt anode sheets and the Pd cathode plate, respectively. The enlarged view of the electrochemical cell is show in the upper part

Table1. Limits on cold fusion rates in Pd

Scatterer	γ-energy (keV)	Efficiency ($x10^{-4}$)	Rate (dd fusion) (n/dd sec)
^{56}Fe	846.8	3.3±0.2	$< 2.4 \times 10^{-24}$
^{74}Ge	595.8	2.9±0.3	$< 3.2 \times 10^{-24}$
^{72}Ge	691	1.6±0.3	$< 5.0 \times 10^{-24}$
^{63}Cu	962.1	0.7±0.1	$< 6.4 \times 10^{-24}$
	669.6	1.0±0.1	$< 5.1 \times 10^{-24}$
^{65}Cu	1115.9	0.3±0.1	$< 1.1 \times 10^{-23}$

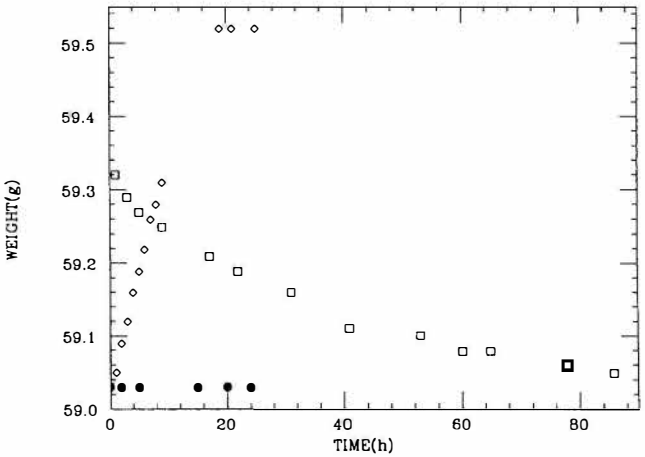

Figure 2. The weight of Pd plate as a function of time during electrolysis. Closed circles show no increase of the weight if the current is off, diamonds show increase of the weight from the begining of electrolysis and the increase of the weight saturates at the fixed weight, and squares show the decreasing of the weight after the current off.

same as the neutron energy from the d+d fusion. A 15mm thick lead plate was inserted between the ^{252}Cf source and the Ge detector to absorb γ-rays from the ^{252}Cf source. Fig. 3(A) shows the energy spectrum of γ-rays following inelastic scattering of neutrons from the ^{252}Cf source. Overall efficiencies were obtained as $k(\gamma_a)=I(\gamma_a)/I_n(E_n)$, where $I(\gamma_a)$ is the peak yield in unit time interval of t=1. The obtained values are given in Table 1. The efficiencies $k(\gamma_a)$ are of the order of 10^{-4}. In order to estimate the minimum neutron flux $S_n(E_n)$ to be detected by the present neutron counter we require the condition that the γ-ray peak yield $Y_\gamma(E_n)=k(\gamma_a)\cdot S_n(E_n)\cdot t$ in a time interval t exceeds the fluctuation of the background $I_\gamma(BG)\cdot t$ in the γ-ray spectrum. The minimum neutron flux to be measured is $S(E_n)=\sqrt{I_\gamma(BG)t}/k(\gamma_a)t$. For the 847 keV γ-ray following the first 2^+ state in ^{56}Fe, $I_\gamma(BG)$ is about 5.5×10^{-5} cps in the γ-ray peak region. The minimum neutron flux to be detected is given by $S_n(E_n)=24.7/\sqrt{t}$ with S_n and t being given in unit of sec. It is $3.2\cdot10^{-2}$ neutrons/sec for t=6.0×10^5sec.

4. Results

The measurement was made for 471 hours of the electrolysis. The average number of the deuterons loaded in the Pd metal was obtained as 0.6 × 3.45 × 10^{23} from the measured excess of the Pd weight. The measured γ-ray spectrum is shown in Fig. 3(C). Before the electrolysis, we also measured the background spectrum from natural radioactivities in the detector system including the scatterers and the electrolytic cell, as shown in Fig. 3(B). There are no significant excess of counts due to the electrolysis at the peak positions of the γ-rays expected from the inelastic neutron scattering.

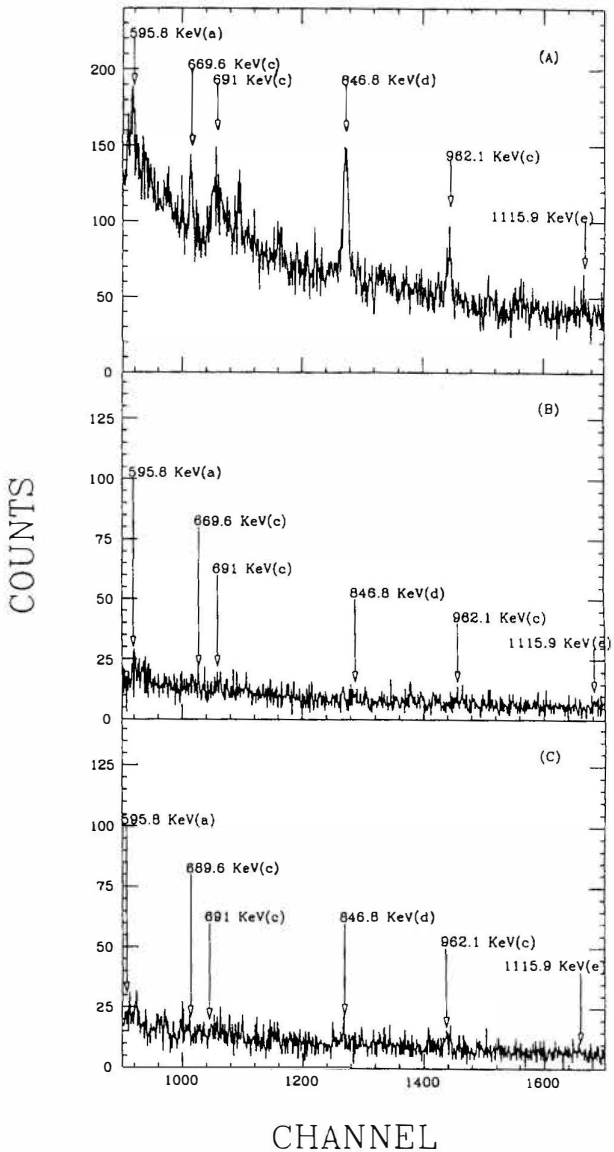

Figure 3. (A):Gamma-ray energy spectrum for the detection efficiency measurement by using the ^{252}Cf neutron source, (B):the spectrum observed before the electrolysis and (C):the energy spectrum observed during the electrolysis. The peaks a, b, c, d and e in the spectrum are the γ-rays from excited states in ^{74}Ge, ^{72}Ge, ^{63}Cu, ^{56}Fe, and ^{65}Cu, respectively.

The reduced upper limits on the fusion rate are summarized in Table 1. Combining all data listed in Table 1, the upper limit on the fusion rate is obtained as $1.6 \cdot 10^{-24}$ (ddn) fusions / [(dd pair) sec].

5. Summary & Discussions

Search for neutrons from any possible deuteron-deuteron fusion during electrolysis was made by using a low background Ge detector. It is emphasized that the present method looking for sharp γ-ray peaks is sensitive to only fast neutrons and thus useful for separating the signal from the continuum background(noise). The upper limit of $1.6 \cdot 10^{-24}$ (ddn) fusions / [(dd pair) sec] is derived. It is one of the severest limits among the recently published results. In fact there are several works which claim finite d+d fusions at the room(cold) temperature. Most of them, however, do not detect directly the fast neutrons nor the neutron energy. Since detection of low-intensity neutrons are rather hard, it is essential to use simultaneously various types of detectors for measuring the neutron energy at several different positions. The present detector, which is a very low-background/noise system sensitive to the fast neutrons from the d+d fusion, is strongly reccommended to be used for checking possible d+d fusions if any.

Acknowledgement

The authors are indebted to Dr. T. Saito for providing them with the ^{252}Cf source. They thank Dr. M. Fujiwara, Mr. K. Matsuoka, Mr. K. Kume and members of ORIS (Osaka university RI center) for kind helps and valuable discussions. The present work is supported by the Grant in Aid of Scientific Research, Ministry of Education, Science and Culture, Japan.

References

[1] Charles J. Horowitz, *Phys. Rev.* **C40**(1989)R1555.
[2] S. E. Koonin and M. Nauenberg, *Nature* **339**(1989)690.
[3] S. Ichimaru, *J. Phys. Soc. Jpn.* **60**(1991)1437.
[4] S. E. Jones et al., *Nature* **338**(1989)737.
[5] M. Fleishmann, S. Pons and M. Hawkins, *J. Electroanalyt. Chem.* **261**(1989)301.
[6] A. de Ninno et al., *Europhys. Lett.* **9**(1989)221.
[7] N. Wada and K. Nizhizana, *Japanese J. of Appl. Phys.* **28**(1989)2017.
[8] R. Taniguchi et al., *Japanese J. of Appl. Phys.* **28**(1989)2021.
[9] J.F.Ziegler et al., *Nature* **338**(1989)737.
[10] N.Lewis et al., *Nature* **340**(1989)525.
[11] M.Gai et al., *Nature* **340**(1989)29.
[12] D. Aberdam et al., *Phys. Rev. Lett.* **65**(1990)1196.
[13] M. M. Broer et al., *Phys. Rev.* **C40**(1989)R1559.
[14] T. Shibata et al., *Nucl. Instr. Meth.* **A316**(1992)337.
[15] J. D. Porter et al., private communication (1989).
[16] H. Ejiri, K. Matsuoka and E. Choi, *Nucl. Instr. Meth.* **A302**(1991)482.
[17] H. Ejiri et al., *Nucl. Phys.* **A448**(1986)271.
[18] N. Kamikubota et al., *Nucl. Instr. Meth.* **A245**(1986)379.

Statistically Significant Increase in Neutron Counts for Palladium Plate Filled with Deuterons by Electrolysis

Masanori FUJIWARA and Koichi SAKUTA

Electrotechnical Laboratory
1-1-4, Umezono, Tsukuba, Ibaraki 305
Japan

ABSTRACT

The comparison of the neutron count rate was executed among the Pd states different in the absorbed deuteron amounts. Charge and discharge of deuterons to the Pd plate was repeated cyclically by electrolysis. Highly significant difference of 1% level in statistics was observed between filled and emptied states in one sample among the four samples tested. This excess neutron count rate corresponds to the fusion rate of 0.8 $\times 10^{-23}$~ 3.2$\times 10^{-23}$ fusions/deuteron pair/sec.

1. Introduction

As the mechanism of the cold fusion phenomena, the fracto-fusion mechanism was proposed[2][4]. In this theory, a strong electric field generated by a crack in the metal induces a local nuclear fusion. Failures in the reproducibility of experimental results can be explained by this theory[3]. Recently, Arata and Zhang[1] reported the positive results using a complex cathode formed by plasma spraying, which contains plenty of microscopic defects.

We adopted an alternating electrolysis, in which charging and discharging of deuterons to the palladium plate were repeated cyclically. This method is expected to enhance the generation of cracks.

2. Methods

The neutron count rate was measured during the alternating electrolysis of D_2O with Pd/Pt electrodes. Two

FRONTIERS OF COLD FUSION

^{3}He proportional counter tubes were used for the neutron detector. In order to shield background neutrons, all the electrolytical devices, ^{3}He counters and water tanks for neutron thermalization were covered with cadmium plate and set in a pile of water tanks, measured $1.5^W \times 1.2^D \times 2.3^H$ (m). The efficiency of the neutron measurement was about 1.6%.

For the noise discrimination in the neutron measurement, the wave form data of ^{3}He amplifier output was analyzed using wave form analysis. Neutron signals were specified by the pulse height analysis.

The size of the Pd plate of 99.9% purity was 50× 12 × 0.1 (mm), which was surrounded by 4 turns of Pt wire of 0.5 mm diameter. D_2O solution of about 0.1 mol/l LiOD was used as the electrolyte. One cycle of the electrolysis consisted of 4 different stages, 2 hours each, totaled 8 hours. Each stage was classified by the Pd states of deuteron absorption, that is, Pd was ① being charged, ② filled, ③ being discharged and ④ emptied with deuterons. Each stage was a constant current electrolysis with different current. It was ① 264 mA (22 mA/cm2), Pd negative, ② 0 mA, ③ 104 mA (8.7 mA/cm2), Pd positive and ④ 0 mA, respectively. The D/Pd ratio in the stage ② was estimated about 0.77. It was measured by discharging all the deuterons in the Pd plate under the gas generating voltage.

3. Results

Hitherto, 4 Pd samples were examined. The results of each sample are summarized in Table 1. The averaged count rate of the sample 4 is decreased because of the rearrangement of the apparatus. To make the difference among the 4 stages clear, the accumulated differences of neutron counts for each sample are shown in Fig.1. In this figure, the difference from the stage ④ (emptied state) are plotted. These data suggests an abnormal increase of neutron counts for the stages ① and ② in sample 1.

4. Discussion

Statistical analysis was executed for these results. Following the standard statistical procedure, the difference of the averages was tested using t-distribution. In Fig.1, the 1% level of significance in the one-sided t-test are plotted by the dash-dotted line. It is indicated that the increase in the stage ② of sample 1 compared with the stage ④ is highly significant in 1% level of significance. It's power of test is 90%. The 90% confidence interval of the neutron count rate difference is estimated to be 0.8 ~ 3.2

Table 1. Summary of experimental results.

	SAMPLE 1	SAMPLE 2	SAMPLE 3	SAMPLE 4
TOTAL RUN TIMES	46	35	36	67
STAGE 1 (CHRAGING)	2394 26.0	1760 25.1	1750 24.3	2715 20.3
STAGE 2 (FILLED)	2432 26.4	1748 25.0	1823 25.3	2781 20.8
STAGE 3 (DISCHARGING)	2280 24.8	1717 24.5	1776 24.7	2721 20.3
STAGE 4 (EMPTIED)	2243 24.4	1744 24.9	1797 25.0	2784 20.8

TOTAL NEUTRON COUNTS
AVERAGED COUNT RATE
(COUNTS/HOUR)

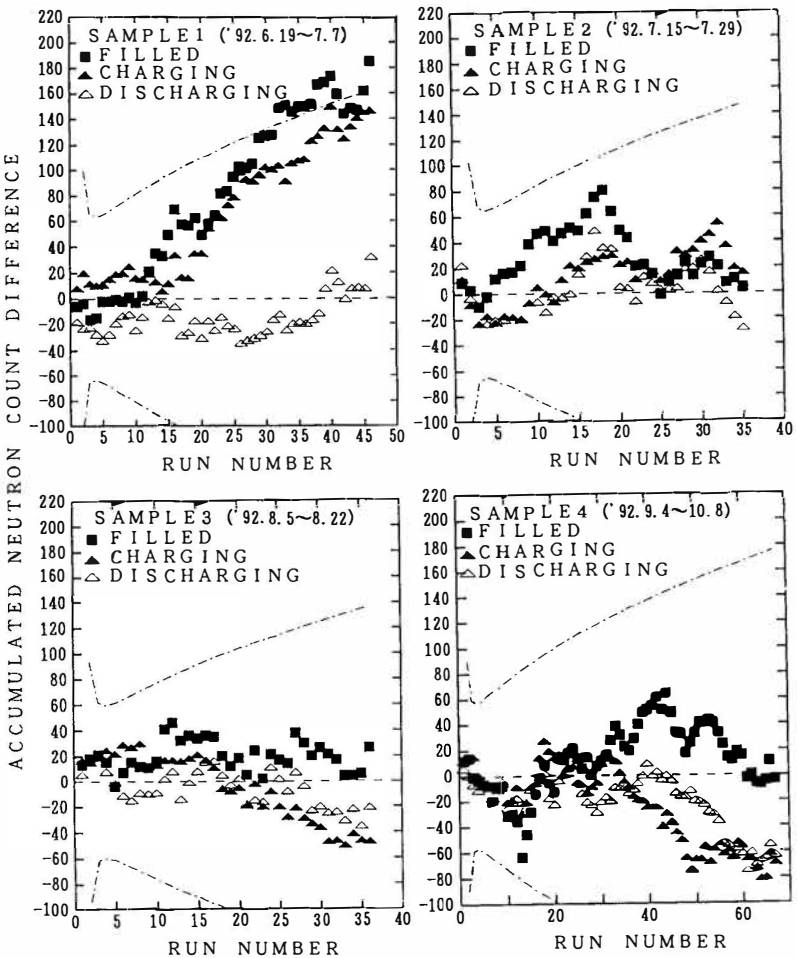

Figure 1. Accumulated neutron count difference from the emptied state.

counts/hour. This corresponds to $0.8\times 10^{-23}\sim 3.2\times 10^{-2}$ fusions/deuteron pair/sec.

It is also indicated that the increase of the stage ① of sample 1 compared with the stage ④ is significant in 5% level of significance. In the stage ①, the effective charging is almost finished in the first 30 minutes. Therefore, it is reasonable that the feature of the stages ① and ② is similar.

The analysis of variance was also applied to the results of sample 1. As a result, the homogeneity of the average count rate of each stage was denied with 2.5% level of significance.

No significant difference was found outside the neutron characteristic region of the pulse height analysis. The number of counts in this region is too small to analyze with the same statistical precision. But it confirms that the increase of the signal in the stages ① and ② was due to neutrons, because the pulse height spectrum as well as the wave shape corresponds to the characteristics of neutron signals.

In order to consider the influence of the atmospheric pressure on the background neutron count rate, the average atmospheric pressure was compared for each stage. No difference requiring further consideration was recognized.

However, the reproducibility is not yet confirmed. No significant difference was found in the experiment of samples 2, 3 and 4. It cannot be denied that the data of the sample 1 was obtained by chance. Therefore, further experiment is required to confirm the cold fusion phenomena.

5. Conclusions

Four Pd samples were tested with alternating D_2O electrolysis. One sample indicates highly significant increase of neutron counts for the deuteron filled state. The level of significance is 1% in statistics. The excess neutron count rate corresponds to the fusion rate of $0.8\times 10^{-23}\sim 3.2\times 10^{-23}$ fusions/deuteron pair/sec. Other samples indicate no significant deference. Further experiments are necessary to confirm the reproducibility.

6. References

1. Arata, Y. and Zhang, Y., KAKUYUGO KENKYU 67, 432.
2. Cohen, J.S. and Davies, J.D., Nature 338,705.
3. Kuhne, R.W., Phys. Let. A 159, 208.
4. Takeda, T. and Takizuka, T., J. Phys. Soc. Japan 58, 3073.

Detection of Neutron and Tritium during Electrolysis of D_2SO_4 - D_2O Solution

Osamu MATSUMOTO, Kan KIMURA, Yuko SAITO, Haruo UYAMA, Tsuyoshi YAITA, Akihiro YAMAGUCHI, and Osamu SUENAGA
Department of Chemistry, Aoyama Gakuin University
Chitosedai, Setagaya-ku, Tokyo 157, JAPAN

ABSTRACT

During the electrolysis of 0.5 M D_2SO_4-D_2O solution using Pd as a cathode material and Pt as an anode material, the emission of neutron was detected by means of the fission track method and the production of tritium was investigated with the liquid scintillation method.

The neutron emission rate was estimated to be compable with natural abundance of neutrons at the surface of the earth which was 2 neutrons cm^{-2} s^{-1} estimated by fission track method comparing with the neutron radiation from the ^{241}Am-^{9}Be neutron source. The tritium production wate was estimated to be 10^4 T atoms cm^{-2} s^{-1} in the Pd metal used as the cathode materials by the liquid scintillation ,ethod. The branching ratio (T/n) was estimated to be 10^4.

1. INTRODUCTION

Branching ratio of tritium production rate to neutron emission rate in the d-d nuclear reaction was estimated to be 10^8 in the discharge of D_2 gas prepared using plasma focus device[4] and this was reported to be 10^4 in the electrolysis of LiOD-D_2O solution[3]. We have measured the neutron emission rate and tritium production rate using fission track method and liquid scintillation method, respectively, during the electrolysis of D_2SO_4-D_2O solution[2]. In this case, it is necessary to obtain the correlation between the fission track number and the absolute neutron emission rate. The relation between the neutron fluence and fission track density was estimated using ^{241}Am-^{9}Be neutron source to determine the absolute neutron emission rate.

FRONTIERS OF COLD FUSION

In the present paper, some results obtained during the electrolysis are reported and the branching ratio (T/n) is briefly discussed.

2. EXPERIMENTAL

The electrolysis of 0.5 M D_2SO_4-D_2O solution was carried out for 5 h using Pd as a cathode material and Pt as an anode material. During the electrolysis, the emission of neutron was detected by means of fission track method. After the electrolysis, the ß-ray radiation from the electrolyte and Pd used as the cathode material was measured by liquid scintillation method using scintillation counter (TRI-CARB 2500TR). The experimental procedures were determined in detail in the previous paper[2].

3. RESULTS

In the neutron detection during the electrolysis of 0.5 M D_2SO_4-D_2O solution and 0.5 M H_2SO_4-H_2O solution using Pd as the cathode material, the fission track metho was applied in order to investigate the effect of the electrolyte solution on the neutron emission. The results obtained are given in Table 1.

Table 1 Fission Track DEnsity Observed in Fission Track Detectors in the Electrolysis

Electrolyte	Detector	Track density[a] (cm^{-2})	B/A
D_2SO_4-D_2O	Dummy	23 (A)	2.6
	Electrolysis	60 (B)	
H_2SO_4-H_2O	Dummy	12 (A)	1.3
	Electrolysis	16 (B)	

a) A fluctuation of neutron levels was observed in some dummy detectors. This may be due partly to slightly difference in treatment conditions. These conditions were the same in set of detectors in each experiment.

The number of fission tracks detected in the detect after electrolysis of D_2SO_4-D_2O solution was 2.6 times higher than that in the dummy detector, though the track density observed after the electrolysis of H_2SO_4-H_2O solution was 1.3 times larger than that in the dummy detector. The increased track number in the electrolysis o D_2SO_4-D_2O solution would be due to the (n,f) reaction of ^{235}U by impinging of neutrons emitted during the electrolysis. The tracks observed in the dummy detector woul correspond to the natural abundance of neutrons.

The relation between the neutron density and the track density was estimated by the determination of the relation between the neutron fluence from the ^{241}Am-^{9}Be neutron source and observed fission track density. The linear relation was obtained between the track density and the neutron fluence. One fission track corresponded to 10^7 neutron fluxes. The natural abundance of neutron was determined using fission track method and it was estimated to be 1.9 neutrons cm^{-2} s^{-1}. This is approximately equal to that reported by Hess et al[1]. Comparing the results obtained during the electrolysis of D_2SO_4-D_2O solution and H_2SO_4-H_2O solution with the natural abundance of neutron, the neutron emission flux during the electrolysis of D_2SO_4-D_2O solution is estimated to be 2 neutrons cm^{-2} s^{-1}.

The ß-ray radiation from the electrolytes and cathode materials after the electrolysis was measured by means of the liquid scintillation method. In the first case, the ß-ray radiation from the electrolytes of D_2SO_4-D_2O solution and H_2SO_4-H_2O solution was measured before and after the electrolysis. The second one is the measurement of the ß-ray radiation from the Pd plate used as the cathode materials in the electrolyses of D_2SO_4-D_2O and H_2SO_4-H_2O solutions. The results obtained are given in Table 2.

Table 2 ß-ray Radiation due to Tritium Formation during the Electrolysis

Sample	cpm[a)]	dpm[a)]
H_2SO_4-H_2O (b)[1)]	0	0
(a)[2)]	6.47	13.77
D_2SO_4-D_2O (b)	117.92	235.84
(a)	193.82	387.64
Pd (b)	0	0
Pd (H_2SO_4-H_2O)[3)]	3.85	9.17
Pd (D_2SO_4-D_2O)[4)]	23.18	65.56

1) Before electrolysis, 2) After electrolysis, 3) After electrolysis in H_2SO_4-H_2O, 4) After electrolysis in D_2SO_4-D_2O, a) Sampling 3 ml

From the results given in Table 2, the activity and the increment of tritium by the electrolysis of D_2SO_4-D_2O solution were estimated as given in Table 3. The tritium production rate in the D_2SO_4-D_2O solution during the electrolysis is estimated to be 10^4 T atoms ml^{-1} s^{-1}. On the other hand, the production rate of tritium in the Pd electrode during the electrolysis of D_2SO_4-D_2O solution is estimated to be 10^4 T atoms cm^{-2} s^{-1}.

Table 3 Estimated Activity and Increment of Tritium during the Electrolysis

Sample	Activity (Bq ml^{-1})	Increment of Tritium
H_2SO_4-H_2O (b)[1]	0	2.5×10^3 atoms ml^{-1} s^{-1}
H_2SO_4-H_2O (a)[2]	0.08	
D_2SO_4-D_2O (b)	1.31	2.7×10^4 atoms ml^{-1} s^{-1}
D_2SO_4-D_2O (a)	2.15	
Pd (b)	0	3.2×10^3 atoms cm^{-2} s^{-1}
Pd (H_2SO_4-H_2O)[3]	0.15	
Pd (b)	0	2.3×10^4 atoms cm^{-2} s^{-1}
Pd (D_2SO_4-D_2O)[4]	1.09	

1), 2), 3), and 4) are used as the same symboles in Table 2.

4. DISCUSSION AND CONCLUSION

The emission rate of the neutron during the electrolysis of D_2SO_4-D_2O solution was estimated to be 2 neutrons cm^{-2} s^{-1} by means of fission track method connecting with the neutron emission from the ^{241}Am-^{9}Be neutron source. The triyium production rate in the Pd used as the cathode material diring the electrolysis of D_2SO_4-D_2O solution was estimated to be 10^4 T atoms cm^{-2} s^{-1}.

The considerably large amounts of tritium observed in the Pd used as the cathode material in the electrolysis of D_2SO_4-D_2O solution would be formed by the d-d nuclear reaction, even if the increment of tritium in the electrolyte should be due to the enrichment of tritium during the electrolysis.

In conclusion, the branching tatio (T/n) estimated in the present experiment is 10^4 like that in the electrolysis of LiOD-D_2O solution[3].

Refernces

1. Hess, W.N. et al., 1961, J. Geophys. Res., 66, 665.
2. Matsumoto, O. et al., 1991, AIP Conference Proceeding: 228, 494.
3. Mizuno, T. et al., 1991, Denki Kagaku, 59, 798.
4. Srinivasan, M. et al., 1991, AIP Conference Proceedings, 228, 514.

Production of Neutron and Tritium from D_2O Electrolysis with Palladium Cathode

G. Y. FAN, X. F. WANG, G. S. HUANG, H. Y. ZHOU, Z. E. HAN, Z. D. WU*
Institute of Low Energy Nuclear Physics
Beijing Normal University, Beijing 100875,
China

ABSTRACT

Anomalous neutron burst and an increase in tritium concentration were observed simultaneously from heavy water electrolysis with palladium cathode. Considered with previous experiment results, we presumed that production of neutron and tritium from D_2O electrolysis depends heavily on the constitution and the state of each cathode.

Keywords: electrolysis, palladium, neutron, tritium

1. Introduction

Since first reports on cold fusion [1, 2], a great number of experiments have been done for verifying these phenomena. Many new positive results have been published which confirm that the claims of cold fusion can not be pushed aside quite easily. However, most of laboratories were not able to reproduce the observations controllablly. It has been realized that some features have not been discovered.

*Department of Chemistry, Beijing Normal University

FRONTIERS OF COLD FUSION

Previous experiments from our laboratory have been reported by Zhou. H.Y, in which a neutron spectrum has been measured from D_2O electrolysis with palladium cathode. Experiment results showed that only one type of palladium tubule which we used in electrolysis experiment is favourable for cold fusion. It will be most interesting to understand the influences of the constitution of material. Repeat experiments have been done in order to verify this assumption.

2. Experimental Aspects

Experimental details regarding this experiment were described previously[3] and will not be elaborated here. Only some important parts would be explained following. In this electrolysis experiment, cathode is a palladium tubule which was used as a deuterium gas filter for a long time. Before we used, no special treatment was done for it except a normal cleaning. Palladium tubule was put in the center of a teflon tube with holes. The diameter of teflon tube was 10 mm. Platinum wire which wound around the teflon tube was used as an anode. The liquid scintillator which was used as a neutron detector was shielded with 30cm thickness of lead and paraffin. In order to regulate the background, n- γ discriminator was well adjusted, and put to the test of stability for several days. The equipments worked quite stably. The average counting rate for background was about 75 counts/hour.

The experiment lasted for five days. The electrolysis current is about 130 mA. The sorrounding temperature always kept at 21° C$\pm$1° C. During the experiment, the temperature measured for reaction cell was shaking around 23° C.

3. Results and Discussion

Experiment results are interesting. Anomalous neutron burst has been observed in this experiment. The details of neutron burst detected were listed in table 1. It is obvious that the counting rates were higher than the average counting rate of background, the variables were beyond the statistical

fluctuation. Compared with previous experiment results[3] , the burst pulses lasted too short time. Amount of neutron detected was significantly small.

Table 1. The details of neutron burst

Event No.	Time (a)	Counting rate (n/min)
1	20 h 05 m	37
2	38 h 02 m	17
3	39 h 12 m	9
4	40 h 09 m	19
5	42 h 39 m	14

a. referred to starting time of electrolysis (t=0).

An increase in tritium concentration was found in the electrolyte after electrolysis with heavy water and palladium cathode. The measurement was taken by comparison between two samples. Sample 1 was 10 ml electrolyte which was taken before the electrolysis. Sample 2 was get from reaction cell after electrolysis. A scintillation counter PACKARD 2250 was used to measure the concentration of tritium in electrolyte. The measurements for two samples were performed under the same conditions and repeated for several times. The data showed that tritium concentration in sample 2 was systematically higher than in sample 1. The average deviation between two samples was about 3 percent, then the statistical error was 1 percent. Quantitative analysis has not been carried out.

We wanted to make a discussion considered with previous experiment results. In our laboratory, electrolysis experiments with heavy water have been done for more than fifty times, using different cathode materials. There were only four experiments (including this one) that we have observed anomalous neutron bursts (among them, there was some doubt for one experiment). Although the behaviours observed for neutron burst are different, one interesting point is that the palladium

tubules were from same type, and were used as deuterium gas filters for a long time. Another point is that if we compared our experiments with others, the time is different when anomalous neutron burst happened. In our experiments, the first burst happened about 20 hours later after electrolysis starting. It was much shorter than others. It led us to presume that whether those palladium tubules have already concentrated deuterium in lattice since it laid in deuterium gas for a long time. If it is so, a new experiment design have to be done. However, it seems to be early to conclude this question. Systematically and critically analyzed experiments will require to make a true understanding of the phenomena.

4. Reference

(1) M. Fleischman and S. Pons, J. Electrolytical Chemistry and Interfacial Electrochemistry, Vol. 261, 301 (1989)
(2) S. E. Jones, et al., Nature, 338, 737 (1989)
(3) Zhou Hongyu, et al., Proceedings of the Ⅱ Annual Conference on Cold Fusion (1991) P49

The FERMI Apparatus and a Measurement of Tritium Production in an Electrolytic Experiment

B. STELLA, M. ALESSIO, M. CORRADI, F. CROCE, F. FERRAROTTO, S. IMPROTA, N. IUCCI, V. MILONE, G. VILLORESI
INFN Roma and Dipart. di Fisica e Chimica,
Universita' "La Sapienza", P. A. Moro 2, 00185 Roma
F. CELANI, A. SPALLONE - INFN Frascati (Roma) -ITALY

ABSTRACT

FERMI is a 7 BF_3, 2 ^3He apparatus with high detection efficiency for moderated neutrons,pulse shape acquisition and good sensitivity to neutron bursts; it also performs a good statistical reconstruction of the average neutron energy. Gamma rays are detected by a complementary low background NaI detector. The total neutron background measured by the apparatus in the Gran Sasso INFN underground laboratory amounts to 0.09 Hz.

A few different experiments have been performed with the same detector (see also the following contribution)..

A D_2O-LiOD electrolysis with Pd cathode has been realized with emphasis on the cleanliness of all components. D_2 and O_2 produced gases were recombined using a room temperature catalyzator and the resulting water was monitored twice a day for tritium content; the same was done for samples of the electrolytical solution.

Loading the Pd with variable currents, an elongation of 130 μ m (with much larger radial broadening)was observed in the first few days accompanied by a 60-100 % tritium excess detected in the recombined water. The measured neutron rate in the same period was consistent with the background.

1. Introduction. The apparatus.

Unambiguous detection of nuclear ashes is fundamental in cold fusion studies. Neutrons,protons,tritium and gamma rays can be individually detected in principle,with larger difficulties for protons. We have set up an apparatus to detect neutrons,gammas and tritium. The name FERMI means (in italian) "Electrochemical Fusion with Interdisciplinary dedicated Research" and refers to the collaboration of specialists in different branches.

A cross section of the apparatus is shown in fig.1. In a big structure of poliethylene moderator seven large BF_3 (2 m long) proportional counters are imbedded. In an inner gap two ^3He are aside of a longitudinal bogie allowing to extract the samples. A big NaI crystal equipped with a spe-

FRONTIERS OF COLD FUSION

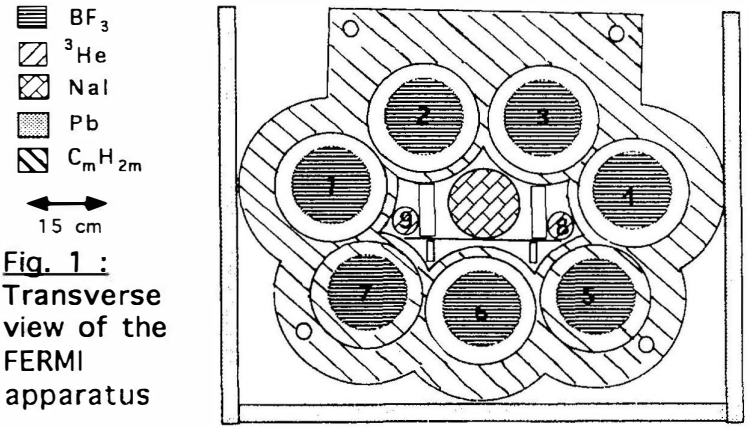

Fig. 1 : Transverse view of the FERMI apparatus

cial low noise photomultiplier, closes the gap axially.

The electronics provides per each counter 1) 100 MHz counting, 2) pulse height analysis, 3) full pulse shape acquisition within 500 μsec (for high multiplicity events). This redundancy allows internal cross checks, discrimination of neutrons from other particles, oscillations and discharges and time resolution from a few μsecs (same counter) to zero (different counters). A full automatic acquisition is performed, including timing for every event.

The detector has been fully simulated by Monte Carlo method (MCNP code), including the moderation and interaction of neutrons. Comparison with various experimental data has been used to improve the reliability of the simulation, which then has been used to compute the efficiency and to optimize various parameters. The thickness of poliethylene in front of every neutron detector (including grains in the cylindrical gap of counters 5 and 7) has been optimized to obtain the maximal efficiency and energy dependence of it (fig.2). This way the 9 rates provide a statistical reconstruction of the average energy of the neutrons by a likelihood algorithm. The final resolution is $\sigma_E/E=(16\pm2)/\sqrt{N}$ (N=total number of detected neutrons).

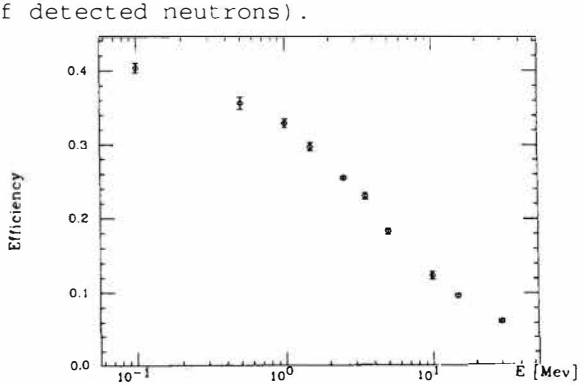

Fig. 2: Total neutron counters efficiency vs energy

To summarize, FERMI's "virtues" are: 1) high neutron efficiencies in a wide range; 2) good energy resolution;

3) low background (0.09 n/sec in the Gran Sasso tunnel); 4) good time resolution and sensitivity to bursts; 5) gammas and tritium detection; 6) multihit feature (we have observed events with up to 16 neutrons); 7) redundancy; 8) automatic acquisition (including pulse shape); 9) slow controls acquisition (temperature, pressure, voltages); 10) full MC simulation (tested).

2. The electrochemical experiment.

We have designed the cells for electrolysis with special care of the cleanliness from impurities, the minimization of systematic errors and the possibility to measure tritium content both in the solution and in the gas. A sketch of the cells is shown in fig.3. The cells body is

1) Pd cathode
2) Teflon cell
3) Entrance D_2O
4) Reference electrode
5) Thermical sensor
6) Mechanical comparator
7) Pt electrode (fine net)
8) Condensation spiral
9) Hole for D_2O pickups
10) Cathalyzator
11) Exit for recombined solution
12) Exit for pickups
13) Mechanical structure
14) Pd mechanical blocking

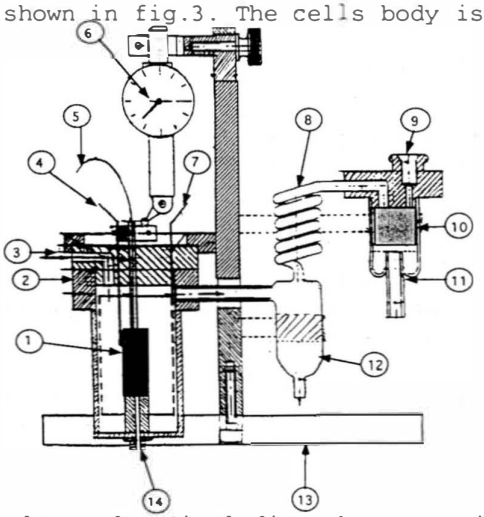

Fig. 3

made of teflon and the electrodes (including the extremities of the Pd cathode) are made of Platinum, to avoid contamination of the Pd sample. The samples (three cylinders 2.5 cm high and 4 mm diameter) were degassed in vacuum (~10^{-5} Torr) at 650 °C. The Pd temperature is measured by a thermocouple directly on the electrode.

The solution is D_2O-LiOD 0.1M and is continously provided by a peristaltic pump. The level is kept constant by the hole at right: the excess solution drops in a small container and the gases flow through a serpentine to a vessel where a room temperature catalyzator recombines D_2 and O_2 with 100% efficiency. The recombined water drops in a temporary container. Both excess solution and recombined water are sampled twice a day for tritium measurements.

The loading of Pd during the electrolysis has been monitored for cell D only, by measuring the elongation of the electrode by a micrometer.

Three cells were individually supplied with current densities up to 300 mA/cm^2. The cells were inserted in FERMI's longitudinal gap and all relevant variables were automatically acquired by computer. The electrolysis lasted about one month, using different current densities.

3. Results

After an initial loading, giving 130±5 μm elongation (together with a much larger radial broadening at center) the length of the monitored electrode came back almost to the original value (see bottom of fig.4). At top of fig.4 we report the measured activity of the samples: the letters indicate the three cells, capital for recombined water, small for solution. We find, as expected due to the isotopic effect in the ion mobility, approximate double activity for the solution respect to the recombined water, but for the four measurements in coincidence with the elongation (loading). Here we find an excess of 60% for D and 100% for A (C was not yet measured, unfortunately).

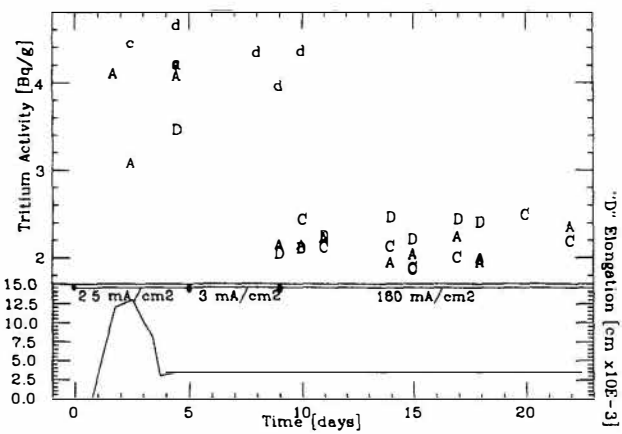

Fig. 4: upper part: specific tritium activity in the solution (lower case letters) and in the recombined gas (upper case) vs time; lower part: electrode D elongation vs time ; used current densities are indicated.

In order to check that the tritium was not accumulated originally in the catalyzer itself, we measured its activity separately. The result has been negative, with upper limit .050 Bq/cm^2 at 5σ level. Other sources of tritium are very unlikely.

The neutron rate measured during all the experiment was consistent with background. The ratio of produced neutrons over the excess tritium atoms is lower than approximately 10^{-7}, in agreement with other results [1].

4. Conclusions

We have observed a clear tritium excess in recombined water from two samples of degassed Pd. The excess happened in coincidence with a clear elongation and enlargement of the monitored sample. The effect is not due to previous enrichment of the catalyzer.

We are analyzing the data of the temperature of the samples and of the gamma rays detected in the same period.

Reference

1) Storms, E.,1991, Fusion Technology 20, 433.

Time-Evolution of Tritium Concentration in the Electrolyte of Prolonged Cold Fusion Experiments and its Relation to the Ti Cathode Surface Treatment

J.SEVILLA, B.ESCARPIZO, F.FERNANDEZ, F.CUEVAS and C.SANCHEZ.
Universidad Autónoma de Madrid
Cantoblanco 28049, Madrid
SPAIN

ABSTRACT

Tritium concentration in the electrolyte has been carefully monitored in more than twenty electrolytic cold fusion experiments accomplished in open cells. In order to distinguish between T-natural enrichment (isotopic enrichment) and any other T source inside the cell a macroscopic theoretical model is proposed to analyze the experimental data. It is concluded that T-concentration variations in the electrolyte above the level due to natural enrichment can be detected with confidence and therefore that open-cell experiments are convenient to investigate T-production. In addition, some empirical correlations between model parameters (measured separation factors) and cathode surface treatments prior to experiment have been found.

1. Introduction

Most of our present knowledge on the processes at the cathode surface and hydrogen generation in an electrolytic cell has been gained by conventional electrochemical experiments accomplished in short time (from minutes to a few hours). Longer electrolysis like those in cold fusion experiments will yield new problems in relation to the cathode behaviour and the electrolysis itself. On the other hand, more discussion is needed to elucidate whether cold fusion experiments with open or closed cells must be accomplished. Closed cells may represent a potential danger whereas results obtained with open cells are, in general, difficult to be analyzed. In relation to T production in cold fusion experiments with open cells some T goes out from the cells with the produced gases and some difficulties may appear on determining possible increases of its concentration due to the nuclear processes. We have faced both problems in our current research. Some of the conclusions obtained about T-production in electrolytic cold fusion experiments and its relation to previous cathode surface treatments are now presented.

FRONTIERS OF COLD FUSION

2. Experimental

Main characteristics (materials and procedures) of our experiments have been already published (Fernández et al. 1990). In all cases electrolysis was carried out in open cells. Measurements of the electrolyte T-content with a scintillation counter have been described in the same paper and only a few details will be given now. Background signal of our measurements is ~ 6 cpm per ml of electrolyte and stability better than 2%. Electrolyte volume in the cells was in all cases 75 or 150 ml. Daily sampling (2 ml) to measure T-concentration was done. Before taking the electrolyte sample, the cell was refilled up to reach the original level in order to compensate losses due to electrolysis and other processes. Sample taken was stored in a vial at low temperature. Chemiluminiscence and other misleading phenomena were eliminated. All Ti and Pd cathodes used in our experiments were treated prior to the experiment. Details of the treatments will be given in the text.

3. Results and discussion

According to our experimental characteristics the following conditions can be accepted to figure out an equation to describe the evolution of T-concentration in the electrolyte:

a) We only consider kinetics of T and D concentrations

b) Different processes contribute to remove electrolyte from the cell. We accept that in all cases the amount removed is proportional to the remaining electrolyte volume.

c) Permanent and continuous refilling of the cell was done to keep

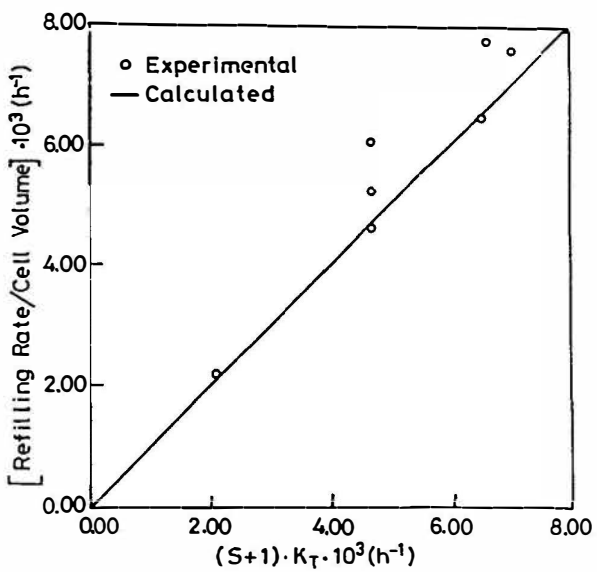

Figure 1. Model parameters (S and K_T) versus refilling rate.

constant the electrolyte volume.

d) T concentration is in all cases much smaller than D concentration.

Under these conditions the following equation can be obtained:

$$C(t)=S\cdot C_r-(S\cdot C_r-C_o)\cdot\exp(-k_T\cdot t)$$

where $S=k_D/k_T$ and C(t) is the T concentration expressed trough the number of counts per minute and ml., C_r are the counts of the refilling electrolyte and C_o those of the initial electrolyte (in most cases $C_r=C_o$). The parameter S will be called "macroscopic separation factor" and it is an average of separation factors from different microscopic processes. Therefore S is not directly comparable to microscopic separation factors from other works. k_D and k_T are proportionality constants between the loss-rate of D and T and their concentrations in the remaining electrolyte. Both S and k_T are obtained by fitting C(t) to those experimental results where no nuclear process took place.

S values from experiments with Ti cathodes show consistent results. In particular a proportionality relationship between $(S+1)\cdot k_T$ and the electrolyte cell refilling rate is deduced from the model and is also well verified by the experimental data as shown in Fig.1. Different S values are obtained for the Ti cathodes according to their nature and surface treatment prior to experiments (Fig. 2). The first group (experiments 6,8 and 9) is formed by experiments accomplished with electrolytic Ti-cathodes which were mechanically polished. The second one (exp. 11,12 and 13) with the same Ti but chemically etched. Finally in the third group (exp. ETi17 and 19) Ti cathodes from commercial grade, cold rolled and chemically etched plates were used.

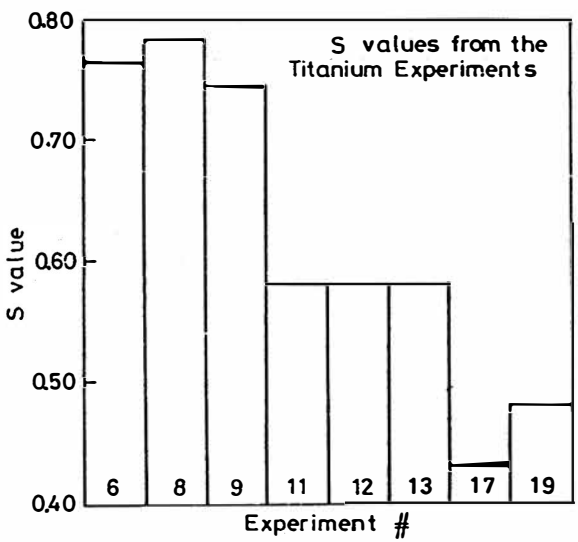

Figure 2. Influence of cathode surface treatment on the S values (see text).

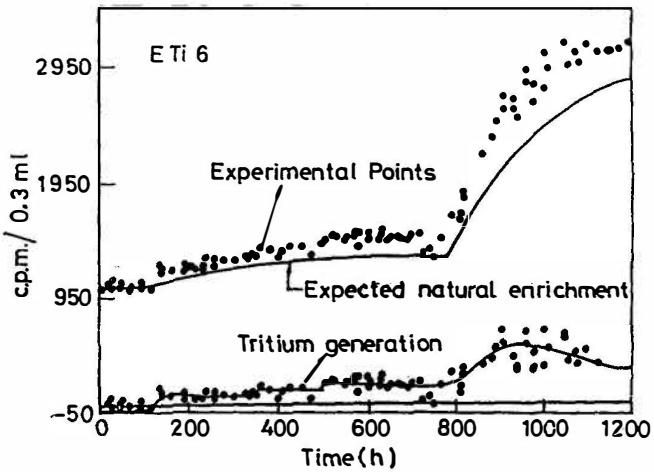

Figure 3. T-excess as measured in experiment ETi6

Finally, the result from experiment ETi6 has been analyzed according to the proposed model and T production due to nuclear processes has been detected and is shown in Fig.3. The total amount of T-atoms produced in the full experiment was $\cong 2.5 \cdot 10^{10}$.

4. References

1. Fernandez, J.F. et al, 1990, AIP Conference proceedings no.228."Anomalous nuclear effects in Deuterium/solid systems", pp.130 - 145. Provo, USA.

5. Acknowledgements

This research has been supported by CICYT (Spain) under contract MAT-90-0053. Support received from Fundación Banco Exterior (FEB), Madrid, is also gratefully recognized. Thanks are given to members of CEDEX (MOPT) for their assistance in the T measurements.

The Change of Tritium Concentration during the Electrolysis of D_2O in Various Electrolytic Cells

Kew-Ho LEE and Young-Mok KIM

Korea Research Institute of Chemical Technology
P.O.Box 9 Daedeog-Danji, Taejeon, Korea 305-606

ABSTRACT

The U-type and bell jar type electrolytic cells were designed using pyrex glass and modified for recombination of gases with platinum catalysts. The electrolysis of $LiOD/D_2O$ in U-type cell yielded more final activities in Pt/Pd system than Pt/Pt system. Some electrolysis of $LiOD/D_2O$ in Pt/Pd showed the increase of ^3T above 100%. The separation factor of D/T in electrolysis was not measured directly but assumed 2~3 from literature. The increase of ^3T can not be explained with the isotope separation effect.

But in the modified cells with recombination, the electrolysis yielded no significant increase of final tritium activities in the total system. In this case, recombined D_2O was collected separately and total ^3T activities were obtained by combining this with residue in D_2O electrolytes.

Finally, bell jar type closed cells were designed with recombination catalysts. And palladium electrode was covered by different porous materials. After 10 days of electrolysis with a change of current density, one cell showed the increase of ^3T activities significantly.

I. INTRODUCTION

The cold fusion reactions were usually confirmed by detection of neutron emission, and the production of tritium and heat.

This study is to observe the tritium which can be produced as a nuclear product in palladium metals that were used as cathode in various electrolytic cells of alkaline electrolytes by following reactions.

$$^2D + {}^2D \rightarrow {}^3T + {}^1H$$
$$(1.0\ \text{Mev})\quad (3.02\ \text{Mev})$$

The production of tritium proves the existence of a nuclear reaction unquestionably and the change of tritium concentration can be measured easily by counting β activities in electrolytes with a liquid scintillation counter.

FRONTIERS OF COLD FUSION

II. EXPERIMENTAL

Galvanostatic electrolysis was conducted in the water bath with different cathodes and electrolytes at different current densities ranging from 50 to 1000 mA/cm^2.

The different U-type and bell jar type electrolytic cells were designed using pyrex glass and modified for the recombination of evolved gases as shown in following figures.

500 $\mu\ell$ of liquid electrolytes were withdrawn for tritium analysis from the cell using a sterile syringe and β activities of electrolytes were counted by liquid scintillation counter.

X-ray, BET, ICP and SEM were used to analyze palladium electrodes before and after reactions.

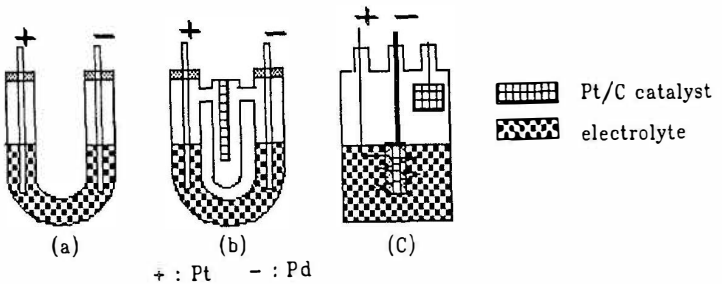

Fig. Electrolytic Cell of Cold Fusion Reactions
(a) U-type cell (open cell) (b) Modified U-type cell (closed cell)
(c) Bell jar type cell with porous materials

III. RESULTS AND DISCUSSION

1. The variation of electrolytes
Electrolysis in $LiOD/D_2O$ (CF-3,4,5) yielded more final ^3T activities than KOH/D_2O (CF-1) and $LiOH/D_2O$ (CF-2) at the Pd working electrode in U-type open cells (Table 1).

TABLE 1. Increase of ^3T concentration in U-type open cell after electrolyis in different electrodes and electrolytes.

Cell Code	Electrode		Electrolyte	Cell Type	Current Density (mA/cm^2)	Before ^3T (dpm/ml)	After ^3T (dpm/ml)
	Cathode	Anode					
CF-1	Pd	Pt	0.1M KOH/D_2O	A	60 - 600	120	140
CF-2	Pd	Pt	0.1M $LiOH/D_2O$	A	60 - 600	105	130
CF-3	Pd	Pt	0.1M $LiOD/D_2O$	A	50 - 500	106	196
CF-4	Pd	Pt	0.1M $LiOD/D_2O$	A	50 - 500	87	165
CF-5	Pd	Pt	0.1M $LiOD/D_2O$	A	50 - 500	187	289
CF-8	Pt	Pt	0.1M $LiOD/D_2O$	A	50 - 600	166	212
CF-9	C	Pt	0.1M $LiOD/D_2O$	A	50 - 600	186	238
CF-15	Pt	Pt	0.1M $LiOD/D_2O$	A	50 - 500	129	132
CF-17	Pt	Pt	0.1M $LiOD/D_2O$	A	50 - 500	124	146
CF-12	Pd	pt	0.1M $LiOH/H_2O$	A	50 - 500	25	29
CF-18	Pd	Pt	0.1M $LiOH/H_2O$	A	50 - 500	33	49

2. The variation of Electrolytes
Under the same electrolysis condition the increase ratio of ^3T at Pd (CF-3,4,5) was larger than that of Pt (CF-8,15,17) and carbon electrodes (CF-9) (Table 2).

3. Blank Test
The electrolysis with $LiOH/H_2O$ was run for the blank test to compare with $LiOD/D_2O$. Almost no increase of ^3T activities was observed even after long peridos of electrolysis (CF-12 and CF-18 in Table 1).

4. The pretreatments of palladium
Torching, quenching, etching and mechanical hammering of Pd metals were carried out. But this pretreatments gave no significant effect on the increase of ^3T activities in this study.

5. Modified closed U-type cell
U-type cells were modified as closed system to recombine the evolved gases by Pt catalysts. (> 98% recovery). As shown in Table 2, small increase of ^3T was observed but was considered within the error bound (CF-25,26) in the total system. The small increase in remained electrolytes and the decrease in recombined D_2O were observed

Table 2. The total ^3T activity in modified U-type closed cell before and after electrolysis.

Cell Code	Electrode		Electrolyte	Cell Type	Current Density (mA/cm^2)	Before ^3T *1 (dpm)	After ^3T *2 (dpm)	Uf *3 (dpm/ml)	Rf *4 (dpm/ml)
	Cathode	Anode							
CF-24	Pd	Pt	0.1M $LiOH/D_2O$	B	50-500	1523 (152)	1545	171	82
CF-25	Pd	Pt	0.1M $LiOD/D_2O$	B	50-500	1604 (160)	1626 -1900	191-241	83-96
CF-26	Pt	Pt	0.1M $LiOD/D_2O$	B	50-500	1391 (139)	1408 -1872	166-237	74-83
CF-27	Pd	pt	0.1M $LiOH/D_2O$	B	50-500	1391 (139)	1459	167	78

* 1 : dpm/ml x initial volum (ml)
2 : Uf x Volum of remained electrolyte + Rf x Volum of recombined D_2O
3 : Uf : ^3T acitivity in remained electrolyte
4 : Rf : ^3T acitivity in recombined D_2O

6. Bell jar type closed cell
Ordinary bell jar type cells with catalyst (F.P cell type) were tested with variation of Pd electrodes. Some Pd electrodes were covered with microporous materials, porous vycor glass and porous Al_2O_3/PS. In most cells no increase of ^3T activities was observed except one cell in which Pd was covered with porous vycor glass. (CF-30). This phenomenon was not reproduced. In this cell silica was dissolved from Vycor and deposited on the surface of Pt electrode.

Table 3. Increase of ^3T concentration at different Pd electrodes in bell jar type closed cell

Cell Code	Electrode		Electrolyte	Cell Type	Current Density (mA/cm^2)	Before ^3T (dpm/ml)	After ^3T (dpm/ml)
	Cathode	Anode					
CF-28	Pd	Pt	0.1M LiOD/D_2O	C	50 - 500	124	115
CF-30	Pd/Vycor	Pt	0.1M LiOD/D_2O	C	100 - 450	112	208
CF-31	Pd/Vycor	Pt	0.1M LiOD/D_2O	C	100 - 800	112	115
CF-32	Pd/Vycor	Pt	0.1M LiOD/D_2O	C	100 - 900	124	120
CF-33	Pd/PS	Pt	0.1M LiOD/D_2O	C	100 - 600	112	127

IV. CONCLUSION

Even though the fusion reaction was not confirmed by the exponential increase of ^3T, the increase of ^3T activity was a real phenomenon during the electrolysis of LiOD/D_2O at Pd electrode in this study. And this increase could not explained only by the concentration effect of D/T separation factor in electrolysis.

V. REFERENCES

1. Chene, J. and Brass, A.M, 1990, J. Electroanal. Chem., 280, 199-205
2. Storms, E. and Talcott, C., 1990, Fusion Technology, 17, 680-694
3. Packham, N.J. et al, 1989, J. Electroanal. Chem., 270, 45-458
4. Schultze, J.W. et al, 1989, Electrochimica Acta, 34(9), 1289-1313
5. Mengoli, G. et al, 1991, J. Electroanal. Chem., 304, 279-287

Comments on Methodology of Excess Tritium Determination

Stanislaw SZPAK and Pamela A. MOSIER-BOSS
NRaD, San Diego, CA 92152-5000, USA
Jerry J. SMITH
Dept. of Energy, Washington, DC 20585, USA

Abstract

Three methods of tritium data analysis are considered – comparison between experimental and theoretical data, total mass balance and curve-fitting.

1.0 Introduction

The evidence for tritium production in electrochemical cells, with few exceptions (Will *et al*, 1992), is based on measurements of tritium increase in the electrolyte phase in excess of that predicted from the isotopic separation factor. Often, this enrichment was computed under conditions of constant electrolyte volume which, in turn, implies continuous additions and withdrawals, a somewhat unrealistic undertaking. In those instances where the total tritium content at the end of an experiment was ten times or more greater than what was present in the beginning, it cannot be disputed that generation of tritium occurred. However, for low levels of tritium production, care must be taken in the analysis, especially if open cells are used. In this communication, we comment on the methodologies of analysis used and point out their advantages and disadvantages.

2.0 Use of Simulated Data to Evaluate Methods of Tritium Analysis

To evaluate the methods of analyzing tritium, we needed data that would show various degrees of tritum production and include measurements of both the electrolyte and gaseous phases over a fairly long period of time. In addition there could be no question of contamination of tritium from the cell, cell components or outside environment or of erroneous tritium measurements resulting from chemical reactions in the scintillator fluid. To meet all of these requirements, it was deemed necessary to use simulated data.

FRONTIERS OF COLD FUSION

2.1 Development of Model

In an open cell, a volume of electrolyte, V, is electrolyzed. Throughout the experiment, electrolyte is being withdrawn for tritium analysis and is being replaced. Assuming sampling is instantaneous, for any given time the rate of change of tritium in the electrolyte, $\frac{dT_L}{dt}$; on the recombining electrode, $\frac{dT_R}{dt}$; and in the gas phase, $\frac{dT_G}{dt}$, are given by:

$$\frac{dT_L}{dt} = -\xi(f_L m_L)\phi - \alpha(f_L m_L) + C \tag{1}$$

$$\frac{dT_R}{dt} = \xi(f_L m_L)\phi - \alpha(f_R m_R) - \xi_R(f_R m_R) \tag{2}$$

$$\frac{dT_G}{dt} = \xi_R(f_R m_R) - \alpha(f_R m_R) \tag{3}$$

where ξ and ξ_R are the isotopic enrichment factor for tritium during electrolysis and on the recombining electrode, respectively; α and C are the radio-active decay rate and generation rate of tritium, respectively, both are in *atoms* sec^{-1}; f_L and f_R are the mass fraction of tritium in the electrolyte and on the recombiner, respectively; and $\phi = \frac{i\epsilon M_{D_2O}}{2F}$ where M_{D_2O} is the molecular weight of D_2O and ϵ is the Faradaic efficiency. In this model the amount of D/T absorbed/desorbed by the Pd-electrode and losses due to evaporation are not considered. Using these differential equations, simulated data for tritium in the gas and liquid phases were calculated under conditions of no production, low continuous production, continuous production near the end of an experiment, and pulse production. In constructing these data sets, the total volume was fixed at 50 ml; $\xi = 1.8$; $\xi_R = 1.0$, which corresponds to 100 % efficiency of the recombiner; $\alpha = 250$ *atoms* sec^{-1}; and Gaussian noise, with a 1 % standard deviation, was superimposed on the calculated values. The simulated data for zero and pulse production are shown in Figure 1.

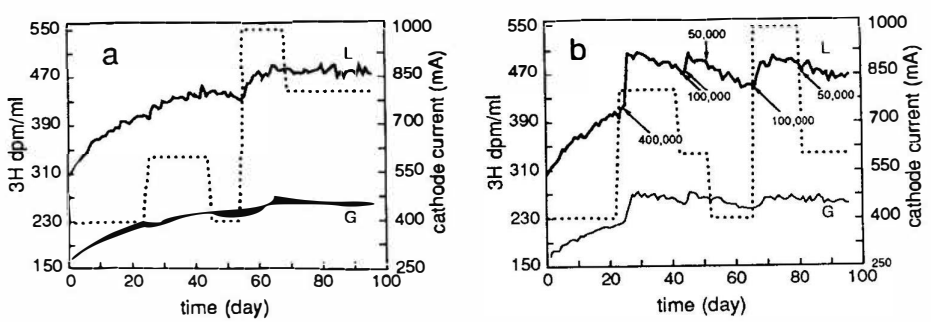

Figure 1. Simulated data for (a) zero tritium production and (b) pulse tritium production. Solid lines are the liquid, L, and gas, G, phase tritium measurements and dotted lines represent the cathodic current profile. Tritium production bursts, in *atoms* sec^{-1}, are indicated.

3.0 Experimental Methods of Analysis

The methods of analysis fall into three general categories. In one method, samples of the gas and liquid are taken, the tritium content is measured and compared with the theoretical value. The second method is one of total mass balance. The third method utilizes curve-fitting.

3.1 Method 1: Comparison of Experimental and Theoretical Values

Usually theoretical values for the liquid and gas phases are calculated using the expression derived by Bockris *et al.* (Lin *et al*, 1990):

$$\frac{a(t)}{a(0)} = \xi - (\xi - 1)\, exp(\frac{-ti}{2F\xi nV}) \tag{4}$$

where $a(0)$ and $a(t)$ are the activity of tritium initially and at time t, respectively, and n is the concentration of D_2O. Equation (4) assumes a constant current, i, and that the number of deuterium atoms far exceeds the number of tritium atoms. It also assumes a constant volume, V; *i.e.*, after electrolysis for a given time period, D_2O is added to restore the volume prior to sampling. The differential equations (1)-(3) were solved for this experimental procedure to yield data sets under the conditions of no tritium production, i=0.4A, ξ=1.8, V=50ml, $a(0)$= 300 $dpm\ ml^{-1}$ and no Gaussian noise on the data. These data sets were compared to the $a(t)$ values calculated using Eqn. (4). Without correcting for sampling, the data agree well with one another for about one week. Afterwards, the values calculated using Eqn. (4) are much higher. When sampling is included, there is good agreement up to the one month period at which time the values calculated using Eqn. (4) were again larger.

3.2 Method 2: Total Mass Balance

In this approach, for a given time interval, the total amount of tritium in the beginning is compared to the total amount in the liquid and gas phases at the end. For the zero production case, the difference between the amount of tritium at the end and the beginning of a time interval (Δ), followed a Gaussian distribution with Δ's evenly divided between positive and negative σ's. In the cases of tritium production, *i.e.*, low continuous production, pulse production and production at the end, the overall distribution of Δ's was not Gaussian and was skewed towards more positive σ's. This skewing towards more positive σ's clearly indicates that tritium was produced.

3.3 Method 3: Curve-fitting

If the initial mass of deuterium and tritium, $m(0)$, is electrolyzed at a constant cell current, i, for a specified period of time, τ, at which time a sample is withdrawn and analyzed for tritium and D_2O is added to restore the initial volume. The tritium

mass fraction in the electrolyte, $f_L(t)$, is given by:

$$f_L(t) = [m(0) - r(i)t]^{\xi-1} \left[\frac{f_L(0)}{m(0)^{\xi-1}} + \int_{t=0}^{\tau} \frac{C dt}{[m(0) - r(i)t]^{\xi}} \right] \quad (5)$$

where $r(i)$ is the rate of removal due to electrolysis. Equation (5) is a general solution of the differential equations (1)-(3) and neglects the radioactive decay and loss by evaporation. As written, Eqn. (5) has two adjuustable parameters which will be stongly coupled to one another – the isotopic separation factor, ξ, and the tritium generation rate, C. The simulated data for all four cases were computer analyzed using Eqn. (5). In the zero tritium and low continuous production cases, there was excellent agreement between the data and the computer analyzed curves. However, the computer analyzed curves did not agree with the remaining two cases especially in the regions where the tritium production occurred.

4.0 Conclusions

All three methods discussed for analyzing tritium data require 100% efficiency of the recombining electrode. Efficiencies less than 100% result in a preferential loss of DT over D_2 in the gas phase. The technique advocated by Bockris and others, that of comparing the measured tritium values with those calculated using Eqn. (4), is valid for short term experiments. This approach requires that the isotopic separation factor, ξ be known. For the Pd/D system, ξ's ranging from 2 to 10 have been reported. Furthermore, it is assumed that ξ remains constant throughout the course of the experiment. This assumption may not be valid since ξ depends upon the kinetics of the system as well as the current density. With the technique of total mass balance, ξ need not be known nor is it required to remain constant. Likewise with curve-fitting, one does not need to know the value of ξ, but ξ is assumed to be constant. Therefore, when the experimental and computer analyzed curves don't agree, it is not known if ξ was affected or if tritium production occurred. However, curve-fitting does indicate that something happened during the course of the experiment. The total mass balance and curve-fitting approaches require long term experiments in order to achieve a statistically significant analysis. Of the three techniques, curve-fitting is the least sensitive to detecting burst production of tritium.

5.0 References

1. Lin, G.H., Kainthla, R.C., Packham, N.J.C., Velev, O. and Bockris, J.O'M, 1990, *International J. Hydrogen Energy*, **15**, 537.

2. Will, F.G., Cedzynska, K., Yang, M-C, Peterson, J.R., Bergeson, H.E., Barrowes, S.C., West, W.J. and Linton, D.C., 1991, Conference Proceedings of the Second Annual Conference on Cold Fusion, June 29- July 4, Como, Italy, pg.373.

The authors would like to acknowledge the contributions of Dr.'s Roger Boss and Cedric Gabriel and the support of Dr. Frank Gordon.

Fine Structure of the Charged Particle Bursts Induced by D_2O Electrolysis

Ryoichi Taniguchi and Takao Yamamoto
Research Institute for Advanced Science and Technology, University of Osaka prefecture
1-2 Gakuen-cho, Sakai, Osaka 593, Japan

Abstract

Internal structures of charged particle bursts induced by the D_2O electrolysis have been studied by use of a fast response measurement system. Charged particles were detected by a NE102a plastic scintillation counter. The electrolysis was continued at low temperature at 4°C for 3 hours. After then, the cell was warmed up to several ten degrees of Celsius scale. During the warming-up, we caught some anomalous pulse emissions of charged particles. The pulse shapes of the bursts were found to be complicated and the duration of the bursts was distributed from 40 to 100 nanosecond. Comparison of these pulse shapes and standard response for a single particle suggests that the burst is a pile-up pulse and consists of many particles.

1. Introduction

Emissions of neutron bursts were reported frequently in the cold nuclear fusion experiment. Especially in the $Ti+D_2$ heat cycle experiments, intense neutron bursts with the time scale of microseconds were reported[1]. However, the detail of the timing structure of the bursts have not been measured. When the duration of the bursts would be short, energy spectra of the bursts are also difficult to be measured. Conventional pulse height analyzing system gives only a total energy of bursts. It can not analyze the pulse height of individual pulses separately. In any case, the timing structures of the bursts are considered to be important for understanding the reaction processes of the cold fusion. The energy spectrum of the particles is also indispensable for identification of the type of the reaction. Previously, we have studied the cold fusion phenomena by use of the charged particle method[2], and observed some charged particle bursts[3]. This paper is concerned with the investigation of the

FRONTIERS OF COLD FUSION

pulse shape of the charged particle burst by use of a fast response measurement system.

2. Experimental System

Figure 1 shows the electrolysis cell used in this experiment. A NE102a scintillation counter as a charged particle detecter was attached to the cathode foil with a gap of 5 mm. Figure 2 shows the pulse analyzing system. Output current pulses of the photo-multiplier are integrated by a charge sensitive amplifier and the pulse-height is analyzed with the PHA(Fig.2(a)). In addition, the fast response measurement system is prepared in the present experiment (FiG.2(b)). The output current pulse of the photo-multiplier is amplified by a wide-band current pulse amplifier without integration. The pulse shapes were recorded in a digital strage oscilloscope. A 20 μm thick palladium foil was used for the cathode and set at the bottom of the electrolysis cell. 0.1 μm thick Ag layer was deposited on the air side surface of the cathode foil. The solution used was D_2O+ 0.1moldm^{-3}LiOD. The temperature control of the D_2O solution was programmed to follow a desired pattern. After the electrolysis at low temperature, 20 mA at 4°C for 3 hours, the cell was warmed up to several ten degrees. Abnormal charged particle emission was observed during the warm-up of the solution. Energy spectrum and the pulse shape of the burst were measured simultaneously.

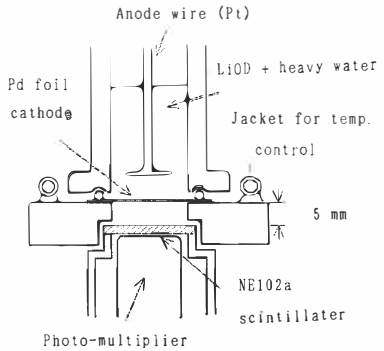

Fig.1 Electrolysis cell and the charged particle detecter.

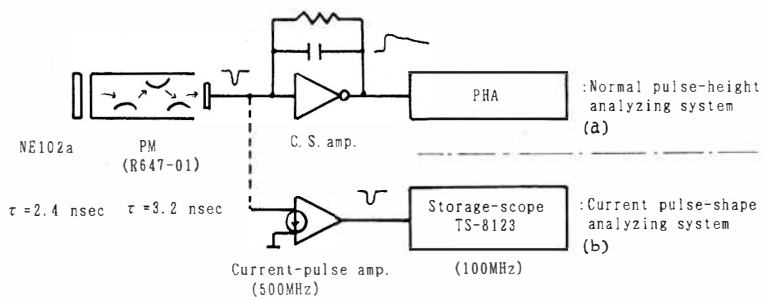

Fig.2 Conventional PHA system and the fast response measurement system.

3. Results and Discussion

Figure 3 shows the energy spectrum measured by the conventional PHA system. The spectrum shape was featureless. The pulse shapes of the slow outputs of the charge sensitive amplifier were not different from the normal response. However, the pulse shape of the burst were completely different from that of the standard alpha particle shown in Fig.4(c). We obtained only two pulse shapes of the burst. Figures 4(a),(b) show the pulse shapes of the bursts. The burst seemes to have some complicated structures. We supposed that the structure of the burst was attributed to the pile-up of many pulses. We restored them to the original timing structure by use of an unfolding method. The restored pulse shapes are shown on the upper side of the Figs.5(a) and (b), respectively. The dotted curves shown in the figures indicate the reconstructed pile-up shapes when the standard responses are appeared and piled-up according to the restored timing strucure. The small dotted curves in the same figures show the burst shape measured in the experiment. Comparison of these curves seems to support our supposition that the burst is the pile-up of the pulses. It is slightly complicated to estimate the energy of the tiny pulses participated in the burst. The light response of the NE102a scintillater is depend on the species of the particles. An energy scales are plotted on the left side of the frames of Figs.5(a) and (b), on the assumption that the particles were electrons. On the opposite side, the scales for protons are plotted. In the case of proton, the energy of the particles should be distributed from 0 to 1.5 MeV, while in the case of electron, that is distributed from 0 to 0.3 MeV. In the proton case, the energy distribution is consistent with that the D-D reaction occured in the palladium foil cathode. The particle identification is indispensable in the study of cold fusion. Futher experiment are in progress.

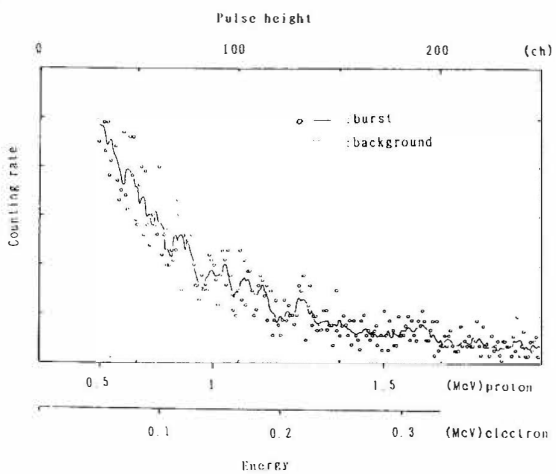

Fig.3 Energy spectrum of the charged particle burst.

Acknowledgment

The authors wish to express their gratitude to Prof. M. Kitagawa for his useful suggestions.

References

1) A.De Ninno, A.Frattolillo, G.Lollobattista, L.Martinis, M.Martone, L.Mori, S.Podda and F.Scaramuzzi, Europh. Let. 9.221(1989).

2) R.Taniguchi, T.Yamamoto and S.Irie, Jpn. J. of Appl. Phys., 28(11),L2021(1989)

3) R.Taniguchi, T.Yamamoto and S.Irie, Bul. of Univ. of Osaka Prefecture, A39, No2, 233(1990)

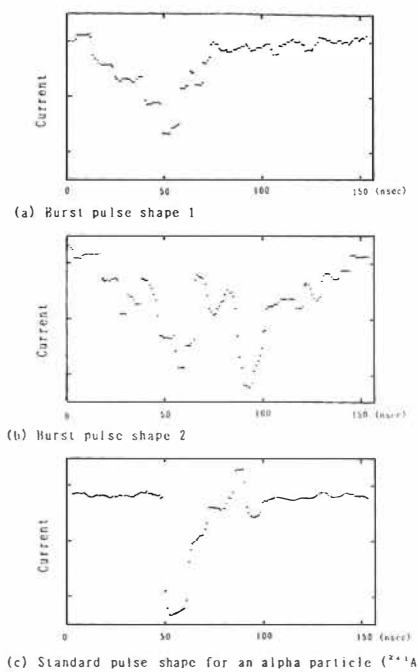

Fig.4 Pulse shapes of the charged particle bursts and a standard pulse shape.

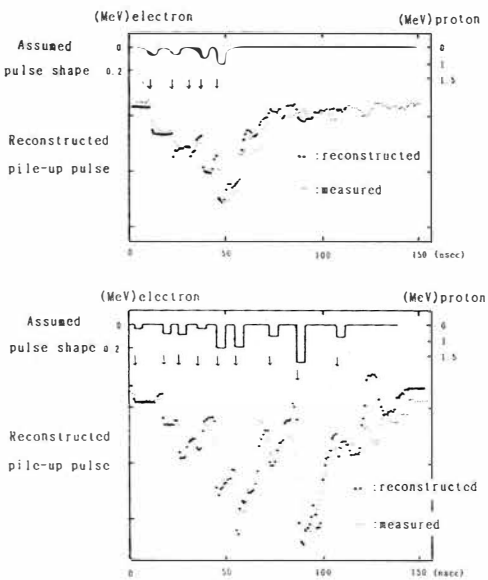

Fig.5 Presumption of the original timing structures of the bursts, and comparison of the reconstructed pile-up shape to the measured pulse shape.

Measurement of Protons and Observation of the Change of Electrolysis Parameters in the Galvanostatic Electrolysis of the 0.1M-LiOD/D_2O Solution

Shinya.MIYAMOTO, Keisuke.SUEKI, Hidekazu.IWAI, Masatoshi.FUJII, Toshiaki.SHIRAKAWA, Hiroaki. MIURA, Toshihiro.WATANABE, Hideyuki.TORIUMI, Torahiko.UEHARA, Yuki.NAKAMITSU, Masami.CHIBA, Tachishige.HIROSE, and Hiromichi.NAKAHARA
Faculty of Science,Tokyo Metropolitan University
Minami-Ohsawa, Hachioji-shi, Tokyo 1-1, JAPAN

Abstract

In order to confirm the cold fusion phenomena, measurements of protons in the galvanostatic electrolysis of the 0.1M-LiOD/D_2O solution have been carried out. The upper limit of fusion rates was deduced to be 1.35×10^{-24} fusion/d-d/sec with an assumption of the atomic ratio D/Pd of unity. No charged particles predicted by Takahashi[1] for d-d-d fusions were observed. The Li content in the electrolyte was measured by ICP-AES after the electrolysis and found to be appreciably reduced in the electrolyte; the rest being found mostly in the 0.5%-Pd alumina catalyst used for recombination of D_2 and O_2 and partly in the Pd cathode.

1.Introduction

In march 1989, M.Fleishmann et al.[2] and S.Jones et al.[3] first reported the cold fusion phenomena which they claimed proceeded through next reactions:

$$d + d \longrightarrow {}^3He\ (\ 0.82MeV\ ) + n\ (\ 2.45MeV\ ) \quad (1)$$

$$d + d \longrightarrow {}^3H\ (\ 1.01MeV\ ) + p\ (\ 3.02MeV\ ) \quad (2)$$

$$d + d \longrightarrow {}^4He + \gamma + 23.4MeV \quad (3)$$

According to the current knowledge of nuclear physics, reactions (1) and (2) occur with the similar probability. A few paper reported to measure charged particles.[4],[5] In the present work, protons were measured to confirm the cold fusion phenomena through the reaction (2). The detection of protons is generally more sensitive than that of neutrons due to the lower background and the higher detection efficiency. But, as the range of 3.02MeV protons is 30μm in palladium, the

FRONTIERS OF COLD FUSION

maximum allowed thickness of a Pd foil is only about 25μm.

2.Methods

Galvanostatic electrolysis of the 0.1M-LiOD/D_2O solution was carried out under a constant current of 200mA (100mA/cm^2) with a 25μm thick Pd foil (Nilaco co., PD343228,) as a cathode whose effective diameter was 1.6cm. (0.0604g as Pd) Six runs were performed until now. In RUNs 001-004, the back side of the Pd foil was coated with about 1.1μm thick SiO_x for prevention of leakage of deuterium. Figure shows the cell especially fabricated for the experiment. In RUN006, the whole system was thermally insulated for the measurement. A 4.5cm^2 surface barrier Si detector (SSD) (EG&G ORTEC, Model No.; BA-21-450-500, Serial No.; 30-531C) was used for detection of protons. The void space in between the Pd foil and the SSD was evacuated with a rotary pump for reducing the background level due to ^{222}Rn and also for avoiding the degradation of proton energy. The 0.5%-Pd alumina pellets (NE Chemcat co. Lot No.: 256-18130) were suspended above the electrolyte solution as a catalyst for recombination of D_2 and O_2 gas into D_2O. The current, input voltage, reference voltage, and the temperature of the electrolyte and the room were monitored. After electrolysis, Li contents in the electrolyte, in the catalyst, and in the Pd foil were measured by ICP-AES. The expected energy spectra of the p, d, ^3H ^3He, and ^4He have been calculated by the Monte Carlo method for various sites of their origin within the Pd foil.

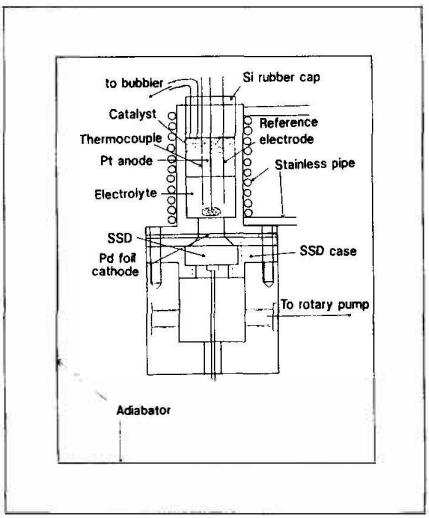

< Figure >
The cell for the experiment.

3.Results

Measurements of protons were performed three times for the $LiOD_{aq}$ (RUNs 001, 002, and 006) and once for $LiOH_{aq}$ (RUN003). No protons were observed above the background level which was 9 counts in 74.39hrs with the effective counting efficiency of 12.4%. From 3σ of the

background counts, the upper limit for the reaction (2) was deduced to $1.59X10^{-24}$ fusion/d-d/sec. No charged particles predicted by Takahashi were detected who proposed the d-d-d fusion in order to explain the T/n ratio of 10^5-10^6 reported the many investigators. Detailed conditions and results of each run are summarized in table 1 and 2.

In RUN001, the electrolyte temperature reached above 353K after 6days. But unfortunately, the input voltage and the room temperature were not measured in this run, and no definitive conclusion can be made as to the excess heat. For observing the excess heat, both input voltage and room temperature were monitored in RUN004, 005. In RUN004, a sudden increase of the input power was observed after 14days, although the electrolyte temperature decreased unsteadily. In RUN005, the space in between the Pd foil and the SSD was not evacuated and then, no such an increase of the input power and a decrease of the electrolyte temperature was observed. In RUN006,the whole electrolysis system was thermally insulated from the environment, and the cell was cooled by the forced flow of water through a stainless pipe. From the difference of the water temperature between IN and OUT, no excess heat was observed.

In RUN001 and 005, atomic ratio of D/Pd was measured. These were 0.652 and 0.705, respectively. From our previous measurement of D/Pd by weight and TPD of Pd rods, D was found to escape from the Pd rod in two stage. The percentage of D that escape quickly after the end of electrolysis is about 30% while that of the slow component is about 70%. The above cited values of about 0.7 is only the amount of the slow component, and so, the total D/Pd ratio is estimated nearly 1.0 in our

Table 1 : Detailed conditions and results of each run.

RUN	Electrolytic time(h)	Measurement of protons(cph) 1501-2400ch	701-1000ch	301-4096ch•	Fusion rate♣ (f/d-d/s)
001	165.5	0.103±0.025	1.01±0.082	31.6±0.437	$1.35X10^{-24}$
002	120	0.125±0.032	1.29±0.104	36.1±0.548	$1.64X10^{-24}$
003♥	74.39	0.121±0.040	1.01±0.117	35.6±0.692	$1.59X10^{-24}$
004♦	503	———	———	———	———
005♦	956.7	———	———	———	———
006♠	247	0.181±0.027	1.61±0.083	74.2±0.562	$2.24X10^{-24}$

♥ : 0.1M-LiOH/H_2O solution was used for electrolyte.
♦ : Protons were not measured.
♣ : For the calculation of fusion rate, D/Pd was assumed To be 1.0.
♠ : In RUN006, the background level is to be higher.
• : 2400ch = 3.02MeV

experiment.
Li contents before and after the electrolysis were measured by ICP-AES. While the volume of electrolyte solution decreased typically from 20ml to 6ml in 22days, the Li concentration reduced to less than half of its initial concentration. In RUN004, presence of a white substance was recognized on the back of the Pd foil and in the vessel of vacuum system. This white substance was found to contain Li. In all run, most of the Li lost from the electrolyte was found in the catalyst, but a small amount of Li was always found also in the Pd cathode. Therefore, it is probable that Li plating on Pd becomes possible after Pd attaining a certain amount of D in the cathode.

Table 2 : Li content in Pd cathode, Li/Pd, D/Pd

RUN	Li content in Pd cathode	Li/Pd	D/Pd
001	$7.914X10^{-6}g$	$2.00X10^{-3}$	0.652
002	$1.970X10^{-6}g$	$5.00X10^{-4}$	———
003	$1.205X10^{-6}g$	$3.07X10^{-4}$	———
004	$1.251X10^{-5}g$	$3.15X10^{-3}$	———
005	$1.293X10^{-6}g$	$3.24X10^{-4}$	0.705

4.Discussion

Measurements of protons and excess heat in the galvanostatic electrolysis in the 0.1M-LiOD/D_2O were carried out, and no protons above the background level and no excess heat were observed. A longer run is being planned for making our conclusion more solid. We found the Li content in the Pd foil increased after electrolysis. The finding may be related to the report[6] that if Pd metal contains Li, deuterium solubility increases. More careful chemical investigations have to be made before ascribing the observed anomalous phenomena to more unrealistic nuclear fusion.

5.Reference

1. A.Takahashi et al., 1991, THE SCIENCE OF COLD FUSION (PROCEEDINGS OF THE II ANNUAL CONFERENCE ON COLD FUSION, Societa Italiana di Fisica), 93
2. M.Fleischmann, S.Pons and M.J.Hawkins, 1989, J.Electroanal. Chem., 261, 301
3. S.E.Jones et al., 1989, Nature, 338, 737
4. P.B.Price et al., 1989, Phys. Rev. Lett., 63, 1926
5. J.F.Ziegler et al., 1989, Phys. Rev. Lett., 62, 2929
6. Y.Sakamoto et al., 1991, Zeitschrift für Physikalische Chemie, 173, 235

Helium Isotopes from Deuterium Absorbed in $LaNi_5$

Hiroki SAKAGUCHI and Gin-ya ADACHI*
Department of Applied Chemistry, Faculty of Engineering, Osaka University, Yamadaoka, Suita, Osaka 565, JAPAN
Keisuke NAGAO
Institute of Study of the Earth's Interior, Okayama University, Misasa, Tottori 682-02, JAPAN
*Author to whom correspondence should be addressed.

ABSTRACT

Helium isotopes(^3He and ^4He) from D_2 or H_2 gases absorbed in $LaNi_5$ were analyzed with a noble gas mass spectrometer. The reproducible increase in ^3He, corre-sponding to a fusion probability of $>8.0\times10^{-24}$ d-d·s^{-1}, was observed on the D_2-experiment, whereas ^3He was not formed by the reaction of H_2 and $LaNi_5$. ^4He production was unreliable, because the reproducibility of the result has not been obtained.

1. Introduction

Helium is a suitable candidate in order to detect the cold fusion product, because helium generated can be accumulated and condensed in a closed system even if the nuclear reaction occurs instantaneously or discontinuously.

From this point of view, we have made a thorough study of the helium isotopes from the D_2 gas absorbed in $LaNi_5$ by using a noble gas mass spectrometer[1-3] since Fleischmann and Pons[4] and Jones et al.[5] reported the occurrence of cold fusion.

It is necessary to measure not only ^3He and ^4He but also other noble gases, because the elemental abundance of these gases suggests the origin of the helium isotopes. The estimation of the increase in ^4He needs the greatest care since the amount of ^4He in the closed system is easy to be affected by the atmospheric ^4He due to the air leakage. Such a work that only ^4He has been measured is out of the question.

We present the results of the precision analysis for the helium isotopes and other noble gases in the D_2 gas

FRONTIERS OF COLD FUSION

absorbed by $LaNi_5$.

2. Experimental details

The reaction vessels(3.23×10^{-5}) sealed with a copper gasket, gas samplers and vacuum-gas connecting lines were made of stainless steel to exclude helium in air. The reaction vessels were previously degassed by heating at 1123 K for half a day in vacuo. After loading in the vessels, the $LaNi_5$ ingots(52.5 g) was heated at 1123 K for 18 h in the evacuated vessels, and then a portion of the resulting gas was collected in a sampler("Degas" in Table 1). The 99.5 % pure D_2 gas or 99.999 % pure H_2 gas were applied to the $LaNi_5$ ingots at a pressure of 7.9×10^5 Pa. Since a large amount of helium was initially contained in the raw D_2 or H_2 gas, the helium gas was removed by evacuating while the applied hydrogen gas was absorbed in the $LaNi_5$ ingot. After removing the helium gas, a part of the residual gas was collected in a sampler("Ante-reacted gas" in Table 1).The temperature fluctuation process (77⇔300 K) to the vessel containing the hydrogenated $LaNi_5$ was repeated 135 times over a period of 130.0 days (2nd run;131 times, 120.4 days), and a portion of the gas separated from the D_2 or H_2 gas was withdrawn into another sampler("Post-reacted gas" in Table 1).

A VG5400 mass spectrometer(Operating in the "static" mode) and a noble gas purification system installed at Okayama University were used for helium isotopic analyses. The detection limit of helium with this apparatus was about 10^{-20} m^3 STP(10^5 atoms). For helium isotopic analyses, the mass resolutions necessary to separate the hydrogen and deuterium peaks are 510, 400 and 100 for ^3He-HD, ^3He-H_3 and ^4He-D_2 respectively, so that the high resolution(600) collector was used for the ^3He analyses and the low resolution(200) collector was used to separate ^4He and D_2. The helium background of the system was about less than 1×10^{-16} m^3 STP(<10^9 atoms) and 1×10^{-20} m^3 STP(<10^5 atoms) for ^4He and ^3He respectively.

Nucleonic helium may be detected as an isotopic ratio different from the ratio of helium initially contained in the D_2 gas. The helium isotopic ratio, however, can be changed by air leakage and physical processes such as diffusional transport. Therefore, to determine such an effect on the helium isotopic ratio, the elemental abundance of neon, argon, krypton and xenon was measured in addition to the helium isotopic ratios in some of the sample gases.

3. Results and Discussion

Elemental abundances of helium, neon, argon, krypton and xenon, and isotopic ratios of ^3He and ^4He are listed

Table 1. Contents and isotopic ratios of He, Ne, Ar, Kr and Xe.

	^{3}He ($\times10^5$)	^{4}He ($\times10^{10}$)	^{3}He/^{4}He ($\times10^{-6}$)	^{20}Ne ($\times10^9$)	^{36}Ar ($\times10^{10}$)	^{84}Kr ($\times10^8$)	^{132}Xe ($\times10^7$)
[First run]							
D_2 Gas Experiment							
Post-reacted gas	27.6(7.53)	43.7(5.99)	6.3(1.9)	2.94(0.42)	489(69)	9.47(1.33)	25.0(3.5)
Ante-reacted gas	0.20(0.72)	2.82(0.39)	0.71(2.6)	1.34(0.20)	106(15)	3.12(0.44)	4.08(0.59)
Increment	27.4(8.3)	40.9(6.4)		1.60(0.62)	383(84)	6.35(1.77)	20.9(4.1)
H_2 Gas Experiment							
Post-reacted gas	<1	2.58(0.36)	<4	3.10(0.49)	0.734(0.104)	1.12(0.16)	0.883(0.125)
Ante-reacted gas	0.83(0.67)	0.26(0.04)	32(26)	3.77(0.55)	1.10(0.15)	3.42(0.49)	2.32(0.33)
Increment	—	2.32(0.40)		—	—	—	—
[Second run]							
D_2 Gas Experiment							
Post-reacted gas	30.8(11.2)	0.111(0.016)	2.78×10^3 (1.09×10^3)	56.1(7.8)	23.7(3.3)	29.0(4.1)	0.171(0.024)
Ante-reacted gas	5.58(1.25)	0.286(0.040)	195(52)	29.9(4.2)	7.31(1.01)	21.4(3.0)	3.17(0.45)
Increment	25.2(12.5)	—		26.2(12.0)	16.4(4.3)	7.6(7.1)	—
H_2 Gas Experiment							
Post-reacted gas	8.80(6.20)	1.46(0.21)	60(43)	0.577(0.0951)	1.71(0.24)	0.316(0.045)	0.171(0.024)
Ante-reacted gas	0.80(1.26)	0.0849(0.0119)	94(149)	1.12(0.16)	0.306(0.043)	0.964(0.137)	0.571(0.086)
Increment	8.00(7.46)	1.37(0.22)		—	1.40(0.29)	—	—
Degas(at 1123 K)	2(2)	14.6(2.5)	14(14)	47.7(8.2)	26.2(4.5)	26.6(4.6)	22.6(3.9)
Air			1.399(0.013)				

· The noble gas contents are given in number of atoms existing in the reaction vessel.
· The standard deviations are shown in brackets.

in Table 1. We assumed that the nuclear reaction occurs at the surface or near surface of $LaNi_5$ and that the generated helium is released from $LaNi_5$ with hydrogen. On the experiment using the D_2 gas, it is noteworthy that the amount of ^{3}He(2.74(0.83)x10^6 atoms) increased in the gas obtained after the repeated temperature cycling, while no enrichment of ^{3}He was observed for the H_2-experiment. The phenomenon was reproduced in the second run. The increase in ^{4}He(4.09(0.64)x10^{11} atoms) was also observed in the first run. The ^{4}He production, however, was unreliable, because the reproducibility of the phenomenon was not obtained in the second run.

The enhancement of ^{3}He as well as ^{4}He may be caused by only the air leakage. If we assume that the increment of ^{4}He originated from the atmosphere, then it should be accompanied by 5.72(0.90)x10^5 atoms of ^{3}He which is derived by using the atmospheric ratio of 1.399x10^{-6}. Thus, the excess of ^{3}He is 2.17(0.92)x10^6 atoms. Assuming that the ~2.2x10^6 atoms ^{3}He generated by the D_2 gas(2.5x 10^{22} molecules) absorbed in $LaNi_5$ during a period of the temperature fluctuation process for 1.1x10^7 s, we obtained a lower limit of ~8.0x10^{-24} fusion/d-d·s^{-1} based on the reaction d + d → ^{3}He + n. The fusion probability is comparable to that given by Jones et al.[5] and Menlove.[6]

Figure 1 shows the noble gas elemental abundance relative to that in air, expressing the following equation,

$$F(m) = ({}^mX/{}^{36}Ar)/({}^mX/{}^{36}Ar)_{atmosphere},$$

where ^mX is the noble gas element with mass m and the subscript "atmosphere" means the atmospheric elemental

abundance.

The elemental abundance patterns provide significant information regarding the isotopic anomaly of helium observed in this work, such as the air leakage and the diffusional transport. If the leakage of air into the vessel occurred during the temperature fluctuation process, the abundance pattern of the post-reacted gas would be close to that of air(logF(m)=0). The increase in ^{3}He was not significantly affected by the air contamination, because the abundance patterns for both ante- and post-reacted gases resembled each other, and were much different from those for air. The possibility of the diffusional transport was also denied due to the coincidence of the two patterns of the ante- and post-reacted gases.

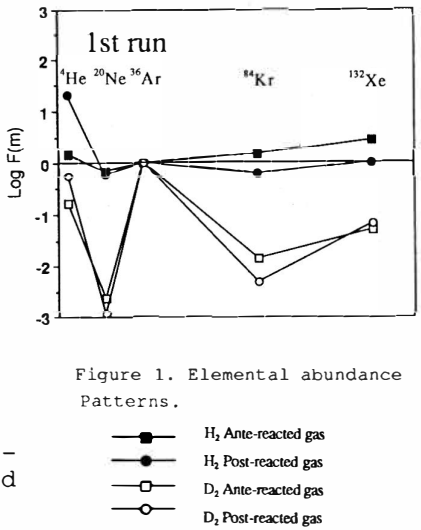

Figure 1. Elemental abundance Patterns.

4. Conclusions

The enrichment of ^{3}He was observed in the D_2 gas absorbed by $LaNi_5$ after the repeated temperature fluctuation cycling. The phenomenon, however, was not obtained from the H_2-experiment. The elemental abundance patterns indicate that the increase of ^{3}He was not obviously caused by the air leakage. The fusion probability estimated by the ^{3}He production was $>8.0\times10^{-24}$ fusion/d-d$\cdot$s^{-1} which is in agreement with the value determined by Jones et al. or Menlove.

References

1. Sakaguchi, H., Nagao, K. and Adachi, G., *Proc. Topical Meet. on Cold Fusion*, Osaka, February 27-28,(1990) p.71.
2. *Sankei Shinbun*, Sangyo Keizai Shinbun, Osaka, 17077, March 8, (1990).
3. Adachi, G., Sakaguchi, H. and Nagao, N., 1992, *J. Alloys & Compd.* **181**, 469.
4. Fleischmann, M. and Pons, S., 1989, *J. Electroanal. Chem.* **261**, 301.
5. Jones, S. E. et al., 1989, *Nature*, **338**, 737.
6. Menlove, H. O., *Workshop on Cold Fusion Phenomena, Santa Fe, NM, Meeting Abstracts LA-UR-89-1974*, (1989).

The Detection of 4He in Ti-Cathode on Cold Fusion

Q. F. Zhang Q. Q. Gou Z. H. Zhu B. L. Xio J. M. Lou F. S. Liu J. X. S.
(The Institute of Atomic and Molecular Science at High-Temperature and High-Pressure, Chengdu Univesity of Science and Technology, Chengdu, 610065, China)
Y. G. Ning H. Xie Z. G. Wang
(Center of Electronic Materials Microanalysis, University of Electronic Science and Technology of China, Chengdu, 610054, China)

Abstract

The Ti- cathode has beeen examined after electrolysis with remarkable phenomenon of "excess heat" by SIMS. The special mass peak of 4 amu in SIMS spectra of Ti-cathode has been detected by a series of experiments. It' s concluded that the mass peak of 4 amu is the mass peak of ^{4}He in Ti-Cathode produced in cold fusion.

To avoid interference of D_2 and H_2D with ^{4}He in SIMS spectra, the negative SIMS spectra are used in the detection of ^{4}He.

I Experimental Condition

The detection of ^{4}He produceed on cold fusion is an important step to determine if a theoretical model or an experimental method on cold fusion is feasible. We designed three experiments to determin the exist of ^{4}He in Ti-cathode after electrolysis. No matter whether the cold fusion occures, H and D which may exist in the forms of D_2 and H_2D may be absorbed in the Ti-cathode. Prof. Ning has found that the negative SIMS method can avoid the interference of D_2 and H_2D with ^{4}He in SIMS spectra. Therefore, the negative SIMS method was applied to detect the presence of ^{4}He in Ti-cathode.

The analysis of ^{4}He has been made on the VG Microlab MK Ⅱ surface analysis instrument with Ga ion gun.

Beam current is 30nA, beam voltage is 10KV.

Target bias voltage is 5. 5V.

Pole bias voltage is 7. 9V.

Base vaccum is 2×10^{-9} mbar.

Flood oxygen gas on sample in analysing process to increase positive ion yields and stabilize the negative ion yields.

Ga^+ ion source is used to raise negative ion yields.

The peaks of D_2 and H_2D will overlap the peak of ^{4}He in produst of cold fusion. We have found that the negative SIMS method can avoid the interference of D_2 and H_2D with ^{4}He in SIMS spectra. Therefore, the negative SIMS method was applied to detect the existence of ^{4}He in Ti-cathode.

FRONTIERS OF COLD FUSION

Ⅱ Experimental method and it's results

1. We examined the Ti-cathode which has undergone electrolysis with remarkable phenomenon of "excess heat" .[2] In the electrolytical experiment, the Ti-rod-cathode was half immersed in the heavy water and the other half above the surface of heavy water. Along the rod, samples a, b, c, d are taken from the segment immersed in and samples a′ , b′ , c′ , d′ are taken from the segment above the surface of it. (Figure 1.)

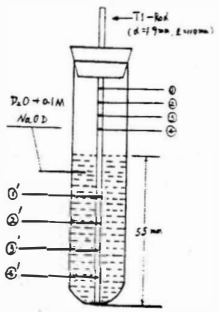

Figure 1. The distribution of Samples taken

Fig 2 (a) and Fig 2 (b) are the negative SIMS mass spectra of samples a, b, c, d and a′ , b′ , c′ , d′ respectively. Comparing these spectra with each other, we found that the peak of D^- (2amu) exist both in Fig 2 (a) and Fig 2 (b), but the peak of 4 amu only exists in spectro of Fig 2(b). It shows that the helium exist exactly in Ti-cathode after producing "excess heat" .

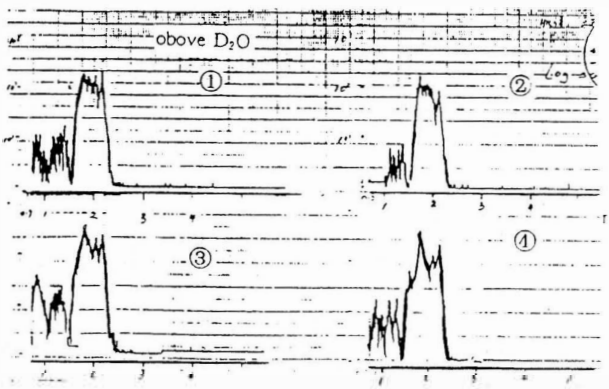

Figure 2 (a) The SIMS Spectra of Ti-rod above D_2O

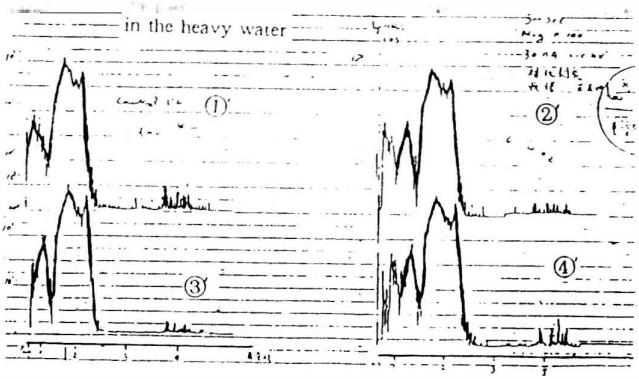

Figure. 2 (b) The SIMS spectra of Ti-rod immersed in D_2o

2. As a comparative experiment, we examine the other Ti-cathode which has undergone electrolysis for fifteen days without any phenomenon of "excess heat" and the electrolyty contained more water (H_2O). The sample (E) is taken from the segment of Ti-rod above the heavy water along the Ti-rod and sample (F) is taken from the segment immersed. The results of negative SIMS detection are shown is Fig 3 (a) and Fig 3 (b).

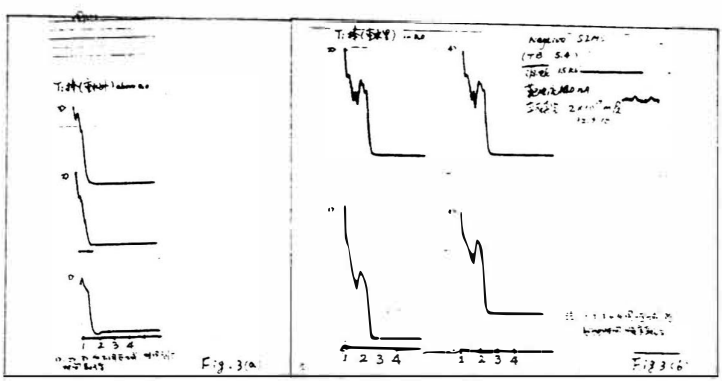

1, 2, 3 are the same deepth and different area

Figure 3(a). The SIMS Spectra of Ti-rod immersed in (D_2O+H_2O).

1, 2, 3, 4 are the same area and different deepth
1. is the minimum deepth
4. in the maximum deepth

Figure 3(b). The SIMS Spectoa of Ti-rod immersed in (D_2O+H_2O).

Fig 3 (a) shows that the hydrogen peak is the only peak, because the capability of hydrogen to be adsorbed by titanium rod is much greater than that of deuterium.

Fig 3 (b) shows that the amount of deuterium in the surface is less than that in the deeper layer, but the deuterium never form the peak of 4amu in the Ti-rod after electrolysis.

3. A clear Ti-rod is placed in a vaccum chamber and heated to give off gas at 600℃. In this process, the vaccum is kept to 2×10^{-5}mbar. While the Ti-rod turns cold, let high purity He gas into the champer. After then, the rod has been placed in He gas for 4 hours. Sample G is taken from it.

After the sample G was detected by negative SIMS, no any hydrogen deuterium and helium peaks can be foumd in the negative SIMS spectra.

Ⅲ Discussion

1. The peak of negative SIMS of helium only exist in titanium rod after "excess heat" experiment as Fig 2 (b) shows. It shows that the helium is formed in the titanium crystal latlice after producing $D+D\rightarrow{}^4He^*\rightarrow{}^4He+Q$.

2. Fig 2 (a) and Fig 2 (b) show that neither Two hydrogen atoms in the crystal lattice of Ti-cathode can form 2 amu peak, nor two deutarium cam form 4 amu peak. under the detection of negative SIMS.

3. Fig 3 (a) and Fig 3 (b) show that if there are no "excess heat", the helium may not be produced in crystal lattice of Ti-rod after electrolysis.

4. From test result of sample G, We found that the helium ion or atom can not enter the crystal lattice of titanium by means of Van der Wadls force. Therefore, if He exist in crystal lattice of titaium, it must be formed by means of: $D+D\rightarrow{}^4He+Q$ process.

Ⅳ Conclusions

Our experiments show:

1. The "excess heat" phenomenon is related to the helium products, so the process of $^2D+{}^2D\rightarrow{}^4He+23.8Mev$ may exist in the cold fusion.

2. The method of negative SIMS is feasible for detecting He in the Ti-rod after "excess heat". And the detailed research report of SIMS technigue will be published later.

3. The further study in this field is underway.

Reference

[1] M. Fleischmann, S. Pons, (1989) J. Electroanal Chem. 261 301—308

[2] Q. Q. Gou, Z. H. Zhu, Q. F. Zhang, (1990) 《Chinese Journal of Atomic and Molecular Physics》 7. 3 1491—1495

Real Time Measurements of the Energetic Charged Particles and the Loading Ratio (D/Pd)*

Da-Wei Mo, Li Zhang, Bo-Xian Chen, Yi-S Liu,
Shi-Yuan Doing, Ming-Yan Yao, Li-Y Zhou,
Hong-Guo Huang, Xing-Zhong Li, Xian-Da Shen,
Shi-Cheng Wang, Tie-Sun Kang, Nai-Zhang Huang.
Tsinghua University, Beijing 100084, CHINA

ABSTRACT

A loading D_2 gas system was built, which can measure the gas pressure, the temperature, the loading ratio, the charged particles and burst, in real time. the charged particles and burst was searched and the reproduece condition was fond preliminary.

1. Introduction

Since ICCF II, we have continued on measuring the energetic charged particles emitted from the deuterized palladium wire in a high pressure vessel. Measurement of charged particles possess distinctive advantages.[1]The experimental arrangement has been developed into a real time measurement system, which can measure the temperature of vessel, the pressure of D_2 gas in vessel, the loading ratio (D/Pd), charged particles number and energy, and charged particles burst, continuously. (Fig.1). This development allows us to identify the charged products and the condition under which they are emitted.

2. Loading Ratio (D/Pd)

There are three methods to check the loading ratio, i.e. the electric resistance method, the volume-pressure method, and weight method in real-time measurement resistance method is the most convenient one.

Fig2 [2] shows the relationship between H_2 and D_2 content-loading ratio and relative resistance.

Fig 3 [2] shows the isothermal curves of Pd-H system, table 1 lists our experiment results.

---

* This work is supported by state commission of science and technology, natural science foundation of China and Tsinghua University.

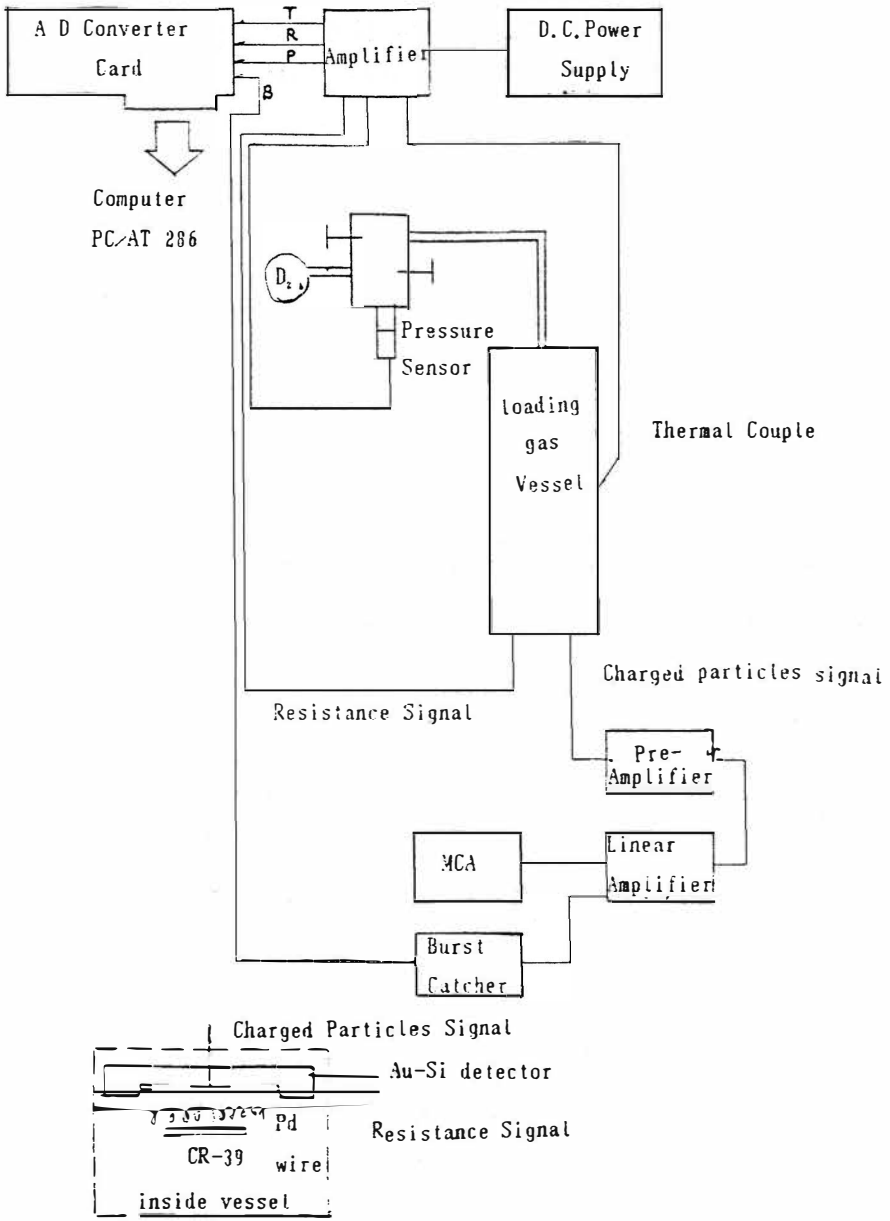

Fig 1. Experimental arrangement

Table 1. Loading Ratio Experiment Results

No.	Surface Treatment	Storing Time	Ro(Ω)	Gas	Pressure (atm)	H/Pd	Loading Time hr.
1	Y	half year	8.15	H	9	0.74	16
2	N		21.47	H	6	0.85	75
3	Y	two days	20.96	H	20	0.89	<4.5
4	Y	five days	16.0	H	16	0.88	6
5	Y	fifteen days	9.2	D	19	0.74	7.5

Sample No.3 was weighted and compared with electric resistance. The results are listed in table 2.

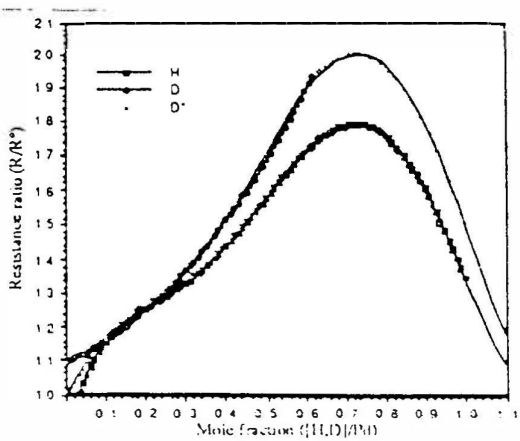

Fig 2. Ralationship between ralative resistance and H_2, D_2 loading ratio

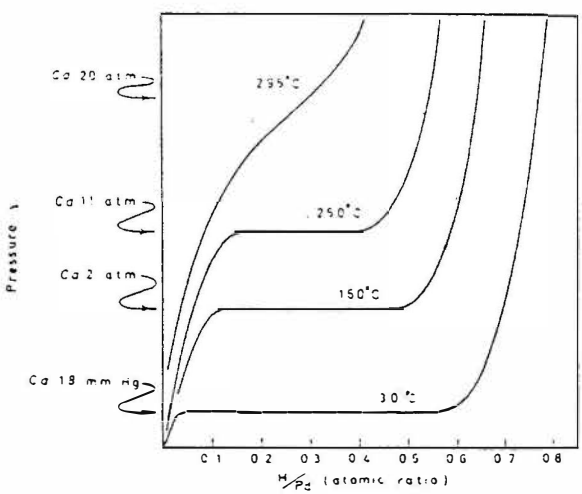

Fig 3. D/Pd system isothermal curves

Table 2 The Loading Ratio Results of Weight Method

Before loading		After loading		Ratios	
Mass (mg)	Electric Resistanc Ro (Ω)	Mass (mg)	Electric Resistance R (Ω)	H/Pd	R/Ro
139.01	20.96	140.17	33.6	0.89	1.6

This result means that the loading ratio has acrossed the peak of Fig2 curve and the result is coincident with electric resistance method. So it can be used to measure the loading ratio in real time.

The No.5 result tells us that the loading ratio 0.74 is obtained.

All of the experiment results is achievable the peak of the loading ratio curve.

3. Experimental results

In gas loading experiment, the emission of charged particles or neutron is connected to thermodynamic transformation taking place (in particular phase transformations), while the temperature of sample, the pressure of gas and related parameter are changing. [4]

Temperature is an important parameter at our previous work [3], temperature was changed from 77° K to 300° K. The results are positive. At this work temperature is changed only from 0° to 25℃ based on Takahashi's experiments (~20℃) and the transform point of Pd-D system (~19℃). The charged particles bursts are observed at about 20℃, when vessel was vacuumed.

Table 3 Shows the results

Table 3 The experimental Results

No	T° K	P	R/Ro	Count of Bursts	Time duration min
1	287.1	tore	1.86	400	10
2	285.7	Vacuum	1.89	400	36
3	289.1		1.88	4200	120

4. Acknowledgements

This work is supported by state commission of science and technology, natural science foundation of China and Tsinghua University.

References

[1] Da-Wei Mo, The Proceedings of the II Annual Conference on Cold Fusion (Como-Italy, 1991) P. 123-127

[2] F. A. Lewis, Palladium/Hydrogen System Academic Press Inc (Loudon) Ltd., 4.

[3] M. C. H. Mckubre , etal. The proceedings of the I Annual Conference on Cold Fusion (SLC USA 1990) P.21

[4] F. Scaramuzzi, The Proceedings of The II Annual Conference Cold Fusion (Como-Italy, 1991) P. 445-452.

Detection of Radioactive Emissions in the Electrolytic Deuteriding-Dedeuteriding Reactions of Pd and Ti

H. UCHIDA, Y. HAMADA, Y. MATSUMURA and T. HAYASHI
Department of Applied Physics, Tokai University, Hiratsuka, Kanagawa 259-12, JAPAN. FAX Japan-463-58-1812

ABSTRACT

This report demonstrates the occurrence of radioactive emissions detected by GM(Geiger-Mueller)counter in the electrolytic deuteriding-dedeuteriding reactions of Pd and Ti. For the Pd samples annealed or cold worked, the excess counts higher than BG(back ground levels=32 ±2 cpm) by factors 1.5 to 2 in average were measured almost continuously and reproducibly during the pules modulated electrolysis over 600 mA/cm². The excess counts were measured for a while even after electrolysis. For the Ti samples annealed or cold worked, the burst-like GM counts over 200 cpm were often measured at low current densities below 10 mA/cm². The much higher burst-like GM counts over 1500 cpm were measured after electrolysis.

1. Introduction

In previous investigations[1-3], we reported that the pulse modulated deuteriding-dedeuteriding reactions of Pd in a KOD cell exhibit distinct excess GM counts and that the cold working of Pd sample is effective to yield higher GM counts. The reactions of Pd deuteride formation-decomposition at the Pd surface seem to be crucial for the radioactive emissions. This work dealt with the similar measurement using Ti which forms more stable deuteride than Pd[4] and the results for Pd and Ti are compared and discussed.

2. Experimental Process[1]

The schematic arrangement of the cell, GM counter(ALOKA Basic Scaler TDC-105), NaI scintillation counter(CANBERRA series 20) and pulse generator used are shown in Fig. 1. BG fluctuations were monitored at real time before, during and after electrolysis using two additional GM counters set at at distances of 6 m(BG. 1) and 45 m(BG. 2) from the cell, respectively as shown in Fig. 2. Electric noises as well as the fluctuations of the GM counters used were strictly checked by switch-on and off of equipments in the laboratory

FRONTIERS OF COLD FUSION

building over one week before each experiment. Wire samples(1mmx1mmx50mm) of Pd and Ti and a Pt plate were used for electrolysis in 0.5 N-KOH or KOD solutions. The purity of D_2O used was 99.8-99.9%.

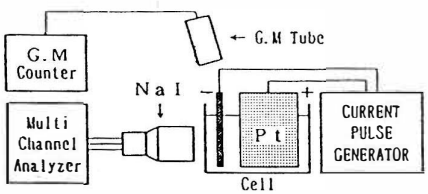

Fig.1 Schematic arrangement of the electrolysis.

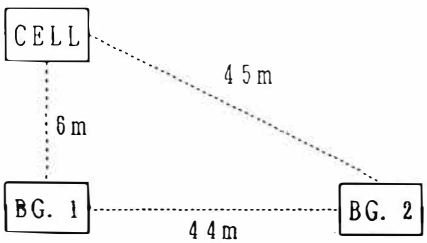

Fig.2 BG measurements at different sites:BG.1 and BG.2.

3. Results

The measured GM counts of BG at the cell are shown in Fig.3 as deflectionin %, $\Delta 1$ from BG.1 and $\Delta 2$ from BG.2 in Fig.3. Each point of deflection displayed was calculated from 10 min average counts. The GM counts at the cell exhibit around 20% steday deflections compared with BG.1 and BG.2. Fig.4 shows an example of the GM counts measured for a Pd sample

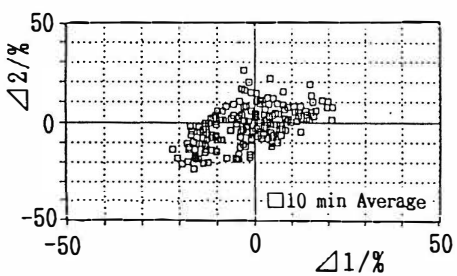

Fig.3 Fluctuation of BG at the cell in comparison with BG.1 and BG.2.

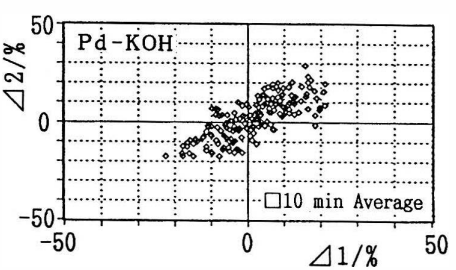

Fig.4 Deflections from BG.1 and BG.2 in pulse modulated hydriding-dehydridings of Pd cold worked 49.4 % in 0.5 N-KOH at 5 A/ cm^2

deformed by 49.4% in a pulse modulated electrolysis at 5000 mA/ cm^2 in a 0.1 N-KOH cell. The measured deflections exhibit an almost identical distribution with BG fluctuations in Fig.3, indicating no occurrence of meaningful phenomenon in the electrolysis of Pd in KOH. However, Fig.5 and Fig.6 show the deflections of GM counts at the cell in pulse modulated electrolysis of two different Pd samples deformed by 49.4% at 4000 mA/cm^2 and 600 mA/cm^2 in KOD cells, respectively. Much higher deflections than BG fluctuations can be seen in the first quadrant, meaning that these pulse modulated reactions yield distinct excess GM counts at the cell in 40-50% positive deflections. The distinct excess counts could be measured in 20-30 min after the initiation of

electrolysis and continued for a while after electrolysis.

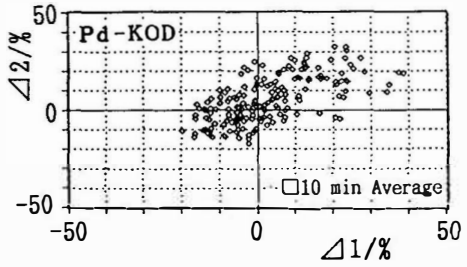

Fig.5 Excess GM counts as positive deflections in pulse modulated deuteriding-dedeuteridings of Pd cold worked by 49.4 % in 0.5 N-KOD at 4 A/ cm².

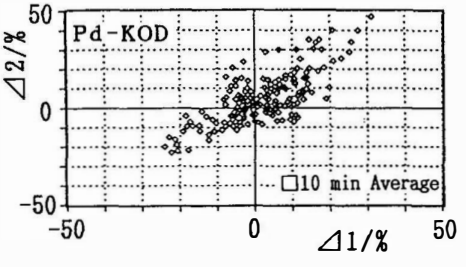

Fig.6 Excess GM counts as positive deflections in pulse modulated deuteriding-dedeuteridings of Pd cold worked by 49.4 % in 0.5 N-KOD at 0.6 A/cm².

The excess GM counts during and after electrolysis of Ti in KOD solution were much higher than those observed with Pd. Therefore, the measured GM counts for Ti are presented in cpm as a function of time t in Fig. 7 and Fig. 8.

Fig. 7 shows burst-like GM counts up to about 300 cpm for a Ti sample cold worked by 32.5% at t=100 to 130 min in an electrolysis at 6.0 mA/cm². Similar burst-like emissions took place also at t=500-540 min after electrolysis after the current had been cut off at t=400 min. At t=200 to 400 min, a pulse modulated current was applied at 0-4600 mA/cm², however, no excess GM count was measured. Fig. 8 shows much higher bursts in GM counts over 200 cpm for a Ti sample deformed by 7.1% at t=20-30 min in an electrolysis at 5 mA/cm² and also burst-like GM counts over 1500 cpm at t=450-460 min after electrolysis. Such burst-like emissions were measured three times in or after electrolysis using seven different Ti samples.

4. Discussion

The average compositions of Ti deuterides were $TiD_{0.6-0.8}$ for Fig. 7 and $TiD_{0.1}$ for Fig. 8 during electrolysis. However, the optical observations on the samples showed that only the surface regions down to a few μm were mainly deuterided, meaning the formations of deuterides with much higher D concentrations at the surface than the calculated average concentrations. Judging from thermodynamic properties of Ti hydrides[4], γ-TiD_2 phase may be formed in the electrolysis at the surface. The burst-like emissions observed seem to be related to the formation and decomposition of the di-deuteride phase in and after electrolysis, respectively, and which is similar to the excess emissions of the Pd-D system by a pulse modulated electrolysis[1-3]. The observations for Pd and Ti imply the occurrence of radioactive emissions like γ- or X-rays detectable by GM counters.

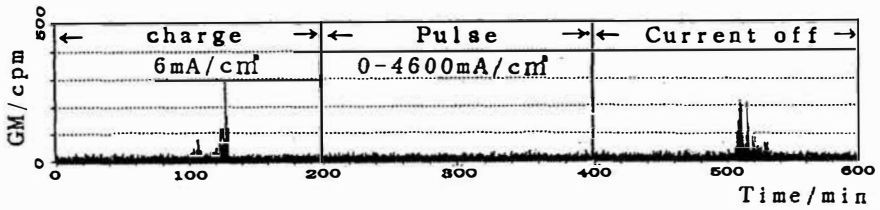

Fig.7 Burst-like GM counts in deuteriding of Ti cold worked by 32.5 % at 6 mA/cm² and in curret-off state after electrolysis.

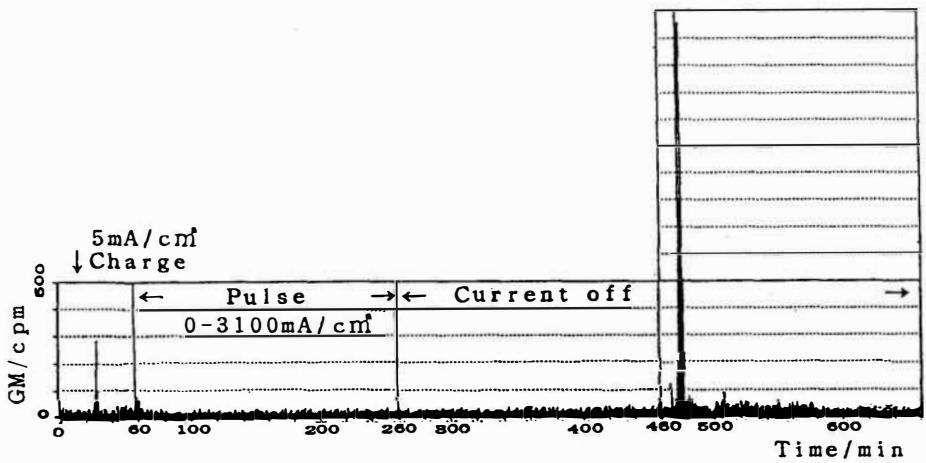

Fig.8 Burst-like GM counts in deuteriding of Ti cold worked by 7.1 % at 5 mA/cm² and in curret-off state after electrolysis.

Acknowledgement

The authors are grateful to Prof.K.Takayama, Prof.Y.Yoneda and Prof. T.Hirayama, Tokai University for their kind support to this work. For kind supply of heavy water to this work, the authors are thankful to Showa Denko Co.

5. References

1. Uchida, H. et al., Proc. 40th Int. Soc. Electrochem. Meeting, Sep. 1989, Kyoto Rept. No. 22-01-13-G.
2. Uchida, H. et al., J. Less-Common Met., 172-174(1991)A40.
3. Uchida, H. et al, Proc. Int. Symp. Metal-Hydrogen Systems, Uppsala, Jun. 1992, PII-38.
4. E. Fromm and E. Gebhardt, Gase und Kohlenstoff in Metallen, Springer Verlag, Berlin 1976, p. 408.

The Sensitizing Phenomenon of X-Ray Film in the Experiment of Metals Loaded with Deuterium

Chen Suhe, Wang Dalun, Chen Wenjang
Li Yijun, Fu Yibei and Zhang Xinwei

Southwest Institute of Nuclear Physics and
Chemistry P.O. Box 525-74, Chengdu, P.R. China

ABSTRACT

The sensitizing phenomenon of X-ray film was studied, in metals loaded with deuterium, by a cycle method of temperature and pressure (CMTP). The experimental results showed that the sensitization of X-ray film was derived from the chemical reaction and the anomalous effect of metals loaded with deuterium.

1. INTRODUCTION

When Italian A. De. Ninno et al. studied the anomalous phenomenon in metals loaded with deuterium using CMTP, neutrons were detected[1]. When X. Zh. Li et al, from Tsinghua Univ, studied the precursor of the "cold fusion" phenomenon using CMTP, it was fornd that X-ray films were sensitized [2]. To clarify the sensitizing reason of X-ray films, we studied the sensitization phenomenon of X-ray films using CMTP of metals loaded with deuterium. The experimental results show that the sensitizing reasons of X-ray film are derived from the chemical reaction and the anomalous effect of metals loaded with deuterium. Recently R.K. Rout et al. From Bhabha Atomic Research Centra, India, systematically studied the sensitization phenomenon of X-ray films. They considered that low energy electrons emitted in metals loaded with deuterium lead to the sensitization of films[3].

2. EXPERIMENT

2.1 Experimental Process

Cu and Fe slices were used as contrasting metal to perform blank

runs on the sensitization of X-ray film. Pd and Ti slices loaded with deuterium were used to perform the experiment on the sensitizing effect. Three kinds of metals loaded with deuterium were used: (1) Pd slice (purity 99.6%) 0.5mm in thickness; (2) Ti slice 0.1mm in thickness; (3) Pd slice on whose two surface 0.5-μm-thick Ti was evaporated.

Metal slices treated and X-ray films were combined, and then sealed into a copper vessel whose vacuum was at about 10^{-4} torr. Under the condition of the temperature of liquid nitrogen (LN_2), the copper vessel was filled with deuterium gas and the cycle of temperature and pressure (CTP) was done.

2.2 Blank Runs

(1) Air was substituted for deuterium gas. Then CTP was performed. The sensitization of films was not found.

(2) Cu and Fe slices were put between films and the cycle of temperature and pressure was done. It was found that films were sensitized in full area.

(3) Two sets of films were used. One was sealed into a small copper vessel (2mm in thickness, filled with air). The other was put between Cu slices 2mm in thickness and wrapped in Al foil 50 μm in thickness (aerated but opaque). The cycle of temperature and pressure was done. The experimental reaults showed that the first set of films didn't sensitize but the second did, this excluded the possibility that high energy X-rays sensitized films which were produced by bremsstrahlung of high energy γ-rays, X-rays or electrons.

(4) Hydrogen gas was substituted for deuterium gas and then Cu slice was used to perform the experiment as described above. It was found that films also sensitized.

To clarify the reasons of film sensitization in blank run, the checking experiments were done and described below.

2.3 Checking Experiments

Considering the reasons of film sensitization mentioned above, we used only films to perform the checking experiments instead of Cu and Fe slices.

(a) Two sets of films were put into a copper vessel. One was sealed in a black paper bag which was 0.3mm in thickness (opaque, but aerated). The other was put between polyethylene foils 50μm in thickness and wrapped in Al foil 50μm in thickness (opaque, but aerated). When vacuum reached 10^{-4}-5×10^{-5}torr in the copper vessel, oxygen in the copper vessel was excluded by using 6 atm argon was over three times. When vacuum reached 10^{-4}-5×10^{-5} torr in the copper vessel again, deuterium gas was let in and the cycle of temperature and pressure was done. It was found that all the films were sensitized in full area. This excluded the possibility that the combination of deuterium and oxygen sensitized films, which was explained as follows. (i) With vacuum 10^{-4}-5×10^{-5} torr and by the treatment of excluding oxygen by argon gas, quantity of oxygen in gas deuterium was very small. Hence few atoms of deuterium and

oxygen could combine. (ii) The combination of deuterium and oxygen produced on the wall of the tube could emit visible and invisible lights (ultraviolet ray). The lights were shut out by a 50 μm-thick polyethylene foil added to a 50 μm-thick Al foil and 0.3mm- thick black paper. If the combination of deuterium and oxygen took place in aluminium oxide, emitted radiation should be shut out by the 50 μm-thick polyethylene foil.

(b) There were two sets of films. One was put in a copper box 3mm in thickness (opaque, but aerated). The other was put between polytetrafluoroethylene 5mm in thickness and wrapped in an Al foil 50 μm in thickness (opaque, but aerated). After vacuum was obtained in the copper vessel, it was filled with deuterium gas and the cycle of temperature and pressure was done. It was found that all of the films were sensitized in full area. This excluded the possibility that electrons, X-rays and so on which were emitted owing to Cu absorbing deuterium resulted in the sensitization of films.

By blank run and checking experiment mentioned above, it was excluded that the combination of deuterium and oxygen, and radiation derived from copper and iron absorbing deuterium resulted in the sensitization of films. By the comparion with the experimental conditions of sensitizing and no sensitizing in blank run and checking experiment, it was shown that the reason of film sensitization was that the combiantion of deuterium and Br in film formed DBr and Ag ion was displaced out.

The repeatability of the experiments mentioned above is 100%.

2.4 Experiment of Sensitizing Effect in Metal Loaded with Deuterium

Ti slices and two kinds of Pd slices loaded with deuterium were used to perform the experiment by the cycle of temperature and pressure. One kind of Pd slice was 0.5mm in thickness and the other was the one plated 0.5 μm Ti on two surfaces. The combination of films and metal loaded with deuterium is shown in Fig. 1.

Experimental results were shown as figures:

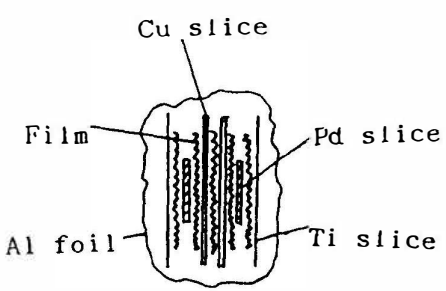

Fig. 1. Combination of X-ray films and the metal slices

Fig. 2. An image of Pd slice

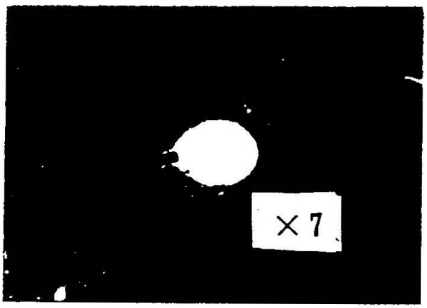

Fig. 3. A sensitized point on a film

Fig. 4. An image of Pd tube

3. DISCUSSIONS

(1) There was an image of Pd slice in full background of sensetized films which were combined with Pd slices. The fac shows that two reasons result in the sensitization of films. One is the chemical reaction. The other is the oneself effect of PaD metal. The even sensitization in full area of films indicates that Br in films chemically react with deuterium. An image of Pd slice in full background of sensitized films indicates that the sensitization is derived from the anomalous effect in Pd slice.

We consider that some effevts in PdD metal may make films sensitize as listed below:

(a) Extraheat and burst heat in PdD metal.

(b) Electron emission in PdD metal.

(c) Br in films reacting with highly active deuterium which was releasted by PdD metal.

(d) Charged particles emitted by PdD metal, electrons and characteristic X-rays imitated by the charged particles.

The sensitizing effect of films in PdD metal will be studied further.

(2) There was a track on the outer membrane of a film, which was formed after Pd slice was peeled off. The track may be a result that Pd slice produced extraheating phenomenon.

(3) There were sensitized points on some films. Do the points indicate whether burst heat was released out in a micro-zone of PdD or lots of deuterium was suddenly released in a micro-zone of PdD?

We consider that the sensitizing effect of films made by PdD metal reflects the anomalous phenomenon in PdD metal. Studying the phenomenon is helpful to understand cold fusion further.

REFERENCES

1. A De Ninno et al. Europhys lett. 9 (1989) 221
2. Li Xingzhong et al. The precursor of cold fusion phenomenon in deuterium/solid system TUFP-90/28
3. R K Rout et al. To be published in Indian Journal of Technology

Phenomenon of Low Energy Emissions from Hydrogen/Deuterium Loaded Palladium

R K Rout, A Shyam, M Srinivasan and A B Garg

Neutron Physics Division
Bhabha Atomic Research Centre
Trombay, Bombay 400 085, INDIA

ABSTRACT

Palladium loaded with either hydrogen or deuterium is found to give a clear autoradiograph on exposure to X–ray film. The phenomena is found to be 100% reproducible and is independent of the technique of loading, be it electrolytic, gas loading, plasma discharge or ion implantation. It appears only if the exposure to X–ray film is done in atmosphere of hydrogen, oxygen or air. These emissions are also detected by TLD measurements. Investigations seeking to identify the nature/energy of the radiation through transmission measurements using various filters tentatively indicate that the radiations could be low energy electrons having an energy of around 300 to 400 ev.

1. Introduction

The occurrence of anomalous emissions from certain metals (such as palladium and titanium), when loaded with deuterium, either electrolytically (Jones 1989) or in gas phase (De Ninno 1989) or in plasma phase (Rout 1991), has been reported by various laboratories. Most of these emissions have been found to be sporadic and are not easily reproducible. We report here emission of some low energy radiations emanating from palladium when loaded either with deuterium or hydrogen, by any loading technique. The phenomenon is reproducible and the low energy radiations have been observed from all the samples loaded so far.

2. Experimental Methods & Results

2.1 Loading of Gas

Majority of the samples used were in the shape of disks, 16 mm diameter and 2 mm thick. These were loaded by affixing them on a plasma focus (PF) (Mather 1971) central electrode or by first degassing in vacuum (600 ^{o}C, 10^{-5} mb) and then allowing them to cool in the D_2 or H_2 atmosphere (at 1 bar pressure, for 2 hours). A few Pd samples (in form of needles) were loaded using the Wada gas discharge technique (Wada 1989). The bulk loading obtained

FRONTIERS OF COLD FUSION

varied between 0.1 and 0.6. It is possible that the loading in the surface layer may be much higher. The H_2 and D_2 gases used for loading had tritium content of $\simeq 10^{-4}$ Bq/ml and $< 10^{-5}$ Bq/ml respectively.

2.2 Measurement of radioactive emissions

The radiations emitted from the samples were predominantly of very soft nature and of comparatively low intensity (as will be evident from subsequent sections). They were short lived (maximum life of a few days).

Autoradiography was the most extensively used diagnostics. For autoradiography the X–ray films were kept in contact or a few mm away from the sample. The exposure time varied from 24 to 120 hours. Fig. 1 shows a contact autoradiograph of a disk loaded with D_2 using a PF device (30 discharge shots, 24 hours exposure). Fig. 2 is an autoradiograph of a similar H_2 loaded sample (30 discharge shots, 90 hours exposure) kept 0.2 mm away from the film. In all the autoradiographs obtained (under any condition), the fogging was always observed only on the side of the film facing the samples, in spite of the fact that the X–ray film is transparent to optical radiation and had sensitive coating on both sides. This confirms the low range of the radiations and absence of optical emissions.

No fogging above threshold could be observed on the autoradiographs when the PdH_x samples were kept in vacuum ($<10^{-2}$ mbar). Some samples were also kept in atmospheres of nitrogen, helium and argon gases. The gas pressure was retained slightly ($\simeq$ 50 mbar) above one atmosphere. The exposure time in all the cases was 96 h. No radiation, above threshold, was observed on any of these autoradiographs.

By means of a sensitive densitometer, it was possible to measure density of even very faint autoradiographs. Some samples were also autoradiographed in an atmosphere of hydrogen ($\simeq$ 50 mbar pressure) for 96 h, the fogging obtained on the autoradiographs was just discernible over threshold (see Table 1). PdH_x samples kept in oxygen atmosphere (pressure $\simeq$ 50 mbar) above atmosphere, for 96 h, fogged the autoradiographs to an average density which was 40 to 60 % less than what was obtained with control samples in air (see Table 1). Fogging was also detected when thin filters (2 μm aluminised polycarbonate foil (0.25 mg/cm^2) in one or several layers) were kept between the film and loaded samples. Weak fogging was always measured with one layer of such a filter (see Table 1). With two layer of filters fogging was observed only in one instance (barely above threshold). No fogging was ever observed, above threshold, with three or more layers of filters.

The autoradiography and TLD ($CaSO_4$ based) measurements were made with and without glass and fused silica filters. Activity observed without filter in case of TLD study was seven times above background. No radiation was observed to cross glass or fused silica, indicating the absence (or very low intensity) of optical, ultraviolet or infrared radiators. These results were confirmed by photomultiplier and photodiode study.

The emissions were also subjected to electric field. The electric field between the loaded sample (disk type) and the film was maintained by a perspex spacer, 1.2 mm thick, having an opening of 12 mm at its centre. In different sets of experiments the voltage was varied from $\pm$ 1.5 V to $\pm$ 400 V (field varying from +3.3 KV/cm to –3.3 KV/cm). Application of the field very much increased the intensity of fogging of the autoradiographs. The

Table 1. Density of autoradiographs under various conditions. Density averaged and normalised to 24 h exposure time.

	Condition for autoradiography	Density (x 10^{-3})
1	In normal air atmosphere	80
2	In oxygen atmosphere	32
3	In hydrogen atmosphere	3.5
4	In air with 0.25 mg/cm^2 filter	6.0
5	In air with +0.67 kV/cm field	230
6	In air with –0.67 kV/cm field	210

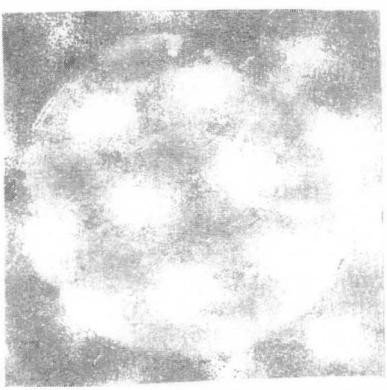

Figure 1. Autoradiograph (sample in contact)

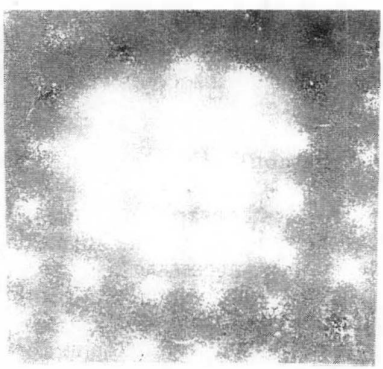

Figure 2. Autoradiograph (sample 0.2 mm away)

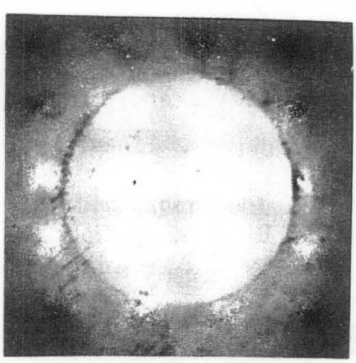

Figure 3. Autoradiograph (+ 0.67 kV/cm field)

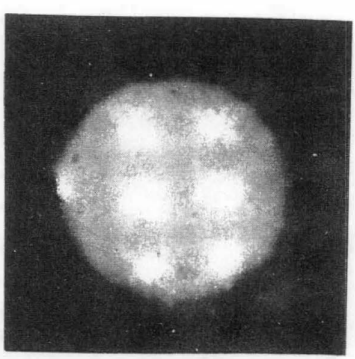

Figure 4. Autoradiograph (– 0.67 kV/cm field)

fogging increased as the voltage was increased, saturating approximately at 100 V. Surprisingly, when positive voltage was applied to the sample (for electrons to be retarded towards the film), the fogging was higher as compared to negative voltage. The Fig. 3 and 4 are the autoradiographs of two identical plasma focus loaded (15 PF shots) disks. The first one was with 100 V positive and the second one with 100 V negative supply. The exposure time for both the cases was 41 hours.

Few samples were also checked for X–ray emission on a low background silicon lithium (SiLi) detector with a thin beryllium window (1 keV energy threshold). The measurement time was typically 18 hours. No sample showed emission of X–rays above background.

Higher energy ($\geq$ 20 keV) radiations emanating from the samples was also measured by a end window type gas flow detector (operating in Geiger Muller mode, 0.8 mg/cm^2 window). The typical background of the detector was 0.01 $\pm$ 0.002 count/s. Samples with D_2 or H_2 loading were observed to give 0.02 $\bullet$ 0.002 counts/s (18 hours of counting). No counts above background were however observed when the sample was kept inside a window less gas flow detector.

3. Discussion & Conclusions

Autoradiographs have been observed in oxygen and air atmospheres but not in helium, argon and nitrogen atmospheres. The presence of oxygen or air appears to be necessary to observe strong radiographs. It is likely that oxygen is assisting the phenomenon (Some other impurity present in oxygen as well as in air causing this phenomena although unlikely, cannot be ruled out). However there appears to be an optimum concentration ($<$ 100 %) of oxygen in atmosphere at which the fogging is maximum.

The energy released in H_2–O_2 recombination reaction is 1.5 eV. If a few hundred to thousand times this energy gets transferred to a D ion then normal hot fusion can take place resulting in emission of energetic charged particles ($\leq 10^{-2}$/s), if there is a pathway to transfer the chemical recombination energy to deuterons. This may be possible only for certain metallurgical compositions and conditions. However there are several other phenomena in condensed matter which suggest that short lived large energy fluctuations (Dasannacharya 1989) do take place. These fluctuations can impart 100 to 1000 times the average energy.

4. References

1. Dasannacharya, B.A. and Rao, K.R., 1989, Remarks on Cold Fusion, C 2, Report BARC–1500, Bhabha Atomic Research Centre, Bombay.
2. De Ninno, A. et.al., 1989, Eurphys Lett, 9, 221.
3. Jones, S.E. et.al., 1989, Nature, 338, 737.
4. Mather, J.W., 1971, Methods of Experimental Physics, Academic Press, NY, USA, 9B, 187.
5. Rout, R.K. et.al., 1991, Fusion Technol, 19, 391.
6. Wada, N. and Nishizawa, K., 1989, Jpn J Appl Phys, 28, 2017.

Electron Impact H-H and D-D Fusions in Molecules Embedded in Al

Kohji KAMADA
National Institute for Fusion Science, Furo-cho, Chikusa-ku, Nagoya 464-01

ABSTRACT

Both H-H and D-D fusion reactions, detected via high energy particle emission on CR-39, are shown to occur when 200 and 400 keV electrons are bombarded onto H^+ or D^+ ion implanted Al thin crystals. Roughly 1-2 x 10^3 particle emissions, including both hydrogen and helium isotopes, in whole space were observed in each case. Collisions between recoiled D atoms due to the high energy electron impact give only 10^{-12} to 10^{-26} times smaller fusion rates than the experimental results. The present observations suggest the presence of a new kind of fusion reaction which occurs with negligible kinetic energy of the reacting nuclei.

1. Introduction

The experiment reported here contains the two new findings: The first is the observation of H-H fusion reaction, which has been elaborated theoretically by Bethe and Critchfield. The second is the fusion reaction which occurs in Al metal. Both were observed on the electron bombardment of the implanted molecular hydrogen isotopes(H_2 or D_2) embedded in Al metal.

In this experiment, hydrogen or deuteron implantation was employed, since it forms coagulation of molecules in Al, then the bombardment with electrons of energies 200 or 400 keV was followed.

2. Experiment

In this experiment, H_3^+ or D^+_3 ions with energy of 90 keV were implanted at room temperature into Al thin films up to the fluence of more than 10^{17} H^+_1 or D^+_1/cm^2 using Cockcroft Walton type accelerator.

After the implantation, the Al specimen, thin enough to pass through for 200 keV electron, was installed into the diffraction chamber of the electron microscope, HITACHI HU-500, and was bombarded with the electron beam with the energies of 200 or 400 keV. The electron beam current was about 300 to 400 nA with the beam size of about 4 x $10^{-5}cm^2$, giving roughly 4 - 6 x 10^{16} electrons/cm^2/s as the flux ϕ_e of the electron beam on the target.

FRONTIERS OF COLD FUSION

For the detection of the high energy emitted particles, the author employed the plastic detector made of CR-39 polymer, supplied by Tokuyama Soda Co. Ltd. The detector size was 10 mm x 15 mm x 1 mm. All detectors were made from the same lot of the plastics, and have been kept with thin plastic films attached on their both sides in a Rn free atmosphere filled with air which has been reserved for several months in an airtight cylinder. Two detectors in the backward side of the electron beam were set parallel to the Al specimen at 20 mm from it with 1 mm slit between them, through which the electron beam comes down to the target. Another two detectors were able to be set parallel to the electron beam at 20 mm from the target. The arrangements of the detectors are shown schematically in Fig.1(X=Z=20 mm). Immediately after the electron bombardment, the vacuum of the electron microscope was broken with the Rn free air, and the detectors were immersed into a salt water to discharge the detector surface which was presumed to have negatively charged with reflected electrons during the bombardment. Then the detectors were etched in 6N KOH solution at 70° C for 2h. The bulk etching rate of the CR-39 in this condition was 2.7 μ m/h. The particle traces thus formed on the target facing surface of the detectors were counted with optical microscope. Further etching was performed for the determinations of both particle species and energies. In exactly the same way,non-implanted Al specimens were also bombarded with the electron beam, and particle traces were counted for the background measurement.

3. Experimental results and discussions

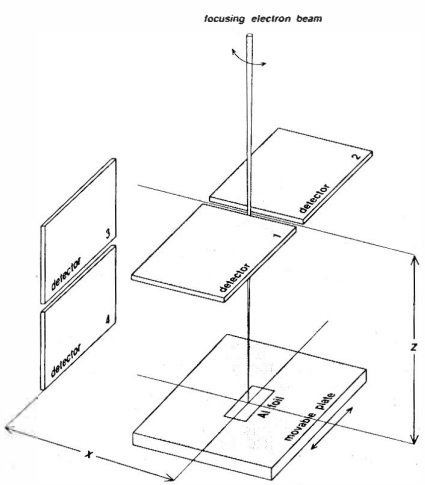

Fig.1 Experimental arrangement

The etching reveals the particle traces on the detector surface as etch pits. Figure 2 shows six typical examples of the etch pits after the two hours' etching of a detector, which was exposed to emitted particles during 200 keV electron bombardment onto H_3^+ implanted Al specimen. All observed pits were able to be sorted with these 6 examples. Particle species and energies were determined by measuring the growth curves of their pits' radii against the bulk etching. They were furtherconfirmed by referring to the sizes of standard etch pits produced by bombardments of p^+ and

$^4He^+$ of known energies onto other CR-39 detectors.

Experimental results are shown in Fig. 3, in which the observed number of the particle traces on a CR-39 detector with the surface area of 1.5cm^2 was plotted against the electron energy(●, ◐, ▲). Also plotted is the background number of traces (○), which was measured with the non-implanted Al specimens. Here, the author would like to note that the pit numbers on the backsides of the detectors, which have not been facing to the Al targets, were also in the background level. This means that the surplus pits observed on the front sides of the detectors were due to the energetic particles from the Al specimens. And also it should be added that the pit numbers of the virgin detectors of the same lot, and of the same treatment, were also within the background level shown in Fig. 3.

It is seen in this figure that the numbers of the particle traces on the both H^+ and D^+ implantation are more than twice, on the average, of the background level at both energies. Reproducibility of the experiment was confirmed in the 200 keV electron bombardment case, in which the four successive experiments gave always the surplus number of traces over the background level.

The reproducibility of the experiment was controlled by two factors. The first was the brightness of the electron beam, namely the number of bombarding electrons per unit area of the beam cross-section. Unfortunately, the brightness was rather hard to be controlled with the electron microscope used in this experiment, specially at the specimen position employed. From the measurement of the beam size on the target surface, more than 3 x 10^{16} electrons/cm^2/s of the brightness was necessary to observe the particle emission. The second factor which controlled the particle emission was the amount of implantation. It was requisite to have formed the so-called tunnel like structure in the subsurface layer of Al specimen. The bubble structure which precedes the formation of the tunnel like structure was not responsible for the particle emissions. Additionally, the author would like to mention that surface contamination of the Al specimen have not affected the particle emission at all. Since the Alspecimens have chemically etched before the implantation, only source of the contamination was that of oxidation during the implantation, due to the water molecules being collected on the Al surface.

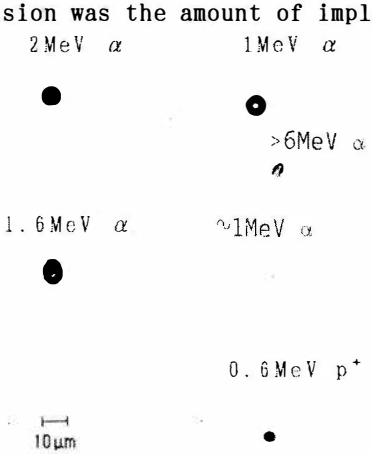

Fig.2 Particle traces

However, even on the heavy contamination, which was experienced when the vacuum of the implantation chamber was worse than about 3 x 10^{-6}Torr, the particle trace remained within the background level when the implantation were not enough to produce the tunnel like structure.

Number of traces on each detector with the same solid angle was not necessarily the same. For example, in D_3^+ implantation case at 400 keV, 470 and 170 traces were observed on the detectors 1 and 2, respectively. Similar inhomogeneity, but to a less extent, was also observed in H_3^+ implantation case. However, when particle number is relatively low, like those points with slashes shown in Fig. 3 at 200 keV, the particle emission seems rather homogeneous. The reason is not clear at present.

It is also seen in this figure that the increase of the particle traces over the background level does hardly depend on the electron energy. Together with the number of traces, this point shows a sharp contrast against the high energy collisional fusion which gives only 10^{-26} to 10^{-12} times smaller fusion rates than the present results as shown in Table 1. The solid angle $\Delta\omega$ of the detector 1 or 2 in Fig 1 was evaluated numerically obtainin g 0.936 each. Using this value and taking roughly 100 as the homogeneous increase of the particle trace over the background level for each detector, total number of the particle emission N in whole space becomes

$$N = 100 \times 4\pi / \Delta\omega = 1340$$

for the H-H reaction case, which is assumed nearly equal to the number of the fusion events R. For the D-D reaction case, if the inhomogeneous emission was taken into account, more particle emission can be estimated.

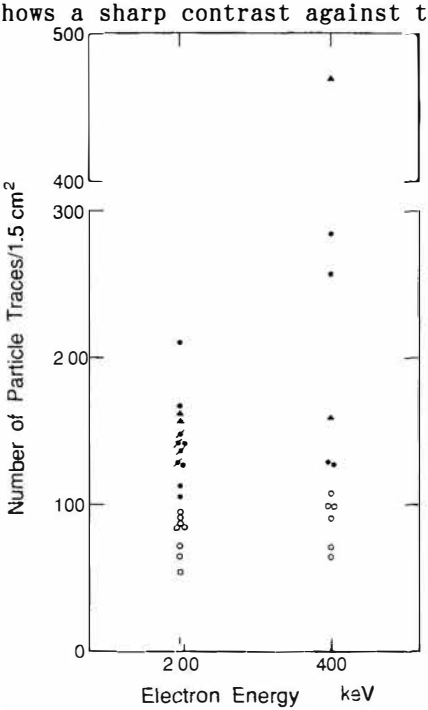

Fig.3 Number of traces

Table I. Evaluation of the collisional fusion from eq. (2).

E (keV)	T_m (eV)	R_0^c (cm$^{-3}\cdot$s^{-1})	R^c
200	262	2.8×10^{-18}	4×10^{-23}
400	611	9.4×10^{-5}	1.4×10^{-9}

Observations on the Biological Cold Fusion or the Biological Transmutation of Elements

Prof. Dr. Hisatoki KOMAKI
The Biological and Agricultural Research Institute.
OTSU, SHIGA-KEN, JAPAN

ABSTRACT

In previous paper [1)~7)], the author, with Prof. Dr. C. Louis KERVRAN, suggested the probable occurrence of the biological cold fusion or the biological transmutation of elements. In order to confirm the phenomena, under the more controlled condition, potassium, magnesium, iron and calcium were determined in cells of *Aspergillus niger* IFO 4066, *Penicillium chrysogenum* IFO 4689, *Rhizopus nigricans* IFO 5781, *Mucor rouxii* IFO 0396, *Saccharomyces cerevisiae* IFO 0308, *Torulopsis utilis* IFO 0396, *Saccharomyces ellipsoideus* IFO 0213 and *Hansenula anomala* IFO 0118 cultured in normal medium and media deficient in one of potassium, magnesium, iron or calcium. Values of potassium 1890~2650 μg, magnesium 380~510 μg, iron 95~120 μg, and calcium 60~95 μg were obtained per g dried cells cultured in each deficient medium, while potassium 8650~11050 μg, magnesium 1920~2160 μg, iron 510~680 μg, and calcium 380~450 μg were found per g dried cells obtained by cultivation in the normal medium.

The author would like to suggest the probable occurrence of the phenomena relevant to biological cold fusion.

1. Introduction

According to the late Prof. Dr. C. Louis Kervran, the probable mechanism of the non-radioactive biological transmutations of the elements non-radioactive (biological cold fusion) is summarized as follows:—

$Na_{23}+O_{16}=K_{39}$
$^{23}Na+^{1}H:=:^{24}Mg$
$Fe_{56}-H\rightarrow Mn_{55}$

$K_{39}+H_{1}\rightarrow Ca_{40}$
$Mg_{24}+O_{16}\rightarrow Ca_{40}$
$Si_{28}+C_{12}\rightarrow Ca_{40}$

In this paper, in order to confirm the phenomena—non-radioactive biological transmutations of elements or non-radioactive biological cold fusion—, my coworkers and I [Hisatoki KOMAKI] determined the amount of potassium, magnesium, iron and calcium in the cells of Aspergillus niger IFO 4066, Penicillium chrysogenum IFO 4689, Rhizopus nigricans IFO 5781, Mucor rouxii IFO 0396, Saccharomyces cerevisiae IFO 0308, Torulopsis utilis IFO 0396, Saccharomyces ellipsoideus IFO 0213 and Hansenula anomala IFO 0118, cultured in normal medium and media deficient in one of potassium, magnesium, iron or calcium, under more controlled condition than the previous papers.

II. Methods and Results

The composition of the normal medium, for mold, and the media for mold deficient in one of potassium, magnesium, iron or calcium.are shown in Table 1.

The composition of the normal medium, for yeast, and the media for yeast deficient in one of potassium, magnesium, iron or calcium, are shown in Table 2.

The microorganisms were cultured with each 200 ml of culture media; shaking culture at 30°C for 27 hours, using IWASHIYA's shaking incubator.

The experimental results are shown in Table 3 and Table 4.

Table 3 shows the comparison of the yield, as the weight of dried cells (mg) of mold and yeast obtained by normal media and potassium-deficient, magnesium-deficient, iron-deficient, and calcium-deficient culture; cultured with each 200 ml of culture media; shaking culture at 30°C for 27 hours.

Table 4 shows the comparison of the contents of potassium, magnesium, iron and calcium (μg) of the whole amount of, and 1g of, the dried cells of mold and yeast obtained by normal culture, and potassium-deficient, magnesium-deficient, iron-deficient and calcium deficient culture: Each 200 ml, 30°C, 72 hours.

Upper shows per-whole-amount of the obtained dried cells.

Lower shows per-1g of the obtained dried cells.

The data in ( ) in Table 4 shows the pure data, in which the influence of the biological concentration is excluded.

III. Discussion and Conclusion

These experimental results led us to conclude the probable accurence of non-radioactive biological transmutations of elements or the non-radioactive biological cold fusion.

In the monograph, presented for 4th International Conference on Biophysics and Synchrotron Radiation (BSR 92, Tsukuba), my coworkers and I [Hisatoki KOMAKI][7] proposed the cooperative research with the research workers of the National Laboratory for High Energy Physics (Tsukuba) to analyze the whole structure of various cell proteins, especially that of the enzyme proteins, in living form, which must be catalyze the non-radioactive biological transmutations of elements (the non-radioactive cold fusion) in cells of Aspergillus niger IFO 4066, Penicillium chrysogenum IFO 4689, Rhizopus nigricans IFO 5781, Mucor rouxii IFO 0396, Saccharomyces cerevisiae IFO 0308, Torulopsis utilis IFO 0396, Saccharomyces ellipsoideus IFO 0213 and Hansenula anomala IFO 0118. The recent developments in studies of macromolecular structure of living cell protein (especially enzyme protein) by X-ray crystallography [8], the recent develop-

ments in soft X-ray radiobiology and synchrotron radiation [9], that in the natural imaging[10] of biological specimens with X-ray microscopes, and the neutrons in studies of biological systems and their complementarity with X-rays, that in the solution scattering[11], that in membranes, that in time-resolved macromolecular crystallography[12], that in small-angle X-ray scattering, and that in spectroscopy (XAFS, CD, fluorescence, etc.) must be the most effective methods to analyze the probable mechanism of the non-radioactive biological cold fusion.

Dr. Goldfein, of the U.S. Army Laboratory, kindly suggested that the biological transmutations of elements (biological cold fusion, we should say) must be catalyzed by Mg-ATP as biological particle accelerator. In this connection, we have much concern with Prof. Dr. Katsuzo Wakabayashi (Osaka University) and Prof. Dr. Takeyuki Wakabayashi (Tokyo University)'s small-angle X-ray scattering analysis of conformational changes of the myosin head (SI) during hydrolysis of ATP (Mg-ATP)[13]

References

1) Hisatoki KOMAKI: Production de proteins par 29 souches de microorganismes et augmentation du potassium en milieu de culture sodique, sans potassium (Revue de Pathologie Comparee 67, 213-216, 1967)
2) Hisatoki KOMAKI: Formation de proteines et variations minerales par des microorganismes en milieu de culture, sort avec ou sans potassium, sort avec ou sans phosphore (Revue de Pathologie Comparee, 69, 83-88, 1969)
3) Hisatoki KOMAKI: C.L.Kervran: Experiences de Komaki, Premiere Serie de Recherches (PREUVES IN BIOLOGIE DE TRANSMUTATIONS A FAIBLE ENERGIE, MALOINE, S.A., PARIS, 1975, P. 116-120)
4) Hisatoki KOMAKI: C Louis Kervran: Deuxieme Serie D'Experiences de KOMAKI (ibid., P. 120-121)
5) Hisatoki KOMAKI: C. Louis Kervran: Troisieme Serie D'Experiences de H. KOMAKI (ibid., p. 122-130)
6) Hisatoki KOMAKI et al.: Proceedings of the 13th International Congress of Biochemistry, Amsterdam, 1986
7) Hisatoki KOMAKI et al: An Approach to the Probable Mechanism of the Non-radioactive Biological Cold Fusion or So-called Kervran Effect, Abstract of 4th International Conference on Biophysics and Synchrotron Radiation (BSR 92), p272, Tsukuba, August 30th ~ September 5th 1992.
8) J. Deisenhofer: Developments in Studies of Macromolecular Structure b y X-ray Crystallography, Abstract of BSR 92, Tsukuba, 1992.
9) D. T. Goodhead: Soft X-ray Radiobiography and Synchrotron Radiation, Ibid., 1992
10) G. Schmahl: Natural Imaging of Biological Speciments with X-ray microscopes, Ibid., 1992
11) H. B. Stuhrmann: Solution Scattering, Ibid., 1992
12) J. R. Helliwell: Time-resolved macromolecular crystallography, IBid., 1992
13) K. Wakabayashi et al.: Small -angle X-ray Scattering Analysis of Conformational Changes of the Myosin Head (S1) during Hydrolysis of ATP Ibid., F107, 1992

Table 1. Composition of the Nonnal, K-deficient, Mg-deficient, Ca-deficient and Fe-deficient Media for Mold

Components	Normal	K-deficient	Mg-deficient	Ca-deficient	Fe-deficient
Sucrose	3%	3%	3%	3%	3%
$NaNO_3$	0. 3%	0.3%	0.3%	0.3%	0.3%
K_2HPO_4	0.1%	—	0.1%	0.108%	0.1%
KCl	0.05%	—	0.05%	0.05%	0.05%
$MgSO_4 \cdot 7H_2O$	0.05%	0.05%	—	0.05%	0.05%
$FeSO_4 \cdot 7H_2O$	0.001%	0.001%	0.001%	0.001%	—
$CaHPO_4$	0.008%	0.008%	0.008%	—	0.008%
Na_2HPO_4	—	0.1%	—	—	—
NaCl	—	0.05%	—	—	—
Na_2SO_4	—	—	0.05%	—	—
$MnSO_4 \cdot 7H_2O$	—	—	—	—	0.001%
Pure Water	to 100%	to100%	to 100%	to 100%	to 100%

All components used are pure chemicals

Table 2. Composition of the Normal, K-deficient, Mg-deficient, Ca-deficient and Fe-deficient media for Yeast

Components	Normal	K-deficient	Mg-deficient	Ca-deficient	Fe-deficient
Sucrose	10%	10%	10%	10%	10%
Ammonium Tartarate	1%	1%	1%	1%	1%
$MgSO_4 \cdot 7H_2O$	0.25%	0.25%	—	0.25%	0.25%
$FeSO_4 \cdot 7H_2O$	0.001%	0.001%	0.001%	0.001%	—
$CaHPO_4 \cdot 2H_2O$	0.008%	0.008%	0.008%	—	0.008%
K_3PO_4	0.5%	—	0.5%	0.5%	0.5%
Na_3PO_4	—	0.5%	—	—	—
Na_2SO_4	—	—	0.25%	—	—
K_2HPO_4	—	—	—	0.08%	—
$MnSO_4 \cdot 7H_2O$	—	—	—	—	0.001%
Pure Water	To 100%	To100%	To 100%	To 100%	To 100%

Table 3. Comparison of the yield, as the weight of dried cells (mg) of mold and yeast obtained by normal media and K-deficient, Mg-deficient, Fe-deficient, and Ca-deficient culture. (Cultured with each 200 *ml* of culture media ; shaking culture at 30℃ for 27 hours.)

Species	Culture media				
	Normal	K-deficient	Mg-deficient	Fe-deficient	Ca-deficient
Aspergillus niger (IFO No. 4066)	574	54	72	56	125
Penicillum chrysogenum (IFO No. 4689)	907	83	99	90	196
Rhizopus nigricans (IFO No. 5781)	496	42	56	45	121
Mucor rouxii (IFO No. 5773)	388	35	40	38	98
Saccharomyces cerevisiae (IFO No. 0308)	1480	141	146	138	281
Torulopsis utilis (IFO No. 0396)	2710	253	263	220	365
Succharomyces ellipsoideus (IFO No. 0213)	1540	155	163	159	294
Hansenula anomala (IFO No. 0118)	1060	98	105	103	215

Table 4. Comparison of the contents of K, Mg, Fe, Ca (μg) of the whole amount of, and 1g of, the dried cells of mold and yeast obtained by normal culture, and K-deficient, Mg-deficient, Fe-deficient and Ca-deficient culture (Each 200 *ml* ; 30℃ ; 72 hours).
(Upper : Per whole amount of the obtained dried cells ; Lower : Per 1g of the obtained dried cells)

Species	Normal culture				K-deficient	Mg-deficient	Fe-deficient	Ca-deficient
	K	Mg	Fe	Ca	K	Mg	Fe	Ca
Aspergillus niger (IFO No. 4066)	5280 9198	1110 1934	390 679	260 453	130 (90) 2407(1667)	34 472	7 125	12 96
Penicillium chrysogenum (IFO No. 4689)	10100 11136	1910 2106	570 628	390 429	150 (110) 1807(1325)	50 905	9 100	14 71
Rhizopus nigricans (IFO No. 5781)	4240 8548	960 1935	250 504	190 383	110 (70) 2619(1667)	21 375	5 111	10 82
Mucor rouxii (IFO No. 5773)	3940 10156	780 2010	210 389	160 412	89 (29) 1971 (879)	18 450	4 105	6 61
Saccharomyces cerevisiae (IFO No. 0308)	14300 11014	2820 1905	1180 797	720 486	310 (270) 2199(1916)	68 466	15 109	29 196
Torulopsis utilis (IFO No. 0396)	23900 8819	1750 645	2020 756	1380 493	490 (450) 1937(1779)	130 494	22 100	29 148
Saccharomyces ellipsoideus (IFO No. 0213)	18400 11948	2990 1949	1220 792	790 513	340 (300) 2194(1935)	62 380	16 101	28 231
Hansenula anomala (IFO No. 0118)	12500 11792	2060 1943	840 792	520 491	120 (130) 1235(1327)	42 117	12 400	15 153

Chapter III
Materials and Hydrogen Behavior

TEM Investigation of Hydrogen Ordering in Pd

C. L. Hsu, F.-R. Chen and C. M. Wan
Materials Science Center, National Tsing Hua University
Hsinchu, Taiwan, R. O. C.

ABSTRACT

TEM was used to study the microstructure of Pd electrodes before and after electrochemical reaction in molten salt and heavy water cells. Hydrogen ordered structure in the non-stoichiometric PH_x was observed in the Pd specimens annealed in air, vacuum and hydrogen furance. On the contrary, high density of dislocations and subgrains and no superlattice structure was observed in the Pd specimens after electrochemical reactions. The reason why no superlattice structure in the electrochemically reacted Pd may be due to traping of hydrogen atoms by defects.

1.Introduction

More than four years ago, thousands of scientists around the world raced to confirmed the claims of electrochemically induced fusion [1,2] especially in the palladium/deuterium system. It is well-known fact that palladium powder at room temperature will absorb hydrogen or deuterium at 1 atm presure to a saturation value which occurs at an atomic ratio H/Pd of about 0.7 which is due to the filling of 4d-band in palladium [3]. Depending on the amount of hydrogen present, x-ray investigation have shown that two different fcc phases exist in the palladium. At low hydrogen concentrations, the α-phase exists and has a lattice constant of 3.89A, very nearly the same as that of pure palladium. However, as the hydrogen concentration is increased, the β-phase (palladium hydride, PH_x) becomes present, in which the lattice is expanded to 4.02A. The hydrogen in the palladium hydride is non-stoichiometric.

Vacancy ordered structures of many non-stoichiometric carbides, nitrides, oxides and silisides of metals [4] were found. However, the vacancy ordered structure in the PdH_x has not been reported yet.

From materials science point of view, the microstructure of the palladium electrode may play a very important role in the case either hydrogen or deuterium

FRONTIERS OF COLD FUSION

absorption is crucial [5]. The distribution of hydrogen in PdH_x (order or random) may be a controlling factor for the fusion. It is, therefore, our motivation to carry out the TEM investigation of the microstructure of palladium including the distribution of the absorbed point defects, dislocations and grain structure before and after the electrochemical reactions in order to understand the correlation between microstructure and fusion. Although the electron microscope itself cannot decide the cold fusion issue, the microstructural details at the μm and atomic level might provide a very powerful perspective insofar as the role of microstructures in altering deuterium absorption, concentration, and proximity.

2.Methods

Palladium rods (99.99 %) with a diameter of 4.5 mm were annealed at 1127 K (850 ^oC) in vacuum of 10^{-2} torr and in air for two hours. Some of annealed palladium rods were then electro-polished with a mixture of 33% (wt%) sulphuric acid, 33% orthophoshorric acid and 34% nitric acid before they were put into electrochemical cells for fusion experiments. Two different fusion cells were used our experiments: 1) the molten salt cell contains Pd anode and Al cathode. The molten salt electrolyte is a eutectic mixture of 113.3 g KCl and 122.3 LiCl. Temperature of this cells was kept at 450 ^oC. 2) second type of cell is composed of heavy water electrolyte, Pd cathode and Pt anode. The heavy water electrolyte is 0.1 M LiOD in D_2O. The temperature of this cell was kept at the room temperature.

The annealed and electrochemically reacted palladium rods were cut into pieces of about 1 to 2 mm thick and punched into discs a diameter of 3 mm. The specimens were then mechanically thinned to about 20 μm. Specimens were dimpled until a small hole appears in the center of disc. A copper mesh was bonded to the sample by epoxy . The sepecimens were finally thined by ion milling for about 4 hours before examination of TEM.

TEM experiment were carried out by using JEOL 200CX and 4000EX microscopes. The MULTI-SLICE program written by Roar Kilaas was used to simulate the diffraction patterns [6].

3. Results and Discussion

We have observed weak superlattice diffraction spots in the annealed Pd specimen (in air, vacuum and hydrogen furance) in many crystallographic zone axes such as [111], [112], [221] and [332] diffraction patterns. The first two diffraction patterns are depicted in the figures 1 (a) to (b) and the superlattice diffraction spots are indicated by arrows. On the contrary, no superlattice diffraction observed in the electrochemically reacted Pd specimens which contain high density of dislocations and subgrains.

We have investigated many possibilities for the origin of these superlattice diffraction spots such as surface incomplete cell, surface reconstruction and hydrogen vacancy ordering in PH_x. Ultra-high vacuum and very thin specimen are required for the superlattice diffraction due to surface effect being able to be observed. We have found the superlattice diffraction in rather thick area of Pd specimen which was not

observed in the ultrahigh vacuum.

There may have little amount of PH_x in the annealed Pd specimen. The hydrogen in the non-stoichiometric PH_x may form order structure like many non-stoichiometric carbide, nitride, oxide and siliside of metals [4]. The hydrogen ordered structures viewing from [111], [112] are given in the figures 2 (a) to (b) and their corresponding computed diffraction patterns are depicted in the figures 3 (a) to (b) which have very good matches with the experimental diffraction patterns in the figures 1 (a) to (b), respectively.

Since the electrochemically reacted Pd specimens contain high density of dislocations and subgrains which may trap the hydrogen/deuterium atoms so that the hydrogen/deuterium atoms may not allowed to diffuse into the Pd lattice to form ordered structure. This may be the reason why we do not observe the superlattice diffraction spots in the electrochemically reacted specimens.

5. Conclusions

Hydrogen atoms were found to form ordered structure in the Pd specimens which were annealed in the air, vacuum and hydrogen furance. On the contrary, no hydrogen ordered structure can be found in the Pd specimens which were electrochemically reacted in the motlen salt and heavy water cells.

6. References

1. M. Fleishmann and S. J. Pons, 1989, J. Electroanalyt. Chem., 261, 301
2. S. E. Jones, et. al., 1989, Nature, 338, 737
3. J. E. Worsham, Jr. et. al., 1957, J. Phys. Chem. Solids, 3, 303
4. T. L. Lee, L. J. Chen and F. R. Chen, 1992, J. Appl. Phys., 71, 3307
5. L.E. Murr, 1990, Scripta Metall. Et Materialia, 24, 783
6. R. Kilaas, Proc. of the 49th Annual Meeting of electron Microscopy society of America, edited by G. W. Bailey and E. L. Hall (San Franciso Press, San Franciso, 1991), p528

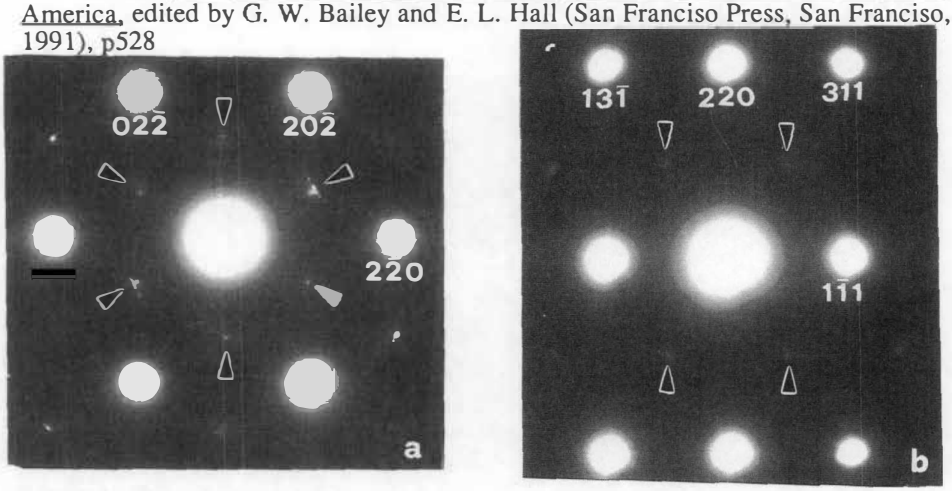

Figure 1. Experimental diffraction patterns of a) [111] zone axis and b) zone axis [112]

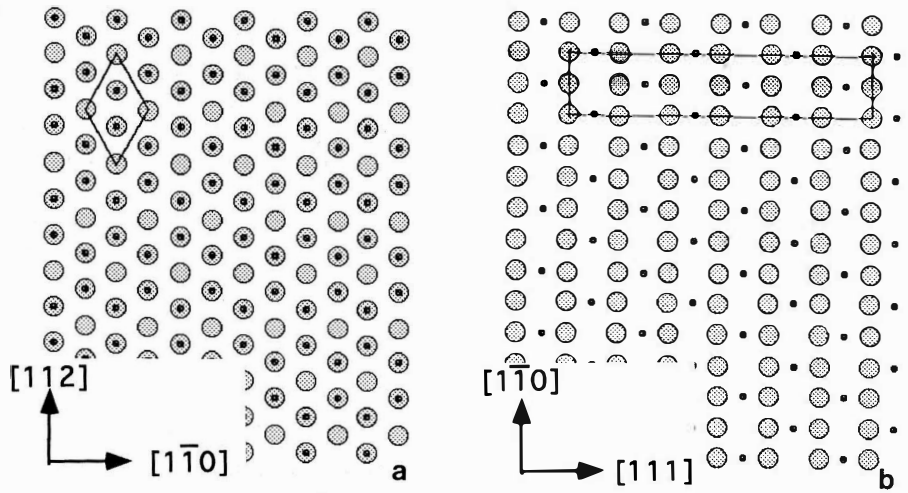

Figure 2. Hydrogen ordered structures viewing along a) [111] direction and b) [112] direction

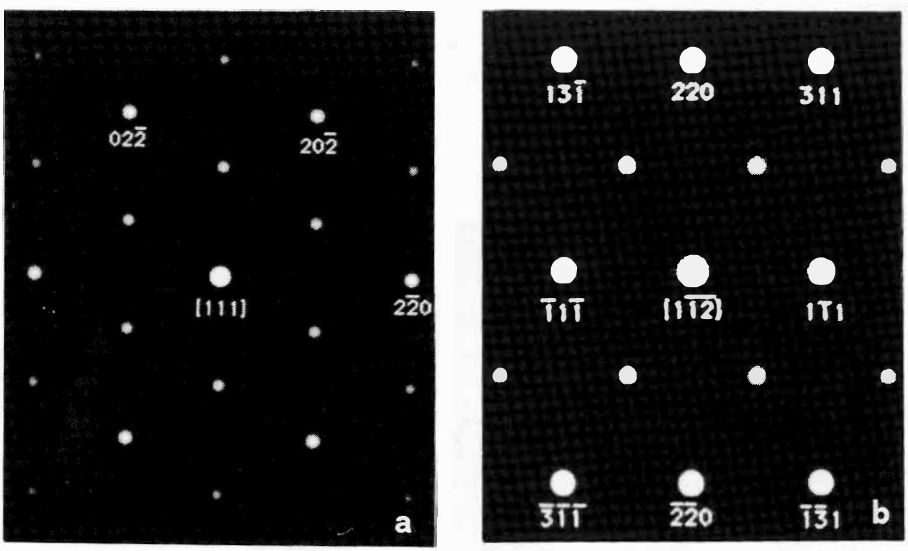

Figure 3. Computer simulated diffraction patterns of a) [111] zone axis and b) [112] zone axis for the projected structures shown in the figures 2

Hydrogen and Deuterium Absorption by Pd Cathode in a Fuel-Cell Type Closed Cell

Akihiko KUBOTA, Hidemi AKITA, Yumiko TSUCHIDA, Toshiya SAITO,
Akiko KUBOTA, Norifumi HASEGAWA, Norio IMAI, Nana HAYAKAWA,
Keiji KUNIMATSU
IMRA JAPAN CO.,LTD.
3-6 Techno Park 2 Cho-me Shimonopporo, Atsubetsu-ku, Sapporo 004,
JAPAN

ABSTRACT

The hydrogen and deuterium loading ratio, H/Pd and D/Pd, in Pd cathode were measured during electrolysis of 1M LiOD, 1M LiOH, 2.8M H_2SO_4, 2.8M D_2SO_4, 14.7M H_3PO_4, 0.57M K_2CO_3 in a fuel-cell type closed cell. Cold worked pure Pd (ϕ 2- ϕ 5 rods) were used for cathodes. A gas-diffusion type fuel cell anode was used for ionization of hydrogen and deuterium gas. H/Pd or D/Pd was calculated from H_2 or D_2 gas pressure decrease and temperature during electrolysis under in-situ conditions.

The result is summarized as follows; the loading ratio depends on hydrogen overvoltage. D/Pd is smaller than H/Pd by 4~8% for a given overvoltage. The loading ratio does not depend on electrolyte, but the overvoltage depends on electrolyte for a given current density.

1. Introduction

After the reports on "Cold Fusion" by Fleischmann, Pons[1] and Jones et al[2], many groups have conducted experiments in order to reproduce either the excess heat generation or to detect nuclear products such as neutron, tritium, helium. In 2nd ACCF in Como, importance of achieving high loadimg ratio close to 0.9 was pointed out by a few groups[3] for successful detection of excess heat and the nuclear products. It has not been reported, however, how one can achieve such a high loading ratio by electrolysis of heavy water using a palladium cathode. The aim of the present study is to measure the loading ratio of both hydrogen and deuterium in Pd as a function of the hydrogen overvoltage at cathode in various media in order to find various factors which have influence on the loading ratio.

2. Experimental

The electrolysis was conducted in a closed cell schematically shown in Fig.1. The cell was pressurized by H_2 or D_2 gas in which a gas diffusion electrode partially immersed in the electrolyte served as an anode in order to avoid oxygen evolution at the counter electrode and to determine the loading ratio from the pressure decrease during the electrolysis. A platinized platinum electrode served as the RHE(Reversible Hydrogen

FRONTIERS OF COLD FUSION

Electrode) for measurement of the hydrogen overvoltage at the Pd cathode. The overvoltage reported in the present report has been corrected for the Ohmic overvoltage due to the solution resistance which has been determined by galvanostatic transient method.

The determination of the loading ratio has been conducted in 1M LiOH, 1M LiOD, 2.8M H_2SO_4, 2.8M D_2SO_4, 14.7M H_3PO_4, 0.57M K_2CO_3 as a function of hydrogen overvoltage at either 10℃ or 30℃. The temperature inside the electrolyte, however, did change at the high current densities due to Joule heating of the electrolyte.

The palladium samples studied were rods of 99.99% purity with 2, 4 and 5mm in diameters. They have different Vicker's hardness, Hv, depending on their history of cold working. All the palladium samples were degassed at 200℃ in vacuum for 3 hours before the measurements. Two palladium wires of 0.5mm in diameter were spot-welded on the palladium rods to make the electrical lead from the cathode.

The initial pressure of H_2 or D_2 before the electrolysis was ca. 5～10kgf/cm², which decreased typically by 1～2kgf/cm² during the electrolysis. Temperature of the electrolyte as well as the gas phase changed at the high current densities, and the temperature change was corrected for by using the temperature measured by a thermocouple placed in the gas phase for the calculation of the loading ratio.

Electrolysis and data acquisition have been conducted by a computer controlled galvanostatic electrolysis system developed in our laboratory.

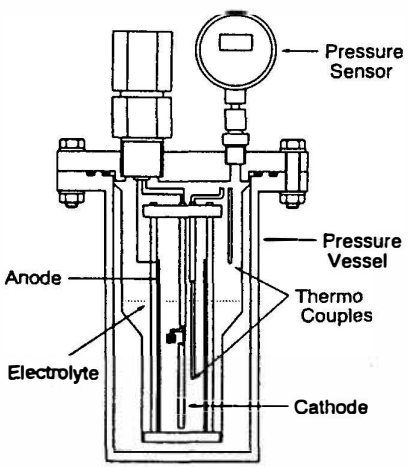

Fig.1 Electrolysis Cell

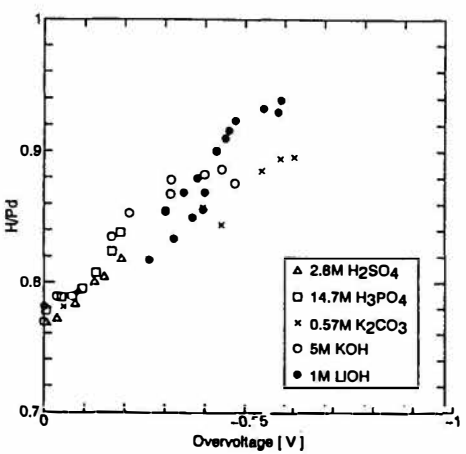

Fig.2 H/Pd vs Overvoltage for φ5 Pd at 30℃

3. Results and Discussion

Effect of the type of electrolyte on the loading ratio

Figure 2 shows the overvoltage dependence of the H/Pd observed in the various electrolytes. The results demonstrate that the loading ratio depends primarily on the hydrogen overvoltage, in other words the loading ratio for a given overvoltage is almost the same irrespective of the type of electrolyte. This means also that the alkaline electrolyte is a better choice for achieving the higher loading ratio simply because the overvoltage at the palladium cathode is higher in the alkaline solutions than in the acidic solutions for a given current density.

Isotope effect on the loading ratio

Figure 3 and 4 demonstrate the difference of the loading ratio between hydrogen and deuterium observed in LiOH, LiOD and H_2SO_4, D_2SO_4 respectively. The figures clearly show that the loading ratio for hydrogen is 4～8% larger than that of deuterium for a given overvoltage. This is interpreted in terms of the higher plateau pressure in the P-C-T curve observed commonly in the gas phase for the Pd/D_2 system than the pressure for the corresponding Pd/H_2 system. The relationship between the hydrogen overvoltage and it's equivalent hydrogen pressure was discussed by Enyo et al.[4] and the interpretation of the isotope effect on the overvoltage dependence of the loading ratio presented in Fig.3 and 4 is supported by their result.

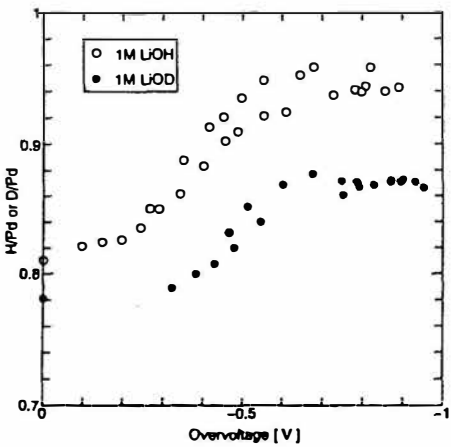

Fig.3 H/Pd or D/Pd vs Overvoltage for ϕ5 Pd at 10℃

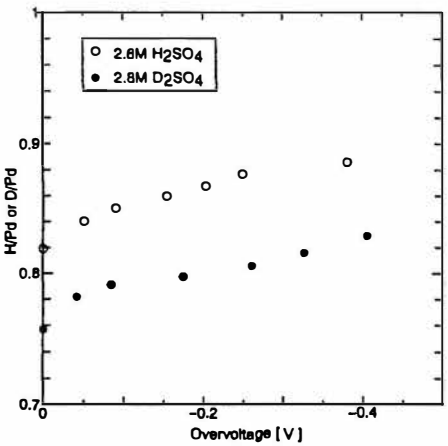

Fig.4 H/Pd or D/Pd vs Overvoltage for ϕ4 Pd at 10℃

Effect of Vicker's hardness of Pd on the loading ratio

Figure 5 demonstrates the overvoltage dependence of D/Pd for three kinds of palladium rods with different Vicker's hardness. The results suggest that the hardness of palladium has little effect on the loading ratio, although it is not clear at the moment if effect still remains small in the region of higher loading ratio than achieved in the present report. In view of the fact that the hardness is determined primarily by the history of the cold working of the palladium samples, we may conclude from the present data that the cold working of the sample has little effect at least on the loading ratio.

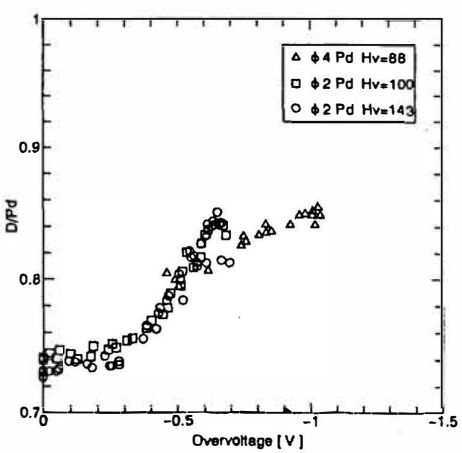

Fig.5 D/Pd vs Overvoltage for ϕ2 and ϕ4 Pd in 1M LiOD at 30℃

Dependence of the loading ratio on the current density

The overvoltage dependence of the loading ratio can be converted to the corresponding dependence of the loading ratio on the electrolysis current density using the relation between the current density and the overvoltage. Figure 6 shows the dependence of the overvoltage on the current density in 2.8M H_2SO_4, 1M LiOH and 1M LiOD. The dependence of the loading ratio on the current density is shown in Fig.7.

The role of the current density demonstrated in Fig.7 strongly suggests that high current density is necessary to achieve and maintain the high loading ratio. The dependence of excess heat generation on the current density reported originally by Fleischmann and Pons and later by Storms[5] can be interpreted in terms of the role of the current density described above.

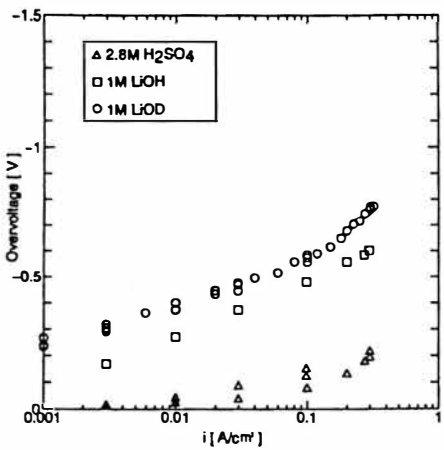

Fig.6 Overvoltage vs Current density for φ2 Pd at 30℃

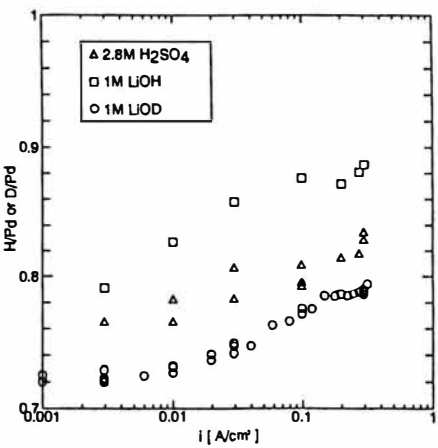

Fig.7 H/Pd or D/Pd vs Current density for φ2 Pd at 30℃

4. Conclusion

The loading ratio does not depend on the type of electrolyte, but depends primarily on hydrogen overvoltage at Pd cathode. D/Pd is smaller than H/Pd by 4～8% for a given overvoltage. The difference of the hardness of Pd cathode have little effect on the loading ratio.

5. Reference

1) M.Fleischmann, S.Pons, J.Electroanal.Chem., 261, 301(1989); errata 263, 187(1989)
2) S.E.Jones and et al., Nature, 338, 737(1989)
3) ICCF2, Conference Proceedings Vol. 33 "The Science of Cold Fusion"(1990)
4) T.Maoka, M.Enyo, Electrochim. Acta., 26, 607(1981)
5) E.Storms, Fusion Technol., 20, 433(1991)

Preparation of Pd Electrodes and Their Hydrogen Loading Ratios

Toshiyuki SANO, Toshihisa TERASAWA, Tamio OHI, and Shinji NEZU

IMRA MATERIAL R&D CO., LTD.
5-50 Hachiken-cho, Kariya, Aichi 448
JAPAN

ABSTRACT

We prepared a series of palladium-based rods with various compositions and processing histories as cathode for water electrolysis. These rods were evaluated in terms of hydrogen loading ratio (H/Pd). The hydrogen loading ratios of Pd-Ag and Pd-Ce alloys are compared with that of a pure Pd rod. The hydrogen loading ratios of Pd rods subjected to annealing and/or cold-working (swaging) are also compared with that of a cast Pd rod. The results show that the alloying markedly reduces the loading ratio, and neither annealing (350-650 °C) nor swaging (up to the processing ratio of 98 %) produces a distinct effect.

1. Introduction

The lack of reproducibility of excess heat generation in heavy water electrolysis might be ascribed to unknown factors which are closely related to the material nature of the palladium cathode. It has been pointed out that attaining a high loading ratio is the key to give rise to excess heat generation [1]. Correlation between the rate of excess heat generation and the hydrogen loading ratio reported recently [2].

It has been known that the amount of hydrogen absorbed by a Pd electrode polarized cathodically is a function of the hydrogen overpotential [3,4]. On the other hand, the relation between palladium characteristics and the amount of absorbed hydrogen is not well understood.

In this study we prepared a series of palladium-based rods with various compositions and processing histories as cathode for water electrolysis, and measured the hydrogen

FRONTIERS OF COLD FUSION

loading ratios in order to investigate the effect of alloying, cold-working, and annealing.

2. Experimental

2-1. Preparation of electrodes

Palladium grain (99.99 %, 3-5 mm in diameter) was used as a mother alloy. Button-shaped mother alloys of Pd-Ag and Pd-Ce were prepared by arc-melting of the palladium grain and the respective metals (Ag: 99.9 %; Ce: 99.7 %). The mother alloys were cast into rods (8 mm in diameter) by high frequency induction melting (1650 °C) under an argon atmosphere. Using these rods, the following four groups of rods were prepared by annealing and/or swaging when necessary:

(1) Rods cast only.
(2) Cast and subsequently annealed rods.
(3) Cast and subsequently swaged rods.
(4) Cast, then annealed, and subsequently swaged rods.

In swaging, the percentage of a reduction in a cross section (processing ratio) was 75 % a swaging process. The final diameters of swaged rods were 4, 2, or 1 mm. The annealing temperatures were 350, 450 or 650 °C. The samples were held at an annealing temperature for 1 hour, and then cooled to room temperature at the rate of 1 °C/min.

2-2. Measurement of Hydrogen Loading Ratio

The rods (1-8 mm in diameter) were washed by acetone before each measurement using a ultrasonic cleaner, and then electrolyzed in H_2O at 25-30 °C (electrolyte temperature) using a cell shown in Figure 1. It should be noted that an evolved hydrogen gas is separated from an oxygen gas by a separator. A platinum black reference electrode was used to measure the hydrogen overpotential. A platinum rod which had the same surface area as a test rod was used as control electrode. All the measurements reported here were made galvanostatically at the current density of 300 mA/cm^2. The amount of the hydrogen absorbed in a test electrode was determined from the difference in evolved gas volume between the test electrode and the Pt control electrode in a subsequent run. Gas volume measurements were made using a mass flow meter (KOFLOC, Model-3710). Output from the mass flow meter was monitored every 5 seconds and integrated into the amount of hydrogen.

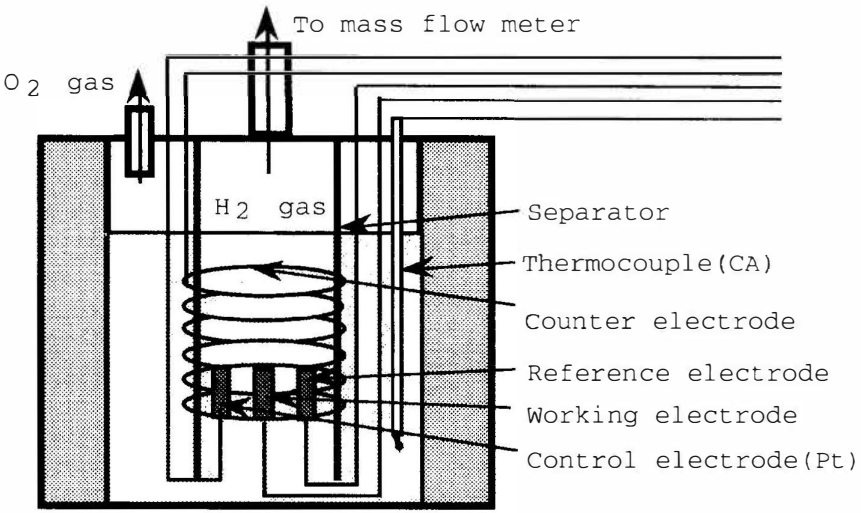

Figure 1. Electrolysis cell used for hydrogen loading ratio measurement.

3. Results and Discussion

Figure 1 shows the hydrogen loading ratios of Pd-based alloys with various Ag or Ce contents. In this experiment, all the electrodes (2 mm in diameter) were prepared by swaging of cast rods (8 mm). As is shown, the loading ratio markedly decreased with the increase of the Ag or Ce content.

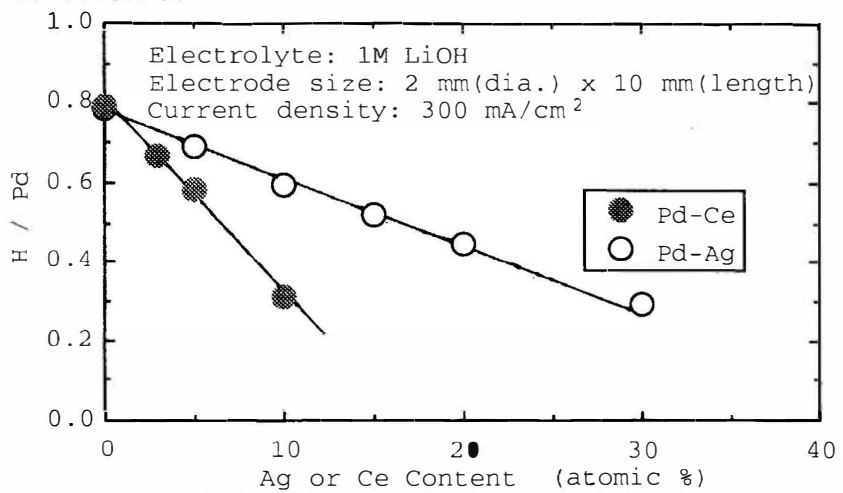

Figure 2. Loading ratios versus Ag or Ce content.

Table 1 shows the hydrogen loading ratios of swaged and/or annealed Pd rods. Although a little variation is seen, a distinct effect of those processing could not be observed under the condition employed in this study. The variation may suggest that other unknown factors are involved in the loading.

Table 1. Hydrogen loading ratios of swaged and/or annealed Pd rods.

Annealing Temp. / °C	Processing Ratio 0 %	75 %	94 %	98%
not annealed	0.776	0.780	0.785	0.767
350	0.746	0.773	0.776	0.778
450	0.782	0.767	0.731	0.759
650	0.774	0.762	0.746	0.748

5. References

(1) M. McKubre et.al.,Conference Proceedings Vol. 33 "The Science of Cold Fusion", p419, SIF, Bologna 1991.
(2) K. Kunimatu et.al.,Proceedings of The Electrochemical Society of Japan 1992 Fall Conference, p77.
(3) T. Maoka and M. Enyo, Surf.Tecnol.,9, 147 (1979).
(4) T. Maoka and M. Enyo, Electrochim. Acta, 26, 607 (1981).

Absorption of Hydrogen into Palladium Foil Electrode: Effect of Thiourea

Toshihide NAKATA, Yumiko TSUCHIDA, Keiji KUNIMATSU
IMRA JAPAN CO.,LTD.
2-3-6 Technopark, Simonopporo, Atsubetsu-ku, Sapporo
JAPAN 004

ABSTRACT

Electrolytic hydrogen absorption into Pd foil (50 μ m thickness) was investigated in the absence and presence of 30 μ M thiourea (THU) in 0.5M H_2SO_4 and 0.4M LiOH. The amount of hydrogen absorbed under cathodic polarization was determined by integrating the ionization current of hydrogen when Pd electrode was polarized anodically.

After THU addition in the acidic and alkaline solution H/Pd increased by about 8% and 5%, respectively.

Further we tried absorption of deuterium into Pd foil and found a similar effect of THU to increase D/Pd only in the acidic solution.

1. Introduction

Cold fusion phenomena in Pd cathode has been said to occur when the deuterium loading ratio, D/Pd, is higher than 0.9. But it is not easy to attain such high value of D/Pd by an ordinary electrolysis method. Therefore it is very important to find the experimental condition to increase the loading ratio higher than 0.9.

Enyo *et al.*[1) 2)] demonstrated that the hypothetical hydrogen pressure $P_{H_2}^*$ acting on the Pd hydrogen electrode was related to the overpotential of the Tafel step by the following Nernst type equation;

$$P_{H_2}^* = P_{H_2} \exp(-2F\eta_2/RT)$$

where P_{H_2} is hydrogen gas pressure in the cell and η_2 the overpotential of Tafel step ($2H(a) \rightarrow H_2$) for hydrogen electrode reaction on palladium, and that thiourea ($(NH_2)_2CS$) in acidic solution poisoned Tafel step and accordingly increased η_2.

FRONTIERS OF COLD FUSION

So we reinvestigated absorption of hydrogen/deuterium into Pd electrode under cathodic polarization in aqueous solutions containing THU in expectation of a rise in H(D)/Pd value.

2. Experimental

The design of a glass cell for electrolysis is shown in Fig.1. We used a palladium foil (50 μ m thickness $\times$ 5mm $\times$ 5mm) which was pretreated in vacuum at 200 ℃ for one hour as a working electrode. A platinum black mesh and a reversible hydrogen electrode (RHE) were used as an auxiliary and a reference electrode, respectively. All the experiments were performed in acidic solutions (0.5M H_2SO_4, D_2SO_4) or in alkaline solutions (0.4M LiOH, LiOD), bubbling nitrogen or argon gas throughout the experiment.

The absorption and desorption of hydrogen into/from Pd foil were carried out at 283K controlling the potential of Pd electrode as shown in Fig.2a. First hydrogen were absorbed into Pd foil under potentiostatic cathodic polarization. After a given period of electrolysis, Pd foil was then polarized anodically and all the absorbed hydrogen were desorbed from Pd. Fig.2b shows typical current response curve to these potential control. The negative and positive currents were integrated to give as "input charge" and "discharge charge", respectively, and loading ratio H/Pd was estimated as follows.

$$\mathrm{H/Pd} = \frac{\text{(discharge charge)/(Faraday constant)}}{\text{(the mole number of Pd in the cathode)}}$$

Hydrogen absorption and H/Pd measurement were performed using the same Pd foil repeatedly before and after the addition of 30 μM THU.

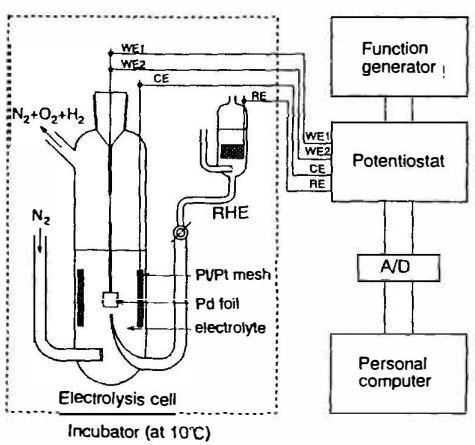

Fig.1. Schematic of experimental device

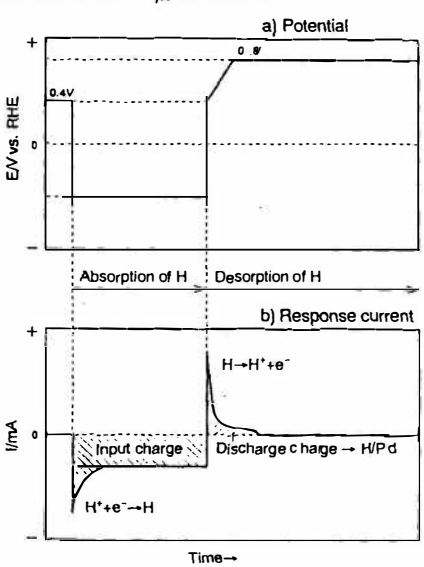

Fig.2. Charging and discharging process

3. Result and Discussion

Cyclic voltammetry of Pd foil electrode

Cyclic voltammograms for the Pd foil electrode in the absense and presense of THU in 0.5M H_2SO_4 are presented in Fig.3. After addition of THU in the electrolyte, two changes in voltammograms were observed; one was a decrease of the negative current peak at approximately +0.7V due to the reduction of the oxydized layer on Pd, and the other was an increase in anodic current above +1.0V. Bucur *et al.*[3] suggested that THU molecules were hydrolized and dissociated on the surface of Pd electrode as follows.

$$Pd \cdot SC(NH_2)_2 \rightarrow Pd \cdot SH_2 + NH_2CN \rightarrow Pd \cdot S^* \cdot (2H^*) + NH_2CN$$

* chemisorbed atom

It was considered that resulting S* atom hindered oxydation of Pd and caused the decrease of the negative peak current due to reduction of the surface oxide, and that the increase in anodic current was due to oxidation of S* atom to SO_4^{2-}.

Figure 4 shows voltammograms of the Pd foil for the extended potential sweep into the cathodic region. The current due to hydrogen evolution and absorption into the Pd foil were observed in the negative potential sweep, and upon the positive potential sweep discharging current due to the ionization of absorbed hydrogen desorbing from Pd was observed. The addition of THU led to the retardation of hydrogen evolution and absorption as well as of hydrogen desorption/ionization upon positive potential sweep.

A similar tendency was observed in 0.4M LiOH containing THU.

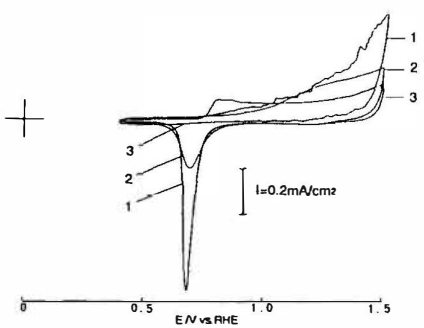

Fig.3.
Cyclic voltammograms for Pd electrode in 0.5M H_2SO_4 containing
1: no THU, 2: 30 μ M THU and
3: 200 μ M THU.

sweep rate: 50mV/sec

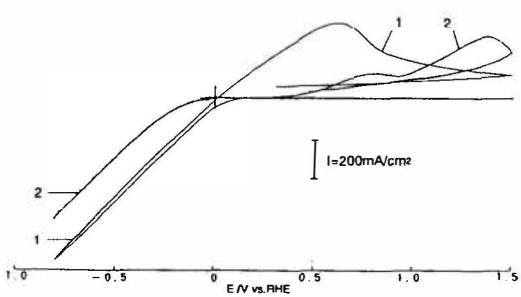

Fig.4.
Linear sweep coltammograms for Pd electrode in 0.5M H_2SO_4 containing
1: no THU and 2: 30 μ M THU.

sweep rate: 50mV/sec

Effect of THU on H/Pd (D/Pd) value

The relationship between H/Pd and input charge measured in 0.5M H_2SO_4 is shown in Fig.5. The amount of the input charge necessary for hydrogen to fill the Pd foil is 13～14 coulomb. While H/Pd in the electrolyte without THU kept nearly a constant value of 0.77 independent of input charge, after the addition of 30 μ M THU in electrolyte the value reached 0.85; approximately 8% increase of H/Pd was observed.

Figure 6 shows the result in 0.4M LiOH. In the alkaline solution H/Pd value tended to rise with increase of input charge. H/Pd went up maximally by 5% after addition of THU. We could not compare the H/Pd values in the acidic solution directly with that in the alkaline solution, because the electrolysis potential was not the same. However the rise in H/Pd was confirmed in both electrolytes.

Further we studied absorption of deuterium into Pd foil in 0.5M D_2SO_4 and 0.4M LiOD. D/Pd value,0.82, obtained in 0.5M D_2SO_4 containing 30 μ M THU was 6～8% higher than in the electrolyte without THU. But little effect of THU on D/Pd was found in 0.4M LiOD at this concentration of THU.

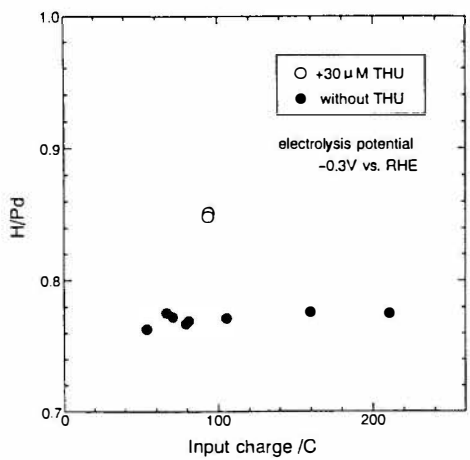

Fig.5. H/Pd vs. Input charge in 0.5M H_2SO_4 at 283K

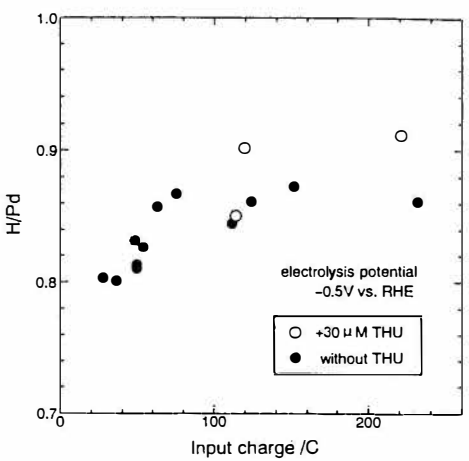

Fig.6. H/Pd vs. Input charge in 0.4M LiOH at 283K

4. Conclusion

The addition of 30 μ M THU into electrolytes except 0.4M LiOD led increase of hydrogen loading ratio in Pd electrode. The effect of THU should be investigated further by varying the hydrogen overpotential on Pd and the concentration of THU.

5. References

1) T.Maoka and M.Enyo, *Surface Tech.*, **9**, 147 (1979)
2) T.Maoka and M.Enyo, *Electrochimica Acta.*, **26**, 607 (1981)
3) R.V.Bucur and P.Marginean, *Electrochimica Acta.*, **29**, 1297 (1984)

In-Situ Electrochemical Quartz Crystal Microbalance Studies of Water Electrolysis at a Palladium Cathode

Noboru Oyama, Nobushige Yamamoto and Tetsu Tatsuma
Department of Applied Chemistry, Tokyo University of Agriculture and Technology
2-24-16 Naka-machi, Koganei, Tokyo 184
Japan

ABSTRACT

The in-situ electrochemical quartz crystal microbalance (EQCM) technique has been applied to study electrolysis of water containing 0.2 M $LiClO_4$ at Pd cathode. Decrease in resonant frequency was observed during the electrolysis. The decrease was attributed to the mass change involving hydrogen absorption into the palladium and lithium underpotential deposition, the mechanical stress change in the electrode, and the change in roughness of the electrode surface. The stress change, which may be caused by hydrogen uptake, was estimated using palladium film-coated AT- and BT-cut quartz crystal oscillators. The surface roughness change was observed by scanning electron microscopy and a number of cracks and holes were found. Underpotential deposition of lithium was observed in propylene carbonate containing 0.1 M $LiClO_4$ and 16 mg L^{-1} water. Contributions of respective factors to the total frequency change was estimated.

1. Introduction

In the studies on electrolysis of $LiOD/D_2O$ or $LiOH/H_2O$ using a Pd cathode, it is important to elucidate the electrochemical reaction of proton and process of hydrogen absorption accompanied by change in mechanical stress and surface morphology of the Pd electrode. Electrochemistry of lithium on the Pd electrode should also be studied because it may play an important role for excess heat generation. These were examined by means of electrochemical quartz crystal microbalance technique.

2. Experimental

5.0 MHz AT- and BT-cut quartz crystal plates were coated with the same thickness (ca. 140 nm) of Pd thin-film by sputtering. Geometrical area of the piezoelectrically active electrode and electrochemically active one are 0.283 and 0.503 cm^2, respectively. Electrochemical measurements were performed with a conventional three-electrode system in a 0.2 M $LiClO_4$ solution, pH of which has been adjusted to be 3.0 with $HClO_4$. An Ag wire was employed as reference

FRONTIERS OF COLD FUSION

electrode. Piezoelectric measurements were carried out as described elsewhere (Oyama *et al.*, 1990).

3. Results and Discussion

Correlation between frequency change (Δf) of a quartz crystal oscillator and mass change on the electrode of the oscillator (Δm) is reportedly as follows:

$$\Delta f = C\Delta m \tag{1}$$

where C is a constant. This equation is valid as long as the electrode is sufficiently rigid and the surface roughness and the mechanical stress of the electrode do not change. When the stress changes in the electrode of a quartz crystal oscillator, specific frequency of an AT-cut oscillator decreases with increasing stress, while that of a BT-cut oscillator increases. Frequency change caused by the lateral stress change (Δs) has been formulated as follows, on the assumption that the vertical stress is negligible (EarNisse, 1973):

$$\Delta f_{AT} = (K_{AT}\Delta s/\tau_{AT} - \Delta m/\rho\tau_{AT})f_{0AT} \tag{2}$$

$$\Delta f_{BT} = (K_{BT}\Delta s/\tau_{BT} - \Delta m/\rho\tau_{BT})f_{0BT} \tag{3}$$

where K is a stress constant, τ is the thickness of the quartz crystal, and ρ is the density of quartz (2.648 g cm^{-1}). In the present experiments, $K_{AT} = -K_{BT} = 2.75 \times 10^{-12}$ cm^2 dyn^{-1}, $\tau_{AT} = 0.0338$ cm, and $\tau_{BT} = 0.0510$ cm. Thus the mass change (Δm) and the stress change (Δs) of the electrode can be evaluated on the basis of the following equations which are derived from equations 2 and 3,

$$\Delta s = \frac{1}{K_{AT} - K_{BT}}\left(\frac{\tau_{AT}\Delta f_{AT}}{f_{0AT}} - \frac{\tau_{BT}\Delta f_{BT}}{f_{0BT}}\right) \tag{4}$$

$$\Delta m = \frac{\rho}{K_{AT} - K_{BT}}\left(\frac{K_{AT}\tau_{AT}\Delta f_{AT}}{f_{0AT}} - \frac{K_{BT}\tau_{BT}\Delta f_{BT}}{f_{0BT}}\right) \tag{5}$$

Resonant frequency of the AT- and BT-cut quartz crystal oscillators was monitored under galvanostatic electrolysis (-20.4 μA cm^{-2}) of a 0.2 M $LiClO_4$ aqueous solution. Figure 1 shows correlations between the frequency change (Δf) and passed charge (ΔQ). Both dependencies are rectilinear and the BT-cut quartz crystal oscillator exhibited a larger slope than the AT-cut oscillator. This difference is attributed to a stress generated in the Pd electrode. Figure 2 depicts the correlations between the mass change (A) or the stress change (B) and the anodic charge passed, evaluated using equations 4 and 5 on the assumption that absorbed hydrogen is homogeneously distributed in the Pd electrode. As seen in the figures, both the mass change and the stress change are proportional to the passed charge. Thus the stress change is proportional to the absorbed amount of hydrogen, on the assumption that the ratio of charge consumed for proton reduction per total charge passed and the

molar ratio of hydrogen absorbed into the Pd electrode per total hydrogen generated are constant. Elongation of the interatomic spacing accompanying hydrogen uptake, which was observed by an X-ray diffraction measurement (Yamamoto *et al.*, 1990), may be responsible for the stress change. On the assumption that the number of reacting electrons is 1, apparent molecular weight of the substance which is deposited on or absorbed into the Pd is estimated as 2.94 g mol^{-1}. This value is much larger than that expected for absorption of hydrogen alone, 1 g mol^{-1}. This results indicates that the frequency change reflects not only the hydrogen absorption but also deposition of other species, change in the surface roughness, and so forth. Then the deposition of lithium is examined next.

Wagner and Gerischer (1989) described about the underpotential deposition of lithium on a gold electrode from acetonitrile solutions containing small amount of water. Here we studied on underpotential deposition of lithium in a propylene carbonate solution containing water by means of electrochemical quartz crystal microbalance technique. Cyclic voltammetric measurements were performed with the Au film-coated At-cut quartz crystal oscillator in propylene carbonate containing 0.1 M $LiClO_4$ and 16 mg L^{-1} water. Figure 3 shows changes in the current and frequency monitored at the first potential scan. Frequency decrease was observed at potentials more negative than -0.6 V vs. Ag; this may reflect the underpotential deposition of lithium because the formal potential of Li/Li^+ couple is -2.96 V vs. Ag. The deposited film blocked the electrode reaction of ferrocene in the solution; this indicates that the film is not conductive. Lithium is speculated to react with water to form insulating compounds, such as lithium hydroxide or lithium hydride, immediately after the deposition. Further, there is another possibility that deposited lithium form an alloy with a substrate electrode. The underpotential deposition of lithium is anticipated to occur even in electrolyte solutions with much higher content of water, though the observation of it is interfered with the hydrogen evolution.

We have reported that a number of cracks and holes were observed on the Pd electrode surface by scanning electron microscopy after a long-time electrolysis (Yamamoto *et al.*, 1990). The increase in roughness of the electrode surface of a quartz crystal oscillator reportedly cause a change in resonant frequency (Schumacher *et al.*, 1985 and 1987). Then, contribution of respective factors, stress change, mass change (hydrogen absorption and lithium deposition), and roughness change, were estimated assuming the ratio of the charge consumed for proton reduction per total charge passed (Table 1). Thus, though some assumptions must be employed, each factor can be estimated by the present technique.

4. References

1. EarNisse, E. P., 1973, *J. Appl. Phys.*, 44, 4482-4485.
2. Oyama, N., Yamamoto, N., Hatozaki, O. and Ohsaka, T., 1990, *Jpn. J. Appl. Phys.*, 29, L818-L821.
3. Schumacher, R., Borges, G. and Kanazawa, K. K., 1985, *Surf. Sci.*, 163, L621-L626.
4. Schumacher, R., Gordon, J. G. and Melroy, O., 1987, *J. Electroanal. Chem.*, 216, 127-135.
5. Wagner, D. and Gerischer, H., 1989, *Electrochim. Acta*, 34, 1351-1356.
6. Yamamoto, N., Ohsaka, T., Terashima, T. and Oyama, N., 1990, *J. Electroanal. Chem.*, 296, 463-471.

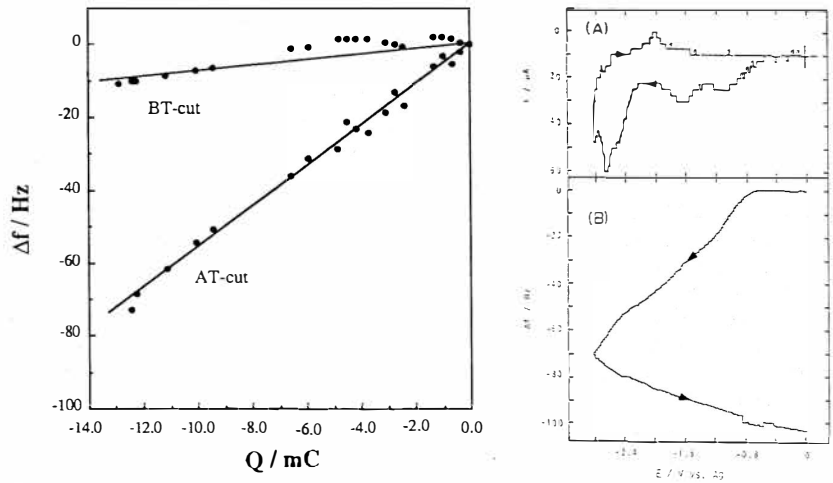

Fig. 1. Plots of the frequency change vs. the anodic charge passed for the galvanostatic electrolysis (-0.02 mA cm^{-2}) at Pd-coated AT-cut and BT-cut quartz crystal (5.0 MHz) in 0.2 M $LiClO_4$ aqueous solution (pH 3.0).

Fig. 3. Cyclic voltammogram (A) and a frequency change-potential curve (B) obtained in propylene carbonate containing 0.1 M $LiClO_4$ at the first potential scan.

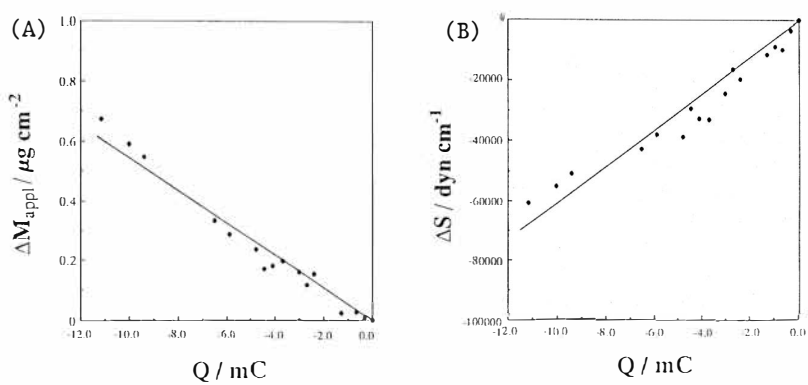

Fig. 2. Correlations between the mass change (A) or the stress change (B) and the anodic charge passed evaluated from the data shown in Fig. 1 using eqs. 4 and 5.

Table 1. Contributions of respective factors to the total frequency change.

$Q_H/(Q_H + Q_{Li})$[a]	Δf_{stress}	Δf_H	Δf_{Li}	Δf_{rough}	Δf_{total}
67	1.43	0.39	1.32	0.00	3.13
90	1.43	0.52	0.40	0.77	3.13

[a] Q_H and Q_{Li} are charges used for reduction of H^+ and Li^+, respectively.

A Role of Lithium for the Neutron Emission in Heavy Water Electrolysis

Mutuhiro NAKADA,* Takehiro KUSUNOKI, Makoto OKAMOTO and Osamu ODAWARA
Tokyo Institute of Technolgy, Ookayama, Meguro-ku, Tokyo, 152 JAPAN

ABSTRACT

The depth plofile analysis of Pd, Li, and D has been perfomed by means of SIMS to clarify the roles of lithium in D_2O Pdelectrolysis for cold fusion research. Very clear differences between the depth profiles of Li and D in the Pd electrode surfaces with the neutron emission and without it. The depth profiles were also found to depend on the mode of the electric currentemployed. Based on the above findings, it is discussedthat the anomalous deutrium accumulation in the surface region of the Pd with the neutron emission attributed to the formation of Pd-Li layer in the surface region and to the Low/High pulse mode electrolysis of heavy water with LiOD.

1. Introduction

Lithium has been recognized as a key element not only for the neutron emission but also for the excess heat in the heavy water elctrolysis method. There has been no clear evidence to discuss the role of lithium in the cold fusion cells.

In the present work, the depth profiles of lithium and deuterium have been deduced from SIMS analysis data of these two elements in the surface region of the Pd electrodes used in the electrolysis of heavy water with LiOD. The depth profiles of the two elements could be enable us to discuss the roles of lithium to accumulate deuterium in the surface region of the Pd cathodes.

* Present address, Hokuriku Electric Power Co. Ltd.

FRONTIERS OF COLD FUSION

2. Experimental

The characteristics of Pd test pieces are listed in Table 1. The test pieces were selected by the following criteria.

(1) Pd electrodes gave the appreciable neutron emission in the Low/High mode electrolysis, Pd-1, Pd-2, Pd-3.
(2) Pd elctrode did not give the neutron emission in Low/High mode electrolysis, Pd-4.
(3) Pd electrode did not give the neutron emission in a consatant current elctrolysis, Pd-5.

The details of the electrolysis experiment and the neutron detection will be described in the proceedings of the present conference [Frontiers of Cold Fusion].

Table 1. The characteristics of the test pieces Pd

Test Piece No.	Electrolysis mode	Current density Low/High	Neutron emission
Pd - 1	L / H	10/200 mA/cm^2	yes
Pd - 2	L / H	10/200 mA/cm^2	yes
Pd - 3	L / H	10/200 mA/cm^2	yes
Pd - 4	L / H	2/40 mA/cm^2	no
Pd - 5	Constant current	40 mA/cm^2	no

The SIMS analysis was performed on a Secondary Ion Mass Spectrometer (IMS-4S, CAMECA/France) at Interdisciplinary Graduate School of Science and Technology, Tokyo Institute of Technology.

3. Results and discussion

As the typical examples of the depth profiles obtained by SIMS analysis are shown in Fig.1 (a) and (b) for the test sample Pd-2 and Pd-5, respectively. In this case the former is a typical sample which gave neutron emission and the latter is a typical sample without neutron emission. Comparing these two profiles, we can find the clear differences in the profiles of lithium and also deuterium between the two graphs. The depth profiles of the two elements at the surface region in Pd-2 have some structures, while the profiles in Pd-5 are monotonous. As will be shown later, the same feature is confirmed in other samples. This point is the first significant difference in the depth profiles of Li and D

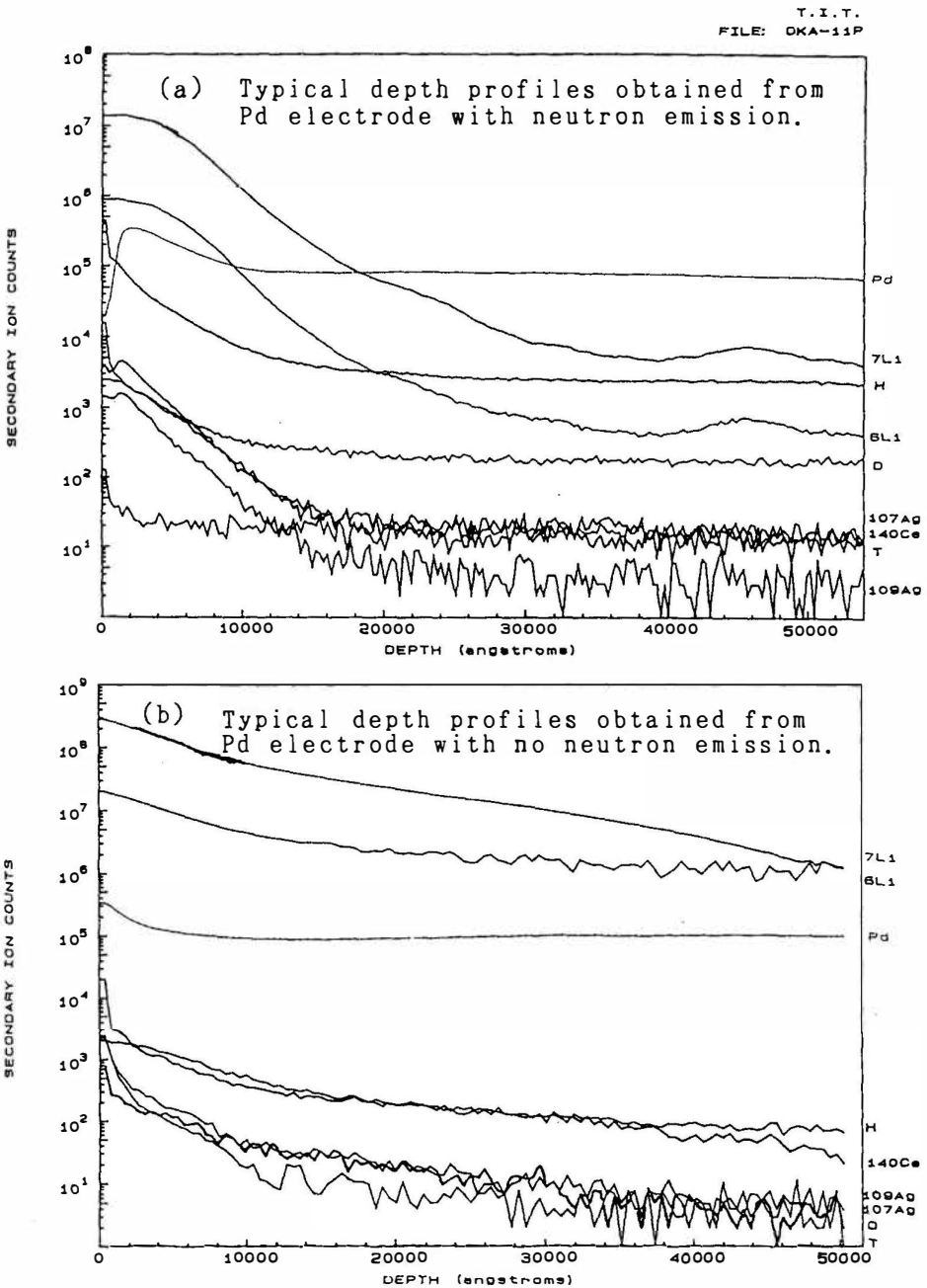

Fig.1 The typical examples of depth profiles obsereved by SIMS analysis.

between the Pd sample with the neutron emission and that without the neutron emission.

The sensitivities for the individual elements in SIMS analysis are very different each other, so the absolute concentration of each elements can not be evaluated from the intensities obtained. The intensity of Pd ions is almost same in the two graphs, we can compare the relative concentration in each element. The lihtium concentration in the surface region in Pd-5 is higher than that of Pd-2, while the concentration of D in the same region in Pd-5 is lower than that of Pd-2. This big difference of deuterium concentartion seems to be the key factor for the occurrence of the neutron emission. This fact is the second siginificant difference found in the depth profiles in the two typical Pd samples.

In Fig.2, the depth profiles of Pd, Li and D are illustrated for the surface region upto 30 μm .The first siginificant difference mentioned above can be evidently foud between the samples with the neutron emission (Pd-1, Pd-2, Pd-3 ; positive group) and those wihtout the neutron emission (Pd-4, Pd-5; negative group). The second point is also clearly confirmed between the positive group and the negative group. We can find that the deuterium concentration in the positive group is much higher than those in the negative group. The anomalous high accumulation of deutrium may have a siginificant contribution to the neutron emission.

The next discussion point is also very important to elucidate the role of lithium for the neutron emission. The depth profiles of lithium have very similar feature to the profiles of deuterium. It means that the deuterium accumulation in the surface region may attribute to the accumulation of lithium in the region. The profiles of Pd also have similar feature to that of lihtium. This fact indicates that Pd-Li compound formation takes place in the surface region.[1] The higher intensities of Pd and Li in the near surface region indicate that the atomic density of Pd and Li in the compound should be larger than that in the bulk of Pd electrode. The layer of the Pd-Li compound works as a barrier to escape the D in the stage of the low current density electrolysis.

Based on the above discussion and the high desorption rate of D from Pd reported by Mizuno[2] a model can be imaged for the mechanism of the anomalous accumulation of deuterium in the surface region.

1) By high current density elctrolysis, lithium and deuterium absorbed into the Pd electrode.
2) Absorbed lihtium formed Pd-Li compound at the surface region.
3) By reducing the current density to the low current density electrolysis, the deuterium moves to the surface with very high migration rate to attain to a

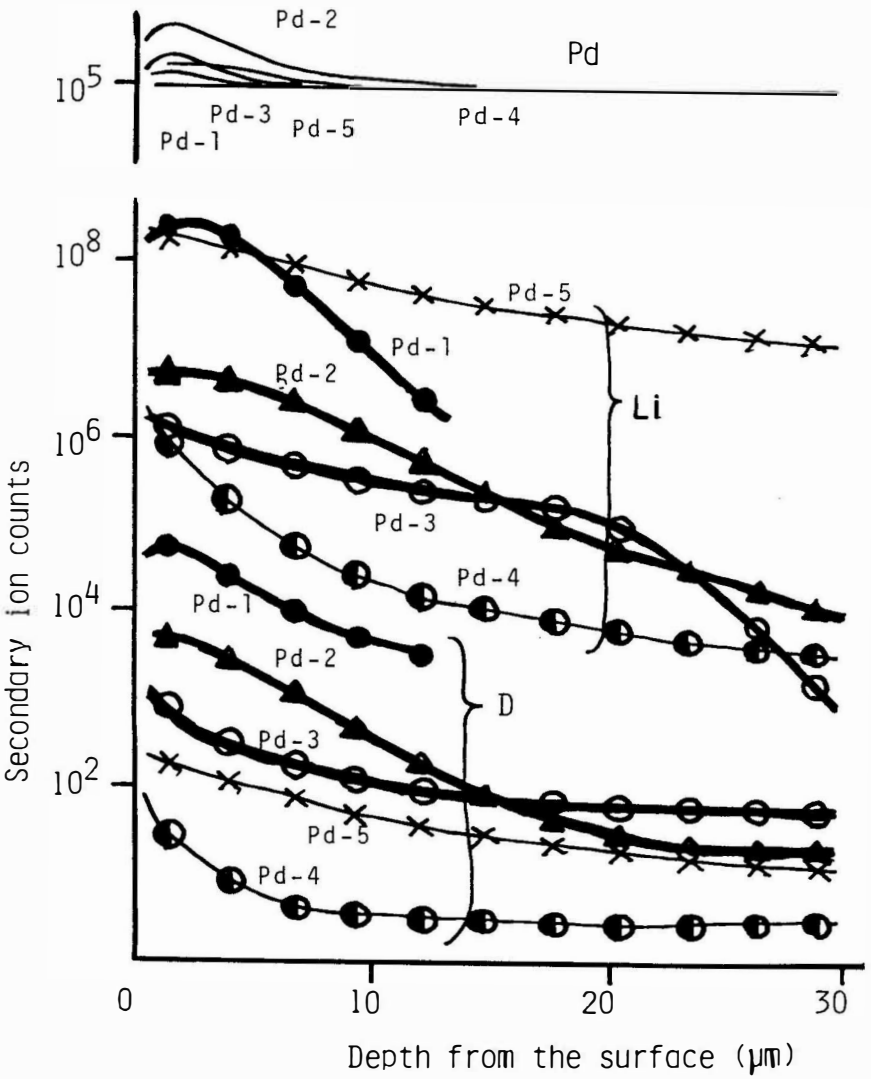

Fig.2 The depth profiles of Li, Pd and D in the surface regio upto 30μm.

In the figure, the bolt lines represent the depth profiles obsereved from the positive Pd samples and the thin lines from the negative Pd samples.

concentration equilibrated to the low current density.
4) The escape of deuterium to the heavy water was disturbed by the Pd-Li compound layer.
5) Thus the deutrium is accumulated anomalously in the surface region. As shown in Fig.2, the concentration of deuterium in the surface region become higher one to two order than that in the bulk.

The SIMS analysis was carried out after the rather long time storage of the electrodes in a sealed glass wear, still then such a depth profile was well kept. It indicates that the Pd-LI-D phase has to be very stable after its formation in the L/H pulse mode electrolysis. In the present work, the neutron emission was found in only the cases of L/H pulse mode electrolysis and the anomalous accumulation of deuterium in the surface region.

4. Conclusion

The depth profiles of Li, D and Pd were obseved by the SIMS technique for several Pd test pieces cut from the Pd electrodes employed in the study of the neutron emission from the heavy water electrolysis using Pd-D_2O-LiOD system. The depth profiles can be classified into two types; one is the profile with a structure and the other is the nomotonous profile. The former was observed on the Pd test piece from the Pd electrode with neutron emission, while the latter was from the Pd electrode wihtout neutron emission.

The structure attributes to the formation of Pd-Li compound in the surface region of the Pd elecrode. The compound works as the barrier to the migration of deuterium from the bulk to the surface at the stage of the low current density electrolysis in L/H pulse mode operation, resulting the anomalous accumulation of deutrium at the surface region of the Pd electrode.

It can be concluded that lihtium forms Pd-Li compound and the formation of the compound causes the high accumulation of deutrium.The anomalous accumulation of deuterium may have an important effect to the neutron emission in Pd-D_2O-LiOD electrolyis.

References

1. Loebich O. Jr. und Raub Ch. J., 1977, J. Less-Common Mtals. 55, 67.

2. Mizuno T. Akimoto T. Azumi K. and Enyo M., 1992, DENKI KAGAKU, 60, No.5, 405.

Chapter IV
Theory and Modeling

Tunnel Disintegration and Neutron Emission Probability

Toyu TANI [1] and Yukio KOBAYASHI [2]

1 Nagase 1194-13, Moroyama-cho, Iruma-gun, Saitama 351-03, JAPAN

2 Frontier Research Program, The Institute of Physical and Chemical Research (RIKEN), Hirosawa 2-1, Wako, Saitama 351-01, JAPAN (Present address : Department of Information Systems Science, Faculty of Engineering, Soka University, 1-236 Tangi-cho, Hachioji-shi, Tokyo 192, JAPAN)

ABSTRACT

It is shown that the main features of the so-called cold fusion, that is, poor reproducibility, high t/n ratio and the energy spectrum of neutrons, can be explained by the "tunnel disintegration" of a deuterium and the subsequent "dipole disintegration" of a deuteron. Especially, the 2.45-MeV peak found in the energy spectrum, which has been considered to be owing to the d-d nuclear fusion, is explained by this mechanism, and therefore the observation of 2.45-MeV neutrons may not be a direct verification of the d-d nuclear fusion.

1. Introduction

Cold nuclear fusion in condensed matter, one of the recent scientific topics which have startled the world, seems to find its reasons in the instability of the deuterium molecule. According to Van Siclen and Jones[1], Koonin and Nauenberg[2] and others, two deuterons in a free deuterium molecule tunnel mutually through the Coulomb barrier to initiate fusion at rates of 10^{-64} to 10^{-74} s^{-1}. However, these estimates of the d-d fusion rate in a free deuterium molecule appear to be not supported by quantum mechanics. First of all, it must be pointed out that the adiabatic approximation, under which estimates of the d-d fusion rate have been made, is not justified at shorter internuclear distances. Second, the electron motion is not correctly taken into consideration in estimating the d-d fusion rate. It is hard to suppose that the electron motion cannot be affected by the tunnel effect. In addition, recent experiments have revealed strange and incomprehensible results from the point of view of the d-d nuclear fusion: That is, high t/n ratio[3] and the neutron energy spectrum showing peaks at about 2.45 and 3 ~ 7 MeV[4]. Theory should be able to explain these experimental results as well as poor reproducibility.

Based on quantum mechanics, one of the authors has shown that the probability of fusion of two nuclei in a composite system, such as a free diatomic molecule, is exactly zero[5]. This implies that as a quantum-mechanical system the composite system should turn into a different system as soon as the two nuclei exceed the range

classically forbidden to approach each other to zero separation. The change considered will be disintegration. From this it has been concluded that when a diatomic molecule interacts so strongly with a metal, such as palladium or titanium, in its surface region that the two nuclei approach each other to exceed the classically forbidden range, it will disintegrate with the transition of the electrons to the states of the continuous spectrum according to the reaction scheme

$$\text{(Dia. Mol.)} + \text{(Metal)} \rightarrow A + B + ne + \text{(Metal)}, \tag{1}$$

where A and B denote the two nuclei of the diatomic molecule, and n is the number of electrons contained in the molecule. We shall call this disintegration "the tunnel disintegration". If this is the case, it is expected that simultaneously with the tunnel disintegration, collective modes will be intensively excited to build up instantaneous strong localized electric fields because the energy released by the tunnel disintegration of a deuterium molecule is of the order of 30 eV. The deuteron is a quite loosely bound nucleus. If, therefore, an isolated deuteron is placed in a strong external electric field, there is a chance that dipole oscillations will be excited between the proton and neutron in the deuteron. If the localized electric field induced by the tunnel disintegration of deuterium ions D_2^+ is relatively slowly varying one (as compared with the characteristic period ($\sim 10^{-21}$s) of the nuclear motion), then it is possible that the deuteron ground state is prepared by the electric field for "dipole disintegration". In the present paper we calculate the probability of dipole disintegration of the deuteron, assuming for the localized electric field a pulse-like variation of the form

$$f(t)=\varepsilon_0 \lambda t(2-\lambda t)\exp(-\lambda t) \tag{2}$$

with $\varepsilon_0 = 1.0\cdot 10^{20}$ (V/m) and $\lambda = 1.0\cdot 10^{17}(s^{-1})$.

2. Tunnel Disintegration

Consider a diatomic molecule with n electrons. Hereafter, a representation in which its center-of-mass coordinates are separated from the other coordinates will be referred to as the center-of-mass representation, and a representation in which the coordinates of the constituent particles are separated from each other will be referred to as the particle representation. It will be a natural requirement that the center-of-mass representation and the particle representation should be equivalent over the whole region of configuration space. It, however, can be shown that we can pass from the center-of-mass representation to the particle representation if and only if the Hamiltonians H_A and H_B of the nuclei A and B of the diatomic molecule are separately Hermitian. In the center-of-mass representation the Hamiltonians H_A and H_B are given by

$$H_A = \frac{\mathbf{p}_R^2}{2M_A} + \frac{1}{2} M_A \mathbf{V}^2 + \mathbf{P}_R \cdot \mathbf{V} \tag{3}$$

$$H_B = \frac{\mathbf{p}_R^2}{2M_B} + \frac{1}{2} M_B \mathbf{V}^2 - \mathbf{P}_R \cdot \mathbf{V} \tag{4}$$

where

$$\mathbf{V} = \frac{\mathbf{P}_1}{M_A+M_B} + \frac{\mathbf{P}_2}{M_A+M_B+m} + \ldots + \frac{\mathbf{P}_n}{M_A+M_B+(n-1)m} \tag{5}$$

In Eqs. (3), (4) and (5) $\mathbf{P}_R$ is the relative momentum of the nucleus B with respect to the nucleus A with M_A and M_B the respective masses of the nuclei A and B and with m

the electron mass, and $\mathbf{P}_i$ the relative momentum of the ith electron with respect to the center of mass of a subsystem consisting of the two nuclei and the 1st, 2nd,..., (i-1)th electrons. We can show that if the wave function describing the nuclear relative motion has a tail which penetrates to the interior of the classically forbidden range, then the Hamiltonians H_A and H_B will cease to be Hermitian separately. Therefore, in such a case, we cannot pass from the center-of-mass representation to the particle representation; in other words, we cannot define any unitary operator connecting the wave functions in both the representations. From the equivalency requirement of both the representations it has been concluded that when the diatomic molecule interacts so strongly with a metal in its surface region that two nuclei approach each other to exceed the classically forbidden range, one should expect the disintegration of the molecule as a quantum-mechanical system. This is what we called "the tunnel disintegration".

3. Dipole Disintegration of a Deuteron and Far-distant Interaction

The tunnel disintegration of deuterium ions is expected to lead to the occurrence of an intense localized electric field in condensed matter. In what follows we shall consider a deuteron from a collapsed ionized deuterium molecule. The localized electric field will act on the proton of the deuteron. If the localized electric field varies quickly, we cannot expect any nuclear phenomenon from this electric action. If it, on the contrary, varies slowly compared with the characteristic period of the nuclear motion, then the deuteron will be capable of absorbing energy from the localized electric field, hence we can expect nuclear phenomena. Considered are nuclear dipole oscillations excited between the proton and neutron in the deuteron. When the localized electric field is relatively slowly varying one, the amplitude of dipole oscillations will be gradually increased, as a result of which there will happen a chance of disintegrating.

For simplicity we assume that the localized electric field is in the z-direction. The Schrödinger equation for the deuteron under the action of the localized electric field is then

$$i\hbar\frac{\partial\Psi}{\partial t} = H_r\Psi \tag{6}$$

with $$H_r = H_0 - \frac{eM_n}{M} f(t)\, z, \tag{7}$$

where H_0 is the unperturbed Hamiltonian with a spin-dependent square-well potential, and the second term represents a time-dependent perturbation due to the localized electric field with z the z-component of the distance $\mathbf{r}$ between the nucleons, f(t) being given by Eq.(2), M being the total mass with M_n the neutron mass, and e being the elementary charge. In the first approximation the solution of Eq.(6) is given by

$$\Psi(\mathbf{r},t) = e^{\frac{-i}{\hbar}E_0 t}\psi_0^{(0)}(\mathbf{r}) + \sum_k a_k^{(0)}(t)\, e^{\frac{-i}{\hbar}E_k^{(0)}t}\psi_k^{(0)}(\mathbf{r}) \tag{8}$$

where $H_0\psi_0^{(0)}(\mathbf{r}) = E_0\psi_0^{(0)}(\mathbf{r})$ and $H_0\psi_k^{(0)}(\mathbf{r}) = E_k^{(0)}\psi_k^{(0)}(\mathbf{r})$. $\psi_0^{(0)}(\mathbf{r})$ represents a $^3S_1$ state and $\psi_k^{(0)}(\mathbf{r})$ ^3P states. At t=T at which the amplitude of dipole oscillations reach a maximum, the "dipole disintegration" of the deuteron is initiated. The Hamiltonian describing this decaying process is given by

$$H_r = \overline{H_0} + V_{res}(r) - \frac{eM_n}{M} f(t)\, z, \tag{9}$$

where $\overline{H_0}$ is a self-consistently constructed Hamiltonian. We here must point out that

a "far-distant" interaction $V_{res}(r)$, which has been hitherto neglected, should be taken into account under the action of the localized electric field. For $t > T$ we expand the solution of Eq.(6) in the form

$$\Psi(r,t) = e^{\frac{-i}{\hbar}E^{(1)}(t-T)}\psi_0^{(1)}(r) + \sum_{l,m}\int a_{Elm}(t)e^{\frac{-i}{\hbar}E(t-T)}\psi_{Elm}^{(0)}(r)dE, \tag{10}$$

where $\overline{H_0}\,\psi_0^{(1)}(r) = E^{(1)}\psi_0^{(1)}(r)$,

$$\psi_0^{(1)}(r) = N\left(\psi_0^{(0)}(r) + \sum_k a_k^{(0)}(T)\, e^{\frac{-i}{\hbar}(E_k^{(0)}-E^{(1)})T}\psi_k^{(0)}(r)\right), \tag{11}$$

and $\overline{H_0}\,\psi_{Elm}^{(0)}(r) = E\,\psi_{Elm}^{(0)}(r)$ $\quad (E > 0).$ (12)

The probability that the neutron is ejected with energy between E and E + dE by nuclear dipole oscillations is

$$\sum_{lm}|a_{Elm}(\infty)|^2\,dE \tag{13}$$

4. Results and Conclusions

As is seen above, our theory reasonably explains the poor reproducibility of the phenomena observed.

Taking, with a view to investigate the validity of the theory, for the Hamiltonian $\overline{H_0}$ spin-dependent square-well potentials with E_0, $E_k^{(0)}$ and the well depths as parameters, and assuming for $V_{res}(r)$ a potential of δ-function type of the form

$$V_{res}(r) = V\,\delta(r - a) \qquad (a \sim 30\ \text{fm};\ V = 1.0\ \text{MeV}), \tag{14}$$

we calculated the probability of dipole oscillations, i.e., the neutron emission probability. Figure 1 shows a result of calculations. From this we find that the neutron emission probability has three peaks at C.M. energies of about 0.01 MeV, 4.9 MeV and ~ 12 MeV, which correspond to laboratory energies of about 0.005 MeV, 2.45 MeV and ~ 6 MeV, respectively. Especially, the ratio of the emission probability at the extremely low energies to that at 4.9 MeV is of the order of 10^5, which will explain the large t/n ratio reported. We therefore conclude that the main features of the observed phenomena can be reasonably explained by the theory of dipole disintegration.

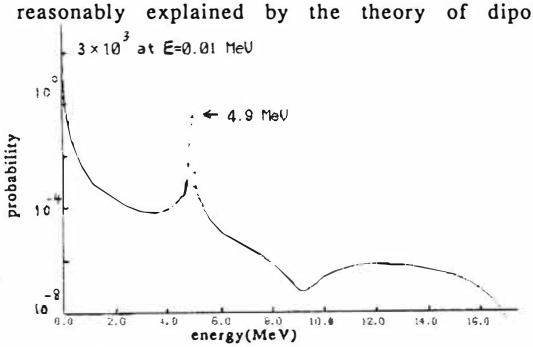

Figure 1. Neutron emission probability by the dipole disintegration.

5. References

1. Van Siclen, C. Dew. and Jones, S. E., 1986, J. Phys. G 12, 213.
2. Koonin, S. E. and Nauenberg, M., 1989, Nature, 690.
3. Proc. 1st Annual Conf. Cold Fusion, 1990, Salt Lake City.
4. Takahashi, A. et al., 1990, J. Nucl. Sci. and Technol. 27, 663.
5. Tani, T., 1990, unpublished paper.

Field Formation of the Condensed Matter Fusion by Electro-Transport of Deuterium in Palladium

Masayoshi TAMAKI and Kanji TASAKA
Department of Nuclear Engineering, Nagoya University
Furo-cho, Chikusa-ku, Nagoya 464-01
JAPAN

ABSTRACT

A model of cold fusion was proposed. Electrotransport effect on deuterium in palladium was crystallographically examined and verified for the field formation of the condensed matter fusion. Electrotransported palladium hydride was analyzed by neutron radiography technique. The effective number of the electric charge of hydrogen in $PdH_{0.67}$ was evaluated to be $+0.30\pm0.05$.

1. Introduction

This paper concerns (1) to propose a model of electrotransport (ET) effect on deuterium (D) in palladium (Pd) for the field formation of the condensed matter fusion (cold fusion), (2) to verify the effectiveness of the D densification in PdD, (3) to visualize the hydrogen (H) distribution in PdH by neutron radiography, and (4) to analyze its intrinsic physical property. PdH (D, T) is a well-known material which shows superconductivity, and its transition temperature depends on its nonstoichiometry [1]. In order to prepare the high H density ((H/Pd) ratio>1) in PdH, electrolysis of water as well as absorption of H under high pressure and cryogenic temperature had been applied by many investigators [2]. On the experiment for the cold fusion, the same approaches had been adopted for the hydrogenation of Pd and Ti. When modeling the system analytically in the case of the electrolysis of heavy water, we must take into account of not only electrolysis process (<1>+<2>) but also ET effect on H in Pd metal under electric field (<3>+<4>) as shown below:

$$D^{+}_{aq}=\langle 1\rangle=[Pd+D]_{ads}=\langle 2\rangle=PdD_{surf}=\langle 3\rangle=PdD(\alpha)_{bulk}=\langle 4\rangle=PdD(\beta)_{bulk}$$

Diffusion of H in bulk Pd under external forces such as ET and thermotransport [3] is an important subject. Especially the ET effect is an essential factor.

FRONTIERS OF COLD FUSION

2. Theory of ET of D in Pd

A model of the ET of D in Pd metal matrix for the field formation of the condensed matter fusion (cold fusion) is shown in Fig. 1. D as well as H and T are transported and compressed at the anodic side (-) of the Pd specimen by the applied electric field (E). The expression of the process was given by force of ET and Fick's second law [4, 5]. The driving force of the ET of D in metal is presented by $F = e E Z^*$. Here e is the electron charge unit, E the applied electric field and Z^* the effective number of the electric charge of D in metal. The H number density in the metal matrix at the anodic side (-) is evaluated to be approximately multiplied by $\exp(-eEZ^*/kT)$ in comparison with that of the cathodic electrode side (+) for specified initial and boundary conditions. This principle has been applied to the transportation and densification of D as well as H in the Pd metal and Pd alloy (Pd (Au, Ag)) in order to verify experimentally its effectiveness and to simulate the field formation of the condensed matter fusion.

3. Experiments

3. 1. ET of D in Pd (Au, Ag)

First experimental run was conducted to verify the ET effect on D in the process of the densification of D in the Pd metal matrix. A special ET Pd alloy electrode was prepared as shown in Fig. 2. The Pd alloy part were plated with Cu and Au thin film to hold D in the bulk Pd alloy. The electrode was set up in the heat pipe temperature control system as shown in Fig. 3. D_2 gas ($2.6 kg/cm^2$) was supplied to be absorbed by the Pd alloy electrode. 40A-7V DC was applied to the Pd electrode at about 100℃ for 21days before Pd-sheet fused down. The typical experimental conditions were indicated in Fig. 3. From the X-ray diffraction analysis of the electrotransported Pd (Au, Ag) D, the D transportation and densification in the electrode was evaluated crystallographically.

3. 2. Neutron Radiography of H in ET Pd Metal

Second run was carried out for the analysis of H distribution in Pd. The experimental condition of the ET was similar to that of the first run. Pd metal wire (2. 0mm in dia.) with heat treatment (1000℃, 2h, in vacuum) was prepared as the ET specimen. The Pd wire about 50mm was attached to Cu electrodes, and hydrogenated at 160℃ for 10h under 0. 2 MPa H_2 gas. Then the hydrogenated Pd wire with Cu electrodes was plated with Cu (0. 02mm) and Au (0. 01mm) double layers by electrolysis. The ET element was set up in the similar manner as shown in Fig. 3. The transportation, redistribution and densification of H in PdH by the ET function was carried out under the experimental conditions; temperature around 120℃, applied DC power of 47A-55mV, and overall operation of 9 weeks. H distribution was tested nondestructively using neutron radiography for the PdH sample electrotransported for 3, 6 and 9 weeks.

4. Results and Discussions

4. 1. PdD Lattice Parameter

The lattice parameter of the fused electrotransported Pd(Au, Ag) element was evaluated as shown in Fig. 4. Axial distribution of the lattice parameter was illustrated with the estimated axial profile of the applied electric potential and Pd(Au, Ag) sheet temperature. The position of the arrow indicated the fused section of the Pd-sheet after 21 days operation. The lattice parameter of the Pd-sheet after annealing at 200℃ was also plotted. The difference of the lattice parameter of Pd alloy sheet between as ET and after annealing is considered to be proportional to the D content in the ET element. This shows that the ET effect in the D absorption of the Pd alloy was confirmed.

4. 2. Neutron Radiographic Analysis of PdH

The redistribution of H in PdH by the ET was visually confirmed by neutron radiography [5]. Fig. 5 shows the time-dependent redistribution of H in PdH by the ET process. The homogeneous H of initial (H/Pd) ratio of 0. 67 was redistributed to the linear distribution from 0. 55 at the positive electrode side to 0. 70 at the negative electrode side after 9 weeks operation. From the H distribution, the effective electric charge number of the H atom in PdH was evaluated to be about 0.30 ± 0.05. This value is lower than the literature value (0. 54) due to much higher H content (0. 55-0. 70 in (H/Pd) ratio) in the present case than 0. 01 in (H/Pd) ratio in the literature cases [3].

5. Conclusions

In conclusions, the ET effect on D in PdD was proposed for the modeling of the field formation of the condensed matter fusion (cold fusion) and verified experimentally. The effectiveness of the ET for the D and H densification in the Pd was confirmed by the X-ray diffraction analysis as well as neutron radiography.

6. Acknowledgement

Authors would like to thank to Mr. H. Matsunaga for his experimental help.

7. References

[1] Lässer, R., Tritium and Helium-3 in Metals (Springer-Verlag, Berlin, 1989), p. 90.
[2] Stritzker, B. and Wühl, H., Hydrogen in Metals II (Springer-Verlag, Berlin, 1978), p. 243.
[3] Wipf, H., Hydrogen in Metals II (Springer-Verlag, Berlin, 1978), p. 273.
[4] Pratt, J. N. and Sellors, R. G. R., Electrotransport in Metals and Alloys (TRANS TECH SA, Switzerland, 1973), p. 26.
[5] Tamaki, M. et al, Neutron Radiographic Analysis of Distribution of Electrotransported Hydrogen in Palladium, 4th World Conference on Neutron Radiography, May 11-16, 1992, San Francisco, USA.

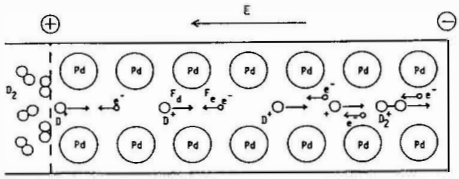

Fig.1 Model of Electrotransport of Deuterium in Palladium Metal

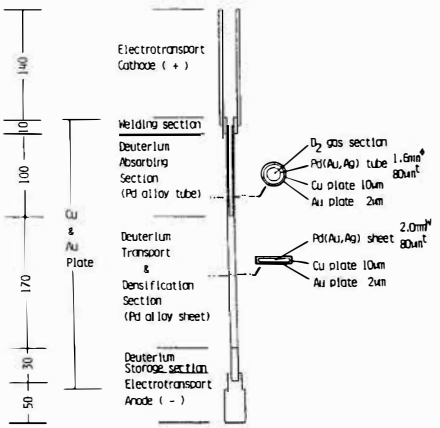

Fig.2 Pd(Au,Ag) Electrotransport Element

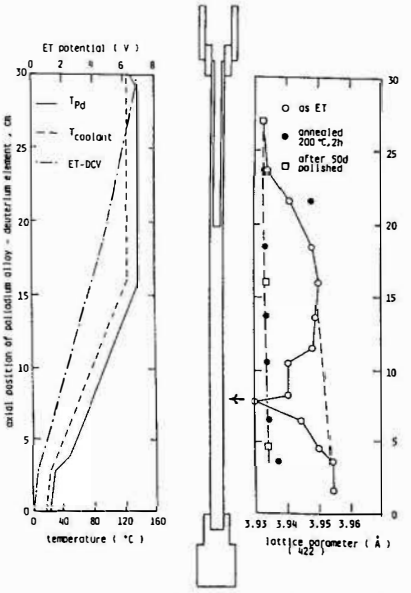

Fig.4 Axial Distribution of Electric Potential, Temperature and Lattice Parameter in the Electrotransported Pd Element

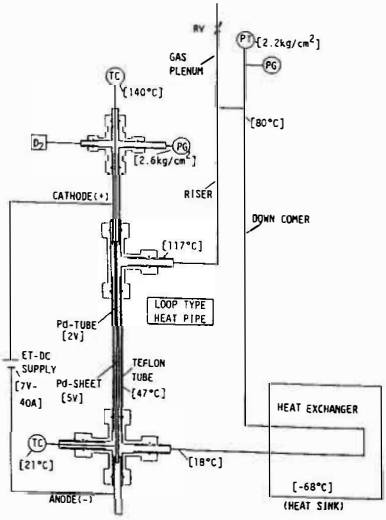

Fig.3 Experimental Setup for Electrotransport of D in Pd

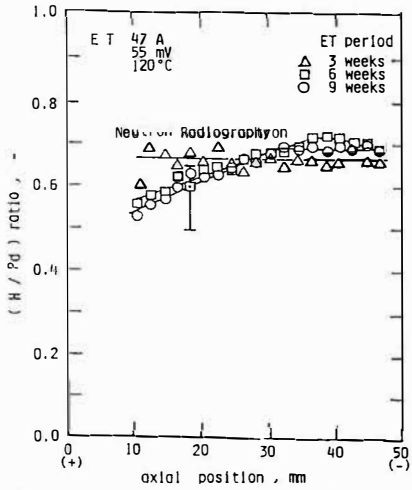

Fig.5 Relation between (H/Pd) and Axial Position in Electrotransported PdH, evaluated by Neutron Radiography

The Combined Resonance Tunneling and Semi-Reasonance Level in Low Energy D-D Reaction

Xing Zhong LI, De Zhe Jin, Lee Chang
Department of Physics, Tsinghua University
Beijing 100084
CHINA

ABSTRACT

When nuclear potential wells are connected by an atomic potential well, a new kind of tunneling may happen even if there is no virtual energy level in nuclear potential wells. The necessary condition for this combined resonance tunneling is the resonance in the atomic potential well. Thus, the nuclear reaction may be affected by the action in atomic scale in terms of combined resonance tunneling. The nuclear spectrum data support this idea.

1. Introduction

While more evidences are confirming the anomalous nuclear phenomena in deuterium / solid system, there are still two puzzels remaining: i.e. the penetration of Coulomb barrier at low energy, and why the process in nuclear scale is affected by the parametric variation in atomic scale.

2. Combined Resonance Tunneling in a New Matrix Formalism

It is well known in quantum mechanics that the potential barriers in Fig.1 may be penetrated without any reflection when the energy of the incident nucleus is in resonance with the virtual energy level of the potential well between the barriers. The penetration may be expressed in a matrix formalism with the new base functions at each interface between the barrier and the well. Under the WKB approximation [1], the solutions of Schrodinger equation in regions Ⅰ, Ⅱ, Ⅲ, Ⅳ and Ⅴ may be written as

$$\psi_{\mathrm{I}} = \frac{1}{\sqrt{k}}\left\{A_a \cos\left[\int_a^x k\,dx - \frac{\pi}{4}\right] + B_a \sin\left[\int_a^x k\,dx - \frac{\pi}{4}\right]\right\}$$

FRONTIERS OF COLD FUSION

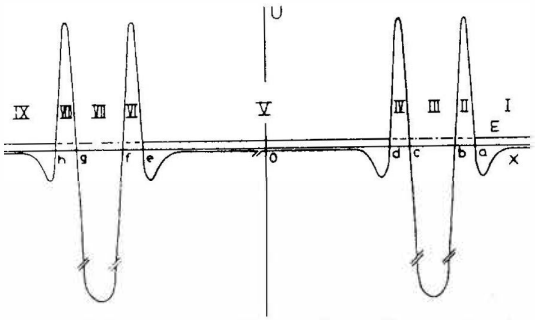

Fig.1 The Combined Resonance Tunneling of Two Barrier–Well–Barriers.

$$\psi_{II} = \frac{1}{\sqrt{\beta}}\left\{C_a \exp[-\int_x^a \beta dx] + D_a \exp[\int_x^a \beta dx]\right\}$$
$$= \frac{1}{\sqrt{\beta}}\left\{C_b \exp[-\int_b^x \beta dx] + D_b \exp[\int_b^x \beta dx]\right\}$$
$$\psi_{III} = \frac{1}{\sqrt{k}}\left\{A_b \cos[\int_x^b k dx - \frac{\pi}{4}] + B_b \sin[\int_x^b k dx - \frac{\pi}{4}]\right\}$$
$$= \frac{1}{\sqrt{k}}\left\{A_c \cos[\int_c^x k dx - \frac{\pi}{4}] + B_c \sin[\int_c^x k dx - \frac{\pi}{4}]\right\}$$
$$\psi_{IV} = \frac{1}{\sqrt{\beta}}\left\{C_c \exp[-\int_x^c \beta dx] + D_c \exp[\int_x^c \beta dx]\right\}$$
$$= \frac{1}{\sqrt{\beta}}\left\{C_d \exp[-\int_d^x \beta dx] + D_d \exp[\int_d^x \beta dx]\right\}$$
$$\psi_V = \frac{1}{\sqrt{k}}\left\{A_d \cos[\int_x^d k dx - \frac{\pi}{4}] + B_d \sin[\int_x^d k dx - \frac{\pi}{4}]\right\}$$

Here $k^2 \equiv (2\mu/h^2)\,(E - U(x))$, $\beta^2 \equiv (2\mu/h^2)\,(U(x) - E)$. μ and E are the mass and the total energy of the particle, respectively. h is the Planck constant divided by 2π. U(x) is the potential energy. Using the WKB connection formula, the relation between coefficients may be expressed in matrix form as

$$\begin{bmatrix} C_a \\ D_a \end{bmatrix} = C_{BW}\begin{bmatrix} A_a \\ B_a \end{bmatrix} = \begin{bmatrix} \frac{1}{2} & 0 \\ 0 & -1 \end{bmatrix}\begin{bmatrix} A_a \\ B_a \end{bmatrix}$$
$$\begin{bmatrix} C_b \\ D_b \end{bmatrix} = B_{ba}\begin{bmatrix} C_a \\ D_a \end{bmatrix} = \begin{bmatrix} 0 & \theta_2 \\ \theta_2^{-1} & 0 \end{bmatrix}\begin{bmatrix} C_a \\ D_a \end{bmatrix}$$
$$\begin{bmatrix} A_b \\ B_b \end{bmatrix} = C_{WB}\begin{bmatrix} C_b \\ D_b \end{bmatrix} = \begin{bmatrix} 2 & 0 \\ 0 & -1 \end{bmatrix}\begin{bmatrix} C_b \\ D_b \end{bmatrix}$$
$$\begin{bmatrix} A_c \\ B_c \end{bmatrix} = W_{cb}\begin{bmatrix} A_b \\ B_b \end{bmatrix} = \begin{bmatrix} \sin\gamma_{cb} & -\cos\gamma_{cb} \\ -\cos\gamma_{cb} & -\sin\gamma_{cb} \end{bmatrix}\begin{bmatrix} A_b \\ B_b \end{bmatrix}$$

$$\begin{bmatrix} C_c \\ D_c \end{bmatrix} = C_{BW} \begin{bmatrix} A_c \\ B_c \end{bmatrix} = \begin{bmatrix} \frac{1}{2} & 0 \\ 0 & -1 \end{bmatrix} \begin{bmatrix} A_c \\ B_c \end{bmatrix}$$

$$\begin{bmatrix} C_d \\ D_d \end{bmatrix} = B_{dc} \begin{bmatrix} C_c \\ D_c \end{bmatrix} = \begin{bmatrix} 0 & \theta_4 \\ \theta_4^{-1} & 0 \end{bmatrix} \begin{bmatrix} C_c \\ D_c \end{bmatrix}$$

$$\begin{bmatrix} A_d \\ B_d \end{bmatrix} = C_{WB} \begin{bmatrix} C_d \\ D_d \end{bmatrix} = \begin{bmatrix} 2 & 0 \\ 0 & -1 \end{bmatrix} \begin{bmatrix} C_d \\ D_d \end{bmatrix}$$

Here $\theta_2 \equiv \exp[\int_b^a \beta dx]$, $\theta_4 \equiv \exp[\int_d^c \beta dx]$, and $\theta_2 = \theta_4 = \theta$ is assumed hereinafter due to the symmetry. Usually, θ is a very large number. $\gamma_{cb} \equiv \int_c^b k dx$. We may define a matrix, T_{da}, to transform the cofficients $\begin{bmatrix} A_a \\ B_a \end{bmatrix}$ in region I to the cofficients $\begin{bmatrix} A_d \\ B_d \end{bmatrix}$ in region V.

$$T_{da} \equiv (C_{WB} B_{dc} C_{BW}) W_{cb} (C_{WB} B_{ba} C_{BW})$$

$$= \begin{bmatrix} -\sin\gamma_{cb} & -(2\theta)^2 \cos\gamma_{cb} \\ -(\frac{1}{2\theta})^2 \cos\gamma_{cb} & \sin\gamma_{cb} \end{bmatrix}$$

An outgoing wave in region I, $\frac{1}{\sqrt{k}} \exp[i(\int_a^x k dx - \frac{\pi}{4})]$, corresponds to $\begin{bmatrix} A_a \\ B_a \end{bmatrix} = \begin{bmatrix} 1 \\ i \end{bmatrix}$. It may be connected to an incident wave in region V, $\frac{1}{\sqrt{k}} \exp[-i(\int_x^d k dx - \frac{\pi}{4})]$, which corresponds to $\begin{bmatrix} A_d \\ B_d \end{bmatrix} = \begin{bmatrix} 1 \\ -i \end{bmatrix}$. When the energy of incident particle, E, is in resonance with the meta-stable energy level in potential well III, then $\gamma_{cb} = (n + \frac{1}{2})\pi$, and this connection is possible, which means a perfect penetration of barrier-well-barrier combination. However, experiments do not show any evidence for this resonance energy level. Instead we propose another possible connection, i.e. the barrier-well-barrier (abcd) is combined to another barrier-well-barrier (efgh) by an atomic well region V. Now, if $\gamma_{cb} = \gamma_{gf} = n\pi$ ($n = 0, 1, 2 \cdots$) and $\gamma_{ed} = (m + \frac{1}{2})\pi$, $(m = 0,1,2\cdots)$, the connection matrix for this combination is

$$T_{ha} \equiv T_{he} W_{ed} T_{da} = (-1)^{n+1} \begin{bmatrix} 1 & 0 \\ 0 & -1 \end{bmatrix}$$

This is again the right connection matrix for a perfect penetration through (hgfe) and (dcba) in Fig. 1. We may call this the combined resonance tunneling, because two semi-resonances in nuclear wells ($\gamma_{cb} = \gamma_{gf} = n\pi$) are combined by an atomic resonance well ($\gamma_{ed} = (m + \frac{1}{2})\pi$).

3. Semi-Resonance Energy Level in D-D System

We must first answer the question whether there is any semi-resonance level near E=0 in Fig.1. Fig.2 shows the experimental data [2] for states of the mass number 4 with charge number 2. It is interesting to notice that there are two energy levels just equally above and below 23.8 MeV, (In Fig.2 E=0 has been set for ^{4}He ground state; therefore, E=23.8MeV in Fig.2 corresponds to E=0 in Fig.1). The energy of these two levels are 25.5MeV and 22.1MeV, respectively. These two resonance levels may correspond to condition

$$\left[\int_c^b k dx\right]_{E=22.1MeV} = (n + \frac{1}{2})\pi \qquad (n = 0,1,2,\cdots\cdots)$$

and $$\left[\int_c^b k dx\right]_{E=25.5MeV} = (n + 1 + \frac{1}{2})\pi$$

The linear interpolation of these two levels would give

$$\left[\int_c^b k dx\right]_{E=23.8MeV} = (n + 1)\pi$$

This is just the condition for semi-resonance energy level in a nuclear potential well.In order to obtain the combined resonance tunneling, a resonance energy level for atomic potential well (region V in Fig.1) is the key point.

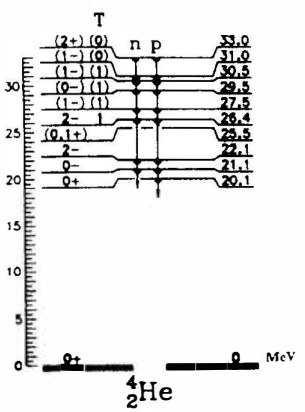

Fig.2 Data Showing Semi-Resonance Level.

---

* This research is supported by the Natural Science Foundation of China, and the State Commission of Science and Technology.

[1.] D.Bohm, Quantum Theory, Prentice-hall Inc. New York (1954).
[2.] C.M.Lederer, and V.S.Shirley, Table of Isotopes (7-th edition), John Wiley & Sons Inc., New York (1978).

Lawson Criterion Made Obsolete by Cold Fusion through the Double Screening Process

Michel RAMBAUT
57H rue De La Hacquinière, 91440, Bures-sur-Yvette, FRANCE

Abstract:

It is shown that the same phenomenon has been observed in Cold Fusion and also in another rather different experiments. The necessity to take into account the electron participation in nuclear fusion process in dense media is ensuing from this result. It implies that the fusion reaction rate, necessary for obtaining the Lawson criterion in the thermonuclear case, is not any valid in those experiments: so a new formula is proposed.

1. Introduction: Correlation between experiments

Nuclear fusion reaction counting data from diverse tentative fusion experiments have been plotted in function of deuteron energy E in logarithmic scale (Figure 1). Those experiments were of three kinds: the D^2O cluster collision experiments, the transitory flow of current pattern in deuterated media, and the so called cold fusion experiments [1]. It turned out that those experiments were non-thermonuclear origin and that the mean square method applied to the experiment representative points, could lead to a fit with a straight line whose slope was bounded between 1.5 and 2.

This correlation suggested that there could be a common cause of the fusion reaction production in very different experiments

The hypothesis which was been made consisted of taking into account the role of all plasma constituents, particularly the electrons, whereas the thermonuclear hypothesis takes only into account the ion existence.[2]

FRONTIERS OF COLD FUSION

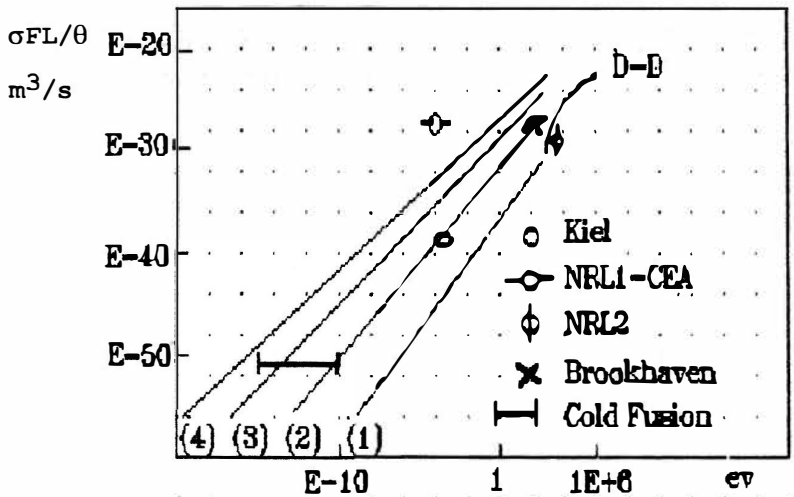

Figure 1. Fusion production factor $\sigma FL/\theta$ in function of deuteron energy in logarithmic scale. The number of electrons per cloud is respectively: (1) 342, (2) 1350, (3) 3374, (4) 5.10^4. The arc D-D corresponds to the thermonuclear case.

2. Double screening process.

There are two causes of modifying the Coulomb barrier between two colliding deuterons. Firstly the cloud of moving electrons, with their great mobility, from the nearby environment towards the positive potential accident created by the two colliding deuterons. Secondly a change of reference potential V_p at the colliding place due to the environmental electron depopulation. The whole phenomenon can be called "Double Screening", inspite the first effect is less important than the second one. This reasoning leads to an effective expression in function of radius r, outside the nuclear well, which has the form,

$$V = f(e/r - V_p) \qquad (1)$$

This potential is close to the one proposed phenomenologically by many authors [2].

$$V = (e^2/4\varepsilon_0)[(1/r) - (1/R)] \ , \ r_1 < r < R \qquad (2)$$

For calculating the barrier transmission factor F, the non relativistic Schrödinger equation is useful. One can drop the L-term, as the wavelength of partial amplitudes is large [2].

One has to take into account the real useful parameters in this process: the nuclear reaction rate R, the nuclear cross section σ, the whole barrier crossing duration θ, the barrier width L, the transmission barrier factor F, the number n of particles which can be involved in a nuclear reaction. Using an improved dimensional analysis method [2], one gets the following formula:

$$R = (n^2/4)\ \sigma FL/\theta \qquad (3)$$

It replaces the customary expression, valid only in the thermonuclear hypothesis and which imply the Lawson criterion:

$$R = (n^2/4)\ \langle\sigma v\rangle \qquad (4)$$

3. Results of calculations.

The results of the barrier transmission factor calculations, give a straight line in the log R diagramm vs log E, for a constant number of electrons contributing to the Double Screening (Figure 1). The slope of those straight lines is close to the slope of the straight regression line, deduced from the experimental points. The most probable number of those electrons is in the range of 10^3 to $2\ 10^3$.

Moreover this number is in agreement with simple ion distribution considerations in dense media, this point of view consisting of assuming that the 3D spatial deuteron distribution obeys Poisson's law [2].

The results of those calculations are also in agreement with several experimental results, the most striking being the Brookhaven results of D^2O colliding clusters [3]. The number of nuclear fusion reactions has a maximum in function of the D^2O molecule number in the cluster (Figure 2). For a D^2O number inferior to the one of maximum there is one unique deuteron collision center. The maximum corresponds to the turning up of two deuteron collision points . Those two collision centers are competitor for attracting the environmental electrons.

A D^2O collision experiment performed with a greater number of D^2O molecules in the cluster would probably give another maximum counting rate followed by a decrease, corresponding to the turning up of three deuteron collision centers.

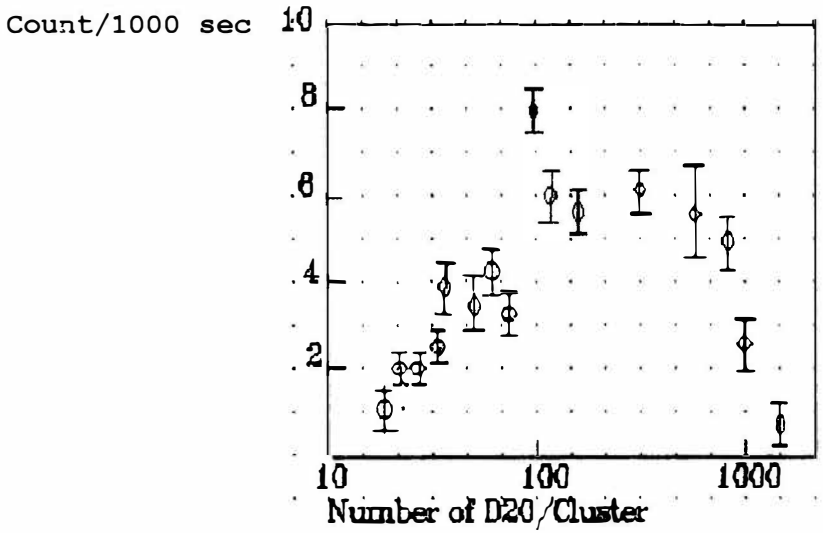

Figure 2. From [3]. The proton yield dependence on the cluster size.is depicted for 300 kev clusters.

4. Ccnclusions

Electrons play a fundamental role in a nuclear process. An experiment performed by M.Fallavier et Al [4] , with pure deuteron clusters has not given any fusion reaction. According the double screening model, clusters must be rich in electrons for sustaining fusion reactions. It builds up the conjecture which consist to suppose, as made J.Schwinger [5], that the D(D,^{4}He)gamma reaction becomes probable. So it could account for the mysterious excess heat production, given that ^{4}He nuclei have a very short range in dense media, and can so produce gammas and heat.

6. References

[1] M.Rambaut, Physics Letters A 163 (1992) 335-342, 30 march 1992.
[2] M.Rambaut, Physics Letters A 164 (1992), 155-163, 13 April 1992.
[3] R.J.Beuhler, G.Friedlander, and L.Friedman, Physical Review Letters, Volume 63, Number 12, 18 September 1989, PP 1292-1295.
[4] M.Fallavier, J.Kemmler, R.Kirsch, J.C.Poizat, J.Remilleux, and J.P.Thomas, Physical Review Letters, Volume 65, Number 5, 30 july 1990.
[5] J.Schwinger, Z.Naturforschung 45a, 756 (1990).

Fractofusion Mechanism

Kyuichi YASUI
Department of Physics, Waseda University
3-4-1 Ohkubo, Shinjuku, Tokyo, JAPAN

ABSTRACT

The fractofusion mechanism of Cold Fusion is investigated theoretically. The conditions necessary for fractofusion are clarified. The origin and quantity of the electrical field inside cracks in the conductor are clarified also. The characteristics of Cold Fusion are explained by the mechanism. Almost all the total neutron yields experimentally observed are smaller than the upper limit predicted by the fractofusion mechanism. It indicates that they can be explained by the fractofusion mechanism.

1. Introduction

In some cold fusion experiments, excess neutrons were clearly observed during electrolysis of D_2O by Pd cathodes, though in many other experiments no excess neutrons were observed. Fractofusion mechanism is that D^+ ions are accelerated by electric field inside cracks and that fusion reactions take place during the penetration of such accelerated D^+ atoms in Pd. In spite of many theoretical investigation of fractofusion mechanism, three important problems remain. One is the origin and the quantity of electric field inside cracks in conductor. Another is what are necessary conditions for fractofusion. The third is whether so called cold fusion experiments are really explained by fractofusion mechanism or not.

2. Electric potential in cracks in conductor

We have concluded that the electric field in cracks in conductor, whose existence is experimentally confirmed, is due to the contact charging at crack surfaces as a result of different work functions between touching two grain surfaces. The

charge density ς on crack surfaces is

$$\varsigma = \frac{\varepsilon}{d}\Delta \tag{1}$$

where ε is the dielectric constant, d is the shut down distance of tunneling current, and Δ is the difference of work functions. The electric potential (V) between two crack surfaces is

$$V = \frac{\varsigma l}{\varepsilon} \tag{2}$$

where l is the width of crack. If we assume d=1(nm) and $\Delta = 0.5$(eV), then $\varsigma = 5 \times 10^{-3}$ (C/m^3). Thus V = 5x10 l where l is in mm(l$\leq$ 1mm), and V is in keV. Here we assumed that no discharge takes place during the separation of two facing crack surfaces. This assumption is valid only when the pressure of gas in a crack is less than 10^{-2} Torr (no breakdown), the velocity of crack propagation is more than 10^2 (m/s) (neglect of prebreakdown current), and the electric resistance around a crack increases to more than $10^6\Omega$(neglect of current around a crack).

3. Conditions necessary for fractofusion

(a) Crack generations at grain boundaries, (b) high orientation angle of grains, (c) rapid crack formation, (d) increase of electric resistance around cracks, (e) wider cracks, and (f) many crack generations.

4. Are the cold fusion experiments really explained by fractofusion mechanism?

A. Characteristics of cold fusion

The results of cold fusion experiments have three qualitative characteristics. The first is that excess neutrons were observed in only a few experiments while in many other experiments no excess neutrons were observed. The second is that excess neutrons were observed often in bursts. The third is that sometimes large deformation of Pd specimen coincides with the excess neutron observation. These three characteristics are explained by fractofusion mechanism successfully as follows. The first one is due to the existence of many required conditions for fractofusion. The second characteristic is explained as follows. Fractofusion occurs incracks. When one crack is generated, some amount of fusion events take place immediately at once. The third characteristic is explained as follows. When a Pd specimen is deformed, many cracks are generated. This is the direct result of fractofusion.

B. Quantity of neutron yield

(1) Fusion yield by E (keV) D^+ ion during the penetration in Pd-D

$$Y = 1 \times 10^{-6} exp(\frac{-44.24}{\sqrt{E}}) \tag{3}$$

(2) Electric potential in a crack

$$E = 50 \times a^2 \tag{4}$$

where a is the grain size in mm and E is in keV.Then

$$Y_{tot} = 5 \times 10^7 \frac{exp(\frac{-2}{a})}{\dot{a}} \tag{5}$$

$$Y^{u.l.}_{tot.max.} = 7 \times 10^6 \tag{6}$$

where $Y^{u.l.}_{tot.max.}$ is the upper limit of the fractofusion yield per 1 cm^3 .The comparison with the experimental data is shown in table 1. Detailed calculations are in Ref.[19].

Table 1. The comparison between the total neutron yield observed in the experiments and the theoretically estimated upper limit

experiments				theory
Ref.	Volume of Pd (cm^3)	Method	Y_{tot}	
1	15.7	electrolysis	10^{11}	1×10^8
2	7	electrolysis	10^4	5×10^7
3	8	electrolysis	7×10^4	6×10^7
4	14	electrolysis	4×10^4	1×10^8
5	1.3	electrolysis	2×10^3	9×10^6
6	1.1	electrolysis	10^4	8×10^6
7	0.8	electrolysis	7×10^5	6×10^6
8	0.01	electrolysis	2×10^3	7×10^4
9	0.4	electrolysis	10^4	3×10^6
10	0.6	electrolysis	3×10^5	4×10^6
11	7.7	electrolysis	4×10^5	5×10^7
12	0.3	electrolysis	10^4	2×10^6
13	0.5	electrolysis	10^3	4×10^6
14	0.5	electrolysis	10^4	4×10^6
15	0.3	electrolysis	6×10^5	2×10^6
16	0.9	electrolysis	10^6	6×10^6
17	0.6	electrolysis	10^8	4×10^6
18	0.9	gas release	10^6	6×10^6

5. References

1. Arata, Y. and Zhang, Y.C., 1990,Fusion Technol.18,95.
2. Bittner, M. et al., 1990, Fusion Technol.18,120.
3. Bittner, M. et al., 1991, Fusion Technol.19,2119.
4. Bittner, M. et al., 1991, Fusion Technol.20,334.
5. Dudu, D. et al., 1989, Rev.Roum.Phys.34,229.
6. Golubnichii, P.I. et al., Sov.Tech.Phys.Lett.16,11,826.
7. Gozzi, D. et al., 1991, Nuovo Cimento 103A,143.
8. Harb, J.N. et al., 1990, Fusion Technol.18,669.
9. Jones, S.E. et al., 1989, Nature 338,737.

10. Lewis, D. and Skold, K., 1990, J.Electroanal.Chem.294,275.
11. Miljanić , Š. et al., 1990, Fusion Technol.18,340.
12. Para,A.F. et al., 1990, Fusion Technol.18,131.
13. Sato, T. et al., 1991, Fusion Technol.19,357.
14. Scott, C.E. et al., 1990, J.Fusion Energy9,115.
15. Sona, P.G. et al., 1990,Fusion Technol.17,713.
16. Takahashi, A. et al., 1991, Fusion Technol.19,380.
17. Venkateswaran, G. et al., 1990, Fusion Technol.18,60.
18. Yamaguchi, E. and Nishioka, T., 1990, Jpn.J.Appl.Phys.29,L666.
19. Yasui, K., 1992, to be published in Fusion Technol.(in November).

Is Sono-Fusion to be a Possible Mechanism for Cold Fusion ?

Kenji FUKUSHIMA
Department of Physics
Tokyo Metropolitan University
Minami-osawa, Hachioji City, Tokyo 192-03
Japan

ABSTRACT

Phenomena of sono-luminescence now appear before the footlights. Recently direct measurement of the temperature of a hot spot created in a liquid by applying a supersonic field was carried out and very large values, $T \sim 0.5$ eV, were obtained.

It seems, therefore, to be an urgent problem to determine the upper bound for temperatures and densities realizable in the hot spot, in connection with cold fusion. In this paper we calculate it by use of the bubble dynamics so far developed by many authors and estimate the fusion rate per bubble.

1. Introduction

Let us start with a brief description of phenomena of sono-luminescence. A supersonic field applied to a liquid yields vapour- and/or gas-filled cavitations in the liquid, which subsequently expand and contract more or less oscillatorilly in phase with the supersonic field. The temperature and density of an adiabatically compressed bubble is so high that atoms or molecules in it are excited and then irradiate photons in its expansion phase.

Recently Flint and Suslick[1)] succeeded in directly measuring the temperature of hot spots and obtained the value

$$T = 5075 \pm 156\text{K}.$$

The aim of this work is to estimate the upper bound of the temperature and density of the hot spot created in a liquid by a supersonic field.

2. Rayleigh-Plesset Equation

The sono-luminescence has a long history of research more than forty-five years and constitutes a well-established branch of physics. We now have a lot of review works, by which one may easily get familiar with it. (For example, see Reference 2)

FRONTIERS OF COLD FUSION

The motion of a bubble in a liquid with radius R is described by the following Rayleigh-Plesset equation

$$\ddot{R} = -\frac{3}{2R}\dot{R}^2 + \frac{1}{\varrho R}\left[(P_0 + \frac{2\sigma}{R_0})(\frac{R_0}{R})^{3\kappa} - \frac{2\sigma}{R} - \frac{4\mu\dot{R}}{R} - P_0 - P_A(t)\right], \tag{1}$$

where P_0 is a hydrostatic pressure of the liquid and R_0 is a radius of the bubble in equilibrium with the pressure P_0. The ϱ, σ and μ are, respectively, the density, surface tension and viscosity coefficient of the liquid. The κ is the polytropic index of the gas (this will vary between the specific heat ratio γ and unity, the limits of adiabatic and isothermal conditions, respectively). It is assumed in (1) that the content of the bubble is an ideal gas, but generalization to a van der Waals gas may be straight-forward. The $P_A(t)$ is the applied supersonic field

$$P_A(t) = -P_A \sin \omega_A t. \tag{2}$$

In deriving (1), several simplification were made. (For details, see Reference 2)

3. An Ideal Gas Case

Let us consider a bubble with radius R_0 and in equilibrium with hydrostatic pressure P_0 at $t = 0$, which will then expand isothermally in the first quarter of a period of the supersonic field (2). If the amplitude P_A of the field is large enough, the radius of the bubble is known to abnormally grow up beyond the Blake radius R_B [2]. Let the maximum value of the radius R be R_{max}. In a subsequent half period, the pressure field increases from $P_0 - P_A$ to $P_0 + P_A$ and the bubble contracts adiabatically with increasing pressure. Let R_{min} be a radius of the minimum bubble, where the gas filling the bubble achieves the maximum temperature T_{max}.

The expansion phase is describable in terms of (1) by putting $\kappa = 1$ (isothermal proccess), since the poccess takes place quasistatically. Neppiras [3] numerically calculated the R_{max} for an air bubble in water, assuming that the air is an ideal gas.

Next turn to the contraction phase. It was numerically ascertained by many authors that the contraction occurs very rapidly around the end of the third quarter of a period of the supersonic field (2), when the pressure field is almost $P_0 + P_A$. We can thereby describe the adiabatic contraction proccess by a couple of following equations

$$\begin{aligned} (P_0 + P_A)(V_{max} - V_{min}) &= -\int_{V_{max}}^{V_{min}} P\, dV, \\ PV^{\gamma} &= \text{constant} \end{aligned} \tag{3}$$

in stead of directly solving the differential equation (1).

After integrating (3), we can get the maximum temperature and minimum radius as follows;

$$\begin{aligned} T_{max} &= T_0 Z^{\gamma - 1}, \\ Z \equiv (\frac{R_{max}}{R_{min}})^3 &\sim \left[(\gamma - 1)\frac{P_0 + P_A}{P_0 + 2\sigma/R_0}(\frac{R_{max}}{R_0})^3\right]^{1/(\gamma - 1)} \end{aligned} \tag{4}$$

if Z is much greater than unity, where T_0 is the initial temperature. Figs. 1(a) and 1(b) depict R_{min} and T_{max} against R_0, where we have used values of R_{max} calculated by Neppiras.

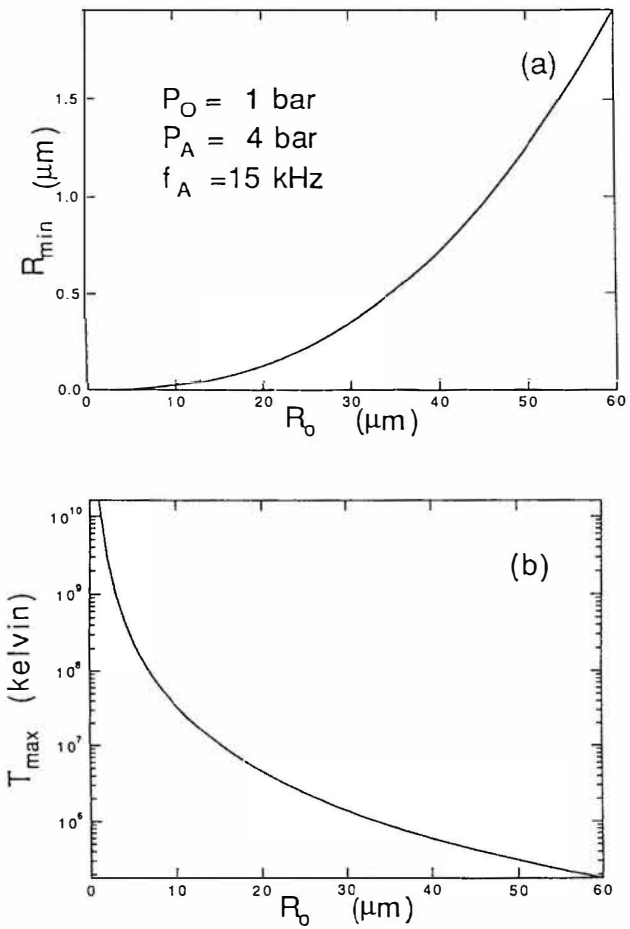

Figure 1

As seen from Fig. 1(b), for initial bubbles of a few microns the maximum temperatures reached are high enough for nuclear fusion to take place. Let the bubble be filled by D_2 gas instead of air. The fusion number per bubble can be calculates as

$$\text{No. of fusions/sec/bubble} = f_\tau (N_e/N)^2 N \varrho v \sigma(E), \tag{5}$$

where f_τ is the fraction of the duration of a minimum bubble to the period of the supersonic field, and N and N_e are the numbers of particles contained in the initial bubble and remaining in the minimum bubble, respectively. The rest of factors on the right hand side of (5)

$$N\varrho v\sigma(E) \tag{6}$$

is a so-called fusion rate per bubble, where ϱ, v and $\sigma(E)$ are the number density of gas in the minimum bubble, averaged relative velocity of gas constituents and fusion cross section, respectively. In (6), $E = (1/2)\mu v^2 = (3/2)k_B T_{max}$, where μ is the reduced mass, k_B the Boltzmann constant. In deriving (5), we postulate that the fusion reaction takes place as in free space, neglecting the dynamical correlation among deuterons, dynamical screening of Coulomb repulsion by electrons etc. We can roughly estimate f_τ and the fraction N_e/N as follows. The speed of wall of the bubble in the contraction phase may be close to the sound velocity v_s. The duration of the minimum bubble, therefore, may be roughly estimated as R_{min}/v_s. On the other hand, the speed of diffusion of the gas content to the liquid is much smaller than that of the wall, so that we may put $N_e/N \sim 1$. The fusion rate per bubble (5) are plotted against R_0 in Fig. 2.

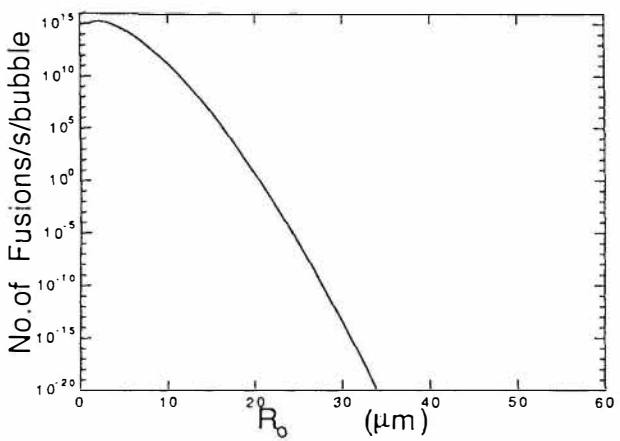

Figure 2

After all, we get a sufficient number of fusions easily detectable in a laboratory.

4. Discussion

Calculations so far made concerns a perfect gas and it is questionable whether such an idealization is valid up to extreme conditions that we are now interested in. To obtain quantitatively acceptable results, we have at least to carrry out calculation similar to the above for a van der Waals gas, and eventually apply molecular dynamics, plasma physics etc. This work only constitutes a preliminary part of the whole task and detailed calculation will appear in another place.

References

1. Flint, E. B. and Suslick, K. S., 1991, Science, 253, 1397.
2. Walton, A. J. and Reynolds, G. T., 1984, Advances in Physics, 33, 595.
3. Neppiras, E. A., 1984, Physics Reports, 61, 159.

Review for "Nattoh" Model and Experimental Findings during Cold Fusion

Takaaki Matsumoto
Hokkaido University
North 13, West 8, Sapporo 060
JAPAN

Abstract

A review is described for the Nattoh model that provides the framework of the mechanisms of cold fusion. The model classifies the reactions into two categories: fundamental and associated reactions. The former involves the new "hydrogen-catalyzed" fusion reaction and the chain-reactions of hydrogens. And extremely exciting physics are invloved in the latter. Furthermore experimental findings are described.

1. Introduction

Since Pons and Fleischmann(1) and Jones et al.(2) independently published cold fusion, many experiments have been performed to verify whether the cold fusion can really take place in a metal. It has been made clear that the phenomena of the cold fusion are too complicated to be explained by the conventional D - D fusion reaction at all. Our thinkings of the cold fusion should be drastically changed.

The author early proposed the Nattoh model ("nattoh" means fermented soybeans) that can well explain the com-

FRONTIERS OF COLD FUSION

plicated phenomena(3,4). This paper describes a review for the Nattoh model and the important experimental findings that have been obtained by using nuclear emulsions.

2. Review for Nattoh model

The framework of the cold fusion is shown in Fig. 1.

2.1 Hydrogen-catalyzed fusion reaction(3, 5)

The hydrogen-catalyzed fusion reaction occurrs in hydrogen-clusters. Many hydrogens are contained in the clusters so that there are many variations for the fusion reaction. The most probables are the fusion reactions between two hydrogens as follow, for heavy water,

$$2D + e + D \longrightarrow {}^{4}He + i_1 + {}^{2}n \quad (1)$$

$$\longrightarrow {}^{4}H + i_1 + d \quad (2)$$

$$\longrightarrow {}^{4}He + e + \bar{\nu} \quad (3)$$

$$2D + 2e + D \longrightarrow {}^{4}n + i_2 + d \quad (4)$$

Here ${}^{2}n$ and ${}^{4}n$ are the di- and quad-neutrons, respectively. The new particle "itons" i that might consist of electrons, positrons and neutrinos cover up the product particles. The emitted energetic hydrogens can make additional fusion reactions, i.e., the chain-reactions of hydrogens can be maintained to predominantly contribute to the excess heat production(4).

2.2 Associated reactions

There are various reactions associated with the hydrogen-catalyzed fusion reaction, shown in Fig. 1. Exciting physics such as the production of the multiple-neutrons, tiny black holes and white holes are also involved.

3. Experimental findings(6 - 19)

Experimental evidences indicating the reactions mentioned above were obtained. Micro-explosions caused by the di- and quad-neutrons were recorded on nuclear emulsions. And the evaporation of the tiny black holes that are produced by heavy mutiple-neutrons was observed. The tiny white holes were also observed.

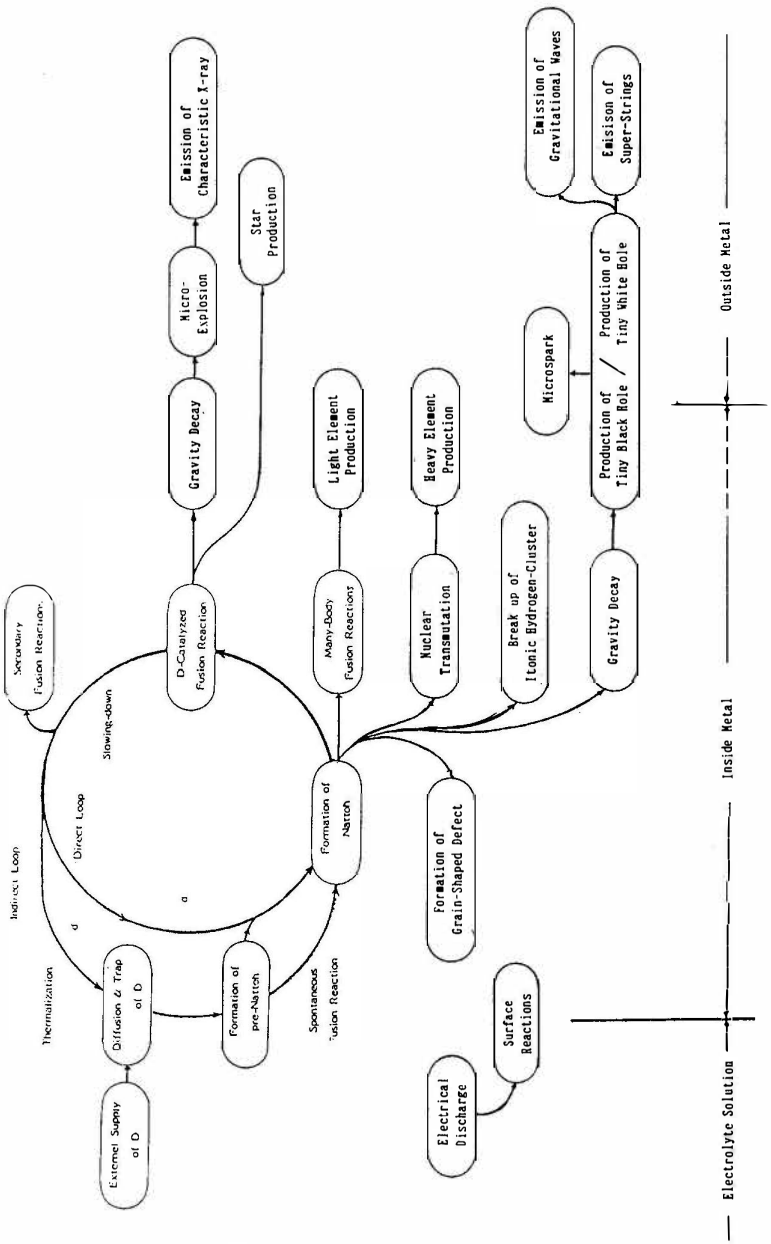

Fig. 1 Framework of cold fusion

References

(1) M. Fleischmann and S. Pons, "Electrochemically induced nuclear fusion of deuterium" J. Electroanal. Chem., 261, 301(1989)
(2) S. E. Jones et al., "Observation of cold nuclear fusion in condensed matter" Nature, 388, 27,737(1989)
(3) T. Matsumoto, "'NATTOH' model for cold fusion" Fusion Technology, Vol 16, p 532 (1989)
(4) T. Matsumoto, "Progresses of the Nattoh model and new particles emitted during cold fusion" Proc. Int. Conf. Provo, (1990)
(5) T. Matsumoto, "Prediction of new particle emission on cold fusion" Fusion Technology, Vol.18, No.4, p 647(1990)
(6) T. Matsumoto, "Observation of new particles emitted on cold fusion" Fusion Technology, Vol.18, No.2, p 356(1990)
(7) T. Matsumoto, "Cold fusion observed with ordinary water" Fusion Technology, Vol 17, p 490 (1990)
(8) T. Matsumoto, "Observation of quad-neutrons and gravity decay during cold fusion" Fusion Technology, Vol.19, No.4, p 2125 (1991)
(9) T. Matsumoto and K. Kurokawa, "Observation of heavy elements produced during explosive cold fusion" Fusion Technology, Vol.20, No.3, p 323 (1991)
(10) T. Matsumoto, "Observation of gravity-decays of multiplied neutron-nuclei produced during cold fusion" Fusion Technology, Vol.22, p 164 (1992)
(11) T. Matsumoto, "Microscopic observation of Pd used for cold fusion" Fusion Technology, Vol.19, No.3, p 567 (1990)
(12) T. Matsumoto, "Interference phenemena observed during cold fusion" Fusion Technology, Vol.21, p 179 (1992).
(13) T. Matsumoto, "Searching for tiny black holes during cold fusion" Fusion Technology, Vol.22, p 281 (1992)
(14) T. Matsumoto, "Observation of stars produced during cold fusion" Fusion Technology, Vol.22, December issue (1992)
(15) T. Matsumoto, "Observation of mesh like traces on nuclear emulsions during cold fusion" Fusion Technology, Vol.23, January issue (1993).
(16) T. Matsumoto, "Cold fusion experiments with ordinary water and thin nickel foil" Fusion Technology, submitted (1992)
(17) I. Yukimura and T. Matsumoto, "Observation of luminescences, spraks and radiations during AC electrolysis cold fusion" Fusion Technology, submitted (1992)
(18) T. Matsumoto, "Experiments of one-point cold fusion" Fusion Technology, submitted (1992)
(19) T. Matsumoto "Photographs of cold fusion; Reproducing the nobles in the universe" private publication (1992)

Thermodynamic Theory of Cold Nuclear Fusion (C.N.F)

Zhongliang Zhang
Institute of Chemistry, Academia Sinica Beijing, 100080, China Fax: 01-2569564
and
Shu-I Liu* University of Science and Technology of China

* Address for Correspondence:
Prof. Dr. Shu-I liu 111 bulding 15, Zhongguancun, beijing 100080 China Phone: Beijing 2561790

Sept. 29, 1992

A new discipline known as STATE-FIELD THEORY OF THERMODYNAMICS (S-F. TOT) had been established in the period (1979-1991) by Shu-I Liu [1-5] [10].

In the present paper, (S-F. TOT) was applied to set up a strict thermodynamic theoretical foundation for the problem of COLD FUSION [6-9].

(I) THE NEW SECOND LAW OF THERMODYNAMICS, THE (law of Coupling) = (LOC)

In article [10], the first law was used to prove the qualitative existence of entropy S ($dS = 0$, when $\delta Q_R = 0$) without knowing the dS equation. This makes it possible to establish a new second law of thermodynamics, the Law Of Coupling (LOC) [1] [2], which states:

FRONTIERS OF COLD FUSION

"It is impossible for a simple system to approach a high entropy state from a low entropy one with evolution of heat at the same time! " ..... (Liu's LOC)

This statement is identical with( ) its 3 branches (I) (II) (III) and 5 small branches as shown by (Liu's Branch Theory of LOC), Equation(I-1) wherein P Process)

Identity (LOC) ≡≡≡ (I-1)

- exothermic P WITHOUT ENTROPY INCREASE (I)
  - exothermic P WITH ENTROPY DECREASE } 1OC(I-1)
  - exothermic P WITHOUT ENTROPY CHANGE } LOC(I-2)
- entropy increase WITHOUT EVOLUTION OF HEAT (II)
  - entropy increase IN ENDOTHERMIC PROCESS } LOC(II-1)
  - entropy increase IN ADIABATIC PROCESS } LOC(II-2)
- (III) ADIABATIC SYSTEM WITHOUT ENTROPY CHANGE } LOC(III-1)

Cold Nuclear Fusion belongs to LOC(I-1): (CNF) is an EXOTHERMIC PROCESS with ENTROPY DECREASE. ..... (I-2)

Entropy S is an extensive function, its value is

proportional to the number of moles (n); n=2 for the reactants (A+B); and n=1 for the product AB with mass defect:

$$\text{LOC (I-1)} \ldots \left\{ \begin{array}{l} \text{A+B} \dashrightarrow \text{AB with mass defect} \\ \text{(mass defect)} \dashrightarrow \text{(heat} < 0\text{)}; \\ S_{A+B} > S_{AB} \end{array} \right\} \ldots\ldots \text{(I-3)}$$

(II) DISSIPATION CRITERIA FOR COLD NUCLEAR FUSION (CNF):

It was proved by using LOC for the process of irreversible charging of an electric cell:

$$\{ \underset{\cdot\cdot}{\triangle} Z_{TP} = - \underset{\cdot\cdot}{A'} - \triangle^{A}) \text{ / mole} \} \ldots\ldots \text{(II-1)}$$

This is the first two laws of thermodynamics for this irreversible cell process wherein:

$$\left. \begin{array}{l} \underset{\cdot\cdot}{\triangle} Z_{T.P} = \text{(increase of free energy)} \\ \quad \text{produced by the charging work} \\ \quad \underset{\cdot\cdot}{A'} < 0 \text{ done to the cell} \end{array} \right\} \cdots\cdots \text{(II-2)}$$

The meaning of the above two equations is:

Bra { In the process of charging, the work input to the cell, $\underset{\cdot\cdot}{A'}$ is converted into the increase of free energy, $\underset{\cdot\cdot}{\triangle} Z_{T.P} > 0$;
Due to IRREVERSIBLE NATURE of the process, the work input $\underset{\cdot\cdot}{A'}$ cannot be completely converted

into free energy increase $\underset{\cdot\cdot}{\triangle} Z > 0$,
PART OF $\underset{\cdot\cdot}{A}'$ IS DISSIPATED AS HEAT:
(Heat Dissipation) $= \triangle^{A} > 0$ } ket... (II-3)

The exists a (CRITICAL VALUE OF $\triangle^{A}$) $= \triangle^{A}_{c}$, such that the following (CRITERIA FOR CNF) hold:

(1) { If: $\triangle^{A} \geq \triangle^{A}_{c}$, Then: (CNF) occurs ; (2) { If: $\triangle^{A} < \triangle^{A}_{c}$, Then: (CNF) cannot occcur .... (II)-4)

Equation (II-4) seems to explain the experimental facts published by some authors. However, more experiments are seriously needed, especially the method of experiment and treatment of the results need serious considerations.

REFERENCES

[1] Shu-I Liu: State-Field Theory for The Laws of Thermodynamics: (III) A New Second Law Of Thermodynamics: the Law of Coupling and Its Deductions For Reversible Processes. Progress in Physics, Chemistry and Mechanics (PPCM) Vol. 1 (1988), PP1-19.

[2] Shu-I Liu: State-Field Theory for the Laws of Thermodynamics: (IV) The Set of Inequalities for Co-terminal Pair of Processes from the New Second Law of Thermodynamics, The Law of Coupling. PPCM Vol. 2 (1990), PP6-25, Hunan Press of Science and Technology.

[3] Shu-I Liu and Meiying Wang: A Comparative Critical Analysis of the Deductions from the Two Carnot Theorems of Thermodynamics, PPCM Vol. 2 (1990) PP96-113

[4] Shu-I Liu: Complete Chinese Text of the Paper: From The New Second Law of Thermodynamics, The Law of Coupling, to dissipation Criteria in Both Directions of Electric Cell Processes. PPCM Vol. 3 (1992), Earthquake Press, Beijing.

[5] Shu-I Liu and Meiying Wang: Complete Chinese Text of The Paper: A New Second Law of Thermodynamics, The Law Of Coupling; The State Rule And Two Gas Models. PPCM Vol. 3 (1992), Earthquake Press, Beijing.

[6] M. Fleischmann and S. Pons, J. Electroanal. Chem. Interfacial Electrochem., 261 (1989) 301

[7] Xu-Wu An et al., Thermochimica Acta 183 (1991) 107

[8] M. Schreiber et al., The First Annual Conference on Cold Fusion, March 28-31, 1990 (Salt Lake City, Utah, U. S. A.), Conference Proceedings P44

[9] Zhongliang Zhang et al., AIP Conference Proceedings 228 (Anomalous Nuclear Effects in Deuterium/Solid Systems) Provo, UT. U. S. A. (1990)

[10] Shu-I Liu: State-Field Theory for the Laws of Thermodynamics: (I) Direction Uniqueness Theorem of Adiabatic Process Vector. Science Exploration, 1 (1987), PP1-12.

Ion Band State Fusion

Scott R. CHUBB and Talbot A. CHUBB
Research Systems, Inc.
5023 N. 38th St.
Arlington, VA 22207
U.S.A.

ABSTRACT

Puska et al.[6] and Astaldi et al.[1] have provided experimental evidence for the existence of hydrogen ion band states in adsorption studies of H and D atoms on metallic surfaces. If a certain view of quantum reality is correct, an ion band state (IBS) D^+ population has wave function overlap and will undergo cold fusion, unlike normal molecules and ionic and covalent solids. Arguments leading to this conclusion and a tabulation of likely IBS reactions are presented.

1. Introduction

IBS fusion assumes a population of energetically-bound band state deuterons. IBS wave function amplitudes have the periodicity of a lattice. The postulated band state is a 3-dimensional analog of the surface H^+ and D^+ band states observed by Puska et al.[6] and Astaldi et al.[1]. The many body wave function describing a D^+ IBS population and its nuclear self-interaction properties are described in Chubb and Chubb[3,4]. The theory predicts reactions which release volume-distributed heat, whereas reactions involving energetic particle emission are forbidden. This paper discusses why and how fusion can occur with a D^+ IBS population and explains why it is not allowed in normal, deuterated chemical compounds.

2. Self-interaction Reactions in Bound Systems

Quantum mechanics describes IBS reactions in terms of a summation over energy-conserving configuration fluctuations (partial reactions) $\dot{N}$ between an initial state $\langle AB|$ and a transitory state $|C\rangle$, namely $\dot{N} = 2\pi/\hbar \langle AB|V|C\rangle\langle C|V|AB\rangle\delta(E_{AB}-E_C)$, where $\hbar$ is Planck's constant/2π, V is the (primarily nuclear) interaction Hamiltonian, E_{AB} and E_C are ISB

FRONTIERS OF COLD FUSION

initial and transitory state energies, and δ is the Dirac delta function. On a longer time scale $|C\rangle$ can interact electromagnetically and irreversibly with the lattice through excitation of electrons and/or phonons. When V involves short range forces, finite N, requires that on the scale of atoms the spatial part of the input-state wave function $\psi_A\psi_B$ must overlap ψ_C and spatial part ψ_A must overlap ψ_B. Self-induced reactions may occur, depending on the correlation properties of the bound system wave function. The wave function is determined by system energy minimization subject to the electromagnetic interactions between particles and system boundary conditions. Consider the helium atom, which consists of the He^{++} nucleus and the two electrons. The energy minimizing solution for the helium electrons is given, to adequate accuracy for our purposes, by the Hylleraas second approximation.[7] With the position of the nucleus being coordinate system origin, the 2-electron wave function consists of a main term, which describes the fall-off of electron charge density with radial distance r, and two correlation factors which modulate the main term so as to reduce the wave function amplitude when $r_1 \approx r_2$. Here r_i is the position vector of electron$_i$. The correlation terms dimple the wave function at $r_1 \approx r_2$, reducing electron-electron overlap. In the helium, atom these dimpling factors are small and the overlap is almost complete. If the electrons had the nuclear properties of deuterons, cold fusion would occur.

3. Non-applicability of Gamow Calculations for Bound Particles

It is instructive to calculate the expected overlap of the two electrons of the helium atom using the Gamow factor[5] G_e. The wave function overlap is proportional to $(G_e)^{1/2}$, where

$$G_e = \exp(-2\pi\alpha\, c/v(T)) \qquad (1)$$

Here $\alpha=1/137$ is the fine structure constant, c is the speed of light and v(T) is the relative speed of electrons (=twice the thermal speed of the single electron) at temperature T, defined by $v(T) = (6K_BT/m_e)^{1/2}$. K_B is the Boltzmann constant and m_e is the electron mass. Using $K_BT \leq .025$ eV, one finds $G_e \leq 10^{-37}$, whereas the correct value is near unity.

4. Why Deuterated Compounds Don't Fuse

The 2-electron wave function of the helium atom is calculated using the principle of energy minimization. More generally, for bound systems involving particles of mass m the kinetic energy density is $\hbar^2|\nabla\psi|^2/(2m)$ and the potential energy density associated with particle$_i$-particle$_j$ repulsion is $e^2|\psi_i|^2|\psi_j|^2/2r_{ij}$, where $|\psi_i|^2$ is the particle density of particle$_i$ and r_{ij} designates $|r_i-r_j|$. Dimpling reduces the wave function as $r_{ij} \to 0$, decreasing potential energy but increasing kinetic energy. The amplitude of the correlation dimpling modulation is the value at which the incremental decrease in potential energy equals the incremental increase

in kinetic energy. In the Hylleraas atom, this balance is achieved with very small dimpling, i.e. large overlap.

However, the balance condition would be very different if the electrons of the helium atom had the mass of D^+, while the size of the helium atom were kept unchanged. Here the increase in kinetic energy for a fixed amount of correlation dimpling is reduced by 3700 relative to the real atom, while the potential energy reduction is unchanged. Energy minimization then occurs with 100% dimpling, i.e. $\psi = 0$ at $r_{12} = 0$ for all r. This example illustrates the reason why nucleus-nucleus overlap does not occur for any deuterated molecule or ionic or covalent solid. Here, the volume of the molecule or solid is set by the deBroglie wavelength of the electrons while the wave-function dimpling of the nucleus-nucleus interactions is set by the nuclear masses. For the nucleus wave functions, correlation dimpling is complete and no nucleus-nucleus overlap occurs. In chemical substances cold fusion is impossible.

5. The Quantum Reality Question for Ion Band State Matter

The possibility of cold fusion depends on the correlation behavior of IBS matter. The wave function of low density electron band state matter describes particles whose charge is partitioned over the many unit cells N_{cell} of a crystal, i.e. the matter state is built from Bloch functions. If D^+ IBS matter acts as if the charge of each D^+ ion is similarly partitioned over N_{cell}, the charge within each unit cell is e/N_{cell}. The coulombic correlation energy density associated with each pair$_{ij}$ of band state D^+ in a given unit cell then is $e^2|\psi_i|^2|\psi_j|^2/(2r_{ij}N_{cell}^2)$. In the sum over N_{cell}, this interaction is much smaller than the comparable $e^2|\psi_i|^2|\psi_j|^2/2r_{ij}$ interaction of the chemical case. Here ψ_i designates a single particle wave function contribution to the many body wave function. The ratio $|\nabla\psi_i|/|\psi_i|$ is independent of N_{cell}. The net effect is that the relative contribution of the kinetic energy increase through dimpling is multiplied by the factor $1/N_{cell}$. Energy minimization then occurs with negligible dimpling, as in the helium atom. With this picture of quantum reality there is no correlation barrier to cold fusion.

6. Band State Fusion

The reactions of D^+ ion band state fusion are of a different character than those of free particle fusion. D^+ ion band state matter is a volumetrically-distributed, collective, exchange-dominated, bosonic matter state described by a many body wave function with Bloch-function symmetry[2]. The mass distribution within each unit cell corresponds to the zero point motion of a D^+ ion in the potential well provided by the lattice. The allowed reactions are transitions from D^+ ion band state matter to other band state matter of the same geometry, preserving the same Bloch symmetry. The reaction possibilities are most easily identifiable if the many body wave function is expressed in terms of transient integer particle occupations of unit cells, as described in the Wannier function representation[4]. This representation contains terms which describe

transient multiple occupations, which we designate n-D^+_{band}. The 2-D^+_{band} undergoes reversible reactions 2-$D^+_{band} \rightleftarrows {}^4He^{++*}_{band}$, in which ${}^4He^{++*}_{band}$ is heliumlike IBS matter with energy = 23.8/Ncell MeV. To preserve periodic order, on a longer time scale ${}^4He^{++*}_{band}$ decays to an IBS ${}^4He^{++}$ through lattice interaction. Subsequent transitions between ion band states are allowed except at surfaces, where ^{4}He is created, as observed[2]. The reactions, reactants, and products are volume distributed. The MeV energy release per reaction is distributed throughout the lattice. In each reaction only a small energy release occurs locally[4]. In PdD_x IBS occupation requires high loading with $x \sim 1$.

7. Reactions

The allowed reactions are those that preserve spatial and bosonic symmetry, e.g.

$$2\text{-}D^+_{band} \rightarrow {}^4He^{++}_{band} \qquad (2)$$

$$3\text{-}D^+_{band} \rightarrow {}^4He^{++}_{band} + {}^2D^+_{band} \qquad (3)$$

$$4\text{-}D^+_{band} \rightarrow 2\ {}^4He^{++}_{band} \qquad (4)$$

$$2\text{-}D^+_{band} + {}^1H^+_{band} \rightarrow {}^3H^+_{band} + H\uparrow H\downarrow^{++}_{band} \qquad (5)$$

Reaction 2 is the primary cold fusion reaction. In Reaction 5 the spin-paired proton $H\uparrow H\downarrow^{++}$ acts as a boson on the length scale of the lattice interaction. Reaction 5 is proposed as the main source of tritium build-up.

There are a number of forbidden reactions which break spatial symmetry, but possibly occur during disruptive events that cause loss of periodic order. These reactions, which produce energetic particles, may be able to take place at surfaces, crystal boundaries, impurity sites, or dislocations, i.e. structures that disrupt periodic order.

8. References

1. Astaldi, C., A. Bianco, S. Modesti, and E Tosatti, 1992, Phys. Rev. Lett., **68**, 90.
2. Bush, B. F., J. J. Lagowski, M. H. Miles and G. S. Ostrom, 1991, J. Electroanal. Chem., **304**, 271.
3. Chubb, T. A. and S. R. Chubb, 1990, Fusion Technology, **17**, 710.
4. Chubb, T. A. and S. R. Chubb, 1991, Fusion Technology, **20**, 93.
5. Merzbacher, E., *Quantum Mechanics* (Wiley and Sons, New York, 1967), p. 124.
6. Puska, M. J. , J., R. M. Nieminen, M, Manninen, B. Chakraborty, S. Holloway, and J.K.Norskov, 1983, Phys. Rev. Lett., **51**, 1081.
7. Seitz, F., *The Modern Theory of Solids* (McGraw-Hill, New York, 1940), pp. 227-234.

Solid State Boson Condensation Model of Cold Fusion

James T. WABER
Michigan Technological University
Houghton, MI 49931
UNITED STATES

ABSTRACT

This theoretical study is based on the second suggestion of Leaf Turner which was independently developed by Chubb and Chubb. It lead to the selection rule, Bosons In, Bosons Out, which helps to explain the low yield of tritons, protons, neutrons and ^{3}He. The production of the boson ^{4}He has now been correlated with simultaneous production of excess heat.

1. Introduction

There is growing evidence which will not be cited here that the formation of ^{4}He is intimately connected with excess heat production in the Cold Fusion experiments. More rigorous standards are now being imposed by investigators in contrast to the euphoric days of March 1989 when poorly characterized palladium samples were immersed in poorly prepared strong alkaline solutions. There is little evidence that the charged particles tritons, protons, neutrons or ^{3}He are the primary products of the reaction. They are fermions. This will become more understandable when the Solid State Paradigm of Chubb and Chubb is applied in place of the commonly used Free Space model.

Leaf Turner[14] at Los Alamos made two suggestions to account for the phenomenon, namely either Transmission Resonance or Boson Condensation. The former is the basis of the Bush-Eagleton[3,4] model. The latter has gone largely ignored. Barry Kunz[10] suggested that there should be a connection between superconductivity and "cold fusion". That is, Cooper pairs of deuterons could approach each

FRONTIERS OF COLD FUSION

other, that the relatively higher mass of the deuterons should significantly reduce the correlation distance, and that the reaction should occur in the vicinity of the Debye temperature of palladium or palladium hydride. He gave no further details. Later he noted that while d-d and d-t fusion does occur in high temperature plasmas and gasses, (where frequent collisions occur) other nuclear reactions such as pair-production and/or electron-positron annihilation require the mediation of a solid in almost all cases.

It noted here that superconductivity involves a boson liquid of electronic Cooper pairs which do not interact with the solid state lattice. Bogoliubov's theory of superconductivity[2] specifically includes the electrostatic interaction between bosons in Einstein-Bose condensation in contrast to the BCS theory. This lead the author to see a connection to superfluidity.

2. Paraphrase of Chubb and Chubb

To achieve some brevity, only a paraphrase of theoretical development by Chubb and Chubb[6] will be given here. They have a more detailed paper[7] at this conference to which the reader is referred. A very important ingredient of their theory and the present extension to temperatures above 0° K is the condensation of bosons into a Bloch state of deuterons and the use of a multi-boson wavefunction formulated in a Wannier representation. They call this a Boson-Bloch-Condensate phase or **BBC**. Born-Oppenheimer separability is another feature. The time evolution of this BBC state leads to the significant selection rule - **bosons in, bosons out,** since the short range nuclear wave-functions are constrained to be independent of the electrostatic (atomic) wave-function **only** during an intermediate time stage when the nuclear portions are constructed of neutron-proton-pair bosonic function Ψ_{np}.

Chubb and Chubb point out that the deuteron charges will be screened and bound by a "sea" of electrons i.e., all regions will be electrically neutral on the macroscopic scale, just as the electrons in a semiconductor are bound by the ion cores. We envision the BBC extending throughout the lattice and interacting only slightly with it. They say, "Just because a deuteron looks and acts like a particle in one situation..." it need not do so in another situation and similarly "...just because the energy is [usually] released entirely in one place .." does not constrain the release to be highly localized in another. Because of the wave nature of matter in a condensed phase the wave-function is spread throughout the material, only a small portion of any atom is located with

any unit cell and only a portion of any nuclear reaction may occur at all periodically equivalent locations.

Note that all the particles are initially bound and the particles resulting from the nuclear reaction remain bound. The kinetic and potential energy portions of the Hamiltonian effectively cancel each out so that the right hand side of the Schrödinger equation remains finite. Because of the nature of the wave function the worrisome "cusp" condition is avoided.

The s- and d- bands of PdD_x must be filled so that the Fermi Level lies very close to the maximum energy of the s- band. Hence x must be $(1-\delta)$: then thermally excited deuterons will occupy "ionic band states." Hence the PdD_x must be thoroughly charged electrolytically and this is a difficult feat since the deuterium diffusion rate in the deuteride falls dramatically when x exceeds about 0.7.

3. Boson Condensation

It is proposed herein that two superfluid rotons (involving deuterons) interact with an interstitial deuterium atom to yield the compound nucleus ^6Li which readily decays to $^4He^{+*}$ plus an excited D^{+*} ion and the resulting energy can be dissipated readily in lattice by well known processes. This differs in small details from the suggestion of Becker[11]. Recently Nieminen[12] pointed out that even on the surface of a metal, hydrogen atoms are delocalized into surface band states.

The energy states of a system of identical bosons interacting weakly by pair-wise forces can be represented by the Hamiltonian

$$\underline{\underline{H}} = \sum{}' _{\mu} \; \underline{E}_{\mu} \, \langle \underline{B}_{\mu}^{\dagger} | \underline{B}_{\mu} \rangle + \underline{\underline{H}}' \qquad (1)$$

where the $\underline{\underline{H}}'$ is a small correction. The double underline has been used here to indicate an operator, and the $|\underline{B}_{\mu}\rangle$ and $\langle \underline{B}_{\mu}^{\dagger}|$ are Bogoliubov's canonically adapted annihilation and creation operators. The prime on the summation indicates that it does not include the value $\underline{k} = 0$. The system energy is $\underline{E}_{\mu}$. The interaction corresponds to the disappearance of particles with momenta $\underline{k}_1\downarrow$ and $\underline{k}_2\uparrow$ (expressed in units of $\hbar$) and the appearance of particles in states with $\underline{k}_1\downarrow$ and $\underline{k}_2\uparrow$. The ground state of such a system of non-interacting bosons corresponds to condensation. The Cooper pair involves the further condition that $E(\underline{k}) = E(-\underline{k})$ and the momenta $\rho(\underline{k}) = \rho(-\underline{k})$ i.e., they are diametrically opposed quantities just outside the Fermi Surface. There is an energy gap and if the electric field is weak, any single particle scattering process - breaking up of the pair - is connected with an increase in the energy of the system of deuterons. The

elementary excitations of a system of bosons between which weak repulsive forces are acting leads to the curve discussed below by Feynman.

The important boson fluid of excitations lies slightly above the Fermi Level and does apparently interacts with the lattice. These D^{+*} are cospatial with the other deuterons in a lattice unit cell.

Feynman[8] notes that the curve connecting the excitation energies as a function of the momentum ρ of the particles in a superfluid has one minimum. States linearly dependent on ρ are called phonons and those with momenta above the minimum ρ_0 are called rotons. The contribution of the phonons to the liquid goes as T^4 and only dominates over rotons at very low temperatures. Feynman sketched a periodic array of rotons in his figure 8. Rotons are created in pairs and attract each other. The correlation distance r in a non-ideal Bose gas is $r \approx \hbar/mu$. Note that the effective mass in the denominator is at least as large at that of the deuteron which in turn is roughly 3500 times the electronic mass. Note that the experimental correlation distance in two high temperature superconductors is given as 10 Å in ref.(5) and 3 Å ref.(11) resp. This would lead, because of the mass effect, to a correlation distance of less than 100 Fermis. There is a further effect.

In the case of electrons, spin information and exchange forces are conveyed by virtual phonons. In the case of nuclear forces, interparticle information is conveyed by means of virtual pions, which are bosons. Kenny[9] points out that binding by spin 0 bosons arises from Yukawa mass correction and the range of these is about seven times that of the usual nuclear components. Such long range forces have the ability to bring about coalescence of two or more deuterons.

The friction is essentially zero when a negative ion (such as D^{-*} which occurs in typical metallic hydrides) is accelerated by an electric field through the superfluid, up to a critical velocity and above this velocity (for roton emission), the number of states into which a roton can be excited grows rapidly.

While the superfluid phenomena in liquid helium occur below 5° K, the superfluid in superconductivity operates at or above the boiling point of liquid nitrogen. The proposal of a third kind of boson state, namely a superfluid of excited deuteron states as in BBC occurring at 300° K does not seem extraordinary.

4. Concluding Remarks

An extension of the ideas involves mild electrostatic interactions between the bosons which can lead to the BBC

and the development of excited ionic band states which lie above the Fermi Level in PdD_{1-x}. The extension involves teachings from two other boson condensates, namely superconductivity and superfluidity. It is proposed that the interaction between a "stationary" interstitial D atom and two rotons rather than phonons give rise to bound reaction particles with a $D^{\cdot}$ carrying away part of the reaction energy.

Note added in proof.

In 1990, Rabinowitz[13] called attention to a possible connection between "cold fusion" and superconductivity, noting that Pd-D_x is a BCS superconductor, but apparently did not pursue this idea. He also discusses the fact that as a superconductor it exhibits a negative isotope effect. He discusses low-dimensional superconductors which may be pertinent to the Bush-Eagleton model.

5. Acknowledgement

This work was supported by the U.S. Army Research Office. The author is very grateful for the counsel and encouragement of Scott Chubb.

6. References

1. Becker, E. W., 1989, Naturwissenschaften, **76**, 214.
2. Bogoliubov, N. N., 1958, "A new method in the theory of superconductivity I and III," Soviet Physics, **34**, 41-50 and 51-53.
3. Bush, R. and Eagleton, R., 1989, **89-WATS-3**, Am. Soc. Mech. Eng., 14 pp.
4. Bush, R. and Eagleton, R., 1991, Fusion Tech., **19** 313-315,
5. Chaudhari, P., Dimos, D. and Mannhart, J., "Earlier and Recent Aspects of Superconductivity," Editors J. G. Bednorz and K. A. Müller, (Springer Verlag, Berlin), 57.
6. Chubb, S. R. and Chubb, T. A., 1990, Fusion Tech., **17**, 710-712.
7. Chubb, S. R. and Chubb, T. A., 1991, Proc. Anomalous Nuclear Effects in Deuterium/Solid Systems, **AIP Conf. Proc. 228**, 691 ff.
8. Feynman, R. P., 1957, Rev. Mod. Phys., **29**, 205-212.
9. Kenny, J. P., 1991, Fusion Tech, **19**, 547-551.
10. Kunz, A. B., 1989, Private Communication.
11. Kitazawa, A, 1991, opus cit., 203.
12. Nieminen, R., 1992, Nature, **356**, 289-291
13. Rabinowitz, M., 1990, Mod. Physics Lett., **4** [4] 233-247.

14. Turner, L., 1989, "Thoughts unbottled by Cold Fusion," Physics Today, Sept. 1989, 140-141. See also comments in the Santa Fe Conference proceedings.

Mechanism of Cold Nuclear Fusion in Palladium

Ken-ichi TSUCHIYA

Department of Electronic Engineering, Tokyo National College of Technology, 1220-2 Kunugida, Hachioji, Tokyo 193 (Japan)

Kazutoshi OHASHI

Faculty of Engineering, Tamagawa University, Machida, Tokyo 193 (Japan)

Mitsuru FUKUCHI

Department of Instrumentation Engineering, Faculty of Science and Technology, Keio University, Hiyoshi, Yokohama, Kanagawa 223 (Japan)

Abstract

A new interpretation of cold nuclear fusion at the center of the boson cluster was given by R.T.Bush et al. The modified theory is given in this paper by adding the effect of screened d-d repulsion. Tunneling probability and power density of cold nuclear fusion in palladium are obtained, and the role of screening effect is found to be very important.

1. Introduction

In 1989, Fleishman and Pons et al [1] reported experimental results suggesting a cold nuclear fusion in palladium. And also in 1989, Jones et al [2] reported similar results. In 1991, we have pointed out the importance of electronic screening around deuteron (d) and obtained d-d pair potential with taking into account the non-linear screening effects [3]. Bush et al [4] have given another approach in 1990 by using the concept of symmetry force for boson cluster, and obtained the transmissivity of tunneling and power density generated from d-d nuclear reaction at the center of the cluster. According to their theory, attractive symmetry force supplies kinetic energy to d and this raises the transmissivity of tunneling through the Coulomb barrier. In the present work, we consider that two forces are effective to d. One is symmetry force and the other is d-d repulsive force. This means that repulsive potential reduces the tunneling effect, however electronic screening around d seems to decrease this reduction. Therefore, linear screened, i.e. Thomas-Fermi, and non-linear screened [3] potentials are tried to use for the calculation of transmissivity and power density as a function of the number of d's in a cluster.

2. Kinetic Energy

As in ref.[4], d's in metals perform as identical bosons and tend to make clusters. The attractive force effective to them is called symmetry force, and it is written as

FRONTIERS OF COLD FUSION

$$F_s(R) = -\Omega R^3 \ , \tag{1}$$

where Ω is a coupling constant and R is a radius of the N boson cluster, which is determined by using degenerate radius r_0 as

$$\frac{4}{3}\pi R^3 = N\frac{4}{3}\pi r_0^3 \ . \tag{2}$$

The coupling constant is given by assuming that attractive symmetry force and repulsive force between two bosons are balanced when the distance between them is r_0 as

$$\Omega R_0^3 = -\left[\frac{d}{dr}V(r)\right]_{r=r_0} \ , \tag{3}$$

where R_0 is the radius of two boson cluster and $V(r)$ is the repulsive potential. The value of degenerate radius r_0 is given in ref.[4] as $r_0=0.23A$.

When a d moves towards the center of the cluster under the effects of force f, kinetic energy E_k is supplied, which is expressed as

$$E_k = \int_R^0 f(R)dR \ . \tag{4}$$

In eq.(4), Bush et al [4] assumed that only symmetry force is effective and f was written as

$$f(R) = F_s(R) \ , \tag{5}$$

which gave

$$E_k = \frac{1}{4}\Omega R^4 \ . \tag{6}$$

In our treatment, we assume that not only symmetry but also repulsive forces are effective, therefore f is expressed as

$$f(R) = F_s(R) + \frac{d}{dR}(NV(R)) \ , \tag{7}$$

which gives

$$E_k = \frac{1}{4}\Omega R^4 - NV(R) \ . \tag{8}$$

If Coulomb repulsion is chosen as V, the second term of eq.(8) is so large that E_k is always negative. However, if screened repulsion is chosen, E_k becomes positive for large N, and the tunneling effect is catalyzed.

3. Transmissivity and Power Density

If a d with kinetic energy E_k penetrates the repulsive barrier ($r_n < r < r_1$) and reachs the nuclear force region ($r < r_n$), the tunneling point r_1 depends on the shape of the repulsive potential and the values of the kinetic energy and taransmissivity of this tunneling are written as

$$E_k = V(r_1) \ , \tag{9}$$

and

$$T = exp(-2G) \ , \tag{10}$$

where the formula of G is well known [5] as

$$G = \frac{\sqrt{2m}}{h}\int_{r_n}^{r_1}(V(r) - E_k)^{1/2}dr \ . \tag{11}$$

In the nuclear force region, the d-d nuclear reaction to produce He^4 is catalyzed, and the power generated from this reaction can be calculated by using the transmissivity T. This gives the power density p as

$$p = \frac{\nu n N T E_1}{2V_a} \ , \tag{12}$$

where ν, n, E_1, and V_a mean frequency factor, average number of d's injected per interstitial site, released energy from this nuclear reaction and volume of a unit cell of fcc palladium, respectively, and the values of them are given in ref.[4] as $\nu=10^{14}s^{-1}$, $n=1.2$ and $E_1=38.4\text{x}10^{-13}J$. The value of lattice constant of fcc palladium is $a=3.89A$, and this gives $V_a=a^3/4$. We regard the radius r_n of nuclear force region as $10^{-5}A$.

4. Results

For the case of using the Thomas-Fermi screening potential as a repulsion, we obtain

$$\Omega = \frac{(kr_0+1)e^2}{2r_0^5}exp(-kr_0) \ , \tag{13}$$

and

$$\frac{e^2}{r_1}exp(-kr_1) = \frac{(kr_0+1)e^2}{8r_0}exp(-kr_0)N^{4/3} - \frac{e^2}{r_0}exp(-kr_0N^{1/3})N^{2/3} \ , \tag{14}$$

where k is a screening constant and the value is given in ref.[3] as $k=1.71A^{-1}$. The value of r_1 is obtained by solving eq.(14) numerically. The results for Transmissivity T and power density p are shown in Table 1. In this case, it is found that E_k is negative for $N<8$ and p is small even for large N.

Table 1. Transmissivity T and power density p as a function of N by using Thomas-Fermi screening potential.

N	$r_1(A)$	$E_k(Ryd.)$	T	$p(W/cm^3)$
8	0.85	0.3	$8.3\text{x}10^{-136}$	$1.0\text{x}10^{-110}$
10	0.27	2.5	$6.6\text{x}10^{-82}$	$1.0\text{x}10^{-55}$
12	0.16	5.0	$8.6\text{x}10^{-64}$	$1.6\text{x}10^{-36}$
13	0.13	6.4	$4.9\text{x}10^{-58}$	$9.9\text{x}10^{-32}$
14	0.11	7.8	$1.9\text{x}10^{-53}$	$4.1\text{x}10^{-27}$
15	0.095	9.3	$1.1\text{x}10^{-49}$	$2.5\text{x}10^{-23}$
16	0.084	10.8	$1.5\text{x}10^{-46}$	$3.8\text{x}10^{-20}$
17	0.074	12.4	$7.3\text{x}10^{-44}$	$1.9\text{x}10^{-17}$
18	0.066	14.1	$1.5\text{x}10^{-41}$	$4.4\text{x}10^{-15}$
19	0.060	15.8	$1.7\text{x}10^{-39}$	$5.0\text{x}10^{-13}$
20	0.054	17.5	$1.1\text{x}10^{-37}$	$3.4\text{x}10^{-10}$

For the case of using non-linear screened d-d pair potential [3], Ω, r_1 and G are obtained through numerical differentiations and integrations. The results for T

and p are shown in Table 2. In this case, E_k is always positive and p is large enough for $N>16$.

Table 2. Transmissivity T and power density p as a function of N by using non-linear screened d-d pair potential [3].

N	$r_1(A)$	$E_k(Ryd.)$	T	$p(W/cm^3)$
2	0.26	0.7	$1.0\text{x}10^{-80}$	$5.6\text{x}10^{-51}$
4	0.16	3.9	$5.6\text{x}10^{-60}$	$3.5\text{x}10^{-34}$
6	0.090	7.7	$4.5\text{x}10^{-49}$	$4.3\text{x}10^{-23}$
8	0.064	11.6	$1.9\text{x}10^{-42}$	$2.4\text{x}10^{-16}$
10	0.053	15.6	$1.7\text{x}10^{-38}$	$2.7\text{x}10^{-12}$
11	0.049	17.7	$8.6\text{x}10^{-37}$	$1.5\text{x}10^{-10}$
12	0.046	19.7	$2.5\text{x}10^{-35}$	$4.6\text{x}10^{-9}$
13	0.043	21.9	$7.3\text{x}10^{-34}$	$1.5\text{x}10^{-7}$
14	0.040	24.1	$1.7\text{x}10^{-32}$	$3.7\text{x}10^{-6}$
15	0.038	26.1	$2.6\text{x}10^{-30}$	$6.0\text{x}10^{-5}$
16	0.035	28.3	$4.4\text{x}10^{-30}$	$1.1\text{x}10^{-3}$
17	0.033	30.6	$6.1\text{x}10^{-29}$	$1.6\text{x}10^{-2}$
18	0.030	32.8	$6.5\text{x}10^{-28}$	$1.8\text{x}10^{-1}$
19	0.027	34.9	$5.0\text{x}10^{-27}$	1.5
20	0.026	36.7	$2.3\text{x}10^{-26}$	7.2

5. Conclusions

Bush et al [4] pointed out the tendency of identical bosons to clump and derived the attractive symmetry force. In our work, we modified their theory by adding the effect of d-d repulsion. And it is found that screening effect is very important, because symmetry force can not catalyze the tunneling effect for the case of using direct Coulomb repulsion in eq.(8). Our results for the case of using non-linear screening in Table 2 show that power density p is large enough to measure for $N>16$. We think that the candidate for the site of such a big cluster is lattice defects in palladium.

Acknowledgements

The authors wish to thank Professors S.Haruyama and S.Masaki for encouragements, suggestions and discussions.

References

1. M.Fleishman, S.Pons and M.J.Hawkins, J.Electroanal. Chem., 261 ,301(1989)
2. S.E.Jones, E.P.Palmer, J.B.Czirr, D.L.Decker, G.L.Jensen, J.M.Throne, S.F.Taylor and J.Rafelski, Nature (London), 338 ,737(1989)
3. K.Tsuchiya, Y.H.Ohashi, K.Ohashi and M.Fukuchi, J.Less-Common Metals, 172-174 ,1371(1991)
4. R.T.Bush and R.D.Eagleton, J.Fusion Energy, 9 ,397(1990)
5. E.Segre, Nuclei and Particles, W.A.Benjamin, N.Y., p324-325(1977)

A Mechanism for Cold Nuclear Fusion: Barrier Reduction by Screening under Transient Coherent Flow of Deuterium

Noriaki MATSUNAMI
Crystalline Materials Science, School of Engineering,
Nagoya University, Furo-cho, Chikusa-ku, Nagoya 464-01,
Japan

ABSTRACT

A mechanism for the cold nuclear fusion is suggested, based on reduction of the barrier penetration factor λ due to screening by enhanced electron density around deuterium at excited/ionic states under transient coherent flow of d in metals. For D^- state, $\lambda \approx 70$ or the rate of ~1 fusion/s•cm^3 is obtained. The effective region and probability of the transient coherent D^- state are discussed.

1. Introduction

The cold fusion reported in 1989 by Fleischmann and Pons[1] and Jones et. al.[2] has been investigated extensively[3-6]. Many of the mechanisms suggested for enhancement over the standard theory (see,e.g., ref.[7]), which fails to explain the anomalous cold fusion rate, are summarized in refs.[3,6]. At present, however, none of these mechanisms is readily satisfactory. Among all, the most striking of the cold fusion phenomena is irreproducibility. This would strongly suggest that the cold fusion involves extreme transient or fluctuating processes as discussed below.

In this paper, a mechanism is suggested based on reduction of the barrier due to screening by enhanced electron density around d at excited and/or ionic states under transient coherent flow of deuterium. The effective region and probability are discussed with emphasis on the irreproducibility and the fusion rate is derived.

FRONTIERS OF COLD FUSION

2. Barrier Reduction by Screening at Transient States

The present model follows that the d-d fusion rate is proportional to the square of the overlap of two deuterium wavefunctions. During electrolysis of D_2O or discharge after charge of d under high pressure or by implantation, the d concentration would be near saturation and hence the coherent (fluid-like) movement of d is expected, unless otherwise no space is available[8,9]. Under these movements, deuterium would pass through the transient,i.e., excited and/or ionic states, at which the electron density around d might be enhanced due to the charge transfer from metal atom to d, like non- and anti-bonding states, and thus reducing the barrier factor. The cohesive energy of the ionic states is comparable with that of metal-hydrides as discussed later. Since there is little information on the transient states, the following potential is used in this study;

$$V(x)=(1-z)/x + (z/x)\exp(-x/b) \quad , \qquad (1)$$

where b is the screening parameter and z is the effective number of electrons around d (z=1 and 2 correspond to D^o and D^- states, respectively). Herein atomic units(au) are used unless specified. In the coherent movement of d, the relative energy ε would be close to zero and the turning point x_o satisfying $V(x_o)=\varepsilon=0$ is given by;

$$x_o=b\log\{z/(z-1)\} \quad . \qquad (2)$$

The barrier factors calculated using the WKB method are given in Table 1 for various b and z, including λ obtained with an approximate formula(error<10%);

$$\lambda=(2\pi k)^{1/2}\{(1/\pi x_o)^2+(1/8b)^2\}^{-1/4} - \log(8kx_o) \quad , \qquad (3)$$

where $k=m_r/m_e$ is the reduced mass m_r of d-d system divided by the electron mass m_e. For z=1(D^o), x_o=0.5 is employed.

Table 1. The barrier factor λ for the screening parameter b (au) and the effective number of electrons z(z=1,2 correspond to D^o,D^-). The values in the parenthesis are obtained with eq.(3).

b	0.05	0.1	0.2	0.3
z=1	59(58)	83(82)	105(105)	113(114)
z=1.5	34(36)	51(53)	74(77)	92(96)
z=2	27(29)	40(42)	59(62)	74(77)
z=3	20(21)	30(32)	45(47)	57(59)

A small contribution from the log term in eq.(3) and WKB formula which should be eliminated to match the Gamow factor for the Coulomb potential($V(x)=1/x$) will not change λ significantly. One sees that λ is close to 70 for $z=2$ or D^- state with the screening parameter $b=0.3$, this b value being close to that in free H_2 molecule[10,11] and the ground state of H in Pd[12].

3. Fusion Rate

Let the probability and fractional volume being at the transient states be f_t and f_v, the fusion rate Y is given by

$$Y(/s \cdot cm^3)=AN\lambda \exp(-\lambda)/a_0^3(f_t f_v), \qquad (4)$$

here $a_0=0.529\times10^{-8}$ cm is the Bohr radius, $A=1.5\times10^{-16}$ cm^3/s is the reaction constant[13,14] and N is the d-d pair concentration. For $\lambda=74$(e.g.,$b=0.3$,$z=2$) with $f_t f_v=1$ and $N=10^{22}/cm^3$, $Y\approx5/s\cdot cm^3$ is obtained. The factors f_t and f_v, which depend on d/metal atom ratio, defect densities and etc, would have values much less than unity and large fluctuations. The parameter b and z may also have fluctuation as contrast to that at the ground state. These would result in "irreproducibility" of the cold fusion.

The cohesive energy E_c for an ionic lattice of MH is given by E_c=(Madelung energy)-(Ionization energy of M)+(Electron affinity of H), neglecting a repulsive contribution. Suppose a hypothetical ionic states of Pd^+H^- (H^- at tetrahedral sites of the fcc Pd lattice), this is equivalent to ZnS structure with $d_{nn}=0.17$ nm, where d_{nn} is the nearest neighbor distance between metal ion and H^-, and one gets $E_c=6.4$ eV[15,16]. Similarly, one finds $E_c=8$ eV for $Ti^{2+}H_2^{2-}$ (H^- at the mid points of the 2nd nearest neighbors of the fcc Ti lattice, equivalent to NaCl structure with $d_{nn}=0.28$ nm). These values are comparable with E_c of metal hydrides, 6.7 and 10 ev for PdH[12] and TiH_2, respectively. The repulsive contribution is small unless d_{nn} is too small and E_c is relatively insensitive to the structure. Thus high probability being at the ionic states is expected for the transient states, if the activation energy into these states is smaller than that of diffusion. The present model does not require contraction of two d nuclei nor acceleration of deuterium. The details will be described elsewhere.

4. Conclusion

The fusion rate is derived based on the reduction of the barrier penetration factor due to screening by enhanced electron density around d at excited ionic states under transient coherent flow of d in metals. The fusion rate can reach to ~ $1/s \cdot cm^3$ and critically depends on the effective time and region of the transient states, resulting in the "irreproducibility" of the cold fusion. More investigations on the transient states would be fruitful.

References

1. M. Fleischmann and S. Pons, J. Electroanal. Chem. 261(1989)301.
2. S. E. Jones, E. P. Palmer, J. B. Czirr, D. L. Decker, G. L. Jensen, J. M.Thorne, S. F. Tayler & J. Rafelski, Nature 338(1989)737.
3. J. O'M. Bockris, G. H. Lin and N. J. C. Packham, Fusion Technol. 18(1990)11.
4. E. Storms, Fusion Technol. 20(1991)433.
5. V. A. Tsarev and D. H. Worledge, Fusion Technol. 20(1991)484.
6. G. Preparata, Fusion Technol. 20(1991)82.
7. C. D. Van. Siclen and S. E. Jones, J. Phys. G12(1986)213.
8. G. Alefeld and J. Völkl, "Hydrogen in Metals I And II", (Springer-Verlag,1987).
9. Y. Fukai, Adv. in Phys. 34(1985)263.
10. T. E. Sharp, Atomic Data 2(1971)119.
11. N. Matsunami, Rad. Effects and Defects in Solids 112(1990)181.
12. Z. Sun and D. Tomanek, Phys. Rev. Lett. 63(1989)59.
13. N. Jarmie and R. E. Brown, Nucl. Instrum. & Methods B10/11(1985)405.
14. A. Krauss, H. W. Becker, H. P. Trautvetter, C. Rolfs and K. Brand, Nucl. Phys. A465(1987)150.
15. C. Kittel,"Introduction to Solid State Physics",(Wiley,1976).
16. W. A. Harrison,"Electronic Structure and The Properties of Solids",(Dover,1989)

Quantum Mechanics on Cold Fusion

Norio YABUUCHI

High Scientific Reseach Laboratory

204, Marusen－Bill Marunouchi Tsu－City Mie－Prefecture 514 JAPAN

ABSTRACT

According to plasma thermonuclear fusion, the deutron collide with target deutron, needs high temperature thermal energy, because the deutron change thermal energy into movement energy.

But, nuclear fusion based on the characteristic of deutron as wave which does not need hightemperature thermal energy. because amplitude of wave cause the nuclear fusion easy. and the amplitude of wave field of deautrons resulting in tunneling effect.

Pd metal including current and deutrons appears at the crack which causing the electric field and the photon field and the deutrons field.

And wave fields of photons and deutrons interact to cause the phenomenon of superconduction.

There for incident accelerated deautron by superconduction collide with target deautron resulting in the nuclear fusion with tunneling effect, on this case nuclear chemistry equations are next example because of experimental value is 2.45MeV～6.MeV

$$D+D\rightarrow n+{}^{3}He+3.27MeV \quad (1)$$

$$D+D\rightarrow p+T+4.03MeV \quad (2)$$

$$D+D+D\rightarrow T+{}^{3}He+9.5MeV \quad (3)$$

$$D+D+D\rightarrow {}^{3}He+d+23.8MeV \quad (4)$$

$$D+D+D\rightarrow {}^{4}He+D+24MeV\rightarrow T+P+D+4MeV\ (\therefore {}^{4}He\rightarrow T+P-20MeV) \quad (5)$$

1. Introduction

Deuterium atoms intruding into Pd metal are subject to excitation due to lattice vibration whem they are packed among lattices of Pd atoms in the saturated state, which separate electrons away and become deutrons. The deutrons violently vibrate further by receiving excitation due to vibration among lattices of Pd atoms, causing cracks among Pd atoms. Thus am intense electric field appcars at the

FRONTIERS OF COLD FUSION

crack, according to Drude's theory, causing the photon field. If so, the field of photon as a Bose particle and that of deutron as another Bose particle interact to give superconduction and the deutrons collide with target nucleus resulting in the nuclear fusion.

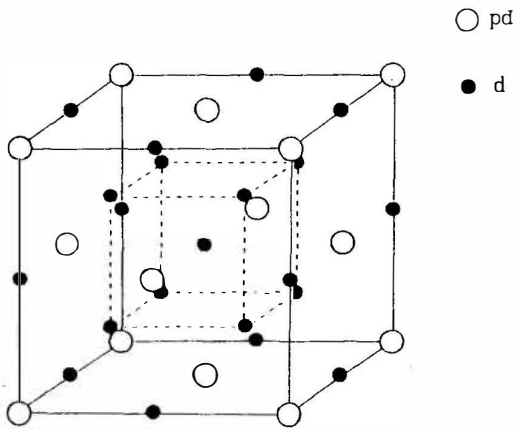

Fig. (1)

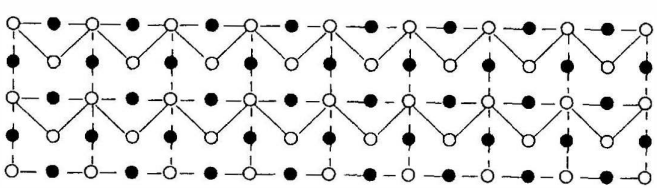

Fig. (2)

2−D model of Fig. (1)

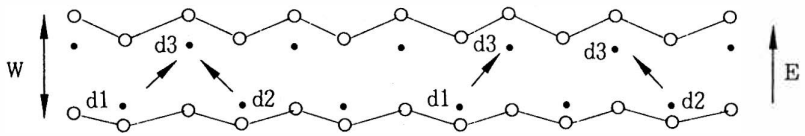

Fig. (3)

creacked model from Fig. (2)

Deuterium atoms intruding into Pd are in the state as shown in Fig. (1). Illustrated in Fig.(2) is an arbitrary section of Pd metal. Fig. (3) illustrates a state that phenomena turned from ionization to cracking,implying expansion of the Pd metal.

Electric field E created in a crack accelerates deutrons in the crack. In additon, created fields of photons and deutrons interact to cause the phenomenon of superconduction. What illustrates wave phenomenon of the field in the crack of Fig.(3) is Fig. (6), and the physical equation is

$$|c_1\Psi_{d1}+c_2\Psi_{d2}|^2=|c_1\Psi_{d1}|^2+|c_2\Psi_{d2}|^2+\underbrace{\bar{c}_1c_2\overline{\Psi_{d1}}\Psi_{d2}+c_1\bar{c}_2\Psi_{d1}\overline{\Psi_{d2}}}_{Z\ \text{term}} \quad (1)$$

Fig. (4) expresses relationship between probabillty distribution and amplitude of deutrons. It is 2−body reaction for one dl, and 3−body reaction including the target nucleus for two. Fig. (5) is a wavy expression of the nuclear reaction, and it becomes a reaction of a kind of compound nucleus and the target nucleus in the cases of 3−body reaction.

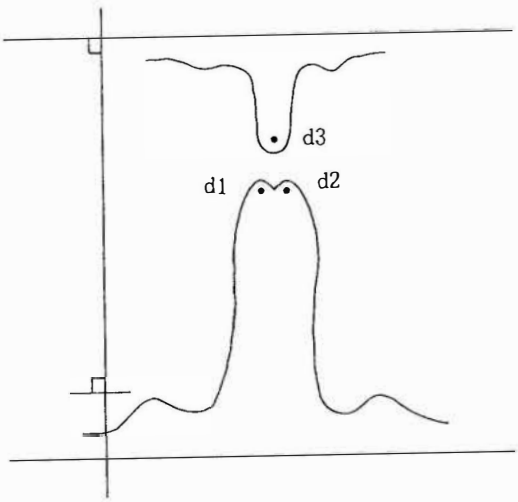

Fig. (4)

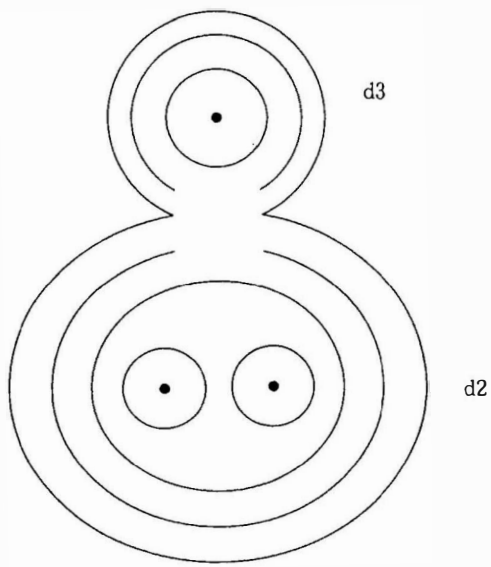

Fig. (5)

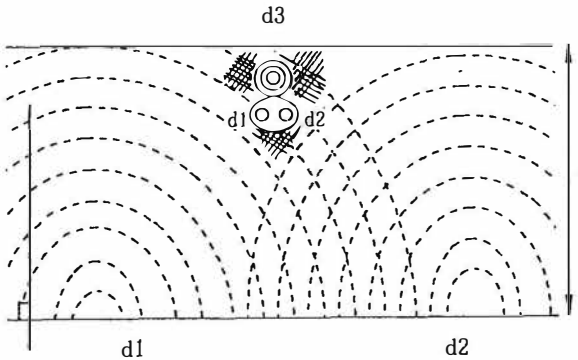

Fig. (6)

Fig. (4), (5) and (6) illustrate nuclear fusions caused by tunneling effect due to the Z term, respectively.

With increased acceleration, superconduction and large amplitude, the target nucleus d3 and incident d particles, d1 and d2, realize the nuclear fusion through tunneling effect. Therefore, the low temperature nuclear fusion is expressed, if expanded with wave equations, as follows:

$$-\left(\frac{\hbar^2}{2\mu_1}\nabla^2+\frac{\hbar^2}{2\mu_2}\nabla^2\right)\Psi_{2d}+(U_1+U_2)\Psi_{2d}+w\Psi_{2d}-\left(\frac{\hbar^2}{2\mu_3}\nabla^2{}_{d3}+U_3\right)\Psi_{d3}$$

$$=-\frac{\hbar^2}{2m_T}\nabla^2\Psi_T+U\Psi_T-\frac{\hbar^2}{2m_{3He}}\nabla^2\Psi_{3He}+U\Psi_{3He}+9.5\mathrm{MeV}$$

This Ψ 2d is a kind of compound nucleus state.
3−body reaction (2)

Because of the 2 body reaction when single nucleus of d1 or d2 is located in z term,

$$-\frac{\hbar^2}{2\mu_1}\nabla^2\Psi_{2d}-\frac{\hbar^2}{2\mu_3}\nabla^2\Psi_{d3}+U_1\Psi_{2d}+U_3\Psi_{d3}$$

$$=\frac{\hbar^2}{2m_n}\nabla^2\Psi_n-\frac{\hbar^2}{2m_T}\Psi_{3He}+U\Psi_n+U\Psi_{3He}+3.27\mathrm{MeV}$$ 2−body reaction (3)

$$\nabla^2=\frac{\partial^2}{\partial x^2}+\frac{\partial^2}{\partial y^2}+\frac{\partial^2}{\partial z^2}$$ This Ψ 2d is an included state

This mixed theory of 2− and 3−body nuclear fusion agreed with experimental value of 2− and 3−body mixture at Osaka university.

In the crack, deutrons give rise to 4− and 5−body reactions stimulated by 2− and 3−body reactions, but if the crack becomes wider, the nuclear fusing reactionstops because electric field disappears. When the crack gets narrower by cooling, however, the nuclear fusion takes place again because the electric field reappears. If the overcurrent is caused by on−off control of current in the crack, the nuclearfusion can be promoted.

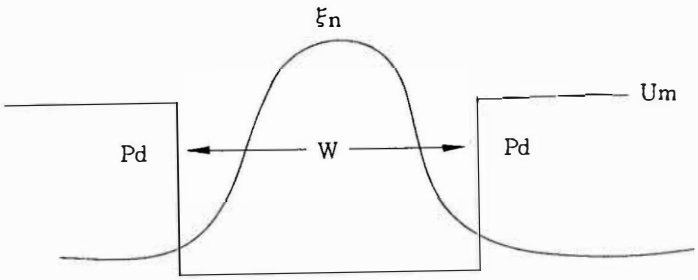

Fig. (7)

crack gets narrower.
or
on. off control of current.

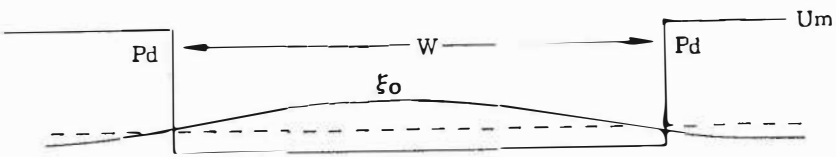

crack becomes wider

Fig. (8)

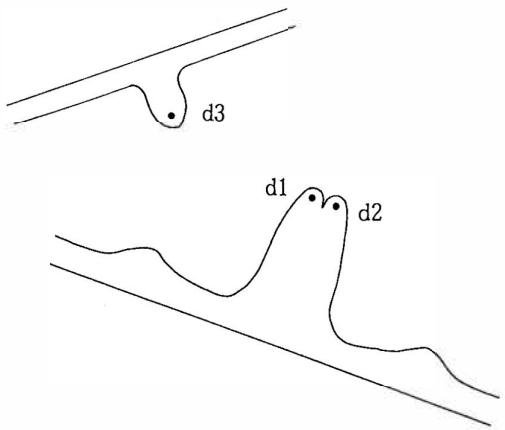

width of crack is not Parallel lines. Fig. (9)

Cold fusion fail in Experiment sometimes, as fig (9). width of cradk is Parallel lines, otherwise the compound nucleus do not collide with target nucleus.
and as fig (2), deuterium atams are Packed among lattiees of Pd atoms in the saturated state, otherwise width of crack is not Parallel lines.

References

1. Takahashi, A. et. al., 1990, J. Electron Soc EP−90−7 P−57.
2. Mizuno, T. et. al., 1992, J. Electro chemical Soc, No. 5 P, 406
3. Yagi, K, 1978, "Nuclear Physics" chap IX.
4. А. И. Блохинцев , 1963. «Основы Квантовой Механики " 2, chap, 16. §101, chap, 18, §101.
5. Aoki, M. 1990, "Solid State Physical Electronics" chap, 11.11•1.
6. Takeda, G. 1991, "Field theory" chap, 8.

Physical Description of Cold Fusion

Evan RAGLAND
6640 Ahekolo Circle
Diamondhead, MS 39525
UNITED STATES of AMERICA

ABSTRACT

Cold nuclear fusion of deuterium in an electrolysis cell with palladium electrodes is described as a comprehensive sequence of physical phenomena.

1. Electrolysis generates many more cations than are necessary to sustain ionization in the cell. The excess cations are adsorbed on the cathode surface where they create an electrical charge Q_o of "overvoltage" E_o.
2. A small fraction (0.01 to 0.1%) of the adsorbed cations, which are thousands of times smaller than typical electrolysis cations and driven by meV adsorption kinetics, penetrate several hundred lattice layers into the cathode metal. These nuclei absorb into the metal until its capacity C (n_t) saturates.
3. Because palladium metal has the property of nucleonic conductance, or "viviance", absorbed nuclei propagate throughout the metal until the internal charge Q_i reaches equilibrium with the adsorbed charge Q_o.
4. For a properly configured cathode, the density of absorbed deuterium nuclei can reach a critical level where the Coulomb force of nuclei crowds those near the cathode center to nuclear fusion.
5. The low kinetic energy of crowded fusion nuclei results in the principal nuclear reaction: [$D^2 + D^2 > H^1 + T^3 + E$]. The [$n + He^3$] reaction product is essentially repressed. Due to the short range of the energetic proton and triton in the metal, only trace product gases escape the cathode. Hence, excess heat is the predominant external evidence of the nuclear reaction.

These physical phenomena are examined in detailed theoretical arguments. It is concluded that the phenomena of cold fusion can and does occur, and that the physical explanations given in this paper reconcile the overwhelming experimental evidence supporting cold fusion.

FRONTIERS OF COLD FUSION

"THROUGHOUT the history of science new discoveries and new ideas have always caused scientific disputes, have led to polemical publications criticizing the new ideas, and such criticism has often been helpful in their development; . . . . . This violent reaction . . . . can only be understood when one realizes that the foundations of physics have started moving; and that this motion has caused the feeling that the ground would be cut from science." Werner Heisenberg, Physics and Philosophy, Harper & Brothers, 1958.

1. Introduction

Since 23 March 1989, when Stanley Pons and Martin Fleischmann startled the scientific world with the announcement of sustained nuclear fusion in an electrolysis cell using heavy water electrolyte and palladium electrodes, controversy worthy of Heisenberg's philosophy has raged. Proponents of this new discovery have determinedly advanced experimental research and in many instances have achieved significant and remarkably encouraging results. Opponents have consistently discounted these results as errors in experimental technique and interpretation. This is peripheral controversy. More significant are the substantive criticisms that there is; 1) no theoretical basis for the reaction, 2) no experimental repeatability, 3) no neutron product from branching reactions, and 4) no neutron or other radiation from secondary reactions.

These negative arguments are helpful in that they identify reasonable scientific concerns and thus define basic questions that must be answered positively. This paper addresses these questions. In response to: 1) it proposes that the Coulomb force of absorbed deuterons crowds those near the center of the palladium cathode to nuclear fusion; 2) it suggests from the mechanics of 1) a sufficiently comprehensive understanding will evolve to explain already reported experimental results and to guide future experiments; 3) it argues that the kinetic energy of the nuclear reaction is so low and the Coulomb repulsion of the protons so high that one or the other deuteron decomposes into a neutron and a proton before the nuclei are close enough to fuse, the neutron suffering no repulsion and continuing on to fusion with the surviving deuteron while the energy of the reaction is carried away by the proton; and 4) it maintains that the low kinetic energy of nuclei in the neighborhood of fusion essentially represses secondary product nuclear reactions and that the only subsequent reaction is the decay of tritons to helium 3 nuclei.

Simply put, cold fusion occurs when deuterons produced by electrolysis absorb into the palladium cathode where accumulation ultimately crowds those near the center of the cathode to [d-d] nuclear fusion. The primary product of the reaction is excess heat; a secondary product is ß radiation from the decay of tritium. Other possible reactions are suppressed by the fusion environment. More explicit explanations follow. Of particular interest may be the theoretical construct for crowding fusion, the postulated mechanics of the nucleonic conduction property of metals (viviance), and the logical extension of the Mayer/Jensen Shell Model of the nucleus to develop an Alternate Model to the generally accepted Standard Model.

2. Theoretical Construct

A space enclosed by a source of kinetic deuterons accumulates deuterons until in equilibrium with the source. Theoretically, a threshold can be reached where deuterons crowd to fusion near the center of the space. The construct envisions a hypothetical fusion cell in which a sustained envelope of deuteron plasma concentrates deuterons inward toward fusion. Fusion diameter, charge volume (C), viviance, and charge time are formulated for the threshold of fusion.

The special case of a spherical source of diameter D_o simplifies description of the physical mechanics of the cell. A constant charge;

$$Q_o = N_o \text{ deuterons, } (= N_o \times e^+ \text{ in esu}), \quad (1)$$

is assumed to be uniformly distributed about a spherical surface of diameter D_o as shown in Figure 1(a). Deuterons emanate from the source until the plasma charge Q_i within the sphere is in equilibrium with the source charge Q_o. Since the charge at the center of the sphere must be zero, the internal charge along any diameter ranges, from q_o to zero to q_o, as shown in Figure 1(b).

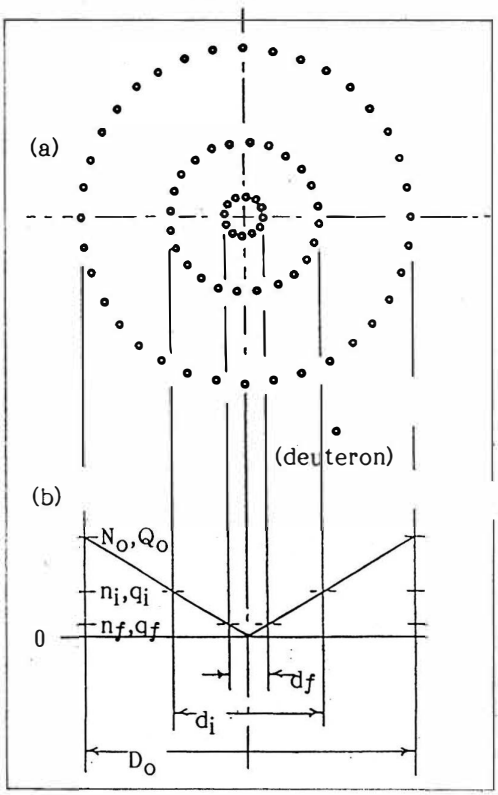

Figure 1. Theoretical construct.

The effective charge at any concentric spherical boundary ($d_i < D_o$) within the plasma is;

$$q_i = d_i Q_o / D_o, \quad (2)$$

and the number of charge elements n_i in that charge is;

$$n_i = d_i N_o / D_o. \quad (3)$$

The charge elements of cross sectional area A_e are uniformly distributed about the spherical area A_i; where,

$$A_e = \pi (d_e)^2/4, \text{ and} \quad (4)$$

$$A_i = \pi (d_i)^2. \quad (5)$$

When the product of the number of deuterons n_i and the cross sectional area of the deuteron A_e equals or exceeds the spherical surface area A_i fusion may occur; i.e. when,

$$n_i \geq 4(d_i/d_e)^2. \quad (6)$$

From (3) and (5) the diameter d_f and the number n_f of fusion elements in terms of the diameter of the deuteron d_e are,

$$d_f = (d_e)^2 N_o / 4D_o, \tag{7}$$

$$n_f = 4d_f^2 / d_e^2. \tag{8}$$

From the logic of these arguments and equations the theoretical conclusion is drawn that; Fusion of deuterons will occur about the center of a spherical space bounded by a constant deuteron charge supply source Q_o when that source exceeds the internal charge element storage capacity Q_i of the space. This is consistent with Coulomb's Law and simply stated is; Crowding Fusion is, f(constant charge source), f(finite charge space) when,

$$Q_o(D_o)^2 \geq q_f(d_f)^2, \tag{9}$$

where q_f is the fusion charge and d_f is the diameter of fusion.

Fusion will occur when,

$$4d_f^2 / d_e^2 = 1. \tag{10}$$

From (12) the critical diameter of fusion for n_f deuterons is,

(FUSION DIAMETER) $$d_f = (n_f d_e^2)^{\frac{1}{2}}/2. \tag{11}$$

The distance separating deuterons λ_i has a rate of change with respect to diameter d_i that is proportional to λ. Thus, the number of deuterons n_d across the diameter D_o is,

$$n_d = (\lambda_o - d_f)/d_e + (d_f/d_e), \tag{12}$$

where the distance between deuterons at source Q_o is λ_o; and the distance between deuterons at d_f (λ_f) is d_e.

Since d_f and d_e are (10^{-5} x λ_o) or smaller,

$$n_d \approx \lambda_o / d_e. \tag{13}$$

The approximate number of deuterons n_t to charge the volume to fusion is then,

(CAPACITY) $$n_t \approx \pi(\lambda_o/d_e)^3/6. \tag{14}$$

Q_o supplies a constant deuteron charging current called j for convenience. The transfer function relating it to the sustaining current i_o of the ionizer; i.e. the liveliness or viviance of diffusion of the deuteron in the charge medium, is designated by the symbol μ where,

(VIVIANCE) $$\mu = j/i_o. \tag{15}$$

It is convenient to measure j in amperes since the ionization of one deuteron D^+ in the source removes one electron e from the source. Then the charge time to fusion t_f is,

(CHARGE TIME) $$t_f \approx n_t/j. \quad (16)$$

This analysis can be extended to any charge medium of any shape that is within a closed charge source. Of particular interest at this time are palladium (Pd) cathodes of cold nuclear fusion electrolysis cells.

3. Viviance

Accumulated absorptivity of energy and matter crowds deuterons to cold fusion. This requires, 1) a sustained source of kinetic deuterons, 2) a field for inward drift of absorbed deuterons, and 3) the cathode bulk property of nucleonic conductance or viviance. The adsorptive kinetics of charge Q_o enveloping the cathode surface of the cold fusion cell; 1) sustain a source of kinetic deuterons, a small fraction of which penetrate the cathode, and 2) develop back voltage E_o which establishes a positive absorptive field gradient. The reversible formation and dissociation of palladium deuterides 3) provides the mechanics of viviance.

Adsorption kinetics at the cathode surface create an ionosphere of randomly moving low meV deuterons. Most capture electrons and escape the electrolyte as deuterium gas or scatter as they collide with the cathode surface. A few with direction of travel either parallel (- 1° of arc) to a crystal plane or coincident (- 0.3° arc) with a crystal channel penetrate the cathode. Repulsion of the nuclei of the crystal tends to confine these to the open space of the plane or channel. They may travel several hundred lattice layers into the crystal before being absorbed. The size of the deuteron relative to other molecules, atoms, and ions present in cell electrolysis, also contributes to the depth of penetration.

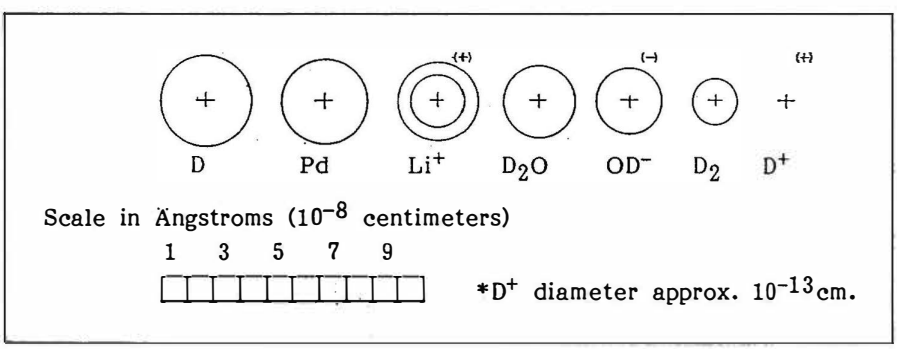

Figure 2. Size of molecules, atoms, and ions in cell electrolysis.

The systematic conditions existing at any moment in a single metal crystal with at least one surface exposed to a deuterium ionosphere include ions, atoms and molecules of deuterium and deuterides of the metal. The electrostatic charge of an individual single crystal is equal

to the totality of charge of the ions extant in the crystal at that moment. These conditions maintained; 1) this charge increases until it reaches equilibrium with the surface charge of the crystal and 2) deuterides ultimately form at all vacancies and at the boundaries of the crystal where incompleteness of crystal structure abound. In summary the single metal crystal might be characterized as a temporary electrical storage cell.

This systematic description of a single metal crystal is inadequate to describe the characteristics of the bulk metal. The composition of metal is grains of polycrystalline structure. This polycrystalline structure is schematically illustrated in Figure 3.

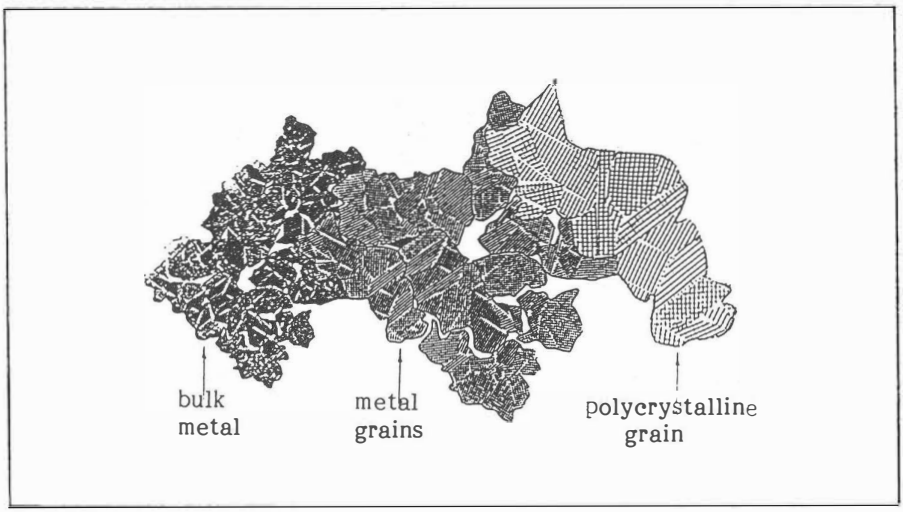

Figure 3. Polycrystalline/grain/bulk metal structure.

The typical grain structure of metals results from uneven solidification. Individual grains are seldom perfect single crystals. Generally numerous crystals of random orientation commence growth as solidification begins. A polycrystalline mass forms as these grow into one another. Disorder and structural incompleteness abound along crystalline boundaries within the polycrystalline mass. Deuterides of the metal may form along these boundaries, grain boundaries, and at other sites of structural incompleteness or irregularity. Further, there is adequate open space within the arrangement of atoms in palladium to accommodate deuterons and/or deuterium as interstitial impurities.

Deuterium exhibits almost metallic properties in alloy like deuterides, is partly positive in character and can act as a connecting bridge between metal atoms. Interstitial deuterons may expand the crystal structure and can change the phase of the structure. In palladium the deuterides may take several distinct phases $Pd_{2n}D_n$ where n is not necessarily an integer.

$Pd_{2n}D_n$ may be explained as a co-ordination compound; i.e., atoms that are united by co-ordinate bonds or valences in accordance with Werner's Co-ordination Theory. The mechanism of these bonds relies on the metallic like properties, small size, and positive charge of the deuteron to attract electrons from neutral palladium atoms which have unshared electrons. The maximum number for the deuteron as the central ion in the co-ordinate compound is 2. Thus the deuteride Pd_2D forms as,

Pd·D·Pd.

The deuteride Pd_4D_2 forms about the deuterium molecule as,

Pd. .Pd
. D·D .
Pd Pd.

Formation of Pd_2D and Pd_4D_2 is enhanced by the square planar complexes formed by covalent complexes of bivalent palladium which configure the four corners of the square coplanar with the central ion. All palladium compounds are easily decomposed and these deuterides are particularly unstable. Dissociation of palladium deuterides is reversible.

When thermal activation or kinetic disturbance causes a deuteride to dissociate deuteron(s) leave behind a negative lattice site and become conducting particle(s) free to drift in the electric field of the lattice. The typical drift path is erratic, being continually interrupted by collisions which the deuteron makes with the atoms of the lattice, with other deuterons, atoms and molecules of deuterium, etc. However, the average of deuteron drifts in the presence of cathode overvoltage E_o is inward toward the center of the cathode. The vacated negative lattice site(s) becomes available as temporary store for other deuteron(s) spent of kinetic energy. This transfer function is the conductive mechanism of viviance; the nucleon is the conducting particle, the fixed lattice sites the conducting medium, and the cumulative absorbed kinetic energy the work.

The argument is advanced that natural thermal dissociation of deuterides at polycrystalline and grain boundaries and at other crystal lattice imperfections is accelerated by kinetic encounter with newly arriving deuterons. This releases secondary deuterons to further propagate within the crystal. These nucleons tend to be repelled from crystals of higher positive charge toward neighbor crystals or grains of lesser charge and to drift along boundaries in the general direction of the field gradient of E_o. Thus nucleon mobility, the interstitial capacity of the individual crystal to absorb nucleons, and the pathways of metallic boundaries to the interior of the metal are the operative mechanics of viviance.

Systematic absorption continues until the internal charge Q_i is in equilibrium with the source charge Q_o. Equilibrium may be reached before deuterons crowd to fusion depending on individual characteristics of palladium cathode specimens.

4. Alternate Model

The fusion of nuclei is more easily visualized from the Alternate Model (a logical extension of the Mayer/Jensen Shell Model) than from the generally accepted Standard Model of the atomic nucleus.

The logic of the Standard Model constructs nucleons, protons (p) and neutrons (n), from sub nucleon particles. Simply explained, each nucleon is constructed of three quarks (electric charges) bound together by three gluons (carriers of the nuclear strong force). According to this model the atomic nucleus is a cluster or clump of nucleons bound together by the nuclear strong force of gluons.

The logic of the Alternate Model constructs the neutron as the complement of the hydrogen (protium) atom; i.e., an electron captured inside a proton. The neutron's resultant internal electric field is the nuclear strong force. According to this model the atomic nucleus is a concentricity of individual nucleon fields, each confined to a distinct shell location by wave length and angular and spin momenta. The structure conforms to the Pauli exclusion principle, the principles of quantum mechanics, and with the exception of the protium nucleus is bound together by the neutron(s) internal field(s).

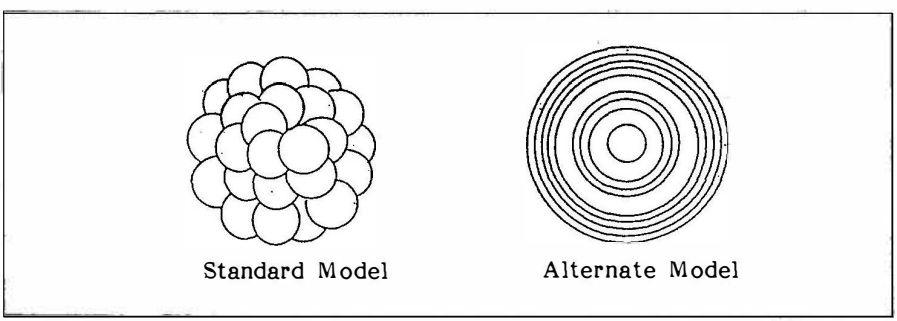

Figure 4. Models of the atomic nucleus.

5. Crowding Nuclear Fusion

Cold fusion in an electrolysis cell is a deuteron to deuteron [d-d] reaction caused by Coulomb crowding. The products of the three possible d-d nuclear reactions are: 1) [p + ^{3}H], 2) [n + ^{3}He], and 3) [^{4}He + gamma ray]. High energy deuteron fusion experiments have shown that reactions 1) and 2) occur in about even proportions. Reaction 3) is not expected as it requires even higher energies to occur. It is generally assumed that reactions 1) and 2) should always produce a 1:1 branching ratio. Reported neutron observations in cold fusion experiments are 10^{-9} to 10^{-6} of the expected product. Hence, it is concluded the absence of neutrons proves there is no nuclear reaction. This conclusion is specious. Reaction 2) does not occur in cold fusion, therefore no neutrons should be observed.

The interaction of the strong forces of the nuclei causes the nuclei to fuse. Fusion occurs when nuclei are crowded to within one nuclear diameter of one another even though they possess no kinetic energy. The [d-d] reaction in a crowded environment ($\lambda \sim 10^{-12}$ cm.) is illustrated (in accordance with the Alternate Model) in Figure 5. Two deuterons D^+, thermally activated, move toward collision at time t_o. Their kinetic energies are small fractions of an electron volt. At time t_{-n+1} the proton (clear) and the neutron (hatched) of each deuteron are concentric about a common center. At some later time t_{-2} they remain centered, but the neutrons internal fields distort in reaction to the Coulomb repulsion of the protons. Later at time t_{-1} one proton overcomes the neutron field and breaks free of the common center. At time t_o the overlap of the neutron strong forces begin to draw the neutrons toward a common center and the Coulomb repulsion of the two protons begins to move them apart. By time t_{+1} the triton has formed and begun to "settle in" and both it and the proton move apart with added kinetic energy from the fusion reaction.

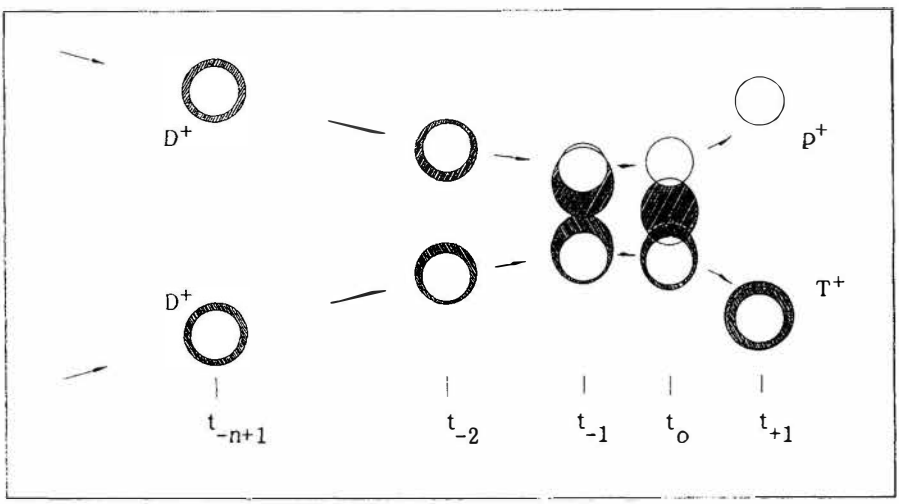

Figure 5. Model illustrating deuteron to deuteron fusion.

The Alternate Model is used for ease of illustration. The same results can be demonstrated using the Standard Model but the conceptualism lends to ambiguity. The argument is that the inertial velocity possible for thermally excited deuterons in the micro dimensions of crowding precludes the collision of the proton components.

6. Conclusion

It is concluded that the phenomena of cold fusion can and does occur. The reaction is a bulk effect. The physical mechanics are simple; almost primitive. Accumulation of absorbed kinetic deuterons can cause Coulomb crowding to reach [d-d] nuclear fusion reaction levels near the

center of high viviance electrolysis cell cathodes. Most transitional metals (Ti to Ni, Zr to Pd, and Hf to Pt) exhibit viviance. The VIIIA metals Pd, Pt, and Ni in its ß phase are unusually viviant. Because of the low kinetic energy of the fusing nucleons only the [d-d] > [p-t] reaction occurs. As a result the primary energy product is heat and the primary radiation product is tritium decay.

The cold fusion cell is inherently small in size and power output as a result of the micro dimensions of the reaction. Large power sources will require batteries of cells. Any disadvantage from this should be largely offset by flexibility of sizing and independence of location. The lack of neutron radiation has positive environmental impact when compared to hot fusion reactions.

Naturally solidified metals are marginally suitable for fusion cell experiments. Cathode metals with controlled and predictable characteristics would accelerate experimental progress.

Cold fusion is one of the great discoveries of natural phenomena. With it comes the potential to open new physical realms beyond just the generation of energy. Much scientific credit is due Pons and Fleischmann for this discovery.

Acknowledgments

The discussions, patient audience, and encouragement of Robert Altenkirch, Bruce Cain, and Albert Gu of Mississippi State University; Mrs. Arlene McGahey Jones of the University of Alabama; and Robert Barton of Scottsdale, Arizona have sustained the research spirit of this paper. Jeb Rothwell of Cold Fusion Research Advocates has helpfully provided news, technical reports, and data from cold fusion activities. Mrs. Theo Vaughey has attended and audited most technical reviews of the work and has been most helpful in the preparation of this paper.

Multilayer Thin Film Electrodes for Cold Fusion

G.H. MILEY, J.U. PATEL and J. JAVEDANI Fusion Studies Lab.
Dept. of Nuclear Engr., University of Illinois, Urbana IL 61801 USA

H. HORA and J. C. KELLY Physics Dept.
University of New South Wales, Sydney, 2033 Australia

J. TOMPKINS Rockford Technology Associates, Inc.
Champaign, IL 61821 USA

ABSTRACT

The application of the "swimming electron layer" theory[1,2] to the design of multilayer electrodes is discussed. A key advantage of this approach is that the enhanced reaction rate at interfaces between select metals results in a high power density throughout the volume of the electrode.

Design criteria and fabrication techniques devised for the multilayer thin films are discussed. Initial experiments using a dense plasma focus (DPF) for loading these targets are described along with the design of an electrolytic cell intended to test scaling to high powers.

1. Introduction

Since the first exciting announcements[3,4] experimental results have lead the theoretical explanations for understanding the mysterious cold fusion phenomena. Many theoretical explanations offered to explain the experimental results on cold fusion were examined critically by Preparata[5], who stresses the key problem of overcoming the coulomb barrier, before the deuterium nuclei could fuse. Most of the theories Preparata reviews, plus his own[5], fully treat the cold fusion as a quantum mechanical tunneling effect. This does not, however, fully explain the high reaction rates observed in recent experiments which are thought to involve surface or interface effects[6,7]. Thus the "swimming electron layer" theory was developed to address this issue. This model is based on the surface

FRONTIERS OF COLD FUSION

tension effects on an exotic plasma at the metal interfaces, which can cause and give enhanced reaction rates. The process of cold fusion in deuterated multilayer targets will be considered according to this model in the following Section whereas, the status of the experiments in progress will be discussed in Section 3.

2. Application of the "Swimming Electron Layer" theory to Cold Fusion

Many experiments so far have indicated that cold fusion is a surface related exothermic phenomena. The "swimming electron layer" theory is consistent with this observation and suggests the use of multilayer thin foils in order to induce reactions throughout the volume of an electrode. This will in turn allow direct scaling to high power levels in minimum size cells.

Multilayer electrodes suggested in this model will have closely spaced interfaces at which cold fusion would occur to provide a high power output. Related experiments using coated electrodes have been reported by Arata and Zhang[6], whereas multiple large volume Pd/Si layers have been studied by T. Claytor[7]. Both experiments were quite successful and thus provides encouragement for the multilayer film concept.

The metal pairs used in the present experiments for fabricating multilayer electrodes is selected so that the metals do not diffuse into each other in order to maintain well-defined interfaces. The differences in Fermi levels of these metals adjust at the interfaces such that an electron layer is created that is most effective in shielding the positive charges of fusing deuterons. The dynamic shielding effect of the electron layer may further be enhanced if the electrode is connected to the negative terminal of a power source that floods the conduction bands of metals with electrons. Thus, when one uses an AC power source or ramps the current from a DC source during the electrolysis, a dynamical non equilibrium condition is created. This effect is related to the enhanced reaction rate observed by others using oscillating or ramped voltages[6,7].

The basic process is viewed as involving colliding thermal deuterons at the interfaces of multilayer electrodes. At the low speeds involved, the D^+ nuclei will be polarized (see Figure 1). The shielding of the positive

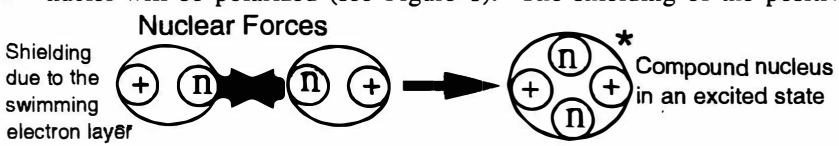

Figure 1. Cold fusion of D^+ shielded by swimming electron layer.

charge in this state by the swimming electron layer allows a very close approach, where the nuclear forces become effective to form a compound nucleus in an excited state.

3. Experimental Methods

Experiments using multilayer electrodes are under way. Thin film foils for DPF experiments are made by electron beam evaporation from water-cooled copper crucibles onto cooled aluminum disks. Layer growth is controlled by a quartz crystal monitor; a deuterium atmosphere can be used if needed to provide preloading. Five such foils have been successfully fabricated to date.

The extension to electrodes for later electrolytic cell experiments is also under study. Nickel cathodes in the shape of hollow cylinders to be used in electrolysis, will be coated with alternating multiple layers.

The selection of metal pairs for multilayer interface effects favors the highest difference for the Fermi energies consistent with adequate diffusion coefficients for loading and an adequate solubility of deuterium in at least one of the pairs. Some potential candidates are tabulated in Table 1. along with their Fermi energies calculated by H. Hora[8] according to formula 6.39 in Reference 8.

Table 1. Table of Fermi Energies for various Metals.[8]

Metal	Ti	Ni	Co	Fe	Pt	Pd	Th	Ce	Zr
E_F eV	5.35	7.35	7.34	7.01	5.91	6.04	3.54	3.35	4.42

The Pd/Ce pair has a difference of 2.96 eV in Fermi energies whereas the Ni/Ce pair has 4.02 eV difference. Thus the Ni/Ce pair offers a maximum difference and will be used extensively in our later experiments. Targets now under study use 10-30 layers of Ti/Fe with layer thicknesses of 10-20 nm. These materials were selected initially based on the ease of handling them and the fact they meet the desired criteria (but are not optimum). Several were fabricated in a deuterium atmosphere to obtain a pre-loading of deuterium.

In some cases a diffusion barrier layer is applied on the outer most surface of the electrode to ensure a sustained high loading ratio of deuterium. A thin layer of Fe-Ni alloy is used for this purpose since it has an extremely low diffusion coefficient for D^+. High currents of D^+ can be driven through such a barrier layer if a minimum thickness is selected as discussed by Uhm and Lee[9].

A 25-kJ DPF device at the University of Illinois is being used to load multilayered foils. The DPF implantation offers distinct advantages[10]: the

plasma cleans the outer surface, eliminating oxide layers; higher energy ions provide good penetration and a number of different foils can be "screened" for performance quickly. The U of I DPF gives a 3 - 5 x 10^5 Ampere 40 ns pulse using a unique axial magnetic field for stabilization. Foils are placed in a special holder with their surface at the base of the pinch plasma. Multiple pulses (80-100) are used for high loading. Various diagnostic techniques including auto radiography[10], charged particle detection and calorimetry are employed. State-of-the-art facilities for sputtering and vacuum evaporation are used for the fabrication of multilayer foils with 50-100 individual layers of 10-30 nm thickness.

The extension of this method to cylindrical electrodes is underway. A unique electrolysis setup with dual cells and hollow cylindrical multilayer cathodes has been designed to study power production in this configuration. Results from the DPF experiments will be used to select optimum metal pairs for the cell electrodes. This cell arrangement is such that a precise measurement of the generation of excess heat can be carried out simultaneously with studies of nuclear particle emissions. The scaling of the design to large powers is also relatively straightforward.

4. Conclusions

The approach proposed here is unique in describing cold fusion as an interface phenomena, consistent with both the "swimming electron layer" theory and with recent experimental results that indicate reaction mainly occur at electrode surfaces. Techniques have been developed to fabricate multilayer thin film electrodes which should produce a high power density throughout the electrode volume. Experiments are in progress to verify this.

5. References

1. H. Hora, G.H. Miley et al., 1990, Nuovo Cimento, **12**, (3), 393.
2. G.H. Miley H. Hora et al., 1990, World Hydrogen Energy Conference #8 in Hawaii, pp. 169.
3. M. Fleischman and S. Pons, 1989, J. Electroanal. Chem., **261**, 301.
4. S.E. Jones et al., 1989, Nature, **338**, 737.
5. G. Preparata, 1991 Fusion Technology, **20**, 82.
6. Y. Arata and Y-C Zhang, 1992, Fusion Technology, **22**, 287.
7. Tom Claytor et al, 1991, 2nd Annual Conference on Cold Fusion, Como, Italy, pp. 395.
8. H. Hora, "*Plasma at high temperature and density*" Springer Verlag, 1992, pp. 101.
9. H. S. Uhm and W. M. Lee, 1991, Physics of Fluids, **B 3**, 3188.
10. R.K. Rout, et al., 1991, Fusion Technology, **19**, 391.

Electrodeless, Multi-Megawatt Reactor for Room-Temperature, Lithium-6/Deuterium Nuclear Reactions

Jerome DREXLER
25440 Becky Lane
Los Altos Hills, California 94022
U.S.A.

ABSTRACT

This paper describes a reactor design to facilitate a room-temperature nuclear fusion/fission reaction to generate heat without generating unwanted neutrons, gamma rays, tritium, or other radioactive products.

The room-temperature fusion/fission reaction involves the sequential triggering of billions of single-molecule, Li^6D "fusion energy pellets" distributed in lattices of a palladium ion accumulator that also acts as a catalyst to produce the molecules of Li^6D from a solution comprising D_2O, Li^6OD with D_2 gas bubbling through it. The D_2 gas is the source of the negative deuterium ions in the Li^6D molecules.

The next step is to trigger a first nuclear fusion/fission reaction of some of the Li^6D molecules, according to the well-known nuclear reaction:

$$Li^6 + D \rightarrow 2\ He^4 + 22.4\ MeV$$

The highly energetic alpha particles (He^4 nuclei) generated by this nuclear reaction within the palladium will cause shock and vibrations in the palladium lattices, leading to compression of other Li^6D molecules and thereby triggering a second series of similar fusion/fission reactions, leading to a third series, and so on. The absorption of the kinetic energy in the palladium will, in turn, generate a continuous flow of heat into the heavy water carrier, which would be removed with a heat exchanger.

FRONTIERS OF COLD FUSION

The reactor apparatus has several potential advantages over the Pons-Fleischmann ("P-F") electrolytic cell structure. In particular, the reactor apparatus allows scaling up the number of reactor cells and the reactor size to meters or even kilometers, to permit multi-megawatt power levels. It also is much safer to work with since there are no electrodes or oxygen gas that could trigger the chemical reaction D + O and an explosion.

1. Introduction

The Pons-Fleischmann experiments, announced in March 1989, brought us a nuclear energy source of significant potential. However, the P-F electrolytic cell does not offer the designer of a high-power reactor much design latitude. It is as simple in its design and power level as the Fleming valve, the first vacuum diode used in radio. Fifty years later, the inventions of the magnetron and klystron, with their large distributed energy interaction areas, enabled multi-megawatts to be generated. The concept of distributed interaction areas for energy generation also can be applied to a room-temperature fusion/fission reactor.

2. Analysis of the Pons-Fleischmann Electrolytic Cell

How does the P-F electrolytic cell achieve room-temperature nuclear reactions? Analysis has led to the conclusion that the P-F electrolytic cell accomplishes two initial functions: (a) it generates deuterium gas and deuterium ions at the palladium cathode surface through electrolysis of the heavy water and (b) the voltage gradient pushes the positive lithium-6 ions into the surface lattices of the palladium cathode.

Such a simple electrolytic cell performing both of these initial functions and also "catalyzing" the room-temperature nuclear reaction as well is truly amazing. How does one optimize the design of such a simple structure when it is accomplishing all of these functions? Any attempt to optimize one of the functions might degrade the others. It is impressive that Pons and Fleischmann found designs that worked at all.

3. The Synthesis of the Electrodeless, Multi-Megawatt, Drexler Reactor

Without electrodes, electrolysis, or voltage gradients in the Drexler reactor, other methods are used to provide the necessary deuterium gas and the essential flow of lithium-6 ions into the palladium lattices. These other methods use (a) a pressurized tank, to feed the deuterium gas into the heavy water at a number of key points and (b) mechanical pump(s), to cause a significant flow of heavy water containing lithium-6 ions through a closed-loop torus (toroid), multi-cell reactor structure, as shown later in Figures 1 and 2.

Without the palladium cathode of the P-F cell, the Drexler reactor must use other ion accumulator designs such as the perforated, palladium-based baffles shown later in Figures 3 and 4. Ionized D_2O (containing D_2 and Li^6OD) is pumped through the torus (doughnut)-shaped, multi-cell reactor structure and through the baffles at pressures and flow rates determined by the number of holes, their sizes, and the pump capacity. The pressure at the palladium-coated surfaces of the baffles will force deuterium and lithium ions into the palladium lattices, where they can chemically react to form large numbers of single-molecule, Li^6D "fusion energy pellets." Shock and vibration from the turbulent heavy-water flow, ultrasonics, or other methods would then trigger some of the Li^6D molecules into the fusion/fission reaction:

$$Li^6 + D \rightarrow 2\ He^4 + 22.4\ MeV$$

The highly energetic alpha particles generated by this nuclear reaction will cause shock and vibrations in the palladium lattices, leading to compression of other Li^6D molecules and thereby triggering a second series of similar fusion/fission reactions, leading to a third series, and so on. The absorption of the kinetic energy in the palladium will, in turn, generate a continuous flow of heat into the D_2O carrier, which would be removed with a heat exchanger.

This reaction is called a fusion/fission reaction since initially it forms the fusion product beryllium-8, which instantly fissions into two energetic alpha particles. The use of lithium-6 deuteride pellets as a nuclear energy source is not new--in fact, they are used in some hydrogen bomb designs to enhance energy output. Also, in generating multi-megawatts, there always is concern about generating undesirable neutrons, gamma rays, tritium, or other radioactive byproducts. This well-known nuclear reaction avoids all of those byproducts.

4. Summary

This room-temperature fusion/fission reactor design overcomes the power-generation limitations of the P-F electrolytic cell and avoids the use of electrodes and electrolysis inherent in the P-F cell design. Its key features are: (a) no electrolysis--deuterium gas is injected, (b) multi-cell structure for large power output, (c) closed-loop reactor for thermal efficiency and to isolate reactants from the atmosphere, (d) energetic alpha particles are the only reaction products, (e) no oxygen gas--threat of explosion is removed.

The author's international patent application, PCT/US91/03503, entitled, "Distributed Deuterium-Lithium Energy Apparatus," [priority date May 25, 1990] describes this torus-shaped reactor, helical-shaped reactor designs, and ion accumulators using beds of palladium particles.

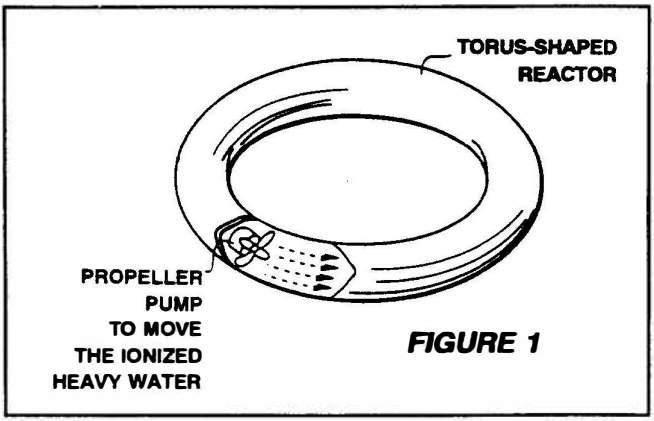

Figure 1. Perspective view of the electrodeless "cold fusion" reactor apparatus, showing a propeller pump for driving the ionized heavy water through a closed-loop torus.

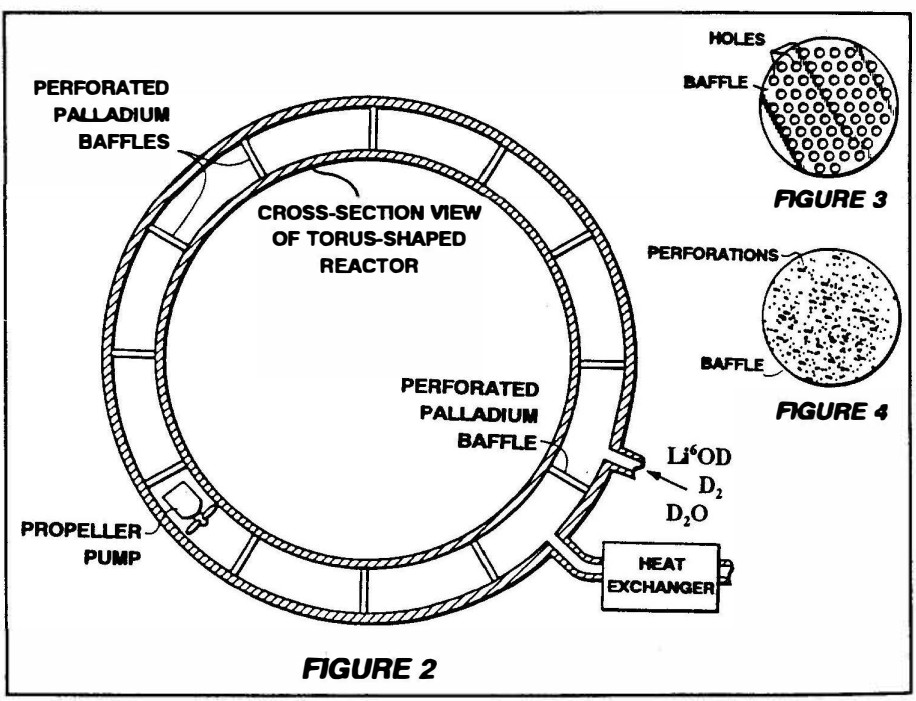

Figures 2 - 4. Figure 2 is a sectional view of the reactor apparatus showing the propeller pump and a sequence of perforated palladium baffles, represented by Figure 3 and Figure 4, which may be used as palladium- or palladium-alloy ion accumulators.

Conference Program

FULL PAPER :
*not accepted
†not received

October 21, Wednesday
Registration
Welcome Party

October 22, Thursday
Registration
Opening Address H. Kakihana

Morning Session I (Oral) Chairpersons : S. Pons and K. Ota

Excess Heat

M. C. H. McKubre, S. Crouch-Baker, A. M. Riley, S. I. Smedley and F. L. Tanzella
Excess Power Observations in Electrochemical Studies of the D/Pd System; in the Influence of Loading

T. N. Claytor (for E. Storms)
Measurement of Excess Heat from a Pons-Fleischmann Type Electrolytic Cell

K. Kunimatsu, N. Hasegawa, A. Kubota, N. Imai, M. Ishikawa, H. Akita and Y. Tsuchida
Deuterium Loading Ratio and Excess Heat Generation during Electrolysis of Heavy Water by a Palladium Cathode in a Closed Cell Using a Partially Immersed Fuel Cell Anode

M. Srinivasan, A. Shyam, T. K. Sankaranarayanan, M. B. Bajpai, H. Ramamurthy, U. K. Mukherjee, M. S. Krishnan, M. G. Nayar and Y. P. Naik
Tritium and Excess Heat Generation during Electrolysis of Aqueous Solutions of Alkali Salts with Nickel Cathode

N. Oyama, T. Terashima, S. Kasahara, O. Hatozaki, T. Ohsaka and T. Tatsuma
Electrochemical Calorimetry of D_2O Electrolysis Using a Palladium Cathode in a Closed Cell System

K. Ota, M. Kuratsuka, K. Ando, Y. Iida, H. Yoshitake and N. Kamiya
Heat Production at the Heavy Water Electrolysis Using Mechanically Treated Pd Cathode

Morning Session II (Oral) Chairpersons: T. P. Perng and N. Oyama

Materials and Hydrogen Behavior

M. Enyo
Hydrogen/Deuterium Concentration in Pd under Cathodic Polarization

D. R. Coupland, M. L. Doyle, J. W. Jenkins, J. H. F. Notton, R. J. Potter and D. T. Thompson
Some Observations Related to the Presence of Hydrogen and Deuterium in Palladium

Y. Fukai
The ABC's of the Hydrogen-Metal System

B. Escarpizo, J. F. Fernandez, F. Cuevas, J. Tornero and C. Sánchez
Deuterium Concentration Profiles and Crystallization Anomalies in Electrolytically Deuterated Titanium Plates

D. L. Wang, S. H. Chen, D. X. Fan, W. J. Chen, Y. J. Li, Y. B. Fu and X. W. Zhang
Experimental Studies on the Anomalous Phenomenon in Pd Metal Loaded with Deuterium

Afternoon Session I (Poster)

Theory and Modeling

†22PI-1 G. Preparata
Theory of Cold Fusion in Deuterated Palladium

22PI-2 V. A. Romodanov, V. I. Savin, Ya. Skuratnik and Yu. M. Timofeev
Nuclear Fusion in Condensed Matter

†22PI-3 P. L. Hagelstein
Coherence Effects: Theoretical Considerations

†22PI-4 P. L. Hagelstein
Coherent and Semi-Coherent Neutron Transfer Reactions

22PI-5 T. Tani and Y. Kobayashi
Tunnel Disintegration and Neutron Emission Probability

†22PI-6 A. Scalia
Anomalies in Nuclear Fusion for Light System at Very Low Energy

*22PI-7 V. A. Chechin and V. A. Tsarev
On a Nonstationary Quantum Mechanical Origin of Cold Nuclear Fusion

22PI-8 T. Matsumoto
Review for "Nattoh" Model and Experimental Findings during Cold Fusion

*22PI-9 J. Yang, X. Chen, L. Tang, D. Xie and L. Gu
"Abnormal" Nuclear Phenomena and Weak Interaction Process

*22PI-10 J. Yang and X. Chen
Dineutron Model of the Cold Fusion

*22PI-11 G. Drăgan
Water-Medium for Natural Nuclear Transmutations

22PI-12 S. Szpak, P. A. Mosier-Boss and J. J. Smith
Comments on Methodology of Excess Tritium Determination

22PI-13 K. Tsuchiya, K. Ohashi and M. Fukuchi
Mechanism of Cold Nuclear Fusion in Palladium

22PI-14 A. de Ninno and V. Violante
"Quasi-Plasma" Transport Model in Deuterium Overloaded Palladium Cathodes

22PI-15 N. Matsunami
A Mechanism for Cold Nuclear Fusion: Barrier Reduction by Screening under Transient Coherent Flow of Deuterium

22PI-16 K. Fukushima
Is Sono-Fusion to be a Possible Mechanism for Cold Fusion ?

22PI-17 X. Z. Li, D. Z. Jin and L. Chang
The Combined Resonance Tunneling and Semi-Resonance Level in Low Energy D-D Reaction

†22PI-18 L. Fonda and G. L. Shaw
Anti-Diquark Catalysis of Cold Fusion

22PI-19 Z. L. Zhang and S. I. Liu
Thermodynamic Theory of Cold Nuclear Fusion (C. N. F)

22PI-20 S. R. Chubb and T. A. Chubb
Ion Band State Fusion

22PI-21 M. Tamaki and K. Tasaka
Field Formation of the Condensed Matter Fusion by Electro-Transport of Deuterium in Palladium

*22PI-22 K. Chukanov and A. Chukanov
Chukanov Cold Fusion Effect

†22PI-23 A. Tenenbaum and E. Tabet
Temporal Sequence of Nuclear Signals in a "Dry" Cold Fusion Experiment

22PI-24 E. L. Ragland
A Physical Description of Cold Fusion

22PI-26 N. Yabuuchi
Quantum Mechanics on Cold Fusion

†22PI-27 P. Glück
"Surfdyn" : Is this Concept Able to Promote Anomalous Nuclear Phenomena to Normal Cold Fusion Science ?

*22PI-28 V. I. Vysotskii and R. N. Kuz'min
Nonthreshold Cold Fusion as a Result of Nonequilibrium Deuterium Fermi-Condensate in Microholes of Crystal

*22PI-29 G. V. Fedorovich
Nuclear Fusion in the E-Cell

22PI-30 K. Yasui
Fractofusion Mechanism

22PI-31 Y. E. Kim, M. Rabinowitz, R. A. Rice and J. -H. Yoon
Condensed Matter Effects for Cold and Hot Fusion

*22PI-32 O. Q. Gou, Z. H. Zhu and Q. F. Zhang, A. P. Ye and B. Y. Miao
The Possible Theoretical Model and it's Experimental Evidences of Cold Fusion

22PI-33 J. T. Waber
Solid State Boson Condensation Model of Cold Fusion

†22PI-34 Y. Chuanzan and Y. F. Chang
Physical Mechanism of Cold Fusion of Nuclei

†22PI-35 Yu. N. Bazhutov and G. M. Vereshkov
New Stable Hadrons in Cosmic Rays, their Theoretical Interpretation and Possible Role in Cold Nuclear Fusion Catalysis

22PI-36 M. Rambaut
Lawson Criterion Made Obsolete by Cold Fusion through the Double Screening Process

†22PI-37 J. R. Huizenga
Cold Fusion Claims

22PI-38 J. -P. Vigier
New Hydrogen Energies in Specially Structured Dense Media: Capillary Chemistry and Capillary Fusion

Afternoon Session II (Poster)

Materials and Hydrogen Behavior

22PII-1 M. Enyo
Hydrogen/Deuterium Concentration in Pd under Cathodic Polarization

22PII-2 D. R. Coupland, M. L. Doyle, J. W. Jenkins, J. H. F. Notton, R. J. Potter and D. T. Thompson
Some Observations Related to the Presence of Hydrogen and Deuterium in Palladium

22PII-3 Y. Fukai
The ABC's of the Hydrogen-Metal System

*22PII-4 A. L. Samgin, V. I. Tsidilkovski and A. N. Baraboshkin
On the Possible Formation of Regions with High Hydrogen Isotope Concentration at Nonlinear Diffusion in Transition Metals

†22PII-5 P. L. Hagelstein
Possible Instabilities in Heat Production

†22PII-6 A. L. Samgin and A. N. Ezin
Nonlinear Diffusion of Deutrium in PdDx under Peaking Regime Boundary Condition

22PII-7 T. Sano, T. Terasawa T. Ohi and S. Nezu
Preparation of Pd Electrodes and Their Hydrogen Loading Ratios

22PII-8 A. Kubota, H. Akita, Y. Tsuchida, T. Saito, A. Kubota, N. Hasegawa, N. Imai, N. Hayakawa and K. Kunimatsu
Hydrogen and Deuterium Absorption by Pd Cathode in a Fuel-Cell Type Closed Cell

22PII-9 T. Nakata, Y. Tsuchida and K. Kunimatsu
Absorption of Hydrogen into Palladium Foil Electrode: Effect of Thiourea

22PII-10 T. Mizuno, T. Akimoto, K. Azumi and M. Enyo
Cold Fusion Reaction Products and Behaviour of Deuterium Absorption in Pd Electrode

22PII-11 B. Escarpizo, J. F. Fernandez, F. Cuevas, J. Tornero and C. Sánchez
Deuterium Concentration Profiles and Crystallization Anomalies in Electrolytically Deuterated Titanium Plates

†22PII-12 E. Palibroda and M. Jalobeanu
Cold Fusion and the Water Electrolysis H-D Separation Factor

†22PII-13 V. A. Goltsov
Structural and Dynamic Effects at Palladium and its Alloys Interaction with Hydrogen

†22PII-14 M. Ragheb, C. O'Connor and M. Shaheen
On the Anomalous Deuterium to Hydrogen and the U235 to U238 Ratios in the Oklo Phenomenon Samples

22PII-15 M. Nakada, T. Kusunoki, M. Okamoto and O. Odawara
A Role of Lithium for the Neutron Emission in Heavy Water Electrolysis

22PII-16 C. L. Hsu, C. M. Wan and F. -R. Chen
TEM Investigation of Hydrogen Ordering in Pd

22PII-17 N. Oyama, N. Yamamoto and T. Tatsuma
In-Situ Electrochemical Quartz Crystal Microbalance Studies of Water Electrolysis at a Palladium Cathode

Miscellaneous

22PII-18 K. Kamada
Electron Impact H-H and D-D Fusions in Molecules Embedded in Al

22PII-19 G. H. Miley, J. U. Patel, J. Javedani, H. Hora, J. C. Kelly and J. Tompkins
Multilayer Thin Film Electrodes for Cold Fusion

†22PII-20 F. E. Cecil, H. Liu and J. S. Yan
Recent Measurements of Deuteron-Induced Nuclear Reactions at Very Low Energies

22PII-21 J. Drexler
Electrodeless, Multi-Megawatt Reactor for Room-Temperature, Lithium-6/Deuterium Nuclear Reactions

22PII-22 H. Komaki
Observations on the Biological Cold Fusion or the Biological Transmutation of Elements

22PII-23 A. B. Karabut, Ya. R. Kucherov and I. B. Savvatimova
Possible Nuclear Reactions Mechanisms at Glow Discharge in Deuterium

*22PII-24 E. Lewis
A Proposal for the Performance of Four Kinds of Experiments to Test My Own Hypotheses and a Statement of a Deduction about Phenomena

Excess Heat I

22PII-25 M. C. H. McKubre, S. Crouch-Baker, A. M. Riley, S. I. Smedley and F. L. Tanzella
Excess Power Observations in Electrochemical Studies of the D/Pd System; the Influence of Loading

22PII-26 E. Storms
Measurement of Excess Heat from a Pons-Fleischmann Type Electrolytic Cell

22PII-27 K. Kunimatsu, N. Hasegawa, A. Kubota, N. Imai, M. Ishikawa, H. Akita and Y. Tsuchida
Deuterium Loading Ratio and Excess Heat Generation during Electrolysis of Heavy Water by a Palladium Cathode in a Closed Cell Using a Partially Immersed Fuel Cell Anode

22PII-28 M. Srinivasan, A. Shyam, T. K. Sankaranarayanan, M. B. Bajpai, H. Ramamurthy, U. K. Mukherjee, M. S. Krishnan, M. G. Nayar and Y. P. Naik
Tritium and Excess Heat Generation during Electrolysis of Aqueous Solutions of Alkali Salts with Nickel Cathode

22PII-29 N. Oyama, T. Terashima, S. Kasahara, O. Hatozaki, T. Ohsaka and T. Tatsuma
Electrochemical Calorimetry of D_2O Electrolysis Using a Palladium Cathode in a Closed Cell System

October 23, Friday

Morning Session I (Oral) Chairpersons : J. O'M. Bockris and K. Kunimatsu

Excess Heat

Panel Discussion on Takahashi Method
A. Takahashi, B. Bush, E. Mallove, F. Celani and A. de Ninno

M. Fleischmann and S. Pons
Calorimetry of the PD·D_2O System: from Simplicity via Complications to Simplicity
S. I. Smedley, S. Crouch-Baker, M. C. H. McKubre and F. L. Tanzella
The January 2, 1992, Explosion in a Deuterium / Palladium Electrolytic System at SRI International
A. Takahashi, A. Mega, T. Takeuchi, H. Miyamaru and T. Iida
Anomalous Excess Heat by D_2O/Pd Cell under L-H Mode Electrolysis
M. H. Miles and B. F. Bush
Calorimetric Principles and Problems in Pd-D_2O Electrolysis
F. Celani, A. Spallone, P. Tripodi and A. Nuvoli
Measurements of Excess Heat and Tritium during Self-Biased Pulsed Electrolysis of Pd-D_2O
A. de Ninno and V. Violante
"Quasi-Plasma" Transport Model in Deuterium Overloaded Palladium Cathodes

Morning Session II (Oral) Chairpersons : Y. Kim and T. Shibata

Theory and Modeling

Panel Discussion on Theoretical Model
P. Hagelstein, G. Preparata, V. Romodanov and J. Vigier

P. L. Hagelstein
Coherent and Semi-Coherent Neutron Transfer Reactions
V. A. Romodanov, V. I. Savin Ya. Skuratnik and Yu. M. Timofeev
Nuclear Fusion in Condensed Matter
J. -P. Vigier
New Hydrogen Energies in Specially Structured Dense Media : Capillary Chemistry and Capillary Fusion

October 24, Saturday

Morning Session I (Oral) Chairpersons : C. Sánchez and K. Nishizawa

Nuclear Products

D. B. Buehler, L. D. Hansen, S. E. Jones and L. B. Rees
Is Reported "Excess Heat" due to Nuclear Reactions ?
E. Yamaguchi and T. Nishioka
Direct Evidence for Nuclear Fusion Reactions in Deuterated Palladium
M. H. Miles and B. F. Bush
Search for Anomalous Effects Involving Excess Power and Helium during D_2O Electrolysis Using Palladium Cathodes
T. Iida, M. Fukuhara, H. Miyazaki, Y. Sueyoshi, Sunarno, J. Datemichi and A. Takahashi
Deuteron Fusion Experiment with Ti and Pd Foils Implanted with Deuteron Beams
J. Kasagi, K. Ishii, M. Hiraga and K. Yoshihara
Observation of High Energy Protons Emitted in the TiD_x + D Reaction at E_d = 150 keV and Anomalous Concentration of ^3He
A. B. Karabut, Ya. R. Kucherov and I. B. Savvatimova
Possible Nuclear Reactions Mechanisms at Glow Discharge in Deuterium
K. Kaliev, A. Baraboshkin, A. Samgin, E. Golikov, A. Shalyapin, V. Andreev and P. Goluburchiy
Reproducible Nuclear Reactions during Interaction of Deuterium with Oxide Tungsten Bronze

D. Gozzi, P. L. Cignini, R. Caputo,M. Tomellini, G. Balducci, G. Gigli, E. Cisbani, S. Frullani, F. Garibaldi, M. Jodice and G. M. Urciuoli
Experiments with Global Detection of Cold Fusion Byproducts

Afternoon Session I (Poster)

Nuclear Products I

24PI-1 D. B. Buehler, L. D. Hansen, S. E. Jones and L. B. Rees
Is Reported "Excess Heat" Due to Nuclear Reactions ?

24PI-2 M. Nakada, T. Kusunoki and M. Okamoto
Energy of the Neutrons Emitted in Heavy Water Electrolysis

24PI-3 E. Yamaguchi and T. Nishioka
Direct Evidence for Nuclear Fusion Reactions in Deuterated Palladium

24PI-4 M. H. Miles and B. F. Bush
Search for Anomalous Effects Involving Excess Power and Helium during D_2O Electrolysis Using Palladium Cathodes

24PI-5 J. Kasagi, K. Ishii, M. Hiraga and K. Yoshihara
Observation of High Energy Protons Emitted in the TiD_x + D Reaction at E_d = 150 keV and Anomalous Concentration of ^3He

24PI-6 K. Kaliev, A. Baraboshkin, A. Samgin, E. Golikov, A. Shalyapin, V. Andreev and P. Goluburchiy
Reproducible Nuclear Reactions during Interaction of Deuterium with Oxide Tungsten Bronze

24PI-7 D. Gozzi, P. L. Cignini, R. Caputo, M. Tomellini, G. Balducci, G. Gigli, E. Cisbani, S. Frullani, F. Garibaldi, M. Jodice and G. M. Urciuoli
Experiments with Global Detection of Cold Fusion Byproducts

†24PI-8 G. K. Hubler and G. P. Chambers
Search for Anomalous Nuclear Emissions by Means of Ion Beam Charging of Metals

24PI-9 D. R. O. Morrison
Review of Cold Fusion Experiments

24PI-10 T. N. Claytor, D. G. Tuggle and S. F. Taylor
Evolution of Tritium from Deuterided Palladium Subject to High Electrical Currents

24PI-11 J. O'M. Bockris, C. Chien, D. Hodko and Z. Minevski
Tritium and Helium Production in Palladium Electrodes and the Fugacity of Deuterium Therein

24PI-13 J. Sevilla, B. Escarpizo, F. Fernandez, F. Cuevas and C. Sanchez
Time-Evolution of Tritium Concentration in the Electrolyte of Prolonged Cold Fusion Experiments and its Relation to the Ti Cathode Surface Treatment

*24PI-14 F. Dalidchik, Yu. Rumyantsev, R. Stukan and A. Shishkov
Hard Emission Generation and Tritium Accumulation during D_2O Electrolysis with Pd Cathode

†24PI-15 A. B. Karabut, Ya. R. Kucherov and I. B. Savvatimova
Gamma-Spectrometry at Glow Discharge in Deuterium

24PI-16 B. Stella, M. Alessio, M. Corradi, F. Croce, F. Ferrarotto, S. Improta, N. Iucci, V. Milone, G. Villoresi, F. Celani, A. Spallone
The FERMI Apparatus and a Measurement of Tritium Production in an Electrolytic Experiment

24PI-17 B. Stella, M. Corradi, F. Ferrarotto, V. Milone, F. Celani and A. Spallone
Evidence for Stimulated Emission of Neutrons in Deuterated Palladium

†24PI-18 R. Zhu, X. Wang, F. Lu, P. Tang, H. Liu, G. Chen, Z. Zou, Y. Liu, Z. Li, Z. Chen and D. Ding
A New Device for Measuring Neutron Burst in Cold Fusion Experiment

24PI-19 T. Shirakawa, M. Chiba, M. Fujii, K. Sueki, S. Miyamoto,Y. Nakamitu, H. Toriumi, T. Uehara, H. Miura, T. Watanabe, K. Fukushima, T. Hirose, T. Seimiya and H. Nakahara
Neutron Emission from Crushing Process of High Piezoelectric Matter in Deuterium Gas

24PI-20 M. Fujii, M. Chiba, K. Fukushima, M. Katada, T. Hirose, K. Kubo, H. Miura, S. Miyamoto, H. Nakahara, Y. Nakamitsu, T. Seimiya, T. Shirakawa, K. Sueki, H. Toriumi, T. Uehara and T. Watanabe
Measurement of Neutrons in Electrolysis at Low Temperature Range

*24PI-21 F. Kayumov, G. Merzon, D. Minasyan, A. Rusetsky, V. Tsarev and G. Tsyrlina
Search for Proton Emission in Cold Fusion Reactions II

†24PI-22 P. I. Golubnichy, N. V. Gribinichenko, V. A. Kurakin, V. V. Litvinenko, V. A. Piven, O. N. Pustovy, A. D. Philonenko, A. A. Tsaric, E. E. Shimko, A. N. Baraboshkin, V. G. Gorodetsky, A. I. Samgin and V. A. Tsarev
Search for Nuclear Emission at Phase Transition of I and II Kind in a Series of Deuterium Carrying Systems

†24PI-23 P. I. Golubnichy, V. V. Litvinenko, A. D. Philonenko, A. A. Tsaric, Y. A. Artemenko, A. F. Volkov, A. V. Goltsov, V. A. Goltsov and V. A. Tsarev
Results of Correlation Experiments on the Problem of Low Temperature Nuclear Fusion in Some Metal and Intermetal System

24PI-24 A. Y. Gavrilyuk, P. I. Golubnichy, N. V. Gribinichenko, V. V. Litvinenko, A. D. Philonemko, A. A. Tsaric, O. A. Bezsheiko, A. P. Degtyarev, I. B. Mikhnitsky, G. A. Prokopets and V. A. Tsarev
High Efficiency Low Background Measuring-Computing Complex for Correlation Experiments on the Problem of Low Temperature Fusion

†24PI-25 P. I. Golubnichy, V. V. Litvinenko, O. N. Pustovy, A. D. Philonenko, A. A. Tsaric, A. N. Baraboshkin, V. G. Gorodetsky, A. I. Samgin and V. A. Tsarev
Correlation Experiment Results on Registration of Neutron Electromagnetic and Acoustic Emission at Hydration of Litium Deuterid in Heavy Water

24PI-26 O. Matsumoto, K. Kimura, Y. Saito, H. Uyama, T. Yaita, A. Yamaguchi and O. Suenaga
Detection of Neutron and Tritium during Electrolysis of D_2SO_4 - D_2O Solution

*24PI-27 S. Y. Duan, S. Q. Cheng, X. M. Chen, Z. G. Yang, Q. Pan and W. S. Guan
The Observation of the Abnormal Nuclear Reaction Phenomenon in the Deuterated Metal

24PI-28 M. Agnello, E. Botta, T. Bressani, D. Calvo, A. Feliciello, P. Gianotti, F. Iazzi, C. Lamberti, B. Minetti and A. Zecchina
Measurement of 2.5 MeV Neutron Emission from Ti/D and Pd/D Systems

†24PI-29 N. Wada and T. Goto
Nuclear Fusion in Solid

24PI-30 E. Choi, H. Ejiri and H. Ohsumi
Limit on Fast Neutrons from DD Fusion in Deuterized Pd by Means of Ge Detector

24PI-31 M. Fujiwara and K. Sakuta
Statistically Significant Increase in Neutron Counts for Palladium Plate Filled with Deuterons by Electrolysis

24PI-32 H. Yamada, N. Sugaya, T. Kamioka, M. Matsukawa, T. Fujiwara and K. Noto
Neutron Emission from Palladium Electrodes in Deuterium Gas under Highly Non-uniform Electric Field

24PI-33 W. X. Liang, D. M. Xu, G. Y. Zhang, Z. L. Yao and E. Y. Wang
Neutron Measurements in a AC-Discharged Tube

24PI-34 L. J. Yuan, C. M. Wan, C. Y. Liang and S. K. Chen
Neutron Monitoring on Cold Fusion Experiments

24PI-35 D. L. Wang, S. H. Chen, D. X. Fan, W. J. Chen, Y. J. Li, Y. B. Fu and X. W. Zhang
Experimental Studies on the Anomalous Phenomenon in Pd Metal Loaded with Deuterium

24PI-36 H. Q. Long, R. S. Xie, S. H. Sun, H. Q. Liu, J. B. Gan, B. R. Chen, X. W. Zhang and W. S. Zhang
The Anomalous Nuclear Effects Inducing by the Dynamic Low Pressure Gas Discharge in a Deuterium/Palladium System

24PI-37 S. Miyamoto, K. Sueki, H. Iwai, M. Fujii, T. Shirakawa, H. Miura, T. Watanabe, H. Toriumi, T. Uehara, Y. Nakamitsu, M. Chiba, T. Hirose and H. Nakahara
Measurement of Protons and Observation of the Change of Electrolysis Parameters in the Galvanostatic Electrolysis of the 0.1M-LiOD/D_2O Solution

24PI-38 Q. F. Zhang, Q. Q. Gou, Z. H. Zhu, B. L. Xio, J. M. Lou, F. S. Liu, J. X. S. , Y. G. Ning, H. Xie and Z. G. Wang
The Detection of ^4He in Ti-Cathode on Cold Fusion

24PI-39 T. Iida, M. Fukuhara, H. Miyazaki, Y. Sueyoshi, Sunarno, J. Datemichi and A. Takahashi
Deuteron Fusion Experiment with Ti and Pd Foils Implanted with Deuteron Beams

24PI-40 K. -H. Lee and Y. -M. Kim
The Change of Tritium Concentration during the Electrolysis of D_2O in Various Electrolytic Cells

24PI-41 H. Uchida, Y. Hamada, Y. Matsumura and T. Hayashi
Detection of Radioactive Emissions in the Electrolytic Deuteriding-Dedeuteriding Reactions of Pd and Ti

24PI-42 S. H. Chen, D. L. Wang, W. J. Chen, Y. J. Li, Y. B. Fu and X. W. Zhang
The Sensitizing Phenomenon of X-Ray Film in the Experiment of Metals Loaded with Deuterium

24PI-43 G. Y. Fan, X. F. Wang, G. S. Huang, H. Y. Zhou, Z. E. Han, Z. D. Wu
Production of Neutron and Tritium from D_2O Electrolysis with Palladium Cathode

†24-PI-44 R. A. Monti
Low Energy Transmutations

Afternoon Session II (Poster)

Nuclear Products II

24PI-1 H. Sakaguchi, G. Adachi and K. Nagao
Helium Isotopes from Deuterium Absorbed in $LaNi_5$

24PI-2 R. Taniguchi and T. Yamamoto
Fine Structure of the Charged Particle Bursts Induced by D_2O Electrolysis

†24PI-3 S. Jin, F. Zhang, Y. Liu and W. Shi
Anomalous Nuclear Effects in Pd/D and YBCO/D Systems

24PI-4 D. W. Mo, L. Zhang, B. X. Chen, Y. S. Liu, S. Y. Doing, M. Y. Yao, L. Y. Zhou, H. G. Huang, X. Z. Li, X. D. Shen, S. C. Wang, T. S. Kang and N. Z. Huang
Real Time Measurements of the Energetic Charged Particles and the Loading Ratio (D/Pd)

†24PI-5 H. Liu and F. E. Cecil
Investigation of Charged Particle Emission from Titanium/Palladium Cathode Glow Discharge Experiments

24PI-6 H. Q. Long, S. H. Sun, H. Q. Liu, R. S. Xie, X. W. Zhang and W. S. Zhang
Anomalous Effects in Deuterium/Metal Systems

†24PI-7 A. B. Karabut, Ya. R. Kucherov, I. B. Savvatimova and A. D. Kurepin
Heavy Charged Particles Registration at Glow Discharge in Deuterium

24PI-8 K. Watanabe, Y. Fukai, N. Niimura and O. Konno
A Search for Fracture-Induced Nuclear Fusion in Some Deuterium-Loaded Materials

24PI-9 R. K. Rout, A. Shyam, M. Srinivasan and A. B. Garg
Phenomenon of Low Energy Emissions from Hydrogen/Deuterium Loaded Palladium

*24PI-10 J. Jorné and E. Granite
Neutron Emission Studies during the Electrolysis of Deuterium Using $BaCeO_3$ Solid Electrolyte and Pd Electrodes

†24PI-11 G. P. Chambers and G. K. Hubler
Search for Anomalous Charged Particle Emissions from Deuterium-Charged Solids Using a Particle Telescope

Excess Heat II

24PI-12 A. Takahashi, A. Mega, T. Takeuchi, H. Miyamaru and T. Iida
Anomalous Excess Heat by D_2O/Pd Cell under L-H Mode Electrolysis

24PI-13 F. Celani, A. Spallone, P. Tripodi and A. Nuvoli
Measurements of Excess Heat and Tritium during Self-Biased Pulsed Electrolysis of Pd-D_2O

24PI-14 M. Fleischmann and S. Pons
Calorimetry of the PD·D_2O System: from Simplicity via Complications to Simplicity

24PI-15 S. I. Smedley, S. Crouch-Baker, M. C. H. McKubre and F. L. Tanzella
The January 2, 1992, Explosion in a Deuterium/Palladium Electrolytic System at SRI International

24PI-16 M. H. Miles and B. F. Bush
Calorimetric Principles and Problems in Pd-D_2O Electrolysis

24PI-17 X. Zhang, W. Zhang, D. Wang, S. Chen Y. Fu, D. Fan and W. Chen
On the Explosion in a Deuterium/Palladium Electrolytic System

24PI-18 C. M. Wan, C. J. Lihn, Z. H. Chin, C. Y. Liang, S. K. Chen, C. C. Wan and T. P. Perng
Repeated Heat Bursts in the Electrolysis of D_2O

24PI-19 N. Hasegawa, K. Kunimatsu, T. Ohi and T. Terasawa
Observation of Excess Heat during Electrolysis of 1M LiOD in a Fuel Cell Type Closed Cell

24PI-20 M. Kobayashi, N. Imai, N. Hasegawa A. Kubota and K. Kunimatsu
Measurements of D/Pd and Excess Heat during Electrolysis of LiOD in a Fuel-Cell Type Closed Cell Using a Palladium Sheet Cathode

24PI-21 L. Bertalot, F. de Marco, A. de Ninno, A. La Barbera, F. Scaramuzzi, V. Violante and P. Zeppa
Study of Deuterium Charging in Palladium by the Electrolysis of Heavy Water: Search for Heat Excess and Nuclear Ashes

24PI-22 H. Miyamaru and A. Takahashi
Periodically Current-Controlled Electrolysis of D_2O/Pd System for Excess Heat Production

24PI-23 M. E. Melich and W. N. Hansen
Some Lessons from 3 Years of Electrochemical Calorimetry

*24PI-24 Y. Tanaka
An ep Particle Theory and Experiments Proving the Theory

*24PI-25 Z. Zhang and F. Tan
Further Examination of Fusion Products and Anomalous Heat Generated during the Electrolysis of Heavy Water

24PI-26 Y. Arata and Y. -C. Zhang
"Cold" Fusion in a Complex Cathode

24PI-27 E. E. Criddle
Implications of Isoperibolic Electrode Calorimetry for Cold Fusion : The Silica Effect

†24PI-28 T. A. Chubb, M. Daehler and K. H. Stern
Electrochemistry of Pd Anodes in Hydrided Molten Salt

24PI-29 C. M. Wan, S. K. Chen, C. Y. Liang, C. J. Linn, C. J. Linn, S. B. Chu and C. C. Wan
Anomalous Heat Generation/Absorption in Pd/Pd/LiOD/D_2O/Pd Electrolysis System

24PI-30 K. Ota, M. Kuratsuka, K. Ando, Y. Iida, H. Yoshitake and N. Kamiya
Heat Production at the Heavy Water Electrolysis Using Mechanically Treated Pd Cathode

24PI-31 S. Isagawa, Y. Kanda and T. Suzuki
Search for Excess Heat, Neutron Emission and Tritium Yield from Electrochemically Charged Palladium in D_2O

24PI-32 R. T. Bush and R. D. Eagleton
Experiments Supporting the Transmission Resonance Model for Cold Fusion in Light Water: I. Correlation of Isotopic and Elemental Evidence with Excess Heat

24PI-33 R. T. Bush and R. D. Eagleton
Experimental Studies Supporting the Transmission Resonance Model for Cold Fusion in Light Water: II Correlation of X-Ray Emission with Excess Power

24PI-34 B. Y. Liaw and B. E. Liebert
A Potential Shuttle Mechanism for Charging Hydrogen Species into Metals in Hydride-Containing Molten Salt Systems

24PI-35 R. Notoya and M. Enyo
Excess Heat Production in Electrolysis of Potassium Carbonate Solution with Nickel Electrodes

24PI-36 T. Ohmori and M. Enyo
Excess Heat Produced during Electrolysis of H_2O on Ni, Au, Ag and Sn Electrodes in Alkaline Media

October 25, Sunday
Morning Session I (Oral) Chairpersons : D. Rolison and M. Okamoto

Nuclear Products

T. N. Claytor, D. G. Tuggle and S. F. Taylor
Evolution of Tritium from Deuterided Palladium Subject to High Electrical Currents

J. O'M. Bockris, C. Chien, D. Hodko and Z. Minevski
Tritium and Helium Production in Palladium Electrodes and the Fugacity of Deuterium Therein

M. Nakada, T. Kusunoki and M. Okamoto
Energy of the Neutrons Emitted in Heavy Water Electrolysis

Activity Report

X. Li : Cold Fusion Researches in China
V. Tsarev : Cold Fusion Researches in Russia
F. Scaramuzzi : Cold Fusion Research in Italy

Round Table Discussion for the Next Step
E. Yamaguchi, M. C. H. McKubre, P. Hagelstein, S. Jones, T. Perng, M. Fleischmann, V. Tsarev, A. Takahashi and T. Bressani

Closing Remarks H. Ikegami

International Advisory Committee

H. Ikegami (Chairman), National Institute for Fusion Science, Japan
J. Bockris, Texas A&M University, U.S.A.
T. Claytor, Los Alamos National Laboratory, U.S.A.
M. Fleischmann, University of Southampton, U.K.
P. Hagelstein, Massachusetts Institute of Technology, U.S.A.
R. Huggins, Zentrum fur Sonnenenergie und Wasserstoff Forschung, Germany
M. Jaendel, Royal Institute of Technology, Sweden
S. Jones, Bringham Young University, U.S.A.
Y. Kim, Purdue University, U.S.A.
X. Li, Tsinghua University, China
B. Liaw, University of Hawaii, U.S.A.
M. McKubre, Stanford Research Institute International, U.S.A.
M. Miles, Naval Air Warfare Center, U.S.A.
K. Nagamine, University of Tokyo, Japan
M. Okamoto, Tokyo Institute of Technology, Japan
N. Oyama, Tokyo University of Agriculture and Technology, Japan
T. Perng, National Tsing Hua University, R.O.C.
S. Pons, IMRA Europe S. A., France
G. Preparata, University of Milan, Italy
D. Rolison, Naval Research Laboratory, U.S.A.
C. Sánchez Lopez, Universidad Autonoma de Madrid, Spain
J. Santucci, Electric Power Research Institute, U.S.A.
F. Scaramuzzi, Energia Nucleare e delle Energie Alternative
M. Srinivasan, Bhabha Atomic Research Centre, India
A. Takahashi, Osaka University, Japan
V. Tsarev, P.N. Lebedev Physical Institute, Russia
F. Will, University of Utah, U.S.A.

Organizing Committee

H. Ikegami (Chairman), Professor, National Institute for Fusion Science, Japan
G. Adachi, Professor, Osaka University, Japan
O. Aizawa, Professor, Musashi Institute of Technology, Japan
Y. Fukai, Professor, Chuo University, Japan
R. Hasiguti, Professor Emeritus, University of Tokyo, Japan
K. Husimi, Professor Emeritus, Nagoya University and Osaka University, Japan
S. Ikezawa, Professor, Chubu University, Japan
H. Kakihana, Professor Emeritus, Tokyo Institute of Technology, Japan
J. Kasagi, Professor, Tohoku University, Japan
Y. Maeda, Professor, Kyoto University, Japan
T. Mizuno, Research Associate, Hokkaido University, Japan
T. Mukaibo, Professor Emeritus, University of Tokyo, Japan
K. Nagamine, Professor, University of Tokyo, Japan
H. Nakahara, Professor, Tokyo Metropolitan University, Japan
M. Nakazawa, Professor, University of Tokyo, Japan
C. Namba, Research Associate, National Institute for Fusion Science, Japan
K. Nishizawa, Associate Professor, Nagoya University, Japan
M. Okamoto, Professor, Tokyo Institute of Technology, Japan
K. Ota, Associate Professor, Yokohama National University, Japan
N. Oyama, Professor, Tokyo University of Agriculture and Technology, Japan
T. Shibata, Professor, University of Tokyo, Japan
A. Takahashi, Professor, Osaka University, Japan
K. Takayama, Professor Emeritus, Nagoya University, Japan
T. Tazima, Associate Professor, National Institute for Fusion Science, Japan
R. Uyeda, Professor Emeritus, Nagoya University, Japan
E. Yamaguchi, Senior Scientist, NTT Basic Research Laboratories, Japan

List of Sponsors

Aichi Prefectural Government
Aisin AW Co., Ltd.
Aisin Seiki Co., Ltd.
Central Research Institute of Electric Power Industry
Daido Steel Co., Ltd.
Digital Equipment Corporation Japan
Godo Steel Ltd.
Kawasaki Steel Corporation
Kobe Steel Ltd.
Kubota Corporation
Kyoei Steel Ltd.
Mitsubishi Materials Corporation
Mitsubishi Research Institute, Inc.
Mitsubishi Steel MFG, Co., Ltd.
Nagoya City Hall
Nakatani Satoshi
Niki Glass Co., Ltd.
Nippon Steel Corporation
Nippon Telegraph and Telephone Corporation (NTT) Basic Research Laboratories
Nisshin Steel Co., Ltd.
Nissho Iwai Corporation
NKK Corporation
Nuclear Fuel Industries, Ltd.
Ohyo Koken Kogyo Co., Ltd.
Osaka Gas Co., Ltd.
R-DEC Co., Ltd.
Seiko EG&G Co., Ltd.
Sumitomo Metal Industries, Ltd.
Tanaka Kikinzoku Kogyo K.K.
The Federation of Electric Power Companies
The Japan Steel Works, Ltd.
The Tokyo Club
Toho Sanso Co., Ltd.
Tokyo Gas Co., Ltd. Fundamental Technology Research Laboratory
Topy Industries, Ltd.
Toshiba Corporation
ULVAC Japan Ltd.

Exhibits and Demonstrations

IMRA Material R&D Co., Ltd.
Nippon Sanso Corporation
ULVAC Japan Ltd.

List of Participants

Abe, Yasushi Department of Energy Engineering, Yokohama National University, 156 Tokiwadai, Hodogaya, Yokohama 240 Japan

Ahmad, Iqbal Army Research Office, Far East, Akasaka Press Center, 7-23-17 Roppongi, Minato, Tokyo 106 Japan

Aizawa, Otohiko Atomic Energy Research Laboratory, Musashi Institute of Technology, 971 Ozenji, Asao, Kawasaki, Kanagawa 215 Japan

Akimoto, Tadashi Department of Nuclear Engineering, Hokkaido University, North 13, West 8, Kita, Sapporo 060 Japan

Amezawa, Koji Department of Nuclear Engineering, Faculty of Engineering, Kyoto University, Sakyo, Kyoto 606 Japan

Ando, Noriyoshi Development Engineering Department 1, System Development Engineering, Nippon Denso Co.,Ltd, 1-1 Showa, Kariya, Aichi 448 Japan

Aoki, Takayoshi Isotope Center, Tsukuba University, 1-1-1 Tennoudai, Tsukuba, Ibaraki 305 Japan

Arakane, Atushi Central Research Laboratoty, Mitsubishi Electric Corporation, 8-1-1 Tukaguchihonmachi, Amagasaki, Hyogo 661 Japan

Asami, Naoto Technology and Information Systems Development Department, Mitsubishi Atomic Power Industries, Inc., 2-4-1 Shibakoen, Minato, Tokyo 105 Japan

Ashidate, Shuichi Tokyo Electric Power Company Inc., 1-1-3 Uchisaiwai, Chiyoda, Tokyo 100 Japan

Barabochkin, Aleksey Institute of High-Temperature Electrochemistry, URAL Division of Academy of Sciences of Russia, S. Kovalevskaya, 20 Ekaterinburg, 620219 Russia

Barrowes, Steven Department of Physics, University of Utah, 201 James Fletcher Bldg., Salt Lake City, UT 84112 USA

Becker, Charles D. Technical Concepts Corporation, 8415 Datapoint Drive, San Antonio, TX 78229 USA

Benson, Thomas Scott Laboratories, Inc., 304 Grand Avenue, Room 208, South San Francisco, CA 94080 USA

Bergeson, Haven E. Department of Physics, University of Utah, 201 James Fletcher Bldg., Salt Lake City, UT 84112 USA

Bockris, John O'M. Department of Chemistry, Texas A & M University, Room 001B Chemistry Bldg., College Station, TX 77843-3255 USA

Boss, Pamela A. Naval Command and Ocean Surveillance Center, RDT&E Division, Code 574 Bldg.1, Bayside, San Diego, CA 92152-5000 USA

Bressani, Tullio Istituto Nazionale Fisica Nucleare-Sezione di Torino, Via Sette Comuni 56-10127 Torino Italy

Buehler, David Bringham Young University, 660 N 200 E ♯7, Provo, UT 84606 USA

Bush, Ben Chemistry Division, Research Department, Code 2353, Naval Air Warfare Center Weapons Division, China Lake, CA 93555-6001 USA

Bush, Robert T. Physics Department, California State Polytechnic University, 3801 West Temple Avenue, Pomona, CA 91768 USA

Calvo, Daniela Laboratorio Tecnologico, Istituto Nazionale Fisica Nucleare-Sezione di Torino, Via Sette Comuni 56-10127 Torino Italy

Celani, Francesco Laboratori Nazionali Frascati, Istituto Nazionale Fisica Nucleare, Via E. Fermi, 00044 Frascati (Roma) Italy

Chambers, George P. Department of the Navy, Naval Research Laboratory, Code 6670, 4555 Overlook Avenue, S.W. , Washington, D.C., 20375-5320 USA

Chen, Su He Southwest Institute of Nuclear Physics and Chemistry, P.O. Box 525-74, Chengdu 610003 China

Chen, Swe-Kai Department of Materials Science and Engineering, Materials Science Center, National Tsing Hua University, 101 Section 2, Kuang Fu Rd., Hsinchu 30043 ROC

Chevrel, Henri 5-9-9 Tokodai, Tsukuba, Ibaraki 300-26 Japan

Chipman, Wilfred L. International Telepresence Corporation, 655 West 7th Avenue Vancouver, British Columbia V5Z 1B6 Canada

Chubb, Scott R. Research Systems, Inc., 5023 North 38th Street, Arlington, VA 22207 USA

Chubb, Talbot A. Research Systems, Inc., 5023 North 38th Street, Arlington, VA 22207 USA

Cilloco, Francesco CNR, Via E. Fermi 38, 00044 Frascati (Roma) Italy

Claytor, Thomas N. Los Alamos National Laboratory, P.O. Box 1663 MS C914, Los Alamos, NM 87545 USA

Combourieu, M. EHESS/CNRS-GERS, 10, Rue Monsieur le Pruice, 75006, Paris France

Corradi, Massimo (Stella) - Dipartimento di Fisica, Universita degli Studi of Roma "La Sapienza", P.le Aldo Moro 2-00185 (Roma) Italy

Criddle, Ernest E. Electrochemical Science & Technology Center, University of Ottawa, 33 Mann Avenue, Ottawa, Ontario K1N 6N5 Canada

Crouch-Baker, Steven SRI International, 333 Ravenswood Ave., Menlo Park, CA 94025-3493 USA

Cuevas, Fermin Departamento de Fisica de Materiales C-IV, Universidad Autonoma de Madrid, Cantoblanco, 28049 Madrid Spain

Daehler, Mark Department of the Navy, Naval Research Laboratory, Code 7215.6, 4555 Overlook Avenue S.W., Washington, D.C., 20375-5000 USA

Dawson, Kirby 1259 El Camino Real ♯332 Menlo Park, CA USA

De Ninno, Antonella. INN-SVIL., ENEA, CRE ENEA-Frascati, Via E. Fermi I-00044 Frascati (Roma) Italy

Del Giudice, Emilio Istituto Nazionale Fisica Nucleare-Sezione di Milano, Fisica Nucleare-Milano, Via Celoria 16-20133 Milano Italy

Dersot, Lionel 1-18-14-301 Nishikubo, Musashino, Tokyo 180 Japan

Dewhirst, Kenneth C. 410 Bayou Cove, Houston, TX 77042 USA

Dodo, Taro Department of Physics, Faculty of Science, Ehime University, 2-5 Bunkyo, Matsuyama 790 Japan

Doe, Hidekazu Department of Chemistry, Faculty of Science, Osaka City University, 3-3-138 Sugimoto, Sumiyoshi, Osaka 558 Japan

Dominguez, Dawn Surface Chemistry Branch, Naval Research Laboratoty, Code 6170, 4555 Overlook Avenue, S.W., Washington, D.C., 20375-5000 USA

Drexler, Jerome c/o Drexler Technology Corporation, 2557 Charleston Road, Mountain View, CA 94043 USA

Eagleton, Robert D. Physics Department, California State Polytechnic University, 3801 West Temple Avenue, Pomona, CA 91768 USA

Eisner, Melvin Department of Physics, University of Houston, 4800 Calhoun, Houston, TX 77204-5504 USA

Endoh, Eiji Kansai R & D Center, Asahi Glass Co., Ltd., 114 Shibata, Kita, Osaka 530 Japan

Enyo, Michio Catalysis Research Center, Hokkaido Universiy, North 11, West 10, Kita, Sapporo 060 Japan

Fan, Guoying Institute of Low Energy Nuclear Physics, Beijing Normal University, Beijing 100875 China

Fitzpatrick, Timothy Salt Lake City Tribune Press, 143 Co. Main SLC, UT 84103 USA

Fleischmann, Martin Department of Chemistry, University of Southampton, Highfield, Southampton, S09 5NH UK

Flores, Ronald 15ch des Colombettes, 1202 Geneva Switzerland

Fox, Hal Fusion Information Center, Inc., P.O. Box 58639, Salt Lake City, UT 84158-0639 USA

Frullani, Salvatore Laboratorio di Fisica, Istituto Superiore di Sanita, Viale Regina Elena, 299-00161 (Roma) Italy

Fujii, Masatoshi Department of Chemistry, Faculty of Science, Tokyo Metropolitan University, 1-1 Minamioosawa, Hachiohji, Tokyo 192-03 Japan

Fujino, Haruyuki Fuji Electric Corporate Research and Development, Ltd., 2-2-1 Nagasaka, Yokosukai, Kanagawa 240-01 Japan

Fujishiro, Shiro Asian Office of Aerospace Research and Development AFOSR (AFMC), Akasaka Press Center, 7-23-17 Roppongi, Minato, Tokyo 106 Japan

Fujita, Hiroharu Faculty of Science and Engineering, Saga University, 1 Honjo, Saga 840 Japan

Fujita, Makoto Sanwa Research Institute, Corp., Sinanobashi Sanwa Bldg., 1-6-1 Awaza, Nishi, Osaka 550 Japan

Fujita, Tomonari Nuclear Fuel Section, Komae, Tokyo Research Laboratory, Central Research Institute of Electric Power Industry, 2-11-1 Iwato Kita, Komae, Tokyo 201 Japan

Fujiwara, Kikuo Refining Test Section, Numazu Factory, N.E Chemcat Corporation, 678 Ipponmatsu, Numazu, Shizuoka 410-03 Japan

Fujiwara, Masami National Institute for Fusion Science, Furo, Chikusa, Nagoya 464-01 Japan

Fujiwara, Masanori Fundamental Energy Technology Section, Energy Fundamental Division, Electrotechnical Laboratory, 1-1-4 Umezono, Tsukuba, Ibaraki 305 Japan

Fukai, Yuh Department of Physics, Faculty of Science and Engineering, Chuo University, 1-13-27 Kasuga, Bunkyo, Tokyo 112 Japan

Fukushima, Kenji Department of Physics, Faculty of Science, Tokyo Metropolitan University, 1-1 Minamioosawa, Hachioji, Tokyo 192-03 Japan

Funasaka, Hideyuki Nuclear Fuel Development Division, Power Reactor and Nuclear Fuel Development Corporation, Tokai, Ibaraki 319-11 Japan

Garibaldi, Franco Istituto Superiore di Sanita-Laboratorio di Fisica, INFN-Sezione Sanita, Viale Regina Elena, 299-00161 (Roma) Italy

George, Russ Cold Fusion Research Advocates 2060 Peachtree Industrial Court, Suite 312-F Chamblee, GA 30341 USA

Gozzi, Daniele Dipartimento di Chimica, Universita di Roma "La Sapienza" , P.le Aldo Moro 5-00185 (Roma) Italy

Grout, Francois Cogema Japan, Urban Toranomon Bldg. 5F., 1-16-4 Toranomon, Minato, Tokyo 105 Japan

Grow, Richard W. Electrical Engineering Department, University of Utah, Merrill Engineering Bldg., Salt Lake City, UT 84112 USA

Grow, Robert J. 9767 South Little Cottonwood Place, Sandy, UT 84092 USA

Haga, Tsuyoshi Energy Apparatus & Systems R & D Department, Electric Power System Technology Research Laboratories, Sumitomo Electric Industries, Ltd., 1-1-3 Shimaya, Konohana, Osaka 554 Japan

Hagelstein, Peter L. Research Laboratory of Electronics, Bldg.38-290, Massachusetts Institute of Technology, 77 Massachusetts Ave., Cambridge, MA 02139 USA

Hamada, Yuzi Department of Applied Physics, Faculty of Engineering, Tokai University, 1117 Kita-kaname, Hiratsuka, Kanagawa 259-12 Japan

Hamano, Michio International Joint Research Division, New Energy & Industrial Technology Development Organization, Sunshine 60-21F., 3-1-1 Higashi-Ikebukuro, Toshima, Tokyo 170 Japan

Hanamoto, Katsumi Faculty of Science and Engineering, Ritsumeikan University, 56-1 Kita-machi, Tojiin, Kita, Kyoto 603-77 Japan

Hanawa, Teruo General Education, Osaka Institute of Technology, Ohmiya, Asahi, Osaka 535 Japan

Hansen, Lee Department of Chemistry, Bringham Young Universtiy, Provo, UT 84606 USA

Hansen, Wilford N. Physics Department, Utah State University, SER Bldg., Room 250, Logan, UT 84322-4415 USA

Harada, Hiroyuki Project Department, Chlorine Engineers Corp., Ltd., Tomiokabashi Bldg., 2-6-11 Fukagawa, Koto, Tokyo 135 Japan

Hasegawa, Kunihiko Radiochemistry Research Laboratory, Shizuoka University, 836 Ohtani, Shizuoka, Shizuoka 422 Japan

Hasegawa, Norifumi IMRA Japan Co., Ltd., 2-3-6 Technopark, Shimonopporo, Atsubetsu, Sapporo 004 Japan

Hasezaki, Kazuhiro Nagasaki Research and Development Center, Mitsubishi Heavy Industries, Ltd., 5-717-1 Fukabori, Nagasai 851-03 Japan

Hashimoto, Akikazu Research Laboratory of Electronics, Massachusetts Institute of Technology, 410 Memorial Dn ♯211e, Cambridge, MA 02139 USA

Hashimoto, Katsushi 3-82 Shimohaba, Hanamaki, Iwate 025 Japan

Hashizume, Arata Sumitomo Chemical Co., Ltd., 2-10-1 Tsukahara, Takatsuki, Osaka 569 Japan

Hatori, Tadatsugu National Institute for Fusion Science, Furo, Chikusa, Nagoya 464-01 Japan

Hauser, Alan SRI International, 333 Rovenswood Avenue, Menlo Park, CA 94025 USA

Hayakawa, Nana IMRA Japan Co.,Ltd., 2-3-6 Technopark, Shimonopporo, Atsubetsu, Sapporo 004 Japan

Higashi, Masao Nuclear Engineering, Ltd., 1-3-7 Tosabori, Nishi, Osaka 550 Japan

Hikita, Tomoji Fundamental Technology Research Laboratory, Tokyo Gas Co., Ltd., 1-16-25 Shibaura, Minato, Tokyo 105 Japan

Himeno, Shunichi Nippon Bunri University, 1727 Ichigi, Oita, Oita 870-03 Japan

Hiromoto, Akira Advanced Technology Research Center, Mitsubishi Heavy Industries, Ltd., 1-8-1 Sachiura, Kanazawa, Yokohama 236 Japan

Hoffman, Nathan P.O. Box 1449, Canoga Park, CA 91304 USA

Honji, Akio Hitachi Research Laboratory, Hitachi, Ltd., 4026 Kuji, Hitachi, Ibaraki 319-12 Japan

Honzawa, Tadao Faculty of Engineering, Utsunomiya University, 2753 Ishii, Utsunomiya, Tochigi 321 Japan

Hosaka, Naoki Scientific News Department, Yomiuri Shimbun, 1-7-1 Otemachi, Chiyoda, Tokyo 100-55 Japan

Hosono, Nagao Products Technology Planning Department, Products Technology Development Head Quarters, Canon Inc., Shinjuku Daiichiseimei Bldg., 2-7-1 Nishi-Shinjuku, Shinjuku, Tokyo 163-07 Japan

Huizenga, John R. Chemistry Department, University of Rochester, Rochester, NY 14627 USA

Hushimi, Kouji Lynx Lyceum, Sanwa-Daiichi Bldg. 2F., 1-17-2 Nishi-Shinbashi, Minato, Tokyo 105 Japan

Ichimura, Eiichi Tokyo Electric Power Company Inc., 1-1-3 Uchisaiwai, Chiyoda, Tokyo 100 Japan

Iida, Toshiyuki Department of Nuclear Engineering, Faculty of Engineering, Osaka University, 2-1 Yamadaoka, Suita, Osaka 565 Japan

Ikegami, Hideo National Institute for Fusion Science, Furo, Chikusa, Nagoya 464-01 Japan

Ikezawa, Shunjiro Department of Electronics, Chubu University, 1200 Matsumoto, Kasugai, Aichi 487 Japan

Imaeda, Hiromasa Central Research Institute of Eletric Power Indusrty, 2-11-1 Iwato-Kita, Komae, Tokyo 201 Japan

Imai, Norio IMRA Japan Co.,Ltd., 2-3-6 Technopark, Shimonopporo, Atsubetsu, Sapporo 004 Japan

Inoue, Noriyuki Science News Section, Chunichi Shinbun, 2-3-13 Kounan, Minato, Tokyo 108 Japan

Ioki, Kimihiro Fusion Development Team, Mitsubishi Atomic Power Industries, Inc., 2-4-1 Shibakoen, Minato, Tokyo 105 Japan

Ippommatsu, Masamichi Fundamental Research Laboratories, Osaka Gas Co., Ltd., 6-19-9 Torishima, Konohana, Osaka 554 Japan

Isagawa, Shigeru Accelerator Department, National Laboratory for High Energy Physics(KEK), 1-1 Oho, Tsukuba, Ibaraki 305 Japan

Ishii, Kazushige National Institute for Fusion Science, Furo, Chikusa, Nagoya 464-01 Japan

Ishii, Keizo Cyclotron and Radioisotope Center, Tohoku University, Aoba, Aramaki, Aoba, Sendai, Miyagi 980 Japan

Ishii, Masami IMRA Material R & D Co., Ltd., 5-50 Hachiken, Kariya, Aichi 448 Japan

Ishimaru, Toshimichi Institute of Applied Energy, Shinbashi SY Bldg., 1-14-2 Nishishinbashi, Minato, Tokyo 105 Japan

Isono, Hideo Shueisha Inc., 2-5-10 Hitotsubashi, Chiyoda, Tokyo 101-50 Japan

Iwamura,Yasuhiro Technical Heavy Quarter Advanced Technology Research Center, Mitsubishi Heavy Industries, Ltd., 1-8-1 Sachiura, Kanazawa, Yokohama 236 Japan

Jones, Steven E. Department of Physics & Astronomy, Bringham Young University, 296 Eyring Science Center, Provo, UT 84602 USA

Jörissen, Ludwig Zentrum fur Sonnenenergie-und Wasserstoff-Forschung, Erich-Rittinghaus-Str. 2, D-W7913 Senden Germany

Kakihana, Hidetake 5-1-21 Hiroo, Shibuya, Tokyo 150 Japan

Kaliev, Kabir Institute of High-Temperature Electrochemistry, URAL Division of Academy of Science of Russia, S. Kovalevskaya, 20 Ekaterinburg, 620219 Russia

Kamada, Kohji National Institute for Fusion Science, Furo, Chikusa, Nagoya 464-01 Japan

Kamei, Atsushi Research Planning Department, Techonova Inc., 13th FL. Fukoku Seimei Bldg., 2-2-2 Uchisaiwai, Chiyoda, Tokyo 100 Japan

Kamiya, Nobuyuki Department of Energy Engineering, Yokohama National University, 156 Tokiwadai, Hodogaya, Yokohama 240 Japan

Kando, Masashi Electrical Eng., Faculty of Engineering, Shizuoka University, 3-5-1 Johoku, Hamamatsu, Shizuoka 432 Japan

Kasagi, Jirohta Laboratory of Nuclear Science, Tohoku University, 1-2-1 Mikamine Sendai, Miyagi 982 Japan

Kato, Kikuo Aisin Seiki Co.,Ltd., 2-1 Kariya, Aichi 448 Japan

Kato, Takahiko IMRA Material R & D Co., Ltd., 58 Ida, Igata, Kariya, Aichi 448 Japan

Kato, Tomohiro Department of Energy Engineering, Yokohama National University, 156 Tokiwadai, Hodogaya, Yokohama 240 Japan

Kawaguchi, Seiichi Tanaka Technical Center, Tanaka Kikinzoku Kogyo, K.K., 2-73 Shin-machi, Hiratsuka, Kanagawa 254 Japan

Kawai, Masao Equos Research Co., Ltd., Gotou Bldg., 2-19-12 Sotokanda, Chiyoda, Tokyo 101 Japan

Kawai, Yoshinobu Graduate School of Engineering Sciences, Kyushu University, 6-1 Kasugakoen, Kasuga, Fukuoka 816 Japan

Kawamoto, Junichi Toyota Central Res. & Develop. Labs., Inc., 41-1 Yokomichi, Nagakute, Nagakute, Aichi, Aichi 480-11 Japan

Kawamura, Takaichi National Institute for Fusion Science, Furo, Chikusa, Nagoya 464-01 Japan

Kim, Yeong E. Department of Physics, Purdue University, West Lafayette, IN 47907-1396 USA

Kobayashi, Isamu Chubu Electric Power Co., Inc., 20-1 Kitasekiyama, Oodaka, Midori, Nagoya 459 Japan

Kobayashi, Masafumi IMRA Japan Co., Ltd., 2-3-6 Technopark, Shimonopporo, Atsubetsu, Sapporo 004 Japan

Kobayashi, Miyoko Department of Energy Engineering, Yokohama National University, 156 Tokiwadai, Hodogaya, Yokohama 240 Japan

Kobayashi, Ryusuke Geosystems Project Department, Nuclear & Advanced Technology Division, JGC Corporation, 1-14-1 Bessho, Minami, Yokohama 232 Japan

Kobayashi, Yukio Frontier Research Program, The Institute of Physical and Chemical Research (RIKEN), 2-1 Hirosawa, Wako, Saitama 351-01 Japan

Kohn, Gustave K. 198 Pine Lane, Los Alto, CA 94022 USA

Koller, Karl Department of Physics, University of Munich, Theresienstr 37, 8000 Muenchen 2 Germany

Komada, Norikazu Planning & Project Coordination Department, Central Research Institute, Mitsubishi Materials Corp., 1-297 Kitabukuro, Ohmiya, Saitama 330 Japan

Komaki, Hisatoki Biological and Agricultural Research Institute, 2-6-18, Sakamoto, Otsu, Shiga 520-01 Japan

Konashi, Kenji Power Reactor and Nuclear Fuel Development Corporation, 4-33 Muramatsu, Tokai, Ibaraki 319-11 Japan

Kondo, Tadashi Aisin Newhard Co., Ltd., 3-2 Showa, Kariya, Aichi 448 Japan

Kosugi, Hisao Chubu Electric Power Co., Inc., 20-1, Kitasekiyama, Oodaka, Midori, Nagoya 459 Japan

Kozima, Hideo Faculty of Science, Shizuoka University, 836 Ohtani, Shizuoka, Shizuoka 422 Japan

Kubota, Akihiko IMRA Japan Co., Ltd., 2-3-6 Technopark, Shimonopporo, Atsubetsu, Sapporo 004 Japan

Kucherov, Yan R. 17 Kargopolskaya Str. Apt. 119, Moscow 127562 Russia

Kunimatu, Keiji IMRA Japan Co.,Ltd., 2-3-6 Technopark, Shimonopporo, Atsubetsu, Sapporo 004 Japan

Kuratuka, Masaki Department of Energy Engineering, Yokohama National University, 156 Tokiwadai, Hodogaya, Yokohama 240 Japan

Kusunoki, Takehiro Research Laboratory for Nuclear Reactors, Tokyo Institute of Technology, 2-12-1 Ookayama, Meguro, Tokyo 152 Japan

Kyotani, Yoshihiro Technova, Inc., 13th FL. Fukoku Seimei Bldg., 2-2-2 Uchisaiwai, Chiyoda, Tokyo 100 Japan

Ladd, Tom Technical Division, U.S. Army Science and Technology Center-Far East, P.O.Box 34, Fussa, Tokyo 197 Japan

Lee, Kew-Ho Korea Research Insutitute of Chemical Technology, P.O. Box 9, Daedeog-Danji, Taejeon, 305-606 Korea

Lewenstein, Bruce V. Department of Communication, Cornell University, 321 Kennedy Hall, Ithaca, NY 14853-4203 USA

Li, Xing Zhong Department of Physics, Tsinghua University, Beijing 100084 China

Liaw, Bor Yann Hawaii Natural Energy Institute, University of Hawaii at Monoa, 2540 Dole Street, Holmes Hall 246, Honolulu, HI 96822 USA

Lin, Chun-Jung Department of Materials Science and Engineering, Materials Science Center, National Tsing Hua University, 101 Section 2, Kuang Fu Rd., Hsinchu 30043 ROC

Long, He Qing Institute of Sichuan Material and Technology, P.O.No.9 Hua Feng Xin Cun, Jiangyou 621700 China

Maeda, Kenji Daikin Industries Ltd., 1304 Kanaoka, Sakai, Osaka 591 Japan

Mallove, Eugene F. Cold Fusion Research Advocates 2060 Peachtree Industrial Court, Suite 312-F Chamblee, GA 30341 USA

Marconi, Umberto Dipartimento di Fisica, Universita di Bologna, Via Irnerio 46, 40126 Bologna Italy

Masai, Kuniaki National Institute for Fusion Science, Furo, Chikusa, Nagoya 464-01 Japan

Matsubara, Takeo Osaka Science & Technology Center, 1-8-4 Utsubo Hommachi, Nishi, Osaka 550 Japan

Matsumoto, Osamu Department of Chemistry, Aoyama Gakuin University, Chitosedai, Setagaya, Tokyo 157 Japan

Matsumoto, Takaaki Department of Nuclear Engineering, Faculty of Engineering, Hokkaido University, North 13, West 8, Sapporo 060 Japan

Matsunami, Noriaki Crystalline Materials Science, School of Engineering, Nagoya University, Furo, Chikusa, Nagoya 464-01 Japan

McKubre, Michael C.H. Energy Research Laboratory, SRI International, 333 Ravenswood Ave., Menlo Park, CA 94025 USA

Melich, Michael E. Naval Postgraduate School, Montery, CA 93943-5000 USA

Miki, Nobuaki Technology Center, IMRA Japan Co., Ltd., 2-3-6 Technopark, Shimonopporo, Atsubetsu, Sapporo 004 Japan

Miles, Melvin H. Chemistry Division, Research Department, Code 2353, Naval Air Warfare Center Weapons Division, China Lake, CA 93555-6001 USA

Miley, George H. Fusion Studies Laboratory, University of Illinois, 103 South Goodwin Avenue, Urbana, IL 61801 USA

Mimura, Mikio Faculty of Engineering, Osaka City University, 3-3-138 Sugimoto, Sumiyoshi, Osaka 558 Japan

Miyamaru, Hiroyuki Department of Nuclear Engineering, Faculty of Engineering, Osaka University, 2-1 Yamadaoka, Suita, Osaka 565 Japan

Miyamoto, Shinya Department of Chemistry, Faculty of Science, Tokyo Metropolitan University, 1-1 Minamioosawa, Hachioji, Tokyo 192-03 Japan

Mizuno, Hideaki 2-101 Ooakicho, Nakamura, Nagoya 453 Japan

Mizuno, Tadahiko Department of Nuclear Engineering, Faculty of Engineering, Hokkaido University, North 13, West 8, Kita, Sapporo 060 Japan

Mochizuki, Mizuho Department of Chemical Engineering, Tokyo University of Agriculture and Technology, 2-24-16 Nakamachi, Koganei, Tokyo 183 Japan

Mochizuki, Takayuki Department of Energy Engineering, Yokohama National University, 156 Tokiwadai, Hodogaya, Yokohama 240 Japan

Momota, Hiromu National Institute for Fusion Science, Furo, Chikusa, Nagoya 464-01 Japan

Monti, Roberto Istituto Tesre-Cnr, Via Castacnoci N1, Bologna Italy

Môri, Nobuo Institute for Solid State Physics, University of Tokyo, 7-22-1 Roppongi, Minato, Tokyo 106 Japan

Moriyama, Kouichi Department of Physics, Faculty of Science and Engineering, Saga University, 1 Honjo-machi, Saga, 840 Japan

Moroni, Cesare Dipartimento di Fisica, Universita di Bologna, Via Irnerio 46, 40126 Bologna Italy

Moroto, Shuzo Aisin AW Co., 10 Takane, Fujii, Anjo, Aichi 444-11 Japan

Morrison, Douglas R.O. CERN, CH-1211 Geneva 23 Switzerland

Nagai, Siro Takasaki Radiation Chemistry Research Establishment, Japan Atomic Energy Research Institute, 1233 Watanuki-machi, Takasaki, Gunma 370-12 Japan

Nagamine, Kanetada Meson Science Laboratory, Faculty of Science, University of Tokyo, 7-3-1 Hongo, Bunkyo, Tokyo 113 Japan

Nagaoka, Kazuhito Tokyo Electric Power Company Inc., 1-1-3 Uchisaiwai, Chiyoda, Tokyo 100 Japan

Nagel, David J. Naval Research Laboratory, Code 4600, Washington, D.C., 20375-5000 USA

Naka, Keisuke Aisin Seiki Co.,Ltd., 2-1, Kariya, Aichi 448 Japan

Nakahara, Hiromichi Department of Chemistry, Faculty of Science, Tokyo Metropolitan University, 1-1 Minamiosawa, Hachioji, Tokyo 192-03 Japan

Nakamura, Hirohiko Frontier Science Institute, Mitsubishi Research Institute, Inc., Time & Life Bldg., 2-3-6 Otemachi, Chiyoda, Tokyo 100 Japan

Nakanishi, Eiji R & D Planning Department, Osaka Gas Co., Ltd., 4-1-2 Hirano, Chuo, Osaka 541 Japan

Nakano, Fujio 1-46-9 Musashi-dai, Hidaka, Saitama 350-12 Japan

Nakata, Toshihide IMRA Japan Co.,Ltd., 2-3-6 Technopark, Shimonopporo, Atsubetsu, Sapporo 004 Japan

Nakatomi, Taizo Electric Power Technology Division, MITI, 1-3-1 Kasumigaseki, Chiyoda, Tokyo 100 Japan

Nakazawa, Masaharu Department of Nuclear Engineering, University of Tokyo, 7-3-1 Hongo, Bunkyo, Tokyo 113 Japan

Namba, Chusei National Institute for Fusion Science, Furo, Chikusa, Nagoya 464-01 Japan

Namba, Kikujiro Technova Inc., 13th FL. Fukoku Seimei Bldg., 2-2-2 Uchisaiwai, Chiyoda, Tokyo 100 Japan

Nezu, Shinji IMRA Material R & D Co., Ltd., 5-50 Hachiken, Kariya, Aichi 448 Japan

Nishida, Nobumichi Department of Energy Engineering, Yokohama National University, 156 Tokiwadai, Hodogaya, Yokohama 240 Japan

Nishiki, Yoshinori Permelec Electrode Ltd., 1159 Ishikawa, Fujisawa, Kanagawa 252 Japan

Nishioka, Takashi NTT Basic Research Laboratories, 3-9-11 Midori, Musashino, Tokyo 180 Japan

Nishizawa, Kunihide Radioisotope Research Center, Nagoya University, Furo, Chikusa, Nagoya 464-01 Japan

Nohira, Toshiyuki Department of Nuclear Engineering, Faculty of Engineering, Kyoto University, Sakyo, Kyoto 606 Japan

Notoya, Reiko Catalysis Research Center, Hokkaido Universiy, North 11, West 10, Kita, Sapporo 060 Japan

Nowak, Robert J. Office of Naval Research, Chemistry Division, Code 1113ES/RJN, Ballston Tower One, 800 North Quincy St., Arlington, VA 22217-5560 USA

Numata, Hiroo Department of Metallurgical Engineering, Tokyo Institute of Technology, 2-12-1 Ookayama, Meguro, Tokyo 152 Japan

Ogata, Tetsusi Department of Energy Engineering, Yokohama National University, 156 Tokiwadai, Hodogaya, Yokohama 240 Japan

Ohi, Tamio IMRA Material R & D Co., Ltd., 5-50 Hachiken, Kariya, Aichi 448 Japan

Ohmori, Tadayoshi Catalysis Research Center, Hokkaido Universiy, North 11, West 10, Kita, Sapporo 060 Japan

Ohsumi, Hideaki Department of Physics, Osaka University, 1-1 Machikaneyama, Toyonaka, Osaka 560 Japan

Okamoto, Makoto Research Laboratory for Nuclear Reactors, Tokyo Institute of Technology, 2-12-1 Ookayama, Meguro, Tokyo 152 Japan

Ona, Katsuya Technova Inc., 13th FL. Fukoku Seimei Bldg., 2-2-2 Uchisaiwai, Chiyoda, Tokyo 100 Japan

Orillion, Michael T. FMC Co., Corporate Technology Center, 1205 Coleman Avenue, Box 580, Santa Clara, CA 95052 USA

Ota, Kenichiro Department of Energy Engineering, Yokohama National University, 156 Tokiwadai, Hodogaya, Yokohama 240 Japan

Oyama, Noboru Department of Applied Chemistry, Tokyo University of Agriculture and Technology, 2-24-16 Naka-machi, Koganei, Tokyo 184 Japan

Oyama, Yukio Department of Reactor Engineering, Fusion Neutronics Laboratory, Japan Atomic Energy Research Institute, Tokai, Naka, Ibaraki 319-11 Japan

Ozawa, Kunio Horiba, Ltd., Miyanohigashi, Kishoin, Minami, Kyoto 601 Japan

Passell, Thomas O. Electric Power Research Institute, P.O.Box 10412, Palo Alto, CA 94303 USA

Perng, Tsong-Pyng Department of Materials Science and Engineering, Materials Science Center, National Tsing Hua University, Kuang Fu Rd., Hsinchu 30043 ROC

Pons, Stanley IMRA Europe S.A., 220, Rue Albert-Caquot, Sophia Antipolis, 06560 Valbonne France

Preparata, Giuliano Dipartimento di Fisica, Universita di Milano, Via Celoria 16, 20133 Milano Italy

Prevenslik, Thomas 3-6-7 Roseheim #613, Azusawa, Itabashi, Tokyo 174 Japan

Ragland, Evan L. 6640 Ahekolo Circle, Diamondhead, MS 39525 USA

Rambaut, Michel 57H, Rue de la Hacquiniere, 91440, Bures-Sur-Yvette France

Rehn, Victor Office of Naval Research Asian Office, Akasaka Press Center, 7-23-17 Roppongi, Minato, Tokyo 106 Japan

Rolison, Debra R. Surface Chemistry Branch, Code 6170, Naval Research Laboratory, 4555 Overlook Avenue, S.W., Washington, D.C., 20375-5320 USA

Romodanov, Vitaliy A. Department of Atomic Industry and Power Engineering of the Russian Federation, Scientific Research Institute of Scientific Production Association Lutch, 142109 Podol'sk, Moscow Region Zheleznodorozhnaya 24 Russia

Rothwell, Jed Cold Fusion Research Advocates 2060 Peachtree Industrial Court, Suite 312-F Chamblee, GA 30341 USA

Saita, Teiji Owners, Engineers Co., 31st FL., Kasumigaseki Bldg., 3-2-5 Kasumigaseki, Chiyoda, Tokyo 100 Japan

Saito, Seiji Department of Energy Engineering, Yokohama National University, 156 Tokiwadai, Hodogaya, Yokohama 240 Japan

Saito, Tadashi Department of Chemistry, Faculty of Science, Osaka University, 1-1 Machikaneyama, Toyonaka, Osaka 560 Japan

Sakaguchi, Hiroki Department of Applied Chemistry, Faculty of Engineering, Osaka University, 2-1 Yamadaoka, Suita, Osaka 565 Japan

Sakaida, Hiroyuki Technology Research Team, Investment Research Department, Nomura Research Institute, Ltd., 2-2-2 Otemachi, Chiyoda, Tokyo 100 Japan

Sakashita, Masao Advanced Materials & Technology Research Laboratories, Nippon Steel Corporation, 1618 Ida, Nakahara, Kawasaki, Kanagawa 211 Japan

Sakiyama, Seikoh U.S. Embassy, 1-10-5 Akasaka, Minato, Tokyo 107 Japan

Sánchez, Carlos Departamento de Fisica de Materiales C-IV, Universidad Autonoma de Madrid, Cantoblanco, 28049 Madrid Spain

Sasabe, Kaoru 1-2-9-305 Oowada, Hachiohji, Tokyo 192 Japan

Sasaki, Shuichi Industrial Technology Department, New Energy & Industrial Technology Development Organization, Sunshine 60-21F., 3-1-1 Higashi-Ikebukuro, Toshima, Tokyo 170 Japan

Sato, Noboru Wako Research Center, Honda R & D Co., Ltd., 1-4-1 Chuo, Wako, Saitama 351-01 Japan

Scaramuzzi, Francesco INN-SVIL., ENEA, CRE ENEA-Frascati, Via E. Fermi I-00044 Frascati (Roma) Italy

Shephard, Francis Technical Division, U.S. Army Science and Technology Center-Far East, P.O.Box 34, Fussa, Tokyo 197 Japan

Shibata, Tetsuya Department of Energy Engineering, Yokohama National University, 156 Tokiwadai, Hodogaya, Yokohama 240 Japan

Shibata, Tokushi Institute for Nuclear Study, University of Tokyo, 3-2-1 Midori, Tanashi, Tokyo 188 Japan

Shigemitsu, Toshinori Nuclear Fuel Industries, Ltd., 1-3-7 Tosabori, Nishi, Osaka 550 Japan

Shimazu, Nobuo NTT LSI Laboratories, 3-1 Morinosato Wakamiya, Atsugi, Kanagawa 243-01 Japan

Shimizu, Okiyasu Nagoya City University, 1 Yamanohata, Mizuho, Mizuho, Nagoya 467 Japan

Shimizu, Susumu Tanaka Kikinzoku Kogyo K.K., 2-6-6 Kayaba, Nihonbashi, Chuou, Tokyo 103 Japan

Shiomi, Hirozo Kansai Electric Power Co., Inc., 3-3-22 Nakanoshima, Kita, Osaka 530-70 Japan

Shiomitsu, Tohru NKK Co., 1-1 Minamiwatarida, Kawasaki, Kawasaki, Kanagawa 210 Japan

Shirakawa, Toshiaki Department of Chemistry, Faculty of Science, Tokyo Metropolitan University, 1-1 Minamioosawa, Hachioji, Tokyo 192-03 Japan

Smedley, Stuart I. Energy Research Center, SRI International, 333 Ravenswood Ave., Menlo Park, CA 94025 USA

Sogi, Tadayuki Fundamental Research Laboratories, Osaka Gas Co., Ltd., 6-19-9 Torishima, Konohana, Osaka 554 Japan

Spallone, Antonio Laboratori Nazionali Frascati, Istituto Nazionale Fisica Nucleare, Via E. Fermi, 00044 Frascati (Roma) Italy

Srinivasan, Mahadeva Neutron Physics Division, Bhabha Atomic Research Center, Trombay, Bombay, 400-085 India

Stella, Bruno Dipartimento di Fisica, Universita degli Studi of Roma "La Sapienza", P.le Aldo Moro 2-00185 (Roma) Italy

Sudo, Shiroshi Electricity Technology Research and Development Center, Tohoku Electric Power Co., Inc., 7-2-1 Nakayama, Aoba, Sendai, Miyagi 981 Japan

Sugai, Hiroshi Tokai Research Center, Sumitomo Metal Mining Co., Ltd., 2600 Ishigamitojuku, Tokai, Naka, Ibaraki 319-11 Japan

Sugihara, Ryo Plasma Science Center, Nagoya University, Furo, Chikusa, Nagoya 464-01 Japan

Sugino, Noboru Mitsubishi Research Institute, Inc., Time & Life Bldg., 2-3-6 Otemachi, Chiyoda, Tokyo 100 Japan

Suzuki, Akio NKK Co., 1-1-2 Marunouchi, Chiyoda, Tokyo 100 Japan

Suzuki, Minoru Fundamental Research Laboratories, Osaka Gas Co., Ltd., 6-19-9 Torishima, Konohana, Osaka 554 Japan

Tabet, Eugenio Laboratorio di Fisica, Instituto Superiore di Sanita, Viale Regina Elena, 299-00161 (Roma)Italy

Takada, Eiji Mitsubishi Research Institute, Time & Life Bldg., 2-3-6 Otemachi, Chiyoda, Tokyo 100 Japan

Takahashi, Akito Department of Nuclear Engineering, Osaka University, 2-1 Yamadaoka, Suita, Osaka 565 Japan

Takahashi, Koji Department of Energy Engineering, Yokohama National University, 156 Tokiwadai, Hodogaya, Yokohama 240 Japan

Takahashi, Ryoji Department of Engineering, University of Tokyo, 7-3-1 Hongo, Bunkyo, Tokyo 113 Japan Home: 2-26-21 Seta, Setagaya, Tokyo 158 Japan

Takai, Takahiro Department of Energy Engineering, Yokohama National University, 156 Tokiwadai, Hodogaya, Yokohama 240 Japan

Takaki, Shinichi Equos Research., Ltd., Goto Bldg., 2-19-12 Sotokanda, Chiyoda, Tokyo 101 Japan

Takayama, Kazuo Tokai University, 1117 Kita-Kaname, Hiratsuka 259-12 Japan

Takeishi, Yasuhiro Department of Energy Engineering, Yokohama National University, 156 Tokiwadai, Hodogaya, Yokohama 240 Japan

Takeuchi, Yasuhito Yokogawa Electric Corporation, 2-9-32, Naka-machi, Musashino, Tokyo 180 Japan

Takuma, Tadasu Komae Research Laboratory, Central Research Institute of Electric Power Industry, 2-11-1 Iwato-Kita, Komae, Tokyo 201 Japan

Tamaru, Takeshi Hiroshima Institute of Technology, 1-1-2 Miyake, Saeki, Hiroshima 731-51 Japan

Tanaka, Yoshihito Research Division, Tokushima Research Center, 537 Kitahata, Okinohama, Tokushima 770 Japan

Tani, Toyu 1194-13 Nagase, Moroyama, Iruma, Saitama 351-03 Japan

Taniguchi, Ryoichi Research Institute for Advanced Science and Technology, University of Osaka Prefecture, 1-2 Gakuen, Sakai, Osaka 593 Japan

Taniguchi, Tomihiro Electric Power Technology Division, MITI, 1-3-1 Kasumigaseki, Chiyoda, Tokyo 100 Japan

Tanimoto, Mitsumori Energy Fundamentals Division, Electrotechnical Laboratory, 1-1-4 Umezono, Tsukuba, Ibaraki 305 Japan

Tarumoto, *Yasumasa* *Kansai Electric* Power Co., Inc., 3-3-22 Nakanoshima, Kita, Osaka 530-70 Japan

Tazima, Teruhiko National Institute for Fusion Science, Furo, Chikusa, Nagoya 464-01 Japan

Thompson, David T. "Newlands", The Village Whitchurch Hill Reading RG8 7PN UK

Tomita, Mitsuru Fusion Power Engineering Group, Advanced Nuclear Systems Engineering Department, Mitsubishi Heavy Industries, Ltd., Shuwa Shiba Park Bldg., 2-4-1 Shibakoen, Minato, Tokyo 105 Japan

Tripodi, Paolo Laboratori Nazionali Frascati, Istituto Nazionale Fisica Nucleare, Via E. Fermi, 00044 Frascati (Roma) Italy

Tsarev, Vladimir A. Department of Nuclear Physics and Astrophysics, Academy of Sciences, P.N. Levedev Physical Institute, Leninsky Prospect, 53 117924, GSP, Moscow Russia

Tsuchiai, Hiroaki Department of Research & Development, Hokkaido Electric Power Co., Inc., 461-6 Satozuka, Toyohira, Sapporo 004 Japan

Tsuchida, Kan *Faculty of Science* and Engineering, Ritsumeikan University, 56-1 Kita-machi, Tojiin, Kita, Kyoto 603 Japan

Tsuchiya, Kenichi Tokyo National College of Technology, 1220-2 Kunugida, Hachioji, Tokyo 193 Japan

Tsukakoshi, Hiroshi IIC., Ltd., 2000-1 Iwai, Iwata, Shizuoka 438 Japan

Tsukui, Katsuyuki Waseda University, 2-8-26 Nishiwaseda, Shinjuku, Tokyo 169 Japan

Tsunoda, Hirokazu Safety Engineering Department, Mitsubishi Research Institute, Inc., Time & Life Bldg., 2-3-6 Otemachi, Chiyoda, Tokyo100 Japan

Tsuruta, Takao Takasago R & D Center, Mitsubishi Heavy Industries, Ltd., 2-1-1 Shinhama, Arai, Takasago, Hyogo 676 Japan

Uchida, Hirohisa Department of Applied Physics, Faculty of Engineering, Tokai University, 1117 Kita-Kaname, Hiratsuka, Kanagawa 259-12 Japan

Uchikawa, Hideo Meijo University, 1-501 Shiogamaguchi, Tenpaku, Nagoya 468 Japan

Ueda, Ryoji 33-5 Maruyama, Yatomi, Mizuho, Nagoya 467 Japan

Ueshima, Masato The Institute of Physical and Chemical Research (RIKEN), 2-1 Hirosawa, Wako, Saitama 351-01, Japan

Urciuoli, Guido Maria INFN- Sezione Sanita, Viale Regina Elena, 299-00161 (Roma) Italy

Veranth, Joe Bose Corporation, The Mountain, Framingham, MA 01772 USA

Vigier, Jean Pierre Laboratoire Physique Theorique, Tour 22 4 Etage, Universite P.et M. Curie(Paris VI), 4 Place Jussier, Paris Ledex 75065 France

Vysotskii, Vladimir I. Kiev State University, 252017, Vladimirskaya 64, Radiophysical dep-t Ukraine

Waber, James Michigan Technological University, 10 Woodland Road, Houghton, MI 49931-9748 USA

Wada, Nobuhiko Faculty of Science, Nagoya University, Furo, Chikusa, Nagoya 464-01 Japan

Wada, Susumu Department of Energy Engineering, Yokohama National University,

156 Tokiwadai, Hodogaya, Yokohama 240 Japan

Ward, Jack F. Fusion Energy Applied Technology, P.O.Box 58639, Salt Lake City, UT 84158 USA

Watanabe, Kenji Department of Physics, Chuo University, Kasuga, Bunkyo, Tokyo 112 Japan

White, Carol 21st Century Science Association, 60 Sycolin Road, Suite 203 Leesburg, VA 22075 USA

Yabuno, Ryohei IMRA Material R & D Co., Ltd., 5-50 Hachiken, Kariya, Aichi 448 Japan

Yabuuchi, Norio High Scientific Research Laboratory, 204 Marusen Bldg., Marunouchi, Tsu, Mie 514 Japan

Yamada, Hiroshi Department of Electrical and Electronic Engineering, Iwate University, 4-3-5 Ueda, Morioka 020 Japan

Yamada, Yasuhiro Production Engineering Development Division, Toyota Motor Co., 1 Toyota, Toyota, Aichi 471 Japan

Yamaguchi, Eiichi NTT Basic Research Laboratories, 3-9-11 Midori, Musashino, Tokyo 180 Japan

Yamaguchi, Sadae Institute for Materials Research, Tohoku University, 2-1-1 Katahira, Aoba, Sendai, Miyagi 980 Japan

Yamamoto, Hisashi Nuclear Power Systems Division, Hitachi, Ltd., 4-6 Kanda-Surugadai, Chiyoda, Tokyo 101 Japan

Yamamoto, Sachio Office of Naval Research Asian Office, Akasaka Press Center, 7-23-17 Roppongi, Minato, Tokyo 106 Japan

Yamamoto, Teiichi Japan Development Bank, 1-9-1 Otemachi, Chiyoda, Tokyo 100 Japan

Yamato, Harumi Research and Development Center, Toshiba Corporation, 4-1 Ukishima, Kawasaki, Kanagawa 210 Japan

Yamazaki, Osamu Department of Energy Engineering, Yokohama National Universaty, 156 Tokiwadai, Hodogaya, Yokohama 240 Japan

Yasui, Kyuichi Department of Physics, School of Science and Engineering, Waseda University, 3-4-1 Ohkubo, Shinju, Tokyo 160 Japan Home: 1593-52, Irumagawa, Sayama, Saitama 350-13 Japan

Yasui, Tsutomu IMRA Europe S.A., 220, Rue Albert-Caquot, Sophia Antipolis, 06560 Valbonne France

Yonezu, Ikuo Functional Materials Research Center, Sanyo Electric Co., Ltd., 1-18-13 Hashiridani, Hirakata, Osaka 573 Japan

Yoshida, Zenko Department of Chemistry, Japan Atomic Energy Research Institute, Tokai, Naka, Ibaraki 319-11 Japan

Yoshikawa, Hiroyuki Faculty of Engineering, University of Tokyo, 7-3-1 Hongo, Bunkyo, Tokyo 113 Japan

Yoshikawa, Nobuharu Institute for Nuclear Study, University of Tokyo, 3-2-1 Midorimachi, Tanashi, Tokyo 188 Japan

Yoshitake, Hideaki Department of Energy Engineering, Yokohama National University, 156 Tokiwadai, Hodogaya, Yokohama 240 Japan

Yuan, Liq-Ji Institute of Nuclear Science, National Tsing Hua University, 101 Section 2, Kuang Fu Rd., Hsinchu 33043 ROC

Zhang, Xin Wei Institute of Applied Physics and Computational Mathematics, No.6 Huayuan Road Hai-Dian District, P.O. Box 8009 Beijing 100088 China

Zhang, Yue Chang Welding Research Institute, Osaka University, 11-1 Mihogaoka, Ibaraki, Osaka 567 Japan

Author Index